

# Hyperbranched Polymers: Multifunctional Flame Retardants for Epoxy Resins

Inaugural-Dissertation

to obtain the academic degree

Doctor rerum naturalium (Dr. rer. nat.)

Submitted to the Department of Biology, Chemistry, and Pharmacy

of the Freie Universität Berlin

by

Alexander Philipp Battig, M.Sc.

2020





The doctoral dissertation presented herein was prepared from February 2016 until January 2020 at the Bundesanstalt für Materialforschung und -prüfung (BAM) in Berlin, Germany, under the supervision of Priv. Doz. Dr. rer. nat. habil. Bernhard Schartel.

1<sup>st</sup> Reviewer: Priv. Doz. Dr. rer. nat. habil. Bernhard Schartel, Bundesanstalt für Materialforschung und -prüfung (BAM), Berlin.

2<sup>nd</sup> Reviewer: Prof. Dr. rer. nat. habil. Rainer Haag, FB Biologie, Chemie, Pharmazie, Freie Universität Berlin

Date of Defense: June 19<sup>th</sup>, 2020



# For Lea

I want to say one word to you. Just one word.

*Yes, sir.*

Are you listening?

*Yes, I am.*

Plastics.

*Exactly, how do you mean?*

There's a great future in plastics. Think about it. Will you think about it?

- The Graduate

## Acknowledgements

My sincere thanks go to Priv. Doz. Dr. habil. Bernhard Schartel for the academic support, fruitful discussions, constructive feedback, and thoughtful guidance throughout the entire PhD process. Your advice, critiques, and expertise were crucial to its completion. Thanks for encouraging me to consistently improve upon my work and myself, and for providing thought-provoking insights into whether one is the cause or the solution to ones' dilemmas. I will strive perpetually to be the latter. I wish to thank Prof. Dr. Rainer Haag for his enduring support throughout my academic pursuits: thank you for your support during my Bachelor thesis in your working group, it inspired me to pursue the Master of Polymer Science, which you also helped supervise. Thanks also for encouraging me to look beyond academia, and now for reviewing this doctoral dissertation.

I have had the privilege of working with exceptional people during my PhD. I would like to thank Jens C. Markwart and Priv. Doz. Dr. habil. Frederik R. Wurm for their crucial roles in the success of the DFG project, and the excellent communication, cooperation, and assistance throughout its course. I would like to thank Patrick Klack for his technical support and the enlightening conversations, also to Dr. Katharina Kebelmann for her technical assistance with the Py-GC/MS. Special thanks to Thomas Rybak for his help with the DSC and CryoMill, and Michael Schneider, Nicolai Schmidt and Tobias Kukofka for their technical support with my polymer samples in the workshop.

I want to give thanks to the amazing friends and colleagues in department 7.5 and beyond with whom I have had the pleasure of working: Tim Rappsilber, Michael Morys, Dr. Aleksandra Sut, Dr. Sebastian Rabe, Lars Daus, Sandra Falkenhagen, Christy Yin Yam Chan, Weronika Tabaka, Dr. Nora Timme, Dr. Sebastian Timme, Melissa Matzen, Marie-Bernadette Watolla, Dr. Daniele Frasca, Analice Turski-Silva Diniz, Dr. Fanni Sypaseuth, Vitus Hupp, Karla Itzel Garfías González, Dr. Tanja Gnutzmann, Dr. Paul Geoerg, Dr. Christian Metz, Philipp Franz, Maren Erdmann, Yi Tan, Xuebao Lin, and my interns Will Harris and Letitia Vasconcelos de Lima. Thank you for your scientific (and non-scientific) insights, thanks for the laughs, and thanks for the memories. A special thank you to Benjamin Zirnstein and Martin Günther for their help, the great coffee, and for making the marathon so memorable.

I would be remiss to thank my friends and family for their continuing encouragement for my academic studies and beyond. Thank you to my mom Elvira and my dad Joachim for their perpetual support for all my endeavors.

My dearest and most sincere thanks go to my wife Lea, who is an enduring inspiration and my greatest source of strength. You have remained a lighthouse in the turbulent seas of this journey. Your patience, love, and encouragement have brought me to this shore.

## Abbreviations

ADMET	Acyclic diene metathesis
AlPi	Aluminum diethylphosphinate
APP	Ammonium polyphosphate
ATMET	Acyclic triene metathesis
CO <sub>2</sub>	Carbon dioxide;
CO	Carbon monoxide
COSY	Correlation spectroscopy
BDP	Bisphenol A diphenyl phosphate
DCM	Dichloromethane
DGEBA	Diglycidyl ether of bisphenol A
DMC	2,2-Dimethyl-4,4'-methylene-bis(cyclohexylamine)
DOPO	9,10-dihydro-9-oxa-10-phosphaphenanthrene-10-oxide
DSC	Differential scanning calorimetry
EHC	Effective heat of combustion
EI	Electron ionization
EP	Epoxy resin
eq.	Equivalent
ESI-MS	Electrospray ionization mass spectrometry
FR	Flame retardant
FIGRA	Fire growth rate
FTIR	Fourier transform infrared spectrometry
hb	Hyperbranched
HRR	Heat release rate
(L)OI	(Limiting) oxygen index
M	Mol(es)
$M_w$	Weight-average molecular weight
MALDI-TOF	Matrix assisted laser desorption / ionization
MARHE	Maximum average rate of heat emission

N	Nitrogen
NMR	Nuclear magnetic resonance
O / O <sub>2</sub>	Oxygen
P	Phosphorus
(hb)-P-FR	(hyperbranched) Phosphorus-based flame retardant
PCFC	Pyrolysis combustion flow calorimeter
PEGE	Pentaerythritol tetraglycidylether
PHRR	Peak of heat release rate
POCl <sub>3</sub>	Phosphoryl chloride
Py-GC/MS	Pyrolysis coupled with gas chromatography and mass spectrometry
S	Sulfur
SEC	Size exclusion chromatography
SEM	Scanning electron microscopy
$T_{5\%}$	Temperature at 5% mass loss (onset temperature)
$T_{dec}$	Decomposition temperature
$T_g$	Glass-transition temperature
TGA	Thermogravimetric analysis
THE	Total heat evolved
THF	Tetrahydrofurane
$T_{max}$	Temperature at maximum mass loss rate
TML	Total mass loss
$t_{ig}$	Time to ignition
UL	Underwriter's Laboratory
wt.-%	weight percent

## Table of Contents

1.	Introduction .....	1
2.	Scientific Background.....	3
2.1.	Fire Behavior and Flame Retardancy .....	3
2.2.	Flame retardants: State of the art, and market analysis .....	7
2.3.	Phosphorus-based flame retardants .....	8
2.4.	Hyperbranched Polymers: Multifunctional Macromolecules .....	10
3.	Scientific Goals and Approach.....	14
4.	Materials and Methods.....	16
4.1.	Polymer matrix: Epoxy resins .....	16
4.2.	Methodology.....	17
4.2.1.	Fire testing: Cone calorimeter .....	18
4.2.2.	Fire testing: Reaction-to-small-flames .....	19
4.2.3.	Thermogravimetric analysis–FTIR (TG-FTIR), Hot-stage FTIR.....	20
4.2.4.	Pyrolysis – Gas chromatography / Mass spectrometry (Py-GC/MS).....	21
4.2.5.	Pyrolysis combustion flow calorimeter (PCFC).....	22
5.	Publications .....	24
5.1.	Molecular Firefighting – How Modern Phosphorus Chemistry Can Help Solve the Flame Retardancy Task.....	24
5.2.	Systematically Controlled Decomposition Mechanism in Phosphorus Flame Retardants by Precise Molecular Architecture: P–O vs P–N.....	44
5.3.	Hyperbranched phosphorus flame retardants: multifunctional additives for epoxy resins.....	93
5.4.	Aromatic vs. Aliphatic Hyperbranched Polyphosphoesters as Flame Retardants in Epoxy Resins .....	130
5.5.	Matrix matters: Hyperbranched flame retardants in aliphatic and aromatic epoxy resins .....	159
5.6.	Sulfur’s Role in the Flame Retardancy of Thio-Ether–linked Hyperbranched Polyphosphoesters in Epoxy Resins.....	189
5.7.	First phosphorus AB <sub>2</sub> monomer for flame-retardant hyperbranched polyphosphoesters: AB <sub>2</sub> vs. A <sub>2</sub> + B <sub>3</sub> .....	213
6.	Summary .....	237
7.	Zusammenfassung.....	240
8.	References .....	243





# 1. Introduction

Polymers are pervasive in almost every facet of modern life; their versatility is derived from their tunable physical and mechanical properties. Consequently, polymeric materials, i.e. plastics, are ubiquitous and indispensable in nearly every aspect of life and every sector of industry.<sup>1</sup> Accordingly, the annual worldwide production was 180 million tons in 2000,<sup>2</sup> and an estimated 8.5 billion tons of virgin plastics have been produced worldwide from the 1950s to 2018.<sup>3</sup> Most plastics are widespread as common commodities or as technical products due to their low production cost and practical properties. High-performance polymers such as epoxy resins, on the other hand, are an interesting alternative to traditional construction materials such as metals and wood due to their unique and tunable properties like low weight and high strength.<sup>4</sup>

Epoxy resins are among the most widely used polymers for high-performance applications due to their high durability, low weight, chemical and thermal resistance, and exceptional mechanical and electrical properties.<sup>5, 6</sup> Their major fields of application include electrical systems and electronics, adhesives, paints and coatings, and especially structural applications as glass or carbon-fiber composite materials.<sup>7</sup> Epoxy resin composites are progressively implemented in automobile, marine, and aerospace design,<sup>8</sup> in part to reduce weight and improve fuel efficiency. Notably, the high strength-to-weight characteristic of epoxy resin composites is used to produce longer and more efficient rotor blades for wind turbine generators.<sup>9</sup> The continued expansion of these markets means increased demand for epoxy resins, and consequently, the global market volume is estimated to grow to US\$ 12.84 billion by 2026.<sup>10</sup>

Most hydrocarbon-based polymeric materials have a high fire load and therefore pose a risk during accidental fires.<sup>1</sup> Especially high-performance materials like epoxy resins are implemented in areas where the material properties are crucial to the design or operation of the product.<sup>8</sup> Both mechanical failure and flammability are equally critical aspects that must be regarded during production and incorporation to ensure the safe usage of these polymers.

It is therefore imperative that the chosen flame retardants affect these material properties in the least impactful way while retaining effective fire protection, and this is where hyperbranched flame retardants can help bridge the gap.<sup>2</sup>

Hyperbranched polymers are a special group of macromolecules that have complex geometries. Their branched structure leads to unique properties: they have a low viscosity, a high functional group content, and are more easily soluble in other polymers.<sup>11</sup> Moreover, they have a high immobility within a polymer matrix, and they may possess high glass-transition temperatures which decreases their overall impact on the glass-transition temperature of the polymer blend.<sup>12</sup> Hyperbranched polymeric flame-retardant additives are multifunctional compounds: their ability to easily blend with and maintain retention in the polymer matrix, exhibit a reduced impact on material properties, and afford effective flame retardancy at low loadings makes them attractive flame retardants for high-performance matrices like epoxy resins.

The aim of this work is the research of hyperbranched polymers as flame retardants for epoxy resins. Several investigations into the way these materials interact with the polymer matrix are presented within the scope of this work, with the aim of gaining a mechanistic understanding of the flame-retardant effect and the underlying structure-property relationship. By utilizing a multi-methodic approach, the specific chemical mechanisms underlying the flame-retardant modes of actions are investigated, the results correlated, and the decomposition pathways identified.

## 2. Scientific Background

### 2.1. Fire Behavior and Flame Retardancy

The prevalence of polymers in everyday life comes at cost: most polymeric materials are easily flammable and burn with a high fire load owing to their hydrocarbon-based composition.<sup>13</sup> In order to curtail the inherent fire risk of these “sliceable petroleum” products, the use of and continued research into flame retardants is of paramount importance to ensure the safe use of plastics.<sup>14</sup> The implementation of a functioning flame retardant can safeguard from unwarranted ignition, prevent the spread of fire, diminish the production of smoke, and increase escape time from dangerous fire scenarios.<sup>1</sup>

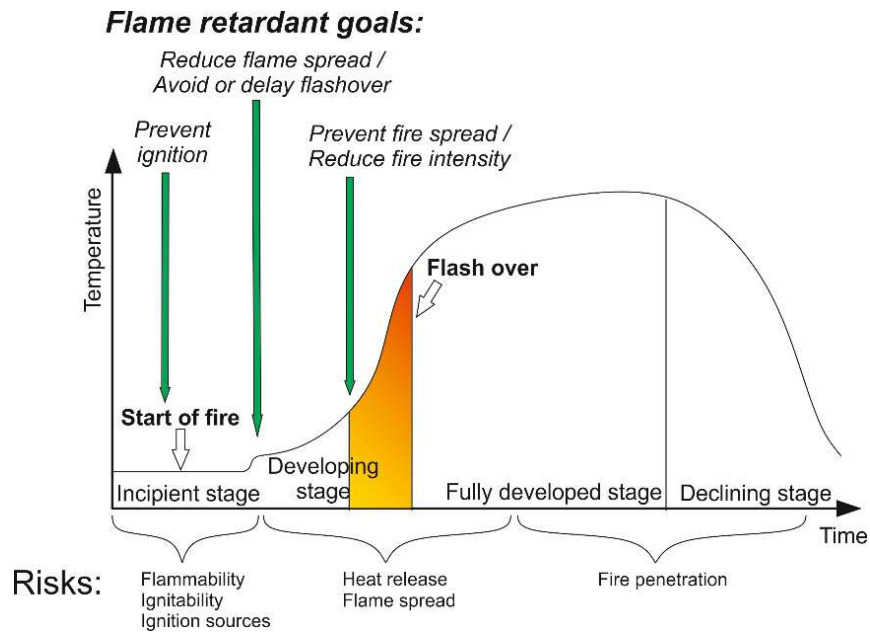


Figure 1. Development of fire temperature over time, material risks at respective fire stages, and fire protection goals for various stages. (adapted from Scharrel et al.<sup>15</sup> and Troitzsch<sup>14</sup>)

Fires may be partitioned into certain stages: incipient, developing, fully developed, and declining (Figure 1).<sup>15</sup> At the start of a fire, the overall temperature remains low, and as the fire continues, increasing amounts of combustible gases fill the area; this comes to a head when their concentration is sufficiently high to cause their sudden ignition. This process is known as the “flash over” and involves a drastic increase in temperature, thus marking the beginning of

the fully developed stage. Here, the overall temperature remains high as increasing amounts of material provide fuel for the fire. As the rate of heat release is nearly constant, the fire is in a steady state. Once the flame cannot be sufficiently sustained with fuel or oxygen, the declining stage begins, the overall temperature drops, and combustion processes begin to decline.

The “fire behavior” of a polymer is not a static material property, but rather the reaction of the material to a specific fire scenario.<sup>16</sup> To understand and characterize the burning behavior of flame-retarded materials, it is important to understand the material’s performance under these specific fire scenarios. Accordingly, fire tests are designed to assess the material’s response under precise circumstances: The reaction-to-small-flames test such as UL-94 or LOI relate to ignition and are aimed at assessing polymer ignitability and flame spread, and a flame-retardant goal is to prevent or delay ignition or prevent or minimize flame spread. For materials used in electrical and electronic equipment, the glow wire test is used to understand the material’s contact response to a glowing hot electrical wire, as may be the case after short-circuits. The cone calorimeter may be used to characterize a material at various fire stages, as the heat flux can be adjusted: between 35 kW m<sup>-2</sup> and 50 kW m<sup>-2</sup>, a developing fire is simulated.<sup>15</sup> Under such forced flaming test, the impact of flame retardants in delaying ignition, reducing flame spread, and reducing the overall fire intensity may be identified and quantified.

Apart from macroscopic fire phenomena, an array of equipment provides further insight into the material behavior during thermal decomposition. For example, thermogravimetric analysis helps to understand mass loss, and Fourier transform infrared spectroscopy (FTIR) or pyrolysis coupled with gas chromatography and mass spectroscopy (Py-GC/MS) may be implemented to characterize decomposition products. Moreover, pyrolysis combustion flow calorimetry (PCFC) and bomb calorimetry measurements can provide insight into thermodynamic processes. By investigating not only the fire behavior of the material on the large scale, but also the thermal decomposition in the milli- and microgram scale, a great deal of knowledge on the function of the flame retardant and how it interacts with the material may be won. The fire phenomena of flame-retarded polymers result from the behavior of the

components in the condensed and/or gas phase, which requires these aspects be looked at separately.

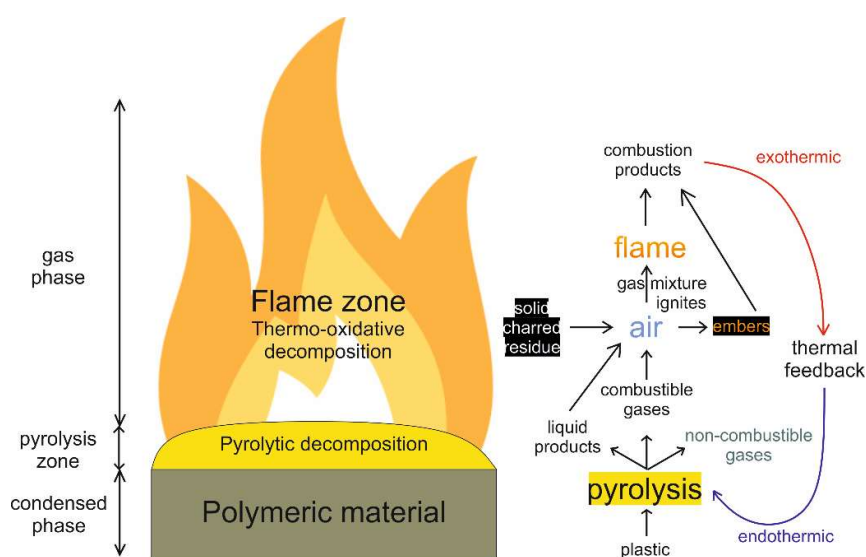


Figure 2. Schematic combustion process, indicating condensed phase, pyrolysis zone, and gas phase (left), and combustion processes (right). (adapted from Troitzsch<sup>14</sup>)

Figure 2 outlines the combustion process of a polymer. Decomposition reactions in the polymeric bulk feeds the flames by the production of combustible fuel. This occurs due to the mass flux caused by the scission of polymer chains, e.g. via random chain-scission, chain-end scission, or elimination of pendant groups.<sup>17</sup> These scission processes produce low molar mass volatiles which liquefy (and ultimately boil) or form new solid particles; hence, this phase is commonly called the condensed phase. Characteristic of diffusion flames is the oxygen gradient between the oxygen-rich periphery, where thermo-oxidative processes occur, and the center, where the decomposition occurs under anaerobic conditions.<sup>13</sup> Hence, this region of anaerobic decomposition is called the pyrolysis zone, and consequently pyrolytic decomposition governs the condensed phase and thus the production of volatiles in the gas phase, including non-combustible gases such as water, carbon dioxide, or ammonia. Volatiles are oxidized in the gas phase by atmospheric oxygen in an exothermic redox reaction known as combustion,<sup>13</sup> which provides sufficient energy to promote additional pyrolytic decomposition in what is known as a “thermal feedback loop”.<sup>14</sup> Several exothermic reactions

occur simultaneously, and the largest contributor to the production of heat is the strongly exothermic reaction of OH· radicals reacting with carbon monoxide to form carbon dioxide and H· radicals.<sup>18</sup> Combustion products include carbon dioxide, carbon monoxide, water, and smoke.<sup>13</sup>

For the steady state burning of a material, the heat release rate (HRR) is described as a function of several specific variables. More importantly, for a material to pass a specific flame retardancy test, the HRR must fall below a specific critical HRR criterion.<sup>19</sup> (Equation 1)

$$\begin{aligned} \text{Equation 1: } \quad HRR &= \chi \cdot \Theta(t) \cdot (1 - \mu) \cdot \frac{h_c^0}{h_g} \cdot \dot{q}''_{net} \\ &= \chi \cdot \Theta(t) \cdot (1 - \mu) \cdot \frac{h_c^0}{h_g} \cdot (\dot{q}''_{ex} + \dot{q}''_{flame} - \dot{q}''_{rerad} - \dot{q}''_{loss}) < HRR_{crit} \end{aligned}$$

HRR: heat release rate;  $\chi$ : combustion efficiency;  $\Theta(t)$ : time-dependent protective layer effects;  $\mu$ : char yield;  $h_c^0$ : heat of complete combustion;  $h_g$ : heat of gasification;  $\dot{q}''_{net}$ : net heat flux;  $\dot{q}''_{ex}$ : external heat flux per material unit area;  $\dot{q}''_{flame}$ : convective heat flux from the flame;  $\dot{q}''_{rerad}$ : heat flux from re-radiation of hot surfaces;  $\dot{q}''_{loss}$ : heat flux loss to environment;  $HRR_{crit}$ : critical heat release rate needed to pass a specific flame retardancy test.

Flame retardants may interact with the polymer matrix or its decomposition products in a variety of ways,<sup>20</sup> and the use of flame retardants affects the key parameters of Equation 1. Some flame retardants are active in the gas phase: they act either by releasing non-combustible gases (flame dilution), by releasing water (cooling), or by interacting with the radicals formed during decomposition (radical scavenging, i.e. flame inhibition).<sup>21, 22</sup> By interrupting the combustion process, diluting the flame zone, or endothermic decomposition, this mode of action affects the combustion efficiency  $\chi$ , the heat of complete combustion  $h_c^0$ , and the heat flux from the flame  $\dot{q}''_{flame}$ , respectively. Other flame-retardant modes of action occur in the condensed phase: the formation of char, a protective char layer, or any other form of thermal or gas barrier can shield the underlying material from further combustion and thus reduce mass flux to the flame.<sup>21, 22</sup> This mode of action affects the time-dependent protective layer function  $\Theta(t)$ , the char yield  $\mu$  and thereby the mass fraction consumer by the fire  $(1-\mu)$ , the

heat of gasification  $h_g$ , as well as the convective heat flux  $\dot{q}''_{\text{flame}}$  and the heat flux from re-radiation of hot surfaces  $\dot{q}''_{\text{rerad}}$ . Many flame retardants may utilize predominantly one mode of action, yet most successful formulations incorporate a combination of both condensed and gas phase modes of action to protect the polymer matrix during fires.<sup>21</sup>

There is no universal flame retardant for polymers, as the interaction between flame retardant, matrix, and the decomposition products of both is the key to effective flame retardancy.<sup>22</sup> Moreover, the flame retardant must suit the specifications of the polymeric material, including polymer type, manufacturing and production specifics, areas of application, and price. Accordingly, a wide range of flame retardants are available,<sup>16</sup> and their implementation and continued research are central to ensure the continued safe use of polymers in everyday life.

## 2.2. Flame retardants: State of the art, and market analysis

In 2015, an estimated 2.25–2.49 million tons of flame retardants (FRs) were consumed.<sup>23</sup> The most common additives were inorganic salts like aluminum (tri)hydroxide (ATH) (approx. 38% of market share<sup>24</sup>) or magnesium (di)hydroxide (MDH), which act by decomposing endothermically and releasing water, thereby removing energy from the fire. While efficient in many types of polymers, one drawback of these additives is that they require high loadings, thus impacting the mechanical and material properties of the polymer matrix. Among the most effective and generally applicable commercial flame retardants are halogenated compounds (approx. 23% market share in 2016<sup>24</sup>). Commonly, chlorinated or brominated organic chemicals are used as additives in combination with antimony oxide (approx. 8% market share in 2016<sup>24</sup>), which enhances the flame retardancy potential via synergism.<sup>25</sup> Alternatively, halogens are used as reactive compounds integrated into the polymer via copolymerization. Their main mode of action is the release of hydrogen halides, which react with hydroxyl and hydrogen radicals formed via bond scission of water molecules during combustion (i.e. flame poisoning).<sup>26</sup> Halogenated flame-retardant systems are functional already at low loadings and their wide field of application have historically made them among the most implemented

formulations. However, the use of halogenated compounds has come under increased scrutiny due to health concerns and their persistence, bioaccumulation, and toxicity in humans and wildlife.<sup>27, 28</sup> Thus, even though several compounds have been forbidden from use in industry,<sup>29</sup> the utilization of halogenated flame retardants, although debatable, remains a current practice in industry.

Among the most prominent alternatives to halogens is the use of phosphorus in flame-retardant formulations. Organophosphorus compounds are promising alternatives to halogenated flame retardants (approx. 18% market share in 2016<sup>24</sup>): they are functional already at low loadings and can maintain crucial material properties such as glass-transition temperature. Moreover, the versatility of phosphorus chemistry allows for a wide array of flame-retardant formulations for a broad field of polymer matrices (see Chapter 5.1).<sup>30</sup>

### 2.3. Phosphorus-based flame retardants

A wide array of flame retardants based on phosphorus exists today, as either reactive or additive compounds.<sup>31</sup> Reactive components are implemented into the polymer backbone via the reaction with functional groups such as alcohols, amines, epoxy groups, etc. and are used primarily in epoxy resins, polyesters, and polyurethane foams.<sup>32, 33</sup> Examples include BAPPO (bis(4-aminophenyl)phenylphosphine oxide) for polyurethanes,<sup>34</sup> or DOPO (9,10-dihydro-9-oxa-10-phosphaphenanthrene-10-oxide) -derivates for epoxy resins.<sup>35-37</sup> Reactive components add “inherent” flame-retardancy to a polymer matrix and are advantageous when material properties are crucial. Despite these advantages, the flame-retardant moiety must be tailored to suit the reactive groups of the material. Thus, additive flame retardants are the most prevalent on the market, as they can be used in a wider array of polymeric materials.

Additive compounds can be divided into inorganic and organophosphorus materials. Inorganic phosphorus flame retardants include red phosphorus, aluminum diethyl phosphinate (AlPi), or ammonium polyphosphate (APP), which have been proven effective in a wide array of matrices, often in multicomponent systems to increase synergism.<sup>38-41</sup> However, organophosphorus compounds are advantageous to particular polymeric systems due to high



effectivity already at very low loadings.<sup>30</sup> Organophosphorus flame retardants vary in molecular mass, phosphorus-content, molecular shape, and oxidation state; especially the latter has been proven to greatly impact the mode of action.<sup>42</sup>

Generally, phosphorus-based flame retardants exhibit both condensed and gas phase modes of action, (Figure 3) although some (such as DOPO) are mainly gas-phase active.<sup>31</sup> Phosphorus-compounds function as char promoters by acting as a net-point to aromatic moieties, leading to carbonaceous char and thereby retaining fuel in the condensed phase. Often, the flame retardants themselves include aromatic groups to promote their incorporation into the residue.<sup>43, 44</sup> Moreover, the production of phosphoric acid groups from phosphorus flame retardants has a catalytic effect on polymer dehydration thus aiding aromatization. The formation of polyphosphates and phosphorus-containing polyaromatic char can act as a protective layer that protects the underlying material from the flame.<sup>45</sup> In the gas phase, phosphorus-based flame retardants often decompose to form radical species which act via flame poisoning, thus reducing the heat of combustion.<sup>46</sup>

Many additive phosphorus-based flame-retardant formulations exist today due to the chemical versatility of phosphorus.<sup>47, 48</sup> Often, synergistic moieties such as nitrogen, sulfur, boron, or silicone compounds are introduced to improve the efficacy or reduce the necessary loading of a material.<sup>49-52</sup> These modifications aim to utilize matrix-specific functional groups. Alternatively, metal ions such as zinc or aluminum (e.g. zinc-borates, aluminum diethyl phosphinate) help catalyze decomposition reactions and promote charring or intumescence, and melamine-based variants, e.g. melamine polyphosphate, or melamine cyanurate-coated red phosphorus, use melamine's gas-phase mode of action in combination with phosphorus to achieve good flame retardancy.<sup>32</sup>

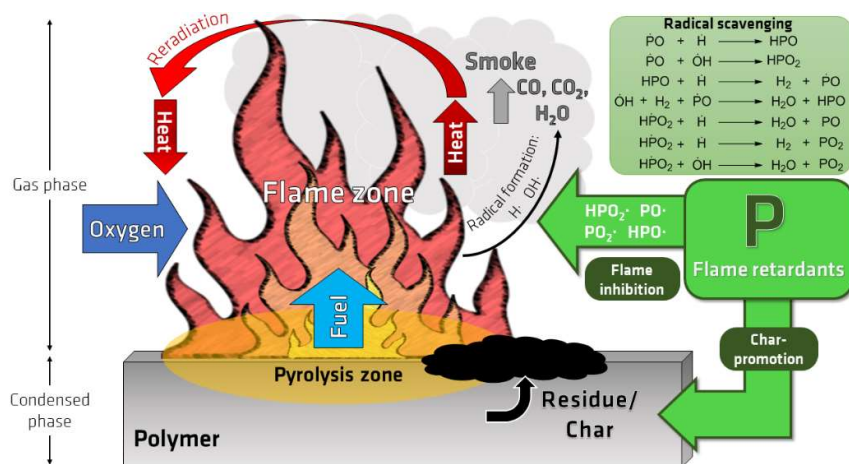


Figure 3. Modes of action of phosphorus-based flame retardants, including char promotion in the condensed phase and flame inhibition in the gas phase.<sup>47</sup>

For both halogenated and non-halogenated flame retardants, there exists an increasing trend toward polymeric formulations. Low molar mass flame retardants are more prone to leach from the matrix or bloom out with time than their polymeric variants, which is a major issue for the REACH (Restriction, Evaluation, Authorization and Restriction of Chemicals) compliance set up by the European Chemical Agency.<sup>53, 54</sup> Polymeric flame retardants are more likely to entangle with the polymer matrix, thus increasing their retention. Furthermore, they decompose at higher temperatures than low molar mass flame retardants, potentially leading to a greater overlap of decomposition temperature ranges of matrix and flame retardants, which improves chemical interaction and leads to greater flame retardancy.<sup>55, 56</sup> Another approach to improve flame retardancy is by utilizing complex architectures:<sup>57, 58</sup> they are amorphous due to their geometry, and thus miscibility with the matrix is improved, and leaching or blooming is decreased due to high immobilization in the matrix. One group of polymers merges the approaches of high molar mass and complex shape: hyperbranched polymers.

#### 2.4. Hyperbranched Polymers: Multifunctional Macromolecules

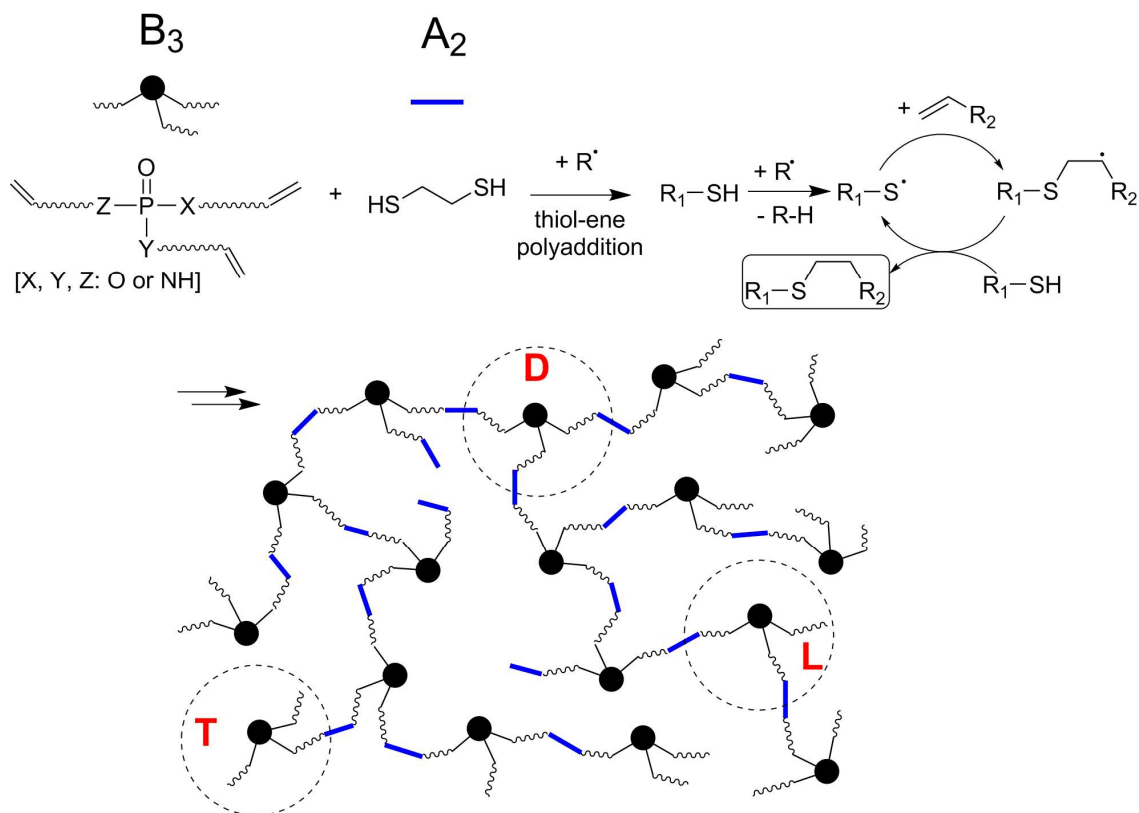
Branching geometries are inherent to a broad range of organic and inorganic objects of all scales<sup>11</sup>, and amylopectin and glycogen are examples for naturally occurring highly branched

polymers. For synthetic polymers, this dendritic pattern may be achieved via polymerization with branching at repeating units, as was first observed by Staudinger and Schulz in 1935 and described with theoretical models by Flory in 1943.<sup>59</sup>

Hyperbranched polymers are a type of specialized macromolecules that are highly branched and related to dendrimers, thus sharing some of their unique properties.<sup>60</sup> One must clearly differentiate between a “perfect” dendrimer, where every repeating unit is branched, to hyperbranched polymers, where the degree of branching is lower than 1.<sup>61</sup> Unlike dendrimers which are monodisperse, spherical, and have a regular three-dimensional topology, hyperbranched polymers have a higher polydispersity, are amorphous, and have an irregular three dimensional topology.<sup>62</sup> They do not require extensive multi-step syntheses and extensive purification steps, which separates them from dendrimers, as these require several protection, purification, and deprotection steps. Instead, hyperbranched polymers may be easily produced in a one-step polymerization,<sup>63</sup> making them attractive for large-scale synthesis, and commercial monomers are readily available.

Their unique characteristics have made these polymers popular in diverse fields, including nanotechnology and the biomedical fields,<sup>64, 65</sup> and growing interest in the field is reflected in the amount of publications over time, which has risen monotonously since 1990.<sup>11</sup> Recently, hyperbranched polymers have been proposed as flame-retardants.<sup>66, 67</sup> More specifically, hyperbranched polyphosphoesters have proven effective in improving the flame retardancy behavior of epoxy resins.<sup>68</sup> This approach combines the use of non-halogenated flame retardants with polymeric formulas as additives to polymer matrices.

Hyperbranched polymers may be prepared in multiple ways, such as the “classic” approach via polycondensation of  $AB_x$  monomers proposed by Flory,<sup>69</sup> the  $A_2+B_y$  approach of which there are several synthesis paths with various combinations,<sup>70, 71</sup> but also via ring-opening multibranching, self-condensing ring-opening, and self-condensing vinyl polymerizations.<sup>72-74</sup>



*Scheme 1. Synthesis route of  $A_2+B_3$  polymers used in this work, including radical initiated thiol-ene polyaddition, and schematic hyperbranched polymer structure, highlighting dendritic (D), linear (L), and terminal (T) units of the macromolecule. (adapted from own work<sup>75</sup>)*

The majority of materials used herein are prepared via polyaddition of  $A_2+B_3$  monomers (Scheme 1), although an  $AB_2$ -type polymer is investigated within this work. For the  $A_2+B_3$  polymers, ethanedithiol acts as an  $A_2$ -unit and a trifunctional phosphoester with three vinyl groups functions as the  $B_3$ -monomer. The thiol-ene polyaddition is efficient and has a fast reaction rate: The radical generator decomposes and initiates the thiol group by abstracting a hydrogen, creating a thiyl-radical which further propagates with the vinyl group in an anti-Markovnikov addition.<sup>76</sup> Finally, in a chain-transfer step, the hydrogen from a new thiol-group is abstracted, forming a thioether bond and a new thiyl-radical which subsequently propagates further polyaddition reactions. The resulting macromolecule contains three types of units: dendritic, linear, and terminal, which differ in the amount of thioether groups, i.e. connections to other monomers. Each branching point is a phosphorus-moiety and all bonds are fully

rotational; thus, the resulting polymer is an amorphous, viscous amber liquid at room temperature.

Phosphorus-based hyperbranched polymers are promising flame retardants because of their multifunctional qualities: their high molar mass and complex geometry increase miscibility with polymer matrices, which increases their efficacy as additive flame retardants due to a more homogenous distribution and lack of agglomeration. Moreover, the high rotational freedom of the hyperbranched structure and the high glass-transition temperature of these polymers reduce the plasticizing-effect most phosphorus-based additives present.<sup>77</sup> Thus, hyperbranched polymers exhibit a less-pronounced impact on the glass-transition temperature of the flame retarded polymer matrix. Furthermore, the high phosphorus-content, and additionally the presence of thioethers as a supplementary functional group, present various modes of action in the gas and condensed phase. Further still, the complex shape and high molar mass decrease health hazards, i.e. persistence, bioaccumulation, and toxicity (PBT), as phosphoesters are hydrolysable, thus reducing their persistence and possibly increasing their biocompatibility.<sup>78</sup> As the REACH regulation monitors the circulation of potentially hazardous chemicals,<sup>53</sup> hyperbranched polymers are interesting compounds for industrial application, and especially interesting for high-performance polymers such as epoxy resins.

As the field of polymeric flame retardants with complex architectures continues to grow and new optimized formulations are investigated, it is crucial to understand the fundamental chemistry at work. By understanding the chemical mechanisms governing the decomposition of these macromolecules, the exhibiting modes of action become clear, and may even be predicted theoretically, thus improving future formulations.

### 3. Scientific Goals and Approach

As described in our review on the subject, there exist several synthesis routes and approaches of implementing phosphorus-based compounds to address the task of flame-retarding polymers. Phosphorus-based chemistry is versatile, and several successful approaches to flame-retardancy implement synergistic-moieties such as nitrogen or sulfur. The specific chemical composition of the phosphorus-containing compounds strongly impacts the flame retardancy performance, and the structure-property relationship between matrix and flame retardant are key. Moreover, compounds with higher molar mass or complex geometries have shown significant results compared to low molar mass analogues (see Chapter 5.1.).

However, it remains unclear what roles specific changes in the chemical composition of hyperbranched polymers play, and how branched architectures or polymerization affect flame retardancy. Moreover, a comprehensive investigation of polymerization type, or aromaticity of either the hyperbranched polymer or its polymer matrix is lacking.

To gain further insight on what role the chemical surrounding of the phosphorus-species plays in flame retardancy, a library of phosphorus-based materials was needed. By systematically controlling the amount of P-O or P-N bonds in the binding pattern of phosphorus during synthesis, variations in the flame-retardant behavior of the resulting materials are identifiable and can thus be attributed to the changes in binding-sphere. Moreover, if the low molar mass  $B_3$  units are compared to their respective  $A_2+B_3$ -type hyperbranched polymer, insight into the function of the complex geometry is attainable. Precisely these approaches were examined in two publications: the first describes the synthesis and investigation of the flame retardancy potential of phosphoramides, phosphorodiamidates, phosphoramidates, and phosphates (see Chapter 5.2.), while the second outlines the polymer synthesis and examines the difference between  $A_2+B_3$ -type hyperbranched polymers and their respective  $B_3$  monomers (see Chapter 5.3.).

The production of carbonaceous char relies on the formation of char-precursors, and while the aliphatic species of monomers and polymers were effective in retaining fuel in the condensed phase via charring, the question remained whether flame-retardancy performance could be enhanced by implementing an aromatic moiety into the carbon chain. This idea was expanded upon in the third publication, where two sets of monomers and polymers, one aliphatic and one aromatic, are produced via acyclic triene metathesis (ATMET) and their flame-retardancy potential assessed (see Chapter 5.4.).

In all cases, an epoxy resin based on diglycidyl ether of bisphenol A (DGEBA) was used as the polymer matrix. However, the structure-property relationship of matrix and flame retardant are the key to effective flame retardancy. While the hyperbranched polymeric flame retardants proved effective for aromatic resins, it was unclear how the compounds would perform in aliphatic resins. This question was addressed in the fourth publication, where the flame-retardant potential of  $A_2+B_3$  polymers and their respective  $B_3$  monomers are compared in an aliphatic and an aromatic resin (see Chapter 5.5).

These investigations provided great insight into the multifunctional capabilities of these novel  $A_2+B_3$  compounds, yet the drawn conclusions were often restricted to comparisons between the polymers and their  $B_3$  monomers; thus, the function of the  $A_2$ -moiety remained uninvestigated. The fifth publication compares sulfur-containing  $B_3$  monomers and the  $A_2+B_3$  hyperbranched polymer to ascertain the part sulfur plays in the flame-retardant efficacy of these materials (see Chapter 5.6.).

Although the thio-ether bonds in hyperbranched polymers contribute to the flame retardancy potential by generating sulfur-radicals which added condensed and gas phase modes of action, the phosphorus content of the polymer may be improved if the polymerization approach were changed from the  $A_2+B_3$  route. The sixth publication compares two types of polymerization types of hyperbranched polymers: By changing the monomer structure and adjusting the reaction conditions, an  $AB_2$ -type monomer and hyperbranched polymer

containing slightly higher phosphorus per repeating unit improved the fire performance compared to an A<sub>2</sub>+B<sub>3</sub>-type polymer and its monomer (see Chapter 5.7.).

An in-depth analysis of phosphorus-based hyperbranched polymeric flame retardants is presented in this work, and the results underline their multifunctional qualities in epoxy resins. This research outlines the function of several components of hyperbranched polymers, which may prove useful in future formulations to further improve the flame-retardant qualities.

## 4. Materials and Methods

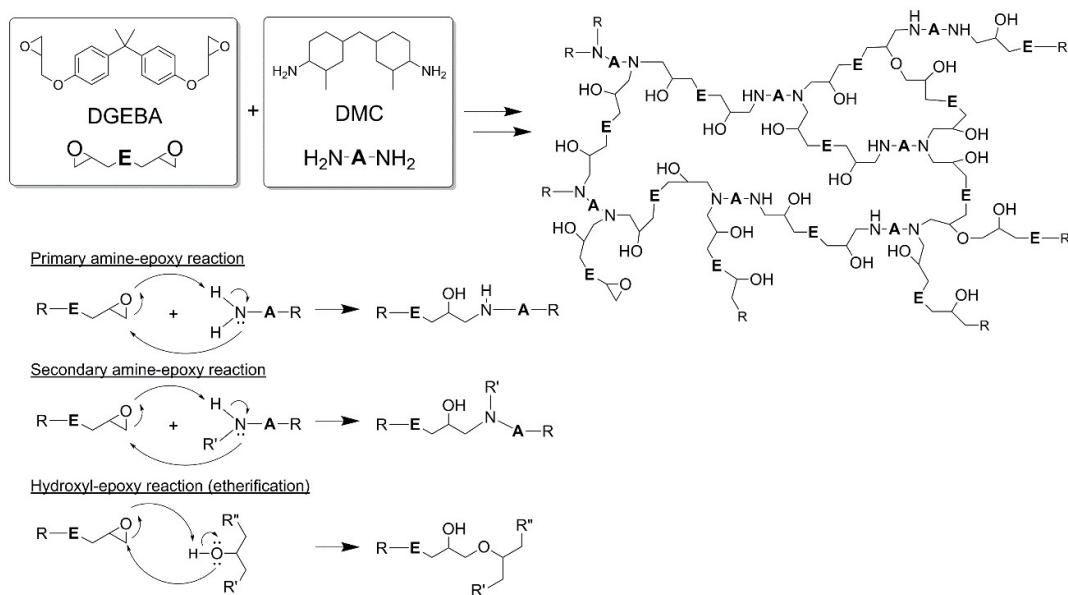
### 4.1. Polymer matrix: Epoxy resins

The main polymer resin matrix implemented within the scope of this work is a type of epoxy resins commonly used in industry: diglycidyl ether of bisphenol A (DGEBA) is produced via the reaction of bisphenol A and epichlorohydrin. The thermosetting epoxy resins are formed by the polyaddition of polyfunctionalized oxirane-containing molecules with nucleophiles to form a three-dimensional network in a process known as curing. While epoxy resins may be cured using anhydrides, phenols, or thiols, one of the most widely commercially used class of hardeners, and the one utilized within the scope of this work, are polyfunctionalized amines. Within this work, 2,2'-dimethyl-4,4'-methylene-bis(cyclohexylamine) (DMC) is used as the hardening agent.

The driving force of the reaction is the nucleophilic ring-opening reaction of the epoxide group (Scheme 2). This reaction may occur in three variants and under both basic and acidic conditions, yet the former is the case for amines: primary amines may initiate the ring-opening reaction via S<sub>N</sub>2 nucleophilic attack, forming a hydroxyl group and a secondary amine bond along the backbone, i.e. β-amino alcohol groups. These secondary amines function as nucleophiles themselves and propagate further ring-opening reactions with other epoxide groups, forming tertiary amines and a hydroxyl group. The hydroxyl groups are also



nucleophilic and may react with epoxide groups to form ether bonds along the backbone (etherification). However, this reaction only becomes significant after an increase of hydroxyl groups from the first two reactions.<sup>79</sup>



Scheme 2. Reaction scheme of an epoxy resin based on diglycidyl ether of bisphenol A (DGEBA) and 2,2'-dimethyl-4,4'-methylene-bis-(cyclohexylamine) (DMC), highlighting the main reactions between hydroxyls, primary, and secondary amines with epoxy groups, respectively. (adapted from own work<sup>80</sup>)

The production of the epoxy resin samples involved the calculation of the correct molar ratio and then the combination of the epoxy and amine components under agitation. For the flame-retarded blends, the epoxy component was first mixed with the additive until homogenous, and then the hardener was added. The compounds were degassed *in vacuo* and then poured into prepared molds of desired dimensions. The final hardening process was performed at elevated temperatures, close to the glass-transition temperature of the final resin at approx. 150 °C.

#### 4.2. Methodology

Using a multi-methodical approach allows insight into a wide range of material properties; thus, the findings of one method are validated with those of another. Generally, the methods

can be divided into investigations of the fire behavior (forced flaming conditions and reaction-to-small-flames) and pyrolytic decomposition (gas and condensed phase analysis) of the flame-retarded material. Moreover, the pyrolytic decomposition of the flame retardants themselves is closely analyzed to understand their decomposition mechanism and thus infer their effect on the polymer matrix during fire. Additionally, changes to the glass-transition temperature ( $T_g$ ) of the polymer matrix by the addition of the flame retardants via differential scanning calorimetry (DSC), as well as microscopy of residues after fire testing via scanning electron microscopy (SEM), offer a broader image of the impact the flame retardants have on the fire behavior of epoxy resins.

#### 4.2.1. Fire testing: Cone calorimeter

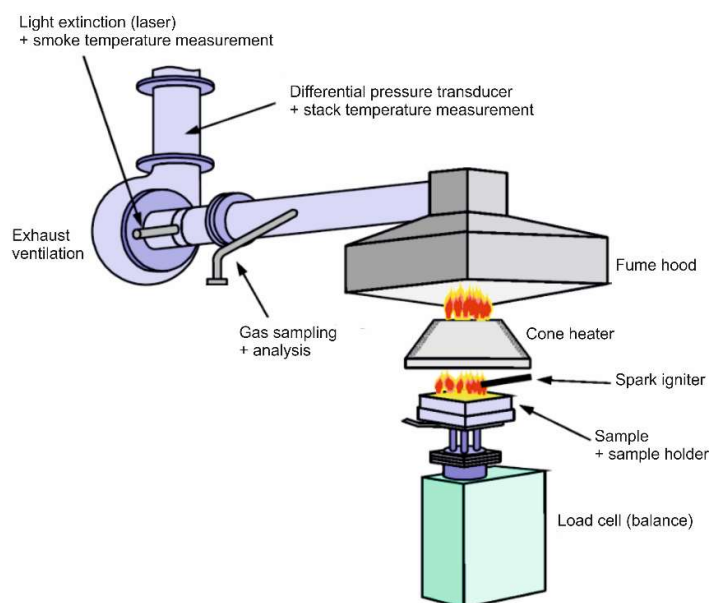


Figure 4. a) Schematic cone calorimeter set-up.<sup>81</sup>

The main method of examining the fire behavior is via the cone calorimeter (Figure 4). A sample placed on a sample holder is positioned on a load cell and subjected to a specific radiation (e.g.  $50 \text{ kW m}^{-2}$ ) from the cone heater. A spark igniter ignites volatile gases, and exhaust fumes pass through the fume hood towards the exhaust ventilation, before which the exhaust gases are sampled and analyzed for  $\text{CO}_2$ ,  $\text{CO}$ , and  $\text{O}_2$  content. The light extinction is

measured by a laser via Lambert-Beer Law, providing smoke production rates. Finally, the difference in pressure and stack temperature are measured in the chimney. The cone calorimeter provides valuable data and parameters essential in understanding the fire phenomena of a given sample, including time of ignition, mass loss over time, CO<sub>2</sub> and CO production over time, O<sub>2</sub> consumption (and consequently heat release rate over time and total heat evolved<sup>82, 83</sup>), smoke production rates, and being able to visually assess specific fire behaviors. Moreover, the data from the cone calorimeter provides valuable information on the burning behavior of a material: when observing the heat release rate over time, the shape of the resulting curve reveals whether the material is thermally thin or thick, or whether there is a protective layer effect of the resulting char layer.<sup>15</sup> By comparing the results of non-flame-retarded to flame-retarded materials, a mode of action may be more easily derived, including charring, protective layer effects, or even flame poisoning effects via the ratio of total heat evolved per mass loss, otherwise known as the effective heat of combustion (EHC).

#### 4.2.2. Fire testing: Reaction-to-small-flames

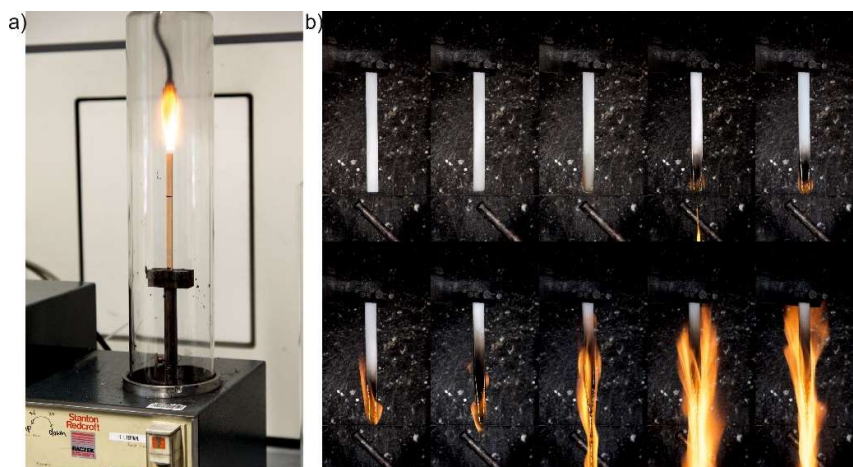


Figure 5. a) Setup and measurement of a specimen with limiting oxygen index (LOI) testing; b) Vertical setup and measurement of a sample in Underwriter's Laboratory 94 test (UL-94).

Among fire tests, a material's ignitability is an important characteristic to assess flame spread. Two reaction-to-small-flames tests, namely limiting oxygen index (LOI) and Underwriter's Laboratory 94 test (UL-94), are utilized within this dissertation. For LOI (Figure

5 a) according to ISO 4589, a sample specimen is supported vertically by a clamp on the bottom in a precise nitrogen/ oxygen mixture flowing upward through a glass chimney. The top of the specimen is ignited, and the burning behavior of the material is observed. Burning times, length of specimen burnt, and oxygen concentration are noted, and the test is repeated at ever decreasing oxygen concentrations until the minimum is estimated. In UL-94 tests according to IEC 60695, a rectangular bar-shaped sample is clamped in either vertical or horizontal position, the former being the more demanding test, and ignited on the free end via a calibrated 50 W burner flame. The material's upward or horizontal flame-spread is assessed, and in vertical setup, a piece of cotton is placed below the sample before measurement to test burning dripping behavior.

#### 4.2.3. Thermogravimetric analysis–FTIR (TG-FTIR), Hot-stage FTIR

While fire tests help to understand the burning behavior of a material, much of the chemistry relevant to flame retardancy occurs in the pyrolysis zone. By measuring the mass of a sample under a constant heating rate via thermogravimetric analysis (TGA), information on decomposition temperature-range, decomposition rate, and temperature at maximum rate ( $T_{\max}$ ) is gained. Understanding the specific changes to the chemical structure of both matrix and flame retardant during decomposition is a crucial step to understanding the chemical mechanisms that govern the flame-retardant modes of action. To that end, FTIR is a useful tool, as specific functional groups and changes in their chemical surrounding can be identified. FTIR works by subjecting a sample to a beam of infrared light, whose wavelength may be altered using a Michaelson interferometer, and measuring how much of the energy is absorbed for each wavelength. Thus, the vibrational-rotational energy working upon a molecule may be measured, and certain functional groups exhibit absorption at unique energies, i.e. wavenumbers.

Two types of FTIR are used herein: one measuring evolved gas (TG-FTIR) and one the condensed phase (Hot-stage) (Figure 7). This way, the decomposition of the material is closely monitored: a few milligrams of the powdered material is heated at a constant rate ( $10 \text{ K min}^{-1}$ )

until it decomposes, and its mass loss is measured by a microbalance (TGA). The ensuing volatile gases pass through a heated transfer-line into the gas cell, where they are measured via FTIR over the duration of the heating period. The condensed phase FTIR is measured by preparing a powdered sample in a potassium bromide platelet, which is placed inside a hot-stage platform under nitrogen atmosphere. The sample is heated at a constant rate ( $10 \text{ K min}^{-1}$ ) and measured via FTIR over the entire heating period. Thus, both the gas and condensed phase of any given sample is analyzed, and by investigating the sample during pyrolysis, information on the fate of a particular functional group can be tracked, providing an insight into the chemical mechanisms at work during pyrolytic decomposition.

#### 4.2.4. Pyrolysis – Gas chromatography / Mass spectrometry (Py-GC/MS)

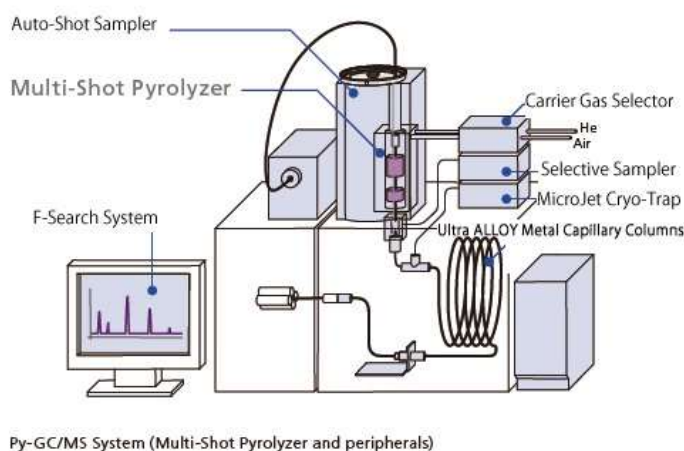


Figure 6. Schematic setup of a pyrolysis coupled with gas chromatography / mass spectrometry (Py-GC/MS) (from Shimadzu<sup>84</sup>).

While FTIR is useful to identify specific groups, the information it gathers is unspecific, as the absorption range of functional groups often overlap, and more complex molecules contain many overlapping signals. A useful method to identify the chemical structure of a material during decomposition is by pyrolysis coupled with gas chromatography and mass spectrometry (Py-GC/MS) (Figure 6).

In the setup used within this dissertation, i.e. single shot analysis, a microgram sample is pyrolyzed at a specific temperature via gravimetric drop into a heated cell. The evolved gases pass through a gas chromatograph, where they are separated through a capillary column running a heating program. The gases pass through a high-energy (70 eV) beam and are ionized before being measured by the mass selective detector.

The output of the combined system provides a mass spectrum of all gas samples passing through the gas chromatograph, which delivers valuable information of the decomposition products of a given material. By combining the findings from FTIR with those from Py-GC/MS, a clearer image of the decomposition mechanism is attainable. An example is presented in Chapter 5.2., where the presence of hex-5-en-1-ol as a decomposition product of a phosphoester-based flame retardant was first stipulated through FTIR analysis, and finally verified by Py-GC/MS measurements. Thus, Py-GC/MS has the strong potential to supplement other pyrolysis investigations.

#### 4.2.5. Pyrolysis combustion flow calorimeter (PCFC)

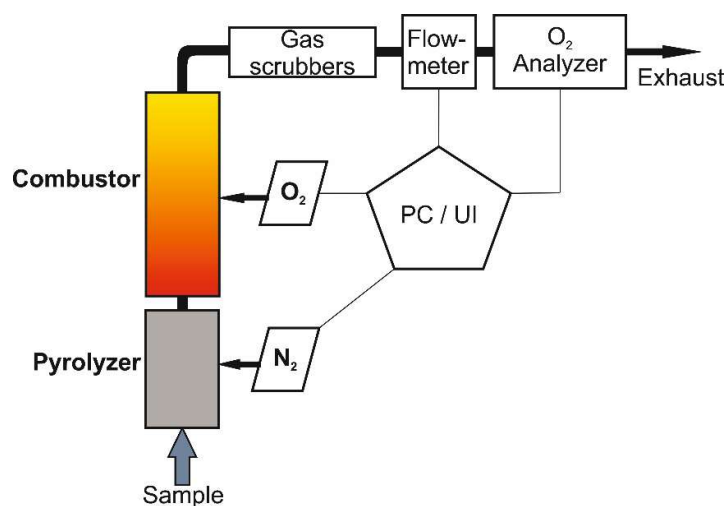


Figure 7. Schematic setup of pyrolysis combustion flow calorimeter (PCFC).

The pyrolysis combustion flow calorimeter is used to determine the heat of combustion of volatile products during the pyrolytic decomposition of a given material. The setup is designed

to mimic the processes in the flame zone, as the specimen is first pyrolyzed under nitrogen atmosphere and the volatile products are combusted in an oxygen rich environment at high temperatures. However, it must be noted that there is no diffusion flame, and the products are fully oxidized in the combustor; thus, the machine is blind to some flame-retardant modes of action, such as flame poisoning via radical scavenging, which is crucial to many phosphorus-based flame retardants.

PCFC provides insight into the heat of complete combustion of the volatiles by measuring the oxygen consumption in the combustor as the material pyrolyzes at a constant heating rate of  $1 \text{ K s}^{-1}$ . The gathered data, which includes the peak of heat release rate (PHRR), the total heat evolved (THE), and the residue yield, validates these value points from cone calorimeter and TGA measurements. However, PCFC is suitable for illuminating flame dilution effects, as the release of incombustible gases yields no oxygen consumption. Therefore, the comparison of a flame-retarded and a non-flame-retarded polymer material via PCFC has the potential to reveal flame dilution as a mode of action.





## 5. Publications

### 5.1. Molecular Firefighting – How Modern Phosphorus Chemistry Can Help Solve the Flame Retardancy Task

Maria M. Veleconso, Alexander Battig, Jens C. Markwart, Bernhard Schartel, Frederik R. Wurm, *Angew. Chem. Int. Ed.* **2018**, 57, 10450-10467.

International Edition: DOI link: <https://www.doi.org/10.1002/anie.201711735>

German Edition: DOI link: <https://www.doi.org/10.1002/ange.201711735>

This article was accepted and published.

#### Author contribution:

- Aided in conceptualizing the frame of the work
- Outlined the main points of each chapter
- Maintained communications between all authors
- Researched articles and literature for each chapter
- Authored the abstract and the introductory chapter
- Authored the conclusion and outlook
- Provided several figures throughout the article
- Proofread and spell-checked all versions of the article

## **Abstract**

The ubiquity of polymeric materials in daily life comes with an increased fire risk, and sustained research into efficient flame retardants is key to ensuring the safety of the populace and material goods from accidental fires. Phosphorus, a versatile and effective element for use in flame retardants, has the potential to supersede the halogenated variants that are still widely used today: current formulations employ a variety of modes of action and methods of implementation, as additives or as reactants, to solve the task of developing flame-retarding polymeric materials. Phosphorus-based flame retardants can act in both the gas and condensed phase during a fire. This Review investigates how current phosphorus chemistry helps in reducing the flammability of polymers, and addresses the future of sustainable, efficient, and safe phosphorus-based flame-retardants from renewable sources.

Phosphorus Flame Retardants

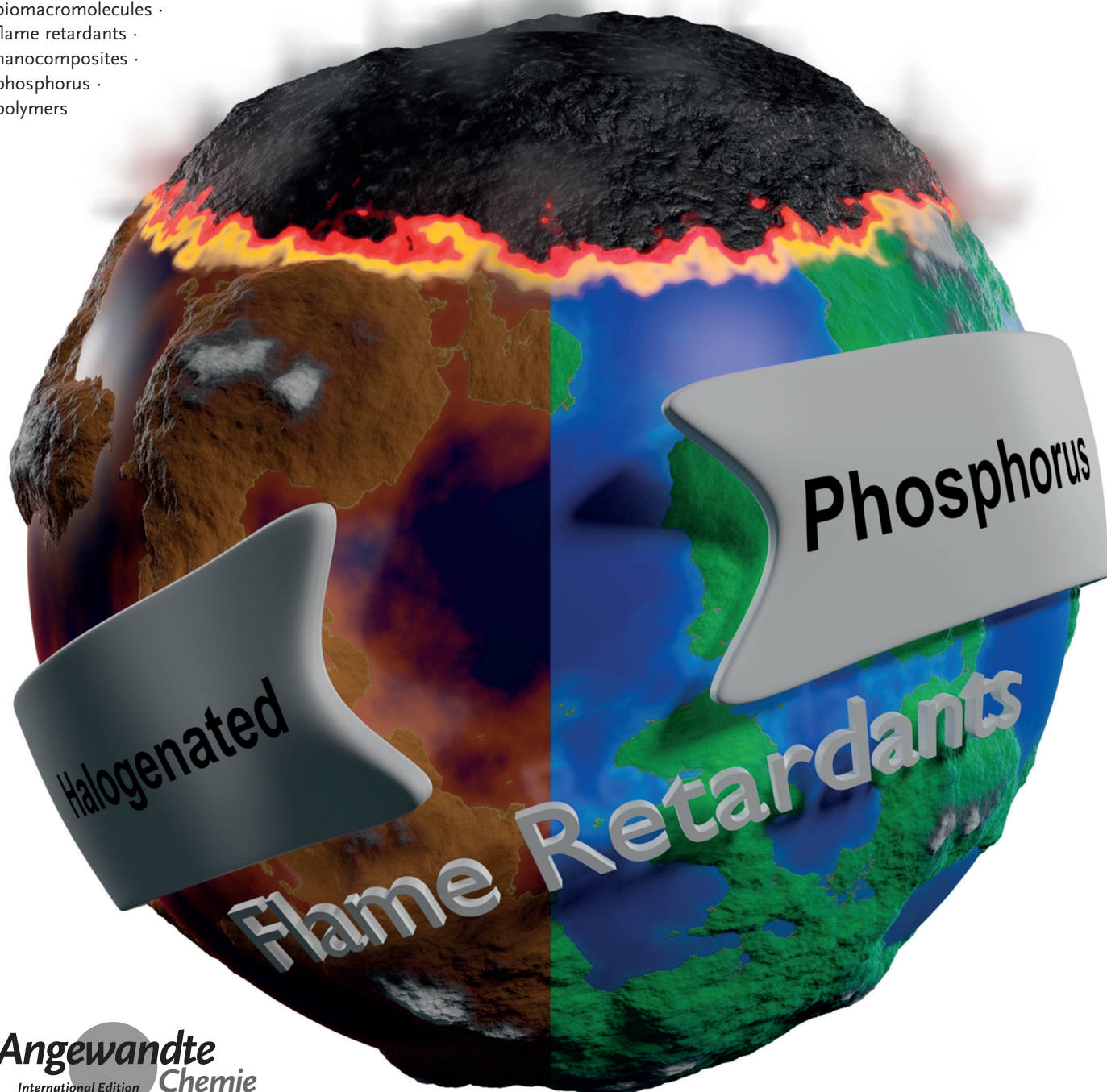
International Edition: DOI: 10.1002/anie.201711735  
German Edition: DOI: 10.1002/ange.201711735

# Molecular Firefighting—How Modern Phosphorus Chemistry Can Help Solve the Challenge of Flame Retardancy

Maria M. Velencoso<sup>+</sup>, Alexander Battig<sup>+</sup>, Jens C. Markwart<sup>+</sup>, Bernhard Schartel, and Frederik R. Wurm\*

**Keywords:**

biomacromolecules ·  
flame retardants ·  
nanocomposites ·  
phosphorus ·  
polymers



The ubiquity of polymeric materials in daily life comes with an increased fire risk, and sustained research into efficient flame retardants is key to ensuring the safety of the populace and material goods from accidental fires. Phosphorus, a versatile and effective element for use in flame retardants, has the potential to supersede the halogenated variants that are still widely used today: current formulations employ a variety of modes of action and methods of implementation, as additives or as reactants, to solve the task of developing flame-retarding polymeric materials. Phosphorus-based flame retardants can act in both the gas and condensed phase during a fire. This Review investigates how current phosphorus chemistry helps in reducing the flammability of polymers, and addresses the future of sustainable, efficient, and safe phosphorus-based flame-retardants from renewable sources.

### 1. The Challenge of Flame Retardancy—Demands of a Good Flame Retardant

Polymeric materials are ubiquitous in nearly all aspects of modern life: from consumer electronics, packaged goods, and construction to transportation, aerospace, industrial machinery, and manufacturing processes. This development comes with an inherent risk of fire: hydrocarbon-based polymeric materials display a large fire load and high flammability. Sustained research on effective flame retardants (FRs) to reduce the risks is pivotal in safeguarding against accidental fires, costly damage to material goods, and in ensuring the health and safety of the populace.

Halogenated flame retardants, which were widely applied in the past, have come under increased scrutiny and prompted increased research into halogen-free and phosphorus-based flame retardants (P-FRs) in particular.<sup>[1]</sup> This development is further attributed to legislation and decisive shifts in market demands, as increased attention has paid to producing more sustainable FRs. P-FRs have now become a prominent alternative to their halogenated counterparts.<sup>[2]</sup> Phosphorus plays the key role in halogen-free flame retardancy as a result of its chemical versatility, multiple FR mechanisms, and high effectivity already at low loadings. As the demand for safe advanced materials grows, the question for material scientists is: what role can current chemistry play in solving the flame retardancy problem? To more closely understand the task at hand, it is necessary to first outline what constitutes a “good” FR:

- 1) Material properties must be conserved to the greatest possible extent, with price as the most determining factor.
- 2) The FR properties must match the polymer processing and pyrolysis characteristics.
- 3) Health regulations and market direction necessitates that formulations must become increasingly environmentally friendly, recyclable, and sustainable.

In the following sections, these aspects are explored in detail. Then, state-of-the-art P-FRs and their modes of action are discussed and show how these features are embraced.

### From the Contents

1. The Challenge of Flame Retardancy—Demands of a Good Flame Retardant	10451
2. Phosphate Rock—A Finite Natural Resource	10454
3. Recent Developments in Reactive Phosphorus Compounds	10456
4. Recent Developments in Additive Phosphorus Compounds	10458
5. Modern Trends and the Future of Phosphorus-Based Flame Retardants	10460
6. Conclusions	10464

Finally, we highlight modern trends of P-FRs and their potential future application. To that end, representative examples for each section were chosen, but this Review is not meant to be a comprehensive summary. For further reading, we recommend the reviews of Weil and Levchik,<sup>[3]</sup> Malucelli et al.,<sup>[4]</sup> and Bourbigot and Duquesne.<sup>[5]</sup>

#### 1.1. Retaining Material Properties: A Question of Price

The chemical composition of the polymer determines the material properties, production routes, application areas, and bulk price (Figure 1). Thermoplastic polyolefins (e.g. poly-


[\*] Dr. M. M. Velencoso,<sup>[†]</sup> M. Sc. J. C. Markwart,<sup>[†]</sup>


Priv.-Doz. Dr. F. R. Wurm  
Physical Chemistry of Polymers  
Max Planck Institute for Polymer Research  
Ackermannweg 10, 55128 Mainz (Germany)  
E-mail: wurm@mpip-mainz.mpg.de

M. Sc. A. Battig,<sup>[†]</sup> Priv.-Doz. Dr. B. Schartel  
Technical Properties of Polymeric Materials  
Bundesanstalt für Materialforschung und -prüfung (BAM)  
Unter den Eichen 87, 12205 Berlin (Germany)

M. Sc. J. C. Markwart<sup>[†]</sup>  
Graduate School Materials Science in Mainz  
Staudinger Weg 9, 55128 Mainz (Germany)

[†] These authors contributed equally to this work.

 The ORCID identification number for one of the authors of this article can be found under:  
<https://doi.org/10.1002/anie.201711735>.

 © 2017 The Authors. Published by Wiley-VCH Verlag GmbH & Co. KGaA. This is an open access article under the terms of the Creative Commons Attribution Non-Commercial License, which permits use, distribution and reproduction in any medium, provided the original work is properly cited, and is not used for commercial purposes.



ethylene, polypropylene, polyvinyl chloride) are common commodities and mass produced at low costs;  $\text{Al}(\text{OH})_3$ , the most common FR, is both effective and inexpensive to produce, but requires high loadings, which affects the material properties (e.g. coloration, opacity, tensile strength).<sup>[6]</sup> Commercially available P-FRs (e.g. ammonium polyphosphate, APP) require significantly lower loadings for similar effectiveness, and thereby retain the respective material properties.<sup>[7]</sup> Moreover, adjuvants and synergists (e.g. metal oxides, charring agents, nanofillers, additional P-FRs) increase the efficacy and further lower the loadings required.<sup>[8]</sup>

Engineering polymers (e.g. polyamides, polycarbonates, polyurethanes, polyethylene terephthalates) are applied in more advanced areas (e.g. electronics/electrical engineering, transport, manufacturing). These materials can be synthe-

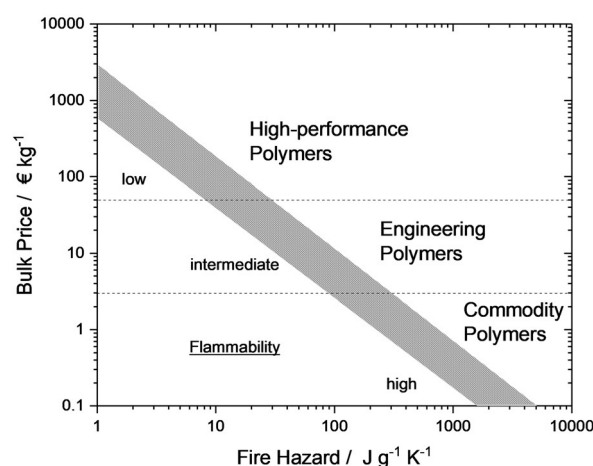


**Figure 1.** Fire hazard versus bulk price of various polymeric material classes.<sup>[14]</sup>

sized as thermoplasts, elastomers, or thermosets in foams, fibers, or foils, and so a wider array of FRs exist. The use of these FRs depend on the polymer's price, quality grade, and precise application.<sup>[9]</sup> Notable formulations contain aluminum diethyl phosphinate, melamine polyphosphate, and Zn borate, or melamine cyanurate-microencapsulated red phosphorus.<sup>[10]</sup>

High-performance polymers (e.g. epoxy/polyester resins, polyetherimides, polysulfones, poly(aryl ether ketones)) are used in specialized fields (e.g. adhesives, coatings, composites)



Dr. Maria M. Velencoso received her M.Sc. in Chemical Engineering from the University of Castilla-La Mancha (Spain) in 2008 and completed her Ph.D. there in 2014 with Prof. Antonio de Lucas Martinez for work on the synthesis and application of phosphorylated polyols as reactive flame retardants. For her research, she maintained a long-term collaboration with HUNTSMAN. She is currently a Marie Skłodowska-Curie Post-doctoral fellow in the group of Prof. Katharina Landfester at the Max Planck Institute for Polymer Research (Germany), where she is working on the development of nanoparticles for flame retardant applications.



Alexander Battig studied Chemistry (B.Sc.) and Polymer Science (M.Sc.) at the Free University Berlin, Germany. After establishing and running his own company, he joined the group of Bernhard Schartel at the Bundesanstalt für Materialforschung und -prüfung (BAM) in Berlin, for his Ph.D. in 2016. He is an active member of the doctoral student network at BAM, a member of its organizing committee, and a representative of the doctoral students. His research, supported by the Deutsche Forschungsgemeinschaft (DFG), focuses on the molecular understanding of hyperbranched polyphosphoesters/-amidates as multifunctional flame retardants.



Jens C. Markwart completed his M.Sc. in Chemistry at the Johannes Gutenberg-University of Mainz, Germany, in 2016, including a stay at the Polymer Science and Engineering Department at the University of Massachusetts in Amherst, USA, in the group of Prof. Alejandro L. Briseno. He joined the group of Dr. Frederik R. Wurm as a Ph.D. student at the Max Planck Institute for Polymer Research, Mainz, Germany. His research focuses on hyperbranched polyphosphoesters as multifunctional flame retardants. His research is supported by a fellowship of the MAINZ Graduate School and by the Deutsche Forschungsgesellschaft (DFG).



Bernhard Schartel is head of the Technical Properties of the Polymeric Materials division at the Bundesanstalt für Materialforschung und -prüfung (BAM). He has been active in the area of flame retardancy of polymers for over 15 years, publishing more than 150 papers. He has served on the editorial boards of *Fire Mater.*, *J. Fire Sci.*, *Polym. Test.*, and *Fire Technol.*, and since 2012 has also edited *Polymer Degradation and Stability* for the topics *Fire Retardants and Nanocomposites*. His main interest is understanding fire behavior and flame-retardancy mechanisms as a basis for future development.



Frederik R. Wurm completed his Ph.D. in 2009 (JGU Mainz, Germany) with Prof. Holger Frey. After a two year stay at EPFL (Switzerland) as a Humboldt fellow, he joined the department "Physical Chemistry of Polymers" at MPIP and finished his habilitation in Macromolecular Chemistry in 2016. He currently heads the research group "Functional Polymers" at the Max Planck Institute for Polymer Research (MPIP). His group designs materials with molecular functions for the development of degradable polymers, nanocarriers with controlled blood interactions, adhesives, and phosphorus flame-retardants.

due to their chemical resistance, temperature stability, and high durability.<sup>[11]</sup> Here, performance outweighs the production costs of the materials and the FRs. Correspondingly, FRs in this material category are the second most important in value terms behind polyolefins: therefore, complex-shaped, multicomponent, and multifunctional FRs are used.<sup>[12]</sup> Notable formulations include 9,10-dihydro-9-oxa-10-phosphaphenanthrene-10-oxide (DOPO) derivatives and variations of P species with synergistic moieties: nitrogen, silicon, sulfur, and boron.<sup>[13]</sup>

### 1.2. Production Specifics: Finding a Match

The FR's mode of action is key when tailoring suitable formulations for polymer materials. Effective flame retardancy depends strongly on the interaction between the FR and the polymer matrix as well as the structure–property relationship between the two during thermal decomposition. The modes of action can generally be classified into condensed- and gas-phase mechanisms (Figure 2), and many successful P-FRs utilize both.<sup>[15]</sup> In the condensed phase, many P-FRs mediate the formation of char by inducing cyclization, cross-linking, and aromatization/graphitization by dehydration of the polymeric structure. The formation of carbonaceous char reduces the release of volatiles, that is, fuel.<sup>[16]</sup> Some P-FRs additionally act through intumescence: a multicellular residue acts as a protective layer, slowing down heat transfer to the underlying material.<sup>[17]</sup> Many FRs alter the melt flow and dripping behavior by promoting either charring combined with a flow limit (non-dripping UL-94 classification) or flame inhibition combined with increased flow, for example, via radical generators (non-flaming dripping UL-94 classification).<sup>[18]</sup> Some inorganic FRs (e.g.  $\text{Al}(\text{OH})_3$ ,  $\text{Mg}(\text{OH})_2$ , Zn borates, boehmite) decompose endothermically and vaporize water, absorbing heat in the condensed phase, and cooling the gas phase.<sup>[19]</sup> Gas-phase modes of action, usually acting in parallel with condensed-phase mechanisms, crucially increase FR effects: releasing non-combustible gases during decomposition reduces the combustion efficiency (fuel dilution).<sup>[20]</sup>

During the combustion of hydrocarbon fuels,  $\text{H}^\bullet$  and  $\text{OH}^\bullet$  radicals are formed, which propagate the fuel combustion cycle most notably through the strongly exothermic reaction  $\text{OH}^\bullet + \text{CO} \rightarrow \text{H}^\bullet + \text{CO}_2$ .<sup>[21]</sup> Many P-FRs decompose to form P radicals which react with  $\text{OH}^\bullet$  radicals and lower their concentration (flame poisoning).<sup>[22]</sup>

These mechanisms crucially depend on the decomposition temperatures of both the matrix and the FR. Therefore, FRs must be chosen to match explicit polymer processing and pyrolysis specifics. To ensure chemical interaction during pyrolysis but not during processing, premature FR decomposition must be avoided, whereas the overlap of the polymer and FR decomposition temperatures should be maximized.<sup>[23]</sup> This is key for high-temperature thermoplastic processes (e.g. compounding, extrusion, injection/blow molding), as well as vulcanization for rubbers, or curing for thermosets.<sup>[24]</sup> For foams, FRs with good foamability are important to maintain mechanical properties, while fiber and textile FRs must undergo spinning, weaving, and washing without loss of material or FR properties.<sup>[25]</sup>

Today, no single FR can be used for the wide range of polymers available; a FR may work well for one matrix but not for another, as the structure–property relationship is specific to the polymer matrix.<sup>[26]</sup> This makes the search for novel FRs with improved mechanisms essential for all fields of polymer applications.

### 1.3. Sustainability: A Regulatory and Market Goal

Health, environmental, and sustainability considerations play increasingly important roles in the development of novel FRs. Increased awareness has been paid to the “PBT” (i.e. persistency, bioaccumulation, toxicity) of FRs.<sup>[27]</sup> Studies on human exposure pathways and ecosystems have highlighted risks of some FRs, thus emphasizing the need for increased control and regulation.<sup>[28]</sup>

To curtail “PBT material” risks, regulatory bodies have enacted legislature to protect the environment and the general population: within the EU, REACH (Registration, Evaluation, Authorization, and Restriction of Chemicals), which acts upon the RoHS (Restriction of Hazardous Substances) and WEEE (Waste Electrical and Electronic Equipment) Directives, evaluates materials hazards and sets health and safety criteria for chemicals, including FRs.<sup>[29]</sup> Notably, the use of penta-, octa-, and decabromodiphenyl ethers was restricted under the Stockholm Convention on Persistent Organic Pollutants because of health risks, thus highlighting the need for halogen-free alternatives.<sup>[30]</sup>

The voluntary ecolabels introduced by ISO help prevent the circulation of PBT material and raise awareness of sustainable, environmentally aware production.<sup>[31]</sup> The “EU Ecolabel” serves to reduce the environmental impact and

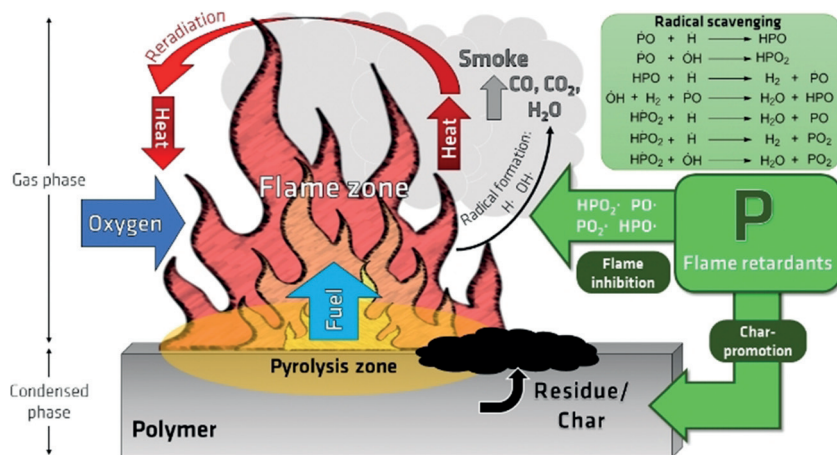


**Figure 2.** Flaming combustion of polymeric material and the role of phosphorus-based flame retardants.<sup>[26]</sup>

health risk of goods, services, and the life cycle of products, much like preexisting labels in Germany and the Nordic countries.<sup>[32]</sup> The Swedish TCO Certification specifically credits the sustainability of IT products, a key industry of non-halogenated FRs. Technology companies such as HP and chemical companies such as ICL-IP have implemented methods (GreenScreen, SAFR) to assess the chemical safety of their products.<sup>[33]</sup>

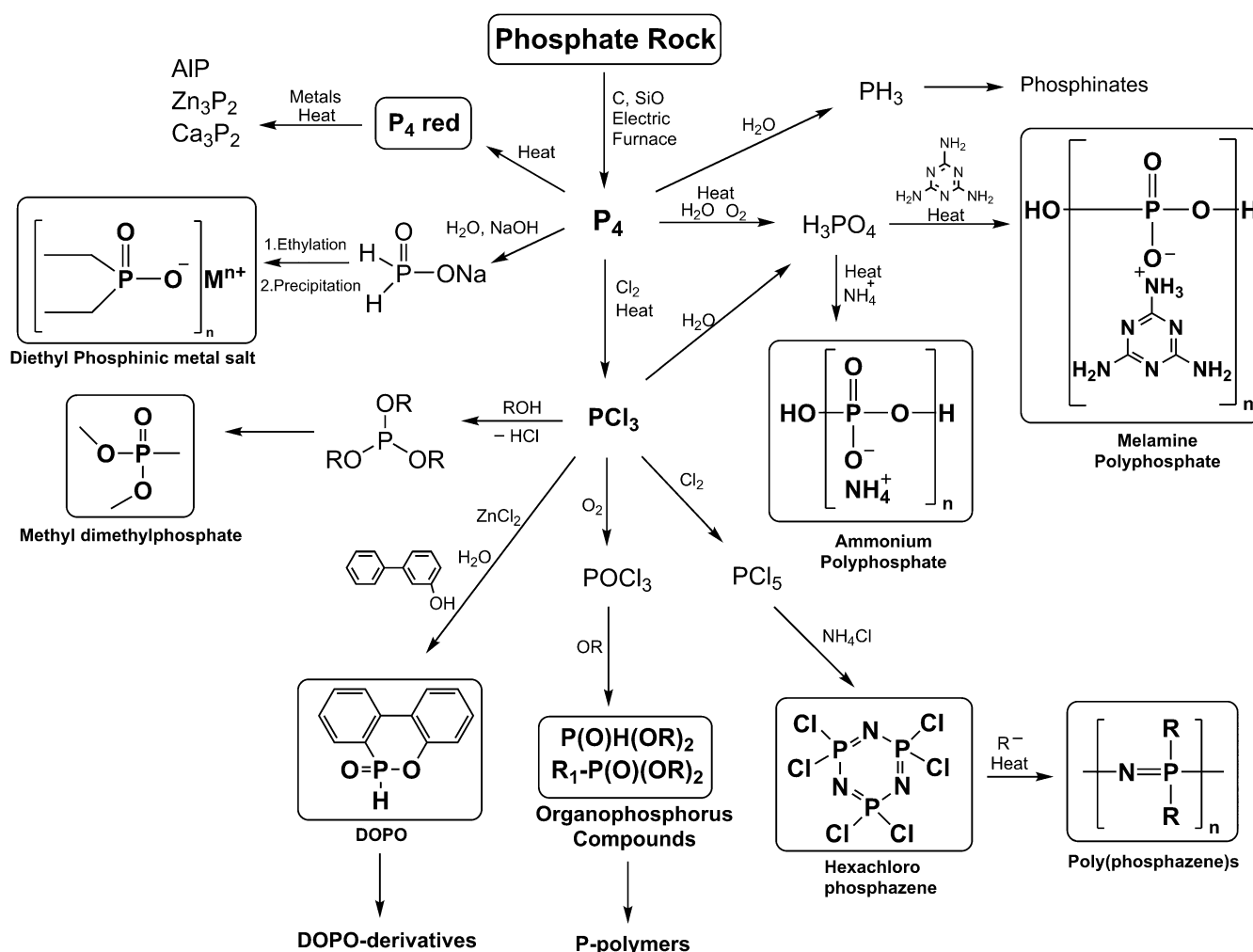
These trends are in line with consumer desires and the market shift toward more environmentally friendly (and ultimately sustainable) products, thus also prompting the use of bio-based materials and green chemistry in FR formulations.<sup>[34]</sup> Currently, attention has been placed on recyclable FR materials, further decreasing the environmental impact.<sup>[35]</sup>

Three key aspects—cost-effective conservation of material properties; matching the thermal stability and mode of action to processing and pyrolysis specifics; increased environmental friendliness with sustainability as a goal—constitute the characteristics of “good” flame retardants. In this respect, novel P-FRs will play a pivotal role in future products: their chemical versatility makes them ideally suited, as will be showcased more closely in the following.

## 2. Phosphate Rock—A Finite Natural Resource

Phosphorus chemistry is one of the oldest areas of chemistry, and involves the continuous development of new methods to improve the safety and sustainability of chemical processes. P-FRs are versatile: 1) the structure of P-FRs can vary from inorganic to organic; 2) the P content in these molecules can vary (e.g. from almost 100% for red P to 14.33% for DOPO); 3) the phosphorus can have different oxidation states, from 0 to +5, thereby resulting in different FR mechanisms (both in the gas and condensed phases). This architectural variation makes phosphorus unique for the design of FRs with tailored property profiles, such as density or glass transition temperatures ( $T_g$ ), by changing the binding pattern (e.g. from alkyl to phenyl groups).

Most compounds that contain phosphorus are manufactured from phosphorite, commonly known as “phosphate rock”. The current industrial pathways for the synthesis of various P-FRs are shown in Scheme 1. Phosphate is reduced by an electrothermal process to elemental phosphorus ( $P_4$ ),<sup>[37]</sup> which serves as a precursor for the production of the main intermediate compounds in industry such as red phosphorus, phosphoric acid ( $H_3PO_4$ ), phosphorus trichloride ( $PCl_3$ ),



Scheme 1. Examples of industrial pathways to various P-based FRs from “phosphate rock”. (M is usually zinc or aluminum.)

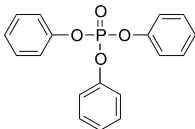
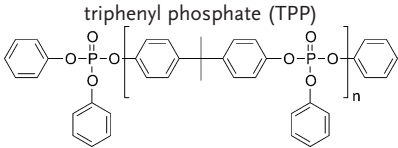
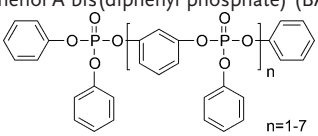
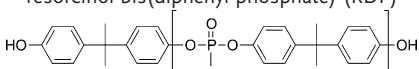
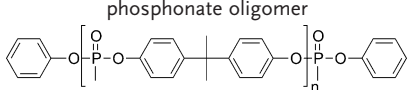
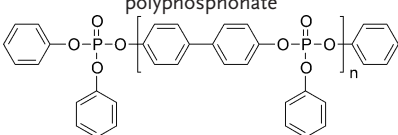
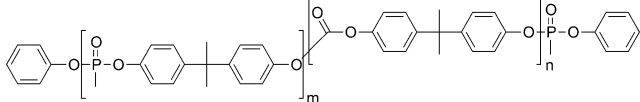
phosphorus pentachloride ( $\text{PCl}_5$ ), phosphine ( $\text{PH}_3$ ), and hypophosphite ( $\text{H}_2\text{PO}_2^-$ ). The exploitation of all these pathways for the synthesis of many FRs, such as ammonium polyphosphate,<sup>[38]</sup> melamine polyphosphate,<sup>[39]</sup> phosphazenes,<sup>[40]</sup> diethyl phosphonic metal salts, or DOPO,<sup>[13b]</sup> validates the versatility of the phosphorus compounds used in FR applications.

Although a large fraction of the  $\text{P}_4$  production is transformed into phosphoric acid, today  $\text{PCl}_3$  is the main intermediate for the production of major industrial organophosphorus FRs such as triphenyl phosphate (TPP), resorcinol bis(diphenyl phosphate) (RDP), and bisphenol A bis(diphenyl phosphate) (BADP), as well as for the production of oligomeric or polymeric FRs (Table 1). The common pathway for the synthesis of phosphorus-containing polymeric FRs is classical polycondensation (polytransesterification or via phosphoric acid chlorides),<sup>[41]</sup> but more modern strategies such as olefin metathesis polycondensation<sup>[42]</sup> or ring-opening polymerization<sup>[43]</sup> (e.g. of cyclic phosphazene derivatives or cyclic phosphoric acid esters) were also studied more recently.

However, phosphorus-based chemicals make up less than 3% of all the phosphorus extracted, with most of phosphate (82%) being used as fertilizer or for other purposes, including animal feed additives (7%), detergents, and cleaning products (8%).<sup>[44]</sup> Phosphate rock is a limited resource that is geographically concentrated in China, the United States, Morocco, Russia, and Jordan (according to the US Geological Survey released in January 2017).<sup>[45]</sup> At current extraction rates, estimates point to phosphate rock reserves being depleted in the next 370 years, with the exception of the reserves in Morocco.<sup>[45]</sup>

Currently, there is no alternative for this element; the phosphorus life cycle needs to be considered for agriculture in particular, but also for FRs. Consequently, the EU introduced phosphate rock to the list of critical raw materials in 2014 and elemental phosphorus followed in 2017.<sup>[46]</sup> Therefore, to ensure that phosphate fertilizers and phosphorus chemicals are preserved for future generations, a sustainable phosphate management, novel methods to better employ feedstock, and recycling strategies are required globally. Possible technolo-

**Table 1:** Commercial P-FR alternatives to decabromodiphenyl ethers (d-PBDE) according to the United States (US) Environmental Protection Agency (released in January 2014).<sup>[a]</sup><sup>[36]</sup>

Commercial P-FR alternatives to d-PBDE	Properties	Polymer applications
	CAS: 115-86-6 $M_w$ : 326.29	PPE-HIPS PC-ABS
triphenyl phosphate (TPP) 	CAS: 181028-79-5 $M_w$ : 693 ( $n=1$ ); > 1000 ( $n=2$ )	PPE-HIPS PC PC-ABS
bisphenol A bis(diphenyl phosphate) (BAPP) 	CAS: 125997-21-9 $M_w$ : 574.46 ( $n=1$ ; CASRN 57583-54-7); $M_w$ : 822.64 ( $n=2$ ; CASRN 98165-92-5)	PPE-HIPS PC-ABS
resorcinol bis(diphenyl phosphate) (RDP) 	CAS: 68664-06-2 $M_w$ : 1000-5000; 25% $M_w < 1000$	thermosets
phosphonate oligomer 	CAS: 68664-06-2 $M_w$ : 10000 to 50000; < 1% $M_w < 1000$	elastomers engineering thermo- plastics
polyphosphonate 	CAS: 1003300-73-9 $M_w$ : 650.6 ( $n=1$ ); 974.8 ( $n=2$ ); > 1000 ( $n \geq 3$ )	PPE-HIPS PC-ABS PC
phosphoric acid, mixed esters with [1,1'-bisphenyl-4,4'-diol] and phenol (BPBP) 	CAS: 77226-90-5 $M_w$ : > 1000; < 1% < 1000	elastomers engineering thermo- plastics
poly[phosphonate-co-carbonate]		

[a] The mode of action in all cases involves chemical action in the condensed phase and char formation.



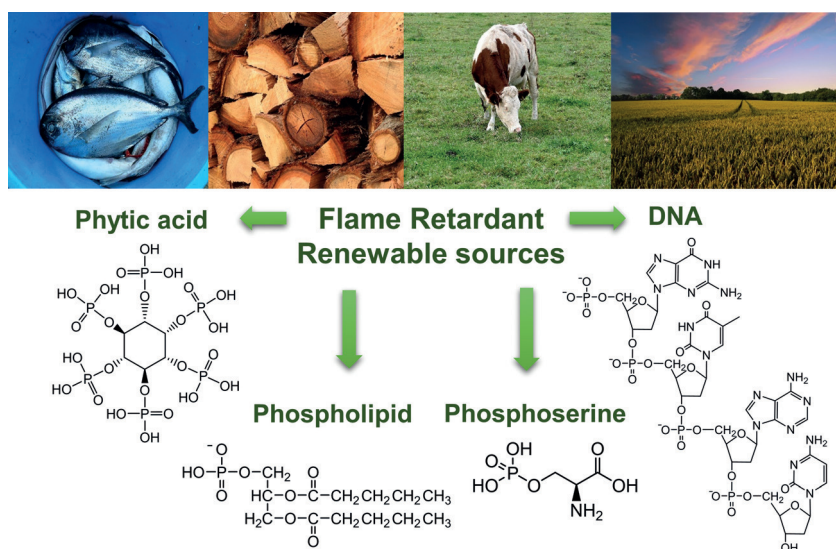


Figure 3. Renewable sources of P-FRs.

gies for phosphorus recovery include a wide range of strategies, such as phytoextraction (optimum annual P removal from Indian mustard seed equal to  $114 \text{ kg P ha}^{-1}$ ), biochar (ca.  $10 \text{ g P kg}^{-1}$  biochar), or extraction from human urine and feces (recovery of over 80% of total P from urine with approximately  $0.5$  and  $1.3 \text{ g capita}^{-1} \text{ day}^{-1}$ ).<sup>[47]</sup> In addition, it is estimated that the extraction of P from manure in the EU may be near to  $1.8 \text{ million t a}^{-1}$ , which would satisfy the annual demand of P required for EU fertilizers.<sup>[48]</sup> On the other hand, as sugars are sometimes referred to as the “new oil” for tomorrow’s materials, the extraction of phytic acid or biomacromolecules (deoxyribonucleic acid and caseins) are also strategies to isolate P derivatives for the valorization of by-products from the agro- or food industry (see Section 5 and Figure 3) and P-FRs can be part of a sustainable phosphorus chemistry.

### 3. Recent Developments in Reactive Phosphorus Compounds

P-FRs can be implemented as either additive or reactive components. The latter allows for the FR to become part of the material’s constitution, thereby leading to “inherently” flame-retardant materials.

Reactive FRs are mainly used in thermosets, such as unsaturated polyesters, epoxy resins, or polyurethane foams. They are equipped with functional groups (alcohols, epoxy, amines, halogens, etc.), which allow incorporation into the polymer matrix during curing.<sup>[1b,49]</sup> In epoxy resins, reactive FRs are preferred since they are covalently attached to the network and thus have a lower impact on the physical properties of the final product. In contrast, additive FRs result in decreased glass transition temperatures ( $T_g$ ) and are prone to leaching (see Section 4). The decreased leaching of reactive FRs also reduces the potential pollution of wastewaters. However, additive FRs dominate the market, as they are easier to use and lower in price. In contrast, reactive FRs are

accompanied by the need for a significant reformulation of the curing process. This presents a disadvantage of reactive FRs, that is, each matrix needs a newly designed and formulated FR, while additives may be used for several polymer matrices.<sup>[50]</sup>

#### 3.1. Polyurethanes (PUs)

As a consequence of the wide use of polyurethanes (PUs) in foams, coatings, etc. and their inherent flammability, FRs are necessary. However, not only are the FR properties important, they also have an impact on the environment and physical properties. Biodegradable PUs are commonly synthesized with hydrolyzable soft segments.<sup>[51]</sup> The use of P-FRs could achieve both, since these materials demonstrate good FR properties and can be both biocompatible and degradable.<sup>[52]</sup> Chiu et al.<sup>[51]</sup> synthesized PUs that achieve a V-0 rating in the UL-94 test (classification for the flammability of plastics) and presented efficient FR properties with limited oxygen indices (LOI, minimum oxygen concentration required to sustain combustion) higher than 27.7%. The authors used 4,4-diphenylmethane diisocyanate (MDI) as the hard segment; 5-hydroxy-3-(2-hydroxyethyl)-3-methylpentyl-3-[2-carboxyethylphenylphosphine] propanoate (HMCPP, Figure 4) and polycaprolactonediol (PCL) as the soft segments; and 1,4-butanediol (BD) was used as a chain extender. By increasing the HMCPP content (7.5, 15.0, and 22.5 mol% with respect to MDI) in the PUs, the decomposition temperatures and the  $T_g$  values were reduced by several degrees.<sup>[51]</sup>

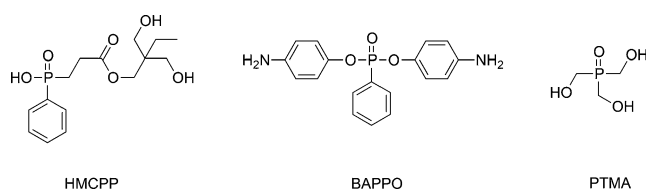


Figure 4. Examples of reactive P-FRs: HMCPP (5-hydroxy-3-(2-hydroxyethyl)-3-methylpentyl-3-[2-carboxyethylphenylphosphine]propanoate) used in PU; BAPPO (bis(4-aminophenyl)phenylphosphine oxide) used in PU; PTMA (phosphoryltrimethanol) used in PU.<sup>[51,53]</sup>

As a water-based example, Çelebi et al.<sup>[53a]</sup> followed a similar approach to synthesize aqueous dispersions of FR PUs, but instead of incorporating the P-FR as a soft segment, they incorporated it in the chain-extension step. Water-based PUs reduce the use of organic solvents and are, therefore, attractive from an environmental perspective. Bis(4-aminophenyl)phenylphosphine oxide (BAPPO, Figure 4) was used for the flame-retardant PU, and ethylenediamine for the non-flame-retardant PU. Poly(propylene-co-ethylene)polyol was used as a co-monomer. The physical properties of the two PUs are almost identical, except their gloss properties. This

was explained by the difference in the chain conformation of the two PUs. Furthermore, BAPPO increased the crystallinity of the hard segment, through its aromatic groups and longer chain length, which contribute to the higher packing capability of the hard segments.<sup>[53a]</sup>

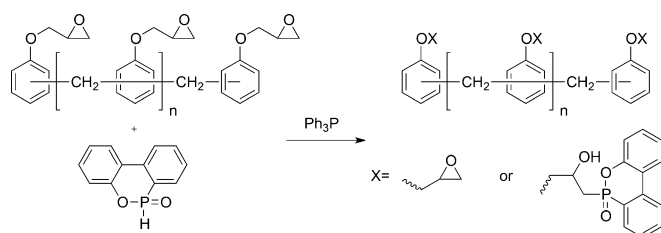
The majority of reactive FRs rely on halogens or phosphorus. Halogenated FRs are substituted nowadays because of toxicity and environmental concerns. It was reported that P-containing polyols are mainly the most appropriate reactive FRs for rigid PU foams, but they are rarely used in flexible PU foams (FPUF).<sup>[54]</sup> Chen et al.<sup>[53b]</sup> presented FPUFs, which contained phosphoryltrimethanol (PTMA, Figure 4) as a cross-linker. They proved that PTMA was mainly active in the condensed phase during a fire scenario. However, PTMA had a negative effect on the cell structure of the foam. With increasing PTMA content, the cell size increased and consequently the number of cell windows decreased. This behavior can be explained by the increased number of closed foam cells arising from the cross-linking nature of the PTMA further influencing the mechanical properties. The FPUF containing 3.2 wt % PTMA showed an increased tensile strength and elongation at break compared to the neat FPUF, because of the change in the foam structure.<sup>[53b]</sup>

### 3.2. Epoxy Resins

The copolymerization of FRs is not limited to PUs; epoxy resins, often used for their thermomechanical properties and processability, also exhibit high flammability and, therefore, require FRs. The FRs can be introduced to the epoxy- or nitrogen-containing compound.

Zhang et al.<sup>[55]</sup> proved that it is possible to achieve high  $T_g$  values, high thermal stability, and an UL-94 V-0/V-1 rating by the addition reaction of DOPO and epoxy phenol-formaldehyde novolac resin (Scheme 2). DOPO was the first efficient halogen-free FR for epoxy resins based on novolac and gained much attention because of its high thermal stability, high reactivity of its P–H bond, and flame-retarding efficiency.<sup>[56]</sup>

An alternative method to incorporate the FR into the polymer network is to use it in the hardener, a process commonly used for epoxy resins. An example of this approach is the work of Artner et al.,<sup>[57]</sup> who compared two DOPO derivatives (Figure 5): one was modified with amine groups and was used as a FR hardener in epoxy resins, the other had



**Scheme 2.** FR-functionalized novolac resin for further use in epoxy resins.<sup>[55]</sup>

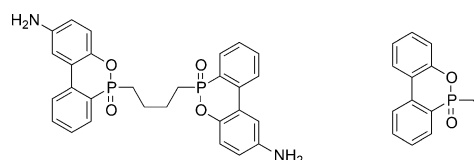


**Figure 5.** DOPO-based hardener (left), nonreactive analogue (right).<sup>[57]</sup>

a similar structure, but was an additive FR. The authors revealed that the reactive FR has the potential to be superior over the additive FR.

By attaching the amine groups directly to DOPO, the solubility of the hardener was increased compared to previous studies. The resin with the DOPO-based diamine hardener presented comparable thermal- and fracture-mechanical properties as the reference epoxy material, namely the diglycidyl ether of bisphenol A with 4,4'-diaminodiphenylsulfone. In contrast to the reactive FR, the non-reactive additive showed a decrease in the  $T_g$  value by about 75 °C and a lower rubber modulus. However, the new hardener revealed a high reactivity, which led to an increase in viscosity during curing, thus posing a problem for application in composite materials because of the reduction in processing time.<sup>[57]</sup>

In contrast, Ciesielski et al. illustrated that it is not necessary to use reactive FR components to maintain superior mechanical performance. By using the DOPO derivatives (DDM-(DOP)<sub>2</sub> and DDM-(DOP)<sub>2</sub>-S) (Figure 6a,b), their epoxy resins achieved a V-0 rating at 1 % P in the resin without significantly lowering the  $T_g$  value. It was reported that phosphoramides can ring-open epoxides,<sup>[58]</sup> so other P–N nucleophiles may also be incorporated into the polymer matrix, depending on the respective reaction kinetics.

Reactive phosphate-based FRs can also decrease the  $T_g$  value, which may be attributed to the flexibility of the P–O bond. However, Wang and Shi<sup>[59]</sup> reported that reactive hyperbranched (*hb*) poly(phosphoester)s (PPEs; Fig-

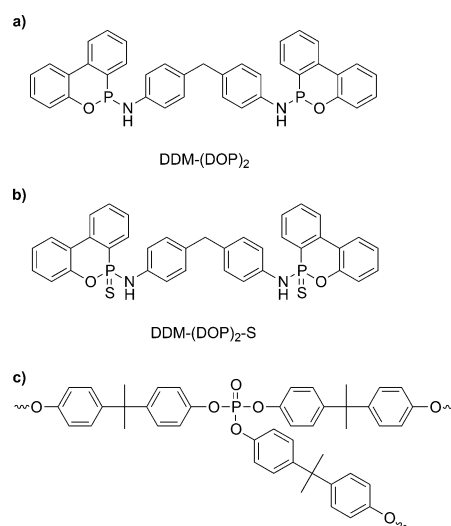


**Figure 6.** a,b) DOPO-based FRs achieving a V-0 rating at 1 % P in the epoxy resin; c) *hb*PPE FR for epoxy resins with a lower impact on the  $T_g$  value.<sup>[58–59]</sup>

ure 6c)—because of their branched structure—reduce the  $T_g$  value to a smaller extent. This was attributed to the higher cross-linking density of the *hbPPE* having a greater influence than the P–O flexibility. The *hbPPE* was synthesized in an  $A_2 + B_3$  approach by polycondensation of bisphenol A and phosphoryl chloride. This *hbPPE* was used to cure a bisphenol A based epoxy resin by  $PPh_3$  catalysis, which led to a resin with a higher  $T_g$  value than the resin cured with only bisphenol A.<sup>[59]</sup>

### 3.3. Phosphorus Oxidation State

The decrease in the  $T_g$  value by the presence of flexible P–O bonds was also reported by Jeng et al.<sup>[60c]</sup> In addition, they stated that the introduction of sterically demanding groups such as P–O–C<sub>6</sub>H<sub>4</sub>–O–P can reduce the cross-linking density, thereby resulting in a further lowering of the  $T_g$  value. In contrast, the  $T_g$  value was reduced less when they used a FR with a more rigid P–Ph group. However, the FR mechanism was also influenced by exchanging a P–O bond by a P–C bond. Most reports indicate that phosphine oxides are rather poor char promoters, but are more active in the gas phase than other P-FRs with higher oxidation numbers such as phosphates.<sup>[60]</sup> The higher gas-phase activity of phosphine oxides was also reported by Braun et al.<sup>[62]</sup> who investigated the impact of the P oxidation state on its FR behavior in epoxy resin composites. They reported, in agreement with previous reports,<sup>[60b]</sup> that the amount of stable residue increased and the release of volatiles containing phosphorus decreased as the oxidation state of P increased (Figure 7). However, in previous reports it was concluded that phosphates are the more efficient FRs, because of their higher efficiency as char promoters compared to phosphine oxides.<sup>[60b]</sup> This conclusion differs from that of Braun et al., who ranked phosphine oxide as the best FR and phosphate as the worst through the observation of an increase in charring and decreased flame inhibition for the phosphates, which significantly accounted for the performance of FR in composites. These conflicting statements can be explained by the fact that Braun et al. investigated composites as a matrix, for which flame inhibition as a main mode of action plus minor charring was a very promising route for flame retardancy.<sup>[12d,61]</sup> They showed that the key role of the oxidation state was in the type of interaction during the pyrolysis. The authors explained the

greater role of the gas-phase activity of composite materials with a high content of carbon fiber through a decrease in the relative impact of the charring.<sup>[60b,62]</sup>

## 4. Recent Developments in Additive Phosphorus Compounds

Most FRs are added as additives during polymer processing steps instead of being built into the polymer backbone.

The major advantage of additive FRs is their cost-effectivity (i.e. performance value of the material) and ease of application in various matrices, thus they are widely used in industry.<sup>[2b,63]</sup> Despite these advantages, additive FRs also exhibit several drawbacks, most notably their impact on physical properties such as the  $T_g$  value or mechanical stability. Leaching of the FRs over time is a major issue, especially for compounds with a low molecular weight. This may be partly prevented by using polymeric substances; however, phase separation needs to be prevented.<sup>[64]</sup> The biggest challenge for additive FRs is, therefore, to find the optimal balance between the FR and the mechanical properties.<sup>[50a,b]</sup>

### 4.1. Inorganic Phosphorus Flame Retardants

The “classic” example of an inorganic P-FR is red phosphorus, but in practice it is only used as an encapsulated substance to process FR thermoplasts, for example, glass-fiber (GF) reinforced PA 6,6, or in many types of multi-component FR systems.<sup>[9a,65]</sup> The main advantages are an unparalleled high P content and efficiency already at small amounts: in GF-reinforced PA 6,6, in combination with metal oxides as synergists, only <7 wt % was necessary to achieve excellent FR performance. While the use of red P alone is declining, it is proposed in combined formulations that include <8 wt % red P, for example, in P + inorganic filler or in P–P mixtures combined with intumescent ammonium polyphosphate (APP) based systems.<sup>[10b,66]</sup>

Tan et al. reported a hardener for epoxy resins based on inorganic APP which was modified with piperazine by cation exchange to later act as a hardener. This approach yielded efficient flame retardancy and showed improved mechanical properties compared to the dispersion of APP in the epoxy resin as a result of homogeneous incorporation without aggregation.<sup>[67]</sup> Duan et al. used APP combined with a *hb*-phosphorus/nitrogen-containing polymer in polypropylene (Scheme 3).<sup>[68]</sup>

Formulations using equal parts (10 wt %) of polymer and APP showed high LOI values of up to 30 %, compared to LOI values of approximately 20 % for 20 wt % of the individual compounds. These results suggested synergism between the *hb* polymer and the APP. Raman spectroscopy revealed that more graphitic char had been formed by the combination of these two compounds. The protective layer effect of the charred layers was also observed in thermogravimetric analysis (TGA) measurements through a higher temperature at maximum weight loss ( $T_{max}$ ).<sup>[68]</sup>

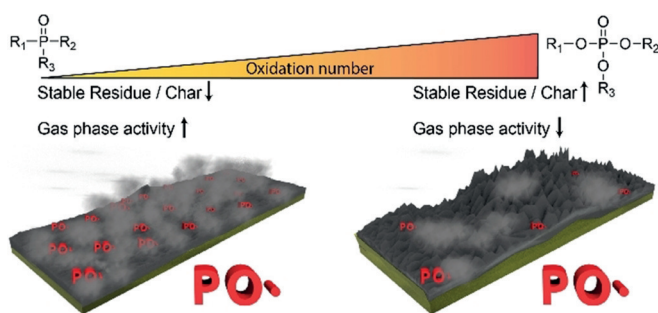
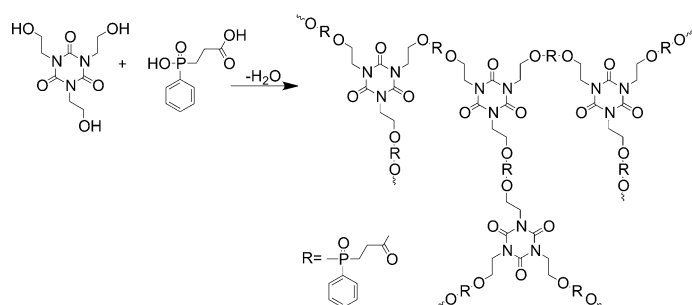


**Figure 7.** The char residue increases and the gas-phase activity decreases as the oxidation state increases.





**Scheme 3.** Synthesis of the *hb* FR polymers containing phosphorus/nitrogen.<sup>[68]</sup>

Braun et al. showed that the reactivity of the P additive with the polymer matrix (here: GF-reinforced PA 6,6) has a great influence on its interaction with other additives as well as the main activity in the condensed or gas phase. This study illustrated that the main mechanism of melamine polyphosphate (MPP) is dilution of the fuel and the creation of a P-based protective layer. Aluminum phosphinate (AlPi), another FR currently widely applied, on the other hand, acts mainly in the gas phase. The combination of the two additives changes the dominant FR mechanism through the formation of a strong protective layer consisting of aluminum phosphate. The addition of zinc borate led to formation of a boron-aluminum phosphate layer, which showed a better protective layer performance than aluminum phosphate and resulted in the best cone calorimeter (most important instrument in fire testing, measuring heat release rate by the amount of oxygen consumed during combustion) performance of the samples, with hardly any ignition evident.<sup>[10a,69]</sup>

The use of various salts of dialkylphosphinates, (e.g. aluminum, calcium, and zinc) as effective FRs for GF-reinforced thermoplasts were investigated by Clariant SE. The aluminum salts AlPi are commercially available under several trade names, such as Exolit OP 930, Exolit OP 935, and Exolit OP 1230. The Exolit OP line of products vary in the AlPi modification (e.g. encapsulation, particle size, etc.).<sup>[13a]</sup>

The synergism between AlPi and nanometric iron oxide or antimony oxide was investigated by Gallo et al., who found different FR behaviors operated: in a redox cycle, Fe<sub>2</sub>O<sub>3</sub> oxidized P to inorganic phosphates and was reduced to magnetite, thereby increasing the amount of P in the condensed phase. However, a catalytic effect on the cross-linking was postulated for Sb<sub>2</sub>O<sub>3</sub>, a nonreducible oxide, as no hint of the same mechanism was detected. The authors proposed that the surfaces of the metal oxides stabilize the oxygen-containing intermediate structures and thereby promote cross-linking reactions between the polymer chains and also the interaction with P-based intermediates.<sup>[70]</sup>

Naik et al., and in a recent study Müller et al., compared the influence of the metals in melamine poly(aluminum phosphate), melamine poly(zinc phosphate), and melamine poly(magnesium phosphate) in epoxy resins. Melamine poly(aluminum phosphate) reduced the peak heat release rate (PHRR) by about 50%, whereas the other two melamine poly(metal phosphates) achieved a reduction of PHRR to less

than 30% compared to the neat epoxy resin. All three materials reduced the fire load by 21–24% and lowered the CO yield and smoke production. The improved fire behavior is explained by their main activity in the condensed phase, with minor signs of fuel dilution. The fire residue increased and, as a result of intumescence, a protective layer was formed. In addition, synergistic combinations with other flame retardants were also studied: here, melamine poly(zinc phosphate) with melamine polyphosphate showed the best overall FR results as a consequence of strong intumescence, with a low heat release rate (HRR) and the lowest PHRR, maximum average rate of heat emission, and fire growth rate index values.<sup>[71]</sup>

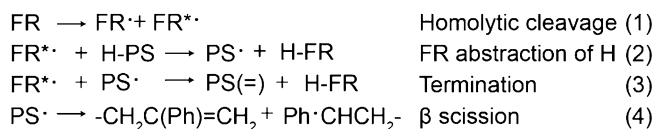
#### 4.2. Organophosphorus Flame Retardants (OPFRs)

Organophosphorus compounds are currently discussed as substitutes for halogenated, mainly brominated, FRs. Most organophosphates are used as additives rather than being chemically bound to the polymer matrix.<sup>[72]</sup> Besides their use as FRs, they work as plasticizers or antifoaming agents and are used in plastics, furniture, textiles, electronics, construction, vehicles, and the petroleum industry. In the following, some examples of these compounds—selected because of their importance to the field (more than 30 citations)—are discussed.

The influence of the chemical structure on the FR mechanism is not only important to small molecules, but also for organophosphorus polymers. Aromatic polyphosphonates exhibit higher thermal stability than aliphatic polyphosphonates, and, at the same time, they have a higher hydrolytic stability than the aromatic polyphosphates. This was explained by the presence of the stable P–C bond in phosphonates, while phosphates carry an additional hydrolyzable P–O–C linkage that results in lower degradation temperatures.<sup>[73]</sup>

The influence of the chemical structure of the FR on its mechanism has been intensively studied. While Beach et al. suggested that the major FR mechanism for bromine- and sulfur-containing FR additives in polystyrene is through enhanced degradation of the polystyrene matrix,<sup>[75]</sup> the phenomenon of radical generation together with flame inhibition was first investigated by Eichhorn in 1964.<sup>[74]</sup> The mechanism of the condensed phase is as follows: a hydrogen atom is abstracted from the polystyrene backbone by the flame retardant, followed by  $\beta$ -scission of the polystyrene radical (Scheme 4).

P-FRs show no such enhanced degradation of polystyrene (PS) and, therefore, exhibit lower performance in LOI tests, the reason being the difference in bond dissociation energies. However, combining sulfur with triphenyl phosphate (TPP)



**Scheme 4.** Mechanism for enhanced degradation of polystyrene.<sup>[75]</sup>

resulted in a performance comparable with that of hexabromocyclododecane (HBCD). Loosening of the polymer network by degradation is an important condensed-phase mechanism which allows mass transfer of gas-phase species to the surface and removes fuel and heat away from the pyrolysis zone via melt flow. According to the authors, the synergism between sulfur and TPP was achieved by the sulfur causing enhanced degradation of the PS network (Scheme 4), which resulted in an improved mass transfer of TPP to the surface.<sup>[75]</sup> More recently, Wagner et al. investigated OPFRs with synergists containing disulfide bridges, further identifying the role of radical generators in the enhanced degradation of polystyrene.<sup>[76]</sup>

As most additive monomeric and oligomeric OPFRs exhibit a plasticizing effect on the polymer matrix and may volatilize or migrate during the processing, alternative FRs are needed. Therefore, academic and industrial studies are increasingly turning to polymeric OPFRs which are designed to be completely miscible with the matrix and, therefore, less likely to migrate over time.<sup>[73]</sup>

The importance of the FR molecular weight was investigated by comparing the monomeric FR TPP with the oligomeric FRs resorcinol bis(diphenyl phosphate) (RDP) and bisphenol A bis(diphenyl phosphate) (BDP) in polycarbonate/acrylonitrile-butadiene-styrene blends. All three compounds showed activity in the gas phase through flame poisoning, with TPP and RDP revealing a slightly better performance than BDP. However, TPP had almost no condensed-phase activity, while RDP showed some, and BDP demonstrated the highest activity. The behavior was explained by the fact that BDP and RDP catalyzed Fries rearrangements in the PC, while TPP volatilized before the decomposition of PC-ABS because of its low molecular weight, thus preventing chemical interaction.<sup>[23c,77]</sup>

The phase separation of polymer blends must always be investigated with respect to the desired material properties. In this context, *hb* polymeric FRs are promising materials. Their key properties include many reactive end groups, a relative low intrinsic viscosity compared to linear polymers, and in most cases a high miscibility and solubility with other polymeric materials. In addition, their straightforward synthesis through “hyperbranching”, that is, statistical branching polymerization, makes them available on a large production scale. Furthermore, this class of polymers also has the potential to have a lower impact on material characteristics such as mechanical properties and  $T_g$  value.<sup>[78]</sup>

Phosphorus combines chemical versatility and FR effectivity, thus allowing for enormous variety in FR formulations. These examples have shown that P shows different modes of action in FR formulations because of many various criteria: oxidation state, reactive or additive, inorganic or organic, low or high molecular weight, etc.

## 5. Modern Trends and the Future of Phosphorus-Based Flame Retardants

### 5.1. Synergistic Multicomponent Systems

Flame-retardant structures containing heteroatoms such as nitrogen, silicon, sulfur, and boron in combination with phosphorus provide a huge range of specific interactions, compared to the decomposition of phosphorus structures or the decomposition of these with pure hydrocarbons,<sup>[26]</sup> thereby reducing the overall load of FRs in a material and maximizing effectivity (Figure 8).<sup>[13d,58,79]</sup>

The combination of phosphorus–nitrogen (P–N) compounds is one of the most promising reported synergisms for halogen-free flame retardants. P–N synergism promotes the formation of cross-linked networks with polymer chains during a fire, thereby encouraging the retention of P in the condensed phase and yielding higher and more thermally stable char formation.<sup>[81]</sup> Two of the most prominent P–N structures include phosphoramidates<sup>[82]</sup> and cyclotriphosphazenes.<sup>[83]</sup>

The main advantages of phosphoramidates over their analogous phosphates are their higher thermal stability,<sup>[84]</sup> lower volatility,<sup>[85]</sup> and higher viscosity as a result of hydrogen bonding.<sup>[82c]</sup> These features can increase the density of the entire system and make them more likely to be retained in the matrix during combustion, thus contributing to a higher condensed-phase activity and affording higher char yields.

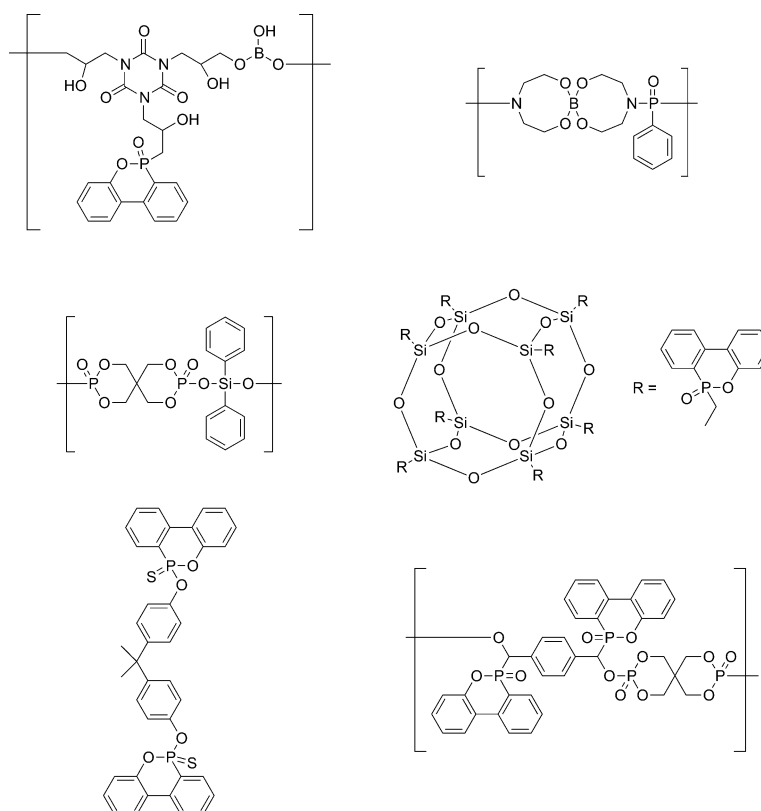
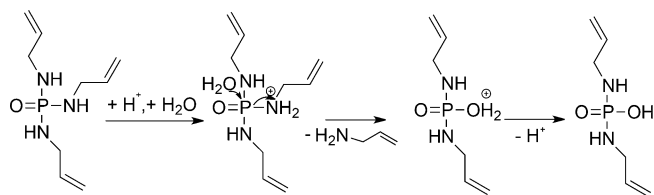


**Figure 8.** Various FR formulations with synergistic moieties. Top row: boron-containing formulations; middle row: silicon-containing formulations; bottom left: P-S-containing formulations; bottom right: formulation containing two types of P.<sup>[13a,80]</sup>

Neisius et al. suggested the hydrolysis of P–N bonds occurred under acidic conditions to form nonvolatile compounds (Scheme 5).<sup>[82c]</sup> Interestingly, they showed that trisubstituted phosphoramidate displayed poor flame-retardant behavior on



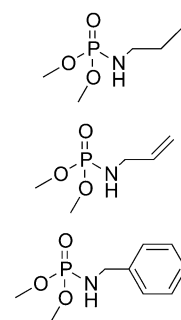
**Scheme 5.** P–N bond hydrolysis under acidic conditions.<sup>[82c]</sup>

flexible polyurethane foams compared to the analogous monosubstituted phosphoramidate (Figure 9). The authors suggest that this is because the trisubstituted phosphoramidate decomposes thermally/hydrolytically to form nonvolatile structures that contribute only to condensed-phase activity. However, the monosubstituted phosphoramidate can decompose to form PO<sup>•</sup> radicals, which might prevent the oxidation of H<sup>•</sup> and OH<sup>•</sup> radicals.

Linear poly(phosphoramidate)s (PPAs) were also studied as FRs.<sup>[86]</sup> The results indicated an enhanced thermal stability, increased formation of char yields at higher temperatures, and higher glass transition temperatures ( $T_g$ ) with respect to the analogous poly(phosphate)s. Improvement in the flammability test (30% limiting oxygen index (LOI)) and dripping resistance (V-0 rating in UL-94) was achieved with a loading of about 30 wt% PPA.

In the last decade, a myriad of chemically and thermally stable phosphazene derivatives has been developed (Figure 10).<sup>[83,86b,87]</sup> Cyclophosphazenes are reported to present even higher thermal stabilities than phosphoramidates: the thermal decomposition of the phosphazene-bound piperazine

Dimethyl mono-substituted secondary phosphoramidates



Diphenyl mono-substituted secondary phosphoramidates

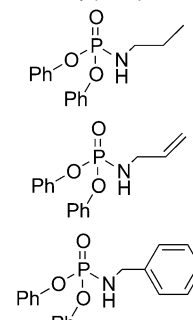


**Figure 9.** Monosubstituted dimethyl/diphenyl phosphoramidates.<sup>[82c]</sup>

has been reported from 350°C up to 500°C (under N<sub>2</sub>) with residues between 50 and 70 wt%, depending on the substituents. This large amount of char indicates cross-linking during pyrolysis, for example, through ring-opening polymerization.<sup>[83a,88]</sup> The hydrolytic lability of P–N bonds limits their application in textiles (washing). Although, recent studies showed self-extinguishing in cotton/polyester blends grafted with allyloxypolyphosphazene.<sup>[89]</sup>

Hexachlorophosphazene is the common starting material for polyphosphazenes, as it allows the introduction of various pendant groups after polymerization, for example, the fully inorganic polyaminophosphazene, or functional inorganic-organic hybrid polymers ranging from linear copolymers<sup>[90]</sup> to branched polymeric structures.<sup>[88]</sup> The cross-linked or *hb*-poly(phosphazene) structure not only acts as a good carbonization agent, but can also stop dripping and reduce the peak heat release rate (PHRR) by 55%, as reported by Tao et al.<sup>[83a]</sup>

Polyphosphazenes usually exhibit low  $T_g$  values (from –100°C to above room temperature).<sup>[91]</sup> Qian et al. synthe-

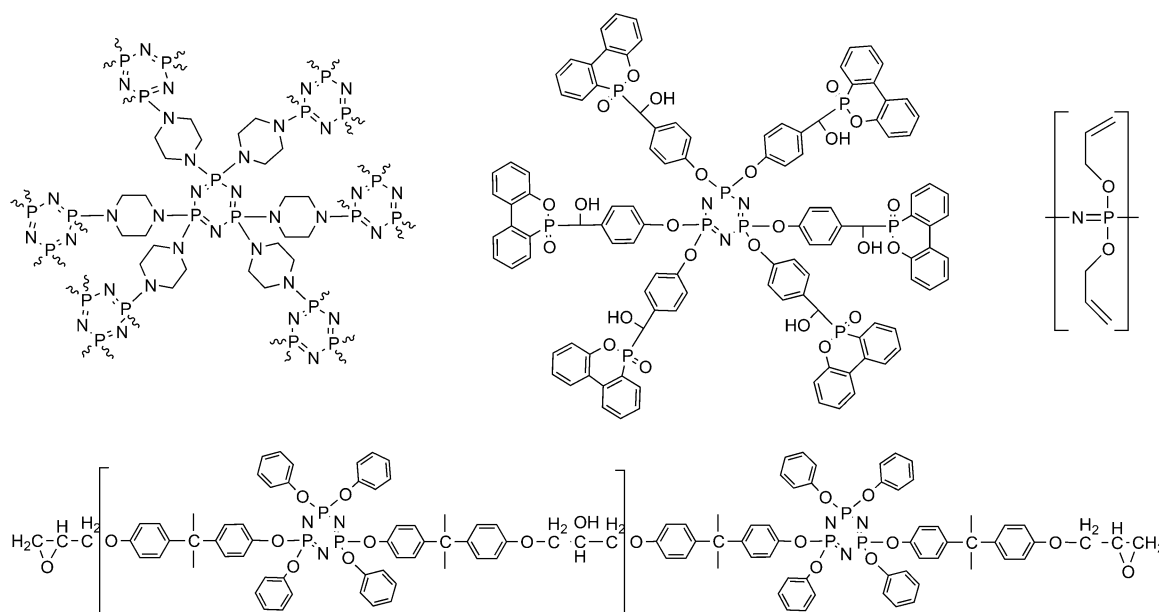


**Figure 10.** Low-molecular-weight and polymeric flame-retardant phosphazenes.<sup>[87–90]</sup>

sized phosphaphenanthrene/cyclotriphosphazene FRs with practically the same  $T_g$  value as the neat diglycidyl ether of bisphenol A (DGEBA) epoxy resin.<sup>[87]</sup> Recently, the Wu research group has been working on the synthesis of several cyclotriphosphazene-linked epoxy resins.  $T_g$  values of 160°C or 145°C were reached by using them as a matrix<sup>[90a]</sup> or loading them into DGEBA resins (20 wt %), respectively.<sup>[83b,90b]</sup> A self-extinguishing UL-94 V-0 rating was achieved with a loading of 30 wt % in the resulting thermosets.

As mentioned in Section 4, a current challenge in the development of new FRs is the retention of the mechanical performance of the matrix and effectiveness of the FR. This was achieved to some extent by reactive *hbPPEs* (see Section 3.2). Another, very promising approach to meeting this requirement is the combination of P compounds either by blending or covalent linkages to nanometric fillers, such as carbon nanotubes,<sup>[92]</sup> graphene,<sup>[93]</sup> polyhedral silsesquioxanes,<sup>[94]</sup> halloysite nanotubes,<sup>[95]</sup> montmorillonite, or metal oxide nanoparticles.<sup>[96]</sup> In some cases, FRs which are covalently grafted onto the nanofillers have higher efficiency than additives at the same concentration.<sup>[97]</sup> Acceptable grafted amounts of P compounds are between 10 and 30 wt %, which equate to less than 1 wt % phosphorus in the final nanocomposite. A UL-94 V-0 classification (Figure 11 a) and an increase in the LOI value have been reported for polypropylene and epoxy resin using DOPO-grafted to SiO<sub>2</sub> nanoparticles,<sup>[98]</sup> exfoliated graphene,<sup>[99]</sup> or glass fabric.<sup>[97a]</sup>

Typically, the synergistic effect of the nanofillers and P-grafted compounds occurs in the condensed phase. Phosphorus promotes the formation of cross-linked structures, which together with the effect of nanofillers of increasing the melt viscosity promotes intensive carbonization (Figure 11 b). However, some studies have suggested that the grafting of chlorinated phosphorus compounds or DOPO-silane deriva-

tives to carbon nanotubes<sup>[92b]</sup> and graphene<sup>[99]</sup> also affected the gas phase. The combination of gas- and condensed-phase activity led to a reduction in the PHRR by around 35 % and an increase in the LOI values in polyamide 6 and epoxy resin, even achieving the V-0 classification in UL-94 tests.

However, the FR effect of the nanofillers depends not only on the formation of a compact network layer at high temperatures, but also on their ability to be dispersed in the nanocomposite (Figure 11). For example, several research groups focused on grafting P compounds such as diphenylphosphinic chloride,<sup>[92a]</sup> hexachlorocyclotriphosphazene,<sup>[92b]</sup> or an oligomeric diaminobisphosphonate<sup>[100]</sup> to carbon nanotubes. These polymers cover the surface of the nanotubes with a thin layer, which impedes the formation of  $\pi$ - $\pi$  interactions and promotes their individual dispersion in polystyrene (PS), polyamide 6 (PA6), or ethylene vinyl acetate (EVA), respectively. Stable dispersions in dimethyl sulfoxide (DMSO), *N,N*-dimethylformamide (DMF), or H<sub>2</sub>O were achieved after ultrasonication. In addition, Qian et al. also obtained stable colloidal dispersions of graphene grafted with DOPO-silane in ethanol, tetrahydrofuran (THF), and DMF (Figure 11 c).<sup>[99]</sup> According to the authors, the introduction of compounds with polar groups on the surface of the carbon nanotubes favored their wettability and compatibility with polymer chains.

It is clear that research on synergistic systems is very active. P-N-based compounds have proved to be a robust alternative to the predominantly halogenated FRs in use today. As shown in Section 5.1, a condensed-phase mechanism is predominant for P-N compounds as well as for P nanocomposites. In the latter, the key role of P-FRs is to favor the dispersion of the nanofillers, thereby enhancing the formation of a protective char layer and lowering the heat release rate (HRR) during the combustion of the polymer.

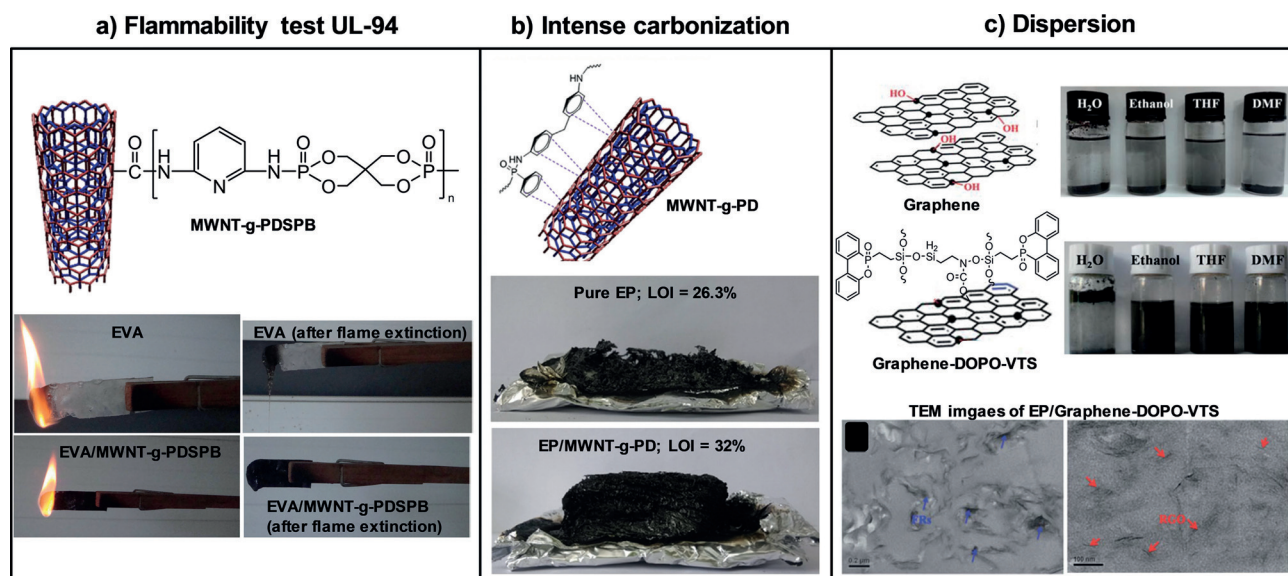


**Figure 11.** Effects of phosphorus-grafted nanofillers in an organic matrix.<sup>[100,111]</sup> a) UL-94 test of ethylene vinyl acetate (EVA) with 1 wt % multiwalled carbon nanotubes (MWNTs) wrapped on the surface with poly(2,6-diaminopyridine spirocyclic pentaerythritol bisphosphonate) (PDSPB); b) carbonization after the cone calorimeter test of epoxy resin (EP) with 2 wt % of the MWNTs wrapped on the surface with poly(phenylphosphonic-4,4'-diaminodiphenylmethane) (PD); c) photographs of dispersions of graphene and graphene wrapped with 9,10-dihydro-9-oxa-10-phosphaphenanthrene-10-oxide (DOPO) modified vinyl trimethoxysilane (DOPO-VTS) in different solvents and transmission electron microscopy (TEM) images of EP with graphene-DOPO-VTS as a flame retardant.



### 5.2. Renewable Sources

Fractions of biomass from different industrial sectors (e.g. paper) are utilized to produce bio-based FRs, such as carbohydrate fractions (starch), oil fractions (triglycerides or fatty acids), and phenolic fractions (lignin).<sup>[101,102]</sup> In some cases, these fractions are modified with P compounds to improve their FR potential.

Since 2006, the group of Cádiz, in particular, have made special efforts in this field.<sup>[103]</sup> They reported new routes to obtain P-containing triglycerides or fatty acids from vegetable oils by cationic polymerization, by cross-metathesis reaction, or by Michael addition. An increase in the LOI values in the final material was detected. More recently, Howell et al.<sup>[104]</sup> reported the esterification of isosorbide (from starch) with 10-undecenoic acid (from castor oil) to provide a difunctional ester which can be modified by a thiol-ene reaction to generate a series of phosphate, phosphonate, and phosphinate esters, which were later incorporated into epoxy resins. Howell et al. further synthesized diethyl esters of tartaric acid, a by-product of the wine industry, using diphenylphosphinic chloride, thereby producing an ester which may serve as a base for further FR agents.<sup>[105]</sup>

Starch, chitin, and chitosan are polysaccharides that carry various chemical functionalities that can undergo reactions such as etherification, esterification, or graft polymerization to produce FRs.<sup>[106]</sup> Cotton fabric is the matrix par excellence for the application of bio-based FRs and is the most commonly used. Polysaccharide cationic polyelectrolytes deposited through layer-by-layer (LbL) assembly can greatly enhance the char-forming ability of cellulose. 20–40 deposition steps are usually necessary to achieve significant flame-retardant properties, which limits the applicability of this technique. However, Carosio et al.<sup>[107]</sup> recently achieved self-extinguishing during a flammability test after only two deposited bilayers (less than 5 wt% deposited on cotton) using a polyphosphoric acid as an anionic polyelectrolyte. The dehydration effect of the polyphosphoric acid promoted the formation of a protective layer from the starch. Xiao et al.<sup>[108]</sup> reported the synergistic effect of a chitosan/urea compound based on a phosphonic acid melamine salt with melamine pyrophosphate and pentaerythritol in polypropylene, thereby accelerating the decomposition and promoting char formation.

Lignocellulosic materials are aromatic-rich polymers that exhibit high thermal stability and very high char yields. The high number of reactive functional groups in their structure allows their chemical functionalization with P to promote dehydration reactions, and with nitrogen compounds to release NH<sub>3</sub> gas. Liu et al.<sup>[109]</sup> reported the modification of lignin by grafting polyethylene imine and diethyl phosphite as well as its incorporation in polypropylene/wood composites. Costes et al.<sup>[110]</sup> modified lignin with PONH<sub>4</sub> to improve its FR action in poly(lactic acid). A V-0 classification in UL-94 fire tests was achieved through the incorporation of 20 wt% of the treated lignin.

Interestingly, the authors showed that the thermal stability of lignin is mainly dependent on the nature and the number of monomer units that constitute the plant, which is not only

affected by the plant origin but also by the extraction process used. Thus, Organosolv lignin was less thermally stable than Kraft lignin. The thermal degradation of lignin started around 230°C with the cleavage of the phenylpropanoid side chain and continued with the further cleavage of the main chain (250°C–450°C), which produced a large quantity of methane. Above 500°C, condensation reactions of the aromatic structure occur, promoting the formation of 50 wt% of a stable char up to 650°C. Lignin-cellulosic derivatives such as coffee grounds<sup>[112]</sup> in poly(butylene adipate-co-terephthalate) or vanillin<sup>[113]</sup> in epoxy resins have also been reported as FR additives.

The use of phytic acid from cereal grains, beans, or seed oil (28 wt% P content) has been reported so far as a bio-based P-FR. Phytic acid (PA) decomposes around 200°C, which ensures the dehydration of a carbon source and makes it a good candidate as an acid source for intumescent systems.<sup>[114]</sup> Laufer et al. used LbL assembly to develop a fully renewable intumescent system which reduced the flammability of cotton.<sup>[114]</sup> The combination of 30 bilayers of PA (anionic polyelectrolyte) with chitosan as a cationic polyelectrolyte succeeded in completely extinguishing the flame in a vertical flame test. Recently, Zheng et al.<sup>[115]</sup> synthesized a melamine phytate (MPA) with a particle size around 1 μm by the reaction of phytic acid with melamine. MPA starts to decompose at around 250°C, releasing water and producing melamine polyphytate by self-cross-linking. At 400°C, the s-triazine ring from melamine decomposes with generation of inert gases. The addition of a charring agent, dipentaerythritol, was necessary to reach 28.5% in the LOI test and a V-0 rating in the UL-94 test (the dripping phenomenon of polypropylene needed to be suppressed).

### 5.3. Biopolymers

The groups of Malucelli and Alongi have recently introduced the use of phosphorylated biomacromolecules such as caseins (from milk products) and deoxyribonucleic acid (from the extraction of salmon milt and roe sacs) as inherent FRs; this was part of a strategy for the valorization of by-products from the agro-food industry.<sup>[4,116]</sup>

$\alpha_{S1}$ -Caseins are phosphorylated proteins containing approximately nine bound phosphate groups per molecule. In cotton fabrics, caseins show thermal degradation profiles analogous to those of ammonium polyphosphate (APP) salts, except that the phosphoric acid is released at lower temperatures compared to the salts, because of the weaker covalent bonds of the phosphate groups in the main chain. The catalytic effect of the phosphoric acid in the dehydration of the cellulose promotes the formation of a thermally stable char at 600°C. In flammability tests, a significant decrease of 35% in the total burning rate and a reduction of the PHRR by 27% were achieved. In polyester fabrics, the decrease in the burning rate was 67%, but dripping was not suppressed.

The structure of deoxyribonucleic acid (DNA) makes it an ideal intumescent material as it carries 1) phosphates as an acid source, 2) deoxyribose units as a char source, and 3) nitrogen-containing aromatic groups as blowing agents.



However, DNA decomposes at lower temperatures (160–200 °C) than the typical intumescent additives (e.g. 300–350 °C).<sup>[117]</sup> In cotton fabrics, the thermal degradation of DNA was similar to that of APP: the combustion data proved a significant decrease in the PHRR by 50 % combined with an intumescent effect.

The application of caseins and DNA to the fabric was carried out by impregnation or by LbL depositions. For significant results, 20 bilayers were necessary to reduce the burning rate and achieve self-extinguishment of the fabric as well as an increase of the final residue after burning. However, the major disadvantage of applying biomacromolecules to fabric is their poor resistance to washing treatments.

Recently, Alongi et al. investigated the potential of DNA coated on different matrices (EVA, PP, PA6) as a “universal” FR.<sup>[118]</sup> Thicknesses of 3 mm (10 wt % DNA) showed good performances and a reduction in the PHRR of more than 50 % in all polymeric matrices (Figure 12).

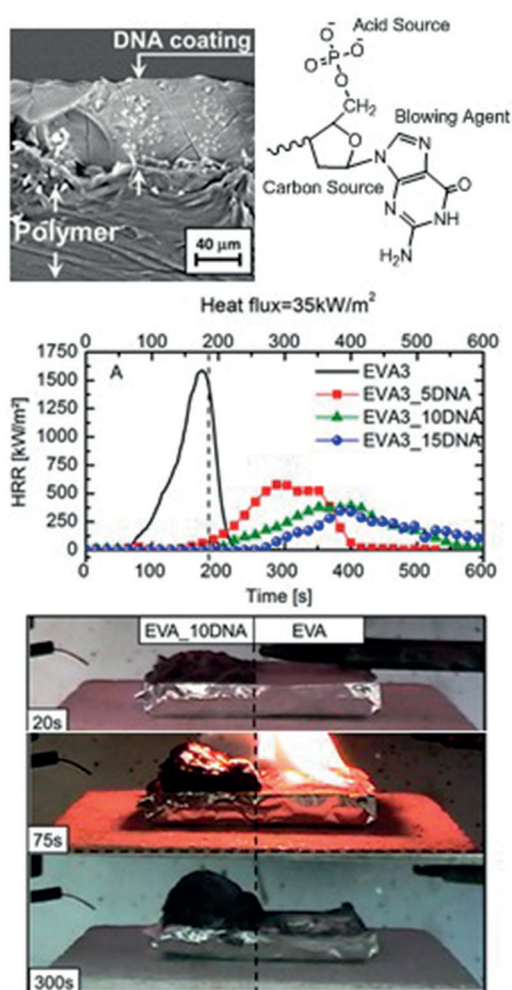


**Figure 12.** Top: DNA-coated polymer surface and chemical structure of a DNA segment and its different compounds acting together to form an intumescent flame retardant. Middle: Heat release rate plots at 35 kW m<sup>-2</sup> for ethylene vinyl acetate (EVA) and EVA treated with 5, 10, and 15 wt% DNA. Bottom: Snapshots taken at different times during cone calorimetry tests on an EVA sample with only 50% of the surface coated with DNA.<sup>[118]</sup>

To summarize, the main mechanism of biopolymers in cotton fabrics is the release of phosphoric acid at lower temperatures to catalyze the formation of a thermally stable char. However, two current limitations to their use are their poor resistance to laundering and their expensive production on a large scale.

## 6. Conclusions

Phosphorus is pivotal to the development of novel efficient flame retardants, mainly because of its chemical versatility: it can act in both the condensed and gas phase, as an additive or as a reactive component, in various oxidation states, and in synergy with numerous adjuvant elements. With increased awareness towards nontoxic, recyclable, and bio-based (or even sustainable) materials, phosphorus has the potential to fulfill all the criteria for future flame retardants. Future FRs will be increasingly tailored to the polymer type and its application, especially for new polymers, including biopolymers. The trend towards high-molecular-weight FRs is apparent, and polymeric, complex, and multifunctional structures will aid in reducing flammability without a loss of valuable properties. Furthermore, investigations into combinations of P with various moieties (P-P, P-Si, P-B, etc.) and multicomponent systems will continue to reduce FR loading and improve FR performance. Finally, the use of renewable resources as effective FRs will ensure a more ecologically aware means of production, thereby increasing the longevity of research into the field of flame retardancy.

“Molecular firefighting” demands the combined efforts of synthetic chemistry, an understanding of FR mechanisms, and knowledge of polymer processing. This interdisciplinary field continues to reveal new insight into the FR mechanisms, which we believe will drive toward a more sustainable P life-cycle for FRs and a new era of polymeric FR materials.

## Acknowledgements

We thank the Deutsche Forschungsgemeinschaft (DFG WU 750/8-1; SCHA 730/15-1) for funding. M. M. V. thanks the Marie Skłodowska-Curie fellowship 705054-NOFLAME. J.C.M. is recipient of a fellowship through funding of the Excellence Initiative in the context of the graduate school of excellence “MAINZ” (Materials Science in Mainz; DFG/GSC 266). F.R.W., M.M.V., and J.C.M. thank Prof. Dr. Katharina Landfester (MPI-P, Germany) for support.

## Conflict of interest

The authors declare no conflict of interest.

**How to cite:** *Angew. Chem. Int. Ed.* **2018**, *57*, 10450–10467  
*Angew. Chem.* **2018**, *130*, 10608–10626

- [1] a) S. Shaw, *Rev. Environ. Health* **2010**, *25*, 261–306; b) S.-Y. Lu, I. Hamerton, *Prog. Polym. Sci.* **2002**, *27*, 1661–1712; c) S. V. Levchik, E. D. Weil, *J. Fire Sci.* **2006**, *24*, 345–364.
- [2] a) Lucintel, Irving, TX, USA, **2016**; b) A. B. Morgan, J. W. Gilman, *Fire Mater.* **2013**, *37*, 259–279.
- [3] E. D. Weil, S. V. Levchik, *Flame Retardants for Plastics and Textiles: Practical Applications*, 2nd ed., Carl Hanser, München, **2015**.
- [4] G. Malucelli, F. Bosco, J. Alongi, F. Carosio, A. Di Blasio, C. Mollea, F. Cuttica, A. Casale, *RSC Adv.* **2014**, *4*, 46024–46039.
- [5] S. Bourbigot, S. Duquesne, *J. Mater. Chem.* **2007**, *17*, 2283–2300.
- [6] a) P. R. Hornsby in *Macromolecular Symposia*, Vol. 108, Wiley Online Library, Chichester, **1996**, pp. 203–219; b) Lucintel, Irving, TX, USA, **2016**, p. 208.
- [7] a) R. W. Nalepa, D. J. Scharf, Hoechst Celanese Corp., **1993**; b) L. J. Chyall, H. A. Hodgen, F. J. Vyverberg, R. W. Chapman, Pabu Services, Inc., **2005**; c) A. Sut, S. Greiser, C. Jäger, B. Schartel, *Polym. Degrad. Stab.* **2015**, *121*, 116–125.
- [8] a) E. D. Weil, *Fire Retard. Polym. Mater.* **2000**, 115–145; b) M. Lewin, *J. Fire Sci.* **1999**, *17*, 3–19.
- [9] a) B. Schartel, R. Kunze, D. Neubert, *J. Appl. Polym. Sci.* **2002**, *83*, 2060–2071; b) S. V. Levchik, G. F. Levchik, A. I. Balabanovich, E. D. Weil, M. Klatt, *Angew. Makromol. Chem.* **1999**, *264*, 48–55; c) P. Catsman, L. C. Govaerts, R. Lucas, C08K 5/521 (2006.01), C08L 69/00 (2006.01) ed. (Ed.: G. E. Company), World Intellectual Property Organization (WIPO), USA, **2000**; d) D. K. Chattopadhyay, D. C. Webster, *Prog. Polym. Sci.* **2009**, *34*, 1068–1133.
- [10] a) U. Braun, B. Schartel, M. A. Fichera, C. Jäger, *Polym. Degrad. Stab.* **2007**, *92*, 1528–1545; b) Y. Liu, Q. Wang, *Polym. Degrad. Stab.* **2006**, *91*, 3103–3109.
- [11] F. L. Jin, X. Li, S. J. Park, *J. Ind. Eng. Chem.* **2015**, *29*, 1–11.
- [12] a) *Additives for Polymers* **2017**, 10–11; b) S. V. Levchik, E. D. Weil, *Polym. Int.* **2004**, *53*, 1901–1929; c) M. Rakotomalala, S. Wagner, M. Döring, *Materials* **2010**, *3*, 4300–4327; d) B. Schartel, A. I. Balabanovich, U. Braun, U. Knoll, J. Artner, M. Ciesielski, M. Döring, R. Perez, J. K. W. Sandler, V. Altstädt, T. Hoffmann, D. Pospiech, *J. Appl. Polym. Sci.* **2007**, *104*, 2260–2269.
- [13] a) M. Ciesielski, B. Burk, C. Heinzmann, M. Döring in *Novel Fire Retardant Polymers and Composite Materials*, Woodhead, Sawston, **2017**, pp. 3–51; b) K. A. Salmeia, S. Gaan, *Polym. Degrad. Stab.* **2015**, *113*, 119–134; c) X. Wang, Y. Hu, L. Song, W. Y. Xing, H. D. A. Lu, P. Lv, G. X. Jie, *Polymer* **2010**, *51*, 2435–2445; d) S. Yang, Q. X. Zhang, Y. F. Hu, *Polym. Degrad. Stab.* **2016**, *133*, 358–366; e) W. C. Zhang, X. M. Li, H. B. Fan, R. J. Yang, *Polym. Degrad. Stab.* **2012**, *97*, 2241–2248.
- [14] R. E. Lyon, M. L. Janssens in *Encyclopedia of Polymer Science and Technology*, Wiley, Chichester, **2002**.
- [15] a) M. Lewin, E. Weil in *Fire retardant materials* (Eds.: A. R. Horrocks, D. Price), Woodhead, Sawston, **2001**, pp. 31–68; b) S. Rabe, Y. Chuenban, B. Schartel, *Materials* **2017**, *10*, 23.
- [16] a) B. Schartel, B. Perret, B. Dittrich, M. Ciesielski, J. Krämer, P. Müller, V. Altstädt, L. Zang, M. Döring, *Macromol. Mater. Eng.* **2016**, *301*, 9–35; b) M. Lewin, *Spec. Publ. R. Soc. Chem.* **1998**, *224*, 3–34; c) S. Levchik, C. A. Wilkie, *Fire Retard. Polym. Mater.* **2000**, 171–215.
- [17] a) G. Camino, S. Lomakin in *Fire retardant materials* (Eds.: A. R. Horrocks, D. Price), Woodhead, Cambridge, **2001**, pp. 318–336; b) J. Alongi, Z. D. Han, S. Bourbigot, *Prog. Polym. Sci.* **2015**, *51*, 28–73; c) S. Bourbigot, M. Le Bras, S. Duquesne, M. Rochery, *Macromol. Mater. Eng.* **2004**, *289*, 499–511.
- [18] a) M. Matzen, B. Kandola, C. Huth, B. Schartel, *Materials* **2015**, *8*, 5621–5646; b) K. Shibuya, H. Hachiya, N. Nanba, (Ed.: J. Asashi Kasei Kabushiki Kaisha), **2002**; c) F. Kempel, B. Schartel, J. M. Marti, K. M. Butler, R. Rossi, S. R. Idelsohn, E. Oñate, A. Hofmann, *Fire Mater.* **2015**, *39*, 570–584.
- [19] S. Bourbigot, M. Le Bras, R. Leeuwendal, K. K. Shen, D. Schubert, *Polym. Degrad. Stab.* **1999**, *64*, 419–425.
- [20] S. Duquesne, M. Le Bras, S. Bourbigot, R. Delobel, F. Poutch, G. Camino, B. Eling, C. Lindsay, T. Roels, *J. Fire Sci.* **2000**, *18*, 456–482.
- [21] G. J. Minkoff, *Chemistry of combustion reactions*, Butterworths, London, **1962**.
- [22] J. Green, *J. Fire Sci.* **1996**, *14*, 426–442.
- [23] a) S. K. Brauman, *J. Fire Retard. Chem.* **1977**, *4*, 38–58; b) G. Camino, L. Costa, M. P. L. di Cortemiglia, *Polym. Degrad. Stab.* **1991**, *33*, 131–154; c) B. Perret, K. H. Pawlowski, B. Schartel, *J. Therm. Anal. Calorim.* **2009**, *97*, 949–958.
- [24] S. V. Levchik, E. D. Weil, *Polym. Int.* **2005**, *54*, 11–35.
- [25] a) M. Modesti, A. Lorenzetti, *Polym. Degrad. Stab.* **2002**, *78*, 167–173; b) K. A. Salmeia, S. Gaan, G. Malucelli, *Polymer* **2016**, *8*, 319; c) A. R. Horrocks, *Polym. Degrad. Stab.* **2011**, *96*, 377–392.
- [26] B. Schartel, *Materials* **2010**, *3*, 4710–4745.
- [27] a) T. Marzi, A. Beard in *Flame Retardants*, Vol. 12, Interscience, London, **2006**, p. 21; b) I. van der Veen, J. de Boer, *Chemosphere* **2012**, *88*, 1119–1153.
- [28] a) J. D. Meeker, H. M. Stapleton, *Environ. Health Perspect.* **2010**, *118*, 318–323; b) A. M. Sundkvist, U. Olofsson, P. Haglund, *J. Environ. Monit.* **2010**, *12*, 943–951; c) G. L. Wei, D. Q. Li, M. N. Zhuo, Y. S. Liao, Z. Y. Xie, T. L. Guo, J. J. Li, S. Y. Zhang, Z. Q. Liang, *Environ. Pollut.* **2015**, *196*, 29–46.
- [29] A. Beard, T. Marzi in Proceedings of Going Green CARE Innovation 2006 Conference. Vienna, Austria, **2006**.
- [30] P. L. Lallas, *Am. J. Int. Law* **2001**, *95*, 692–708.
- [31] I. ISO, International Org. for Standardization, Geneva **2000**.
- [32] a) U. Landmann, Freie Universität Berlin **1999**; b) T. B. Bjørner, L. G. Hansen, C. S. Russell, *J. Environ. Econ. Manag.* **2004**, *47*, 411–434.
- [33] a) A. Beard, M. Klimes, U. Wietschorke, *2012 Electronics Goes Green 2012 + (Egg)* **2012**; b) H. Wendschlag, H. Holder, C. Robertson, C. Wray in *2nd International Conference on ICT for Sustainability (ICT4S 2014)*, Atlantis Press, **2014**, pp. 306–310; c) G. Ondrey, *Chem. Eng.* **2015**, *122*, 19–23.
- [34] a) G. Marosi, B. Szolnoki, K. Bocs, A. Toldy in *Polymer Green Flame Retardants*, 1st ed. (Eds.: C. Papaspyrides, P. Kiliaris), Elsevier, Amsterdam, **2014**, pp. 181–220; b) A. Sakharov, P. Sakharov, S. Lomakin, G. Zaikov in *AIP Conf. Proc.*, Vol. 1459, AIP, **2012**, pp. 316–318; c) M. Zammarano, D. M. Fox, S. Matko, T. Kashiwagi, J. W. Gilman, R. D. Davis, *Fire Mater.* **2011**, 337–342.
- [35] a) P. F. Sommerhuber, J. L. Wenker, S. Ruter, A. Krause, *Resour. Conserv. Recycl.* **2017**, *117*, 235–248; b) D. Hoang, T. Nguyen, H. An, J. Kim, *Macromol. Res.* **2016**, *24*, 537–546; c) M. Schlummer, A. Maurer, T. Leitner, W. Spruzina, *Waste Manage. Res.* **2006**, *24*, 573–583.
- [36] EPA, in *An Alternatives Assessment for the Flame Retardant Decabromodiphenyl ether (DecaBDE)*, [https://www.epa.gov/sites/production/files/2014-05/documents/decabde\\_final.pdf](https://www.epa.gov/sites/production/files/2014-05/documents/decabde_final.pdf), **2014**.
- [37] J.-L. Montchamp, *Acc. Chem. Res.* **2014**, *47*, 77–87.
- [38] K. T. Carter, Vol. US3464808 A (Ed.: S. Co), **1969**.
- [39] J. D. Leman, A. J. Robertson, Vol. US4117200 (Ed.: A. C. Company), **1978**.
- [40] N. Fukuoka, H. Yasuda, M. Nishimatsu, Y. Ohmae, Vol. EP1403273 A1 (Ed.: L. Chemipro Kasei Kaisha), **2004**.
- [41] L. K. Müller, T. Steinbach, F. R. Wurm, *RSC Adv.* **2015**, *5*, 42881–42888.
- [42] a) F. Marsico, A. Turshatov, R. Peköz, Y. Avlasevich, M. Wagner, K. Weber, D. Donadio, K. Landfester, S. Balushev,

- F. R. Wurm, *J. Am. Chem. Soc.* **2014**, *136*, 11057–11064; b) M. Steinmann, J. Markwart, F. R. Wurm, *Macromolecules* **2014**, *47*, 8506–8513; c) G. Becker, L. Vlaminc, M. M. Velencoso, F. E. Du Prez, F. R. Wurm, *Polym. Chem.* **2017**, *8*, 4074–4078.
- [43] a) T. Wolf, T. Steinbach, F. R. Wurm, *Macromolecules* **2015**, *48*, 3853–3863; b) T. Steinbach, S. Ritz, F. R. Wurm, *ACS Macro Lett.* **2014**, *3*, 244–248.
- [44] R. W. Scholz, A. H. Roy, F. S. Brand, D. T. Hellums, A. E. Ulrich, *Sustainable Phosphorus Management: A Global Transdisciplinary Roadmap*, Springer, Dordrecht, Heidelberg, New York, London, **2014**.
- [45] J. Cooper, R. Lombardi, D. Boardman, C. Carliell-Marquet, *Resour. Conserv. Recycl.* **2011**, *57*, 78–86.
- [46] EU, [http://ec.europa.eu/growth/sectors/raw-materials/specific-interest/critical\\_es](http://ec.europa.eu/growth/sectors/raw-materials/specific-interest/critical_es), **2017**.
- [47] E. D. Roy, *Ecol. Eng.* **2017**, *98*, 213–227.
- [48] A. Ehmann, I.-M. Bach, S. Laoeamthong, J. Bilbao, I. Lewandowski, *Agriculture* **2017**, *7*, 1.
- [49] A. H. Landrock, *Handbook of Plastic Foams: Types, Properties, Manufacture and Applications*, Noyes Publications, Park Ridge, **1995**.
- [50] a) G. Marosi, B. Szolnoki, K. Bocz, A. Toldy in *Polymer Green Flame Retardants*, Elsevier, Amsterdam, **2014**, pp. 181–220; b) B. Szolnoki, A. Toldy, P. Konrád, G. Szebényi, G. Marosi, *Period. Polytech. Chem. Eng.* **2013**, *57*, 85–91; c) S. V. Levchik, *J. Fire Sci.* **2006**, *24*, 345–364.
- [51] S.-H. Chiu, C.-L. Wu, H.-T. Lee, J.-H. Gu, M.-C. Suen, *J. Polym. Res.* **2016**, *23*, 205.
- [52] M. Steinmann, M. Wagner, F. R. Wurm, *Chem. Eur. J.* **2016**, *22*, 17329–17338.
- [53] a) F. Çelebi, O. Polat, L. Aras, G. Gündüz, I. M. Akhmedov, *J. Appl. Polym. Sci.* **2004**, *91*, 1314–1321; b) M.-J. Chen, C.-R. Chen, Y. Tan, J.-Q. Huang, X.-L. Wang, L. Chen, Y.-Z. Wang, *Ind. Eng. Chem. Res.* **2014**, *53*, 1160–1171.
- [54] L. Chen, C. Ruan, R. Yang, Y.-Z. Wang, *Polym. Chem.* **2014**, *5*, 3737–3749.
- [55] X.-H. Zhang, F. Liu, S. Chen, G.-R. Qi, *J. Appl. Polym. Sci.* **2007**, *106*, 2391–2397.
- [56] a) C. Klinkowski, L. Zang, M. Döring, *Mater. China* **2013**, *32*, 144–158; b) M. Rakotomalala, S. Wagner, M. Döring, *Materials* **2010**, *3*, 4300.
- [57] J. Artner, M. Ciesielski, O. Walter, M. Döring, R. M. Perez, J. K. W. Sandler, V. Altstädt, B. Schartel, *Macromol. Mater. Eng.* **2008**, *293*, 503–514.
- [58] M. Ciesielski, A. Schäfer, M. Döring, *Polym. Adv. Technol.* **2008**, *19*, 507–515.
- [59] Q. F. Wang, W. F. Shi, *Polym. Degrad. Stab.* **2006**, *91*, 1289–1294.
- [60] a) P. M. Hergenrother, C. M. Thompson, J. G. Smith, J. W. Connell, J. A. Hinkley, R. E. Lyon, R. Moulton, *Polymer* **2005**, *46*, 5012–5024; b) S. Monge, G. David, B. Z. Tang, A. S. Abdel-Aziz, S. Craig, J. Dong, T. Masuda, C. Weder, *Phosphorus-Based Polymers: From Synthesis to Applications*, Royal Society of Chemistry, London, **2014**; c) R.-J. Jeng, J.-R. Wang, J.-J. Lin, Y.-L. Liu, Y.-S. Chiu, W.-C. Su, *J. Appl. Polym. Sci.* **2001**, *82*, 3526–3538.
- [61] a) U. Braun, B. Schartel, *Macromol. Mater. Eng.* **2008**, *293*, 206–217; b) B. Perret, B. Schartel, K. Stoss, M. Ciesielski, J. Diederichs, M. Döring, J. Krämer, V. Altstädt, *Macromol. Mater. Eng.* **2011**, *296*, 14–30.
- [62] U. Braun, A. I. Balabanovich, B. Schartel, U. Knoll, J. Artner, M. Ciesielski, M. Döring, R. Perez, J. K. W. Sandler, V. Altstädt, T. Hoffmann, D. Pospiech, *Polymer* **2006**, *47*, 8495–8508.
- [63] J. H. Song, *J. Vinyl Addit. Technol.* **1995**, *1*, 46–50.
- [64] C. Vasile, *Handbook of Polyolefins, 2nd ed.*, CRC, Boca Raton, **2000**.
- [65] U. Braun, B. Schartel, *Macromol. Chem. Phys.* **2004**, *205*, 2185–2196.
- [66] H. Q. Yin, D. D. Yuan, X. F. Cai, *J. Therm. Anal. Calorim.* **2013**, *111*, 499–506.
- [67] Y. Tan, Z.-B. Shao, L.-X. Yu, J.-W. Long, M. Qi, L. Chen, Y.-Z. Wang, *Polym. Chem.* **2016**, *7*, 3003–3012.
- [68] L. J. Duan, H. Y. Yang, L. Song, Y. B. Hou, W. Wang, Z. Gui, Y. Hu, *Polym. Degrad. Stab.* **2016**, *134*, 179–185.
- [69] E. Gallo, U. Braun, B. Schartel, P. Russo, D. Acierno, *Polym. Degrad. Stab.* **2009**, *94*, 1245–1253.
- [70] E. Gallo, B. Schartel, D. Acierno, P. Russo, *Eur. Polym. J.* **2011**, *47*, 1390–1401.
- [71] a) A. D. Naik, G. Fontaine, F. Samyn, X. Delva, Y. Bourgeois, S. Bourbigot, *Polym. Degrad. Stab.* **2013**, *98*, 2653–2662; b) A. D. Naik, G. Fontaine, F. Samyn, X. Delva, J. Louisy, S. Bellayer, Y. Bourgeois, S. Bourbigot, *Fire Saf. J.* **2014**, *70*, 46–60; c) A. D. Naik, G. Fontaine, F. Samyn, X. Delva, J. Louisy, S. Bellayer, Y. Bourgeois, S. Bourbigot, *RSC Adv.* **2014**, *4*, 18406–18418; d) P. Müller, B. Schartel, *J. Appl. Polym. Sci.* **2016**, *133*, 43549; e) P. Müller, M. Morys, A. Sut, C. Jäger, B. Illerhaus, B. Schartel, *Polym. Degrad. Stab.* **2016**, *130*, 307–319.
- [72] G.-L. Wei, D.-Q. Li, M.-N. Zhuo, Y.-S. Liao, Z.-Y. Xie, T.-L. Guo, J.-J. Li, S.-Y. Zhang, Z.-Q. Liang, *Environ. Pollut.* **2015**, *196*, 29–46.
- [73] L. Chen, Y.-Z. Wang, *Materials* **2010**, *3*, 4746–4760.
- [74] J. Eichhorn, *J. Appl. Polym. Sci.* **1964**, *8*, 2497–2524.
- [75] M. W. Beach, N. G. Rondan, R. D. Froese, B. B. Gerhart, J. G. Green, B. G. Stobby, A. G. Shmakov, V. M. Shvartsberg, O. P. Korobeinichev, *Polym. Degrad. Stab.* **2008**, *93*, 1664–1673.
- [76] J. Wagner, P. Deglmann, S. Fuchs, M. Ciesielski, C. A. Fleckenstein, M. Doring, *Polym. Degrad. Stab.* **2016**, *129*, 63–76.
- [77] K. H. Pawlowski, B. Schartel, *Polym. Int.* **2007**, *56*, 1404–1414.
- [78] K. Täuber, F. Marsico, F. R. Wurm, B. Schartel, *Polym. Chem.* **2014**, *5*, 7042–7053.
- [79] a) B. Liang, X. D. Hong, M. Zhu, C. J. Gao, C. S. Wang, N. Tsubaki, *Polym. Bull.* **2015**, *72*, 2967–2978; b) S. Q. Song, J. J. Ma, K. Cao, G. J. Chang, Y. W. Huang, J. X. Yang, *Polym. Degrad. Stab.* **2014**, *99*, 43–52; c) W. C. Zhang, X. M. Li, R. J. Yang, *Polym. Degrad. Stab.* **2011**, *96*, 2167–2173; d) X. Wang, Y. Hu, L. Song, H. Y. Yang, W. Y. Xing, H. D. Lu, *Prog. Org. Coat.* **2011**, *71*, 72–82.
- [80] S. Hörold in *Polymer Green Flame Retardants, 1st ed.* (Eds.: C. Papispyrides, P. Kiliaris), Elsevier, Amsterdam, Oxford, Waltham, **2014**, pp. 221–254.
- [81] F. Laoutid, L. Bonnaud, M. Alexandre, J. M. Lopez-Cuesta, P. Dubois, *Mater. Sci. Eng. R* **2009**, *63*, 100–125.
- [82] a) A. Toldy, B. Szolnoki, I. Csontos, G. Marosi, *J. Appl. Polym. Sci.* **2014**, *131*, 40105; b) B. Edwards, S. Rudolf, P. Hauser, A. El-Shafei, *Ind. Eng. Chem. Res.* **2015**, *54*, 577–584; c) M. Neisius, S. Liang, H. Mispereuve, S. Gaan, *Ind. Eng. Chem. Res.* **2013**, *52*, 9752–9762; d) X. Zhao, F. R. Guerrero, J. Llorca, D.-Y. Wang, *ACS Sustainable Chem. Eng.* **2016**, *4*, 202–209.
- [83] a) K. Tao, J. Li, L. Xu, X. Zhao, L. Xue, X. Fan, Q. Yan, *Polym. Degrad. Stab.* **2011**, *96*, 1248–1254; b) H. Liu, X. Wang, D. Wu, *Polym. Degrad. Stab.* **2014**, *103*, 96–112.
- [84] K. N. Bauer, H. T. Tee, M. M. Velencoso, F. R. Wurm, *Prog. Polym. Sci.* **2017**, *73*, 61–122.
- [85] S. Gaan, G. Sun, K. Hutches, M. H. Engelhard, *Polym. Degrad. Stab.* **2008**, *93*, 99–108.
- [86] a) B. Li, Z. Zhan, H. Zhang, C. Sun, *J. Vinyl Addit. Technol.* **2014**, *20*, 10–15; b) D. Freitag, P. Go, Y. JEONG, L. Kagumba, Google Patents, WO2013071230A1, **2013**; c) W. Zhao, J. Liu, H. Peng, J. Liao, X. Wang, *Polym. Degrad. Stab.* **2015**, *118*, 120–129.
- [87] L. J. Qian, L. J. Ye, G. Z. Xu, J. Liu, J. Q. Guo, *Polym. Degrad. Stab.* **2011**, *96*, 1118–1124.



- [88] P. Wen, Q. Tai, Y. Hu, R. K. K. Yuen, *Ind. Eng. Chem. Res.* **2016**, *55*, 8018–8024.
- [89] T. Mayer-Gall, D. Knittel, J. S. Gutmann, K. Opwis, *ACS Appl. Mater. Interfaces* **2015**, *7*, 9349–9363.
- [90] a) Y. Bai, X. Wang, D. Wu, *Ind. Eng. Chem. Res.* **2012**, *51*, 15064–15074; b) H. Liu, X. Wang, D. Wu, *Polym. Degrad. Stab.* **2015**, *118*, 45–58.
- [91] S. Rothmund, I. Teasdale, *Chem. Soc. Rev.* **2016**, *45*, 5200–5215.
- [92] a) W. Xing, W. Yang, W. Yang, Q. Hu, J. Si, H. Lu, B. Yang, L. Song, Y. Hu, R. K. K. Yuen, *ACS Appl. Mater. Interfaces* **2016**, *8*, 26266–26274; b) J. Sun, X. Gu, S. Zhang, M. Coquelle, S. Bourbigot, S. Duquesne, M. Casetta, *Polym. Adv. Technol.* **2014**, *25*, 1099–1107; c) S. Qiu, X. Wang, B. Yu, X. Feng, X. Mu, R. K. K. Yuen, Y. Hu, *J. Hazard. Mater.* **2017**, *325*, 327–339.
- [93] B. Yu, Y. Shi, B. Yuan, S. Qiu, W. Xing, W. Hu, L. Song, S. Lo, Y. Hu, *J. Mater. Chem.* **2015**, *3*, 8034–8044.
- [94] a) M. Raimondo, S. Russo, L. Guadagno, P. Longo, S. Chirico, A. Mariconda, L. Bonnaud, O. Murariu, P. Dubois, *RSC Adv.* **2015**, *5*, 10974–10986; b) A. Lorenzetti, S. Besco, D. Hrelja, M. Roso, E. Gallo, B. Schartel, M. Modesti, *Polym. Degrad. Stab.* **2013**, *98*, 2366–2374.
- [95] D. C. O. Marney, W. Yang, L. J. Russell, S. Z. Shen, T. Nguyen, Q. Yuan, R. Varley, S. Li, *Polym. Adv. Technol.* **2012**, *23*, 1564–1571.
- [96] E. Gallo, B. Schartel, U. Braun, P. Russo, D. Acierno, *Polym. Adv. Technol.* **2011**, *22*, 2382–2391.
- [97] a) J. Jiang, Y. Cheng, Y. Liu, Q. Wang, Y. He, B. Wang, *J. Mater. Chem.* **2015**, *3*, 4284–4290; b) S. Pappalardo, P. Russo, D. Acierno, S. Rabe, B. Schartel, *Eur. Polym. J.* **2016**, *76*, 196–207.
- [98] Q. Dong, M. Liu, Y. Ding, F. Wang, C. Gao, P. Liu, B. Wen, S. Zhang, M. Yang, *Polym. Adv. Technol.* **2013**, *24*, 732–739.
- [99] X. Qian, L. Song, B. Yu, B. Wang, B. Yuan, Y. Shi, Y. Hu, R. K. K. Yuen, *J. Mater. Chem.* **2013**, *1*, 6822–6830.
- [100] G. Xu, J. Cheng, H. Wu, Z. Lin, Y. Zhang, H. Wang, *Polym. Compos.* **2013**, *34*, 109–121.
- [101] R. Ménard, C. Negrell, M. Fache, L. Ferry, R. Sonnier, G. David, *RSC Adv.* **2015**, *5*, 70856–70867.
- [102] P. Jia, L. Hu, M. Zhang, G. Feng, Y. Zhou, *Eur. Polym. J.* **2017**, *87*, 209–220.
- [103] a) M. Sacristán, J. C. Ronda, M. Galià, V. Cádiz, *J. Appl. Polym. Sci.* **2011**, *122*, 1649–1658; b) M. Moreno, G. Lligadas, J. C. Ronda, M. Galià, V. Cádiz, *J. Polym. Sci. Part A* **2012**, *50*, 3206–3213.
- [104] B. A. Howell, Y. G. Daniel, *J. Therm. Anal. Calorim.* **2015**, *121*, 411–419.
- [105] B. A. Howell, K. E. Carter, *J. Therm. Anal. Calorim.* **2010**, *102*, 493–498.
- [106] H. Pan, W. Wang, Y. Pan, L. Song, Y. Hu, K. M. Liew, *Carbohydr. Polym.* **2015**, *115*, 516–524.
- [107] F. Carosio, G. Fontaine, J. Alongi, S. Bourbigot, *ACS Appl. Mater. Interfaces* **2015**, *7*, 12158–12167.
- [108] Y. Xiao, Y. Zheng, X. Wang, Z. Chen, Z. Xu, *J. Appl. Polym. Sci.* **2014**, *131*, 40845.
- [109] L. Liu, M. Qian, P. A. Song, G. Huang, Y. Yu, S. Fu, *ACS Sustainable Chem. Eng.* **2016**, *4*, 2422–2431.
- [110] L. Costes, F. Laoutid, M. Aguedo, A. Richel, S. Brohez, C. Delvosalle, P. Dubois, *Eur. Polym. J.* **2016**, *84*, 652–667.
- [111] a) C. Bao, Y. Guo, B. Yuan, Y. Hu, L. Song, *J. Mater. Chem.* **2012**, *22*, 23057–23063; b) S. Wang, F. Xin, Y. Chen, L. Qian, Y. Chen, *Polym. Degrad. Stab.* **2016**, *129*, 133–141.
- [112] H. Moustafa, C. Guizani, A. Dufresne, *J. Appl. Polym. Sci.* **2017**, *134*, 44498.
- [113] S. Wang, S. Ma, C. Xu, Y. Liu, J. Dai, Z. Wang, X. Liu, J. Chen, X. Shen, J. Wei, J. Zhu, *Macromolecules* **2017**, *50*, 1892–1901.
- [114] G. Laufer, C. Kirkland, A. B. Morgan, J. C. Grunlan, *Biomacromolecules* **2012**, *13*, 2843–2848.
- [115] Z. Zheng, S. Liu, B. Wang, T. Yang, X. Cui, H. Wang, *Polym. Compos.* **2015**, *36*, 1606–1619.
- [116] J. Alongi, F. Carosio, G. Malucelli, *Polym. Degrad. Stab.* **2014**, *106*, 138–149.
- [117] J. Alongi, A. Di Blasio, J. Milnes, G. Malucelli, S. Bourbigot, B. Kandola, G. Camino, *Polym. Degrad. Stab.* **2015**, *113*, 110–118.
- [118] J. Alongi, F. Cuttica, F. Carosio, *ACS Sustainable Chem. Eng.* **2016**, *4*, 3544–3551.

Manuscript received: November 15, 2017

Revised manuscript received: January 8, 2019

Accepted manuscript online: January 9, 2018

Version of record online: June 29, 2018

## 5.2. Systematically Controlled Decomposition Mechanism in Phosphorus Flame Retardants by Precise Molecular Architecture: P–O vs P–N

Jens C. Markwart, Alexander Battig, Lisa Zimmermann, Martin Wagner, Jochen Fischer, Bernhard Schartel, Frederik R. Wurm, *ACS Appl. Polym. Mater.* **2019**, 1, 1118-1128.

DOI link: <https://www.doi.org/10.1021/acsapm.9b00129>;

Direct link: <https://pubs.acs.org/doi/10.1021/acsapm.9b00129>

This article was accepted and published. Further permissions related to the material excerpted here should be directed to the publishers (ACS).

Author contribution:

- Aided in conceptualizing the frame of the work
- Chose the polymer materials, approach, loading, sample preparation and testing
- Pyrolytic investigations of the flame retardants (FRs)
  - Thermogravimetric analysis
  - Evolved gas and condensed phase FTIR
  - Pyrolysis gas chromatography / mass spectrometry
  - Pyrolysis combustion flow calorimeter
- Material and fire testing of FR-containing epoxy resins
  - Differential scanning calorimeter
  - Cone calorimeter, LOI and UL-94
  - Scanning electron microscopy, photography
- Collection, analysis, and interpretation of the data.
- Provided figures throughout the article, including decomposition mechanism
- Authored the results and discussion chapter with respect to flame-retardancy
- Scientific discussion, conclusions, maintained communication of all authors
- Proofread and spell-checked all versions of the article

## Abstract

Flame retardants (FR) are inevitable additives to many plastics. Halogenated organics are effective FRs but are controversially discussed due to the release of toxic gases during a fire or their persistence if landfilled. Phosphorus-containing compounds are effective alternatives to halogenated FRs and have potential lower toxicity and degradability. In addition, nitrogen-containing additives were reported to induce synergistic effects with phosphorus-based FRs. However, no systematic study of the gradual variation on a single phosphorus FR containing both P–O and P–N moieties and their comparison to the respective blends of phosphates and phosphoramides was reported. This study developed general design principles for P–O- and P–N-based FRs and will help to design effective FRs for various polymers. We synthesized a library of phosphorus FRs that only differ in their P-binding pattern from each other and studied their decomposition mechanism in epoxy resins. Systematic control over the decomposition pathways of phosphate ( $\text{P}=\text{O}(\text{OR})_3$ ), phosphoramidate ( $\text{P}=\text{O}(\text{OR})_2(\text{NHR})$ ), phosphorodiamidate ( $\text{P}=\text{O}(\text{OR})(\text{NHR})_2$ ), phosphoramidate ( $\text{P}=\text{O}(\text{NHR})_3$ ), and their blends was identified, for example, by reducing cis-elimination and the formation of P–N-rich char with increasing nitrogen content in the P-binding sphere. Our FR epoxy resins can compete with commercial FRs in most cases, but we proved that the blending of esters and amides outperformed the single-molecule amidates/diamidates due to distinctively different decomposition mechanisms acting synergistically when blended.

# Systematically Controlled Decomposition Mechanism in Phosphorus Flame Retardants by Precise Molecular Architecture: P–O vs P–N

Jens C. Markwart,<sup>†,§</sup> Alexander Battig,<sup>‡,§</sup> Lisa Zimmermann,<sup>||,§</sup> Martin Wagner,<sup>⊥,§</sup> Jochen Fischer,<sup>#</sup> Bernhard Schartel,<sup>\*,‡,§</sup> and Frederik R. Wurm<sup>\*,†,§</sup>

<sup>†</sup>Physical Chemistry of Polymers, Max Planck Institute for Polymer Research, Ackermannweg 10, 55128 Mainz, Germany

<sup>‡</sup>Bundesanstalt für Materialforschung und -prüfung (BAM), Unter den Eichen 87, 12205 Berlin, Germany

<sup>§</sup>Graduate School Materials Science in Mainz, Staudinger Weg 9, 55128 Mainz, Germany

<sup>||</sup>Department of Aquatic Ecotoxicology, Goethe University Frankfurt, Max-von-Laue-Str. 13, 60438 Frankfurt/Main, Germany

<sup>⊥</sup>Department of Biology, Norwegian University of Science and Technology, 7491 Trondheim, Norway

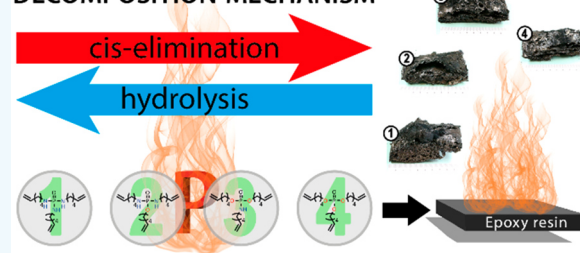
<sup>#</sup>Institute for Biotechnology and Drug Research gGmbH (IBWF), Erwin-Schrödinger-Str. 56, 67663 Kaiserslautern, Germany

## Supporting Information

**ABSTRACT:** Flame retardants (FR) are inevitable additives to many plastics. Halogenated organics are effective FRs but are controversially discussed due to the release of toxic gases during a fire or their persistence if landfilled. Phosphorus-containing compounds are effective alternatives to halogenated FRs and have potential lower toxicity and degradability. In addition, nitrogen-containing additives were reported to induce synergistic effects with phosphorus-based FRs. However, no systematic study of the gradual variation on a single phosphorus FR containing both P–O and P–N moieties and their comparison to the respective blends of phosphates and phosphoramides was reported. This study developed general design principles for P–O- and P–N-based FRs and will help to design effective FRs for various polymers. We synthesized a library of phosphorus FRs that only differ in their P-binding pattern from each other and studied their decomposition mechanism in epoxy resins. Systematic control over the decomposition pathways of phosphate ( $P=O(OR)_3$ ), phosphoramidate ( $P=O(OR)_2(NHR)$ ), phosphorodiamidate ( $P=O(OR)(NHR)_2$ ), phosphoramidate ( $P=O(NHR)_3$ ), and their blends was identified, for example, by reducing *cis*-elimination and the formation of P–N-rich char with increasing nitrogen content in the P-binding sphere. Our FR epoxy resins can compete with commercial FRs in most cases, but we proved that the blending of esters and amides outperformed the single-molecule amidates/diamidates due to distinctively different decomposition mechanisms acting synergistically when blended.

**KEYWORDS:** phosphorus, flame retardants, epoxies, mechanistic study, toxicity

## DECOMPOSITION MECHANISM



## INTRODUCTION

Polymers are omnipresent in our everyday life. However, their inherent risk of fire makes the use of flame retardants (FRs) inevitable. For this purpose, halogenated organics were used as effective FRs, but today these are controversially debated due to the release of toxic gases during a fire or their persistence if discarded. Currently, organophosphates are discussed as promising alternatives to halogenated FRs due to their effective flame-retardant properties and potential to design nontoxic and biodegradable FRs.<sup>1</sup>

The combination of phosphorus FRs (P-FRs) with additional nitrogen-containing additives resulted in synergistic effects during a fire by forming phosphorus–nitrogen intermediates or an increased charring.<sup>2</sup> However, a systematic study of precisely synthesized P-FRs with a variable number of P–N bonds (such as phosphoramidates and phosphorodiamidates, Figure 1) has not been performed. We prepared a series

of aliphatic organophosphates/-amides (1–4) with a precise binding pattern around the central phosphorus and used them as a FR additive in epoxy resins. Their *in vitro* toxicity was also assessed and compared to commercial halogenated or other organophosphate-based FRs. Importantly, the effects of the P-binding pattern (1–4) have been studied during a fire scene to understand their decomposition pathway and compared to blends of phosphate and phosphoramidate (these are 1 and 4) on the performance during a simulated fire scenario.

These P-FRs mainly differ in their main mode of action, which are gas and condensed phase activity. In the condensed phase, phosphorus-containing materials exhibit FR properties due to the enhanced formation and stabilization of carbona-

Received: February 12, 2019

Accepted: April 23, 2019

Published: April 23, 2019

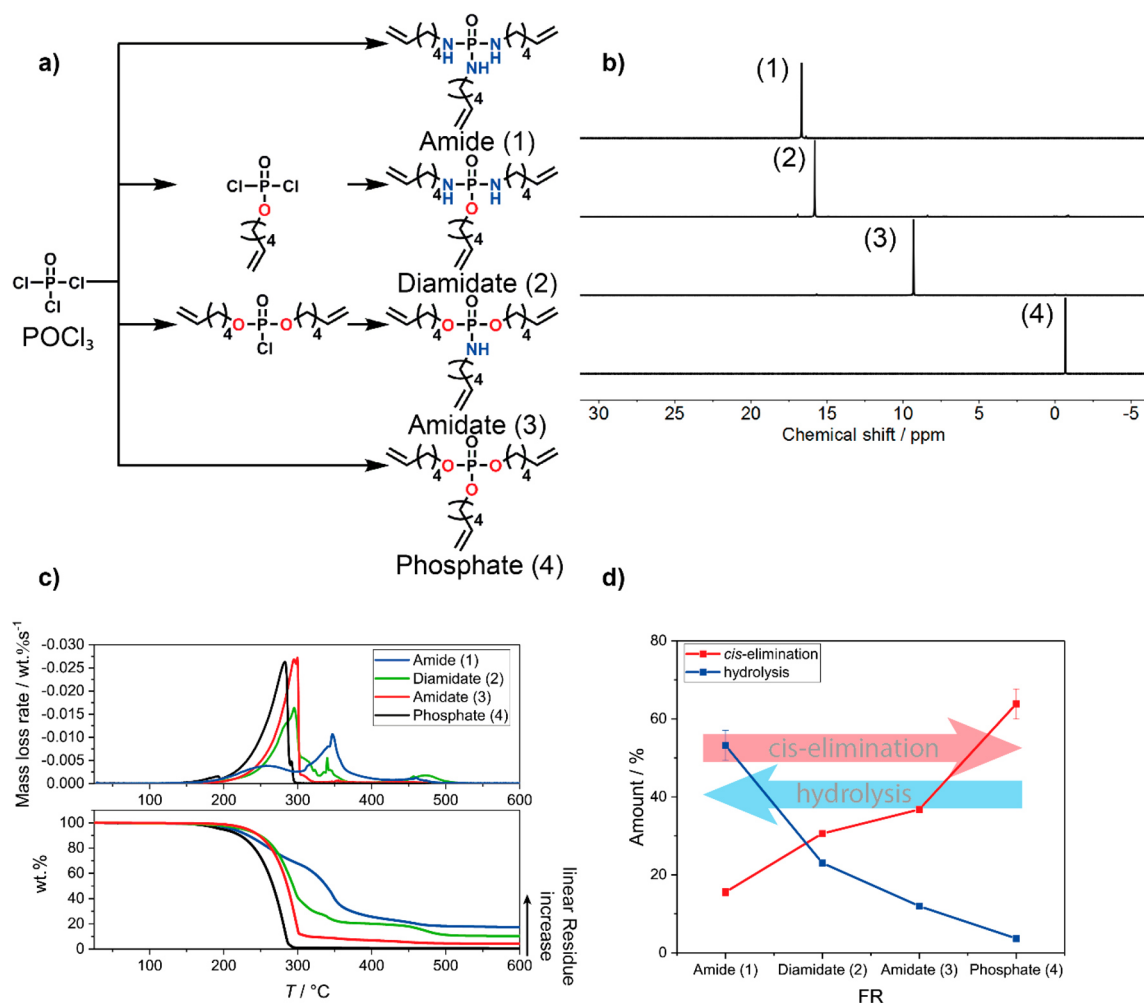


**Figure 1.** Characterization of flame retardants: amide (1), diamidate (2), amidate (3), and phosphate (4) (a) Schematic representation of the synthesis: the amide (1) and phosphate (4) are a one-step synthesis and the diamidate (2) and amidate (3) are a two-step synthesis. (b) <sup>31</sup>P-<sup>1</sup>H NMR of the flame retardants in CDCl<sub>3</sub>. (c) Mass loss of the flame retardants in thermogravimetric tests; char yield increase with increasing nitrogen content. (d) Correlation of relative amount of *cis*-elimination and hydrolysis in the released gases during pyrolysis GC-MS (connection between the data points are only to guide the eye).

ceous char, which retains fuel in the condensed phase. Additionally, an intumescent multicellular char may protect the underlying polymer from heat, acting as a heat shield.<sup>3–5</sup> The increased charring is explained by dehydration of the polymer and the formation of phosphoric acid derivatives, leading to cross-linking and aromatization.<sup>6</sup> Activity in the gas phase is mainly due to the formation of PO radicals, slowing down the exothermic radical process in the combustion zone, leading to a reduced combustion efficiency and therefore reducing the heat release.<sup>4,7,8</sup>

The phosphorus–nitrogen synergism accelerates the polymer phosphorylation by increasing the *in situ* production of phosphoric acid due to catalyzing *cis*-elimination.<sup>9</sup> The same is true for P–N bonds, which are more reactive than P–O bonds regarding the phosphorylation process. This retains phosphorus in the condensed phase and therefore promotes char formation and stabilization.<sup>10</sup> Furthermore, P and N react to form thermally stable polymeric compounds in the condensed phase.<sup>9</sup> While studies have shown the impact of nitrogen- and phosphorus-containing FRs,<sup>11,12</sup> systematic studies on the gradual variation of the phosphorus binding pattern and its impact on the FR mechanism are rare.<sup>6</sup> In addition, the comparison of phosphoramidates and phosphordiamidates

produced via chemical synthesis against blending the respective phosphate and phosphoramidate, hitherto uninvestigated, is presented herein. The P-FRs are synthesized and characterized in detail on the molecular level; for example, degradation temperature and pathway are assessed. They are used as additive FRs in epoxy resins and are investigated in a simulated fire scenario with state-of-the-art techniques (LOI, UL-94, and cone calorimeter).

The knowledge about the varying decomposition mechanisms for combined P–O- and P–N-based FRs will help the future preparation of biofriendly and effective FRs for various polymer materials since there is no universal FR design. FRs are optimized for a special application and matrix. For this task, it is important to know how the FR degrades to estimate possible interactions between matrix and FRs during a fire scenario.<sup>13</sup>

## RESULTS AND DISCUSSION

**Synthesis and Design of Materials.** To investigate the influence of the P–O vs P–N ratio on FR efficiency, a systematic library of organophosphates/-amidates is necessary. Four P-FRs with a central phosphorus atom and three *o*-



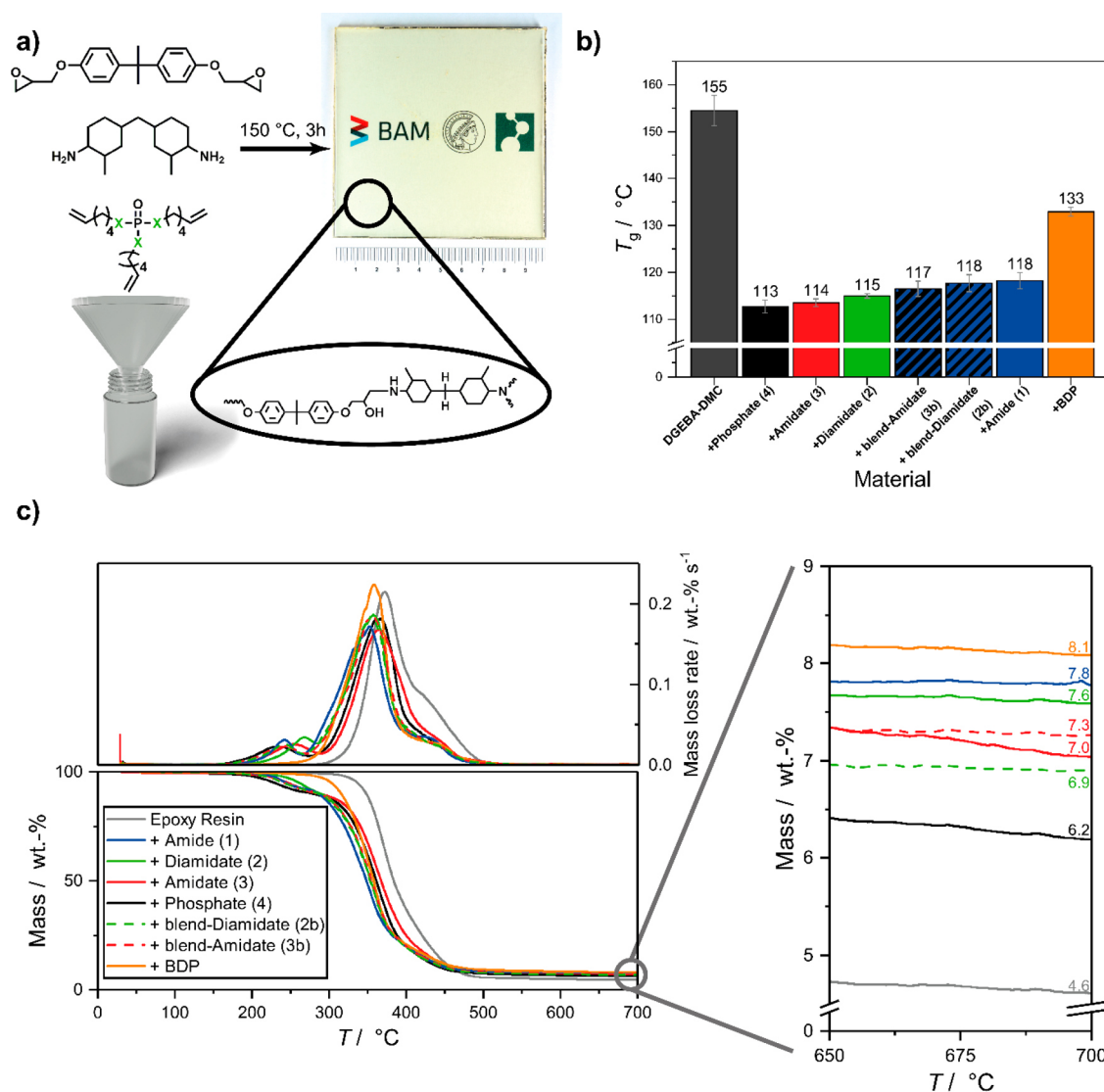


**Figure 2.** Characterization of flame-retarded epoxy resins. (a) Schematic representation of the epoxy resin synthesis. (b) Glass transition temperature of epoxy resin and flame-retarded composites. (c) Thermogravimetry (10 K min<sup>-1</sup>; N<sub>2</sub>) of the epoxy resins with FRs; increase of char yield with increasing nitrogen content of the flame retardant.

hexenyl chains were synthesized. The organic side chains ensure miscibility with the epoxy matrix, and the double bonds were introduced to increase the charring performance.<sup>14,15</sup> Tri(hex-5-en-1-yl)phosphoramidate (1), tri(hex-5-en-1-yl)phosphorodiamidate (2), tri(hex-5-en-1-yl)phosphoramidate (3), and tri(hex-5-en-1-yl)phosphate (4) were synthesized starting from POCl<sub>3</sub> via esterification with 5-hexen-1-ol or amidation with hex-5-en-1-amine (Figure 1a). The phosphoramidate (1) and the phosphate (4) were prepared in a single step. In contrast, the phosphorodiamidate (2) and the phosphoramidate (3) were synthesized in two steps to guarantee the correct binding pattern, first by esterification followed by the amidation (the amidation as the first step may result in multiple amidations). All P-FRs were of sufficient purity after the synthesis without the need for additional purification steps as proven by <sup>1</sup>H and <sup>31</sup>P NMR spectra (Figures S2–S13 and Figure 1b). <sup>31</sup>P NMR spectroscopy is a precise technique to control the correct binding pattern and purity of the compounds: the phosphate exhibited a single resonance at −0.67 ppm, whereas the signal shifted downfield with increasing nitrogen content (Figure 1b). By these

procedures, all P-FRs were easily available up to at least 50 g with standard university lab equipment.

Organophosphorus compounds are currently considered as alternatives for halogenated FRs<sup>16,17</sup> due to their potentially lower toxicity.<sup>18–20</sup> To evaluate their toxicity, we tested 1–4 in fungi and plant cells. Additionally, we used reporter gene assays based on yeast and human cells to assess their baseline toxicity and endocrine activities (estrogenic and antiandrogenic). Compounds 1, 2, and 4 induced baseline toxicity increasing in the following order (4 < 2 < 1) but were less toxic than the halogenated commercial tetrabromo bisphenol A (see the Supporting Information for details). While none of the compounds were estrogenic, 3 and 4 induced some antiandrogenic activity (4 < 3). Although the compounds partly induced toxicity, the actual concentrations of FRs leaching from finished products still need to be determined.

**Decomposition Studies.** Phosphoramides exhibit higher thermal stability, lower volatility, and higher viscosity due to additional hydrogen bonding compared to their analogue phosphates.<sup>21</sup> These properties may increase the overlap of the decomposition temperatures of both matrix and flame

retardant. This overlap leads to higher reactivity during the pyrolysis and an increased residue amount as a higher phosphorus content is maintained in the condensed phase due to interactions of the FR with the matrix and their respective decomposition products.<sup>22,23</sup>

The combination of TGA, FTIR, and pyrolysis GC-MS gave a deeper insight into how the FRs decompose under pyrolytic conditions.

For the pure FRs (1–4) mass loss under pyrolysis, measured by thermogravimetric analysis (TGA, Figure 1c), proved the gradual change of the decomposition behavior according to the structure variation from 1 to 4; this already suggests a possible effect on the FR mechanism during a fire. The phosphoramidate (1) proved the highest decomposition temperature ( $T_{\max}$ ) at 317 °C, which decreased with increasing O content of the FR to 274 °C for 2, 269 °C for 3, and 250 °C for 4. In addition, the char yield (measured at 600 °C) decreased from 1 with 17 wt % to <1 wt % for 4, indicating a different activity of the pure compounds in the gas and/or condensed phase. The phosphate decomposition curve followed a typical behavior of a vaporizing material with a clear boiling point while with increasing nitrogen content the degradation occurs via multiple decomposition steps over a broader temperature range. As P–N bonds are present in the FR, they can form more stable intermediates through a polymerization process that require higher amounts of thermal energy to vaporize, if at all, as is noticeable by the subsequent increase in  $T_{\max}$  and higher amount of residue for each additional nitrogen introduced.

The FTIR spectra from the evolved gases (measured at  $T_{\max}$ , Figure S18) proved the presence of several decomposition products, among them those that correspond to hydrolysis products, i.e., 5-hexen-1-ol and hex-5-en-1-amine (after scission of the P–O or P–N bond, respectively). The spectra also indicated the presence of derivatives containing P=O and P–O moieties at 1299 and 1030  $\text{cm}^{-1}$  for the phosphate (4), while we detected additional vibrations for the  $(\text{NH}_2)\text{--P=O}$  band at 1159  $\text{cm}^{-1}$  during the decomposition of 2 and 3. In addition, all nitrogen-containing P-FRs exhibited C–N bands at 1075  $\text{cm}^{-1}$ , P–N–C or P–N–P bands at 980  $\text{cm}^{-1}$ , and N–H bands at 769  $\text{cm}^{-1}$ . For all nitrogen-containing FRs at higher temperatures ( $T > T_{\max}$ ) P–N bands between 1330 and 1300  $\text{cm}^{-1}$  and two characteristic bands for ammonia at 965 and 930  $\text{cm}^{-1}$  were detected, albeit shifted or overlapped with other signals, pointing to the formation of incombustible gas resulting in flame dilution.

Pyrolysis GC-MS supports these results and further proves the presence of the major decomposition products. Compound 4 decomposed mainly by a *cis*-elimination during pyrolysis as indicated by the high amount of 1,5-hexadiene which was detected at a retention time of 2.6 min (Figure S29). Also, the other P–O-containing FRs (2 and 3) released 1,5-hexadiene during decomposition, but the amount of *cis*-elimination decreased with increasing P–N content (Figure 1d). Additionally, 5-hexen-1-amine and 5-hexen-1-ol were detected for 2 and 3 (retention at 6.1 and 6.7 min in Figure S29). Additionally, for 2–4, phosphoric acid derivatives at retention times of 23.7, 24.6, and 25.8 min were identified, corresponding to the gas-phase activity of such compounds. Because of transesterifications during the decomposition, in the GC elugrams of 3, also compound 4 was detected, while in the elugram of the pyrolysis GC-MS of 2, transesterification leads to the formation of 3 and 4. In stark contrast, during the decomposition of 1, almost no *cis*-elimination occurred, and

only little amounts of phosphoric acid derivatives were observed, indicating the formation of nonvolatiles and thus underlining the condensed phase activity of the phosphoramidate. This was further supported by solid-state  $^{31}\text{P}$  NMR of the char residues, which exhibited distinct signals for P–N compounds (Figure S46).

**Flame-Retardant Behavior in Epoxies.** The FR performances of 1–4 and blends of 1 and 4 were studied in an epoxy resin based on bisphenol A diglycidyl ether (DGEBA) and 2,2'-dimethyl-4,4'-methylenebis(cyclohexylamine) (DMC). The epoxy plates were prepared by mixing DGEBA with DMC in the presence of 10 wt % of each FR in an aluminum mold and curing for 3 h at 150 °C (Figure 2a). As the P–NHR bond may also act as a curing agent under certain conditions, we performed a control experiment with 1 and phenyl glycidyl ether at the curing conditions for the epoxy. Under the cross-linking conditions, no ring-opening of the epoxide occurred from the P–NHR bond (cf. Figures S14–S16), proving that 1–3 act as additive, and not reactive, FRs. As a benchmark, the commercially available and industrially used FR bisphenol A diphenyl phosphate (BDP) was chosen, as it was already used successfully in epoxy resins.<sup>24,25</sup>

Typically, additive FRs act as plasticizers of the epoxy resin and reduce the glass transition temperature ( $T_g$ ). All flame-retarded epoxy resins with 10 wt % 1, 2, 3, or 4 also exhibited lower  $T_g$ s by 36–42 °C compared to the neat epoxy resin. 4 shows the highest decrease of  $T_g$  (to 113 °C), while with increasing amount of NH bonds an increase of the  $T_g$ s was detected, probably due to hydrogen-bonding effects (Figure 2b). Blending of 1 and 4 in a 1:2 or 2:1 molar ratio to “simulate” the elemental composition of a phosphoramidate (3b) and phosphorodiamidate (2b) resulted in a slightly higher  $T_g$  compared to the pure 2 and 3 was detected. For BDP, the  $T_g$  of the neat epoxy (155 °C) was reduced to 133 °C. In all cases, the aliphatic FRs 1–4 result in a higher decrease of  $T_g$  compared to the stiff aromatic BDP.<sup>26</sup>

To understand the differences of 1–4 (and 2b and 3b) on the behavior of the loaded epoxies during combustion, we elucidated the FR mode of actions and mechanisms. A crucial step toward understanding the FR mechanisms is analyzing the pyrolysis of the epoxy resins with FRs by TGA. The burning with a stable flame is dominated by an anaerobe pyrolysis, producing volatile fuel that is combusted in the flame. This model suits most polymeric materials in most fire scenarios such as ignition and developing fires and thus for all the important fire tests for polymeric materials, such as UL 94, LOI, and flaming combustion in the cone calorimeter. Although the heating rate is relatively slow, thermogravimetry under nitrogen is the best common analytical method to investigate the pyrolysis controlling the burning of polymeric materials.<sup>27</sup> A lower onset temperature of the degradation for the FR epoxies was detected compared to the neat epoxy. This was attributed to volatilization of the FRs and is indicated by an additional decomposition step equal to ~10 wt %. Notably, however, the main decomposition step shifts to higher temperatures with increasing amount of P–O bonds in the additive. Importantly, for all FR epoxy resins, an increased char yield was detected, which further increased slightly with increasing P–N bonds in the FRs (Figure 2c).

While microscale experiments aid in understanding certain aspects of a material's fire-retardant properties, they do not fully evaluate fire behavior on a macroscopic scale. Two reaction-to-small-flame tests were conducted, namely limiting

a) Material composition	DGEBA-DMC	+ Amide (1)	+ Diamidate (2)	+ Amidate (3)	+ Phosphate (4)	+ BDP
<b>LOI</b>						
[c(O <sub>2</sub> )] / %	18.7 ± 0.3	22.9 ± 0.2	23.3 ± 0.2	22.8 ± 0.2	23.2 ± 0.3	24.0 ± 0.2
<b>UL-94</b>						
Classification	HB	HB	HB	HB	HB	HB
Burn speed / mm s <sup>-1</sup>	31.7 ± 3.6	38.3 ± 2.9	29.5 ± 1.9	34.0 ± 1.8	30.0 ± 1.6	19.6 ± 3.6

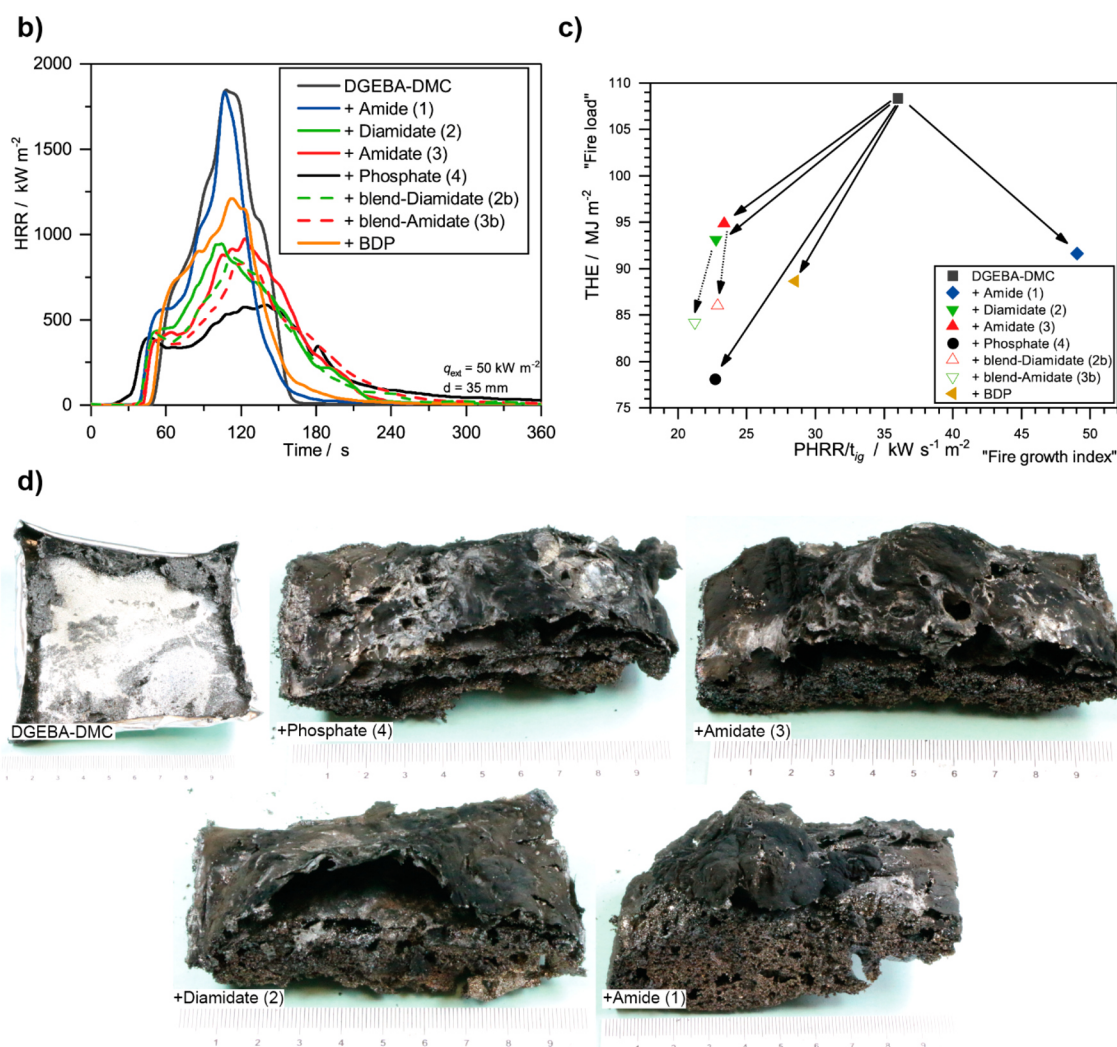


**Figure 3.** Cone calorimeter, UL-94, and limiting oxygen index (LOI) tests of the epoxy resins. (a) Summarized results of LOI and UL-94 tests, with all flame retardants increasing the OI and achieving HB classification in the UL-94 test. (b) Heat release rate over time of epoxy resins, with the phosphate (4) presenting the lowest peak heat release and the amide (1) the highest. (c) Petrella plot of the different epoxy resins with all flame retardants having a positive effect (lowering THE), especially the phosphate (4) lowering both fire load and fire growth index and the amide (1) only lowering the former. (d) Photos of char residue after cone calorimeter test: the epoxy resin has almost no residue; pore size decreases from phosphate (4) to amide (1) along with an increase in char residue.

oxygen index (LOI) and the Underwriter's 94 (UL-94) test, as well as forced-flaming conditions via cone calorimetry. LOI measures the lowest oxygen concentration necessary to sustain combustion in a candle-like setup, while UL-94 measures dripping and flame-spread behavior in vertical and horizontal positions.

The pure epoxy resin exhibited an oxygen index (OI) of OI = 18.7 vol %, proving the inherent flammability of these materials. When a FR was incorporated, the OI increased to

approximately OI = 23–24 vol %, corresponding to a relative increase of ca. 22–28%. The addition of any of the tested FRs increased the OI and slowed down the flame spread and thereby reduced the fire hazard. However, the differences between all tested materials are minimal, mostly due to the relatively low FR loading (10 wt %) and low P content of a sample (~1% P in each resin). The P-FRs performed on an equal level to the benchmark epoxy resin with BDP, indicating that the burning behavior in OI tests can only be altered with



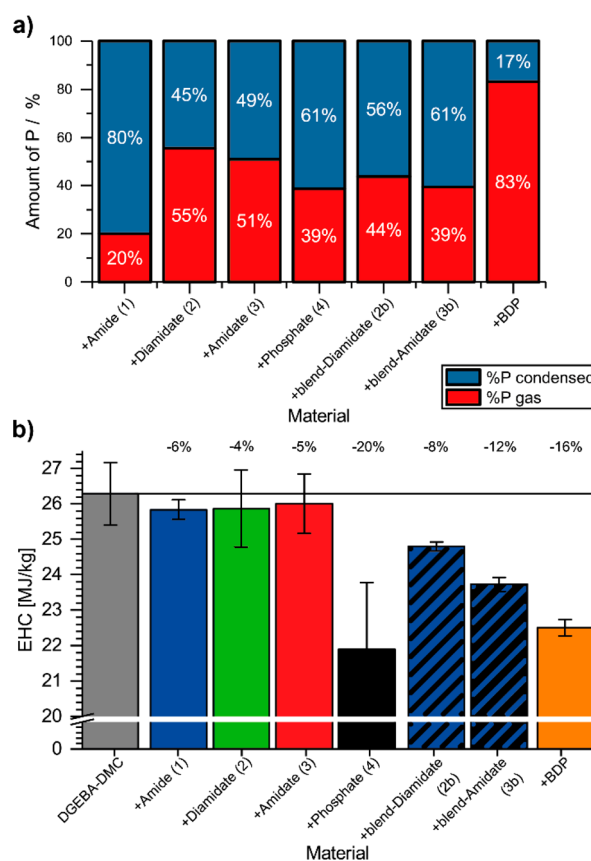
higher loading/higher P content in order attain  $OI > 27-29$  vol %. This is needed to fulfill the demands of diverse flame-retardancy requirements.<sup>14</sup> A similar behavior was obtained from UL-94 tests, where the benchmark BDP-loaded epoxy resin failed vertical tests and only achieved an HB rating in horizontal tests (lowest rating before not passing) due to the high flammability of epoxy resins. The herein-prepared resins with P-FRs achieved the same rating, although not all FRs managed to reduce the horizontal burn speed; most noticeably, the resin with phosphoramidate (1) was barely within the margin of error of passing HB classification. In all UL-94 tests, the strong formation of char was visible for the prepared resins with P-FRs, yet the increase of viscosity of the epoxy resin resulted in the protective char dripping away from the sample. These results illustrate that at 10 wt % loading the FRs cannot stop vertical flame spread due to melt dripping although a strong char formation is visible. Similar to LOI, better classification can be achieved with higher FR loading or higher P content of the sample.

Cone calorimetry measurements proved a significant effect of all P-FRs on epoxy resins during a simulated fire scenario. The epoxy plates ( $10 \times 10 \times 0.4$  cm<sup>3</sup>) were irradiated with a heat flux of  $50$  kW m<sup>-2</sup> at a distance of 35 mm, simulating a developing fire.<sup>28</sup> The results of the forced-flaming condition experiments underlined that the epoxy resin burned with a high heat release rate (HRR) and lost 99.3 wt % of its mass, presenting nearly no residue (Figure 3d). All flame-retarded resins exhibited a clear reduction of peak or heat release rate (PHRR), an increase in residue yield, a lowering of the total heat evolved (THE = total heat released (THR) at flame out), and a reduction of fire growth rate (FIGRA = maximum (HRR/t)) (Figure 3b,c and Table S4). The epoxy resin loaded with the phosphate (4) demonstrated the lowest PHRR ( $855$  kW m<sup>-2</sup>, reduced by 48%) and THE ( $78.1$  MJ m<sup>-2</sup>, reduced by 28%) and displayed a HRR curve corresponding to a charring material with a protective layer. This behavior was clearly visible during the experiments as well as in the cross sections of the residues, as the decomposition of the resin with 4 and the volatilization of its products acted as blowing agents, creating a voluminous intumescent char that shielded the underlying material from the heat source. With increasing P-N content of the FR, a lower reduction of PHRR and THE was detected. 1, 2, and 3 showed a small plateau at  $t = 60$  s, but the lack of blowing agent created a char layer, which was unable to shield the underlying material, leading to additional decomposition of the epoxy and thus a higher PHRR. Epoxy resins with 1 as the additive even had a higher PHRR ( $1832$  kW m<sup>-2</sup>) than the neat epoxy resin ( $1696$  kW m<sup>-2</sup>). However, the residue yields of epoxy resins loaded with 1 (8.4 wt %) was in a similar range as the best performing epoxy loaded with 4 (9.2 wt %).

All flame-retarded epoxy resins revealed an increase in residue yield compared to the epoxy resin without FRs. In pyrolysis investigations, TGA experiments of the pure FRs demonstrated that 1 presented a large amount of residue while 4 hardly left any. The increase in residue was proportional to the increase in P-N bonds, i.e.,  $4 < 3 < 2 < 1$ . In forced flaming conditions, this trend was not clearly visible. However, as has been proven in previous experiments,<sup>29</sup> the residue yields of pure FRs in TGA experiments do not necessarily correlate with the residue yields of flame-retarded resins. Specifically, the interactions between FR and matrix govern the residue yield. For the flame-retarded epoxy resins, although

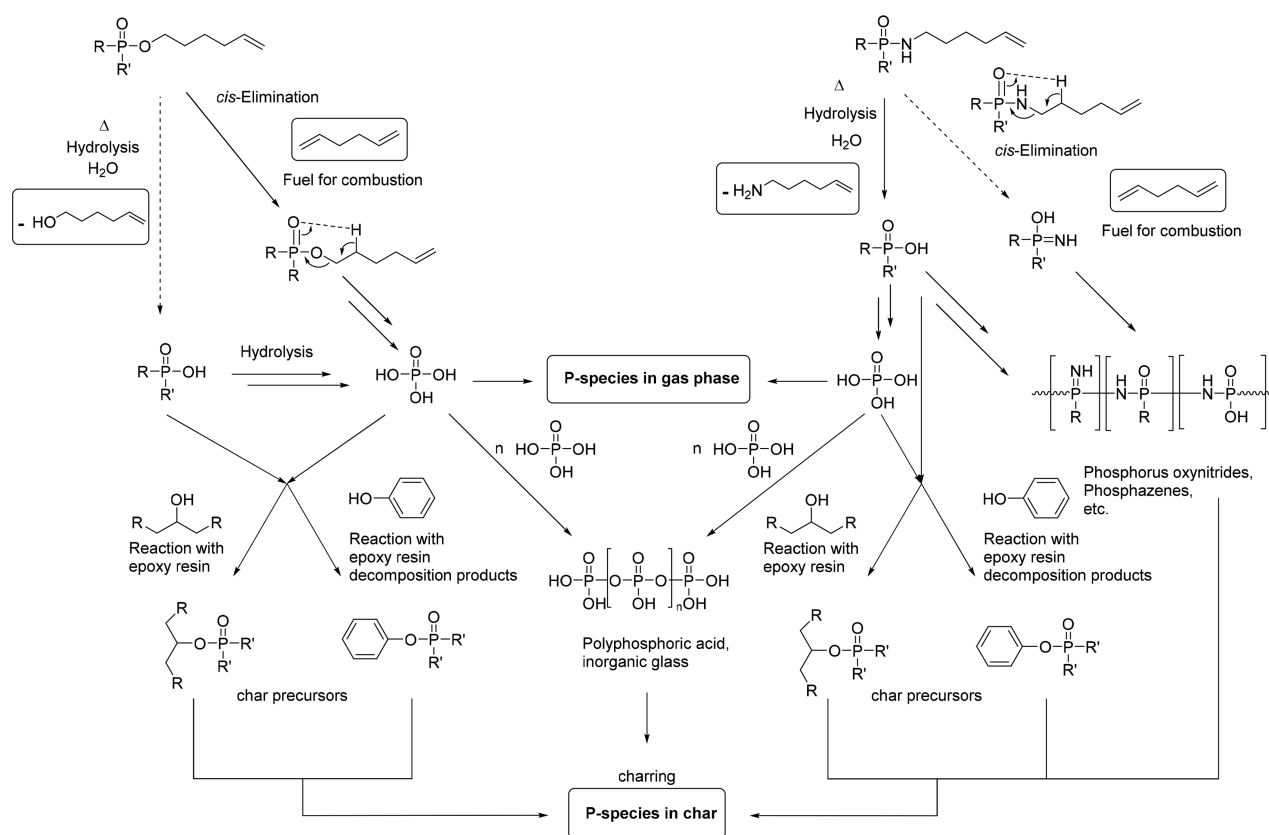
residue yields were in the order  $4 > 2 > 1 > 3$ , the increased residue amount for resins with 4 can be explained by the formation of a protective layer which reduces the mass transfer of combustible material into the flame zone and shields underlying material from thermal radiation. For the nitrogen-containing compounds, the previously noted trend was also seen, especially given the margin of error for resins with 2, illustrating that residue yields increase with increasing nitrogen content in the binding sphere of phosphorus.

The effective heat of combustion (EHC) is the quotient of the total heat evolved and the total mass loss; therefore, it is a ratio between these two values. In cone calorimetry experiments, the EHC relates to flame dilution and flame inhibition, and a reduction in EHC is a parameter for the gas phase activity of a FR.<sup>23</sup> The phosphate (4) displayed a reduction in EHC of  $\sim 20\%$ , from  $29.6$  MJ kg<sup>-1</sup> for the epoxy resin to  $21.6$  MJ kg<sup>-1</sup> for the resin with 4, which points to gas phase activity of the FR (Figure 4b). Noticeably, this effect is



**Figure 4.** (a) Phosphorus content determined by elemental analysis from the residues after cone calorimeter tests (blue bars). Calculated amount of phosphorus in the gas phase (red bars). (b) Comparison of effective heat of combustion (EHC) of epoxy resins with and without FRs. The numbers above the bars represent the relative change to the non-flame-retarded epoxy resin.

minimized if P-N bonds were installed into the FR, as 1, 2, and 3 reduced the EHC only by ca. 4–5%, indicating that the gas phase activity of the synthesized P-FRs decreased with the presence of nitrogen in the chemical structure. Although residue yields of resins with 1, 2, 3, and 4 are within the same range (ca. 8–10 wt % mass loss), the ratios between the THEs and total mass loss changed. This change resulted from flame dilution and flame inhibition effects which affect THE. The

Scheme 1. Scheme of Proposed Decomposition and Reaction Pathways of P–O- and P–N-Containing Phosphorus Flame Retardants<sup>a</sup>

<sup>a</sup>P–O containing P-FRs are more prone to *cis*-elimination, resulting in the formation of phosphoric acid and enabling transesterification reactions. P–N-containing P-FRs are more to hydrolysis, resulting in the formation of phosphorus oxynitrides and phosphazenes. Products in squares were identified via TG-FTIR and pyrolysis GC-MS.

blended FRs (**2b** and **3b**) were also tested in epoxy resins, and the results were compared to resins with **2** and **3**. The results show that the blended FRs achieved higher residue yields a lower PHRR, decreased THE, and a lower EHC than resins with only **2** or **3**. In fact, the PHRR of the resins with **2b** or **3b** are comparable to the resins loaded with **4** which showed the strongest reduction of this value compared to the epoxy resin. Resins with **3b** had a 15% lower PHRR than resins with **3**, while resins with **2b** or **3b** demonstrated 8% or 11% lower THE values and residue yields 47% or 49% higher than resins with only **2** or **3**, respectively. Consequently, the EHCs of resins with **2b** or **3b** are 4% or 7% lower than resins with **2** or **3**, respectively. Noticeably, the fire growth rate (FIGRA) of resins with **2b** are 20% lower than resins with **2**. These results clearly demonstrate that the presence of two types of P-FRs in epoxy resins increases FR efficacy compared to a single P-FR with the same O:N ratio. In the case of **2** and **3**, the P–N linkages retain the phosphorus in the condensed phase, forming char during decomposition (Scheme 1, right pathway). This retention of P in the char reduces flame inhibition as P retention in the condensed phase competes with P release in the gas phase.<sup>23</sup>

The residues after cone calorimeter tests were analyzed for their phosphorus content via elemental analysis, indicating the largest amount of P (80%) in the condensed phase for resins loaded with **1** (Figure 4a). The difference in gas and condensed phase activity is explained by the different decomposition mechanisms as discussed previously.

In epoxy resins, the phosphate (**4**) readily forms phosphoric acid via *cis*-elimination and creates networks with aromatic char in the condensed phase and is present at the main decomposition step due to incorporation into the decomposing matrix via esterification (Scheme 1). In contrast, the phosphoramidate (**1**) was hydrolyzed under these conditions. However, **1** also generated polymeric compounds containing phosphazene or phosphorus oxynitride components in the condensed phase, as indicated by solid-state NMR (Figure S46), leading to an increased residue and high P content in the char. The phosphoramidate (**3**) and phosphordiamidate (**2**), containing both P–O and P–N bonds, exhibit both decomposition mechanisms with decreasing *cis*-elimination when the P–N content increases and transesterification (compare the pyrolysis GC-MS data).

The effect of combining phosphate and amide led to synergistic flame-retardant effects, which were not observed for the combination of P–O and P–N in a single FR additive. The exchange of P–O bonds with P–N bonds reduced the effectiveness of one mechanism but did not sufficiently promote the other. This conclusion was exemplified in the amount of residue in cone calorimeter tests as well as the P content of the residue (Figure 4a): the residue amounts in epoxy resins were ordered  $4 \geq 2 > 1 > 3$  (i.e.,  $9.2\% \geq 5.0\% > 8.4\% > 7.6\%$ ) and  $2b > 3b > 4 > 1$  (i.e.,  $13.4\% > 11.3\% > 9.2\% > 8.4\%$ ) for the blended materials, showing an increase in residue for the blended FRs. As for P content in the condensed phase, the amidate (**3**) and diamidate (**2**) showed lower

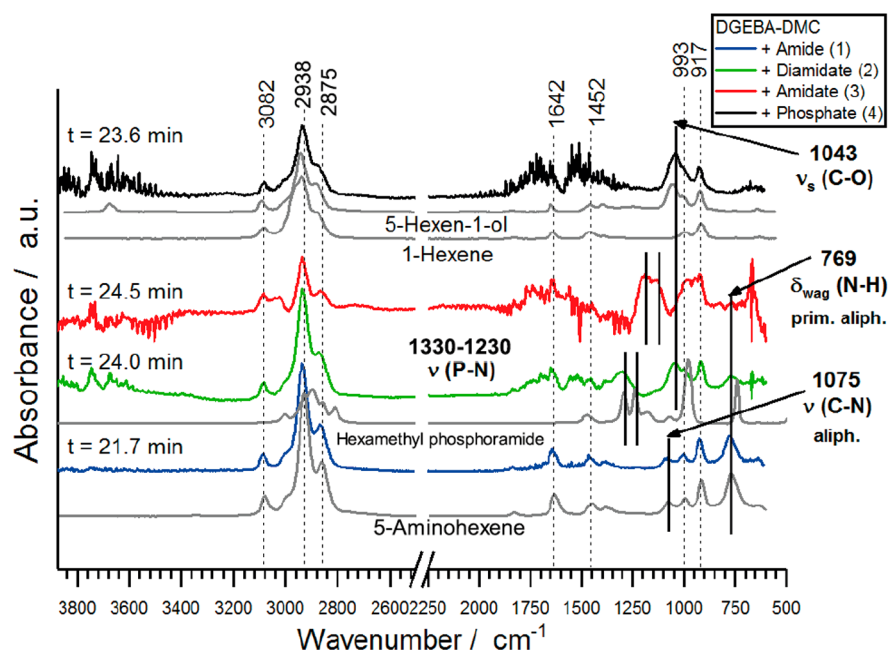


**Figure 5.** TG-FTIR spectra of the first decomposition step of flame-retarded epoxy resins.

amounts of P in their residues (49% and 45%, respectively) than the blended FRs **3b** and **2b** (61% and 56%, respectively).

The FTIR spectra of the evolved gases during the first decomposition step (Figure 5) showed that the FRs decompose above 200 °C, and some decomposition products enter the gas phase, which is a typical behavior for low molecular weight FRs.<sup>22</sup> Looking at the main decomposition step at around 360 °C (Figure S21), TG-FTIR showed the DGEBA-DMC decomposition pattern,<sup>30</sup> pointing to the degradation of the resin matrix. An exception was the epoxy resin with **4**, where the phosphate still displayed characteristic bands during the main decomposition step, implying the presence of phosphate beyond the FR's boiling point. This phenomenon was caused by the reaction between matrix and phosphate (Scheme 1), as the phosphate was more likely to produce phosphoric acid than the nitrogen-containing counterparts due to the difference in bond dissociation energies, leading to incorporation of phosphates into the polymer matrix by transesterification.

Hot stage FTIR spectra (Figure S27) of the condensed phase at various temperatures implied the presence of phosphorus species in the residue (Table S3). All resins containing FRs exhibited bands corresponding to various phosphorus species at 600 °C, i.e., at end of the test. These bands were not detected in the epoxy resin, indicating condensed phase activity for all tested FRs. For **4**, the presence of medium intensity bands at 1181 cm<sup>-1</sup>, corresponding to C–O stretching vibration of phenols, and at 828 cm<sup>-1</sup>, corresponding to C–H bonds of aromatic rings, point to the formation of substituted aromatic compounds in the condensed phase. The band was strongest for **4**, which points to the ability of the phosphate to bind hydroxyl-functionalized aromatic rings during the decomposition of the matrix into the condensed phase. In contrast, all nitrogen-containing FRs (**1–3**) demonstrated a medium intensity band at 1398 cm<sup>-1</sup>, which corresponds to P=N–P or P–N–Ph vibrations, which are probably attributed to polyphosphazenes or phosphor oxynitride in the condensed phase, as underlined by a higher

amount of residue after the TGA experiments for N-containing FRs.

## CONCLUSION

A systematic library of phosphorus-containing flame-retardant (FR) additives (**1–4**) with precisely adjusted P/N/O ratio were synthesized. Compounds **1–4** were less toxic than their halogenated counterpart for most end points, and compounds **2** and **4** represented the best alternatives. With this library, the decomposition pathway of the FRs in an epoxy resin during combustion was controlled.

By a combination of different techniques, we were able to elucidate the degradation mechanism of the different P-FRs and proved a gradual change of the decomposition depending on the chemical structure. In a simulated fire scenario, the phosphate (**4**) exhibited the highest efficiency in epoxy resins and was active in both the gas and the condensed phase effectively. The gas phase activity was explained by the predominant *cis*-elimination mechanism during the combustion (from pyrolysis GC-MS). With an exchange of P–O bonds with P–N bonds, the amount of *cis*-elimination decreased and hydrolysis increased as a decomposition pathway. The amide (**1**) with three P–N bonds proved the highest condensed phase activity of the investigated structures due to cleavage of the P–N bonds during the combustion. This also resulted in the lowest FR performance of **1**. Notably, the blends of phosphate and phosphoramidate (**2b** and **3b**) outperformed the pure **2** and **3**. We believe this is an effect of combining different decomposition mechanisms, which leads to synergistic flame retardancy. These findings will further contribute to the development of systematic libraries of P-based FRs with low toxicity and high efficiency.

## EXPERIMENTAL SECTION

**Tri(hex-5-en-1-yl)phosphate (4).** To a dried three-necked, 2 L round-bottom flask fitted with a dropping funnel, 5-hexen-1-ol (274.2 mL, 2.28 mol, 3.5 equiv) and triethylamine (318.6 mL, 2.28 mol, 3.5 equiv) were added under an argon atmosphere in dry dichloromethane (500 mL). Then phosphoryl chloride (60.6 mL, 0.65 mol,



1.0 equiv) dissolved in dry dichloromethane (50 mL) was added dropwise to the solution, keeping the temperature at 0 °C. The reaction was allowed to stir overnight at room temperature and was then filtered. Afterward, the crude mixture was concentrated at reduced pressure, dissolved in toluene and then filtered to remove most of the ammonium salt byproduct. Then, the crude product was washed with 10% aqueous hydrochloric acid solution, a saturated solution of calcium carbonate, and brine. The organic layer was dried over anhydrous sodium sulfate, filtered, and dried *in vacuo*.

For the biological tests the compound **4** was purified by chromatography over neutral alumina oxide using diethyl ether as eluent to give a clear, slight yellow oil (yield: 95%). The purity and chemical structure were determined by  $^1\text{H}$  NMR,  $^{13}\text{C}$  {H} NMR, and  $^{31}\text{P}$  {H} NMR spectroscopy as well as electrospray ionization mass spectrometry (ESI-MS).

$^1\text{H}$  NMR (300 MHz, chloroform-*d*,  $\delta$ ): 5.83–5.70 (m, 3H, e), 5.02–4.93 (m, 6H, f), 4.02 (q, 6H, a), 2.10–2.03 (td, 6H, d), 1.68 (tt, 6H, b), 1.46 (tt, 6H, c).  $^{31}\text{P}$  {H} NMR (121 MHz, chloroform-*d*,  $\delta$ ): –0.67 (s, 1P, 1).  $^{13}\text{C}$  {H} NMR (75 MHz, chloroform-*d*,  $\delta$ ): 138.17 (s, 3C, e), 114.85 (s, 3C, f), 67.38 (d, 3C, a), 33.11 (s, 3C, d), 29.60 (d, 3C, b), 24.67 (s, 3C, c). ESI-MS: 345.21 [M + H] $^+$  (calculated M $^+$ : 344.21).

**Tri(hex-5-en-1-yl)phosphoramidate (1).** To a dried three-necked, 2 L round-bottom flask fitted with a dropping funnel, hex-5-en-1-amine (286.2 mL, 2.28 mol, 3.5 equiv) and triethylamine (318.6 mL, 2.28 mol, 3.5 equiv) were added under an argon atmosphere in dry dichloromethane (500 mL). Then, phosphoryl chloride (60.6 mL, 0.65 mol, 1.0 equiv) dissolved in dry dichloromethane (50 mL) was added dropwise to the solution, keeping the temperature at 0 °C. The reaction was allowed to stir overnight at room temperature and was then filtered. Afterward, the crude mixture was concentrated at reduced pressure and then filtered for the second time. The crude product was redissolved in diethyl ether (200 mL) and stored overnight at –20 °C. The solution was filtered again to remove the triethylamine hydrochloride completely. The crude product was washed with 10% aqueous hydrochloric acid solution, a saturated solution of calcium carbonate, and brine. The organic layer was dried over anhydrous sodium sulfate, filtered, and dried *in vacuo*.

For the biological tests the compound **1** was purified by chromatography over silica using DCM and methanol (9:1) as eluent to give a clear, slight yellow oil (yield: 92%). The purity and chemical structure were determined by  $^1\text{H}$  NMR,  $^{13}\text{C}$  {H} NMR, and  $^{31}\text{P}$  {H} NMR spectroscopy as well as electrospray ionization mass spectrometry (ESI-MS).

$^1\text{H}$  NMR (300 MHz, chloroform-*d*,  $\delta$ ): 5.81–5.68 (m, 3H, e), 4.98–4.89 (m, 6H, f), 2.85 (quint, 6H, a), 2.36–2.29 (q, 3H, g), 2.05–1.98 (td, 6H, d), 1.48–1.34 (m, 12H, b, c).  $^{31}\text{P}$  {H} NMR (121 MHz, chloroform-*d*,  $\delta$ ): 16.67 (s, 1P, 1).  $^{13}\text{C}$  {H} NMR (75 MHz, chloroform-*d*,  $\delta$ ): 138.50 (s, 3C, e), 114.67 (s, 3C, f), 41.09 (s, 3C, a), 33.39 (s, 3C, d), 31.69 (d, 3C, b), 26.09 (s, 3C, c). ESI-MS: 342.24 [M + H] $^+$ , 683.44 [2M + H] $^+$  (calculated: 341.26).

**Hex-5-en-1-yl Phosphorodichloridate.** To a dried three-necked, 250 mL round-bottom flask fitted with a dropping funnel, phosphoryl chloride (18.7 mL, 205.00 mmol, 10.0 equiv) was added under an argon atmosphere in dry toluene (50 mL). Then triethylamine (2.8 mL, 20.50 mmol, 1.0 equiv) and 5-hexen-1-ol (2.5 mL, 20.50 mmol, 1.0 equiv) dissolved in dry toluene (5 mL) were added dropwise to the solution, keeping the temperature at 0 °C. The reaction was stirred 1 h at room temperature. Afterward, the crude product was concentrated at reduced pressure and filtered to remove the triethylammonium chloride. Then, all byproducts and starting material were removed under reduced pressure (RT,  $5 \times 10^{-2}$  mbar). The product was used without any further purification.

**Di(hex-5-en-1-yl)phosphorochloridate.** To a dried three-necked 250 mL round-bottom flask fitted with a dropping funnel, phosphoryl chloride (8.1 mL, 88.89 mmol, 1.0 equiv) was added under an argon atmosphere in dry toluene (80 mL). Then triethylamine (22.2 mL, 160.00 mmol, 1.8 equiv) and 5-hexen-1-ol (19.2 mL, 160.00 mmol, 1.8 equiv) dissolved in dry toluene (20 mL) were dropwise to the solution, keeping the temperature at 0 °C. The

reaction was allowed to stir overnight at room temperature and was then filtered. Afterward, the crude mixture was concentrated at reduced pressure.

The compound was purified by distillation (90 °C,  $<10^{-1}$  mbar 30 min; 110 °C,  $<10^{-1}$  mbar 15–20 min) to give a clear, slight yellow oil (yield: 82%). The purity and chemical structure were determined by  $^1\text{H}$  NMR and  $^{31}\text{P}$  {H} NMR spectroscopy.

$^1\text{H}$  NMR (300 MHz, chloroform-*d*,  $\delta$ ): 5.78–5.65 (m, 2H, e), 4.98–4.89 (m, 4H, f), 4.21–1.09 (m, 4H, a), 2.02 (td, 4H, d), 1.69 (tt, 4H, b), 1.45 (tt, 4H, c).  $^{31}\text{P}$  {H} NMR (121 MHz, chloroform-*d*,  $\delta$ ): 4.73 (s, 1P, 1).

**Tri(hex-5-en-1-yl)phosphorodiamidate (2).** To a dried three-necked 250 mL round-bottom flask fitted with a dropping funnel, hex-5-en-1-yl phosphorodichloridate (4.5 g, 20.50 mmol, 1.0 equiv) was added under an argon atmosphere in dry toluene (50 mL). Then hex-5-en-1-amine (5.4 mL, 43.05 mmol, 2.1 equiv) and triethylamine (6.0 mL, 43.05 mmol, 2.1 equiv) were added dropwise to the solution, keeping the temperature at 0 °C. The reaction was allowed to stir overnight at room temperature and was then filtered. The crude mixture was concentrated at reduced pressure, and the crude product was dissolved in diethyl ether to wash it with 10% aqueous hydrochloric acid solution, a saturated solution of calcium carbonate, and brine. The organic layer was dried over anhydrous sodium sulfate, filtered, and concentrated on the rotary evaporator.

For the biological tests the compound **2** was purified by chromatography over silica using ethyl acetate, petroleum ether, and methanol (9:1:0.1) as eluent to give a clear, slight yellow oil (yield: 95%). The purity and chemical structure were determined by  $^1\text{H}$  NMR,  $^{13}\text{C}$  {H} NMR, and  $^{31}\text{P}$  {H} NMR spectroscopy as well as electrospray ionization mass spectrometry (ESI-MS).

$^1\text{H}$  NMR (300 MHz, chloroform-*d*,  $\delta$ ): 5.76–5.63 (m, 3H, f, l), 4.94–4.84 (m, 6H, g, m), 3.83 (q, 2H, h), 2.78 (q, 4H, b), 2.61 (br, 2H, a), 1.98 (m, 6H, e, k), 1.57 (m, 2H, i), 1.44–1.29 (m, 6H, c, d, j).  $^{31}\text{P}$  {H} NMR (121 MHz, chloroform-*d*,  $\delta$ ): 15.81 (s, 1P, 1).  $^{13}\text{C}$  {H} NMR (75 MHz, chloroform-*d*,  $\delta$ ): 138.44 (s, 2C, f), 138.36 (s, C, l), 114.73 (s, C, m), 114.65 (s, 2C, g), 64.61 (d, C, h), 41.01 (s, 2C, b), 33.32 (s, 2C, e), 33.25 (s, C, k), 31.43 (d, 2C, c), 29.99 (d, C, i), 25.96 (s, 2C, d), 24.97 (s, C, j). ESI-MS  $m/z$ : 343.24 [M + H] $^+$ , 685.42 [2M + H] $^+$  (calculated: 342.24).

**Tri(hex-5-en-1-yl)phosphoramidate (3).** To a dried three-necked 250 mL round-bottom flask fitted with a dropping funnel, di(hex-5-en-1-yl)phosphorochloridate (25.0 g, 88.9 mmol, 1.0 equiv) was added under an argon atmosphere in dry toluene (80 mL). Then triethylamine (13.6 mL, 97.78 mmol, 1.1 equiv) and 1-hexene-5-amine (12.3 mL, 97.78 mmol, 1.1 equiv) were added dropwise to the solution at room temperature. The reaction was stirred overnight and filtered. The crude mixture was concentrated at reduced pressure, and the crude product was dissolved in diethyl ether to wash it with 10% aqueous hydrochloric acid solution, a saturated solution of calcium carbonate, and brine. The organic layer was dried over anhydrous sodium sulfate, filtered, and dried *in vacuo*.

For the biological tests the compound was purified by chromatography over silica using ethyl acetate and petroleum ether (6:4) as an eluent to give a clear, slight yellow oil (yield: 63%). The purity and chemical structure were determined by  $^1\text{H}$  NMR,  $^{13}\text{C}$  {H} NMR, and  $^{31}\text{P}$  {H} NMR spectroscopy.

$^1\text{H}$  NMR (300 MHz, chloroform-*d*,  $\delta$ ): 5.83–5.69 (m, 3H, e, l), 5.01–4.91 (m, 6H, f, m), 3.95 (m, 4H, a), 2.70 (br, H, g), 2.85 (br, 2H, h), 2.04 (td, 6H, d, k), 1.66 (m, 4H, b), 1.50–1.35 (m, 8H, c, i, j).  $^{31}\text{P}$  {H} NMR (121 MHz, chloroform-*d*,  $\delta$ ): 9.48 (s, 1P, 1).  $^{13}\text{C}$  {H} NMR (75 MHz, chloroform-*d*,  $\delta$ ): 138.47 (s, C, l), 138.41 (s, 2C, e), 114.87 (s, 2C, f), 114.81 (s, C, m), 66.06 (d, 2C, a), 41.33 (s, C, h), 33.37 (s, C, k), 33.29 (s, 2C, d), 31.21 (d, C, i), 29.90 (d, 2C, b), 25.92 (s, C, j), 24.95 (s, 2C, c). ASAP-MS  $m/z$ : 689.2 (2M + H) (calculated: 344.21).

## ■ ASSOCIATED CONTENT

### Supporting Information

The Supporting Information is available free of charge on the ACS Publications website at DOI: 10.1021/acsapm.9b00129.

Thermal properties (DSC, TGA); ESI-MS; TG-FTIR, PCFC; UL-94; LOI; cone calorimeter details; residue morphology; NMR; biological assays (PDF)

## ■ AUTHOR INFORMATION

### Corresponding Authors

\*E-mail: wurm@mpip-mainz.mpg.de.

\*E-mail: bernhard.schartel@bam.de.

### ORCID

Alexander Battig: 0000-0002-9461-1368

Lisa Zimmermann: 0000-0001-6801-6859

Martin Wagner: 0000-0002-4402-3234

Bernhard Schartel: 0000-0001-5726-9754

Frederik R. Wurm: 0000-0002-6955-8489

### Author Contributions

J.C.M. and A.B. contributed equally to this work.

### Notes

The authors declare no competing financial interest.

## ■ ACKNOWLEDGMENTS

The authors thank the Deutsche Forschungsgemeinschaft (DFG WU 750/8-1; SCHA 730/15-1) for funding. J.C.M. is the recipient of a fellowship through funding of the Excellence Initiative (DFG/GSC 266) in the context of the graduate school of excellence "MAINZ" (Materials Science in Mainz). F.R.W. and J.C.M. thank Prof. Dr. Katharina Landfester (MPI-P, Germany) for support. We thank Robert Graf (MPI-P, Germany) for the solid-state NMR measurements. A.B. thanks William Harris and Leticia Lima for their assistance in measuring and preparing samples. L.Z. and F.R.W. thank the German Federal Ministry for Education and Research (BMBF) for their support of the program "Research for sustainable development (FONA)", "PlastX-Plastics as a systemic risk for social-ecological supply systems" (Grant 01UU1603A).

## ■ REFERENCES

- (1) Velencoso, M. M.; Battig, A.; Markwart, J. C.; Schartel, B.; Wurm, F. R. Molecular Firefighting - How Modern Phosphorus Chemistry Can Help Solve the Flame Retardancy Task. *Angew. Chem., Int. Ed.* **2018**, *57* (33), 10450.
- (2) Nishihara, H.; Tanji, S.; Kanatani, R. Interactions between Phosphorus- and Nitrogen-Containing Flame Retardants. *Polym. J.* **1998**, *30*, 163.
- (3) Lindsay, C. I.; Hill, S. B.; Hearn, M.; Manton, G.; Everall, N.; Bunn, A.; Heron, J.; Fletcher, I. Mechanisms of action of phosphorus based flame retardants in acrylic polymers. *Polym. Int.* **2000**, *49* (10), 1183–1192.
- (4) Schartel, B. Phosphorus-based Flame Retardancy Mechanisms—Old Hat or a Starting Point for Future Development? *Materials* **2010**, *3* (10), 4710–4745.
- (5) Green, J. A Review of Phosphorus-Containing Flame Retardants. *J. Fire Sci.* **1992**, *10* (6), 470–487.
- (6) Braun, U.; Balabanovich, A. I.; Schartel, B.; Knoll, U.; Artner, J.; Ciesielski, M.; Döring, M.; Perez, R.; Sandler, J. K. W.; Altstädt, V.; Hoffmann, T.; Pospiech, D. Influence of the oxidation state of phosphorus on the decomposition and fire behaviour of flame-retarded epoxy resin composites. *Polymer* **2006**, *47* (26), 8495–8508.

(7) Täuber, K.; Marsico, F.; Wurm, F. R.; Schartel, B. Hyper-branched poly(phosphoester)s as flame retardants for technical and high performance polymers. *Polym. Chem.* **2014**, *5* (24), 7042–7053.

(8) Minkoff, G. J.; Tipper, C. F. H. *Chemistry of Combustion Reactions*; Butterworths: 1962.

(9) Gaan, S.; Sun, G.; Hutches, K.; Engelhard, M. H. Effect of nitrogen additives on flame retardant action of tributyl phosphate: Phosphorus–nitrogen synergism. *Polym. Degrad. Stab.* **2008**, *93* (1), 99–108.

(10) Laoutid, F.; Bonnaud, L.; Alexandre, M.; Lopez-Cuesta, J. M.; Dubois, P. New prospects in flame retardant polymer materials: From fundamentals to nanocomposites. *Mater. Sci. Eng., R* **2009**, *63* (3), 100–125.

(11) Gao, F.; Tong, L.; Fang, Z. Effect of a novel phosphorous–nitrogen containing intumescent flame retardant on the fire retardancy and the thermal behaviour of poly(butylene terephthalate). *Polym. Degrad. Stab.* **2006**, *91* (6), 1295–1299.

(12) Gaan, S.; Sun, G. Effect of phosphorus and nitrogen on flame retardant cellulose: A study of phosphorus compounds. *J. Anal. Appl. Pyrolysis* **2007**, *78* (2), 371–377.

(13) Morgan, A. B.; Gilman, J. W. An overview of flame retardancy of polymeric materials: application, technology, and future directions. *Fire Mater.* **2013**, *37* (4), 259–279.

(14) Grand, A. F.; Wilkie, C. A. *Fire Retardancy of Polymeric Materials*; CRC Press: 2000.

(15) Cho, Y.-H.; Kim, K.; Ahn, S.; Liu, H. K. Allyl-substituted triazines as additives for enhancing the thermal stability of Li-ion batteries. *J. Power Sources* **2011**, *196* (3), 1483–1487.

(16) Lu, S.-Y.; Hamerton, I. Recent developments in the chemistry of halogen-free flame retardant polymers. *Prog. Polym. Sci.* **2002**, *27* (8), 1661–1712.

(17) Levchik, S. V.; Weil, E. D. A Review of Recent Progress in Phosphorus-based Flame Retardants. *J. Fire Sci.* **2006**, *24* (5), 345–364.

(18) Zheng, X.-B.; Wu, J.-P.; Luo, X.-J.; Zeng, Y.-H.; She, Y.-Z.; Mai, B.-X. Halogenated flame retardants in home-produced eggs from an electronic waste recycling region in South China: Levels, composition profiles, and human dietary exposure assessment. *Environ. Int.* **2012**, *45*, 122–128.

(19) Xiao, H.; Shen, L.; Su, Y.; Barresi, E.; DeJong, M.; Hung, H.; Lei, Y.-D.; Wania, F.; Reiner, E. J.; Sverko, E.; Kang, S.-C. Atmospheric concentrations of halogenated flame retardants at two remote locations: The Canadian High Arctic and the Tibetan Plateau. *Environ. Pollut.* **2012**, *161*, 154–161.

(20) Windham, G. C.; Pinney, S. M.; Sjodin, A.; Lum, R.; Jones, R. S.; Needham, L. L.; Biro, F. M.; Hiatt, R. A.; Kushi, L. H. Body burdens of brominated flame retardants and other persistent organo-halogenated compounds and their descriptors in US girls. *Environ. Res.* **2010**, *110* (3), 251–257.

(21) Nguyen, T.-M.; Chang, S.; Condon, B.; Slopek, R.; Graves, E.; Yoshioka-Tarver, M. Structural Effect of Phosphoramidate Derivatives on the Thermal and Flame Retardant Behaviors of Treated Cotton Cellulose. *Ind. Eng. Chem. Res.* **2013**, *52* (13), 4715–4724.

(22) Perret, B.; Pawlowski, K. H.; Schartel, B. Fire retardancy mechanisms of arylphosphates in polycarbonate (PC) and PC/acrylonitrile-butadiene-styrene. *J. Therm. Anal. Calorim.* **2009**, *97* (3), 949.

(23) Schartel, B.; Perret, B.; Dittrich, B.; Ciesielski, M.; Krämer, J.; Müller, P.; Altstädt, V.; Zang, L.; Döring, M. Flame Retardancy of Polymers: The Role of Specific Reactions in the Condensed Phase. *Macromol. Mater. Eng.* **2016**, *301* (1), 9–35.

(24) Rakotomalala, M.; Wagner, S.; Döring, M. Recent Developments in Halogen Free Flame Retardants for Epoxy Resins for Electrical and Electronic Applications. *Materials* **2010**, *3* (8), 4300.

(25) Ciesielski, M.; Schäfer, A.; Döring, M. Novel efficient DOPO-based flame-retardants for PWB relevant epoxy resins with high glass transition temperatures. *Polym. Adv. Technol.* **2008**, *19* (6), 507–515.

(26) Cowie, J. M. G.; Arrighi, V. *Polymers: Chemistry and Physics of Modern Materials*, 3rd ed.; CRC Press: 2007.



(27) Schartel, B.; Wilkie, C. A.; Camino, G. Recommendations on the scientific approach to polymer flame retardancy: Part 1—Scientific terms and methods. *J. Fire Sci.* **2016**, *34* (6), 447–467.

(28) Schartel, B.; Hull, T. R. Development of fire-retarded materials—Interpretation of cone calorimeter data. *Fire Mater.* **2007**, *31* (5), 327–354.

(29) Wawrzyn, E.; Schartel, B.; Ciesielski, M.; Kretzschmar, B.; Braun, U.; Döring, M. Are novel aryl phosphates competitors for bisphenol A bis(diphenyl phosphate) in halogen-free flame-retarded polycarbonate/acrylonitrile–butadiene–styrene blends? *Eur. Polym. J.* **2012**, *48* (9), 1561–1574.

(30) Schartel, B.; Perret, B.; Dittrich, B.; Ciesielski, M.; Krämer, J.; Müller, P.; Altstädt, V.; Zang, L.; Döring, M. Flame Retardancy of Polymers: The Role of Specific Reactions in the Condensed Phase. *Macromol. Mater. Eng.* **2016**, *301* (1), 9–35.

## Supporting Information

### Systematically controlled decomposition mechanism in phosphorus flame retardants by precise molecular architecture: P-O vs. P-N

Jens C. Markwart<sup>‡[a, c]</sup>, Alexander Battig<sup>‡[b]</sup>, Lisa Zimmermann<sup>[d]</sup>, Martin Wagner<sup>[e]</sup>, Jochen Fischer<sup>[f]</sup>, Bernhard Schartel<sup>\*[b]</sup>, Frederik R. Wurm<sup>\*[a]</sup>

[a] Physical Chemistry of Polymers, Max Planck Institute for Polymer Research, Ackermannweg 10, 55128 Mainz, Germany, E-mail: [wurm@mpip-mainz.mpg.de](mailto:wurm@mpip-mainz.mpg.de)

[b] Technical Properties of Polymeric Materials, Bundesanstalt für Materialforschung und -prüfung (BAM), Unter den Eichen 87, 12205 Berlin, Germany

[c] Graduate School Materials Science in Mainz, Staudinger Weg 9, 55128 Mainz, Germany

[d] Department of Aquatic Ecotoxicology Goethe University Frankfurt, Max-von-Laue-Str. 13, 60438 Frankfurt/Main, Germany

[e] Department of Biology, Norwegian University of Science and Technology, 7491 Trondheim, Norway

[f] Institute for Biotechnology und Drug Research gGmbH (IBWF), Erwin-Schrödinger-Str. 56, 67663 Kaiserslautern, Germany

#### Corresponding author:

\*E-mail: [wurm@mpip-mainz.mpg.de](mailto:wurm@mpip-mainz.mpg.de); [bernhard.schartel@bam.de](mailto:bernhard.schartel@bam.de)

#### Table of Contents

Table of Contents .....	1
Materials .....	2
DSC .....	2
TGA .....	2
ESI-MS .....	2
TG-FTIR .....	2

PCFC .....	3
Hot Stage FTIR .....	3
UL-94, LOI .....	3
Cone Calorimeter .....	4
Residue morphology .....	4
NMR .....	4
Sample preparation .....	4
Bacterial and fungal strains .....	5
Antibacterial and Antifungal Assays .....	6
Additional: Results and Discussion .....	6
References .....	33

## **Experimental Procedures**

### **Materials**

All chemicals were purchased from commercial suppliers as reagent grade and used without further purification.

### **DSC**

Differential scanning calorimetry measurements were performed using a Netzsch 204 F1 “Phoenix” differential scanning calorimeter (DSC) (Netzsch Instruments, Selb, Germany), using 5 mg sample and three heating and two cooling runs at  $10 \text{ K min}^{-1}$  from  $-80$  to  $180 \text{ }^\circ\text{C}$ . The data was evaluated as an average of the 2<sup>nd</sup> and 3<sup>rd</sup> heating run, if  $p < 5\%$ .

For Differential Scanning Calorimetry (DSC), a Mettler Toledo DSC 823<sup>e</sup> was used. With a heating and cooling rate of  $10 \text{ K min}^{-1}$  three measurements of heating, cooling and heating were performed. The measurements were done in a nitrogen atmosphere with a flow rate of  $30 \text{ mL min}^{-1}$ .

### **TGA**

For the thermogravimetric analysis (TGA) of the neat flame retardants, a Mettler Toledo TGA/DSC 3+ in a nitrogen atmosphere was used. Using 10 mg of the sample, the measurements were performed in a range from  $25 \text{ }^\circ\text{C}$  to  $600 \text{ }^\circ\text{C}$  with a heating rate of  $10 \text{ K min}^{-1}$ .

### **ESI-MS**

Electrospray ionization mass spectrometry (ESI-MS) was performed on a Q-ToF Ultima 3 from Waters Micromass, Milford, Massachusetts. 1 mg of the sample was dissolved in 1 ml of THF. The prepared solution was injected into the ionization chamber of the ESI-MS instrument at  $120 \text{ }^\circ\text{C}$ .

### **TG-FTIR**

Both decomposition and evolved gases were investigated under pyrolytic and thermo-oxidative conditions via Fourier transform infrared (FTIR) spectroscopy coupled with thermogravimetric analysis. For epoxy resins with and without FRs, 10 mg of powder attained from cryomilling were used for measurements, while 5 mg samples were measured for pure FRs. Using a TG 209 F1 Iris (Netzsch Instruments, Selb, Germany), samples were heated at a rate of  $10 \text{ K min}^{-1}$  from  $30$  to  $900 \text{ }^\circ\text{C}$  under a nitrogen or synthetic air (80:20) gas flow of  $30 \text{ ml min}^{-1}$ . The evolved gases were analyzed using a Tensor27 infrared spectrometer (Bruker Optics, Ettlingen, Germany), which was coupled to the TG via a transfer line heated to  $270 \text{ }^\circ\text{C}$ .

### **Pyrolysis–Gas Chromatography–Mass Spectrometry (Py-GC-MS)**

Py-GC-MS measurements were conducted as follows: a micro-furnace double-shot pyrolyzer (PY3030iD, Frontier Laboratories, Japan) was connected via a split-/splitless inlet port to a gas chromatograph (7890B, Agilent Technologies, USA) combined with a mass selective detector (5977B, Agilent Technologies, USA). The EI ionization energy of the MSD was 70 eV, the scan range was 15–550 amu. 300 µg samples were inserted by gravimetric fall into the pyrolysis zone at 500 °C and pyrolyzed in a helium atmosphere. The evolved pyrolysis products were separated with an Ultra Alloy +5 capillary column (l = 30 m, iD = 0.25 mm, film thickness = 0.25 µm) with a helium flow of 1 ml min<sup>-1</sup>. The column temperature was kept at 40 °C for 2 min and increased at a rate of 10 °C min<sup>-1</sup> to 300 °C where it was held for 10 min. The temperature of the GC injector was 300 °C and it was operated in a split mode of 1:300. Peak assignments were made with the help of the NIST14 MS library.

### **Gas Chromatography–Mass Spectrometry (GC-MS)**

GC-MS measurement was conducted on Shimadzu GC-2010 plus gas chromatography and QP2010 ultra mass spectrometer with fused silica column (122-5532, DB-5MS) and flame ionization detector.

### **PCFC**

The heat release capacity, total heat released, and heat of combustion of the volatiles were determined using pyrolysis combustion flow calorimetry (PCFC) using a microscale combustion calorimeter (MCC) (Fire Testing Technologies Ltd., East Grinstead, UK). 5 mg powdered samples were pyrolyzed from 150 to 750°C and combusted at 900°C at a heating rate of 1 K s<sup>-1</sup> under a total gas flow of 100 ml min<sup>-1</sup> (80 ml min<sup>-1</sup> nitrogen, 20 ml min<sup>-1</sup> oxygen).

### **Hot Stage FTIR**

The condensed phase activity was monitored using hot-stage FT-infrared spectroscopy using a Vertex70 FTIR spectrometer (Bruker Optics, Ettlingen, Germany), equipped with an FTIR600 Linkam hot-stage cell (Linkam Scientific Instruments Ltd., Chilworth, UK). The samples were pressed into a KBr plate, loaded into the Linkam cell, and heated at a rate of 10 K min<sup>-1</sup> from 30 to 600 °C under a nitrogen gas flow of 300 ml min<sup>-1</sup>.

## **UL-94, LOI**

Two separate tests, namely Underwriter's Laboratory 94 (UL-94) and limiting oxygen index (LOI), were performed to determine and characterize the flammability in terms of the flame retarded resins' reaction-to-small-flames. UL-94 was performed in accordance with the standard DIN EN 60695-11-10 in horizontal and vertical orientation. LOI was performed according to DIN EN ISO 4589-2. All samples were conditioned at 23°C and 50% relative humidity for at least 80 hours.

## **Cone Calorimeter**

All epoxy resin samples were subjected to bench-scale forced flaming combustion using a cone calorimeter (Fire Testing Technology Ltd., East Grinstead, UK) at a distance of 35 mm between specimen and cone heater and a heat flux of 50 kW m<sup>-2</sup> and in accordance with ISO 5660. Specimens sized 100 x 100 x 4 mm<sup>3</sup> were conditioned at 23°C and 50% relative humidity for at least 48 hours and then subjected to irradiation.

## **Residue morphology**

The fire residue surfaces and core interiors were examined via scanning electron microscopy (SEM) using a Zeiss EVO MA10 (Zeiss, Oberkochen, Germany) with an acceleration voltage of 10 kV. Prior to the investigation, the residues were sputtered with gold to reduce the degradation of the images due to sample charging.

## **NMR**

Nuclear magnetic resonance (NMR) analysis, <sup>1</sup>H, <sup>31</sup>P {H} and <sup>13</sup>C {H} NMR spectra were recorded with Bruker Avance spectrometers operating with 250, 300, 500 and 700 MHz frequencies in deuterated chloroform, deuterated dimethyl sulfoxide or deuterated *N,N*-dimethylformamide as a solvent. The calibration of the spectra was done against the solvent signal. The spectra were analyzed using MestReNova 9 from Mestrelab Research S.L.

## **Solid-state NMR**

<sup>31</sup>P CP/MAS NMR measurements were performed with a standard 4 mm magic angle spinning MAS double resonance probe head at 121.5 MHz Larmor frequency.

## **Sample preparation**

All epoxy resins were prepared using bisphenol A diglycidylether (DGEBA) (Araldite MY740, Bodo Möller Chemie GmbH, Offenbach am Main, Germany) as the epoxide agent and 2,2'-dimethyl-4,4'-methylene-bis-(cyclohexylamine) (DMC) (Sigma Aldrich Co. LLC/ Merck KGaA, Darmstadt, Germany)

as the amine hardener. The materials were mixed, poured into aluminum molds of desired dimensions, then hardened at 150°C for 3h. The flame retarded epoxy resins were produced in the same manner, except 10 wt.-% of the mixture was replaced with the respective flame retardant.

### **Baseline toxicity – microtox assay**

In the Microtox assay, the potential of compounds to inhibit the bioluminescence of *Aliivibrio fischeri* is determined by observations of e.g. the bacteria's metabolism or growth. The assay was performed according to the International Organization for Standardization (ISO 11348-3, 2007)(ISO 2017) modified to a 96-well plate format as previously described by Escher et al. and Völker et al.<sup>1,2</sup> Stock solutions were prepared in dimethyl sulfoxide (DMSO) and further diluted in the assay to concentrations ranging from 0.02 to 3.00 mM (<1 % DMSO v/v). All compounds were tested in five independent experiments with two technical replicates each. We used GraphPad Prism 5.0 (GraphPad Software, San Diego, CA) for nonlinear regressions (four-parameter logistic function) to calculate the concentration inducing 20 % luminescence inhibition (EC<sub>20</sub>).

### **Endocrine activity – yeast-based reporter-gene assays**

In order to investigate whether compounds influence the endocrine system, we tested their relative agonistic activity at the human estrogen receptor  $\alpha^3$  and antagonistic activity at the human androgen receptor<sup>4</sup> as previously described with minor modifications regarding the measurement of the reporter gene activity.<sup>5, 6</sup> In brief, we determined the reporter gene activity at 540 nm 40 min after adding 50  $\mu$ l *lacZ* buffer (supplemented with 50 % w/v 4-methylumbelliferyl-beta-D-glucuronide and 15.4 % w/v dithiothreitol) to 30  $\mu$ l sample solution. Depending on the compound's cytotoxicity, concentrations ranging from 0.8 nM to 3 mM were tested. Each assay was repeated three to six times resulting in 24 to 48 replicates. Data analysis was performed using GraphPad Prism 5.0. Estrogenic and antiandrogenic activities were normalized to the pooled negative and solvent controls (0%) and the maximal assay response induced by the references compounds 17 $\beta$ -estradiol and flutamide, respectively. Relative activities at highest noncytotoxic concentrations are given. If possible, dose-response relationships and respective EC<sub>20</sub> values were calculated using a four-parameter logistic function, constrained to a bottom level of zero.

### **Bacterial and fungal strains**

The strains of *Bacillus subtilis* subsp. *spizizenii* (ATCC 6633) and *Staphylococcus aureus* (ATCC 11632) were cultivated at NB (Difco™ Nutrition Broth, BD, France) at 37°C. All fungal strains (*Candida albicans*, ATCC 90028; *Rhizomucor miehei*, Tü 284; *Penicillium notatum*, IBWF gGmbH and



*Paecilomyces variotii*, ETH 114646) were cultured on YMG (4 g/L yeast extract, 10 g/L malt extract, 4 g/L glucose, pH 5.5) at 27°C or 37°C, respectively.

*Pyricularia oryzae*<sup>7</sup> and *Botrytis cinerea*<sup>8</sup> were cultured on CM<sup>9</sup> and malt medium (20 g/L malt extract, pH 5.5) at 27°C for 3 to 4 weeks, respectively.

HeLa-S3 (DSMZ ACC 161) were grown as described previously by Schöffler et al.<sup>10</sup>

### **Antibacterial and Antifungal Assays**

The disk diffusion method was performed to determine the antibacterial and antifungal properties of the chemical compounds. It was mainly based on published methods.<sup>11-13</sup> All agar plates were prepared in 90 mm sterile Petri dishes (PS Sarstedt, 82.1472 Germany) with 20 mL of agar (Difco™ Nutrition Broth, BD, France for bacteria and Difco™ potato dextrose Broth, BD, France for fungi). The bacterial inoculum suspension was diluted in the liquid agar media at 45°C. The inoculated medium was poured into the Petri dishes. For fungi, a spore solution was added to the liquid agar medium at 45°C. The mixture was also poured into Petri dishes. The plates were stored at 4°C until further use. Sterilized assay paper disks (MN 827, #484000; 6.0 mm in diameter, Macherey-Nagel, Germany) were soaked with 10 and 50 µg of the compound solved in DMSO and placed on inoculated plates. The plates were incubated at 37°C overnight for bacteria and at 27°C for 48 h for fungi, respectively. Afterward, the diameters of inhibition zones were measured. As a control, standard antibiotics (50 µg streptomycin for bacteria or 50 µg hygromycin B for fungi), as well as pure DMSO, were included. Each assay was performed thrice. *Pyricularia oryzae* was used for the spore germination test as previously published by Kettering et al. (2005).<sup>14</sup> The method was slightly adapted for the spore germination assay of *Botrytis cinerea*.<sup>8</sup> The cytotoxicity was analyzed as described previously.<sup>15</sup> Phytotoxicity was tested with *Setaria italic* and *Lepidium sativum* with minor alterations.<sup>16</sup> The tested compounds were prepared in aliquots of 10, 20 and 50 µg per 48-well solved in DMSO. The plates were freeze-dried afterward to remove the solvent. To each well 12 seeds and 200 µL H<sub>2</sub>O were added. Afterward, the plates were incubated in a plant humidity chamber for 5 to 7 days. As a control 5% H<sub>3</sub>PO<sub>4</sub> was added to the water poured onto the seeds. All tests were prepared as triplicates.

## **Additional: Results and Discussion**

### ***In vitro* bioassays**

We compared the *in vitro* toxicity of the compound **1-4** with tributyl phosphate (TBP) and halogenated tetrabromo bisphenol A (TBBPA). We investigated the compounds' baseline toxicity as well as their estrogenic and antiandrogenic activities. In concentrations of up to 3 mM, FRs 1-4 showed baseline toxicity in a concentration-dependent manner (Figure S20). However, TBBPA was the most potent in inhibiting bacteria luminescence followed by **1**, **2** and TBP (Table S1). Compared to that, **4** and **3** were less toxic. We observed an interesting structure-toxicity relationship: The luminescence inhibition induced by the phosphoramides increases with the number of P-N bonds.

Three of the alternative FRs showed a relative antiandrogenic activity of up to 40.59% (**4**). Here, we observed the opposite pattern as for the baseline toxicity: **4** and **3** induced a higher effect (Table S1) as the FRs with more P-N bonds, TBP was the most potent antiandrogen. None of the alternative FRs activated the estrogen receptor in the tested concentrations. TBBPA induced a slight estrogenic activity of 6.01% at 3.1  $\mu$ M, the highest noncytotoxic concentration.

In conclusion, the alternative FRs induced both a certain baseline toxicity and antiandrogenic effects at the investigated concentrations but **2** and **4** represent a good alternative for their halogenated counterparts.

### **Biological activities in fungi, bacteria, hela, and plant cells**

In the agar diffusion assay, only TBBPA and **3** inhibited the germination of *P. oryzae* at 5  $\mu$ g/mL and 50  $\mu$ g/mL when dissolved in DMSO. **3**, when dissolved in water also inhibited the rice blast pathogen at 10  $\mu$ g/mL. Furthermore, we were able to detect a cytotoxic activity of TBBPA, **1**, **3** and **4** of 50%, 25%, 75% and 100% cell death when 50  $\mu$ g/mL of the compounds were added, respectively. The cytotoxicity effects were interestingly not detectable when the compounds were solved in DMSO. No phytotoxic effect of all tested compounds (50  $\mu$ g per disc) was observed against *Setaria italica* and *Lepidium sativum*, regardless of the used solvent.

The toxic effects of TBBPA were already discussed and investigated during the last decade.<sup>17-19</sup> The degradation of brominated flame retardants by microorganisms was assayed in recent years.<sup>20, 21</sup> In our study, we determined whether brominated flame retardants show a higher toxicity on a wide range of microorganisms and plants as well as a cytotoxic effect than the herein developed phosphorus flame retardants. Especially the fungicidal effect on *Pyricularia oryzae* was perspicuously lower for **1**, **2** and **4** than for TBBPA.

Additional data:

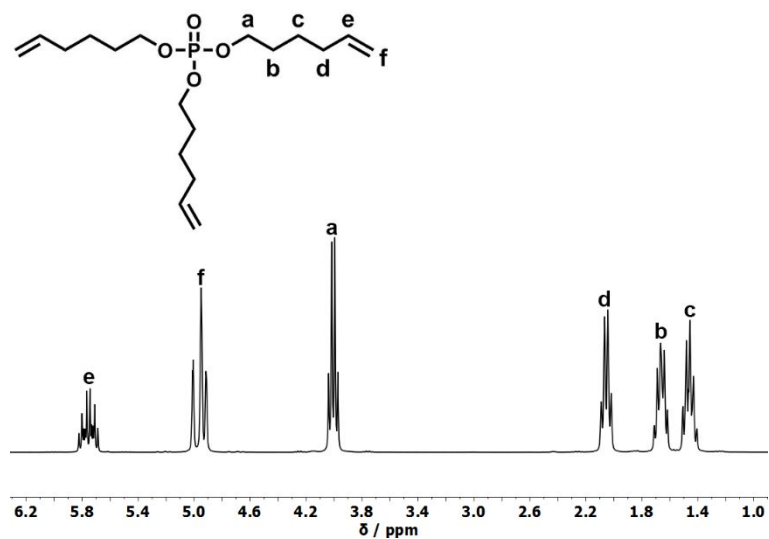


Figure S1. <sup>1</sup>H-NMR (300 MHz in CDCl<sub>3</sub> at 298 K) of 4.

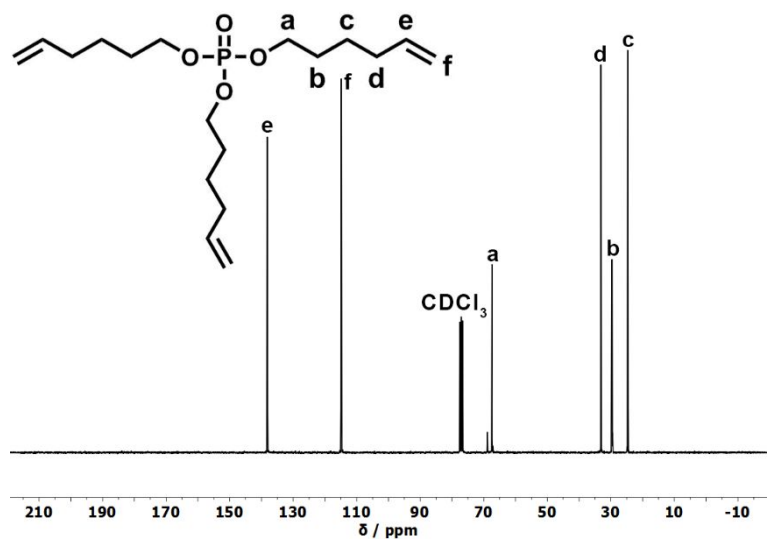
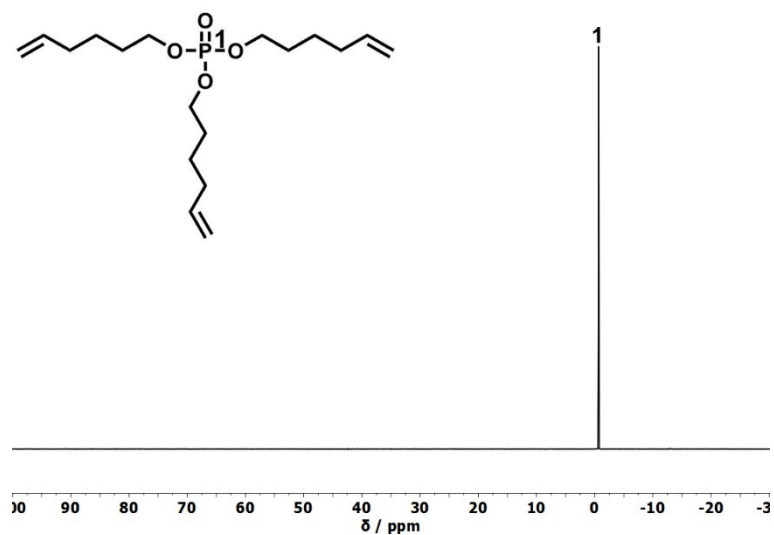
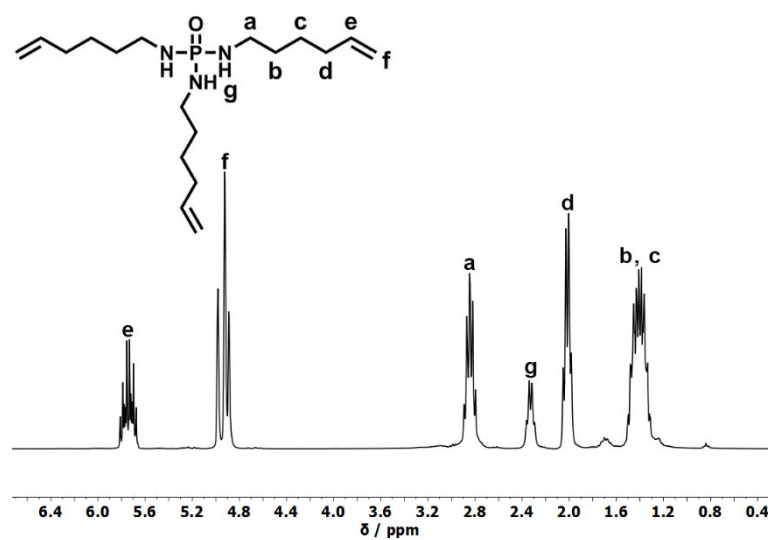


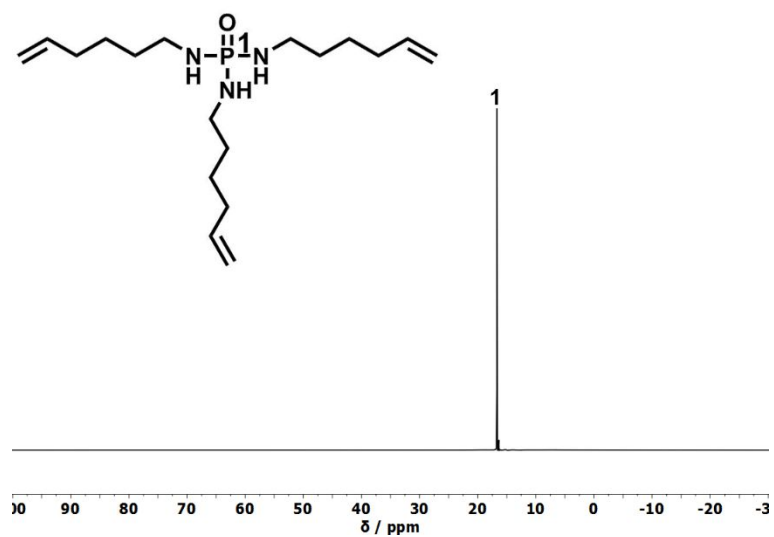
Figure S2. <sup>13</sup>C {<sup>1</sup>H}-NMR (75 MHz in CDCl<sub>3</sub> at 298 K) of 4.



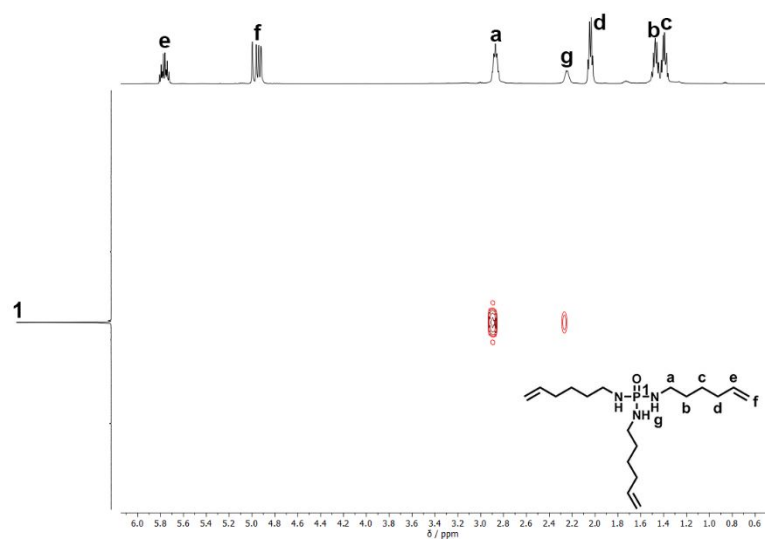
**Figure S3.**  $^{31}\text{P}$  {H}-NMR (121 MHz in  $\text{CDCl}_3$  at 298 K) of 4.



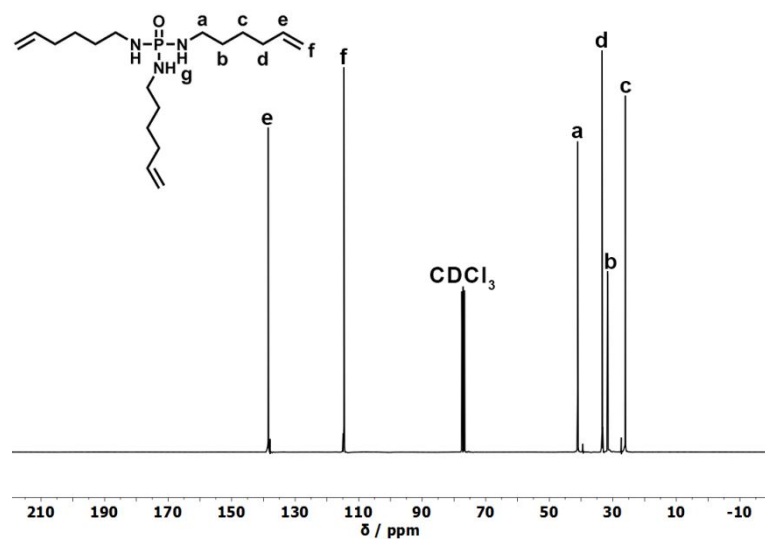
**Figure S4.**  $^1\text{H}$ -NMR (300 MHz in  $\text{CDCl}_3$  at 298 K) of 1.



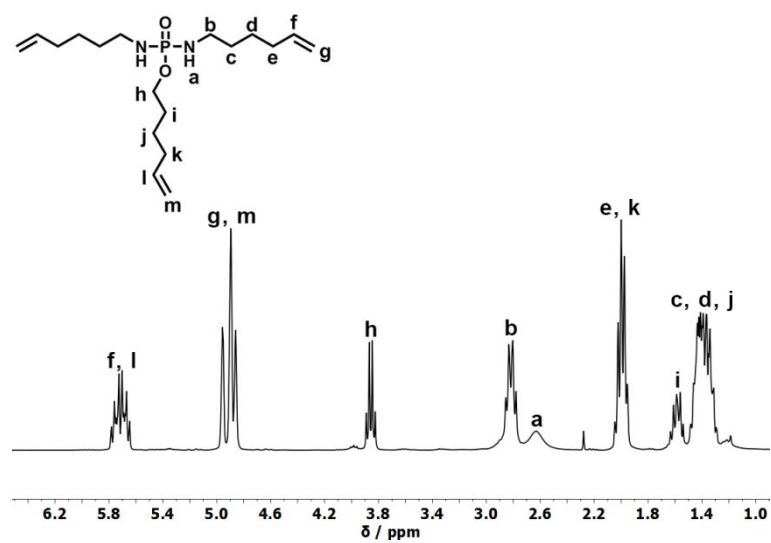
**Figure S5.**  $^{31}\text{P}$  {H}-NMR (121 MHz in  $\text{CDCl}_3$  at 298 K) of **1**.



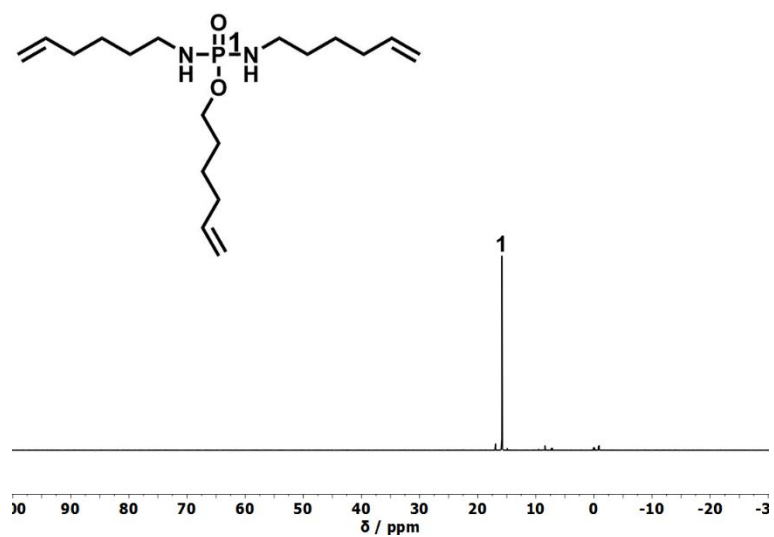
**Figure S6.**  $^{31}\text{P}$  {H}- $^1\text{H}$ -HMBC (200/500 MHz in  $\text{CDCl}_3$  at 298 K) of **1**.



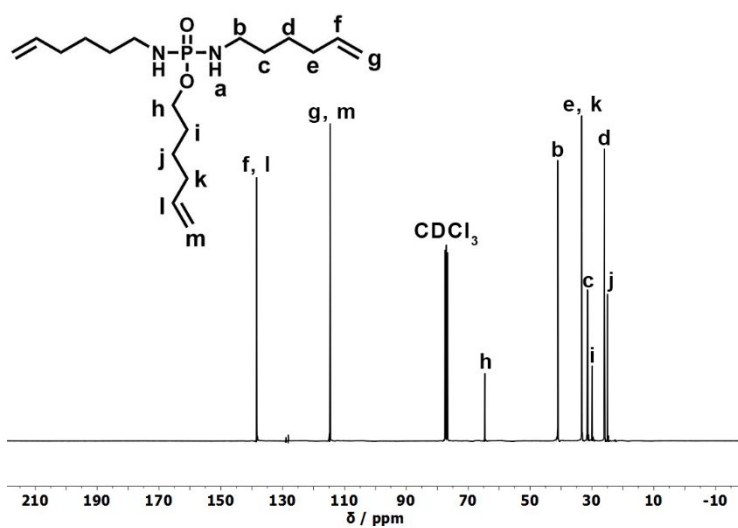
**Figure S7.**  $^{13}\text{C}$   $\{^1\text{H}\}$ -NMR (75 MHz in  $\text{CDCl}_3$  at 298 K) of **1**.



**Figure S8.**  $^1\text{H}$ -NMR (300 MHz in  $\text{CDCl}_3$  at 298 K) of **2**.

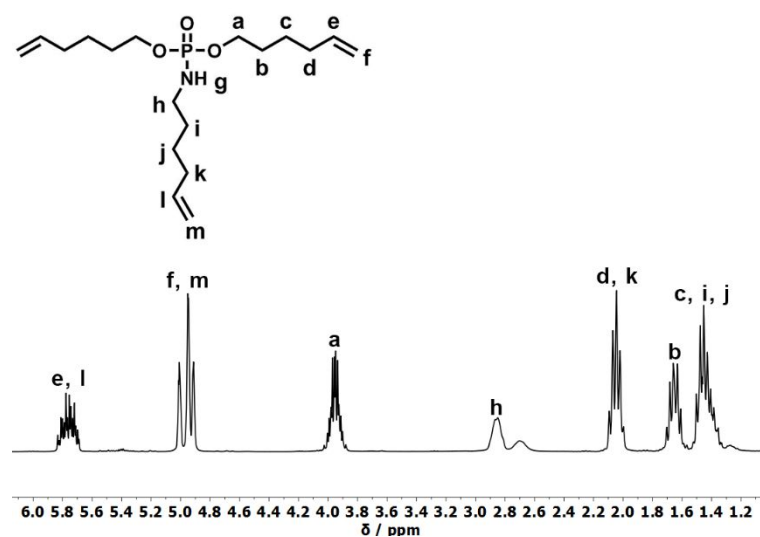


**Figure S9.**  $^{31}\text{P}$   $\{^1\text{H}\}$ -NMR (121 MHz in  $\text{CDCl}_3$  at 298 K) of 2.

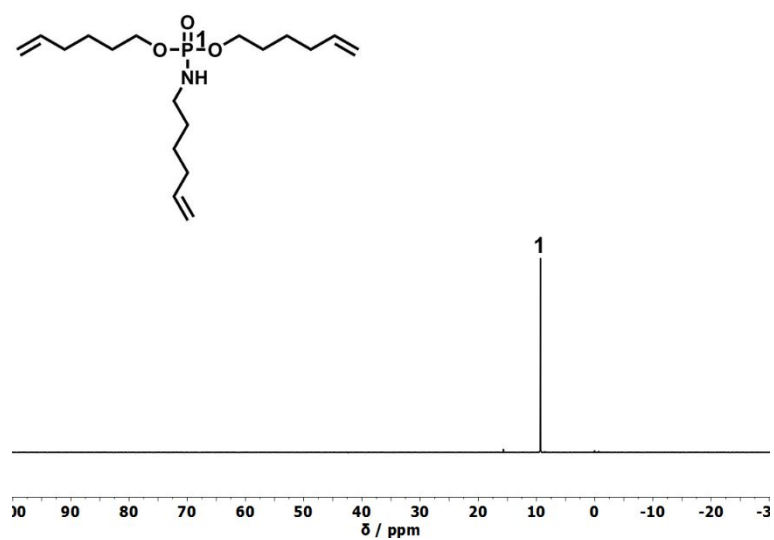


**Figure S10.**  $^{13}\text{C}$   $\{^1\text{H}\}$ -NMR (75 MHz in  $\text{CDCl}_3$  at 298 K) of 2.

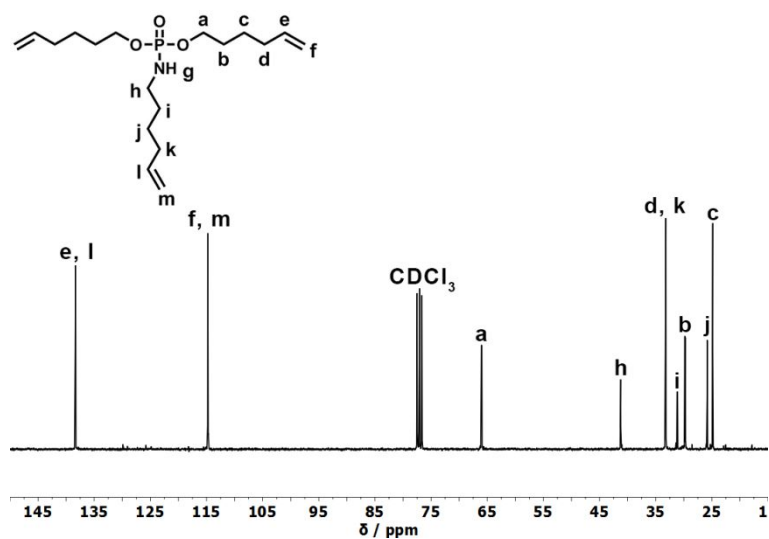




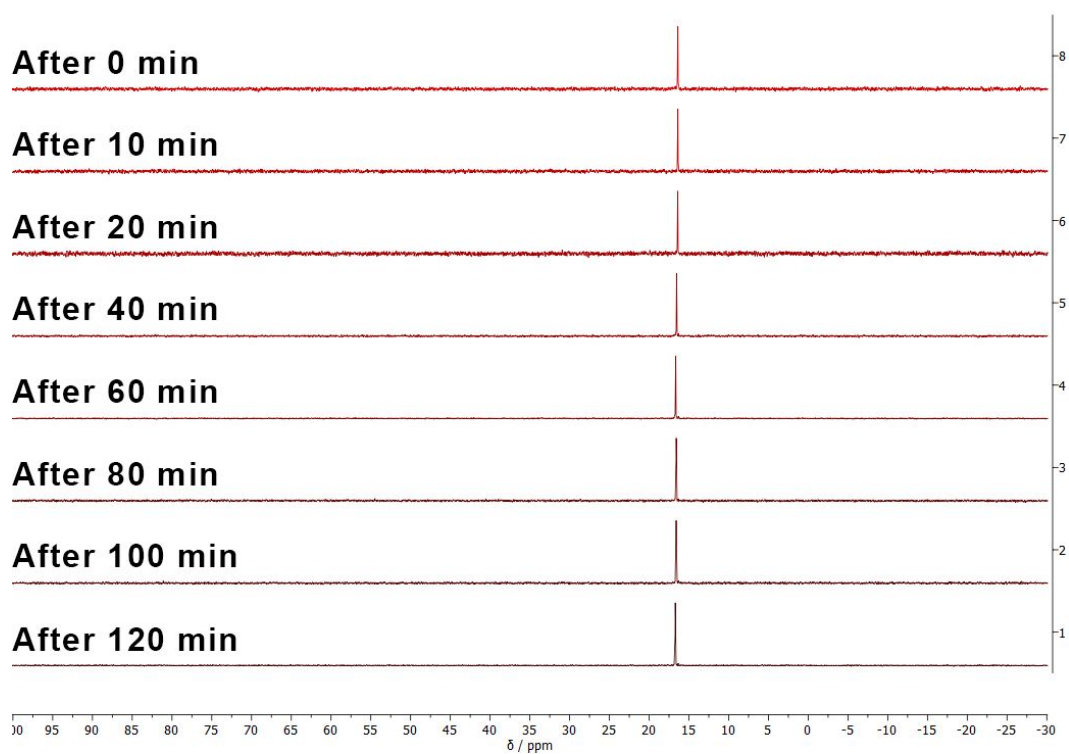
**Figure S11.**  $^1\text{H-NMR}$  (300 MHz in  $\text{CDCl}_3$  at 298 K) of 3.



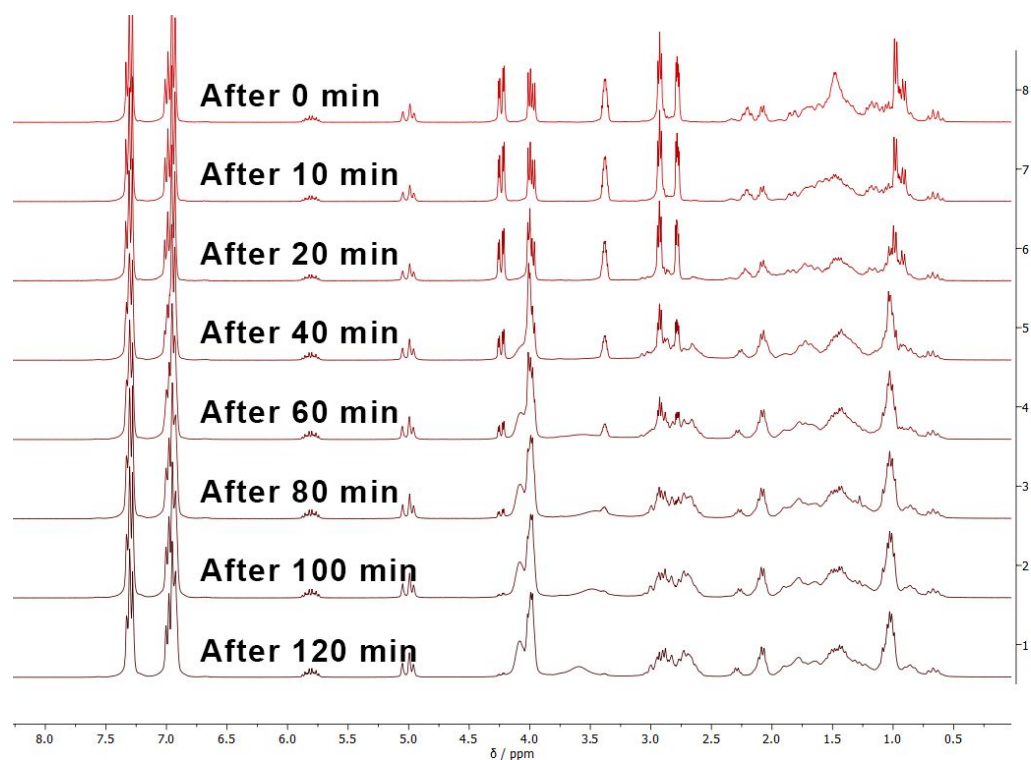
**Figure S12.**  $^{31}\text{P} \{^1\text{H}\}$ -NMR (121 MHz in  $\text{CDCl}_3$  at 298 K) of 3.



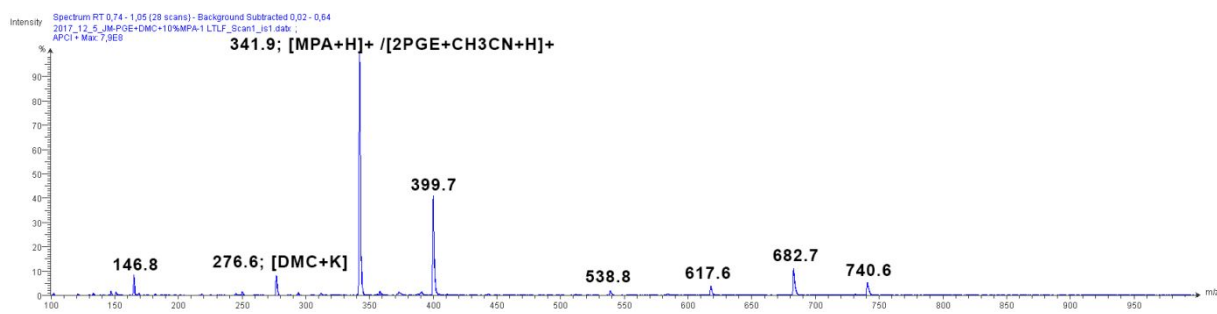
**Figure S13.**  $^{13}\text{C}$  { $^1\text{H}$ }-NMR (75 MHz in  $\text{CDCl}_3$  at 298 K) of 3.



**Figure S14.**  $^{31}\text{P}$  { $^1\text{H}$ }-NMR (121 MHz in  $\text{CDCl}_3$  at 298 K): No reaction of 1 with PGE and DMC under the used epoxy curing conditions.



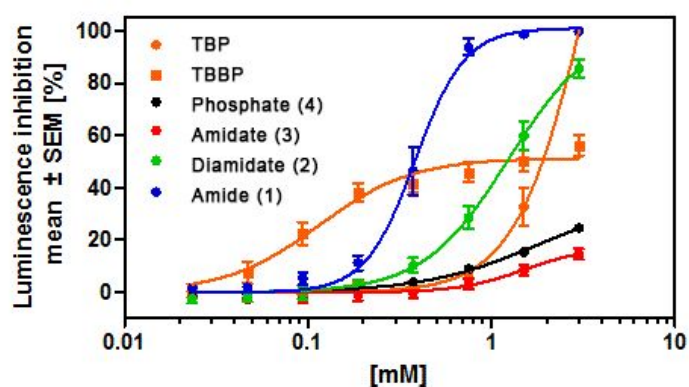
**Figure S15.**  $^1\text{H-NMR}$  (300 MHz in  $\text{CDCl}_3$  at 298 K): No reaction of **1** with PGE and DMC under the used epoxy curing conditions.



**Figure S16.** After the reaction of **1**, PGE and DMC under the used epoxy curing condition MS still shows the unreacted **1**.

**Table S1.** Baseline toxicity (EC<sub>20</sub>, of five experiments run in duplicates), relative antiandrogenic and estrogenic activity (EC<sub>20</sub> and/or relative activity at highest non-cytotoxic concentration (in brackets), n=24-48) of conventional and alternative flame retardants.

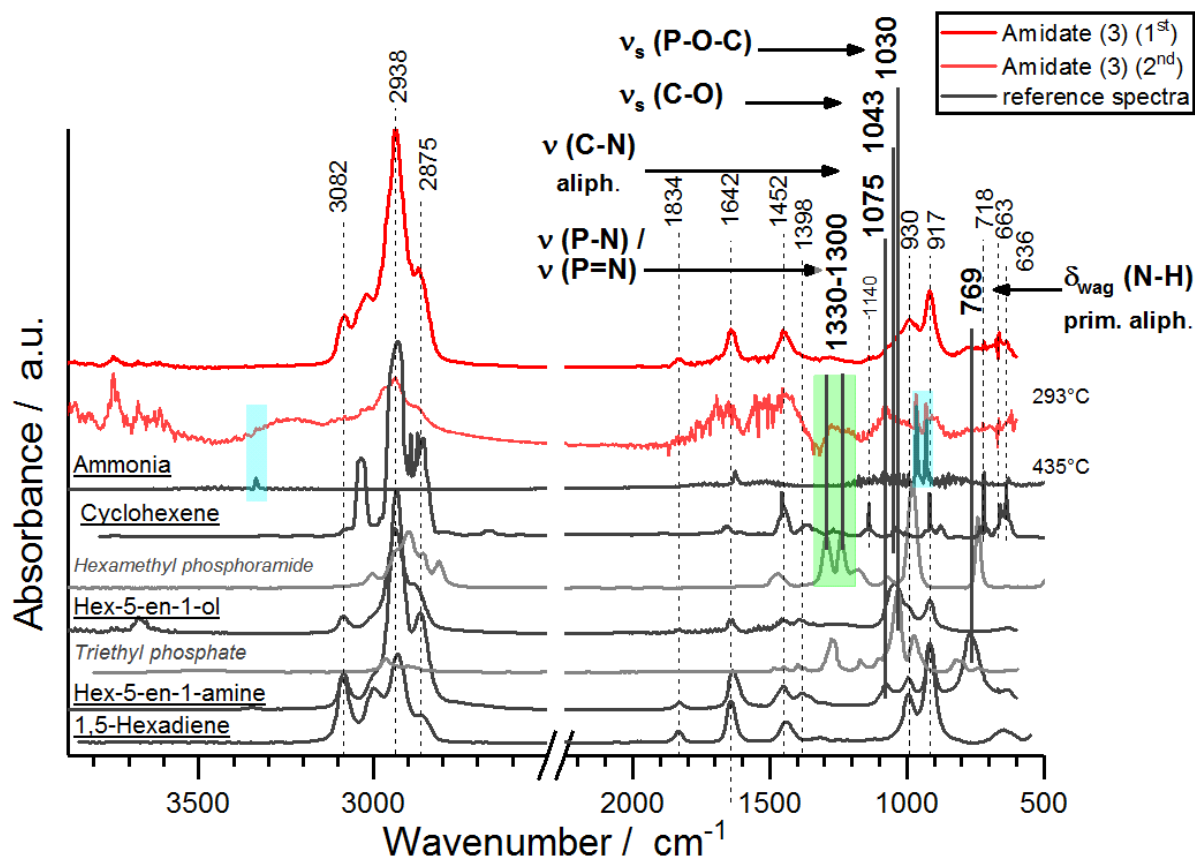
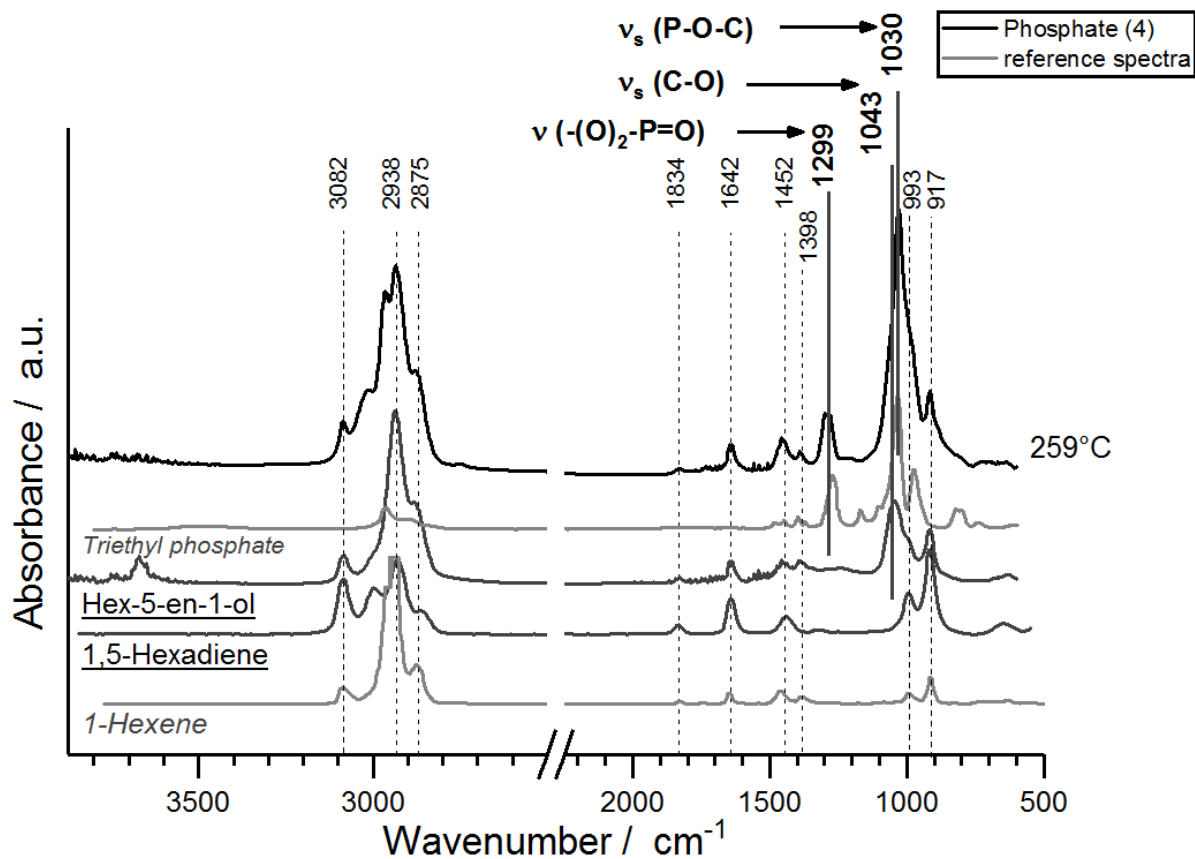
	4	3	2	1	TBP	TBBPA
Baseline toxicity, EC <sub>20</sub> [mM]	2.07	> 3.00	0.59	0.25	1.17	0.09
Relative antiandrogenic activity, EC <sub>20</sub> [mM]	1.43	0.31	> 3.00	> 3.00	0.04	> 3.00
Relative antiandrogenic activity [%]	40.59 ± 3.33	35.02 ± 2.92	7.41 ± 2.03	-	45.32 ± 2.31	-
Relative estrogenic activity [%]	-	-	-	-	-	6.01 ±



**Figure S17.** Baseline toxicity of conventional and alternative flame retardants (0.02 – 3 mM) as mean luminescence inhibition ± SEM in the Microtox assay. Data were pooled from five independent experiments run in duplicates.

**Table S2.** Summarized raw data of the biological assays.

samble name	solvent	Pyricularia oryzae in H <sub>2</sub> O				Pyricularia oryzae in CM				Botrytis cinerea in H <sub>2</sub> O	Hela S3		Setaria italica	Lepidium sativum	B. brevis		S. aureus		C. albicans		R. miehei		P. notatum		P. variotii	
		5 µg/ml	10 µg/ml	25 µg/ml	50 µg/ml	5 µg/ml	10 µg/ml	25 µg/ml	50 µg/ml	50 µg/ml	5 µg/ml	50 µg/ml	50 µg/R	50 µg/R	10 µg/R	50 µg/R	10 µg/R	50 µg/R	10 µg/R	50 µg/R	10 µg/R	50 µg/R	10 µg/R	50 µg/R	10 µg/R	50 µg/R
TBBPA	DMSO	+++	+++	+++	+++	+++	+++	+++	+++	-	-	50%	-	-	-	-	-	-	-	-	-	-	-	-	-	-
	H <sub>2</sub> O	-	-	-	-	-	-	-	-	-	-	-	-	-	-	-	-	-	-	-	-	-	-	-	-	-
4	DMSO	-	-	-	-	-	-	-	-	-	-	-	-	-	-	-	-	-	-	-	-	-	-	-	-	-
	H <sub>2</sub> O	-	-	-	-	-	-	-	-	-	-	100%	-	-	-	-	-	-	-	-	-	-	-	-	-	-
1	DMSO	-	-	-	-	-	-	-	-	-	-	-	-	-	-	-	-	-	-	-	-	-	-	-	-	-
	H <sub>2</sub> O	-	-	-	-	-	-	-	-	-	-	25%	-	-	-	-	-	-	-	-	-	-	-	-	-	-
2	DMSO	-	-	-	-	-	-	-	-	-	-	-	-	-	-	-	-	-	-	-	-	-	-	-	-	-
	H <sub>2</sub> O	-	-	+	+	-	-	-	-	-	-	-	-	-	-	-	-	-	-	-	-	-	-	-	-	-
3	DMSO	-	-	-	+++	-	-	-	++	-	-	-	-	-	-	-	-	-	-	-	-	-	+	-	-	-
	H <sub>2</sub> O	-	+	+++	+++	-	-	+++	+++	-	-	75%	+/-	-	-	-	-	-	-	-	-	-	-	-	-	-



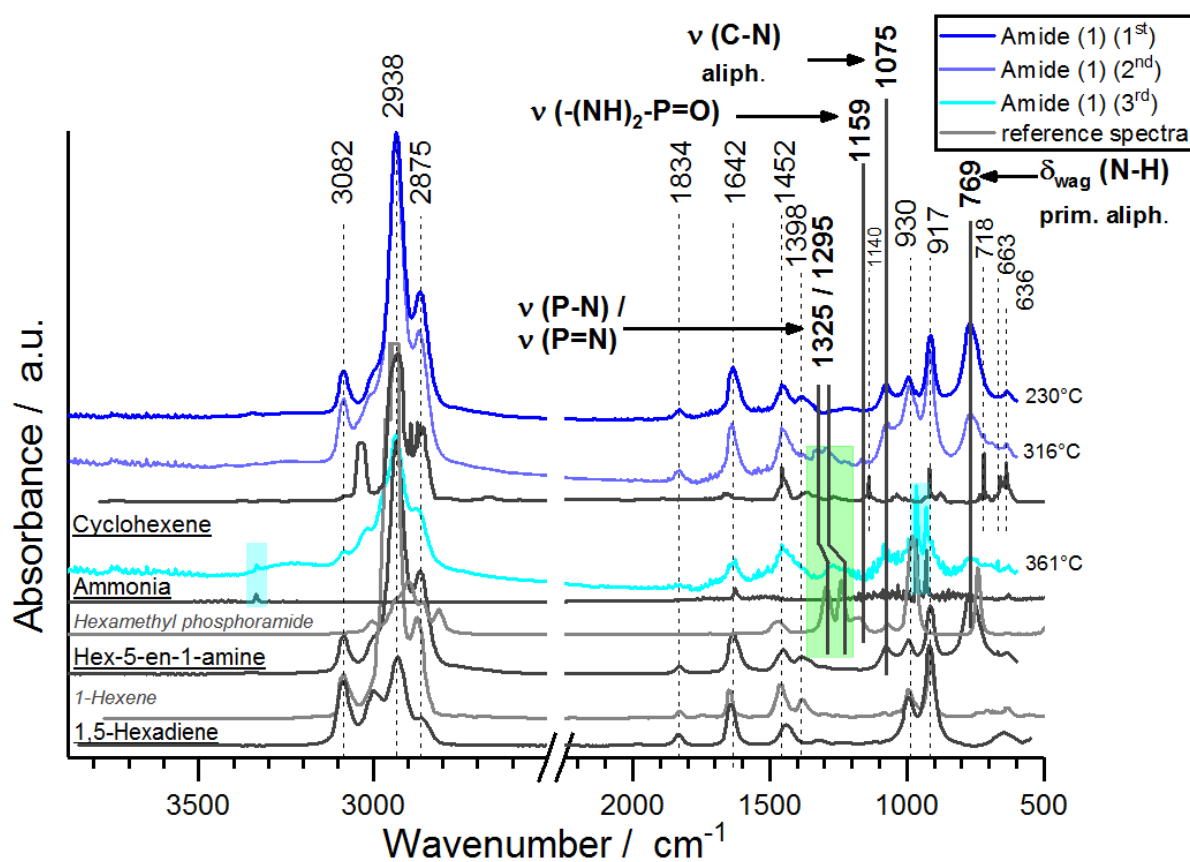
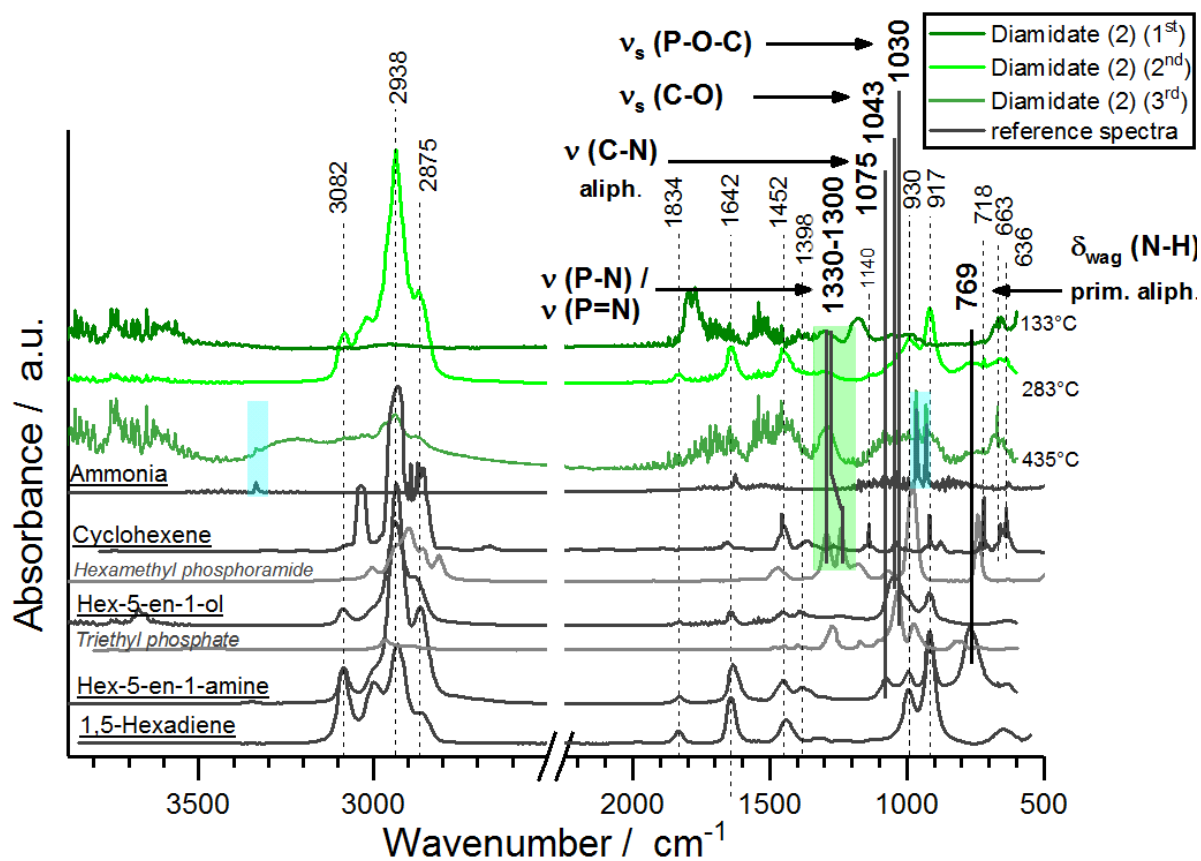


**Figure S18.** Pyrolysis products at  $T_{\max}$  of raw flame retardants and comparative spectra in N<sub>2</sub> via TG-FTIR. Heating rate: 10 K min<sup>-1</sup>.



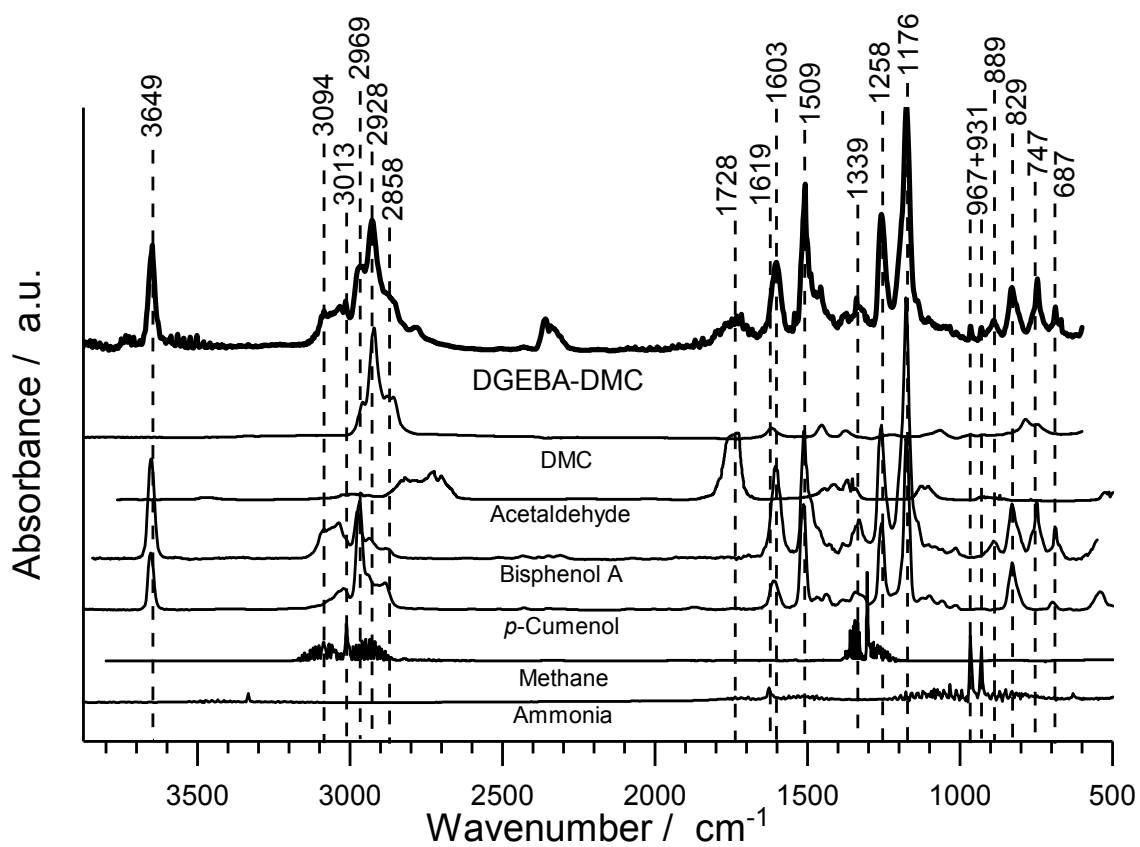


**Figure S19.** FTIR spectrum of pyrolysis products of EPR DGEBA-DMC at  $T_{\max}$  ( $T = 372^{\circ}\text{C}$ ,  $t = 34.4$  min). Below: comparative spectra, taken from NIST.

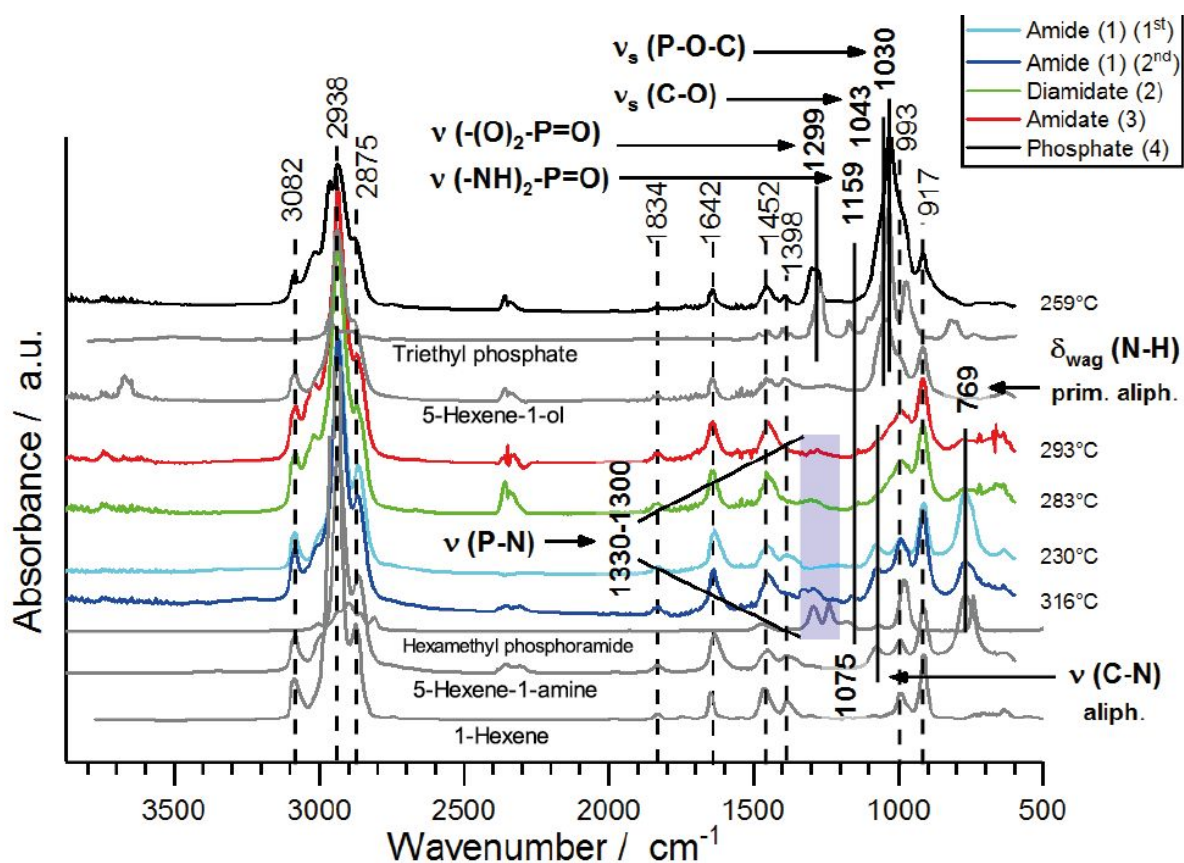


Figure S20. TG-FTIR spectra of the first decomposition step of flame retardants.

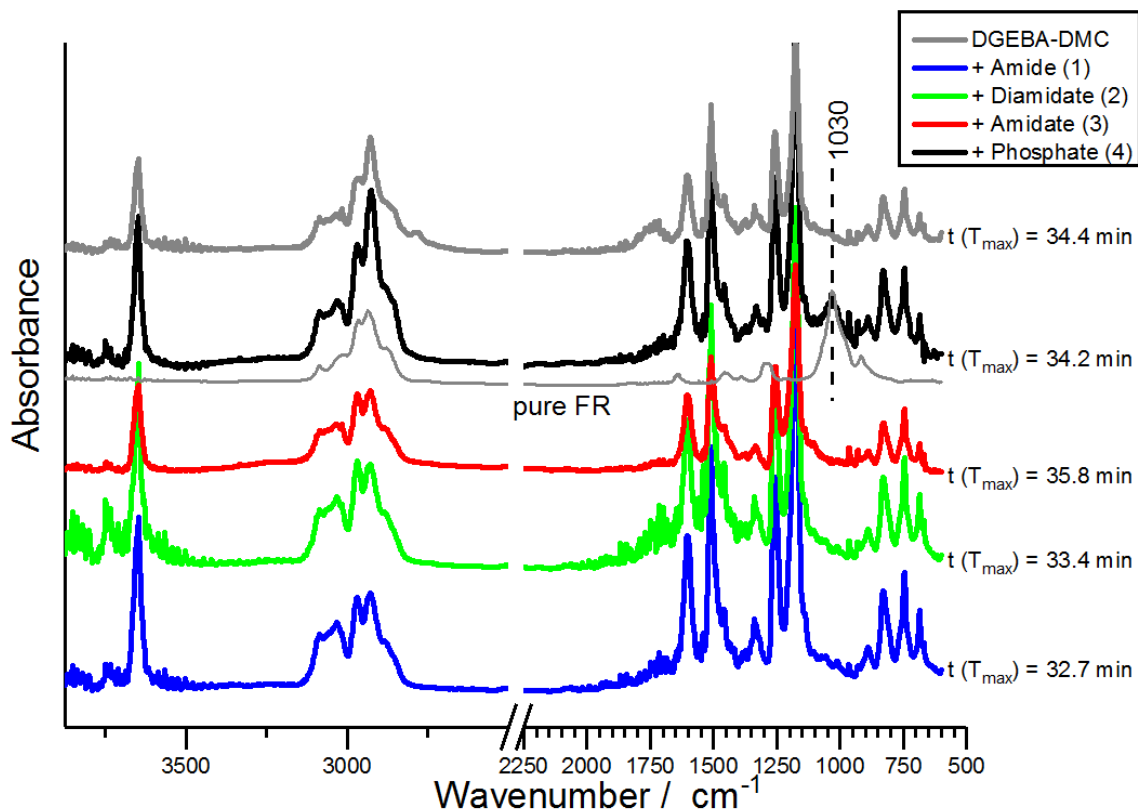
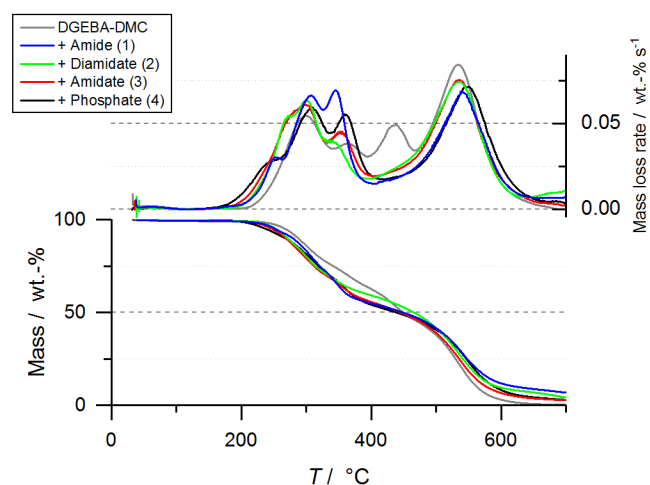
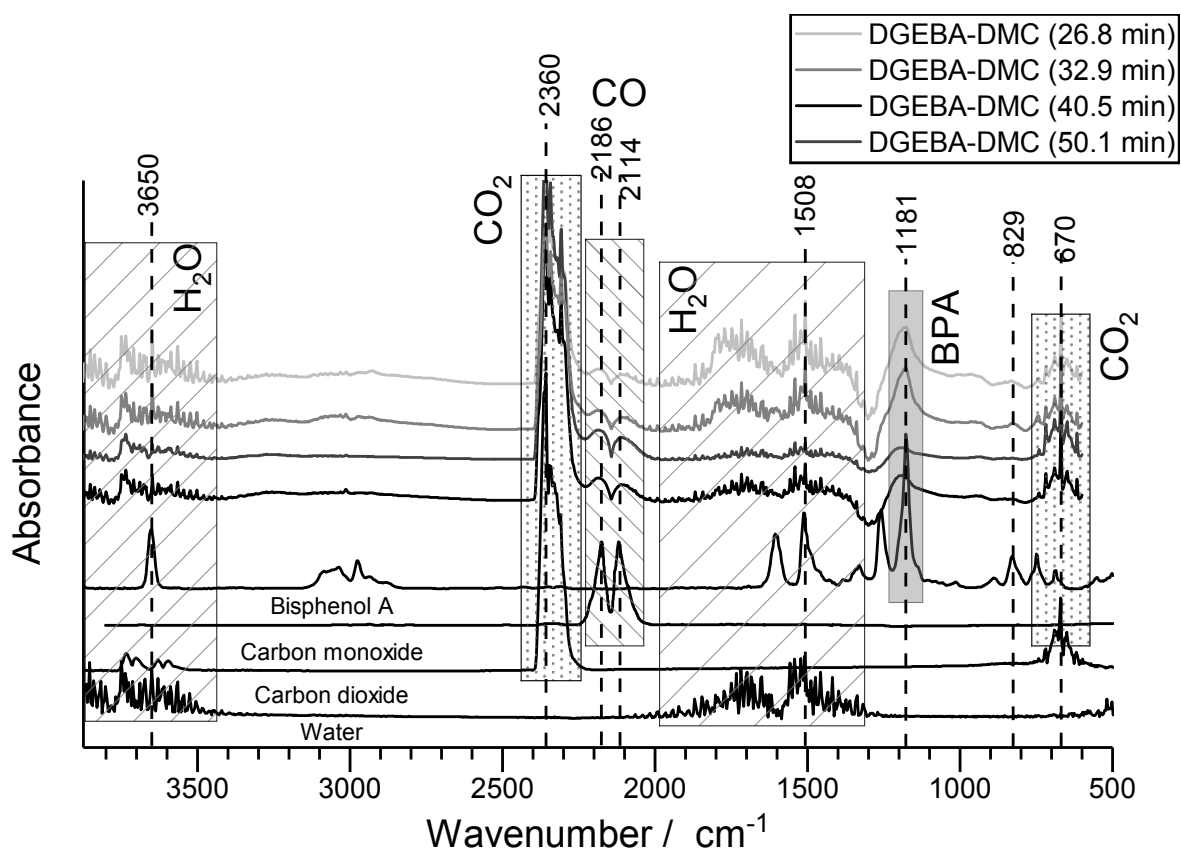


Figure S21. Main decomposition step of DGEBA-DMC + FRs.



**Figure S22.** Mass loss (bottom) and mass loss rate (top) curves of neat and flame retarded DGEBA-DMC epoxy resins in synthetic air (80:20) via TGA. Heating rate: 10 K min<sup>-1</sup>.



**Figure S23.** Decomposition products at decomposition steps of neat DGEBA-DMC epoxy resin and comparative spectra in synthetic air via TG-FTIR. Heating rate: 10 K min<sup>-1</sup>.

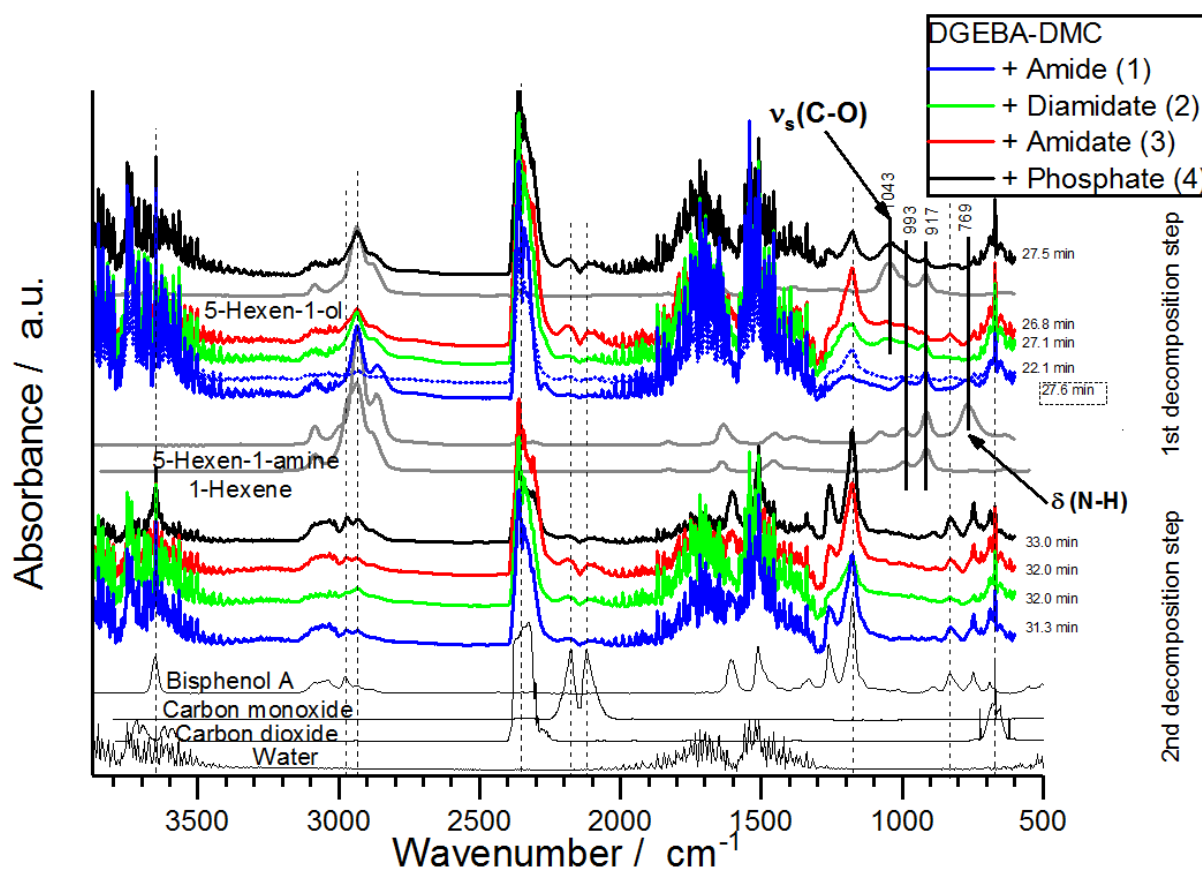


**Figure S24.** Decomposition products at decomposition steps of flame retarded DGEBA-DMC epoxy resin and comparative spectra in synthetic air via TG-FTIR. Heating rate: 10 K min<sup>-1</sup>

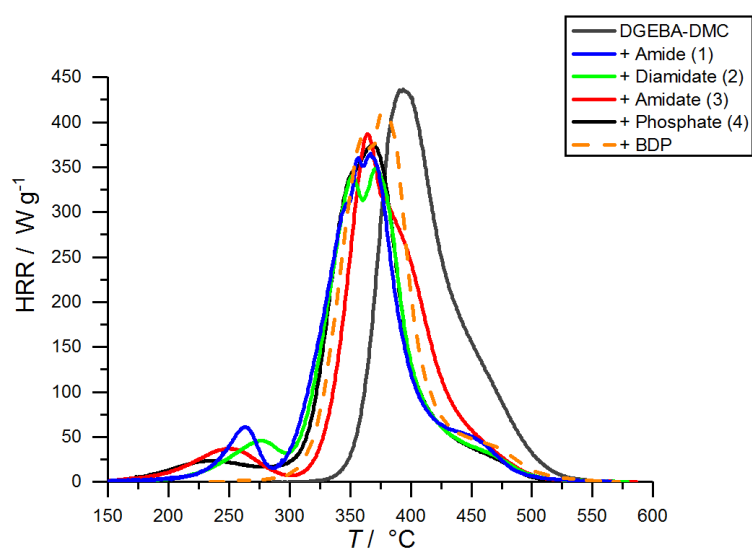


**Figure S25.** Heat release rate curves of neat and flame retarded DGEBA-DMC epoxy resins in N<sub>2</sub> via PCFC. Heating rate: 1 K s<sup>-1</sup>.

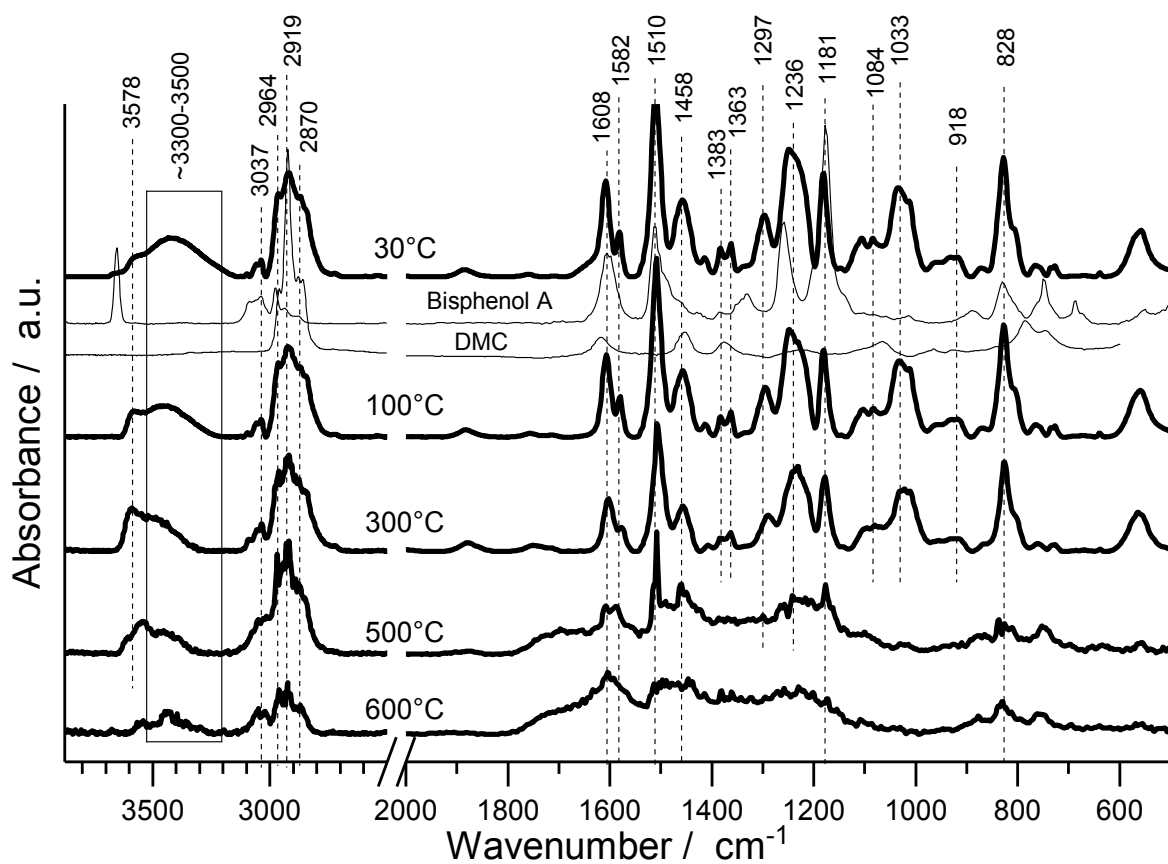


Figure S26. Hot stage FTIR spectra of condensed phase of DGEBA-DMC at 30-600 °C.

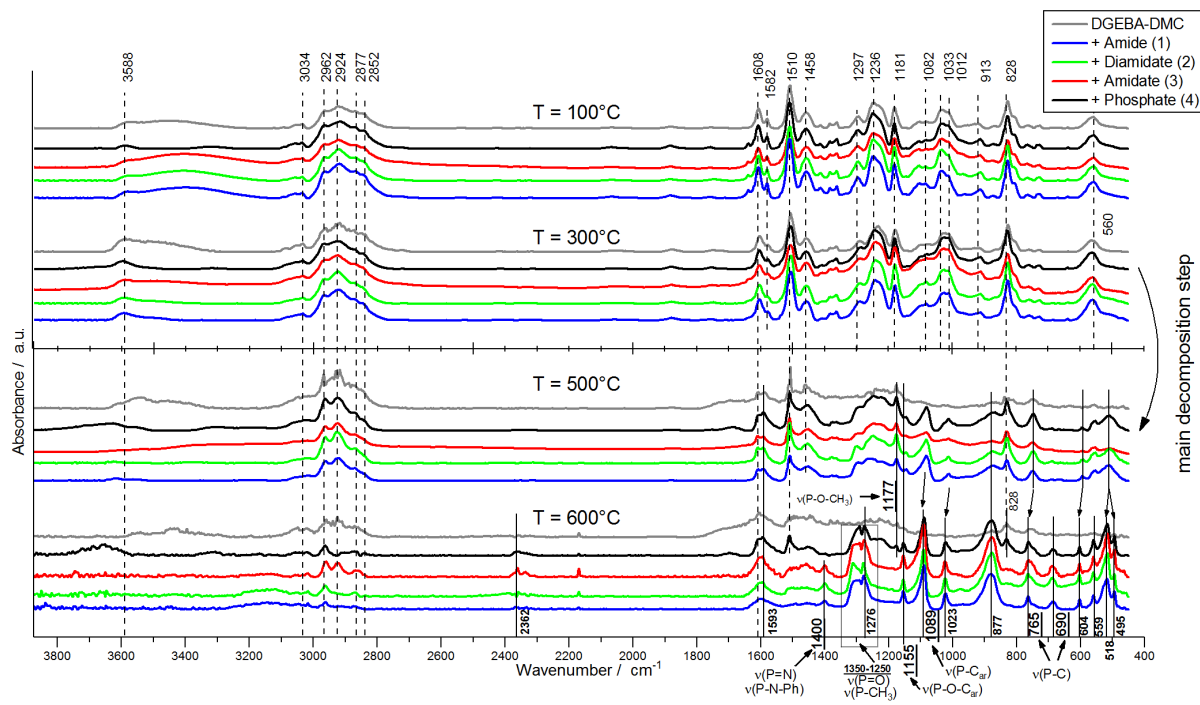
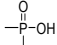
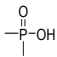


Figure S27. Linkam Hot stage FTIR shows clear P-based signals in all FR epoxy resins, but not in pure polymer.

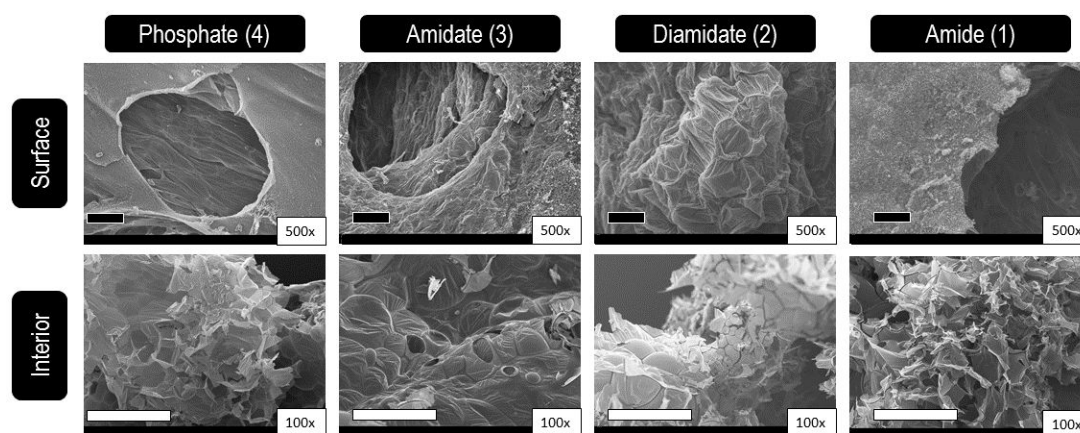
**Table S3.** Assignment of characteristic P bands observed in S29.

Group	Range Literature [cm <sup>-1</sup> ]	Measured [cm <sup>-1</sup> ]
P-H	2400 – 2350 <sup>a)</sup>	2362
P-CH <sub>3</sub> (asym)	1450 – 1395 <sup>b)</sup>	1400
P-CH <sub>2</sub> -R	1440 – 1400 <sup>b)</sup>	1400
P-Phenyl	1440 (s) <sup>a)</sup>	(1400)
P=O	1300 – 1250 <sup>a)</sup>	1276
P-CH <sub>3</sub> (sym)	1346 – 1255 <sup>b)</sup>	1276
	1240 – 1180 (P=O) <sup>a)</sup>	(1276), (1177), (1155)
P-O-Aryl	1240 – 1190 <sup>a)</sup>	(1177)
P-Phenyl	1130 – 1090 <sup>b)</sup>	1089
Phosphate (inorganic)	1100 – 1000 <sup>a)</sup>	1089, 1023
	1 OH: 1040 – 909 (P=O) <sup>b)</sup>	
	2 OH: 1030 – 972	1023
	950 – 917	
P-O-Alkyl	1050 – 1030 <sup>a)</sup>	1089, (1023)
P-O-P	970 – 910 (wide) <sup>a)</sup>	(~877)
	990 – 885	
P-H (wag)	interacts with C-O-P <sup>b)</sup>	~877
P-CH <sub>3</sub>	977 – 842 <sup>b)</sup>	~877
P-C	754 – 634 <sup>b)</sup>	(765), 690
C-C skeletal vibr. (Branched alkanes)	540 – 485 <sup>c)</sup>	518, 495

- a) M. Hesse, H. Meier, B. Zeeh; Spektroskopische Methoden in der organischen Chemie; 4. überarbeitete Auflage; Georg-Thiem Verlag Stuttgart- New York b) [https://faculty.missouri.edu/~glaserr/8160f10/A03\\_Silver.pdf](https://faculty.missouri.edu/~glaserr/8160f10/A03_Silver.pdf), c) George Socrates "Infrared and Raman Characteristic Group frequencies" John Wiley & Sons, 18.06.2004

**Table S4.** Summary of the data gained via cone calorimetry.

Material composition	DGEBA-DMC	+	+	+	+	+ BDP
		Phosphate (4)	Amidate (3)	Diamidate (2)	Amide (1)	
THR / MJ m <sup>-2</sup>	108.4 ± 2.6	78.1 ± 6.5	94.9 ± 2.7	93.1 ± 2.5	91.6 ± 1.2	87.5 ± 1.2
PHRR / kW m <sup>-2</sup>	1696 ± 180	885 ± 16	982 ± 14	889 ± 70	1832 ± 96	1180 ± 41
t <sub>ig</sub> / s	47 ± 1	39 ± 0	42 ± 1	39 ± 0	38 ± 2	42 ± 6
ML / wt.-%	99.3 ± 0.1	90.9 ± 0.1	92.4 ± 0.4	90.9 ± 2.5	91.6 ± 0.2	96.9 ± 0.2
Residue / wt.-%	0.7 ± 0.1	9.2 ± 0.1	7.6 ± 0.4	9.1 ± 2.6	8.4 ± 0.2	3.1 ± 0.2
EHC / MJ kg <sup>-1</sup>	26.9 ± 1.0	21.6 ± 1.8	25.6 ± 0.6	25.9 ± 1.1	25.3 ± 1.0	22.7 ± 0.2
χ / -	0.82 ± 0.02	0.65 ± 0.06	0.80 ± 0.02	0.82 ± 0.04	0.75 ± 0.03	0.69 ± 0.01
MARHE / kW m <sup>-2</sup>	732 ± 24	404 ± 20	481 ± 4	477 ± 1	630 ± 27	546 ± 12
FIGRA / kW m <sup>-2</sup> s <sup>-1</sup>	15.5 ± 2.3	9.0 ± 0.2	8.2 ± 0.6	8.0 ± 0.4	9.8 ± 0.7	11.0 ± 0.7
TSP / m <sup>-3</sup>	28.5 ± 1.1	24.4 ± 6.1	24.1 ± 1.5	29.8 ± 1.9	23.8 ± 0.1	23.8 ± 0.1

**Figure S28.** Morphology (top row: surface; bottom row: interior) of flame retarded DGEBA-DMC epoxy resin residues via SEM; black bar is equal to 100 μm, white bar is equal to 1 mm.



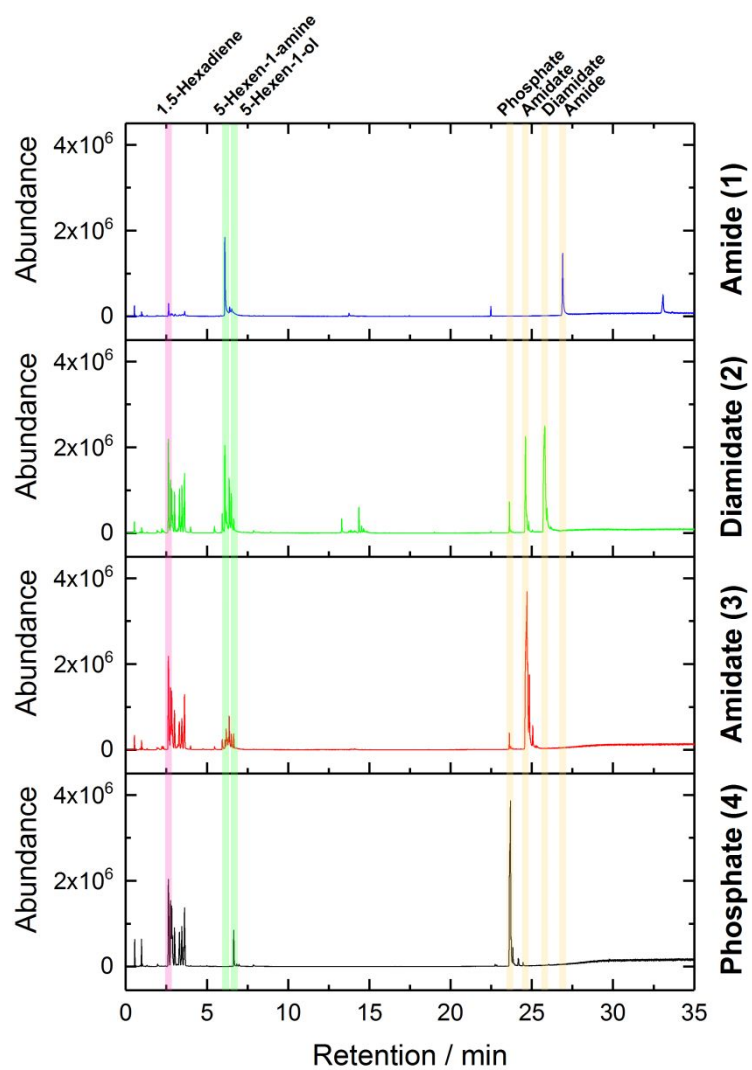


**Figure S29.** Total ion chromatogram of pyrolysis GC MS of the monomeric FRs. Relevant compounds are highlighted and were assigned using NIST14 MS library and GC MS reference spectra of the neat FRs.

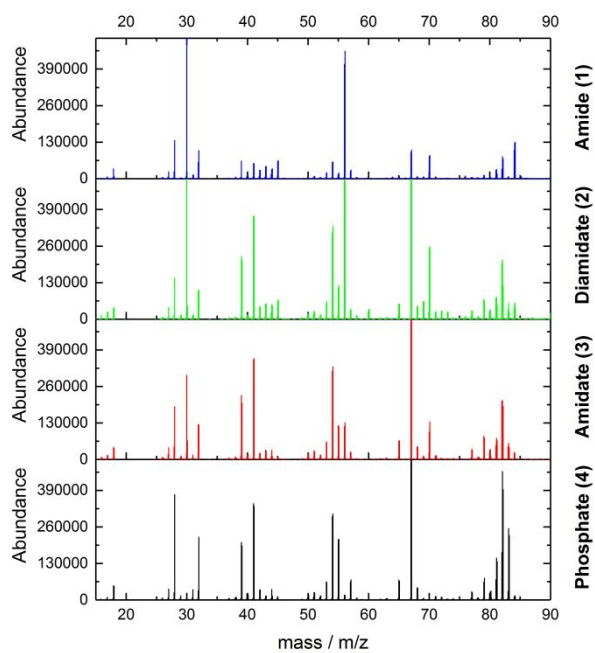


**Figure S30.** Section 1 (red) at 2.63 min in the pyrolysis GC MS total ion chromatogram was assigned to 1,5-hexadiene.

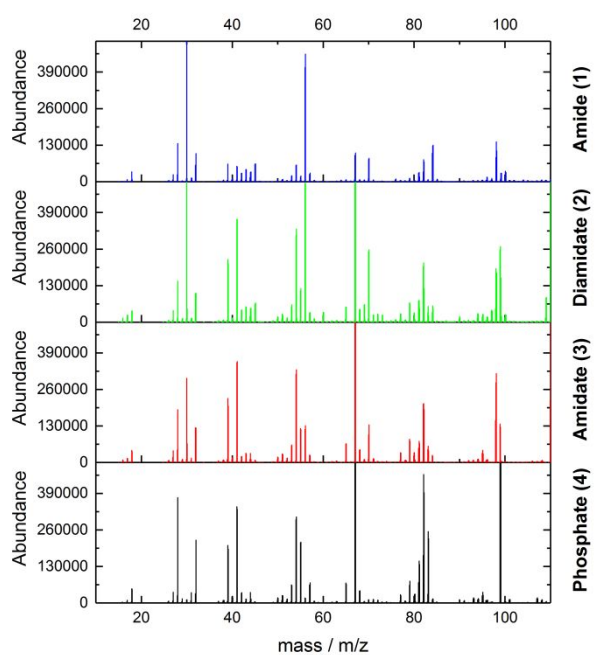


**Figure S31.** Section 2 (green) at 6.1 min in the pyrolysis GC MS total ion chromatogram was assigned to 5-hexen-1-amine.

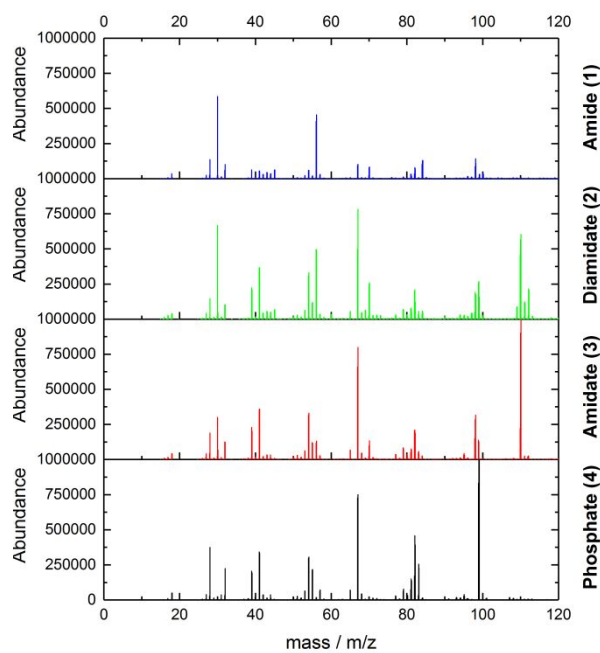


**Figure S32.** Section 3 (green) at 6.7 min in the pyrolysis GC MS total ion chromatogram was assigned to 5-hexen-1-ol.

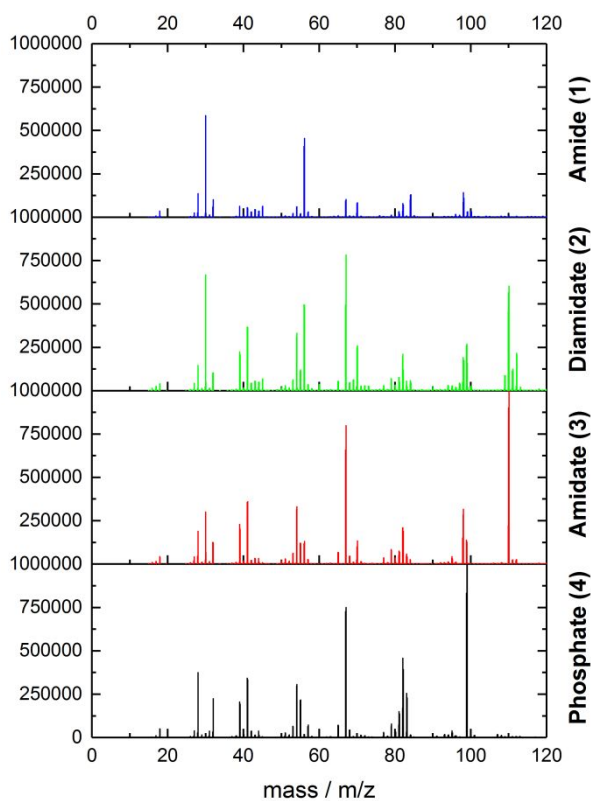


**Figure S33.** Section 4 (orange) at 23.7 min in the pyrolysis GC MS total ion chromatogram was assigned to 4.

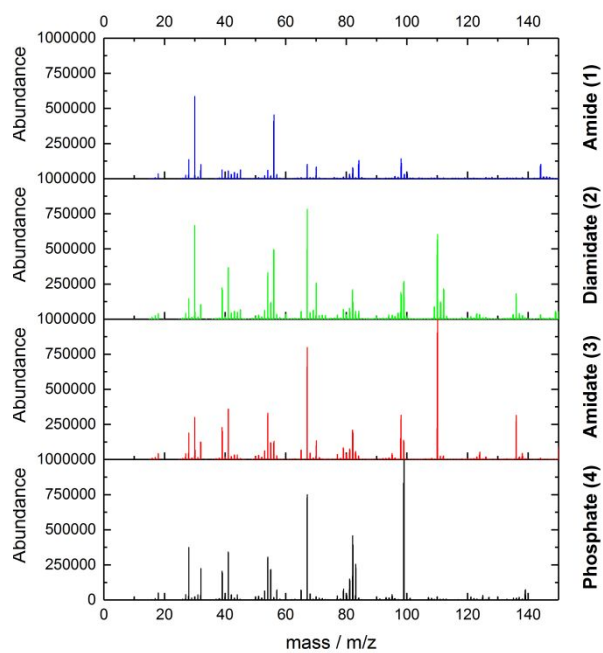


**Figure S34.** Section 5 (orange) at 24.6 min in the pyrolysis GC MS total ion chromatogram was assigned to **3**.

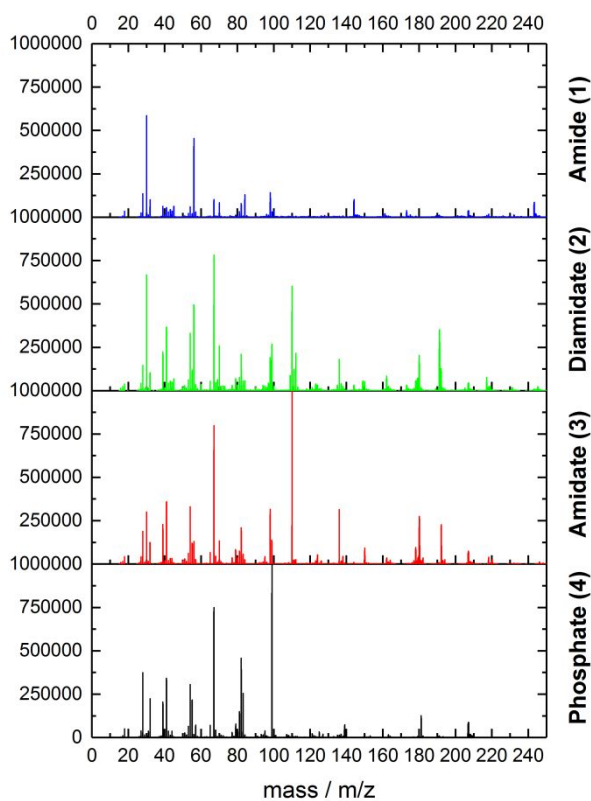


**Figure S35.** Section 6 (orange) at 25.8 min in the pyrolysis GC MS total ion chromatogram was assigned to **2**.

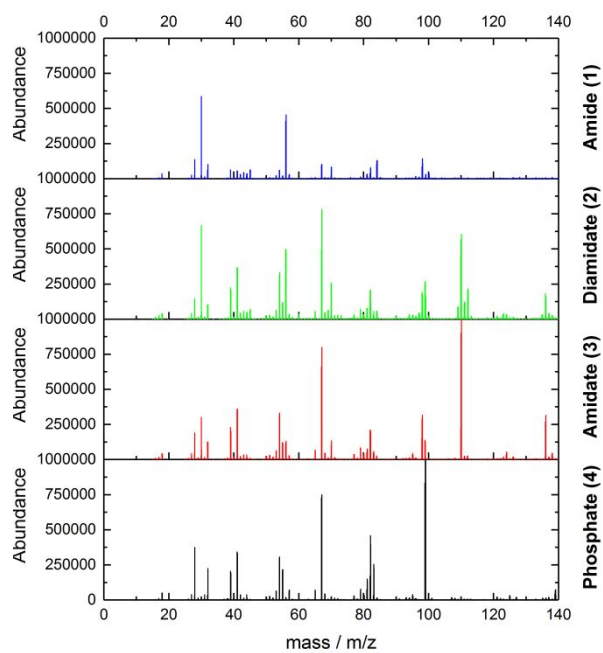


**Figure S36.** Section 7 (orange) at 26.9 min in the pyrolysis GC MS total ion chromatogram was assigned to **1**.

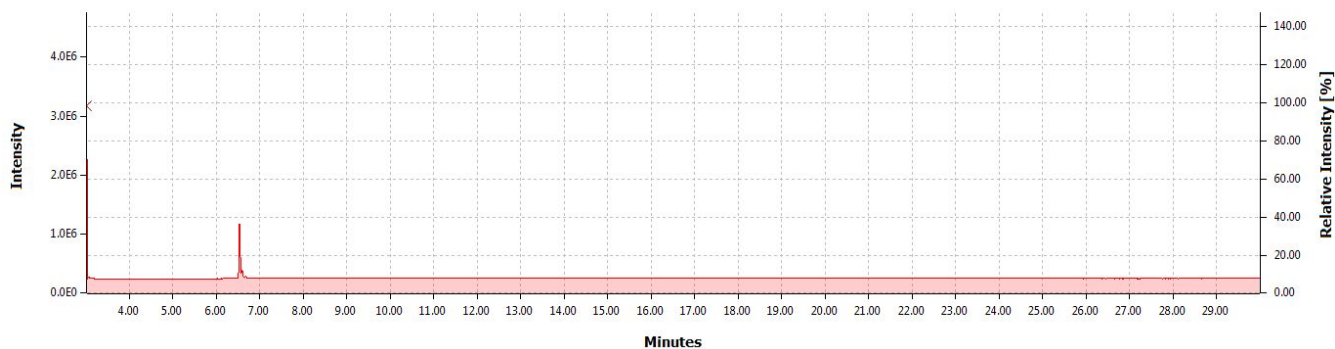


**Figure S37.** Total ion chromatogram of GC MS of **4**.

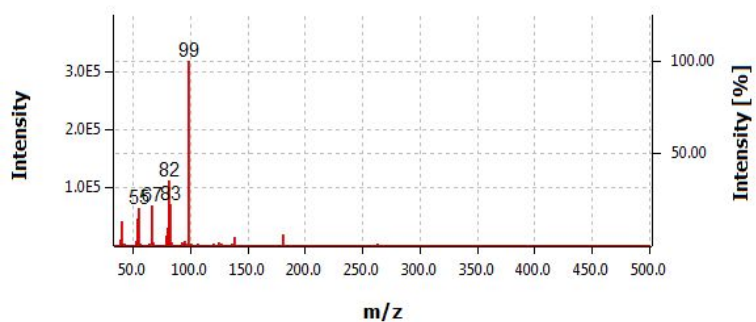


**Figure S38.** Mass spectrum of **4** at 6.53 min.

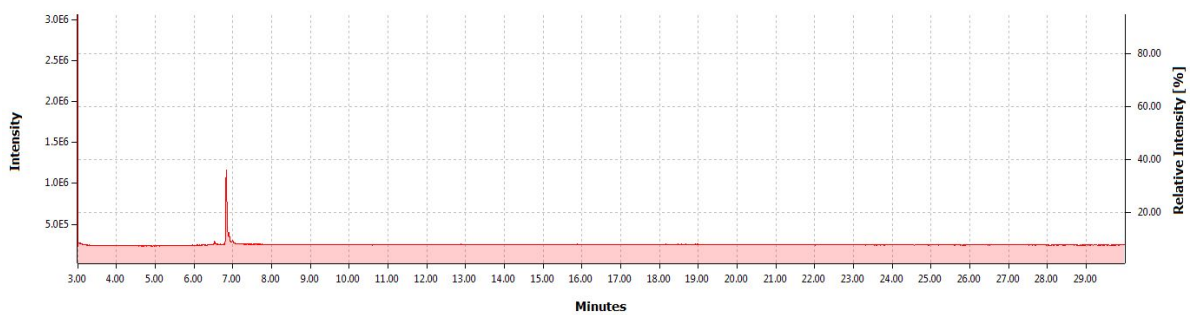


Figure S39. Total ion chromatogram of GC MS of **3**.

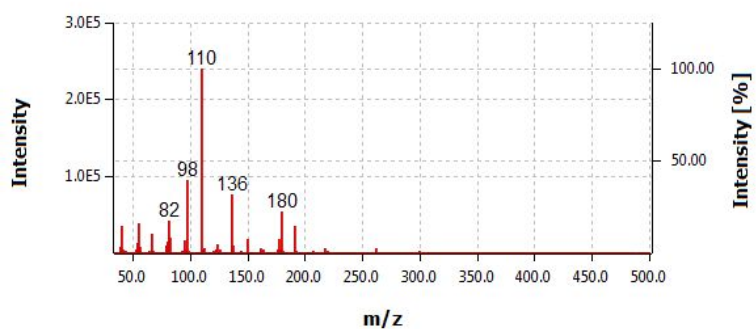


Figure S40. Mass spectrum of **3** at 6.83 min.



Figure S41. Total ion chromatogram of GC MS of **2**.

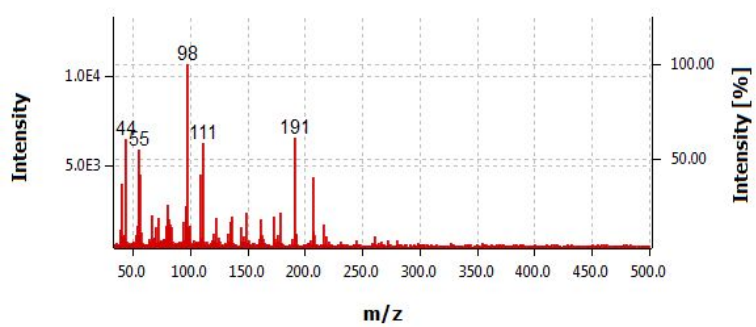
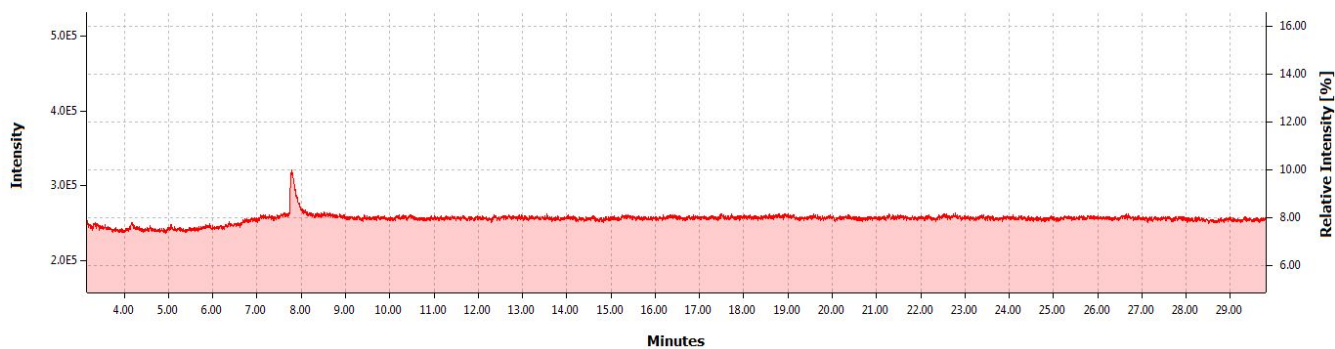
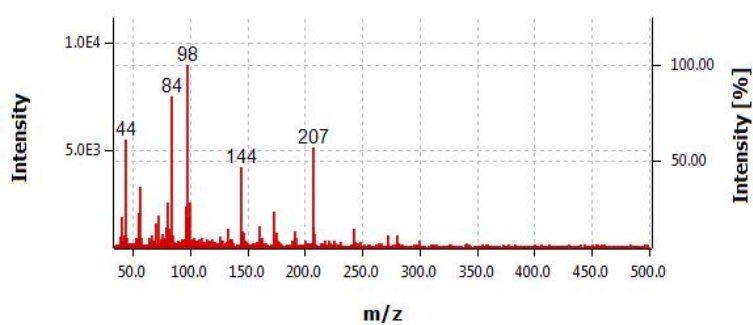


Figure S42. Mass spectrum of **2** at 7.25 min.



**Figure S43.** Total ion chromatogram of GC MS of **1**.



**Figure S44.** Mass spectrum of **1** at 7.78 min.

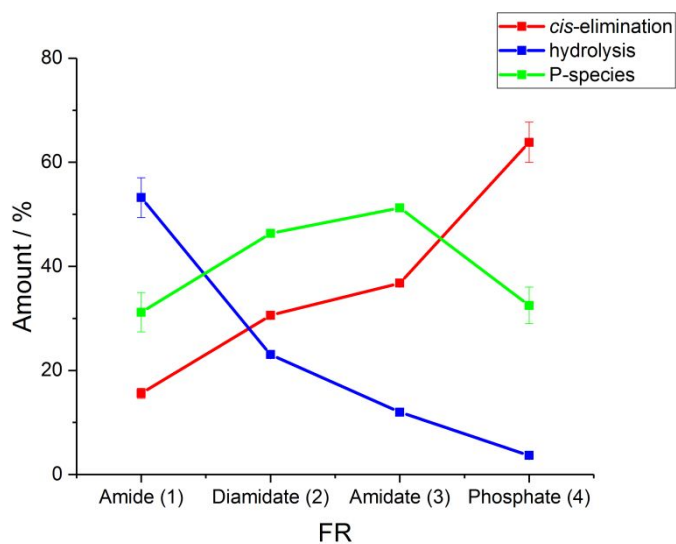


**Figure S45.** Relative amount of *cis*-elimination, hydrolysis and P-species in the released gases during pyrolysis GC-MS.



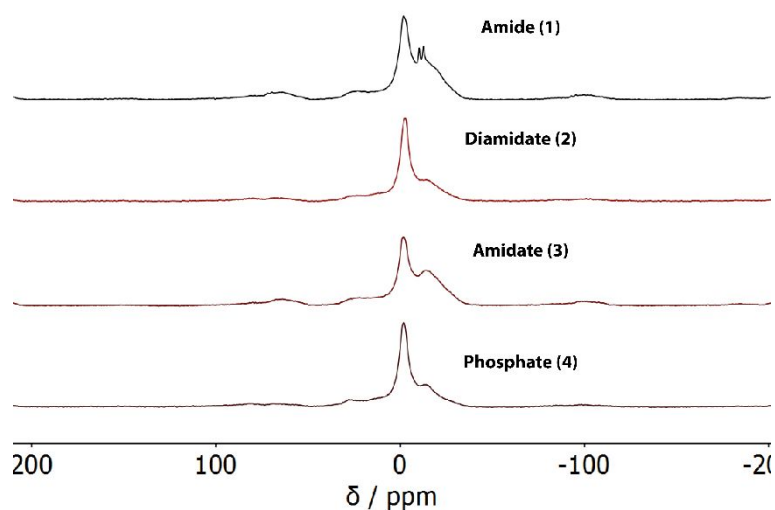


**Figure S46.**  $^{31}\text{P}$  CP/MAS solid state NMR (10 kHz) of the char residue after cone calorimeter test.

## References

1. Escher, B. I.; Bramaz, N.; Mueller, J. F.; Quayle, P.; Rutishauser, S.; Vermeirssen, E. L. M., Toxic equivalent concentrations (TEQs) for baseline toxicity and specific modes of action as a tool to improve interpretation of ecotoxicity testing of environmental samples. *J. Environ. Monit.* **2008**, *10*, 612-621.
2. Völker, J.; Vogt, T.; Castronovo, S.; Wick, A.; Ternes, T. A.; Joss, A.; Oehlmann, J.; Wagner, M., Extended anaerobic conditions in the biological wastewater treatment: Higher reduction of toxicity compared to target organic micropollutants. *Water Res.* **2017**, *116*, 220-230.
3. Routledge, E. J.; Sumpter, J. P., Estrogenic activity of surfactants and some of their degradation products assessed using a recombinant yeast screen. **1996**, *15*, 241-248.
4. Sohoni, P.; Sumpter, J. P. J. T. J. o. e., Several environmental oestrogens are also anti-androgens. **1998**, *158* 3, 327-39.
5. Wagner, M.; Oehlmann, J. J. E. S.; Research, P., Endocrine disruptors in bottled mineral water: total estrogenic burden and migration from plastic bottles. **2009**, *16*, 278-286.
6. Völker, J.; Castronovo, S.; Wick, A.; Ternes, T. A.; Joss, A.; Oehlmann, J.; Wagner, M., Advancing Biological Wastewater Treatment: Extended Anaerobic Conditions Enhance the Removal of Endocrine and Dioxin-like Activities. *Environmental Science & Technology* **2016**, *50*, 10606-10615.
7. Odenbach, D.; Breth, B.; Thines, E.; Weber, R. W. S.; Anke, H.; Foster, A. J., The transcription factor Con7p is a central regulator of infection-related morphogenesis in the rice blast fungus *Magnaporthe grisea*. **2007**, *64*, 293-307.
8. Schüffler, A.; Kautz, D.; Liermann, J. C.; Opatz, T.; Anke, T., Allantofuranone, a new antifungal antibiotic from *Allantophomopsis lycopodina* IBWF58B-05A. *The Journal Of Antibiotics* **2009**, *62*, 119.
9. Talbot, N. J.; Ebbolle, D. J.; Hamer, J. E., Identification and characterization of MPG1, a gene involved in pathogenicity from the rice blast fungus *Magnaporthe grisea*. **1993**, *5*, 1575-1590.
10. Schüffler, A.; Liermann, J. C.; Kolshorn, H.; Opatz, T.; Anke, H., Isolation, structure elucidation, and biological evaluation of the unusual heterodimer chrysoxanthone from the ascomycete IBWF11-95A. *Tetrahedron Lett.* **2009**, *50*, 4813-4815.

11. Anke, H.; Bergendorff, O.; Sterner, O., Assays of the biological activities of guaiane sesquiterpenoids isolated from the fruit bodies of edible lactarius species. *Food Chem. Toxicol.* **1989**, *27*, 393-397.
12. Talontsi, F. M.; Facey, P.; Tatong, M. D. K.; Tofazzal Islam, M.; Frauendorf, H.; Draeger, S.; Tiedemann, A. v.; Laatsch, H., Zoosporicidal metabolites from an endophytic fungus *Cryptosporiopsis* sp. of *Zanthoxylum leprieurii*. *Phytochemistry* **2012**, *83*, 87-94.
13. Li, G.; Kusari, S.; Lamshöft, M.; Schöffler, A.; Laatsch, H.; Spiteller, M., Antibacterial Secondary Metabolites from an Endophytic Fungus, *Eupenicillium* sp. LG41. *J. Nat. Prod.* **2014**, *77*, 2335-2341.
14. Kettering, M.; Valdivia, C.; Sterner, O.; Anke, H.; Thines, E., Heptemerones A~G, Seven Novel Diterpenoids from *Coprinus heptemerus*: Producing Organism, Fermentation, Isolation and Biological Activities. *The Journal Of Antibiotics* **2005**, *58*, 390.
15. Schoettler, S.; Bascope, M.; Sterner, O.; Anke, T., Isolation and Characterization of Two Verrucarins from *Myrothecium roridum*. In *Zeitschrift für Naturforschung C*, 2006; Vol. 61, p 309.
16. Stärk, A.; Anke, T., Omphalone, an Antibiotically Active Benzoquinone Derivative from Fermentations of *Lentinellus omphalodes* [1]. In *Zeitschrift für Naturforschung C*, 1991; Vol. 46, p 989.
17. Van der Ven, L. T. M.; Van de Kuil, T.; Verhoef, A.; Verwer, C. M.; Lilienthal, H.; Leonards, P. E. G.; Schauer, U. M. D.; Cantón, R. F.; Litens, S.; De Jong, F. H.; Visser, T. J.; Dekant, W.; Stern, N.; Håkansson, H.; Slob, W.; Van den Berg, M.; Vos, J. G.; Piersma, A. H., Endocrine effects of tetrabromobisphenol-A (TBBPA) in Wistar rats as tested in a one-generation reproduction study and a subacute toxicity study. *Toxicology* **2008**, *245*, 76-89.
18. Kefeni, K. K.; Okonkwo, J. O.; Olukunle, O. I.; Botha, B. M., Brominated flame retardants: sources, distribution, exposure pathways, and toxicity. *Environmental Reviews* **2011**, *19*, 238-253.
19. Yang, J.; Chan, K. M., Evaluation of the toxic effects of brominated compounds (BDE-47, 99, 209, TBBPA) and bisphenol A (BPA) using a zebrafish liver cell line, ZFL. *Aquat. Toxicol.* **2015**, *159*, 138-147.
20. Eljarrat, E.; Barceló, D., *Brominated Flame Retardants*. Springer Berlin Heidelberg: 2011.
21. Sun, F.; Kolvenbach, B. A.; Nastold, P.; Jiang, B.; Ji, R.; Corvini, P. F.-X., Degradation and Metabolism of Tetrabromobisphenol A (TBBPA) in Submerged Soil and Soil-Plant Systems. *Environmental Science & Technology* **2014**, *48*, 14291-14299.

### 5.3. Hyperbranched phosphorus flame retardants: multifunctional additives for epoxy resins

Alexander Battig, Jens C. Markwart, Frederik R. Wurm, Bernhard ScharTEL, *RSC Polym. Chem.*, **2019**, 10, 4346-4358. - Published by The Royal Society of Chemistry

DOI link: <https://www.doi.org/10.1039/c9py00737g>

This article was accepted and published.

#### Author contribution:

- Conceptualizing the frame of the work
- Chose the polymer materials, approach, loading, sample preparation and testing
- Pyrolytic investigations of the flame retardants (FRs)
  - Thermogravimetric analysis
  - Evolved gas and condensed phase FTIR
  - Pyrolysis gas chromatography / mass spectrometry
  - Pyrolysis combustion flow calorimeter
- Material and fire testing of FR-containing epoxy resins
  - Differential scanning calorimeter
  - Cone calorimeter, LOI and UL-94
  - Scanning electron microscopy, photography
- Collection, analysis, and interpretation of the data.
- Provided figures throughout the article, including decomposition mechanism
- Scientific discussion, conclusions, and writing the manuscript
- Proofread and spell-checked all versions of the article

## Abstract

We successfully synthesized multifunctional P-based hyperbranched polymeric flame retardants (*hb*-FRs) with varying oxygen-to-nitrogen (O : N) content and characterized them via  $^1\text{H}$  and  $^{31}\text{P}$  NMR and GPC. Their miscibility in epoxy resins (EP) and impact on glass-transition temperatures ( $T_g$ ) were determined *via* differential scanning calorimetry (DSC). Using thermogravimetric and evolved gas analysis (TGA, TG-FTIR), pyrolysis gas chromatography/mass spectrometry (Py-GC-MS), hot stage FTIR, flammability tests UL-94 and LOI, fire testing *via* cone calorimetry, residue analysis *via* scanning electron microscopy (SEM) and elemental analysis, detailed decomposition mechanisms and modes of action are proposed. *hb*-polymeric FRs have improved miscibility and thermal stability, leading to high FR performance even at low loadings. Polymeric, complex FRs increase flame retardancy, mitigate negative effects of low molecular weight variants, and can compete with commercial aromatic FRs. The results illustrate the role played by the chemical structure in flame retardancy and highlight the potential of *hb*-FRs as multifunctional additives.



Cite this: *Polym. Chem.*, 2019, **10**, 4346

## Hyperbranched phosphorus flame retardants: multifunctional additives for epoxy resins†

Alexander Battig,<sup>†</sup> Jens C. Markwart,<sup>‡</sup> Frederik R. Wurm<sup>\*,b</sup> and Bernhard Schartel<sup>\*,a</sup>

We successfully synthesized multifunctional P-based hyperbranched polymeric flame retardants (*hb*-FRs) with varying oxygen-to-nitrogen (O : N) content and characterized them *via* <sup>1</sup>H and <sup>31</sup>P NMR and GPC. Their miscibility in epoxy resins (EP) and impact on glass-transition temperatures (*T*<sub>g</sub>) were determined *via* differential scanning calorimetry (DSC). Using thermogravimetric and evolved gas analysis (TGA, TG-FTIR), pyrolysis gas chromatography/mass spectrometry (Py-GC-MS), hot stage FTIR, flammability tests UL-94 and LOI, fire testing *via* cone calorimetry, residue analysis *via* scanning electron microscopy (SEM) and elemental analysis, detailed decomposition mechanisms and modes of action are proposed. *hb*-polymeric FRs have improved miscibility and thermal stability, leading to high FR performance even at low loadings. Polymeric, complex FRs increase flame retardancy, mitigate negative effects of low molecular weight variants, and can compete with commercial aromatic FRs. The results illustrate the role played by the chemical structure in flame retardancy and highlight the potential of *hb*-FRs as multifunctional additives.

Received 21st May 2019,  
Accepted 2nd July 2019

DOI: 10.1039/c9py00737g

rs.c.li/polymers

### Introduction

Polymeric materials are pervasive throughout almost all aspects of modern life. Their tunable properties promote a wide range of applications, from packaging, transport, and construction to consumer electronics, automotive, and aeronautics. In particular, high-performance polymers are increasingly used to reduce weight and improve fuel efficiency in aviation and automobiles, and their material properties are paramount to their effective use. However, plastics are intrinsically flammable and carry a large fire load, consequently prompting the use and continued research into flame retardants (FRs). Due to environmental and toxicological concerns,<sup>1</sup> efforts into

developing halogen-free alternatives to improve safety and reduce risks have led to the formulation of effective phosphorus-based FRs (P-FRs).<sup>2–5</sup>

Moreover, there exists a trend towards polymeric FRs, as the blooming out or leaching of low molar mass FRs is undesirable in consumer products.<sup>6</sup> Low molar mass FRs usually possess low thermal stability, thus limiting their processability. Furthermore, the overlap between the decomposition temperatures of the FR and matrix is crucial to achieving good performance.<sup>7,8</sup> In comparison, oligomeric or polymeric FRs are more effective due to their increased thermal stability which leads to improved chemical interactions during decomposition, yielding higher char yields and better overall flame retardancy.<sup>9,10</sup> In addition, FRs with novel architectures have been investigated, highlighting the impact of the complex chemical structure on the mechanical properties and glass-transition temperature (*T*<sub>g</sub>) of the polymer matrix.

One group of polymers which has the potential to merge the approaches of utilizing high molar mass and complex molecular architecture is hyperbranched (*hb*) polymers. *hb* polymers are a group of specialized macromolecules that exhibit a high branching density and are more easily synthesized *via* a one-pot synthesis than other complex polymers.<sup>11,12</sup> A wide array of synthesis routes and applications has been extensively investigated.<sup>13–15</sup>

Due to their unique characteristics, these complex macromolecules have found use in the biomedical field,<sup>16–18</sup> and recently, they have been proposed as FRs for polymers.<sup>19–21</sup> *hb*

<sup>a</sup>Bundesanstalt für Materialforschung und -prüfung (BAM), Unter den Eichen 87, 12205 Berlin, Germany. E-mail: bernhard.schartel@bam.de

<sup>b</sup>Max Planck Institute for Polymer Research, Ackermannweg 10, 55128 Mainz, Germany. E-mail: wurm@mpip-mainz.mpg.de

<sup>c</sup>Graduate School Materials Science in Mainz, Staudinger Weg 9, 55128 Mainz, Germany

† Electronic supplementary information (ESI) available: NMR spectra (Fig. S1–S7); polymerization study (Table S1); DSC results (Table S2); TGA results of *hb*-FRs (Table S3); hydrolysis decomposition (Scheme S1); elimination decomposition (Scheme S2); inter- and intramolecular decomposition (Scheme S3); sulfur decomposition (Scheme S4); mass spectra of Py-GC-MS (Fig. S8–15); surface etching (Fig. S16); DSC (Fig. S17 and 18); TGA results of EP-*hb*-FRs (Table S4); condensed phase FTIR (Fig. S19 and Table S5); LOI & UL-94 measurements (Table S6); MARHE & FIGRA of cone calorimeter (Table S7); CO-yields (Fig. S20 and Table S8); residue analysis (Fig. S21). See DOI: 10.1039/c9py00737g

‡ These authors contributed equally.

flame retardants (*hb*-FRs) combine the potential of polymeric FRs with the advantages of complex geometries.<sup>22,23</sup> Their high molar mass and complex architecture lead to high solubility and miscibility with other materials.<sup>24</sup> Chiefly among *hb*-FRs, *hb*-polyphosphoesters have been recently proposed as effective FRs,<sup>25</sup> also in epoxy resins (EP).<sup>26</sup> Additionally, phosphorus (P) and nitrogen (N) containing *hb*-FRs have been investigated,<sup>27,28</sup> as the synergistic qualities of P–N compounds have been widely discussed.<sup>29,30</sup>

In a recent study, we have investigated the flame retardancy effect of P-FRs by systematically varying the structure, namely phosphates, phosphoramidates, phosphorodiamidates, and phosphoramides, and have proven the differences in the decomposition mechanism and mode of action.<sup>31</sup>

In this article, we synthesized *hb*-FRs from the previously investigated corresponding monomeric FRs by a radical  $A_2 + B_3$  thiol–ene polyaddition (Scheme 1) and investigated their decomposition mechanism. The aim is to compare the FR potential of *hb*-FRs with varying P–O and P–N contents, and the high molar mass variants are compared to their monomers in terms of flame retardancy mechanisms, mode of action, and efficacy in epoxy resins. The  $A_2 + B_3$  strategy was chosen due to its ease of synthesis and potential for up-scaling.<sup>32,33</sup> As P–O and P–N-bonds possess different stabilities and degradation pathways, an optimized FR performance can be obtained by a precise synthesis of P-FRs.<sup>31</sup>

However, the polymerization process alters the end-group functionality and may affect gas-phase activity. It is unclear which flame-retardant affects the *hb* polymeric variants of previously investigated P-FRs. Moreover, the role of complex molecular architecture in the FR's chemical mechanism remains unclear. With this study, investigating the decomposition pathway of distinctively different *hb*-FRs and their mode of action in EP becomes possible, allowing for a deeper understanding of these multifunctional additives as effective FRs for high-performance polymers. Crucially, the material properties of epoxy resins must be conserved, and by comparing these aliphatic *hb*-FRs to a state-of-the-art, commercially available benchmark FR, their performance can be more accurately estimated. While there have been many reports on P-FR formulations for epoxy resins,<sup>34</sup> of which some studied one type of

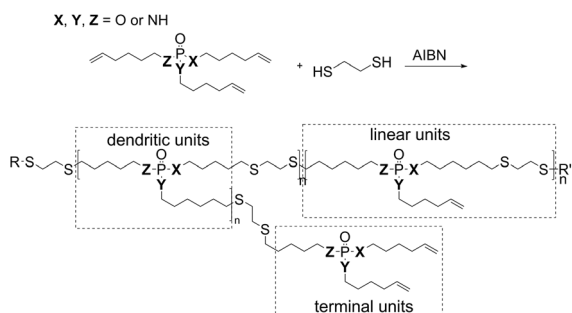
*hb*-FR,<sup>35,36</sup> this study aims at investigating four high-molar mass *hb* P-FRs with systematically varying P–O and P–N contents which are able to retain the material properties of DGEBA-based EP. The results of material and flame retardancy studies aid in optimizing future design of P-FRs.

## Results and discussion

### Hyperbranched flame retardants (*hb*-FRs)

**Chemical synthesis and structure identification.** The influence of the P–O vs. P–N ratio on the FR efficiency of low molecular weight P-FRs has been studied recently.<sup>38</sup> To explore the influence of polymeric materials in comparison with monomeric materials, we extended this systematic library with the respective *hb*-polymers. *hb*-Polyphosphoramidate (1), *hb*-polyphosphorodiamidate (2), *hb*-polyphosphoramidate (3), and *hb*-polyphosphate (4) were synthesized starting from the respective  $B_3$ -monomers in a radical thiol–ene polyaddition using 1,2-ethanedithiol as an  $A_2$ -comonomer and AIBN followed by precipitation into *n*-hexane or toluene (Scheme 1). The successful  $A_2 + B_3$  polymerization was indicated by a reduction in the double-bond resonances in the  $^1\text{H}$  NMR spectra and the detection of a new singlet at 2.71 ppm and a triplet at 2.55 ppm (see the ESI†). By these procedures, all P-FRs were easily available up to at least 80 g with standard university lab equipment. Fig. S1–S3† show the  $^1\text{H}$  NMR spectra of the *hb*-polymers with varying oxygen-to-nitrogen (O : N) ratios. The spectrum of the monomeric phosphate in Fig. 1a highlights the change from the monomeric to polymeric structure. Here, the appearance of a  $\text{CH}_2$  group (triplet) at 2.55 ppm signified a successful polymerization, as it corresponds to the methylene group adjacent to the thioether. The singlet at 2.71 ppm belongs to the two methylene groups between the two thioether linkages. The signals from 1.70 to 1.38 ppm were attributed to the methylene groups of the alkyl chain. Fig. S4–S7† show the  $^{31}\text{P}$  {H} NMR spectra of the hyperbranched polymers with varying O : N ratios. The resonance of the P-atom shifted depending on its chemical surroundings to lower field with increasing nitrogen content surrounding P (from 17.13 ppm for 1 to  $-0.66$  ppm for 4).

As an  $A_2 + B_3$  polymerization can produce both cross-linked and soluble *hb*-polymers,<sup>24</sup> depending on the polymerization conditions and monomer feed ratios, we optimized the polymerization conditions using 4 as an example. Table S1† summarizes the conditions which were varied to produce soluble polymers compared to cross-linking, yield and molecular weights for different monomer feed ratios. For all molar feed ratios up to 8 : 5 (thiols of the  $A_2$  vs. double bonds of the  $B_3$ ), cross-linking was observed. For molar ratios 5 : 9, 5 : 10 and 5 : 11, no gelation occurred, and soluble polymers were obtained. The molecular weights decreased with increasing excess of the  $B_3$ -monomer. Also, the 5 : 9 ratio did not always prevent cross-linking, most probably due to variations in the mixing process by the mechanical stirrer. GPC elugrams also sometimes exhibited shoulders to lower elution volumes, indi-



**Scheme 1** Synthesis of *hb*-FRs via an  $A_2 + B_3$  thiol–ene polyaddition, and schematic representation of dendritic, linear, and terminal units of the *hb*-structure.

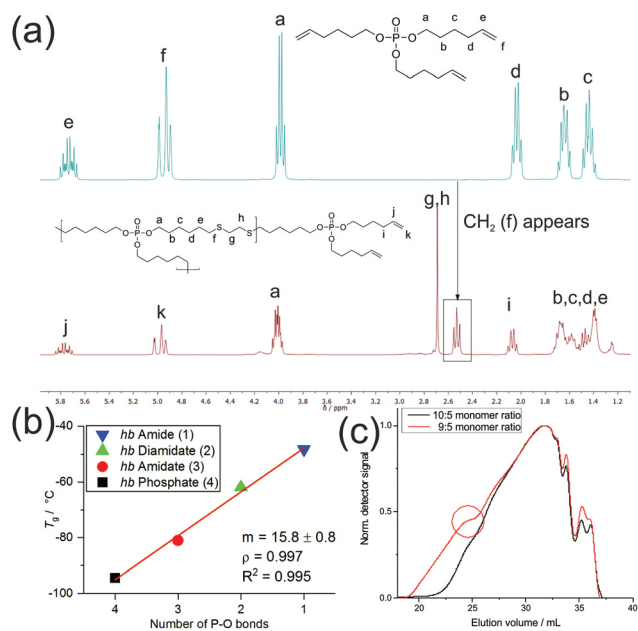


**Fig. 1** (a)  $^1\text{H}$  NMR (300 MHz in  $\text{CDCl}_3$  at 298 K) of tri(hex-5-en-1-yl)phosphate (top) and *hb*-polyphosphate (4) (bottom). The appearance of the singlet (g and h) and the triplet (f) signifies successful thiol–ene reactions. (b) Relationship between the number of P–O bonds in *hb*-FRs and their glass transition temperature ( $T_g$ ) via differential scanning calorimetry (DSC). Linear fit (red line) with a slope ( $m$ ), Pearson's correlation coefficient ( $\rho$ ) and its square ( $R^2$ ). (c) GPC-elugrams (RI detection) of  $\text{A}_2 + \text{B}_3$  polymerization to 4 at different monomer feed ratios. The red circle indicates the beginning of gelation.

cating an onset of gelation under these conditions (Fig. 1c). Although the 5 : 9 ratio provided the highest molecular weights after 24 h of polymerization, the broadest molar mass dispersity with *ca.*  $M_w/M_n = 12$  was obtained. The 5 : 11 and 5 : 10 ratios both prevented gelation and resulted in lower molar masses. We chose the 5 : 10 ratio for the following studies as it prevented gelation effectively and resulted in higher molar masses than the 5 : 11 ratio. All polymers were obtained in yields of 76–89% as off-white and viscous oils.

**Material properties.** The glass-transition temperatures ( $T_g$ ) of the *hb*-polymers were investigated via differential scanning calorimetry (DSC), indicating the fully amorphous behavior of all synthesized polymers (Fig. S17 and Table S2†). The glass-transition temperature increased linearly with the reduction of P–O bonds, *i.e.* an increase of P–N bonds, in the *hb*-polymer structure (Fig. 1b). The  $T_g$  of the *hb*-polyphosphate was detected at  $-94$  °C and increased by approx. 16 °C for each subsequent N bound to P to *ca.*  $-48$  °C for 1.

**Pyrolysis.** The decomposition behaviors of the *hb*-FRs under pyrolytic conditions were investigated using TGA (Fig. 2a and Table S3†). The mass loss curve of the *hb*-phosphate (4) exhibited a main single decomposition step at 274 °C (81 wt% mass loss) with a gradual decomposition thereafter. The *hb*-amidate (3) displayed a mass loss curve similar to 4: its onset temperature ( $T_{5\%}$ ) and temperature of maximum mass loss rate ( $T_{\text{max}}$ ) were in a similar range (242 °C and 281 °C, respectively);

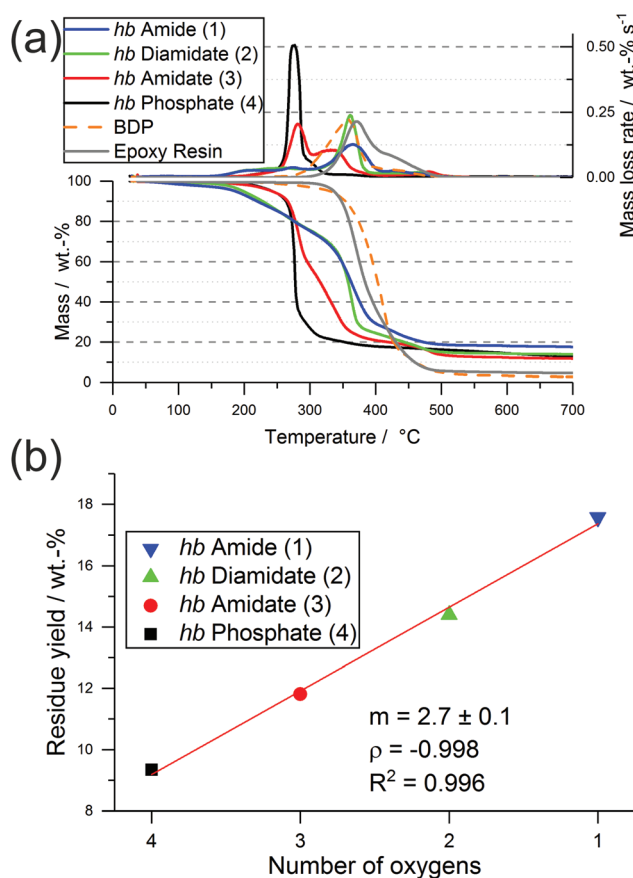


**Fig. 2** Pyrolysis investigations via thermogravimetric analysis (TGA) of *hb*-FRs: (a) mass loss (bottom) and mass loss rate (top) over  $T$  of *hb*-FRs; (b) linear relationship between the number of oxygen atoms in the P-binding sphere of *hb*-FRs and their residue yield at 700 °C (red line: linear fit;  $m$ : slope;  $\rho$ : Pearson's correlation coefficient or PCC;  $R^2$ : PCC squared).

however, the main decomposition step presented an additional shoulder that extended over a range of approx. 40 °C and peaked at 335 °C. Additionally, a small decomposition step (approx. 8 wt%) appeared at 481 °C. The *hb*-diamidate (2) exhibited a decomposition step which extended over a large temperature range from  $T_{5\%}$  at 194 °C to just before  $T_{\text{max}}$  at 359 °C. Similarly, the *hb*-amide (1) also showed a steady decomposition between  $T_{5\%}$  at 190 °C until shortly before  $T_{\text{max}}$  at 361 °C. For both 1 and 2, a small decomposition step (approx. 10 wt%) occurred at 463 °C and 428 °C, respectively. The amount of residue increased from 11.2 wt% for 4 to 17.6 wt% for 1.

Interestingly, the residue amount after pyrolytic decomposition increased with increasing N content by approx. 2.7 wt%, and Fig. 2b illustrates the linear increase between the number of O in the P-binding sphere and the residue yield. The increase in residue yield with increasing P–N bonds in the *hb*-FRs results from the formation of thermally stable intermediates that decompose over a broad temperature range. When comparing 3 and 4, the replacement of a P–O bond with a P–N bond increased residue yield and introduced an additional



decomposition step at elevated temperatures. When comparing 1 and 2 to 3 and 4, the mass loss behavior changed drastically from a single-step decomposition with a shoulder to a multi-step decomposition over a large temperature range, pointing to a crucial influence of the number of P-N bonds in the polymer on its decomposition pathway.

To better understand the decomposition mechanisms of the FRs under pyrolytic conditions, the materials were investigated *via* evolved gas analysis using TGA-FTIR (Fig. 3a-d) and pyrolysis gas chromatography/mass spectrometry (Py-GC/MS) (Fig. 4). The evolved gas FTIR spectra of decomposition products correspond to specific decomposition steps during pyrolysis of *hb*-FRs. For *hb*-FRs, either 5-hexene-1-ol and/or 5-hexene-1-amine was detected during the decomposition, depending on the O:N ratio, which correlates well with previous investigations for low molar mass P-FRs.<sup>31</sup> 5-Hexene-1-ol was identified *via* the vibration band at  $1054\text{ cm}^{-1}$  from the stretching vibration of (C-O). 5-Hexene-1-amine was identified *via* the stretching vibration band at  $1068\text{ cm}^{-1}$  from (C-N) and the wagging deformation band at  $769\text{ cm}^{-1}$  from (N-H). Additionally, 1,5-hexadiene was identified as a decomposition product (*via* a  $\beta$ -elimination) for all *hb*-FRs *via* the bands at  $3082\text{ cm}^{-1}$  from unsaturated hydrocarbons and those at  $1642\text{ cm}^{-1}$ ,  $1452\text{ cm}^{-1}$ ,  $998\text{ cm}^{-1}$  and  $917\text{ cm}^{-1}$  belonging to

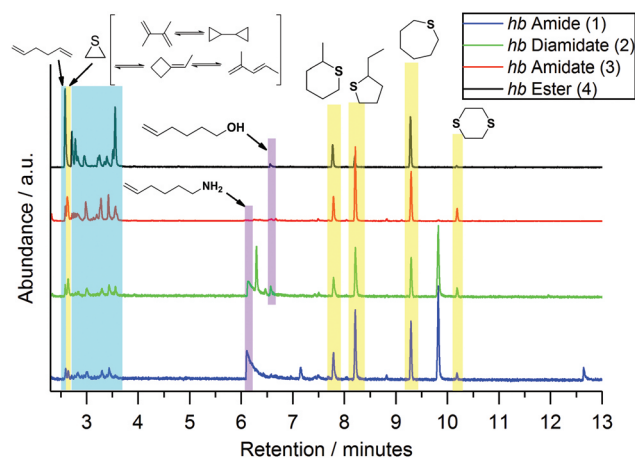


Fig. 4 Ion chromatograms of *hb*-FRs from pyrolysis gas chromatography/mass spectrometry (Py-GC-MS) measurements. Highlighted areas correspond to relevant compounds identified *via* the NIST14 MS library.

various C-H vibrations of the hexene moiety, which were also observed in 5-hexene-1-amine and 5-hexene-1-ol. Interestingly, at  $T > 330\text{ }^{\circ}\text{C}$ , all spectra showed few if any bands for unsaturated hydrocarbons (bands  $> 3000\text{ cm}^{-1}$ ). Furthermore, 2, 3,

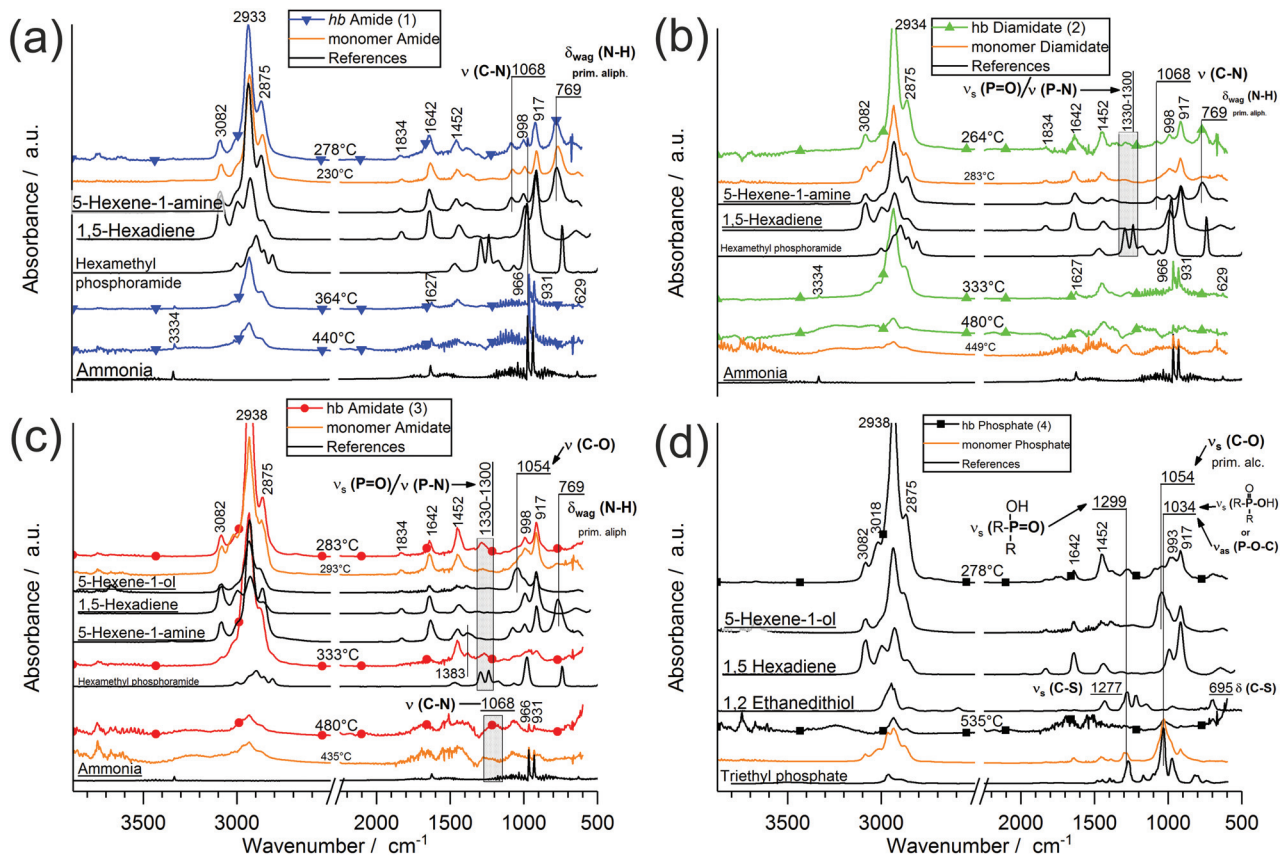


Fig. 3 Evolved gas analysis *via* FTIR (TG-FTIR) of *hb*-FRs: (a-d) FTIR spectra of *hb*-FRs at specific decomposition steps, their monomeric variants (orange) and comparative spectra.

and **4** exhibited the production of a P-species at  $T = 260\text{--}280\text{ }^{\circ}\text{C}$ : for **2** and **3**, the bands at  $1330\text{--}1300\text{ cm}^{-1}$  from the overlapping stretching vibrations of  $\text{P}=\text{O}$  or  $\text{P}-\text{N}$ , and for **4**, the bands at  $1299\text{ cm}^{-1}$  from the stretching vibration  $\text{R}_2\text{-(P=O)-OH}$ , and  $1034\text{ cm}^{-1}$  from  $\text{R}_2\text{-(P-OH)=O}$  or the stretching vibration of  $(\text{P}-\text{O}-\text{C})$ . During the decomposition of the *hb*-FRs with  $\text{P}-\text{N}$  bonds, the evolution of ammonia at  $T = 330\text{--}360\text{ }^{\circ}\text{C}$  and temperatures above  $440\text{ }^{\circ}\text{C}$  was identified by the bands at  $3334\text{ cm}^{-1}$ ,  $1642\text{ cm}^{-1}$ ,  $966\text{ cm}^{-1}$ ,  $931\text{ cm}^{-1}$ , and  $629\text{ cm}^{-1}$ .

The FTIR spectra, TGA mass loss curves, and residue amounts after pyrolysis point toward a certain behavior during pyrolysis: all units of the *hb*-FR undergo several types of decomposition reactions, and several mechanisms occur simultaneously or in tandem with one another. A general decomposition pathway is described in Scheme 2, and hydrolysis (Scheme S1†), elimination (Scheme S2†), and intra- or intermolecular reactions (Scheme S3†) are described more in depth in the ESI.†

For Py-GC/MS,  $\mu\text{g}$  samples were pyrolyzed at a specific temperature and the evolved gases passed through a GC separation column and an MS detector. Measurements at  $500\text{ }^{\circ}\text{C}$  (Fig. 4) revealed additional information on the decomposition mechanism of *hb*-FRs: the production of 1,5-hexadiene was identified by the mass spectrum at 2.6 min (Fig. S8†) and the signals at retention times of 2.7–3.7 min (areas highlighted in blue) were assigned to various  $\text{C}_6\text{H}_{10}$ -species formed by the high-temperature rearrangement of 1,5-hexadiene. Moreover, 5-hexene-1-amine and 5-hexene-1-ol (areas highlighted in purple) were observed at retention times of 6.1 min (Fig. S10†) and 6.6 min (Fig. S11†), respectively. Additionally, all *hb*-FRs formed cyclic sulfur-containing compounds (areas highlighted in yellow). The mass spectra of all *hb*-FRs at retention times of 2.63 min (corresponding to thiirane), 7.8 min (corresponding to 4-methylthiane), 8.2 min (corresponding to 2-ethylthiophane), 9.3 min (corresponding to thiepane), and 10.2 min (corresponding to 1,4-dithiane) are summarized in Fig. S9, S12, S13, S14 and S15,† respectively. A mechanism leading to the production of these products is proposed in Scheme S4.†

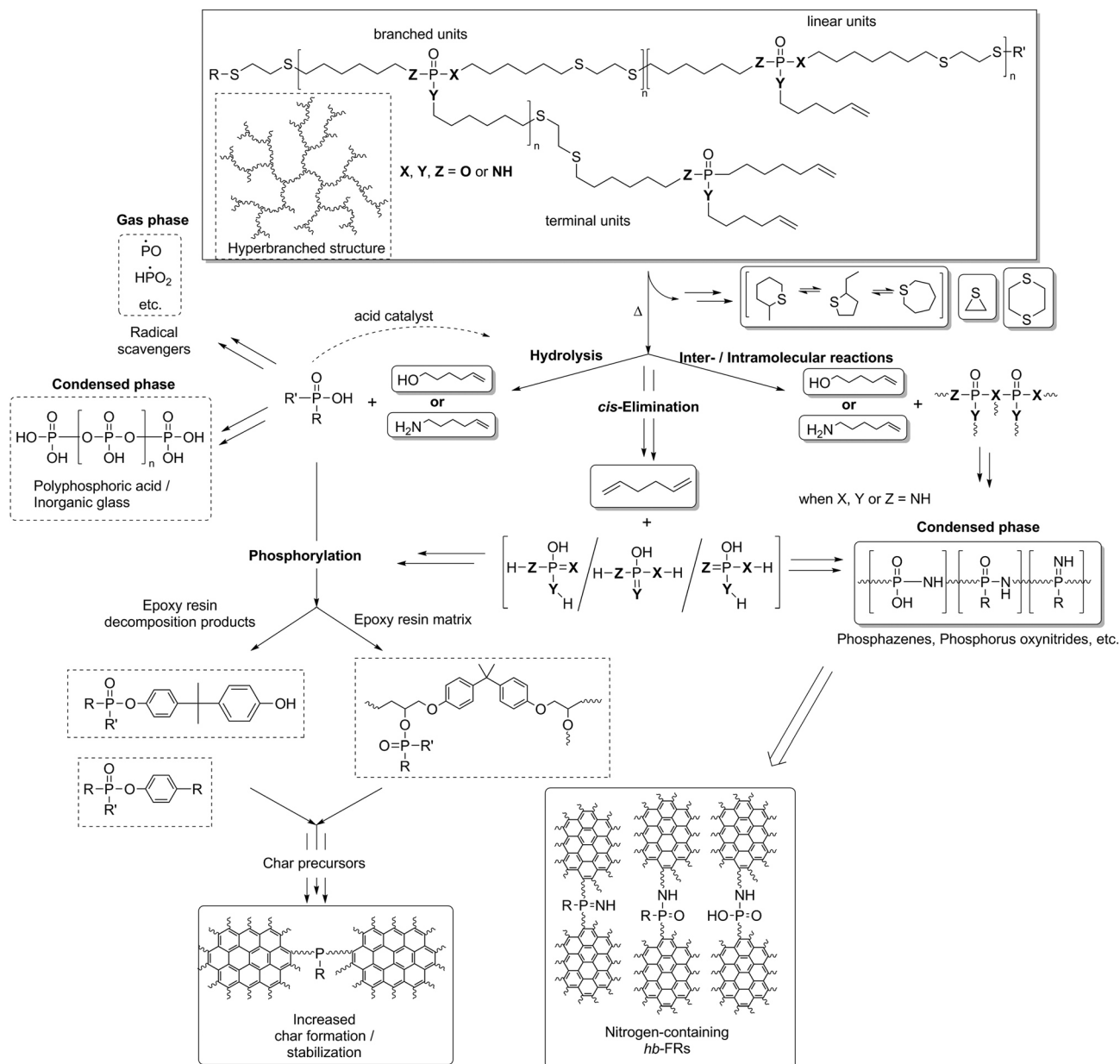
### Flame retardant epoxy resins (EP-FRs)

**Material properties.** The miscibility of **1** and **4** with EP was studied from 0 up to 40 wt%: all samples were translucent and showed no sign of macro-phase separation (Fig. 5a). The miscibility of **4** with EP is further supported by SEM and TEM images (Fig. S21†). A homogeneous surface of a section of EP with 10 wt% of **1** is shown in Fig. S16a.† There is no obvious indication of phase separation. Fig. S16b† displays the surface of EP fractured under cryogenic conditions and etched in dichloromethane according to the method of Meng *et al.*,<sup>37</sup> who studied the phase separation within EP by fracturing the sample under cryogenic conditions and etching it in dichloromethane for thirty minutes. The filler used by Meng *et al.* was soluble in dichloromethane like **4** used in this experiment. The cut block surface which was etched in dichloromethane is illustrated in Fig. S16c† and showed no signs of phase separ-

ation as indicated by the absence of grooves on the surface. These results are supported by a sample stained with ruthenium tetroxide and analyzed by TEM (Fig. S16d†), in which a homogeneous surface is visible, indicating no sign of phase separation. Differential scanning calorimetry (DSC) measurements (Fig. S17†) presented only one glass-transition temperature ( $T_g$ ), further supporting the absence of macro phase separation.

All *hb*-FRs were used as additive flame retardants and under the curing conditions no side-reactions of the phosphoramidate-bond with the epoxy were reported.<sup>31</sup> The impact of *hb*-FRs on the  $T_g$  of EP (Fig. S18†) is presented in Fig. 5b, and the change of  $T_g$  relative to EP is noted. When comparing the  $T_g$  of EP with the monomer of **4** with the  $T_g$  of EP-**4**, the *hb*-FR exhibited a relative increase of 17%, which showcases the decreased effect of *hb*-FRs over their low molecular weight P-FR counterparts. All *hb*-FRs except **1** lowered  $T_g$  of EP at a similar level to the benchmark material BDP, *i.e.* by 14%. **1** had the lowest impact on  $T_g$  compared to the other FRs, lowering  $T_g$  by only 8% to  $142.5\text{ }^{\circ}\text{C}$ . The  $T_g$  values are ordered  $4 < 3 < 2 < 1$ , following the trend visible in the  $T_g$  of pure *hb*-FRs. It should be noted that *hb*-FRs are composed of aliphatic hydrocarbons as opposed to BDP, which contains aromatic rings. The reduced effect on  $T_g$  that these aliphatic FRs exhibit is comparable to that by aromatic compounds, which speaks for the ability of *hb*-FRs to mitigate the plasticizing effect of conventional aliphatic FRs. The *hb*-polymers present significantly higher  $T_g$  values in EP than their monomeric analogues (16–21% increase),<sup>31</sup> highlighting their character as multifunctional FRs.

**Pyrolysis – mass loss and evolved gas analysis.** To understand the decomposition behavior of EP-*hb*-FRs, the mass loss and evolved gas analysis of the pyrolytic decomposition was investigated *via* TGA coupled with gas FTIR. The results are summarized in Table S4.† The mass loss and mass loss rate curves of EP and EP-FRs (Fig. 6a) and the change in residue yields at  $700\text{ }^{\circ}\text{C}$  (Fig. 6b) signify a significant change in the decomposition of EP when *hb*-FRs are added, providing evidence for their interaction during pyrolysis. EP began to decompose at  $T_{5\%} = 338\text{ }^{\circ}\text{C}$  and reached  $T_{\text{max}}$  at  $372\text{ }^{\circ}\text{C}$ . The material decomposed in a single main step equal to a mass loss of 62 wt%, with a shoulder beginning at  $424\text{ }^{\circ}\text{C}$  equal to a mass loss of 33 wt%. The residue at  $700\text{ }^{\circ}\text{C}$  was 4.5 wt%. The mass loss and evolved gas analysis of the resin DGEBA-DMC has been previously reported and will not be discussed in further detail here.<sup>38,39</sup> The resin with the benchmark material BDP (EP-BDP) decomposed in a single step with a shoulder, analogously to EP. However,  $T_{5\%}$  was  $33\text{ }^{\circ}\text{C}$  and  $T_{\text{max}}$  was  $15\text{ }^{\circ}\text{C}$  lower than that of EP, which is attributed to a reduction in cross-linking density of the flame retardant EP system. The shoulder starting at  $423\text{ }^{\circ}\text{C}$  showed a lower decomposition rate compared to EP. The mass loss at  $T_{\text{max}}$  increased to 75 wt% and decreased to 16 wt% at the shoulder. This results from the interaction of BDP with the decomposing matrix, more closely the binding of phenol-derivatives and cycloalkanes which exhibit a maximum in the production rate in this temperature



**Scheme 2** Proposed decomposition mechanism of *hb*-FRs and FR interaction with EP during thermal decomposition of EP-*hb*-FRs. Solid squares: identified products (TG-FTIR, hot stage FTIR, etc.).

range.<sup>9</sup> This interaction also explains the increased residue yield of EP-BDP, which nearly doubled to 8.2 wt%.

All EP-*hb*-FRs exhibited a similar decomposition behavior to EP-BDP:  $T_{5\%}$  was lower than EP by an average of approx. 47 °C, while  $T_{max}$  was lowered by an average of approx. 21 °C. The residue yields of the EP-*hb*-FRs varied depending on the O : N ratio of the *hb*-FRs (Fig. 6b): EP with *hb*-phosphate (EP-4) and EP with *hb*-amidate (EP-3) showed a similar residue yield (7.7 and 6.8 wt%, respectively), while EP with *hb*-diamidate (EP-2) and *hb*-amide (EP-1) exhibited residue yields similar to EP-BDP (8.1 wt% and 8.0 wt%, respectively). Although EP-3 exhibited a lower residue yield, all *hb*-FRs increased residue

yields by the same margin as the benchmark FR, signifying their ability to interact with the decomposing matrix, forming thermally stable residues. The mass loss of *hb*-FRs in EP was strikingly different from their monomeric FR variants: whereas the latter exhibited a mass loss equal to approx. 10 wt% near 220 °C (Fig. 3b, dotted line), all *hb*-FRs are significantly more thermally stable than their low molar mass counterparts in this temperature range and exhibited only minor decomposition.<sup>31</sup> This higher decomposition temperature increased the overlap of FRs and matrix decomposition, leading to higher reactivity and interaction during pyrolysis,<sup>9,40</sup> further illustrating the multifunctional capabilities of *hb*-FRs and the ability

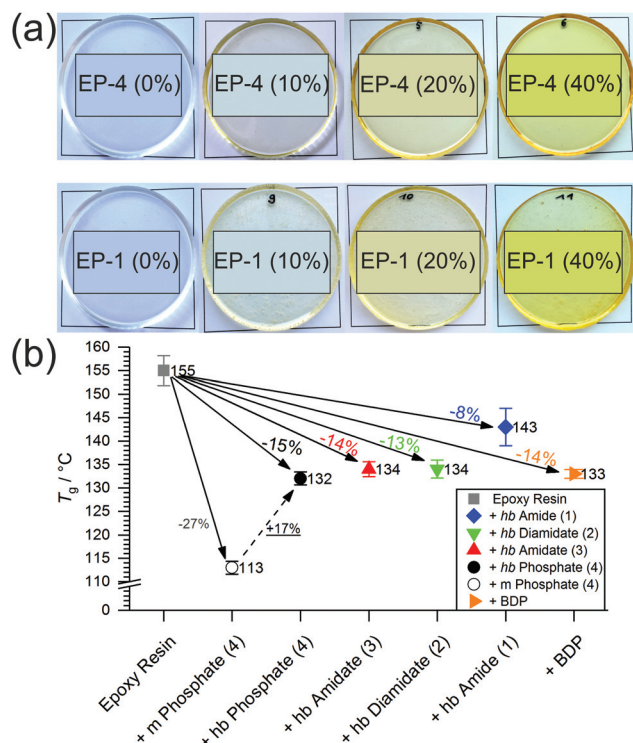


**Fig. 5** (a) EPs with increasing FR loadings (top row: EP-4; bottom row: EP-1; left to right: 0, 10, 20, 40 wt%), phase separation not visible regardless of loading; (b)  $T_g$  values of EP and EP-FRs and change in  $T_g$  relative to EP (in %), (dotted line: relative change in  $T_g$  from EP with the monomer of 4 to EP-4).

of polymeric FRs to overcome the impediments of their monomeric FR variants as well as perform equally to aromatic compounds.

When comparing the FTIR spectra of evolved gases near  $T_{5\%}$  for EP-*hb*-FRs with monomeric FR variants in EP (Fig. 7a), the distinct similarities in the spectra indicate analogous decomposition products, namely 5-hexene-1-ol, 5-hexene-1-amine, cyclohexene, 1,5-hexadiene, and acetaldehyde. The spectra of EP-2, EP-3, and EP-4 exhibited the (C–O) stretching vibration band at  $1054\text{ cm}^{-1}$  assigned to 5-hexene-1-ol. EP-2 and EP-3 produced cyclohexene as identified *via* the C–H bending vibration at  $1140\text{ cm}^{-1}$ . The spectra of EP-1 showed the (C–N) vibration band of aliphatic hydrocarbons at  $1068\text{ cm}^{-1}$  and the (N–H) wagging deformation of primary amines of aliphatic molecules at  $769\text{ cm}^{-1}$ , pointing to the production of 5-hexene-1-amine. Moreover, the (C=O) stretching vibration at  $1730\text{ cm}^{-1}$ , corresponding to acetaldehyde, was visible for EP-1, EP-3, and EP-4, while it was concealed under noise for EP-2. Acetaldehyde is a product of the decomposition of unreacted epoxide groups from EP.<sup>39</sup> The band at  $3082\text{ cm}^{-1}$  belonging to the (C=C) stretching vibration was visible in all EP-*hb*-FR spectra at  $T_{5\%}$  and indicated that the decomposition products are unsaturated. When investigating the evolved gas spectra of EP, EP-*hb*-FRs, and EP-BDP at  $T_{\text{max}}$  (Fig. 7b), all spectra were identical to the spectrum of EP, sig-

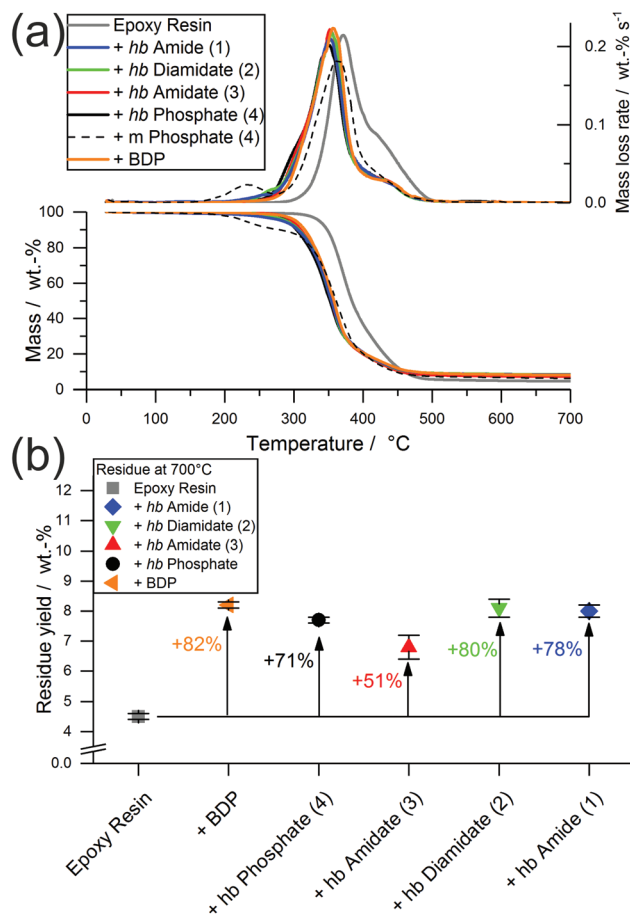


**Fig. 6** (a) Mass loss (bottom) and mass loss rate (top) over  $T$  of EP-FRs from TGA measurements (dotted line: EP with the monomer of 4); (b) residue yields at  $700\text{ °C}$  from TGA measurements of EP and EP-FRs and change relative to EP (in %).

nifying that EP-*hb*-FRs did not exhibit gas evolution at this point. This correlates well with the mass loss curves of the *hb*-FRs under pyrolytic conditions (Fig. 2a), as the *hb*-FRs have nearly completely decomposed at the  $T_{\text{max}}$  of EP. These FTIR spectra provide further evidence that terminal and linear units of the *hb* structure decomposed near  $T_{5\%}$  as evidenced by the presence of unsaturated hydrocarbons present solely on these units and 5-hexene-1-ol and/or 5-hexene-1-amine, respectively. As previously mentioned, this can be rationalized by the lower thermal stability of the  $\omega$ -hexenyl side chains compared to the thiol-linked main chain.

The decomposition pathway is a complex interaction of the FR, the matrix and the decomposition species thereof.<sup>40</sup> The detection of various P-species in the condensed phase (Fig. S19<sup>†</sup>) confirms that *hb*-FRs interact with the decomposing matrix. The incorporation of P into the residue increases charring *via* enhanced cyclization of the hydrocarbon chains and stabilizes the carbonaceous char by acting as cross-linking points between the polyaromatic hydrocarbons.<sup>41</sup> The proposed mechanism is presented in Scheme 2: the decomposition of *hb*-FRs leads to the formation of O=(P–OH) groups



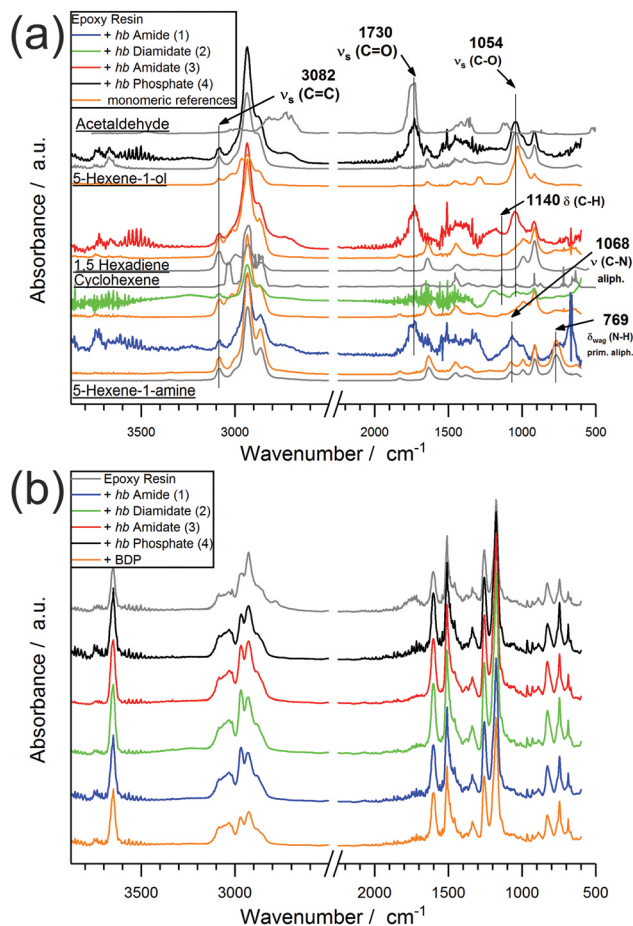


Fig. 7 Evolved gas spectra of EP-*hb*-FRs via TG-FTIR at  $T_{5\%}$ ; (orange: monomeric FR spectra at  $T_{max}$ ; gray: comparative spectra) (b) evolved gas spectra of EP and EP-*hb*-FRs via TG-FTIR at  $T_{max}$ .

via hydrolysis of the (P–N) or (P–O) bond, respectively, resulting in the production of phosphoric acid and acid derivatives. These P-based acids interact with EP in three ways: acting as acid catalysts for further hydrolysis,<sup>42</sup> aiding in the phosphorylation process of the EP matrix via esterification and dehydration,<sup>43</sup> and forming an inorganic glass via polyphosphoric acid, thus affording thermal stability to the residue.<sup>7,44</sup> For N-containing *hb*-FRs, the formation of phosphazenes, phosphorus oxynitrides, and other  $P_xN_yO_z$  species further increased cross-linking of the aromatic char, and the presence of N can accelerate phosphorylation through synergy.<sup>45–47</sup>

**Fire behavior.** EP and all EP-FRs were investigated for their reaction-to-small-flame behavior via UL-94 and LOI (Table S6†) and under forced-flaming conditions in a cone calorimeter to determine their fire load, residue yields, smoke and gas production, and heat release rate (HRR). The HRR of a “steady state” burning polymer is described by the following equations:<sup>48</sup>

$$\text{HRR} = \chi \cdot \theta(t) \cdot (1 - \mu) \cdot (h_c^0 / h_g) \cdot \dot{q}''_{\text{eff}} \quad (1)$$

$$\dot{q}''_{\text{eff}} = (\dot{q}''_{\text{ex}} + \dot{q}''_{\text{flame}} - \dot{q}''_{\text{rerad}} - \dot{q}''_{\text{loss}}) \quad (2)$$

where  $\chi$  is the combustion efficiency,  $\theta(t)$  is the time-dependent protective layer effect,  $\mu$  is the residue yield,  $h_c^0$  is the heat of complete combustion,  $h_g$  is the heat of gasification,  $\dot{q}''_{\text{eff}}$  is the effective heat flux,  $\dot{q}''_{\text{ex}}$  is the external heat flux,  $\dot{q}''_{\text{flame}}$  is the heat flux due to thermal feedback,  $\dot{q}''_{\text{rerad}}$  is the heat flux from reradiation, and  $\dot{q}''_{\text{loss}}$  is the loss of heat flux out of the flame.

The results of the cone calorimeter experiments are summarized in Table 1 and Fig. 8 plots the HRR and total heat released (THR) as functions of time. The shape of the HRR-curves gives insight into the behavior of the material during flaming combustion and highlights the modes of action of the FRs.<sup>49</sup> For EP, the shape was typical of non-charring, thermally intermediately thick samples: after ignition, the material began to decompose with a strong initial increase in the HRR.

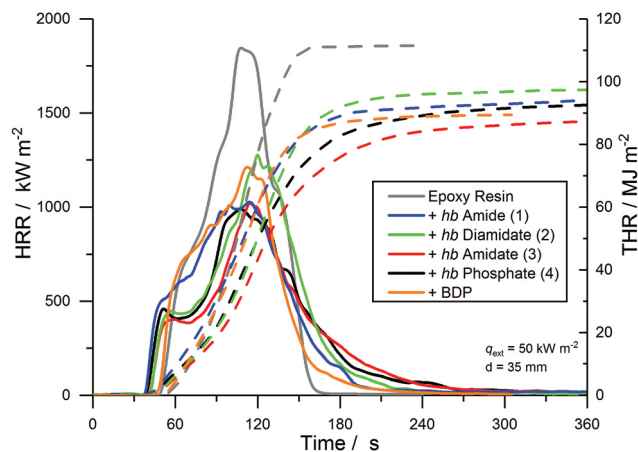


Fig. 8 Heat release rate (HRR, full line) and total heat released (THR, dotted line) over  $t$  of EP and EP-FRs.

Table 1 Results from cone calorimeter experiments of EP and EP-FRs

	EP	EP-1	EP-2	EP-3	EP-4	EP-BDP
THE [ $\text{MJ m}^{-2}$ ]	108.4 ± 2.6	95.5 ± 2.3	99.1 ± 2.7	86.6 ± 0.1	89.8 ± 3.0	87.5 ± 1.2
PHRR [ $\text{kW m}^{-2}$ ]	1696 ± 180	1189 ± 155	1325 ± 10	1019 ± 17	953 ± 41	1180 ± 41
Residue [wt%]	0.7 ± 0.1	12.1 ± 2.7	7.0 ± 0.1	13.6 ± 0.5	7.5 ± 0.6	3.1 ± 0.2
EHC [ $\text{MJ kg}^{-1}$ ]	26.9 ± 1.0	25.5 ± 0.5	26.8 ± 0.8	25.1 ± 0.1	24.3 ± 0.6	22.7 ± 0.2

THE = total heat evolved (=THR at flame-out).

The quasi-static HRR corresponding to the steady state HRR is marked only by a shoulder and disappears near the peak of heat release rate (PHRR). The peak results from a reduction of  $\dot{q}''_{\text{loss}}$  caused by the glass wool under the sample preventing heat transfer to the sample holder as the pyrolysis zone approaches. EP had a PHRR of  $1696 \text{ kW m}^{-2}$  and a total heat evolved (THE = THR at flame-out) of  $108.4 \text{ MJ m}^{-2}$ . It exhibited an effective heat of combustion (EHC = total heat evolved/total mass loss) of  $26.9 \text{ MJ kg}^{-1}$  and a residue yield of 0.7 wt%. For EP-BDP, the HRR-curve resembled a mixture of thermally thick charring materials and thermally intermediately thick non-charring materials: while it retained the characteristic shape of EP, the addition of a charring mode of action was visible, resulting in a 30% reduction of the PHRR ( $1180 \text{ kW m}^{-2}$ ). THE and EHC were also 19% and 16% lower than EP (THE =  $87.5 \text{ MJ m}^{-2}$ ; EHC =  $22.7 \text{ MJ kg}^{-1}$ ), respectively. The residue yield was 3.1 wt%.

All EP-*hb*-FRs reduced the fire load of EP by 9–20% and the PHRR by 22–44% and increased residue yields in the order EP-2 < EP-4 < EP-1 < EP-3. EP-2 showed the lowest residue amount (7.0 wt%) and EP-3 exhibited the highest amount (13.6 wt%). EP-3 and EP-4 displayed the greatest reduction in PHRR and THE, while EP-1 and EP-2 did not achieve the same reduction in these indices. Nearly all *hb*-FRs exhibited a plateau-like shape approx. 20–30 s after ignition, which was caused by the formation of a protective char layer on the sample surface, shielding the underlying material from irradiation and reducing the PHRR. Additionally, the release of P-containing volatiles, observed in pyrolysis investigations (Fig. 2), acted in the gas phase as radical scavengers or fuel diluters, thus reducing THE. As combustion continued, the protective layer effect rescinded, and the decomposition of the underlying material increased towards the PHRR. After flame-out, the char layer underwent thermo-oxidation as evidenced by the slow increase of THR over time in the plateau-state at  $t > 240 \text{ s}$ .

Petrella-plots are a way to assess fire behavior and flame retardancy:<sup>50</sup> the fire load (THE) is plotted over the fire growth index (PHRR/ $t_{\text{ig}}$ ), as THE quantitatively describes heat released but lacks a description of release rate, while PHRR/ $t_{\text{ig}}$  describes the flashover potential (severity of a fire, or peak heat release potential) but is not quantitative. The Petrella-plot of EP and EP-FRs (Fig. 9) displays that, while the PHRR/ $t_{\text{ig}}$  of EP was  $36 \text{ kW m}^{-2} \text{ s}^{-1}$  and the THE was  $109.6 \text{ MJ m}^{-2}$ , all EP-FRs exhibited a lower PHRR/ $t_{\text{ig}}$  and THE, as indicated by the shift to the lower left corner of the coordinate system. 2 displayed the lowest flame retardancy, lowering THE by only 10% to  $99.1 \text{ MJ m}^{-2}$  and PHRR/ $t_{\text{ig}}$  by only 7% to  $33.6 \text{ MJ m}^{-2}$ , while 3 showed the greatest reduction in both THE (21% reduction to  $86.6 \text{ MJ m}^{-2}$ ) and PHRR/ $t_{\text{ig}}$  (31% reduction to  $24.9 \text{ kW m}^{-2} \text{ s}^{-1}$ ). The plot visualizes the ability of 3 and 4 to act more effectively in forced-flaming conditions than 1 and 2, providing further evidence that a critical O : N ratio determines decomposition behavior due to changes in the flame-retardancy mechanism and mode of action. Moreover, 3 and 4 outperform BDP, providing further evidence that *hb*-FRs can compete with aromatic compounds.

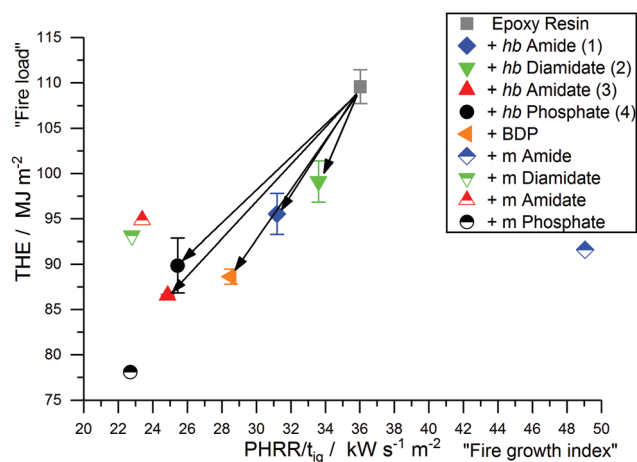


Fig. 9 Petrella-plot of EP and EP-FRs, assessing fire load (THE) versus fire growth (PHRR/ $t_{\text{ig}}$ ).

Furthermore, Fig. 9 also visualizes the change in fire behavior from the monomer to polymer: the low molar mass variants exhibited very scattered results, where the monomer of 4 had a very different impact compared to the monomer of 1 in terms of lowering the fire load and fire growth index of EP. Although the *hb*-FRs presented varied results based on their O : N ratio, in general they displayed significantly less disperse values for fire growth and fire load, the result of a more pronounced chemical interaction between the FR and matrix during decomposition.

## Experimental

### Materials

**Chemicals.** All chemicals were purchased from commercial suppliers as reagent grade and used without further purification. The monomers were prepared according to the literature.<sup>31</sup>

### Methods

**NMR.** Nuclear magnetic resonance measurements ( $^1\text{H}$ ,  $^{31}\text{P}$ -{H} and  $^{13}\text{C}$ -{H} NMR) were performed on a Bruker Avance (Bruker, Ettlingen, Germany) spectrometer at 250, 300, 500, and 700 MHz on samples solved in deuterated chloroform, deuterated dimethyl sulfoxide or deuterated *N,N*-dimethylformamide. Calibration spectra were measured against the solvent signal. All spectra were analyzed using MestReNova 9 (Mestrelab Research S.L., Santiago de Compostela, Spain).

**GPC-MALS.** For gel permeation chromatography with multi-angle laser light scattering online detection (GPC-MALS), a light scattering detector combined with a suitable concentration detector was connected to the output of the GPC columns for the direct determination of the molecular weight. The refractive index increment ( $dn/dc$ ) was determined online under the assumption that 100% of the sample mass is injected and elutes from the column. For the P–N containing polymers, DMAc as the mobile phase with  $2 \text{ g L}^{-1}$  LiBr and

2 g L<sup>-1</sup> TRIS was used. As the stationary phase, a GRAM linear M column with a particle size of 10 μm from PSS Polymer Standards Service GmbH was used. The operation temperature was 60 °C. For the phosphate, the mobile phase was THF. As the stationary phase, three SDV columns with a porosity of 10<sup>6</sup>, 10<sup>4</sup> and 500 Å and a particle size of 10 μm from PSS Polymer Standards Service GmbH were used. The operation temperature was 30 °C.

**DSC.** For *hb*-FRs, a Mettler Toledo DSC 823e (Mettler Toledo, Columbus OH, USA) was used at a heating and cooling rate of 10 K min<sup>-1</sup> under a nitrogen atmosphere with a flow rate of 30 ml min<sup>-1</sup>. Three measurements of a heating-cooling-heating cycle were performed. Measurements of the flame retardant epoxy resins were performed on a Netzsch 204 F1 “Phoenix” (Netzsch Instruments, Selb, Germany) using a 5 mg solid sample. Three heating and two cooling runs were performed at a rate of 10 K min<sup>-1</sup> in the temperature range from -80 to 180 °C for epoxy resins. The *T*<sub>g</sub> of a material was taken as an average of the 2<sup>nd</sup> and 3<sup>rd</sup> heating run.

**TGA/TG-FTIR.** Thermogravimetric analysis and evolved gas analysis *via* FTIR measurements were performed on a TG 209 F1 Iris (Netzsch Instruments, Selb, Germany) coupled to a Tensor27 Infrared Spectrometer (Bruker Optics, Ettlingen, Germany) *via* a heated (*T* = 270 °C) transfer-line. Samples sized 5 mg (*hb*-FR) or 10 mg (epoxy resins, powdered) were heated at a rate of 10 K min<sup>-1</sup> from 30 to 900 °C under a nitrogen atmosphere *via* gas flow at 30 ml min<sup>-1</sup>. The epoxy resins were powdered using a CryoMill (RETSCH, Germany) under liquid nitrogen.

**Hot-stage-FTIR.** FTIR spectra of the condensed phase during pyrolysis were recorded on a hot-stage FTIR using a Vertex70 FTIR spectrometer (Bruker Optics, Ettlingen, Germany) fitted with an FTIR600 Linkam hot stage cell (Linkam Scientific Instruments Ltd, Chilworth, UK). Powdered samples were pressed into a platelet with potassium bromide as the carrying agent and heated at a rate of 10 K min<sup>-1</sup> from 30 to 600 °C under a nitrogen purge at 300 ml min<sup>-1</sup>. The scan resolution was 0.4 cm<sup>-1</sup> and samples were measured between 4000 and 400 cm<sup>-1</sup>.

**LOI.** Limiting oxygen index measurements were performed in accordance with ISO 4589-2. The samples corresponded to type IV of the standard (dimensions: 130 mm × 6.5 mm × 3 mm). All samples were stored at 23 °C and 50% relative humidity for at least 80 hours before measurements.

**UL-94.** Underwriter's Laboratory 94 measurements were performed on samples stored at 23 °C and 50% relative humidity for at least 80 hours in vertical and horizontal orientation according to EN 60695-11-10. The samples were sized 125 mm × 13 mm × 3 mm.

**Cone calorimetry.** All forced-flaming measurements were performed on a cone calorimeter (Fire Testing Technology Ltd, East Grinstead, UK) using a heat flux of 50 kW m<sup>-2</sup> on samples sized 100 mm × 100 mm × 4 mm, conditioned for at least 48 hours at 23 °C and 50% relative humidity, in accordance with ISO 5660 thus simulating a developing fire.<sup>49</sup> As the standard distance of 25 mm caused the sample residues to

touch the heating coil due to intumescence, thus interfering with the measurement results, a distance to the cone heater of 35 mm was chosen.<sup>51</sup> The measurements were conducted in duplicate, and a third measurement was performed if the margin of error was greater than 10%.

**Elemental analysis.** All cone calorimetry residue samples were ground into powder with a mortar and pestle for homogenization purposes and approx. 5 g of material was collected. All elemental analysis measurements were performed by Mikroanalytisches Labor Kolbe (c/o Fraunhofer Institut UMSICHT, Oberhausen, Germany). Phosphorus-contents were determined chromatographically *via* a UV/VIS Specord 90 (Analytik Jena AG, Jena, Germany). For statistical purposes, all measurements were repeated twice.

**SEM.** Scanning electron microscopy measurements were performed on a Zeiss EVO MA10 (Carl Zeiss AG, Oberkochen, Germany) using an acceleration voltage of 10 kV. The samples were glued to the sample holder, and then sputtered with gold prior to measurements to avoid charging effects.

**Py-GC-MS.** Pyrolysis gas chromatography/mass spectrometry measurements were conducted using a micro-furnace double-shot pyrolyzer (PY3030iD, Frontier Laboratories, Japan) connected *via* a split/splitless inlet port to a gas chromatograph (7890B, Agilent Technologies, USA) combined with a mass selective detector (5977B, Agilent Technologies, USA). The scan range was 15–550 amu and the EI ionization energy of the MSD was 70 eV. *Via* gravimetric fall into the pyrolysis zone (*T* = 500 °C), 300 μg samples were pyrolyzed under a helium atmosphere. Using an Ultra Alloy±5 capillary column (*l* = 30 m, iD = 0.25 mm, film thickness = 0.25 μm), all evolved pyrolysis products were separated under a helium flow of 1 ml min<sup>-1</sup>. The column temperature was held at *T* = 40 °C for 120 s, then increased at a rate of 10 K min<sup>-1</sup> to *T* = 300 °C and held there for 10 min. The GC injector temperature was *T* = 300 °C and it was operated in a split mode of 1 : 300. Peak assignments were made using the NIST14 MS library as a reference.

**Synthesis of *hb*-polyphosphoramidate (1), *hb*-polyphosphorodiamidate (2), *hb*-polyphosphoramidate (3), and *hb*-polyphosphate (4).** 1, 2, 3 and 4 were prepared by a radical thiol-ene polyaddition (Scheme 1). For 1, 2, and 3, 234 mmol of the previously synthesized monomer<sup>31</sup> (1 eq.) and 16.7 g of 1,2-ethanedithiol (177 mmol; 0.76 eq.) were dissolved in 240 ml *N,N*-dimethylformamide and added to a reactor fitted with a mechanical stirrer under an argon atmosphere. As a radical initiator, 690.5 mg azobisisobutyronitrile (AIBN) (4.1 mmol; 0.02 eq.) was used. For 4, 80.00 g of 4 (232 mmol; 1 eq.) and 16.57 g of 1,2-ethanedithiol (176 mmol; 0.75 eq.) were dissolved in 240 ml toluene and added to a reactor fitted with a mechanical stirrer under an argon atmosphere. For 2, 3, and 4, 686.5 mg of AIBN (4.18 mmol; 0.02 eq.) was used as a radical initiator, and for 1, 686.5 mg of AIBN (4.18 mmol; 0.02 eq.) was used. The solution was heated at 100 °C for 24 hours. The crude mixture was then concentrated at reduced pressure. 3 and 4 were precipitated twice into toluene. 1 and 2 were precipitated twice into *n*-hexane. Finally, the polymers were dried at reduced pressure until constant weight (yield 2, 3, 4: 73 g,



76%; yield **1**: 86 g, 89%). The purity and chemical structure were determined by  $^1\text{H}$  NMR and  $^{31}\text{P}$  {H} NMR spectroscopy.

### Structure characterization

**hb-Polyphosphoramidate (1).**  $^1\text{H}$  NMR (300 MHz, chloroform-*d*):  $\delta$  [ppm] = 5.84–5.71 (m); 5.02–4.94 (m); 4.02 (m); 2.70 (s); 2.54 (t); 2.06 (td); 1.69 (m); 1.59 (m); 1.40 (m); 1.39 (m); (Fig. 1a).

$^{31}\text{P}$  {H} NMR (121 MHz, chloroform-*d*):  $\delta$  [ppm] = -0.66 (s) (Fig. S4†).

**hb-Polyphosphorodiamidate (2).**  $^1\text{H}$  NMR (300 MHz, chloroform-*d*):  $\delta$  [ppm] = 5.85–5.72 (m); 5.03–4.93 (m); 3.98 (m); 2.87 (br); 2.70 (s); 2.64 (br); 2.54 (t); 2.06 (td); 1.70–1.36 (m); (Fig. S1†).

$^{31}\text{P}$  {H} NMR (121 MHz, chloroform-*d*):  $\delta$  [ppm] = 9.24 (s) (Fig. S5†).

**hb-Polyphosphoramidate (3).**  $^1\text{H}$  NMR (300 MHz, chloroform-*d*):  $\delta$  [ppm] = 5.84–5.71 (m); 5.04–4.93 (m); 3.93 (m); 2.87 (br); 2.70 (s); 2.54 (t); 2.07 (td); 1.64–1.25 (m); (Fig. S2†).

$^{31}\text{P}$  {H} NMR (121 MHz, chloroform-*d*):  $\delta$  [ppm] = 15.49 (s) (Fig. S6†).

**hb-Polyphosphate (4).**  $^1\text{H}$  NMR (300 MHz, chloroform-*d*):  $\delta$  [ppm] = 5.85–5.72 (m); 5.03–4.93 (m); 2.88 (br); 2.70 (s); 2.54 (t); 2.07 (td); 1.58–1.24 (m); (Fig. S3†).

$^{31}\text{P}$  {H} NMR (121 MHz, chloroform-*d*):  $\delta$  [ppm] = 17.13 (s) (Fig. S7†).

**Preparation of FR thermosets.** The polymer resin was based on diglycidyl ether of bisphenol A (DGEBA) (Araldite MY740, Bodo Müller Chemie GmbH, Offenbach am Main, Germany) and the amine component 2,2'-dimethyl-4,4'-methylene-bis(cyclohexylamine) (DMC) (Sigma Aldrich Co. LLC/Merck KGaA, Darmstadt, Germany). The needed ratios of DGEBA and DMC (see Table 2) were calculated using epoxy equivalent weights (ratio 100 : 35), and 10 wt% of the total batch size was replaced with *hb*-FRs or the benchmark FR Bisphenol A bis(diphenyl phosphate) (BDP) (ICL-IP, Tel-Aviv, Israel). All samples needed for measurements were prepared in one batch in the following manner: the respective *hb*-FR was placed in a 1 L polypropylene cup, then DGEBA was added and the chemicals were blended with a wooden spatula until they became homogeneous. DMC was added, and the mixture was thoroughly mixed. Any resulting bubbles were removed *in vacuo*. The compounds were poured into prepared aluminum molds, and then cured in an oven at 90 °C for 30 minutes, at 120 °C for 30 minutes, and at

150 °C for 1 hour. UL-94 and LOI samples were cut into specified dimensions and stored under climate control prior to testing for at least 48 hours according to the respective standards.

## Conclusions

Phosphorus-containing hyperbranched polymers for use as multifunctional flame-retardant additives for epoxy resins were synthesized *via*  $\text{A}_2 + \text{B}_3$  thiol-ene polymerization. A systematic library of P-O and P-N containing polymers allowed the adjustment of the decomposition mechanism. Results from DSC and TGA experiments showed that  $T_g$  and residue yield after pyrolysis increased linearly with the N-content of the *hb*-FRs, and those FRs with a higher N-content were thermally more stable than those with a higher O-content. This was determined to result from a change in the decomposition mechanism which was proposed herein, and that a crucial O:N-ratio determined the pathway. Investigations of flame-retardant epoxy resins provided further evidence of the shift in the chemical decomposition mechanism and ultimately mode of action: all materials exhibited a condensed phase mechanism, as exemplified by the appearance of P-signals in hot stage FTIR measurements, the increase in residue yields in cone calorimeter measurements, and the high amount of the P-content in these residues as determined by elemental analysis. However, *hb*-FRs with a higher O-content exhibited a stronger reduction in the effective heat of combustion, signifying a more pronounced gas phase mechanism. This was supported by CO-yield comparison (see the ESI†) which showed that *hb*-FRs with a higher N-content more strongly affected the combustion efficiency. SEM and residue analysis also illustrated the intumescent characteristic of these FR additives. All *hb*-FRs were compared to the benchmark FR BDP and the results from all measurements demonstrated the ability of these aliphatic FRs to perform at a similar or superior level to an aromatic compound, even at low loadings (P-content in EP < 1%). The *hb*-FRs' ability to mitigate some of the drawbacks of low molecular weight aliphatic FR additives, such as high volatility, low miscibility, poor cohesion in the matrix (leaching or blooming), or strong impact on  $T_g$ , speaks for their practical use as multifunctional flame retardant additives and showcases the enormous potential hyperbranched polymers can have in developing future materials in the field of flame retardancy.

## Conflicts of interest

There are no conflicts to declare.

## Acknowledgements

The authors thank the Deutsche Forschungsgemeinschaft (DFG) for funding (DFG SCHA 730/15-1; WU 750/8-1).

**Table 2** Composition of FR thermosets

Material	Content [g]				
	EP	EP-1	EP-2	EP-3	EP-4
DGEBA	222.2	200	200	200	200
DMC	77.8	70	70	70	70
<b>1</b>	—	30	—	—	—
<b>2</b>	—	—	30	—	—
<b>3</b>	—	—	—	30	—
<b>4</b>	—	—	—	—	30

Alexander Battig thanks Patrick Klack for his assistance with the cone calorimeter measurements, Martin Günther, and Michael Morys for their help with SEM images, Dr Katharina Kebelmann for her help with Py-GC-MS measurements, and Leticia V. Lima for her aid in sample preparation and measurements. Jens C. Markwart is the recipient of a fellowship through funding of the Excellence Initiative (DFG/GSC 266) in the context of the graduate school of excellence "MAINZ" (Materials Science in Mainz). Frederik R. Wurm and Jens C. Markwart thank Prof. Dr Katharina Landfester (MPI-P, Germany). Open Access funding provided by the Max Planck Society.

## Notes and references

- 1 S. Shaw, *Rev. Environ. Health*, 2010, **25**, 261–306.
- 2 M. M. Velencoso, A. Battig, J. C. Markwart, B. Schartel and F. R. Wurm, *Angew. Chem., Int. Ed.*, 2018, **57**, 10450–10467.
- 3 X. Wang, W. Xing, X. Feng, B. Yu, L. Song and Y. Hu, *Polym. Chem.*, 2014, **5**, 1145–1154.
- 4 S. V. Levchik and E. D. Weil, *J. Fire Sci.*, 2006, **24**, 345–364.
- 5 B. Perret, B. Schartel, K. Stöß, M. Ciesielski, J. Diederichs, M. Döring, J. Krämer and V. Altstädt, *Eur. Polym. J.*, 2011, **47**, 1081–1089.
- 6 M. Rakotomalala, S. Wagner and M. Döring, *Materials*, 2010, **3**, 4300–4327.
- 7 G. Camino, L. Costa and M. P. Luda di Cortemiglia, *Polym. Degrad. Stab.*, 1991, **33**, 131–154.
- 8 S. K. Brauman, *J. Fire Retard. Chem.*, 1977, **4**, 38–58.
- 9 B. Perret, K. H. Pawlowski and B. Schartel, *J. Therm. Anal. Calorim.*, 2009, **97**, 949–958.
- 10 K. H. Pawlowski and B. Schartel, *Polym. Int.*, 2007, **56**, 1404–1414.
- 11 B. I. Voit and A. Lederer, *Chem. Rev.*, 2009, **109**, 5924–5973.
- 12 C. J. Hawker, R. Lee and J. M. J. Frechet, *J. Am. Chem. Soc.*, 1991, **113**, 4583–4588.
- 13 A. Sunder, R. Hanselmann, H. Frey and R. Mülhaupt, *Macromolecules*, 1999, **32**, 4240–4246.
- 14 C. Chen, G. Liu, X. Liu, S. Pang, C. Zhu, L. Lv and J. Ji, *Polym. Chem.*, 2011, **2**, 1389–1397.
- 15 R. Hu, J. W. Y. Lam, J. Liu, H. H. Y. Sung, I. D. Williams, Z. Yue, K. S. Wong, M. M. F. Yuen and B. Z. Tang, *Polym. Chem.*, 2012, **3**, 1481–1489.
- 16 S. E. Stiriba, H. Frey and R. Haag, *Angew. Chem., Int. Ed.*, 2002, **41**, 1329–1334.
- 17 M. Calderon, M. A. Quadir, S. K. Sharma and R. Haag, *Adv. Mater.*, 2010, **22**, 190–218.
- 18 K. Y. Pu, K. Li, J. B. Shi and B. Liu, *Chem. Mater.*, 2009, **21**, 3816–3822.
- 19 P. Y. Wen, X. F. Wang, W. Y. Xing, X. M. Peng, B. Yu, Y. Q. Shi, G. Tang, L. Song, Y. Hu and R. K. K. Yuen, *Ind. Eng. Chem. Res.*, 2013, **52**, 17015–17022.
- 20 J. Li, C. H. Ke, L. Xu and Y. Z. Wang, *Polym. Degrad. Stab.*, 2012, **97**, 1107–1113.
- 21 K. C. Cheng, C. C. Wang, J. L. Ruan, C. H. Wu and C. W. Li, *Polym. Adv. Technol.*, 2018, **29**, 2529–2536.
- 22 L. Zang, S. Wagner, M. Ciesielski, P. Müller and M. Döring, *Polym. Adv. Technol.*, 2011, **22**, 1182–1191.
- 23 B. Schartel and J. H. Wendorff, *Polym. Eng. Sci.*, 1999, **39**, 128–151.
- 24 F. Wurm and H. Frey, in *Polymer Science: A Comprehensive Reference*, ed. K. Matyjaszewski and M. Möller, Elsevier, Amsterdam, 2012, ch. 6.05, vol. 6, pp. 177–198.
- 25 D. H. Zhang, H. Y. Wu, T. C. Li, A. Q. Zhang, Y. L. Peng and F. X. Jing, *Polym. Compos.*, 2011, **32**, 36–43.
- 26 X. L. Chen, C. M. Jiao, S. X. Li and J. Sun, *J. Polym. Res.*, 2011, **18**, 2229–2237.
- 27 L. J. Duan, H. Y. Yang, L. Song, Y. B. Hou, W. Wang, Z. Gui and Y. Hu, *Polym. Degrad. Stab.*, 2016, **134**, 179–185.
- 28 Z. Li, P. Wei, Y. Yang, Y. G. Yan and D. A. Shi, *Polym. Degrad. Stab.*, 2014, **110**, 104–112.
- 29 S. Gaan, G. Sun, K. Hutches and M. H. Engelhard, *Polym. Degrad. Stab.*, 2008, **93**, 99–108.
- 30 G. F. Levchik, Y. V. Grigoriev, A. I. Balabanovich, S. V. Levchik and M. Klatt, *Polym. Int.*, 2000, **49**, 1095–1100.
- 31 J. C. Markwart, A. Battig, L. Zimmermann, M. Wagner, J. Fischer, B. Schartel and F. R. Wurm, *ACS Appl. Polym. Mater.*, 2019, **1**, 1118–1128.
- 32 H. Chen and J. Kong, *Polym. Chem.*, 2016, **7**, 3643–3663.
- 33 T. Emrick, H. T. Chang and J. M. J. Frechet, *Macromolecules*, 1999, **32**, 6380–6382.
- 34 M. Ciesielski, B. Burk, C. Heinzmann and M. Döring, in *Novel Fire Retardant Polymers and Composite Materials*, ed. D.-Y. Wang, Woodhead Publishing, 2017, ch. 2, pp. 3–51, DOI: 10.1016/B978-0-08-100136-3.00002-9.
- 35 J. Deng and W. F. Shi, *Eur. Polym. J.*, 2004, **40**, 1137–1143.
- 36 K. Täuber, F. Marsico, F. R. Wurm and B. Schartel, *Polym. Chem.*, 2014, **5**, 7042–7053.
- 37 F. L. Meng, S. X. Zheng and T. X. Liu, *Polymer*, 2006, **47**, 7590–7600.
- 38 L.-H. Lee, *J. Polym. Sci., Part A: Gen. Pap.*, 1965, **3**, 859–882.
- 39 D. P. Bishop and D. A. Smith, *J. Appl. Polym. Sci.*, 1970, **14**, 205–223.
- 40 B. Schartel, B. Perret, B. Dittrich, M. Ciesielski, J. Krämer, P. Müller, V. Altstädt, L. Zang and M. Döring, *Macromol. Mater. Eng.*, 2016, **301**, 9–35.
- 41 U. Braun, A. I. Balabanovich, B. Schartel, U. Knoll, J. Artner, M. Ciesielski, M. Döring, R. Perez, J. K. W. Sandler, V. Altstädt, T. Hoffmann and D. Pospiech, *Polymer*, 2006, **47**, 8495–8508.
- 42 M. Steinmann, M. Wagner and F. R. Wurm, *Chem. - Eur. J.*, 2016, **22**, 17329–17338.
- 43 J. W. Lyons, *J. Fire Flammability*, 1970, **1**, 302–311.
- 44 B. Schartel, *Materials*, 2010, **3**, 4710–4745.
- 45 S. V. Levchik, in *Flame Retardant Polymer Nanocomposites*, ed. A. B. Morgan and C. A. Wilkie, John Wiley & Sons, Inc., 2006, pp. 1–29, DOI: 10.1002/9780470109038.ch1.
- 46 E. D. Weil, *Fire Retard. Polym. Mater.*, 2000, 115–145.

- 47 S. V. Levchik, G. F. Levchik, A. I. Balabanovich, E. D. Weil and M. Klatt, *Angew. Makromol. Chem.*, 1999, **264**, 48–55.
- 48 R. Lyon, in *Handbook of Building Materials for Fire Protection*, ed. C. Harper, McGraw-Hill, New York, New York, 2004, pp. 3.1–3.51.
- 49 B. Schartel and T. R. Hull, *Fire Mater.*, 2007, **31**, 327–354.
- 50 R. Petrella, *J. Fire Sci.*, 1994, **12**, 14–43.
- 51 B. Schartel, M. Bartholmai and U. Knoll, *Polym. Degrad. Stab.*, 2005, **88**, 540–547.

## Supporting Information

For

### Hyperbranched Phosphorus Flame Retardants: Multifunctional Additives for Epoxy Resins

Alexander Battig,<sup>a†</sup> Jens C. Markwart,<sup>b,c†</sup> Frederik R. Wurm,<sup>b</sup> and Bernhard Schartel<sup>a\*</sup>

<sup>a</sup> Bundesanstalt für Materialforschung und -prüfung (BAM), Unter den Eichen 87, 12205 Berlin, Germany.

<sup>b</sup> Max Planck Institute for Polymer Research, Ackermannweg 10, 55128 Mainz, Germany.

<sup>c</sup> Graduate School Materials Science in Mainz, Staudinger Weg 9, 55128 Mainz, Germany.

#### Structure Characterization: <sup>1</sup>H and <sup>31</sup>P NMR

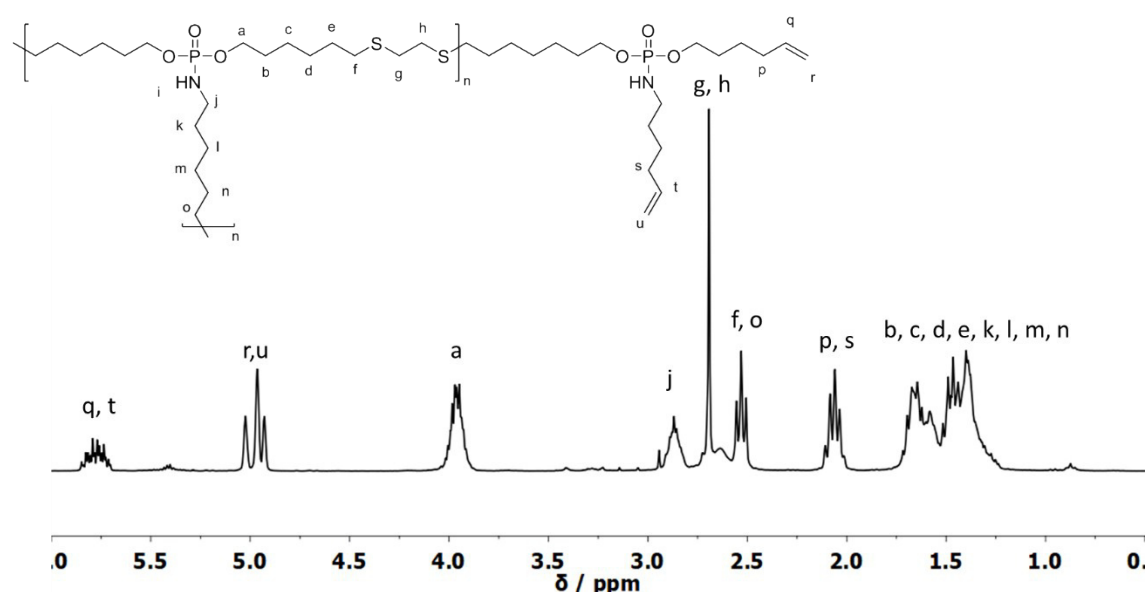


Figure S1. <sup>1</sup>H NMR (300 MHz in CDCl<sub>3</sub> at 298 K) of *hb*-polyphosphoramidate (**3**).

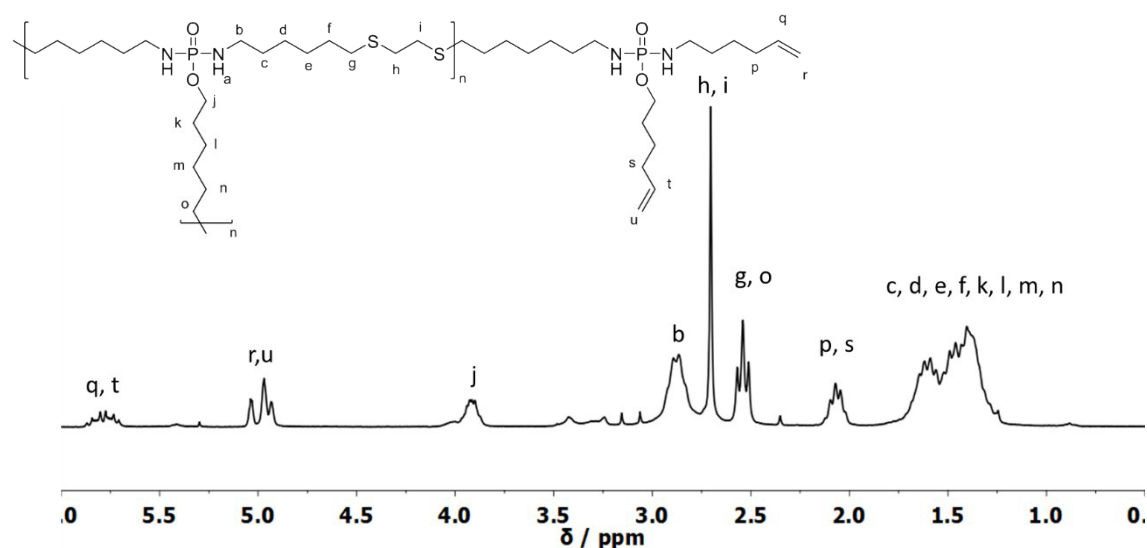


Figure S2. <sup>1</sup>H NMR (300 MHz in CDCl<sub>3</sub> at 298 K) of *hb*-polyphosphordiamidate (**2**).

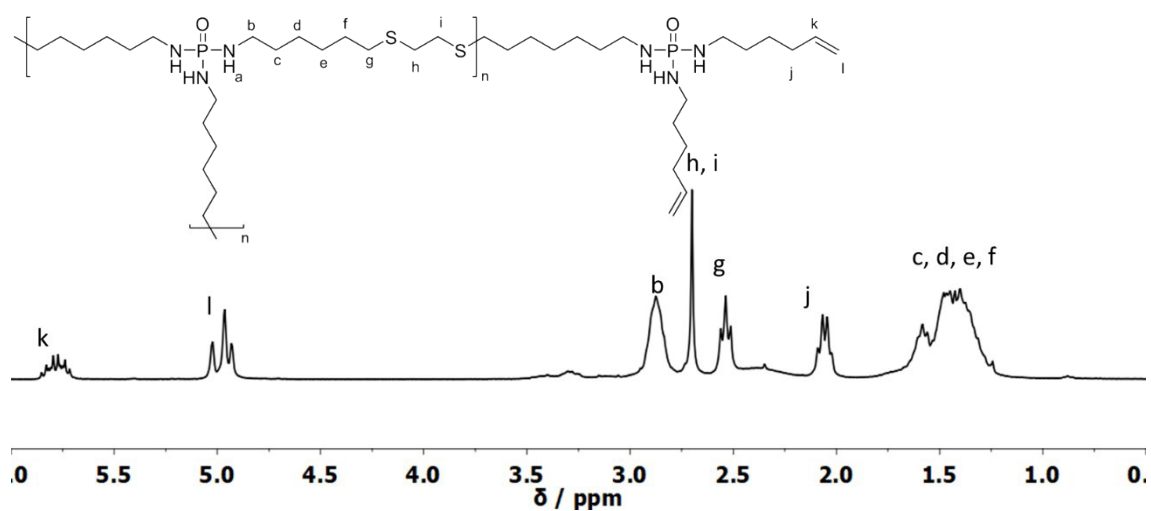


Figure S3.  $^1\text{H}$  NMR (300 MHz in  $\text{CDCl}_3$  at 298 K) of *hb*-polyphosphoramidate (1).

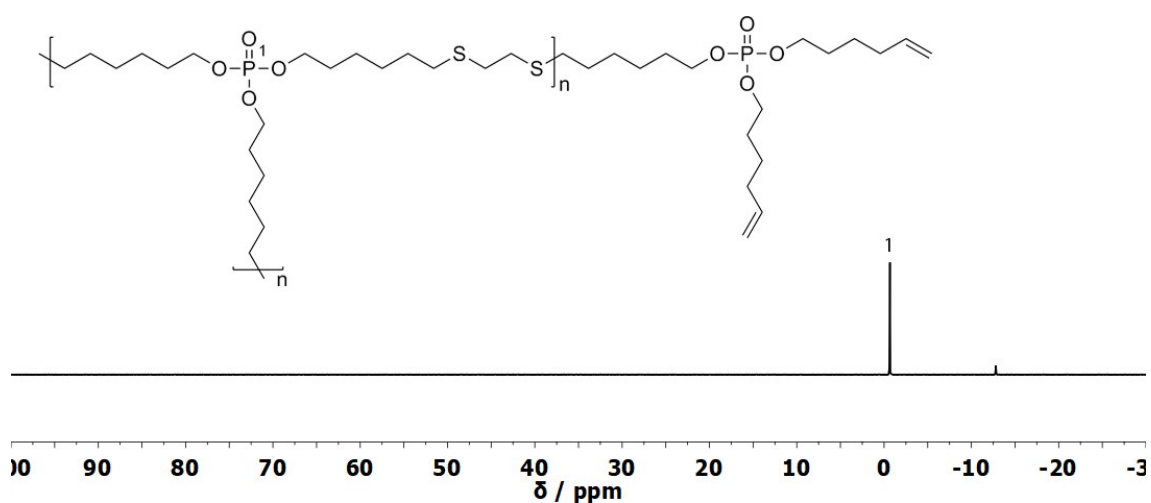


Figure S4.  $^{31}\text{P}$  {H} NMR (121 MHz in  $\text{CDCl}_3$  at 298 K) of *hb*-polyphosphate (4).

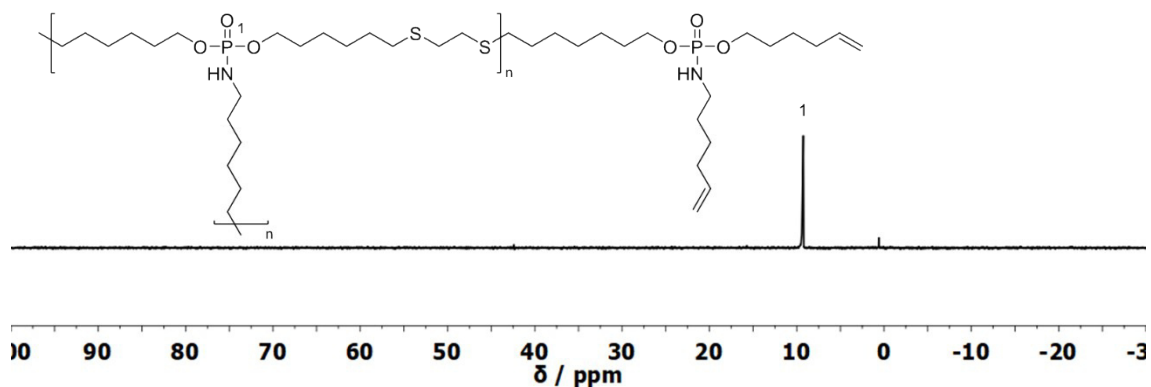


Figure S5.  $^{31}\text{P}$  {H} NMR (121 MHz in  $\text{CDCl}_3$  at 298 K) of *hb*-polyphosphoramidate (3).

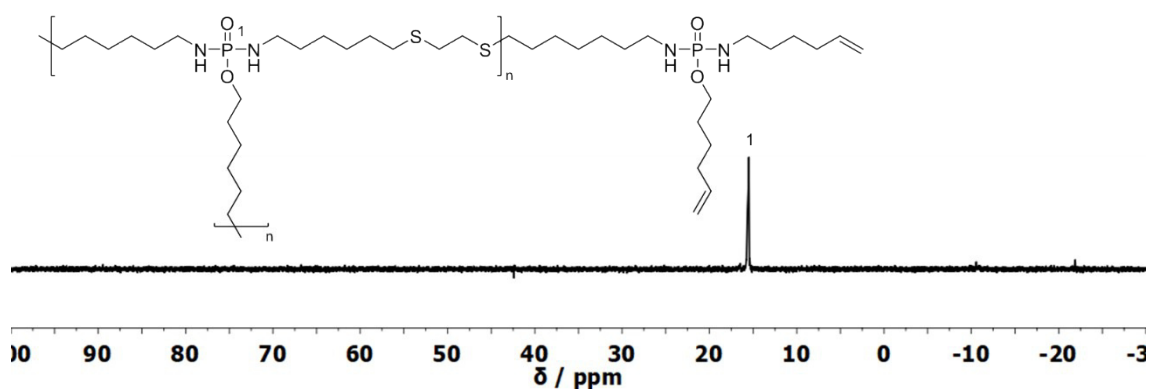
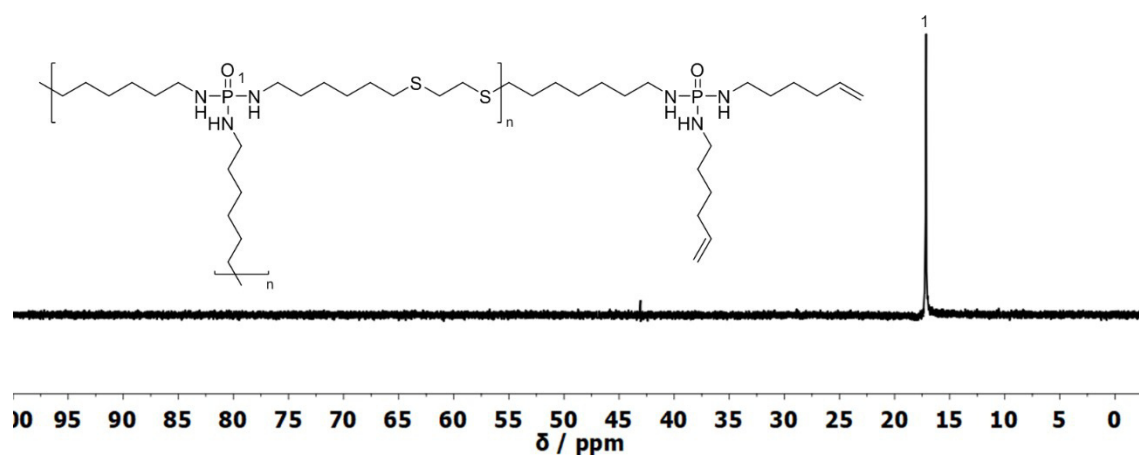


Figure S6.  $^{31}\text{P}$  {H} NMR (121 MHz in  $\text{CDCl}_3$  at 298 K) of *hb*-polyphosphorodiamidate (2).



**Figure S7.**  $^{31}\text{P}$  {H} NMR (121 MHz in  $\text{CDCl}_3$  at 298 K) of *hb*-polyphosphoramidate (**1**).

### Polymerization study

**Table S1.** Variation of polymerization conditions at different  $\text{A}_2:\text{B}_3$  ratios.  $\text{A}_2$  is 1,2-ethanedithiol and  $\text{B}_3$  is tri(hex-5-en-1-yl)phosphate.

Ratio*	CL	time until CL / min	$M_n$ / $\text{g mol}^{-1}$	$M_w$ / $\text{g mol}^{-1}$	PDI	Yield / %
10:5	Yes	180	-	-	-	-
5:6	Yes	24	-	-	-	-
5:7	Yes	103	-	-	-	-
5:8	Yes	120	-	-	-	-
5:9	No	-	4,300	53,400	12.44	87
5:10	No	-	3,400	11,300	3.29	82
5:11	No	-	3,000	7,900	2.66	79

\* molar feed ratio of functional groups, i.e. thiols : double bonds.

### Material Properties: Differential Scanning Calorimetry

**Table S2.** Glass-transition temperatures ( $T_g$ ) of *hb*-FRs determined *via* differential scanning calorimetry (DSC).

	<i>hb</i> phosphate ( <b>4</b> )	<i>hb</i> amidate ( <b>3</b> )	<i>hb</i> diamidate ( <b>2</b> )	<i>hb</i> amide ( <b>1</b> )
$T_g$ / $^{\circ}\text{C}$	-94	-81	-62	-48

### Pyrolysis: Thermogravimetric Analysis of *hb*-FRs

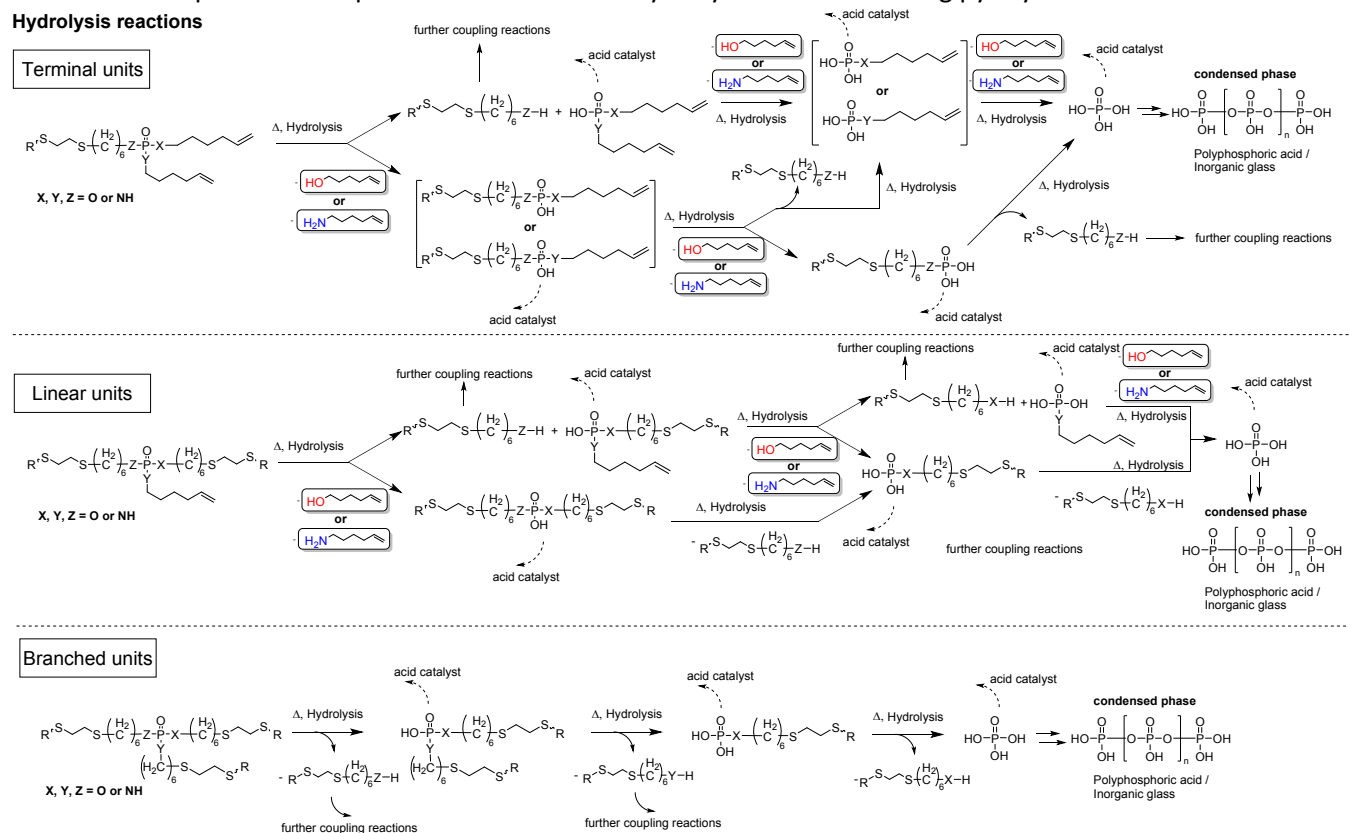
**Table S3.** Results from thermogravimetric analysis (TGA) of *hb*-FRs under pyrolytic conditions ( $\text{N}_2$  flow =  $30 \text{ ml min}^{-1}$ , heating rate =  $10 \text{ K min}^{-1}$ ).

Material	<i>hb</i> Phosphate ( <b>4</b> )	<i>hb</i> Amidate ( <b>3</b> )	<i>hb</i> Diamidate ( <b>2</b> )	<i>hb</i> Amide ( <b>1</b> )
$T_{5\%}$ / $^{\circ}\text{C}$	$241 \pm 2$	$245 \pm 3$	$194 \pm 5$	$190 \pm 3$
$T_1$ / $^{\circ}\text{C}$ (preceding main decomposition step)	-	-	$257 \pm 5$	$273 \pm 3$
$T_{\text{max}}$ / $^{\circ}\text{C}$ [main decomposition step]	$274 \pm 3$	$281 \pm 0$	$359 \pm 2$	$361 \pm 4$
$T_2$ / $^{\circ}\text{C}$ [1 <sup>st</sup> subsequent decomposition step]	-	$335 \pm 4$	-	-
$T_3$ / $^{\circ}\text{C}$ [2 <sup>nd</sup> subsequent decomposition step]	-	$481 \pm 0$	$461 \pm 3$	$428 \pm 3$
Residue / wt.-% (at $700 \text{ }^{\circ}\text{C}$ )	$11 \pm 1$	$12 \pm 0$	$14 \pm 1$	$18 \pm 0$

## Proposed decomposition mechanisms: Hydrolysis

Scheme S1. Proposed decomposition mechanism of hydrolysis reactions during pyrolysis.

### Hydrolysis reactions

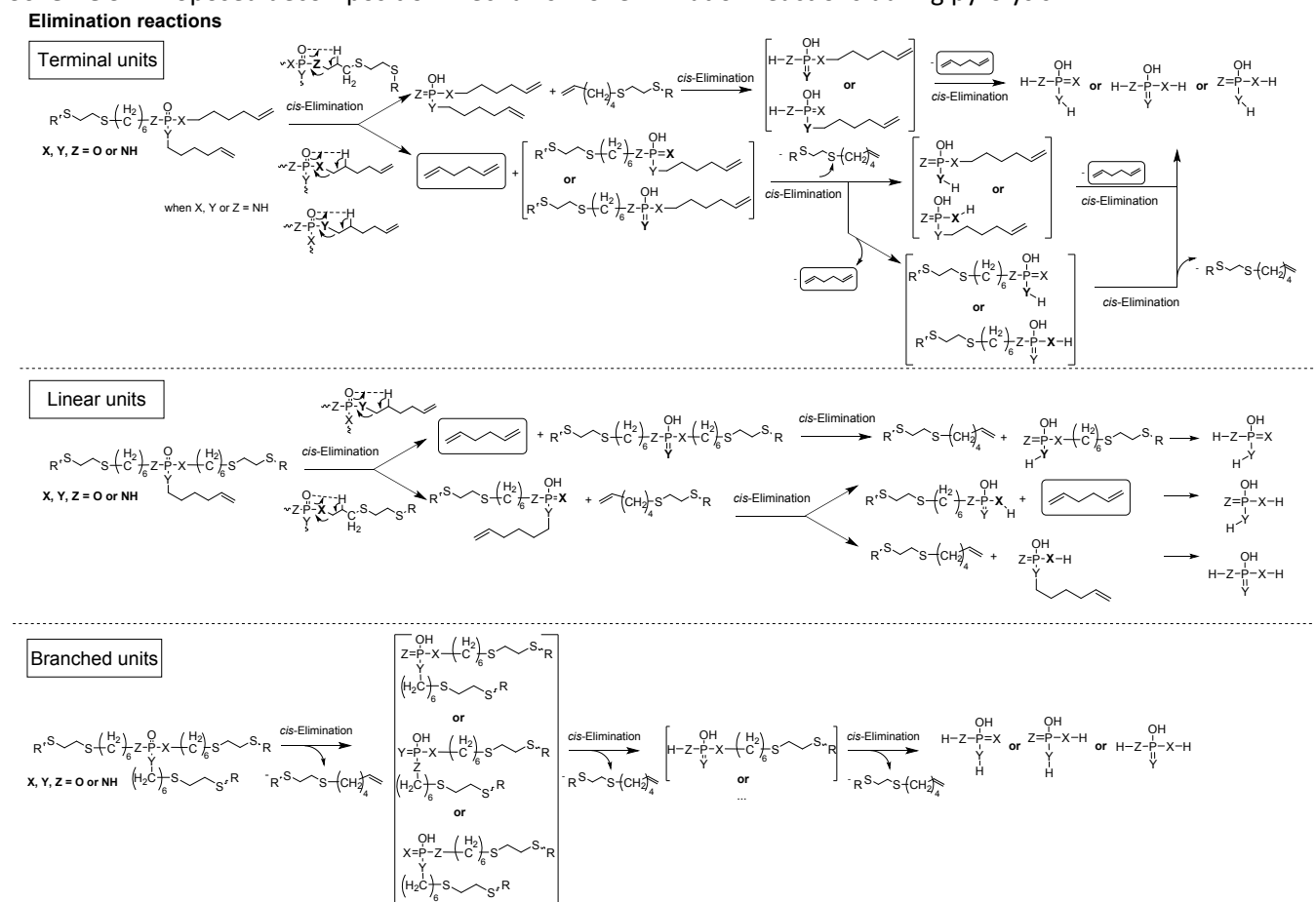


Hydrolysis reactions of phosphates/-amides (Scheme S2) produce phosphates that act as acid catalysts, thereby promoting further hydrolysis reactions.<sup>1</sup> For terminal units and linear units in our P-FRs, two hydrolysis pathways could occur: either the P-(O-C<sub>6</sub>H<sub>11</sub>) or P-(NH-C<sub>6</sub>H<sub>11</sub>) bond can be hydrolyzed, leading to the production of 5-hexene-1-ol or 5-hexene-1-amine, respectively (side chain reaction in linear and terminal units), or alternatively, the P-(O-R) or P-(NH-R) bond connecting the unit to the polymer backbone is hydrolyzed (main chain reaction). Main chain reactions yield new functional groups which could undergo further coupling reactions, e.g. transesterification.<sup>2</sup> Sufficient hydrolysis reactions lead to the cleavage of the phosphorus-containing moiety from the main chain. Complete hydrolysis leads to the formation of phosphoric acid,<sup>3</sup> which typically polymerizes under these conditions to polyphosphoric acid or inorganic glasses in the condensed phase.<sup>4</sup>



## Proposed decomposition mechanisms: *cis*-Elimination

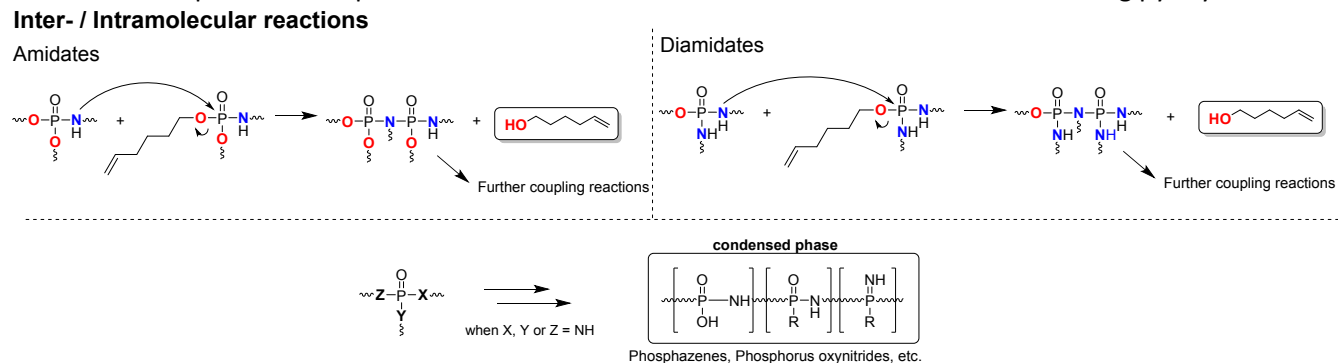
**Scheme S2.** Proposed decomposition mechanism of elimination reactions during pyrolysis.



Besides hydrolysis, elimination reactions (Scheme S3) involve the hydrogen atom in the *cis*-position (relative to the P=O bond) of the  $\beta$ -CH<sub>2</sub> moiety of the hydrocarbon chain.<sup>5-7</sup> Here, hydrogen bonding facilitates the cleavage of the (O-C) or (N-C) bond, generating either 1,5-hexadiene (side chain reaction) or a terminal allyl group (main chain reaction), the latter forming new vinyl groups that undergo cross-linking reactions during decomposition, e.g. *via* radical initiation or cyclization. For N-containing *hb*-FRs, elimination reactions could produce P=N bond, which could further lead to the formation of phosphazenes, phosphorus oxynitrides, or other (P-O-N)<sub>x</sub> compounds in the condensed phase through rearrangement and polymerization processes during thermal decomposition.<sup>8,9</sup>

## Proposed decomposition mechanisms: Inter-/intramolecular reactions

**Scheme S3.** Proposed decomposition mechanism of inter- and intramolecular reactions during pyrolysis.

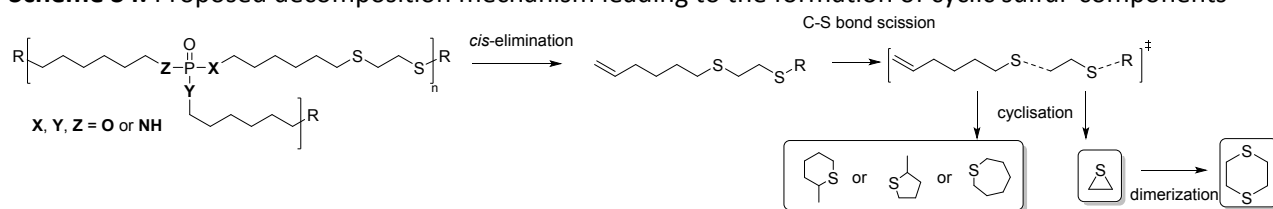


Additionally, inter- and intramolecular reactions (Scheme S4) can occur between two separate molecules, two moieties of the same hyperbranched polymer, or between the FR and matrix. These reactions occur in nitrogen-containing compounds like phosphoramidates, -diamidates, and amides. While the secondary amine acts as a base, the amine hydrogen attacks the pentavalent P of a P-N bond in the vicinity.<sup>10</sup> As a result, 5-hexene-1-ol is produced in an addition-elimination-type reaction. For nitrogen-containing compounds, inter- and intramolecular reactions, as well as rearrangements, may also lead to the formation of thermally stable phosphazenes, phosphorus-oxynitrides, and other (P-O-N)<sub>x</sub> species.<sup>11,12</sup>



## Proposed decomposition mechanisms: Sulfur components

**Scheme S4.** Proposed decomposition mechanism leading to the formation of cyclic sulfur-components



The scission of C-S-bonds of *cis*-elimination products (see Scheme S2) could lead to C<sub>6</sub>H<sub>12</sub>S and C<sub>2</sub>H<sub>4</sub>S fragments. Cyclisation of the former leads to 4-methylthiane, 2-ethylthiophane, or thiepane, and cyclisation of the latter yields thirane, which may dimerize to form 1,4-dithiane.

## Mass spectra from Py-GC-MS

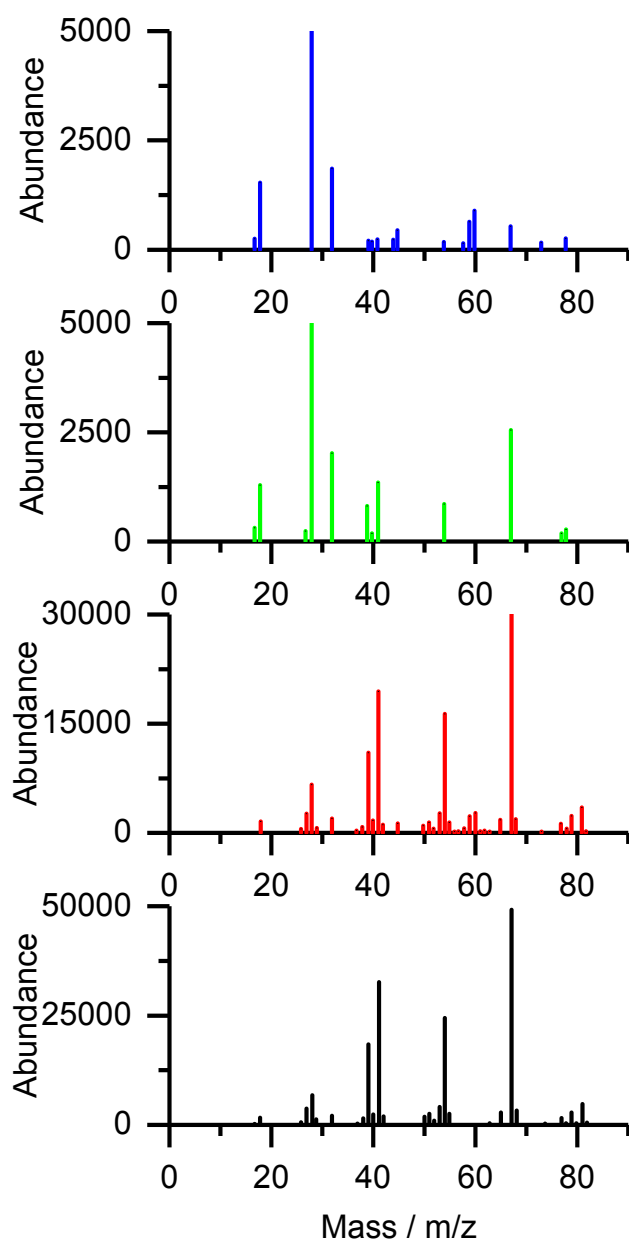


**Figure S8.** Mass spectra from Py-GC-MS measurements at a retention time of 2.6 min (blue region in Figure 4), assigned to 1,5-hexadiene.

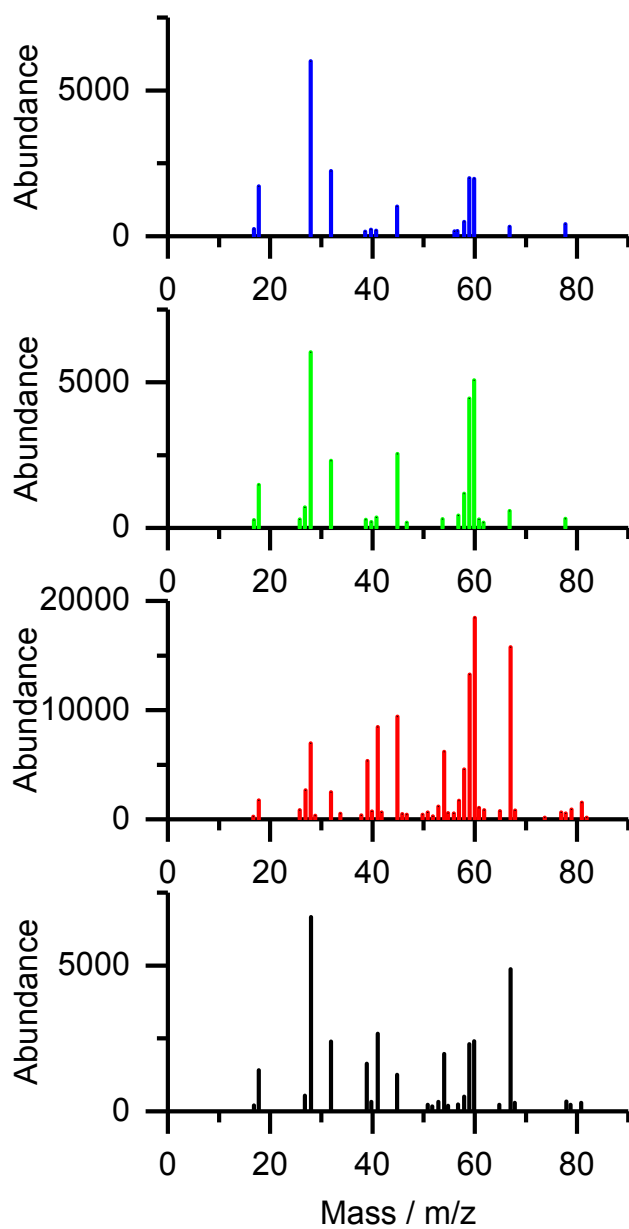


**Figure S9.** Mass spectra from Py-GC-MS measurements at a retention time of 2.63 min (yellow region in Figure 4), assigned to thiirane.

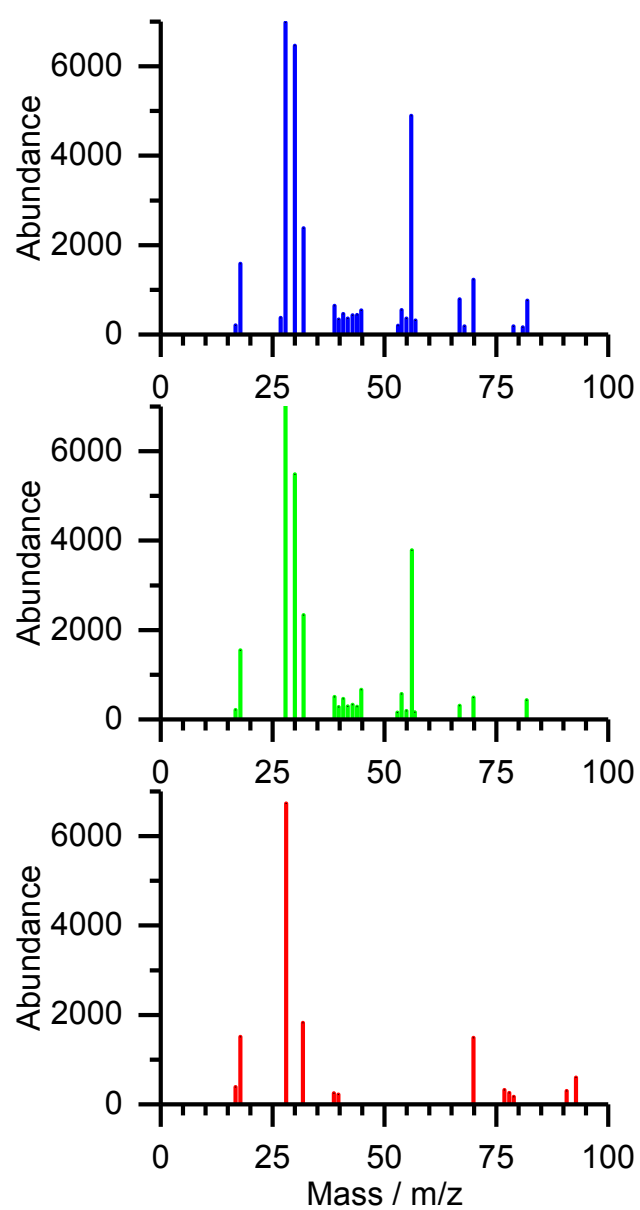


**Figure S10.** Mass spectra from Py-GC-MS measurements at a retention time of 6.1 min (purple region in Figure 4), assigned to 5-hexene-1-amine.

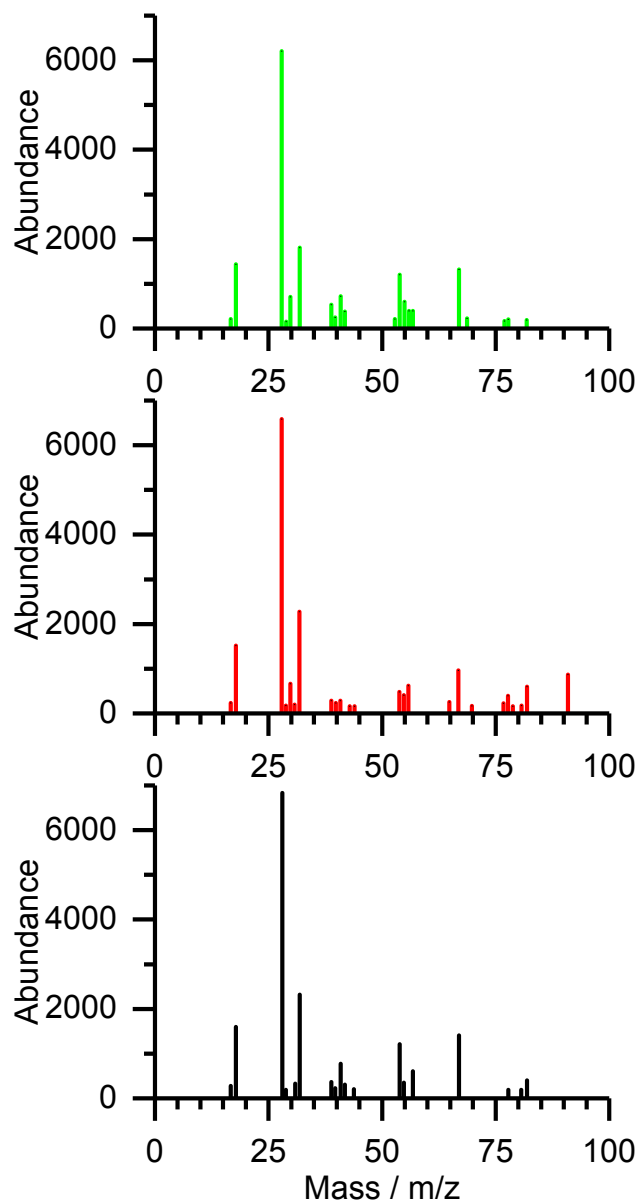


**Figure S11.** Mass spectra from Py-GC-MS measurements at a retention time of 6.6 min (purple region in Figure 4), assigned to 5-hexene-1-ol.

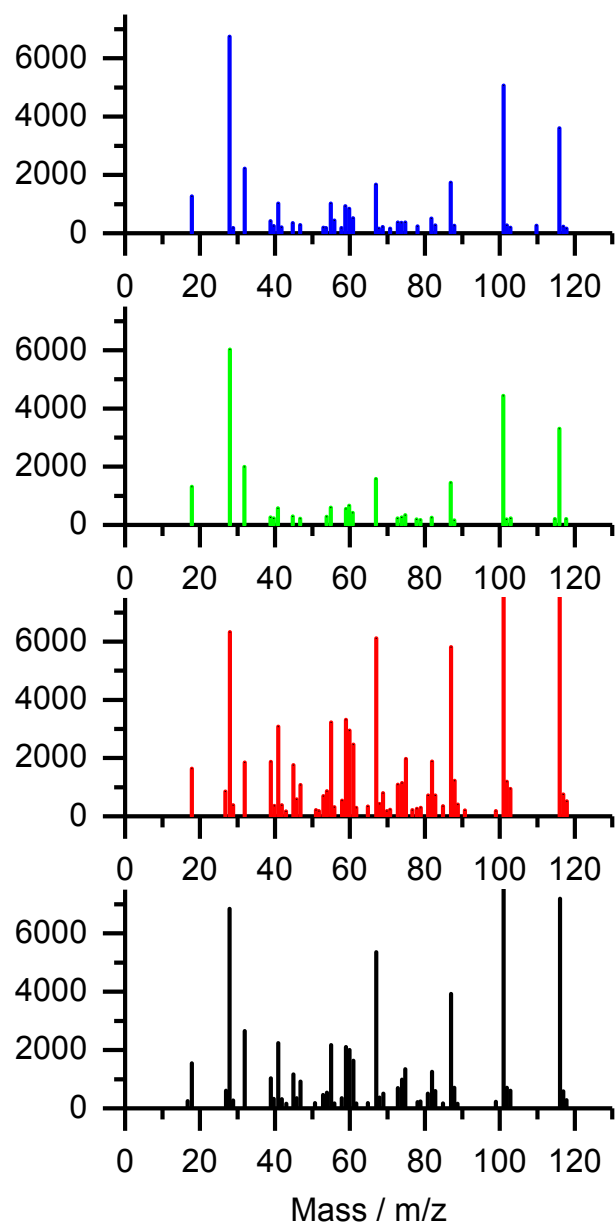


**Figure S12.** Mass spectra from Py-GC-MS measurements at a retention time of 7.8 min (yellow region in Figure 4), assigned to 4-methylthiane.



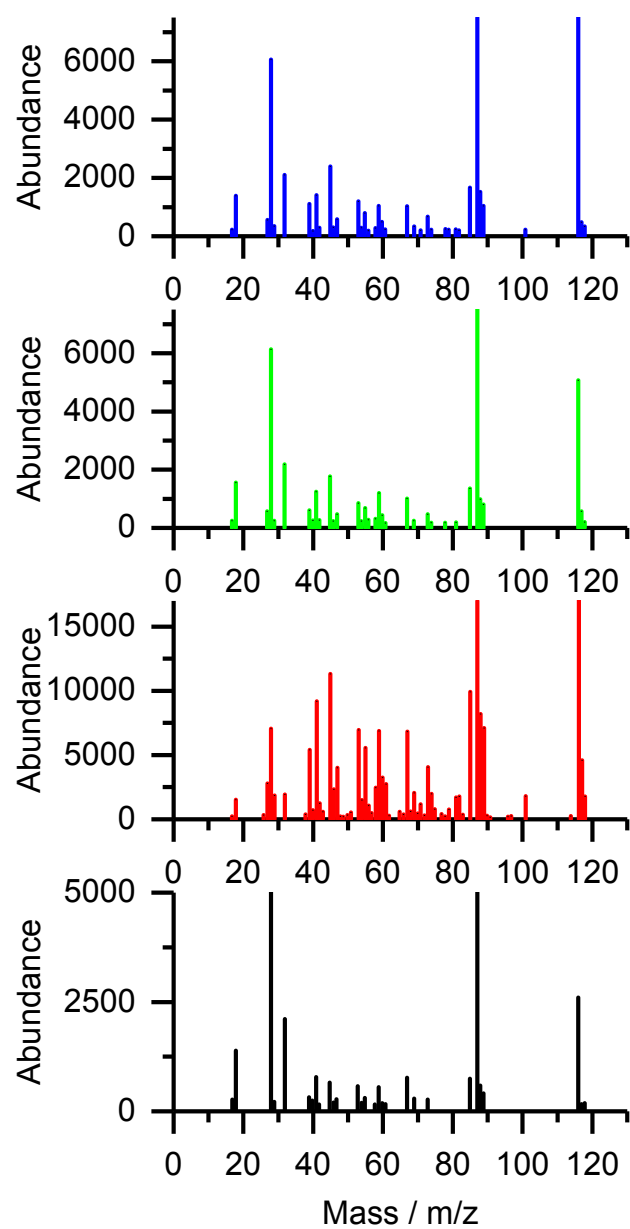


**Figure S13.** Mass spectra from Py-GC-MS measurements at a retention time of 8.2 min (yellow region in Figure 4), assigned to 2-ethylthiophane.

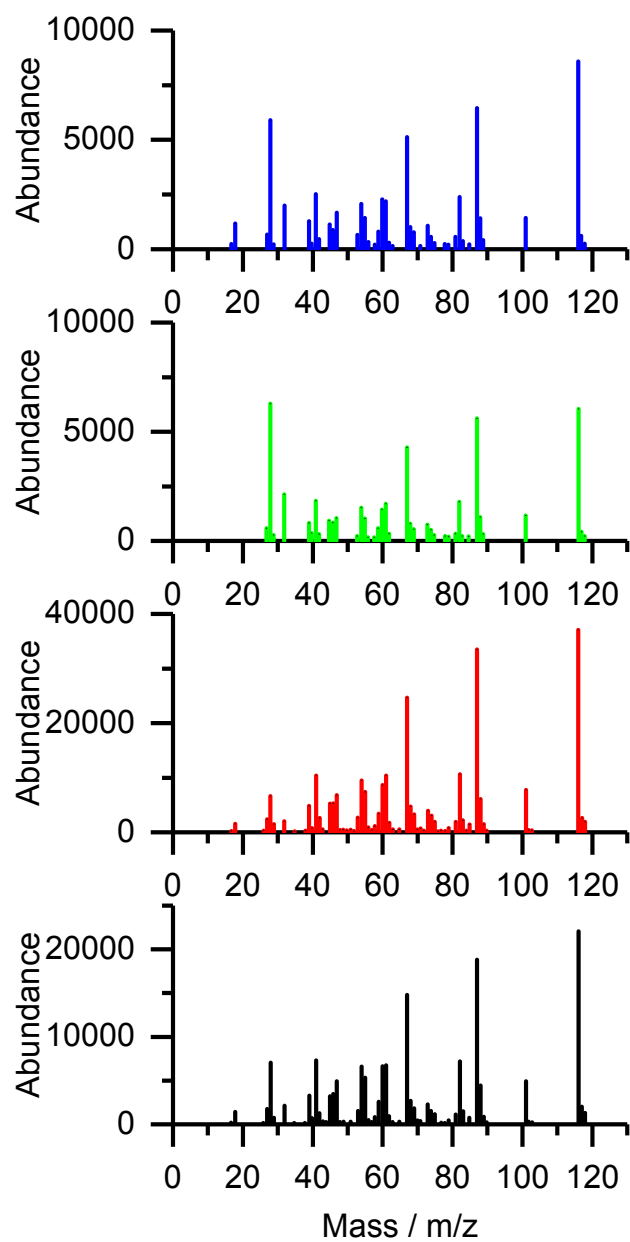


**Figure S14.** Mass spectra from Py-GC-MS measurements at a retention time of 9.3 min (yellow region in Figure 4), assigned to thiepane.

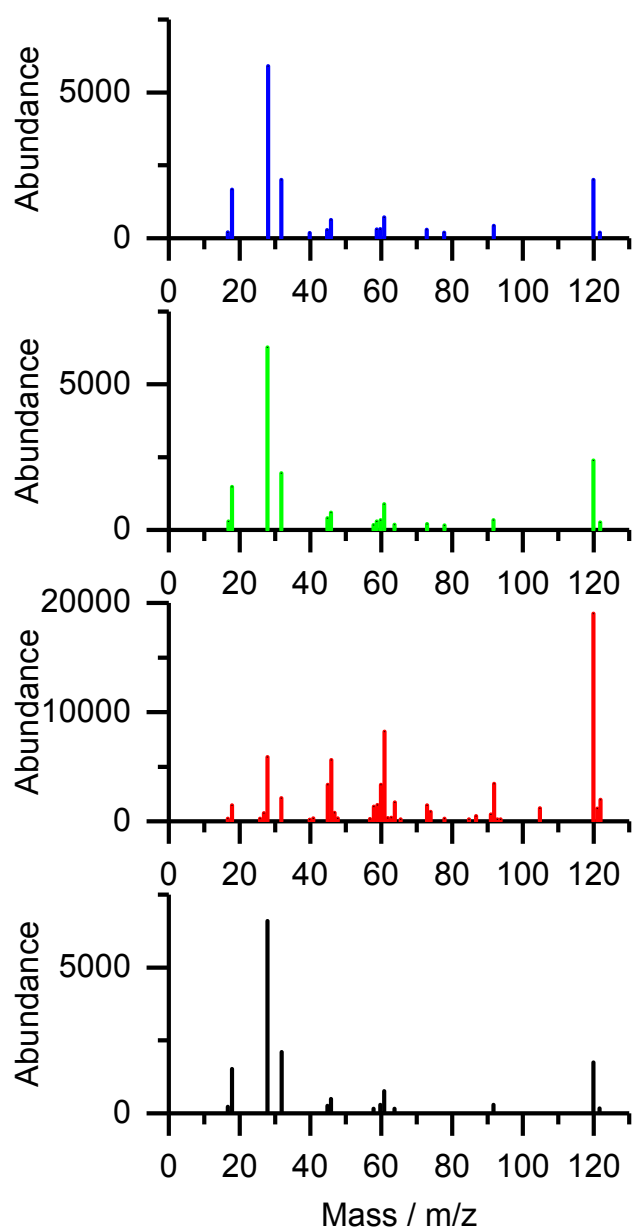


**Figure S15.** Mass spectra from Py-GC-MS measurements at a retention time of 10.2 min (yellow region in Figure 4), assigned to 1,4-dithiane.

## Surface Etching

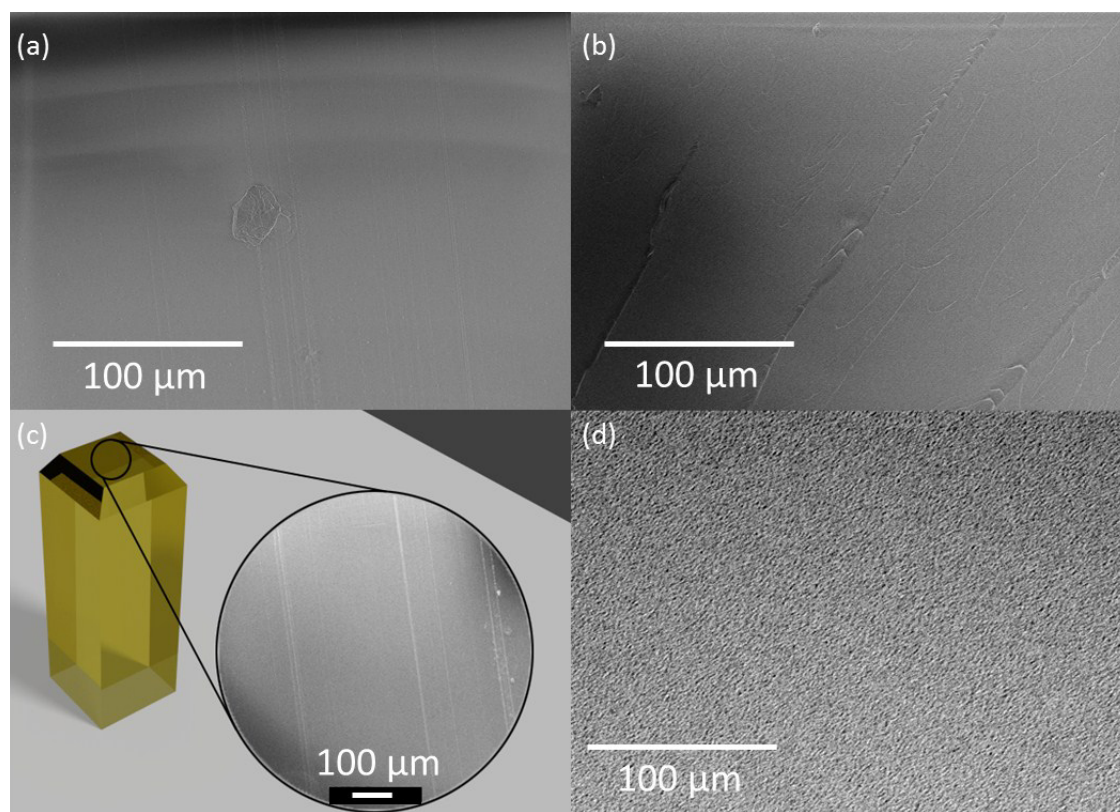


**Figure S16.** Electron microscopy images of EP-4: (a) SEM image of surface; (b) SEM image of surface after etching in dichloromethane under cryogenic conditions; (c) illustrated cut block used in etching experiments; (d) TEM image of surface stained with ruthenium tetroxide, showing no phase separation.

## Glass-transition temperature from Differential Scanning Calorimetry

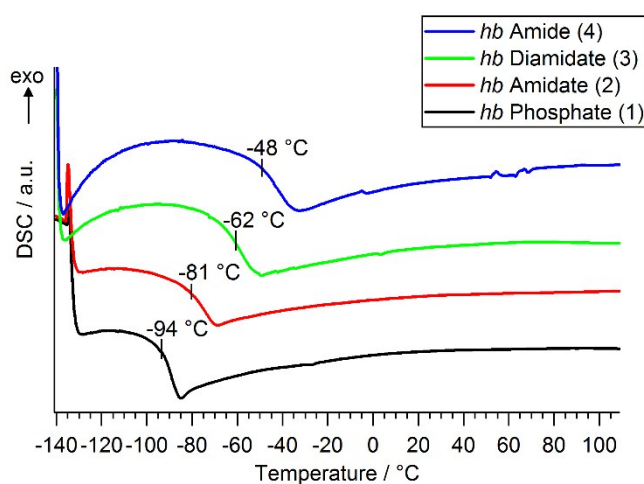


**Figure S17.** DSC curves of *hb*-FRs and noted glass-transition temperature ( $T_g$ )

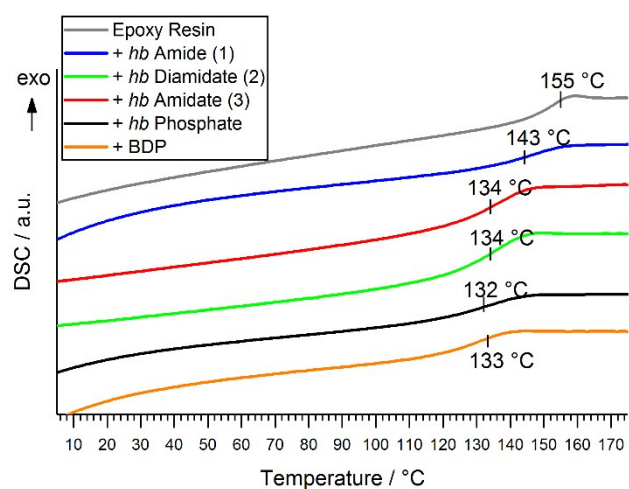


**Figure S18.** DSC curves of EP-*hb*-FRs and noted glass transition temperature ( $T_g$ ).

## Pyrolysis: Thermogravimetric Analysis of EP-*hb*-FRs

**Table S4.** Summary of TGA mass loss experiments of epoxy resins and flame retarded variants.

Material	$T_{5\%} / ^\circ\text{C}$	$T_{\text{max}} / ^\circ\text{C}$	$T_{\text{shoulder}} / ^\circ\text{C}$	Mass loss / wt.-% (pre-main step)	Mass loss / wt.-% (main step)	Mass loss / wt.-% (shoulder)	Residue / wt.-% (700 °C)
DGEBA-DMC	337.6 ± 0.9	372.4 ± 1.0	424.0 ± 5.0	-	62.0 ± 0.8	33.2 ± 0.3	4.5 ± 0.1
+ BDP	304.1 ± 1.2	357.3 ± 0.3	423.2 ± 0.1	-	74.6 ± 0.2	16.1 ± 0.3	8.2 ± 0.1
+ <i>hb</i> Phosphate (4)	288.6 ± 1.4	350.8 ± 1.2	423.8 ± 5.8	19.9 ± 0.1	54.6 ± 0.1	23.2 ± 0.7	7.7 ± 0.1
+ <i>hb</i> Amidate (3)	293.8 ± 3.2	351.8 ± 0.3	421.3 ± 3.9	-	77.8 ± 0.4	15.0 ± 0.2	6.8 ± 0.4
+ <i>hb</i> Diamidate (2)	286.6 ± 2.3	351.9 ± 2.0	423.2 ± 0.1	4.4 ± 0.2	69.8 ± 0.1	16.8 ± 0.2	8.1 ± 0.3
+ <i>hb</i> Amide (1)	282.6 ± 0.9	350.7 ± 1.2	420.5 ± 0.5	3.0 ± 0.1	74.7 ± 0.3	12.9 ± 0.2	8.0 ± 0.2

## Pyrolysis: Condensed Phase Analysis

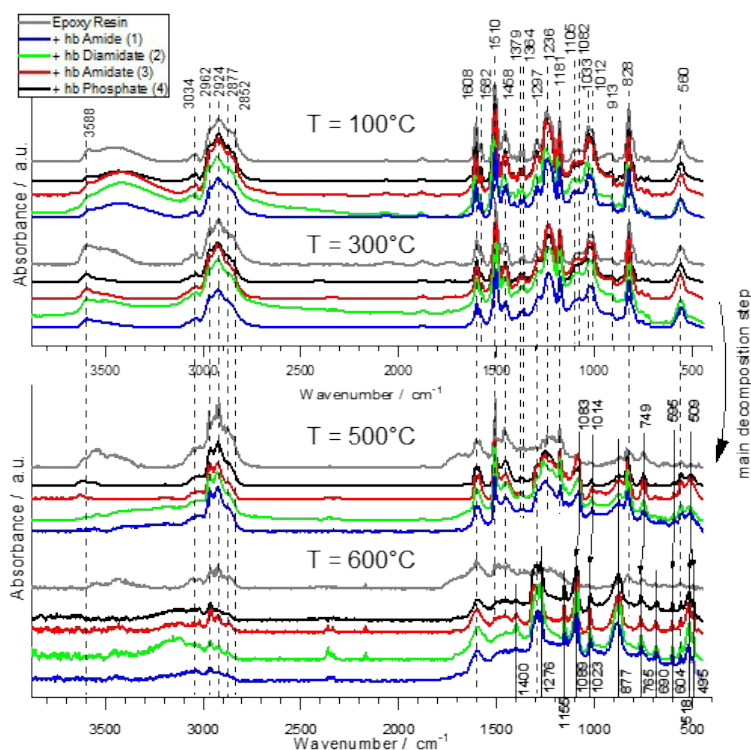


**Figure S19.** Condensed phase FTIR spectra of EP and EP-FRs at specific  $T$  via hot stage FTIR measurements. Dotted lines: EP signals; solid lines: P signals.

**Table S5.** Various phosphorus FTIR signals from literature compared to measured signals.

Measured [ $\text{cm}^{-1}$ ]	Literature [ $\text{cm}^{-1}$ ]	Group
2362	2200–2360 <sup>13</sup>	$\text{R}_2\text{-(P=S)=O}$
	2600–2540 <sup>13</sup>	$\text{R-(S-H)}$
1400	1100–1400 (cyclic compound) <sup>14</sup>	$\nu(\text{P=N})$
	1230–1500 (acyclic compound) <sup>14</sup>	
1400	1380–1425 <sup>15</sup>	(P-N-Ph)
1297–1276	1300–1250 <sup>15</sup>	$\nu(\text{P=O})$ ;
1297–1276	1346–1255 <sup>13</sup>	$\nu_{\text{sym}}(\text{P-CH}_3)$
1155	1240–1180 <sup>15</sup>	$\text{R}_2\text{-(P=O)-OH}$
	1240–1190 <sup>15</sup>	P-O-(Aryl-C)
1089	1130–1090 <sup>13</sup>	$\nu(\text{P-Ph})$
	1050–1030 <sup>15</sup>	P-O-(Alkyl-C)
1023	1130–1090 <sup>15</sup>	Phosphate (inorganic)
	1040–909 <sup>13</sup>	$\nu(\text{P-OH)=O}$
877 (wide)	990–885 <sup>15</sup>	P-O-P
	977–842 (interacts with P-O-C) <sup>13</sup>	$\delta_{\text{wag}}(\text{P-H})$
765, 690	754–634 <sup>13</sup>	$\nu(\text{P-C})$
604, 518, 495	540–485 <sup>14</sup>	$\nu_{\text{skel}}(\text{C-C})$

Hot Stage FTIR analysis was used to determine the changes in chemical structure of EP-*hb*-FRs in the condensed phase; spectra are from 100 °C, 300 °C (between  $T_{5\%}$  and  $T_{max}$ ), 500 °C (after  $T_{max}$ ), and 600 °C (Figure S19). At  $T > T_{max}$ , i.e. the spectra at 500 and 600 °C, the disappearance of characteristic DGEBA-DMC bands of the EP was detected, due to thermal decomposition of the matrix as previously reported.<sup>16</sup> At  $T = 600$  °C, there were only very few characteristic bands visible and the spectrum was very noisy due to complete decomposition. Especially bands at 1510  $\text{cm}^{-1}$  (bisphenol A) and at 1224 and 1028  $\text{cm}^{-1}$  (2-hydroxytrimethylene) showed a strong decrease in absorption due to volatilization of bisphenol A units. The EP-*hb*-FR spectra revealed the appearance of bands which were assigned to various phosphorus-containing species at  $T = 500$  °C and especially at  $T = 600$  °C (Table S5). Crucially, the band at 1400  $\text{cm}^{-1}$  corresponding to (P=N) or (P-N-Ph) stretching vibrations and is visible for the resins with N-containing FRs, which correlates with previous investigations of the monomeric FR variants. This band was visible for EP-**4** as well, indicating that **4** interacts with the decomposing EP's amine component. The broad band between 1350–1250  $\text{cm}^{-1}$  was assigned to the (P=O) or (P-CH<sub>3</sub>) stretching vibration. The bands at 1155  $\text{cm}^{-1}$  and the strong signal at 1089  $\text{cm}^{-1}$  belong to (P=O) or aromatic hydrocarbons bound to phosphorus. The absorption band at 1089  $\text{cm}^{-1}$  has also been noted in (-P-O-P-O) containing structures.<sup>17</sup> The broad band at 877  $\text{cm}^{-1}$  was identified as those from di-substituted aromatic rings,<sup>18, 19</sup> but may also indicate the presence of (P-O-P) bonds.<sup>20</sup> The two bands at 765 and 690  $\text{cm}^{-1}$  indicated the formation of (P-C) bonds.

### **Flammability: Reaction to Small Flames**

EP and all EP-FRs were tested *via* UL-94 and limiting oxygen index (LOI) experiments to ascertain their flammability characteristics and reaction-to-small-flame behavior. The results of these experiments are summarized in Table S6. EP exhibited an oxygen index (OI) of 18.7 vol.-% in LOI experiments and the addition of FRs increased OI above 22 vol.-%. The benchmark FR BDP increased OI to the highest value of all tested materials (24.0 vol.-%). For *hb*-FRs, EP-**4** displayed the lowest OI of all tested materials (22.1 vol.-%), and the OI increased with increasing N-content in the P-binding sphere, with EP-**1** presenting the highest OI of all *hb*-FRs (23.3 vol.-%). Although the change in OI is not very pronounced, it is explained by the decomposition mechanism described in Scheme 2: *hb*-FRs with more (P-N) bonds form thermally stable char and suppress flammability more effectively than those materials with higher amounts of (P-O) bonds.

**Table S6.** Results of reaction-to-small-flame tests LOI and UL-94 for EP and EP-FRs.

	EP	EP-1	EP-2	EP-3	EP-4	EP-BDP
<b>LOI</b>						
O <sub>2</sub> / vol.-%	18.7 ± 0.3	23.3 ± 0.2	22.6 ± 0.2	22.5 ± 0.2	22.1 ± 0.2	24.0 ± 0.2
<b>UL-94</b>						
Classification	HB	HB	HB	HB75	HB	HB
Burn speed / mm s <sup>-1</sup>	31.7 ± 3.6	22.0 ± 0.7	27.0 ± 0.1	41.8 ± 1.5	27.7 ± 4.4	19.6 ± 3.6

The UL-94 test results highlighted that all materials fail to attain a V-classification due mainly to the intense burning and the flaming dripping of the EP matrix. In horizontal tests, all materials achieved an HB classification, except EP-**3**. EP showed a burn speed of 31.7 mm s<sup>-1</sup>, and EP-BDP attained the lowest burning speed at 19.6 mm s<sup>-1</sup>. EP-*hb*-FRs exhibited lower burning speed than EP, and EP-**1** had the lowest value (22.0 mm s<sup>-1</sup>). The reduction in burning speed in UL-94 tests also point to a reduction of flammability with increasing P-N bonds of the *hb*-system for the same reason. The reaction-to-small-flames experiments highlight that higher loadings than the chosen FR load (10 wt.-%) are necessary to attain OI-values and V-classification required for high-performance materials.<sup>21</sup> However, it must be stated that the results exemplify that a reduction of burning speed and a relative increase in OI of approx. 18–26% was possible already at relatively low loadings, signifying the efficacy of *hb*-FRs in EP.

### **Fire Behavior**

**Table S7.** Maximum average rate of heat emission (MARHE) and fire growth rate (FIGRA) of EP and EP-FRs via cone calorimeter measurements.

	EP	EP-1	EP-2	EP-3	EP-4	EP-BDP
MARHE / kWm <sup>-2</sup>	732 ±24	571 ±25	560 ±16	439 ±3	466 ±14	546 ±12
FIGRA / kWm <sup>-2</sup> s <sup>-1</sup>	15.5 ±2.3	10.0 ±0.1	8.1 ±0.1	7.5 ±0.6	9.0 ±0.2	11.0 ±0.7

The maximum average rate of heat emission (MARHE, from DIN CEN/TS 45545) and fire growth rate (FIGRA, from EN 13823) are used to assess fire protection behavior and help to quantify combustion and flame inhibition into tangible values (Table S7). For EP, the MARHE was 732 kW m<sup>-2</sup> and the FIGRA was 15.5 kW m<sup>-2</sup> s<sup>-1</sup>. EP-BDP displayed a 25% lower MARHE (546 kW m<sup>-2</sup>) and a 29% lower FIGRA (11.0 kW m<sup>-2</sup> s<sup>-1</sup>). Furthermore, all EP-*hb*-FRs exhibited a 22–36% reduction in MARHE and a 35–48% lower FIGRA. All *hb*-FRs reduced FIGRA more strongly than BDP, while only **3** and **4** lowered the MARHE more strongly than BDP. Although there are differences among the respective *hb*-FRs in terms of lowering PHRR, THE, MARHE, and FIGRA, the results speak for the ability of the chemical superstructure of the *hb*-FRs to perform on equal terms to an aromatic benchmark FR under forced flaming conditions, further illustrating their multifunctional abilities.

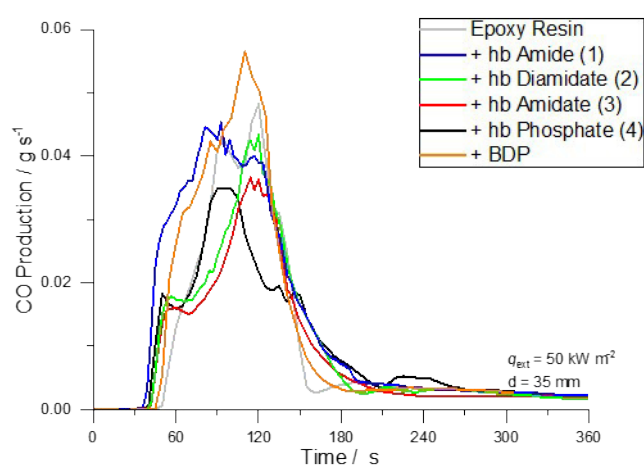


**Figure S20.** Carbon monoxide (CO) production over  $t$  of EP and EP-FRs during cone calorimeter measurements.

**Table S8. CO yields (COY)**

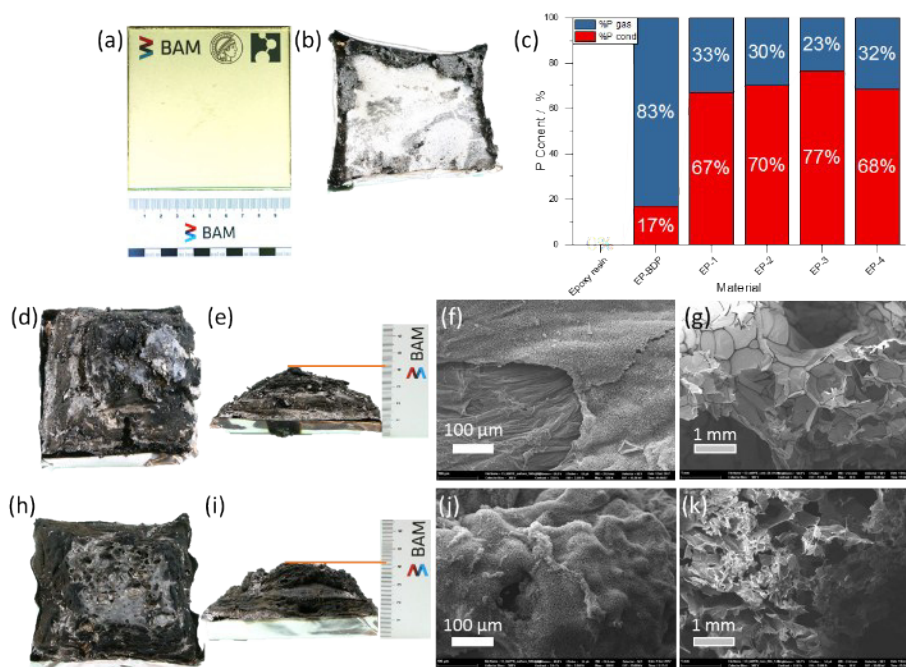
	EP	EP-1	EP-2	EP-3	EP-4	EP-BDP
COY / 10 <sup>-2</sup> g g <sup>-1</sup>	9.0 ±1.0	12.9 ±0.5	9.8 ±0.2	9.4 ±0.1	9.9 ±0.1	11.3 ±0.7

Figure S20 shows the carbon monoxide (CO) production during cone calorimeter measurements, and CO yields (COY) are displayed in Table S8. The CO production during combustion is crucial to understanding the FR effect: a reduction in  $\chi$  (combustion efficiency) is accompanied by an increase in CO and smoke production, as they are byproducts of an incomplete combustion. Consequently, efficient flame inhibition is intrinsically accompanied by an increase in COY.<sup>22</sup> EP showed a CO yield of  $9.0 \cdot 10^{-2} \text{ g g}^{-1}$ , while EP-BDP exhibited a 26% increase in COY. The *hb*-FRs increased COY by 4–43%: EP-1 showed the largest COY increase (43%), indicating the most incomplete combustion for this material, while EP-3 displayed the lowest relative COY increase at 4%. Table 1 also compares the material's EHC, which is a parameter for gas phase activity, and a reduction in EHC signifies effective flame inhibition.<sup>23</sup> BDP, **3**, and **4** lowered EHC in EP by 16, 6 and 10%, respectively, while **2** had no effect on EHC of EP, and **1** actually increased EHC by 5%. These results provide further evidence that *hb*-FRs with higher O-content in the binding sphere of P show a stronger gas phase mechanism resulting in lower EHC, while those with higher N-content present a more pronounced condensed phase mechanism that leads to a decreased combustion efficiency and higher CO yield. These findings correlate well with the mass loss behavior of *hb*-FRs under pyrolysis, where a critical O:N ratio governed the decomposition behavior.



## Residue analysis:

The residues from cone calorimeter tests were investigated *via* scanning electron microscopy (SEM) and elemental analysis to understand the micro- and macroscopic effects of *hb*-FRs on EP. The residues in Figure S21 exemplify the condensed phase effect of *hb*-FRs: Figure S21a shows an EP specimen before and Figure S21b displays the residue after cone calorimeter measurements. EP combusted almost completely with only a very small residue amount (0.7 wt.-%). For EP-*hb*-FRs (Figure S21d,e,h,i), the formation of char fixed fuel into the condensed phase leading to increased residue yields (7–12 wt.-%). The residues had a puffy, foam-like structure. The voluminous structure pointed to an intumescent system, as evidenced by the swollen characteristic of the char-structure averaging at 4 cm in height (Figure S21e,i). Cross-sections of the residues revealed a multicellular structures, and SEM images from the residue surfaces (Figure S21f,j) and cores (Figure S21g,k) provided further evidence of an intumescent system.<sup>24,25</sup> The morphology of the residue cores consisted of a 3-D network of bubble-like surfaces with an open cell structure.<sup>26</sup> The bubbles' diameter ranged from <300  $\mu\text{m}$  for EP-1 to roughly 500  $\mu\text{m}$  for EP-4. The surface images exemplify that the protective layer of the intumescent char relied on the formation of bubbles insulating the underlying material from irradiation. The bubbles near the top of the sample were exposed to radiation and thermo-oxidation after flame-out, leading to a fusing of the cells and the formation of a rough carbonaceous surface topography. This explains the phenomenon seen in cone calorimeter measurements, where a decline in HRR and a small plateau-like shape of the HRR(*t*) curve roughly 20–30 s after the ignition was observed. The decomposing material formed an intumescent foam and when the top layer decomposed, its insulating properties diminished, resulting in renewed decomposition of the underlying material. Notably, the bubble-size for EP-4 were larger than those in EP-1. This phenomenon results from increased partial pressure inside the material caused by the higher gas production of EP-4 during decomposition, which led to better thermal insulation and lower PHRR.



**Figure S21.** Residue analysis of samples after cone calorimeter experiments; (a) Image of EP specimen before measurement; (b) EP specimen after measurement, exhibiting little residue; (c) P-content in gas (blue) and condensed (red) phase, calculated *via* elemental analysis of residues; (d,h) Residue image (top view) of EP-4 and EP-1; (e,i) Residue image (profile view) of EP-4 and EP-1; (f,j) SEM images of EP-4 and EP-1 residue surface; (g,k) SEM image of EP-4 and EP-1 residue core.

Figure S21c portrays the P-content in the condensed phase (red) of residues after cone calorimeter measurements *via* elemental analysis. The amount of P present in the gas phase (blue) was calculated by subtracting the measured mass of P in the residue from the calculated mass of P in the initial EP-FR. As Figure S21c shows, BDP had 17% P-content in the condensed phase, meaning 83% of P went into the gas phase, which is in accordance with previous findings.<sup>8, 27</sup> Figure S21c also displays that, while there are differences in the P-content among them, all *hb*-FRs exhibited between 67–77% P-content in the condensed and 23–33% in the gas-phase. This corresponds well with the increase in residue yields of EP-*hb*-FRs in forced-flaming tests and showcases the ability of *hb*-FRs to retain fuel *via* specific reactions of P in the condensed phase. It should be noted that the elemental analysis was performed on residue samples

taken after cone calorimeter measurements (end of test) and not specifically at flame-out, meaning there is substantial thermo-oxidation of the sample. As many (P-N)-containing species are not thermally stable, their decomposition during thermo-oxidation explains the lower P-content of EP-1 and EP-2 samples.

However, when comparing *hb*-FRs to their low molar mass monomers, the results from elemental analysis point to a shift in mode of action. In previous findings, the monomer of **1** exhibited an 80% P-content in the condensed phase, while the monomer of **2** displayed 55% P-content in the gas phase.<sup>28</sup> This change in condensed phase activity can be rationalized by the increase in chemical interaction between EP and FR during combustion due to the higher thermal stability of *hb*-FR, further highlighting the multifunctional capabilities of P-FRs with complex molecular architectures.

## References

1. D. Marsh, *The Kinetics of the Thermal Decomposition of Isopropyl Methylphosphonofluoridate*, Chemical Defence Experimental Establishment Porton Down (United Kingdom), 1954.
2. K. N. Bauer, L. Liu, D. Andrienko, M. Wagner, E. K. Macdonald, M. P. Shaver and F. R. Wurm, *Macromolecules*, 2018, **51**, 1272-1279.
3. P. A. Glaude, C. Melius, W. J. Pitz and C. K. Westbrook, *P Combust Inst*, 2002, **29**, 2469-2476.
4. S. Hörold, *Polymer Degradation and Stability*, 1999, **64**, 427-431.
5. W. Gerrard, *J Chem Soc*, 1944, DOI: DOI 10.1039/jr9440000085, 85-90.
6. R. W. Baier and S. W. Weller, *Ind Eng Chem Proc Dd*, 1967, **6**, 380-&.
7. S. Gaan, G. Sun, K. Hutches and M. H. Engelhard, *Polymer Degradation and Stability*, 2008, **93**, 99-108.
8. S. V. Levchik and E. D. Weil, *Journal of Fire Sciences*, 2006, **24**, 345-364.
9. S. V. Levchik, G. F. Levchik, A. I. Balabanovich, E. D. Weil and M. Klatt, *Angew Makromol Chem*, 1999, **264**, 48-55.
10. C. Nguyen and J. Kim, *Polymer Degradation and Stability*, 2008, **93**, 1037-1043.
11. S. V. Levchik, in *Flame Retardant Polymer Nanocomposites*, eds. A. B. Morgan and C. A. Wilkie, John Wiley & Sons, Inc., 2006, DOI: 10.1002/9780470109038.ch1, pp. 1-29.
12. E. D. Weil, *Fire retardancy of polymeric materials*, 2000, 115-145.
13. C. Hampton, D. Demoin and R. E. J. O. S. Glaser, 2010.
14. G. Socrates, *Infrared and Raman characteristic group frequencies: tables and charts*, John Wiley & Sons, 2004.
15. M. Hesse, H. Meier and B. Zeeh, *Spektroskopische Methoden in der organischen Chemie*, Georg Thieme Verlag, 2005.
16. B. Perret, B. Schartel, K. Stöß, M. Ciesielski, J. Diederichs, M. Döring, J. Krämer and V. Altstädt, *European Polymer Journal*, 2011, **47**, 1081-1089.
17. L. C. Thomas, *Interpretation of the infrared spectra of organophosphorus compounds*, Heyden London, 1974.
18. A. S. Politou, C. Morterra and M. J. D. Low, *Carbon*, 1990, **28**, 529-538.
19. M. C. Despinasse and B. Schartel, *Thermochimica Acta*, 2013, **563**, 51-61.
20. U. Braun, A. I. Balabanovich, B. Schartel, U. Knoll, J. Artner, M. Ciesielski, M. Döring, R. Perez, J. K. W. Sandler, V. Altstädt, T. Hoffmann and D. Pospiech, *Polymer*, 2006, **47**, 8495-8508.
21. A. F. Grand and C. A. Wilkie, *Fire retardancy of polymeric materials*, CRC Press, 2000.
22. B. Schartel, *Materials*, 2010, **3**, 4710-4745.
23. B. Schartel, B. Perret, B. Dittrich, M. Ciesielski, J. Krämer, P. Müller, V. Altstädt, L. Zang and M. Döring, *Macromolecular Materials and Engineering*, 2016, **301**, 9-35.
24. J. Alongi, Z. D. Han and S. Bourbigot, *Progress in Polymer Science*, 2015, **51**, 28-73.
25. P. Müller, M. Morys, A. Sut, C. Jäger, B. Illerhaus and B. Schartel, *Polymer Degradation and Stability*, 2016, **130**, 307-319.
26. S. Bourbigot and M. Le Bras, in *Plastics Flammability Handbook*, ed. J. Troitzsch, Carl Hanser Verlag GmbH & Co. KG, Munich, 2004, DOI: 10.3139/9783446436695.005, pp. 133-172.
27. S. Rabe, Y. Chuenban and B. Schartel, *Materials*, 2017, **10**, 23.
28. J. C. Markwart, A. Battig, L. Zimmermann, M. Wagner, J. Fischer, B. Schartel and F. R. Wurm, *ACS Applied Polymer Materials*, 2019, **1**, 1118-1128.



Cite this: *Polym. Chem.*, 2019, **10**, 4621

DOI: 10.1039/c9py90116g  
rsc.li/polymers

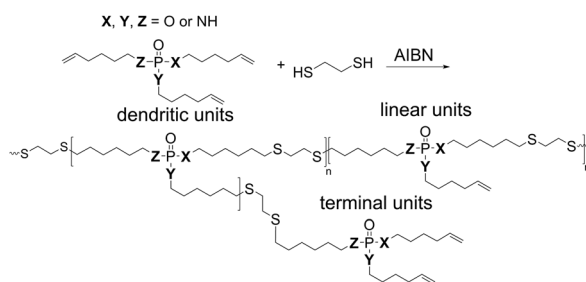
## Correction: Hyperbranched phosphorus flame retardants: multifunctional additives for epoxy resins

Alexander Battig,<sup>a</sup> Jens C. Markwart,<sup>b,c</sup> Frederik R. Wurm<sup>\*b</sup> and Bernhard Schartel<sup>\*a</sup>

Correction for 'Hyperbranched phosphorus flame retardants: multifunctional additives for epoxy resins' by Alexander Battig *et al.*, *Polym. Chem.*, 2019, DOI: 10.1039/c9py00737g.

The authors regret that the following points were not included/corrected in the original manuscript:

1. Author Jens C. Markwart's ORCID is missing in the original manuscript, the correct ORCID is 0000-0002-2796-7380.
2. In Scheme 1 in the original manuscript, there was an error in the amount of carbon atoms in the polymer-backbone. Furthermore, the bracket was not clearly visible. A corrected version of Scheme 1 is presented here.



**Scheme 1** Synthesis of *hb*-FRs via an  $A_2 + B_3$  thiol-ene polyaddition, and schematic representation of dendritic, linear, and terminal units of the *hb*-structure.

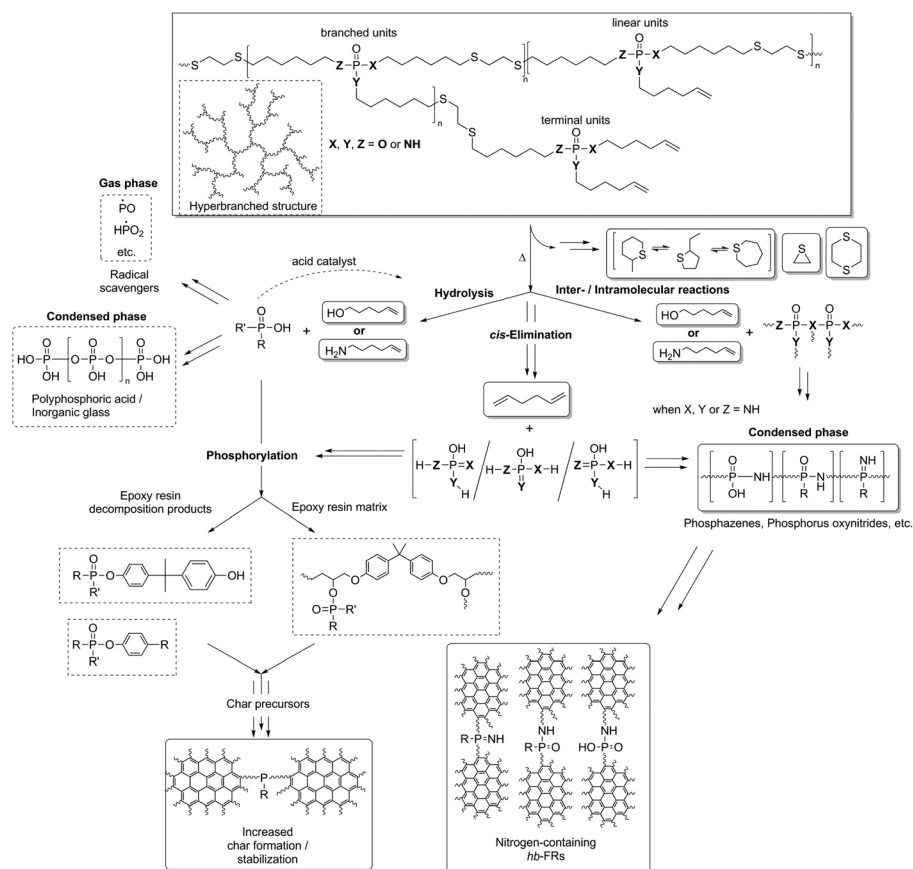
<sup>a</sup>Bundesanstalt für Materialforschung und -prüfung (BAM), Unter den Eichen 87, 12205 Berlin, Germany. E-mail: bernhard.schartel@bam.de

<sup>b</sup>Max Planck Institute for Polymer Research, Ackermannweg 10, 55128 Mainz, Germany. E-mail: wurm@mpip-mainz.mpg.de

<sup>c</sup>Graduate School Materials Science in Mainz, Staudinger Weg 9, 55128 Mainz, Germany



3. In Scheme 2 in the original manuscript, there was an error in the amount of carbon atoms in the polymer-backbone. Additionally, some atoms were missing a label. A corrected version of Scheme 2 is presented here.



**Scheme 2** Proposed decomposition mechanism of *hb*-FRs and FR interaction with EP during thermal decomposition of EP-*hb*-FRs. Solid squares: identified products (TG-FTIR, hot stage FTIR, etc.).

4. The following sentence is missing from the Acknowledgements section in the original manuscript: Jens C. Markwart and Frederik R. Wurm thank Christine Rosenauer (MPIP) for the GPC/MALS analysis.

The Royal Society of Chemistry apologises for these errors and any consequent inconvenience to authors and readers.



#### 5.4. Aromatic vs. Aliphatic Hyperbranched Polyphosphoesters as Flame Retardants in Epoxy Resins

Jens C. Markwart, Alexander Battig, Maria M. Velencoso, Dennis Pollock, Bernhard Schartel, Frederik R. Wurm, *Molecules* **2019**, 24(21), 3901.

DOI link: <https://www.doi.org/10.3390/molecules24213901>

This article was accepted and published.

Author contribution:


- Aided in conceptualizing the frame of the work
- Chose the polymer materials, approach, loading, sample preparation and testing
- Pyrolytic investigations of the flame retardants (FRs)
  - Thermogravimetric analysis
  - Evolved gas and condensed phase FTIR
  - Pyrolysis gas chromatography / mass spectrometry
  - Pyrolysis combustion flow calorimeter
- Material and fire testing of FR-containing epoxy resins
  - Differential scanning calorimeter
  - Cone calorimeter, LOI and UL-94
  - Scanning electron microscopy, photography
- Collection, analysis, and interpretation of the data.
- Provided figures throughout the article, including decomposition mechanism
- Authored the results and discussion chapter with respect to flame-retardancy
- Scientific discussion, conclusions, maintained communication of all authors
- Proofread and spell-checked all versions of the article

## **Abstract**

The current trend for future flame retardants (FRs) goes to novel efficient halogen-free materials, due to the ban of several halogenated FRs. Among the most promising alternatives are phosphorus-based FRs, and of those, polymeric materials with complex shape have been recently reported. Herein, we present novel halogen-free aromatic and aliphatic hyperbranched polyphosphoesters (hbPPEs), which were synthesized by olefin metathesis polymerization and investigated them as a FR in epoxy resins. We compare their efficiency (aliphatic vs. aromatic) and further assess the differences between the monomeric compounds and the hbPPEs. The decomposition and vaporizing behavior of a compound is an important factor in its flame-retardant behavior, but also the interaction with the pyrolyzing matrix has a significant influence on the performance. Therefore, the challenge in designing a FR is to optimize the chemical structure and its decomposition pathway to the matrix, with regards to time and temperature. This behavior becomes obvious in this study, and explains the superior gas phase activity of the aliphatic FRs.

Article

# Aromatic vs. Aliphatic Hyperbranched Polyphosphoesters as Flame Retardants in Epoxy Resins

Jens C. Markwart <sup>1,2,†</sup>, Alexander Battig <sup>3,†</sup>, Maria M. Velencoso <sup>1</sup>, Dennis Pollok <sup>1</sup>, Bernhard Schartel <sup>3,\*</sup>  and Frederik R. Wurm <sup>1,\*</sup>

<sup>1</sup> Max-Planck-Institut für Polymerforschung, Ackermannweg 10, 55128 Mainz, Germany; markwart@mpip-mainz.mpg.de (J.C.M.); maria.mvelencoso@gmail.com (M.M.V.); pollok@uni-mainz.de (D.P.)

<sup>2</sup> Graduate School Materials Science in Mainz, Staudinger Weg 9, 55128 Mainz, Germany

<sup>3</sup> Bundesanstalt für Materialforschung und-prüfung (BAM), Unter den Eichen 87, 12205 Berlin, Germany; alexander.battig@bam.de

\* Correspondence: bernhard.schartel@bam.de (B.S.); wurm@mpip-mainz.mpg.de (F.R.W.)

† These authors contributed equally to this work.

Received: 4 October 2019; Accepted: 23 October 2019; Published: 29 October 2019



**Abstract:** The current trend for future flame retardants (FRs) goes to novel efficient halogen-free materials, due to the ban of several halogenated FRs. Among the most promising alternatives are phosphorus-based FRs, and of those, polymeric materials with complex shape have been recently reported. Herein, we present novel halogen-free aromatic and aliphatic hyperbranched polyphosphoesters (hbPPEs), which were synthesized by olefin metathesis polymerization and investigated them as a FR in epoxy resins. We compare their efficiency (aliphatic vs. aromatic) and further assess the differences between the monomeric compounds and the hbPPEs. The decomposition and vaporizing behavior of a compound is an important factor in its flame-retardant behavior, but also the interaction with the pyrolyzing matrix has a significant influence on the performance. Therefore, the challenge in designing a FR is to optimize the chemical structure and its decomposition pathway to the matrix, with regards to time and temperature. This behavior becomes obvious in this study, and explains the superior gas phase activity of the aliphatic FRs.

**Keywords:** phosphorus; metathesis; dendritic; cone calorimeter; fire test

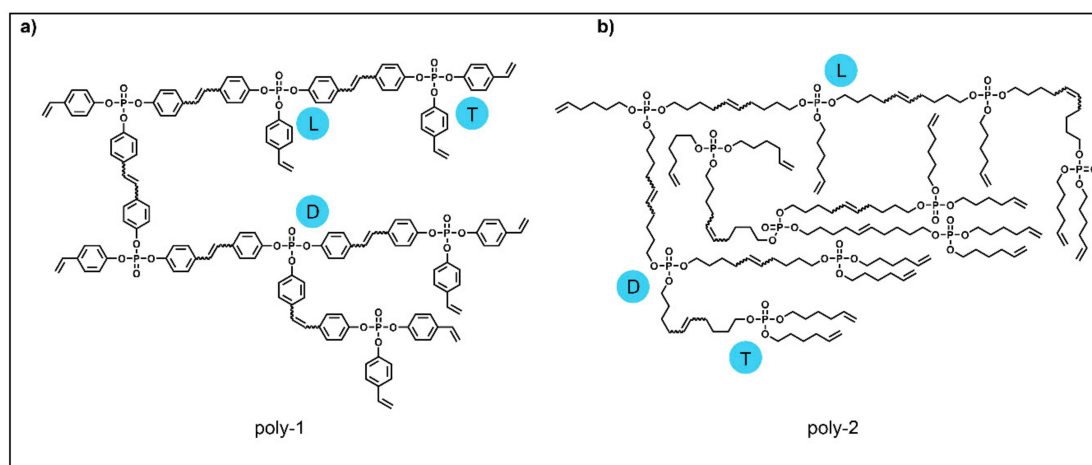
## 1. Introduction

The overlap of the decomposition temperatures of a flame retardant (FR) and its polymer matrix is essential for its effectiveness in the case of fire [1–4]. Aromatic polymers typically have higher thermal stability than aliphatic polymers. In the case of a FR, this higher thermal stability influences at which temperatures the active species are available in the gas phase. An important example of this behavior was reported for brominated aromatic and aliphatic FRs in polypropylene. The thermal decomposition of aliphatic FRs starts below the thermal decomposition of polypropylene, which leads to a good performance in this matrix. Aromatic FRs decompose after polypropylene and therefore, at the decomposition temperature of polypropylene, no optimal debromination is achieved, resulting in mediocre performance [5].

Here, we compared an aromatic with an aliphatic hyperbranched polyphosphoester (hbPPE) prepared via acyclic triene metathesis (ATMET) polymerization as additive FRs in epoxy resins (Scheme 1). We discuss the structure-property relationship and utilize thermal analysis to understand



the flame-retardant mechanism and investigate the influence of the higher thermal stability of the aromatic compounds and the resulting availability of phosphorus in the gas phase [5].



**Scheme 1.** Chemical structures of the investigated polymers: a) the aromatic poly-1 and b) the aliphatic poly-2.

In spite of their high flammability, the excellent mechanical and insulating properties of epoxy resins have led to their widespread application as lightweight material products for construction or electrical equipment. In 2016, the market for epoxy resins had a volume of US\$ 21.5 billion [6]. Typically, epoxy resins are treated with FRs in many applications.

For several decades, halogenated FRs were used as effective FRs. However, in recent years, due to their potential harm to health and environment, their use has been legislatively restricted around the world, promoting a growing demand for halogen-free alternatives, of which phosphorus is an attractive alternative [7]. Phosphorus in the gas phase is reported to be similar or even superior to hydrogen halides like HBr [8], has attractive plasticizing properties [9], adjustable hydrophilicity [10] and potential degradability [11] and biocompatibility [12].

The versatility of polymer chemistry was used to address problems of low molar mass FRs, such as poor matrix compatibility, leaching or migration out of the polymer matrix. In the literature, polyphosphoesters are gaining increased attention as a promising class of polymeric FRs because of the aforementioned reasons and their versatile chemistry that allows tuning their chemical structure to control degradation behavior and matrix compatibility. Branched polymers with their high number of reactive or end-groups, lower intrinsic viscosities and higher matrix compatibility compared to linear polymers are interesting candidates for flame retardant additives [13–16]. Also, PPEs can be prepared as branched polymers, typically relying on the pentavalency of phosphorus [17]. However, the majority of hbPPEs reported in literature are aliphatic materials, only a few publications have reported on aromatic hbPPEs [18–22]. The field is dominated mostly by classical linear aromatic phosphates, such as resorcinol bis(diphenyl phosphate) or bisphenol A bis(diphenyl phosphate) due to their good flame retardant performance, but typically with relatively low molar mass and definition [23–25]. To further understand the flame retardant mechanism and improve performance, additional research in the field of hbPPEs is necessary and this work contributes to this development.

## 2. Results

Acyclic diene metathesis polymerization (ADMET) is a versatile technique to prepare a broad range of linear functional polymers [26–30]. Olefin metathesis is also able to polymerize an  $A_3$  monomer without any complementary  $B_2$  monomer needed to give a hyperbranched structure [15]. For the synthesis of aromatic hbPPEs via acyclic triene metathesis (ATMET) polymerization, an aromatic phosphoester with vinyl groups is mandatory. In this study, the synthesis of tris(*p*-vinylphenyl)phosphate (1) was performed in a single reaction step from  $POCl_3$  and 4-vinylphenol

without further purification such as distillation or chromatography, thus obtaining the A<sub>3</sub>-monomer in high purity and yield (Figure 1a). The resulting monomer is a liquid at room temperature and has a phosphorus content of 7.66 wt.-%. 1 is soluble in aromatic solvents (e.g., toluene) and halogenated solvents (e.g., dichloromethane and chloroform), and insoluble in water. 1 proved thermally stable until a temperature of 127 °C (measured by TGA), at which the vinyl groups undergo radical cross-linking, due mainly to the electron-withdrawing resonance effect of the adjacent phosphate at the ring. The cross-linking-reaction was proven by heating 1 to 300 °C in a silicon form for 2 h producing a hard, cross-linked PPE (Figure S23).

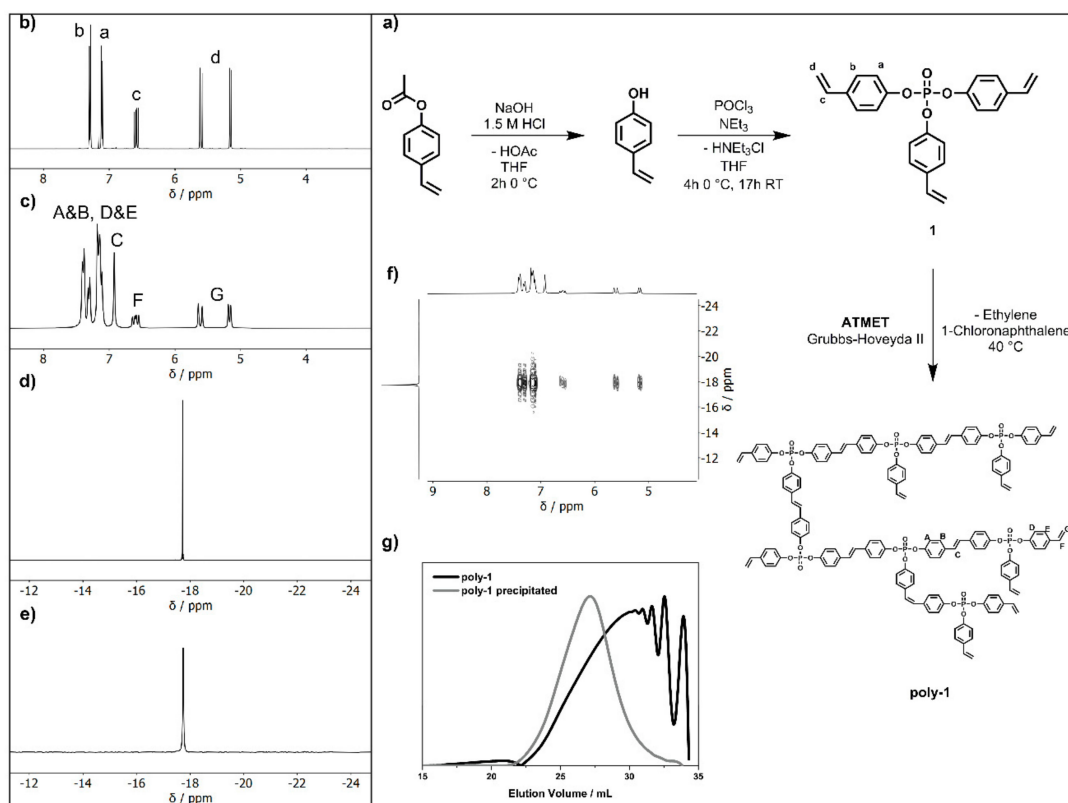


**Figure 1.** (a) Synthesis scheme of tris(p-vinylphenyl)phosphate (1) and poly(tris(p-vinylphenyl)phosphate) (hbPPE); (b) <sup>1</sup>H NMR spectra of 1; (c) <sup>1</sup>H NMR spectra of poly-1; (d) <sup>31</sup>P NMR spectra of 1; (e) <sup>31</sup>P NMR spectra of poly-1; (f) <sup>1</sup>H<sup>31</sup>P HMBC spectra of poly-1; (g) SEC curves of poly-1 before and after precipitation in Toluene.

1 was used as a novel A<sub>3</sub> monomer for the ATMET polymerization to produce poly-1. The protocol of the ATMET polymerization of 1 is described in Figure 1 a and in detail in the Experimental Part. The monomer was dissolved together with the respective Grubbs catalyst in a 37 wt.-% solution of 1-chloronaphthalene at 40 °C and the polymerization was conducted for 5 min in vacuo. Poly-1 was used as a flame-retardant additive in epoxy resins after precipitation into cold hexane. No polymerization in the bulk conditions at 60 °C was observed, probably due to the high viscosity of the monomer. We carried out polymerizations with Grubbs 1<sup>st</sup> generation catalyst at 40 °C and 60 °C, but almost only oligomers were observed ( $M_n < 1200 \text{ g mol}^{-1}$  from size exclusion chromatography (SEC), Figure S1). When Grubbs Hoveyda 2<sup>nd</sup> generation catalyst was used, a broad range of molecular weights was obtained, depending on the reaction conditions (Table S1 and Figure 1g). SEC showed a molar mass of ca.  $M_n 3000 \text{ g mol}^{-1}$  with dispersity  $M_w/M_n \approx 3$  after 120 min of reaction. However, when the addition of the catalyst was carried out in two phases, higher apparent molar masses of ca.  $M_n 4800 \text{ g mol}^{-1}$  with broad molar mass distribution ( $M_w/M_n \approx 11$ ) were obtained. Longer reaction times led to cross-linking of the material. To prevent cross-linking, the reaction can be terminated by the

addition of ethyl vinyl ether or methyl acrylate. The resulting polymer was partially soluble in aromatic solvents (e.g., toluene) but proved highly soluble in halogenated solvents (e.g., dichloromethane and chloroform). Extraction of the crude polymer with toluene resulted in the precipitation of the high molecular weight fractions, providing a poly-1 sample with a molar mass of ca.  $M_n$  11,500 g mol<sup>-1</sup> and  $M_w/M_n = 1.7$  from SEC (Figure 1g).

The polymerization of 1 was followed by <sup>1</sup>H NMR spectroscopy (Figure 1b,c). After polycondensation, the resonances of the terminal double bonds at 5.16 ppm, 5.61 ppm and 6.59 ppm decreased, and a new signal at 6.92 ppm for the internal double bonds was detected. The <sup>31</sup>P NMR spectrum revealed a distinct signal at the same chemical environment (−17.73 ppm) of the monomer (Figure 1d,e).

In addition to the aromatic poly-1, we also synthesized the aliphatic analogue from tri(hex-5-en-1-yl)phosphate (2) by ATMET polymerization (cf. Figure 2a and Experimental Part). Grubbs 1st generation catalyst was used for the polymerization which was terminated after ca. 15 min by the addition of ethyl vinyl ether, before cross-linking occurred and precipitated into hexane. The reaction was performed at 1 g and several polymer batches were combined to conduct the flame retardancy tests (after combining the different batches, SEC of the mixture showed a molar mass of ca.  $M_n$  4400 g mol<sup>-1</sup> (Figure S24)).

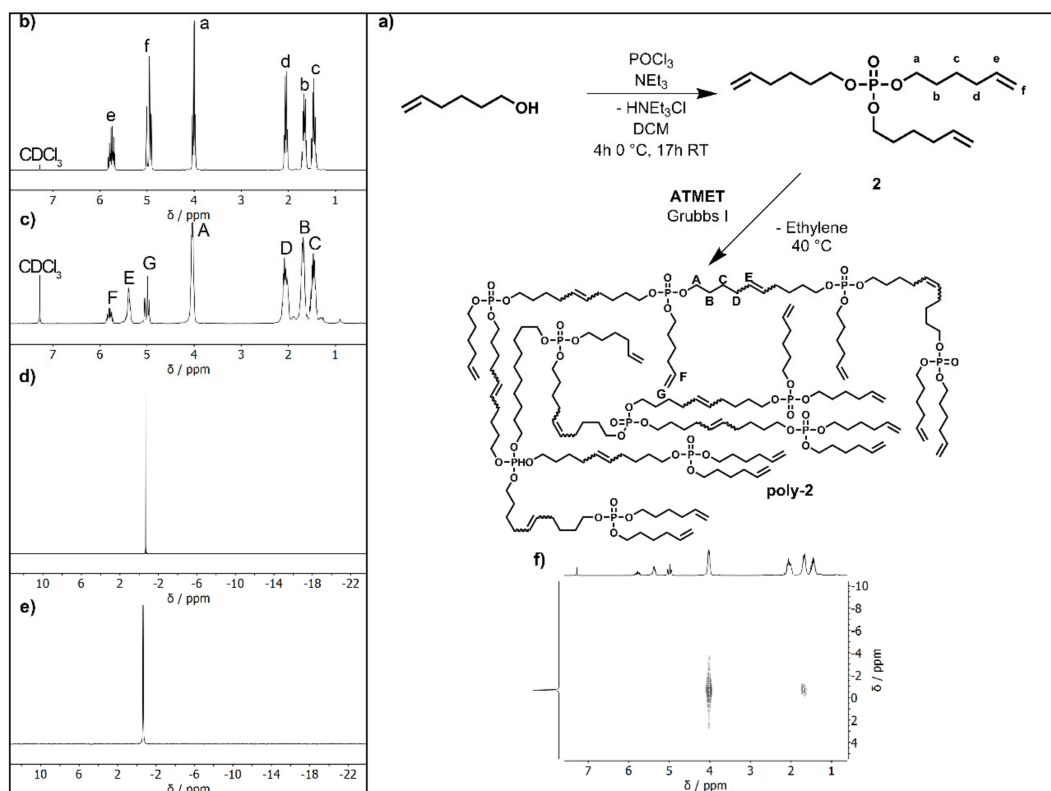


**Figure 2.** (a) Synthesis scheme of tri(hex-5-en-1-yl)phosphate (2) and poly(tri(hex-5-en-1-yl)phosphate) (poly-2); (b) <sup>1</sup>H NMR spectra of 2; (c) <sup>1</sup>H NMR spectra of poly-2; (d) <sup>31</sup>P NMR spectra of 2; (e) <sup>31</sup>P NMR spectra of poly-2; (f) <sup>1</sup>H<sup>31</sup>P HMBC spectra of poly-2.

The successful polymerization of 2 was followed by <sup>1</sup>H NMR spectroscopy. The signals of the terminal double bonds at 5.81 ppm and 5.15 ppm decreased, whereas an additional signal for the internal double bonds at 5.40 ppm was detected (Figure 2b,c). No shift in the phosphorus signal was observed, as the distance between the reactive olefins and the phosphorus is separated by the long alkyl chain (Figure 2d,e). The increase in thermal stability of poly-2 compared to 2 was marginal ( $T_{on, 10\%}$ ; poly-2 = 206 °C and  $T_{on, 10\%}$ ; poly-2 215 °C).

### 2.1. Thermal Characterization of FRs

The analysis of both polymers by differential scanning calorimetry (DSC) revealed a large difference in the glass transition temperatures ( $T_g$ ): poly-2 with its long and flexible aliphatic chains between the phosphate groups exhibited a low  $T_g$  of  $-66$  °C. In contrast, poly-1 exhibited a  $T_g$  which was  $126$  °C higher ( $T_{g, \text{poly-1}} = 60$  °C) due to the rigid aromatic groups [31]. This difference in  $T_g$  also impacts the  $T_g$  of the final FR-containing epoxy resins and therefore must be considered. If a plasticizing-effect on the final FR epoxy resin is desired, the aliphatic FR may eliminate the need for additional plasticizer.

### 2.2. Pyrolysis: Thermal Decomposition via Thermogravimetric Analysis

The decomposition of the FRs under pyrolytic conditions was investigated using thermogravimetric analysis (TGA) (Figure 3). During a fire, the burning is dominated by anaerobic pyrolysis producing volatile fuel, which is then combusted in the flame. This model is accurate for most polymeric materials in fire scenarios such as developing fires [32]. Therefore, it is also applicable for fire tests of polymeric materials like flaming combustion in the cone calorimeter. Moreover, the model applies to reaction to small flame tests such as limited oxygen index (LOI) and UL 94, where the extinguishment of a flame is monitored. TGA under nitrogen is the most common analytical method to investigate the pyrolysis controlling the burning of polymeric materials [32]. The mass loss curve of 1 has two distinct decomposition steps: the first mass loss step of 1 at  $T_{\text{dec}} = 143$  °C is likely due to the cleavage of PO-Ar or P-OAr bonds. This behavior is indicated by the release of aromatic compounds which were identified by TGA coupled with FTIR spectroscopy (Figure S11). The resulting radicals of the bond cleavage initiate a radical polymerization reaction of the vinyl groups, resulting in a cross-linked polymer. This increase in molar mass prevents any further release into the gas phase. In contrast, poly-1 has a steady decrease in mass; it has only few free double bonds available which allow for further cross-linking. Consequently, end-groups are continually eliminated. The second decomposition step is the main decomposing step of the material, which is at the maximum degradation temperature  $T_{\text{max}} = 470$  °C for 1 and at  $T_{\text{max}} = 435$  °C for poly-1. The slight reduction in  $T_{\text{max}}$  for poly-1 is explained with the fact that poly-1 has only few vinyl groups for post cross-linking available; therefore, 1 is more efficient in its cross-linking reaction during the first mass loss step, resulting in a high molar mass, cross-linked network. The aliphatic compounds only experience one decomposition step, which is at much lower temperatures compared to the aromatic compounds. The difference between 2 and poly-2 is only marginal with  $19$  °C ( $T_{\text{max}, 2} = 250$  °C,  $T_{\text{max}, \text{poly-2}} = 269$  °C).

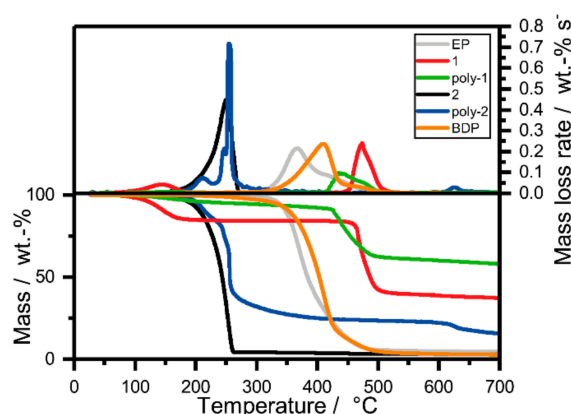


**Figure 3.** Top: Mass loss rate over temperature of pure flame retardants and the pure epoxy resin. Bottom: Pyrolysis investigations via thermogravimetric analysis (TGA;  $10 \text{ K min}^{-1}$ ;  $\text{N}_2$ ); increase of residue yield from aliphatic to aromatic and from monomeric to polymeric.

Considering the decomposition temperature of the epoxy resin (EP, based on bisphenol A diglycidylether (DGEBA) and 2,2'-dimethyl-4,4'-methylene-bis-(cyclohexylamine) (DMC), ( $T_{\text{max}, \text{epoxy}} = 366$  °C)), another important observation was made: The aliphatic FRs decomposed at lower

temperatures than the matrix, whereas the aromatic compounds decomposed at a higher temperatures than the matrix, resulting in potentially less interaction between matrix and FR (Figure 3). As a benchmark, the commercially available and industrially-used FR bisphenol-A diphenyl phosphate (BDP) was chosen, as it was already used successfully in epoxy resins [33,34]. BDP has a decomposition temperature which is similar to the one of the epoxy resin ( $T_{\max, \text{BDP}} = 409 \text{ }^\circ\text{C}$ ).

There is also a clear difference in residue amounts between the aliphatic and the aromatic materials: the residue increases from aliphatic to aromatic and from monomer to polymer. Residues increased from 3 wt.-% (2) to 37 wt.-% for 1 and from 24 wt.-% (poly-2) to 60 wt.-% for poly-1. The large difference in residues between aliphatic and aromatic compounds is explained by the interaction of phosphorus species with aromatic components, resulting in polyaromatic residue [35].

### 2.3. Pyrolysis: Evolved Gas Analysis via TGA-FTIR

During TGA, the evolved gases were analyzed via FTIR (TGA-FTIR), giving insight into the decomposition products and therefore the process as a whole (Figure S9–S12). 2 decomposed in a single step at  $259 \text{ }^\circ\text{C}$ : its main decomposition products were 5-hexen-1-ol, 1,5-hexadiene, and a phosphate-species, as has been previously reported (Figure S9) [36]. poly-2 exhibited disparate products during decomposition: at  $216 \text{ }^\circ\text{C}$ , the spectrum shares most similarities to 1,3-hexadiene (c,t), especially by the bands at  $999$  and  $905 \text{ cm}^{-1}$ , but also those at  $1806$ ,  $1605$ ,  $1460$ ,  $1316$ , and  $1174 \text{ cm}^{-1}$  (Figure S10) [37]. At  $259 \text{ }^\circ\text{C}$ , 2-octene (c,t) and *trans*-1,4-hexadiene were identified, the former by those bands at  $1460$ ,  $1405$ , and  $692 \text{ cm}^{-1}$ , and the latter by the bands at  $971$  and  $919 \text{ cm}^{-1}$ . The FTIR spectra of monounsaturated hydrocarbons share many similarities, and the spectra are likely caused by the overlap of several species. For 1, the spectrum at  $143 \text{ }^\circ\text{C}$  revealed the production of aromatic products including *p*-Cresol, 4-ethylphenol, and *p*-tolyl acetate, the latter a product of rearrangement reactions, and identified by the bands at  $1786$  (C=O) [38,39],  $1372$ ,  $1011$ , and  $908 \text{ cm}^{-1}$  (Figure S11). [37] At  $470 \text{ }^\circ\text{C}$ , the spectrum revealed the presence of bisphenol A, characteristically seen in the decomposition of epoxy resins [40–43], providing evidence for cross-linking reactions occurring at elevated temperatures. For poly-1, two distinct decomposition products were identified at  $T_{\max}$ : at  $447 \text{ }^\circ\text{C}$ , the main product was phenol, while at  $487 \text{ }^\circ\text{C}$ , the production of benzene was clearly visible by the band at  $672 \text{ cm}^{-1}$  (Figure S12).

### 2.4. Thermal Characterization of FRs in Epoxy Resins

The FR-performance of the aliphatic and aromatic FRs was studied in an epoxy resin (EP) based on DGEBA and DMC. The epoxy plates were prepared by mixing DGEBA with DMC in the presence of 10 wt.-% of each FR, pouring the mixture into aluminum molds of desired dimensions, followed by curing for 3 h at  $150 \text{ }^\circ\text{C}$ . The  $T_g$  of the epoxy resin was  $155 \text{ }^\circ\text{C}$ . Typically, additive FRs act as plasticizers of the epoxy resin and reduce the glass transition temperature ( $T_g$ ) [44]. All flame-retarded epoxy resins with 10 wt.-% 1, poly-1, 2 and poly-2 exhibited lower  $T_g$ s by 6–28  $^\circ\text{C}$  compared to the epoxy resin. 1 had almost no influence on the  $T_g$  of EP due to its ridged aromatic structure ( $T_g$  of EP-1:  $149 \text{ }^\circ\text{C}$ ), poly-1 reduced the  $T_g$  to  $127 \text{ }^\circ\text{C}$  and EP-BDP lies in between with a  $T_g$  of  $133 \text{ }^\circ\text{C}$ . In all cases, the addition of aliphatic FRs 2 and poly-2 resulted in a higher or equivalent decrease in  $T_g$  compared to the aromatic FRs ( $T_{g, 2} = 127 \text{ }^\circ\text{C}$ ,  $T_{g, \text{poly-2}} = 149 \text{ }^\circ\text{C}$ ). This difference in influence on the  $T_g$  was already expected due to the large difference in  $T_g$  of the pure FRs.

### 2.5. Pyrolysis: Evolved-Gas Analysis via TGA/TGA-FTIR

A crucial step towards understanding the FR mechanisms is analyzing the pyrolysis of the epoxy resins with FRs by TGA. The epoxy resin had a main decomposition step at  $366 \text{ }^\circ\text{C}$  and therefore no overlap with the aliphatic or aromatic FRs (except the reference BDP). This behavior is not ideal, since it reduces the interaction between the matrix and FR. The mass loss curves of EP-2 and EP-poly-1 have two distinct signals. In the case of EP-2, the low molecular weight compound already boils from the matrix before the matrix decomposes. This is indicated by the mass loss of approx. 10 wt.-%, which



is equal to the amount of FR in the epoxy resin. For EP-poly-1, the first mass loss step is explained with the loss of terminal groups. The temperatures of highest decomposition rate ( $T_{\max}$ ) of EP-2 ( $T_{\max} = 367\text{ }^{\circ}\text{C}$ ), EP-1 ( $T_{\max} = 359\text{ }^{\circ}\text{C}$ ), EP-poly-1 ( $T_{\max} = 361\text{ }^{\circ}\text{C}$ ) and EP-BDP ( $T_{\max} = 357\text{ }^{\circ}\text{C}$ ) are very close to the  $T_{\max}$  of the neat epoxy resin. However, poly-2 reduced  $T_{\max}$  of EP to  $334\text{ }^{\circ}\text{C}$ . The broad range of decomposition is caused by the broad poly dispersity and the high number of low molecular weight fractions, which leave the matrix earlier compared to the higher molecular fragments.

The residue at  $700\text{ }^{\circ}\text{C}$  increased for all tested FR containing EPs. EP-2 had a low increase to 5.1 wt.-% compared to 4.5 wt.-% of EP. EP-BDP had a residue of 8.2 wt.-%, which was notably higher. EP-1 had a residue of 9.1 wt.-%, while EP-poly-2 and EP-poly-1 were in a similar range with 13.3 wt.-% and 14.7 wt.-%, respectively, the latter presenting the greatest increase in residue yield.

The evolved-gas analysis of FR-containing resins during pyrolysis (Figure S13–S16) revealed the development of decomposition products unique to the individual FRs. All materials exhibited the spectrum of DGEBA-DMC at  $371\text{--}375\text{ }^{\circ}\text{C}$  except EP-poly-2, where this spectrum appeared at  $349\text{ }^{\circ}\text{C}$ . The EP-spectrum contained signals from Bisphenol A (e.g.,  $1603, 1510, 1255, 1176\text{ cm}^{-1}$ ) and ammonia ( $965, 930\text{ cm}^{-1}$ ). Only EP-2 contained a phosphate signal ( $1033\text{ cm}^{-1}$ ) [45] at  $373\text{ }^{\circ}\text{C}$  (Figure S13). Both EP-2 and EP-poly-2 exhibited gas production at  $T < T_{\max}$  ( $266$  and  $287\text{ }^{\circ}\text{C}$ , respectively): while for EP-2, the spectrum contained signals from 5-hexen-1-ol ( $3082, 2936, 1043, 918\text{ cm}^{-1}$ ) and a phosphate species ( $1033\text{ cm}^{-1}$ ) (Figure S13), the spectrum of EP-poly-2 displayed overlapped signals from 5-hexen-1-ol as well as longer-chained monounsaturated alcohols, as exemplified by the spectrum of oct-2-en-4-ol which contains the band at  $967\text{ cm}^{-1}$  (Figure S14). These species resulted from the scission of the aliphatic chain between phosphate-moieties and then rearrangement reactions. For EP-1, the spectrum at  $203\text{ }^{\circ}\text{C}$  revealed the evolution of alkyl-substituted phenols such as *p-n*-propyl phenol, as identified by the bands at  $1255, 1176$  and  $830\text{ cm}^{-1}$  which are prevalent throughout substituted aromatic molecules (Figure S15) [38,39]. Moreover, the spectrum at  $437\text{ }^{\circ}\text{C}$  displayed other substituted phenols that are unlike Bisphenol A, providing further support that 1 forms thermally stable polyaromatic compounds at elevated temperatures. EP-poly-1 also displayed similar polyaromatic molecules not stemming from Bisphenol A such as 4-(3-hydroxyisoamyl) phenol at  $482\text{ }^{\circ}\text{C}$  (Figure S16), as identified by the lack of signals at  $1332, 747$ , and  $686\text{ cm}^{-1}$  [37].

## 2.6. Pyrolysis: Condensed Phase Analysis via Hot-Stage FTIR

Investigations via hot-stage FTIR into the condensed phase activity of the FRs in EP revealed many similarities and some subtle differences between the individual FRs (Figure S17–S10). At  $100\text{ }^{\circ}\text{C}$  (Figure S17), the spectrum of EP is clearly visible in all materials, yet some additional bands are visible: for EP-2 and EP-poly-2, the band at  $1025\text{ cm}^{-1}$  was pronounced and may correspond to (P-O) signals which are strong for the aliphatic FRs [45]. The bands at  $1639$  and  $914\text{ cm}^{-1}$  were present in EP-2 and EP-1, as these corresponds to  $\nu_s(\text{C}=\text{C})$  and  $\delta_{\text{oop}}(\text{C}-\text{H})$  of the vinyl groups, respectively [37,38]. EP-poly-2, EP-1, and EP-poly-1 contained a distinctly strong band at  $961\text{ cm}^{-1}$  from  $\delta_{\text{oop}}(\text{C}-\text{H})$  of vinylene groups. The band at  $734\text{ cm}^{-1}$  in EP-poly-1 may belong to  $\delta_{\text{oop}}(\text{C}-\text{H})$  of *cis*-vinylene groups; these may show higher absorbance in aromatic systems [38,39]. At  $300\text{ }^{\circ}\text{C}$  (Figure S18), the spectrum of EP-poly-2 exhibited the most changes due to advanced decomposition ( $T_{5\%} = 249\text{ }^{\circ}\text{C}$ ) compared to the other materials. Here, the band at  $1083\text{ cm}^{-1}$  became pronounced; it may correspond to  $\delta_{\text{as}}(\text{P}-\text{O}-\text{C})$  or  $\nu(\text{P}=\text{O})$  of  $\text{Ar}_2(\text{P}=\text{O})-\text{OH}$ , especially because this band was prominent for EP-1 at  $300\text{ }^{\circ}\text{C}$ , but also all FR-containing spectra at  $500\text{ }^{\circ}\text{C}$ , thus implying the formation of aromatic P-compounds [38,39,45]. For EP-poly-2, the appearance of the strong band at  $521\text{ cm}^{-1}$  may signify the evolution of monounsaturated hydrocarbons, as *cis*- and *trans*-alkenes as well as alkyl-substituted vinylenes exhibit strong signals from skeletal vibrations here. At  $500\text{ }^{\circ}\text{C}$  (Figure S19), the band at  $1293\text{ cm}^{-1}$  appeared for all materials other than EP, and most prominently for EP-poly-2. This band may belong to  $\nu(\text{P}=\text{O})$  of  $(\text{ArO})_3\text{P}=\text{O}$ , providing more evidence for the binding of aromatic rings by P-species of the FRs. Moreover, this band was clearly visible at  $600\text{ }^{\circ}\text{C}$  for all materials except EP, as the aromatic species are not stabilized by phosphorus. At  $600\text{ }^{\circ}\text{C}$  (Figure S20), many absorption bands were visible which were not present in

EP, implicating a strong condensed phase mechanism of all tested FRs. Many of these bands have been characterized previously (Markwart et al., Battig et al.) [36,46]. Furthermore, the presence of several DGEBA-DMC typical bands (underlined in Figure S20) at 1593, 880, 823, 764, and 688  $\text{cm}^{-1}$  suggest that the aromatic structures of DGEBA and its decomposition products were held intact through the formation of stable P-species.

### 2.7. Fire Behavior: Cone Calorimeter

Investigations with the cone calorimeter proved a significant effect of all FRs on epoxy resins (Figure 4b). The epoxy plates ( $100 \times 100 \times 4 \text{ mm}^3$ ) were irradiated with a heat flux of  $50 \text{ kW m}^{-2}$ , simulating a developing fire [47]. The results of the forced-flaming condition experiments underlined that the epoxy resin burned with a high heat release rate (HRR) and lost 99.3 wt.-% of its mass, presenting nearly no residue (Figure 4a and Table S4). The aliphatic FRs in resins exhibited a reduction of peak or heat release rate (PHRR), as well as reduction of fire growth rate ( $\text{FIGRA} = \max. (\text{HRR}/t)$ ). Especially 2 reduced the PHRR of EP significantly ( $885 \text{ vs. } 1696 \text{ kW m}^{-2}$ ) due to the formation of a voluminous char layer that insulated the underlying polymer. This behavior was clearly visible during the experiments as well as in the cross-sections of the residues, as the decomposition of the resin with 2 and the volatilization of its products acted as blowing agents, creating a voluminous intumescent char that shielded the underlying material from the heat source (Figure 4c,d). Moreover, it was very active in the gas phase, as evidenced by a reduction in the effective heat of combustion ( $\text{EHC} = \text{total heat evolved}/\text{total mass loss}$ ), which is a parameter for gas phase activity [4]. The polymeric poly-2 did not exhibit the same type of FR efficacy due to a lower reactivity with the matrix. Notably, it only slightly lowered PHRR ( $1248 \text{ kW m}^{-2}$ ) and was less active in the gas phase ( $\text{EHC} = 24.9 \text{ MJ kg}^{-1}$ ). The aromatic FRs in resins did not exhibit a clear reduction in PHRR and FIGRA like 2. On the contrary, PHRR increased for EP-poly-1, and FIGRA was only slightly lowered. The epoxy resins loaded with 1 had a PHRR of  $1194 \text{ kW m}^{-2}$  and a FIGRA of  $11.2 \text{ kW m}^{-2} \text{ s}^{-1}$  (pure epoxy:  $1696 \text{ kW m}^{-2}$  (PHRR)  $15.5 \text{ kW m}^{-2} \text{ s}^{-1}$  (FIGRA)). Both values are on par to those of EP with the commercial FR BDP. Moreover, EP-1 exhibited a moderate 13% reduction of EHC ( $23.3 \text{ MJ kg}^{-1}$ ) EP-poly-1 showed a PHRR of  $1969 \text{ kW m}^{-2}$  and a FIGRA of  $15.0 \text{ kW m}^{-2} \text{ s}^{-1}$ . The high PHRR is caused by the high decomposition temperature of the FR compared to the matrix, as seen in TGA measurements (Figure 3). All flame-retarded resins exhibited an increase in residue yield and a lowering of the total heat evolved (THE = total heat released (THR) at flame out) (Figure S22 and Table S4). The THE for the epoxy resins containing hb polymers were all comparable to EP-BDP ( $87.5 \text{ MJ m}^{-2}$ -  $94.6 \text{ MJ m}^{-2}$ ). The THE of EP-1 ( $88.4 \text{ MJ m}^{-2}$ ) was comparable to that of EP-2 ( $78.1 \text{ MJ m}^{-2}$ ). The epoxy resin loaded with 2 demonstrated the lowest PHRR ( $885 \text{ kW m}^{-2}$ , reduced by 48%) and THE ( $78.1 \text{ MJ m}^{-2}$ , reduced by 28%) and displayed a HRR curve corresponding to a charring material with a protective layer (Figure 4 a). For EP-poly-2 and EP-1, the HRR curves were nearly identical to EP-BDP: The shape of the HRR curves suggest a quasi-static HRR above ca. 60 s after ignition, indicating the formation of an insulating char layer. However, the insulating properties were soon overcome and additional fuel was transported into the flame, coming to a head shortly thereafter at PHRR. The HRR curve of EP-poly-1 illustrates that the sample ignited earlier than the pure EP, due to a reduced cross-linking density caused by the presence of FRs. Thereafter, fuel was continually fed into the flame before the FR could interact with EP, leading to a poor char layer production. For the polymers and especially for EP-poly-1, a lower reduction of PHRR and THE was detected, most probably due to the lower reactivity. The residue yields of epoxy resins loaded with 1 ( $5.3 \pm 0.0 \text{ wt}\%$ ) were higher than the neat epoxy ( $0.7 \pm 0.1 \text{ wt}\%$ ), yet much lower compared to the aliphatic monomeric phosphate ( $9.2 \pm 0.1 \text{ wt}\%$ ), most likely due to the high reactivity of 2. The resin with poly-1 had an increase in char residue ( $7.0 \pm 1.5 \text{ wt}\%$ ) compared to EP-1 ( $5.3 \pm 0.0 \text{ wt}\%$ ). Although the aromatic FRs were less effective in lowering PHRR and FIGRA in cone calorimeter measurements than the aliphatic counterparts, their efficacy in creating high residue yields in pyrolysis measurements should not go unnoted.



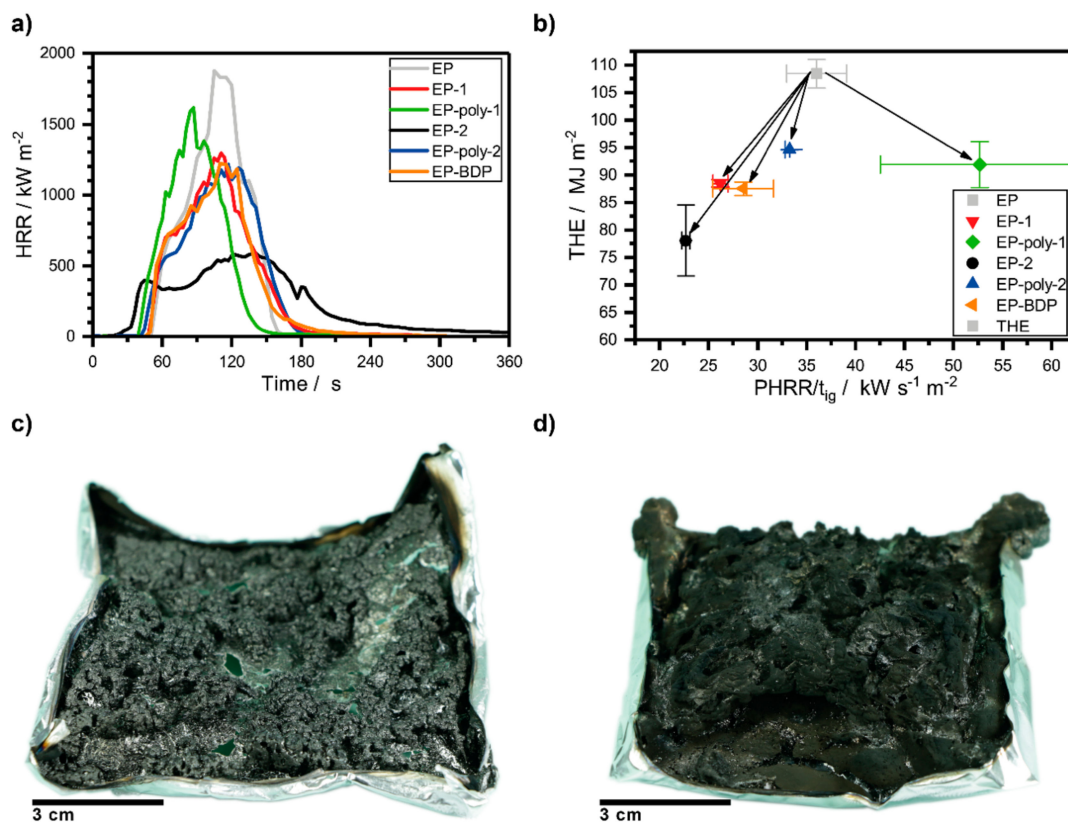


**Figure 4.** (a) Heat release rate (HRR) of epoxy resin and epoxy resin with flame retardants (FRs) measured by cone calorimeter. (b) Petrella plot of the different epoxy resins with all FRs having a positive effect (lowering total heat evolved (THE)), especially 2. (c) Residue of EP-poly-1 after cone calorimeter measurement, presenting a high graphitic residue yield but poor protective layer. (d) The residue of EP-poly-2 after cone calorimeter measurements, presenting a good protective layer by the production of voluminous, multicellular char.

### 3. Materials and Methods

#### 3.1. Materials

All chemicals were purchased from commercial suppliers as reagent grade and used without further purification. The monomer 2 was prepared according to literature [36].

#### 3.2. Instrumentation and Characterization Techniques

##### 3.2.1. Size Exclusion Chromatography (SEC)

Size exclusion chromatography (SEC) measurements were performed in DMF at 60 °C with a PSS SecCurity system (Agilent Technologies 1260 Infinity, Santa Clara, CA, USA). Sample injection was performed by a 1260-ALS autosampler (Agilent) at 60 °C. GRAM columns (PSS) with dimensions of 300 × 80 mm, 10 μm particle size, and pore sizes of 100, 1000, and 10,000 Å were employed. The DRI Shodex RI-101 detector (ERC, Kawaguchi, Japan) and UV-vis 1260-VWD detector (Agilent) were used for detection. Calibration was achieved using PS standards provided by Polymer Standards Service.

##### 3.2.2. Nuclear Magnetic Resonance (NMR)

Nuclear magnetic resonance (NMR) was performed in a Bruker Avance III 300 MHz and 500 MHz spectrometer (Billerica, MA, USA). All spectra were measured in either *d*<sub>6</sub>-DMSO or CDCl<sub>3</sub> at 298 K. The spectra were calibrated against the solvent signal (CDCl<sub>3</sub> (7.26 ppm) or *d*<sub>6</sub>-DMSO (2.50 ppm)) and

analyzed using MestReNova 11 from Mestrelab Research S.L. (Santiago de Compostela, Spain) and Bruker Topspin 3.0 software (Billerica, MA, USA).

### 3.2.3. Electrospray Ionization Mass Spectrometry (ESI-MS)

Electron spray ionization mass (ESI-MS) was performed by a Q-ToF Ultima 3 from Waters Micromass Milford Massachusetts spectrometer (Milford, MA, USA). 1 mg of the sample was dissolved in 1 mL of solvent (THF or DCM) and injected into ionization chamber at 120 °C which operated with a stream of 100 L h<sup>-1</sup> and a reference voltage of 35 V.

### 3.2.4. Differential Scanning Calorimetry (DSC)

Differential scanning calorimetry (DSC) measurements were performed using a Mettler Toledo instrument (Columbus, OH, USA) 1/700 or DSC823 under nitrogen atmosphere at a heating rate of 10 °C min<sup>-1</sup> starting from -140 °C.

### 3.2.5. TGA-FTIR

Both decomposition and evolved gases were investigated under pyrolytic and thermo-oxidative conditions via Fourier transform infrared (FTIR) spectroscopy coupled with thermogravimetric analysis. For epoxy resins with and without FRs, 10 mg of powder attained from cryomilling were used for measurements, while 5 mg samples were measured for pure FRs. Using a TG 209 F1 Iris (Netzsch Instruments, Selb, Germany), samples were heated at a rate of 10 K min<sup>-1</sup> from 30 to 900 °C under a nitrogen or synthetic air (80:20) gas flow of 30 mL min<sup>-1</sup>. The evolved gases were analyzed using a Tensor27 infrared spectrometer (Bruker Optics, Ettlingen, Germany), which was coupled to the TGA via a transfer line heated to 270 °C.

### 3.2.6. Hot Stage FTIR

The condensed phase activity was monitored using hot-stage FT-infrared spectroscopy using a Vertex70 FTIR spectrometer (Bruker Optics, Ettlingen, Germany), equipped with an FTIR600 Linkam hot-stage cell (Linkam Scientific Instruments Ltd., Chilworth, UK). The samples were pressed into a KBr plate, loaded into the Linkam cell, and heated at a rate of 10 K min<sup>-1</sup> from 30 to 600 °C under a nitrogen gas flow of 300 mL min<sup>-1</sup>.

### 3.2.7. Cone Calorimeter

All epoxy resin samples were subjected to bench-scale forced flaming combustion using a cone calorimeter (Fire Testing Technology Ltd., East Grinstead, UK) at a distance of 35 mm between specimen and cone heater and a heat flux of 50 kW m<sup>-2</sup> and in accordance with ISO 5660. Specimens sized 100 × 100 × 4 mm<sup>3</sup> were conditioned at 23 °C and 50% relative humidity for at least 48 h and then subjected to irradiation.

## 3.3. Synthetic Procedures

### 3.3.1. Synthesis of the 4-Vinylphenol

Preparation of 4-vinylphenol was realized according to the method of Ricks-Laskoski et al [48]. To a dried three-necked, 2 L round bottom flask fitted with a dropping funnel and a mechanical stirrer 4-acetoxystyrene (53.36 g, 0.33 mol, 1 eq.) and tetrahydrofuran (200 mL) were added under an argon atmosphere and ice-cooling. Ice-cooling was continued throughout the process. 5 M solution of aqueous sodium hydroxide (100 mL, 0.8 mol, 2.4 eq.) was added dropwise to this solution. The yellow solution was stirred for 2 h under ice-cooling until the reaction was completed as indicated by TLC (SiO<sub>2</sub>: R<sub>f</sub> = 0.75, 30 vol.% ethyl acetate/hexane). Then 1.5 M hydrochloric acid (340 mL) was added slowly to the crude reaction mixture until a pH of 7–5 was reached. The product was extracted with cold ethyl acetate (5 × 50 mL), washed with distilled water (3 × 50 mL), dried over magnesium sulfate

and filtered. The product was distilled at reduced pressure while cooling with an ice bath to yield a crystalline solid (30.9 g, 78%). The product was stored at  $-20\text{ }^{\circ}\text{C}$  under argon atmosphere and light exclusion to suppress self-initiated polymerization.

$^1\text{H}$  NMR (300 MHz, 298 K, DMSO- $d_6$ ):  $\delta/\text{ppm} = 9.53$  (s, 1H), 7.28 (d, 2H,  $J = 9$  Hz), 6.74 (d, 2H,  $J = 9$  Hz), 6.61 (dd, 1H,  $J = 12$  Hz/18 Hz), 5.68 (d, 1H,  $J = 18$  Hz), 5.04 (d, 1H,  $J = 12$  Hz).

$^{13}\text{C}\{\text{H}\}$  NMR (75.48 MHz, 298 K, DMSO- $d_6$ ):  $\delta/\text{ppm} = 157.3, 136.4, 128.2, 127.4, 115.3, 110.6$ .

### 3.3.2. Synthesis of the Tris(p-vinylphenyl)phosphate (1)

To a dried three-necked, 1 L round bottom flask fitted with a dropping funnel and an mechanical stirrer, 4-vinylphenol (15 g, 0.125 mol, 4 eq.) dissolved in THF (300 mL) and triethylamine (12.63 g, 0.125 mol, 4 eq.) in THF (10 mL) at  $0\text{ }^{\circ}\text{C}$  and under an argon atmosphere. Then phosphoryl chloride (4.79 g, 0.031 mol, 1 eq.) in THF (30 mL) was added to the solution dropwise at  $0\text{ }^{\circ}\text{C}$ . Then the reaction was allowed to warm up to room temperature and stirred overnight at room temperature. The mixture was filtered and concentrated at reduced pressure while cooling in an ice-bath. The product was dissolved in DCM (100 mL) and extracted with water and a 1 M potassium hydroxide solution. The organic layer was dried over  $\text{MgSO}_4$ , filtered and concentrated at reduced pressure yield a colorless viscous liquid (8.4 g, 67%). The product was stored at  $-20\text{ }^{\circ}\text{C}$  under argon atmosphere and light exclusion to suppress self-initiated polymerization.

$^1\text{H}$  NMR (500 MHz, 298 K,  $\text{CDCl}_3$ ):  $\delta/\text{ppm} = 7.29$  (d, 2 H,  $J = 10$  Hz), 7.11 (d, 2 H,  $J = 10$  Hz), 6.58 (dd, 1 H,  $J = 10$  Hz/15 Hz), 5.60 (d, 1 H,  $J = 15$  Hz), 5.16 (d, 1 H,  $J = 10$  Hz).

$^{13}\text{C}\{\text{H}\}$  NMR (75.48 MHz, 298 K,  $\text{CDCl}_3$ ):  $\delta/\text{ppm} = 149.9$  (d,  $J = 30$  Hz), 135.6 (s), 135.2 (s), 127.6 (d,  $J = 6$  Hz), 120.2 (d,  $J = 21$  Hz), 114.3 (s).

$^{31}\text{P}\{\text{H}\}$  NMR (121.5 MHz, 298 K,  $\text{CDCl}_3$ ):  $\delta/\text{ppm} = -17.72$  (s). ESI MS: 405.14.

### 3.3.3. ATMET Polymerization to Poly(1)

In a Schlenk tube fitted with a magnetic stirring bar, tris(p-vinylphenyl)phosphate (1) (1 g, 2.47 mmol) dissolved in 1-chloronaphthalene (1.67 g) was placed under an argon atmosphere at  $40\text{ }^{\circ}\text{C}$ . Then, the Grubbs-Hoveyda catalyst 2<sup>nd</sup> gen. (4.65 mg, 0.007 mmol, 0.3 mol%) was added. The polymerization was carried out at a controlled vacuum of  $5 \times 10^{-2}$  mbar to remove the evolving ethylene. When the viscosity increased (typically after ca 5 min), the flask was filled with argon and the reaction was terminated by adding ethyl vinyl ether or methyl acrylate (5 mL). The brown solution was stirred for 1 h at  $40\text{ }^{\circ}\text{C}$  and then the mixture was concentrated at reduced pressure. The product was precipitated twice into hexane and dried at reduced pressure to give an off-white powder (yields 50–90%).

$^1\text{H}$  NMR (500 MHz, 298 K,  $\text{CDCl}_3$ ):  $\delta/\text{ppm} = 7.57$  (d,  $J = 16$  Hz), 7.39 (m), 7.30 (d,  $J = 5$  Hz), 7.16 (m), 6.92 (s), 6.59 (dd,  $J = 10$  Hz/17 Hz), 5.61 (d,  $J = 17$  Hz), 5.16 (d,  $J = 10$  Hz).

$^{13}\text{C}\{\text{H}\}$  NMR (75.48 MHz, 298 K,  $\text{CDCl}_3$ ):  $\delta/\text{ppm} = 149.8, 135.6, 134.8, 129.7, 127.9, 120.4, 118.3, 114.4$ .

$^{31}\text{P}\{\text{H}\}$  NMR (202.46 MHz, 298 K,  $\text{CDCl}_3$ ):  $\delta/\text{ppm} = -17.73$ .

### 3.3.4. Tri(hex-5-en-1-yl)phosphate (2)

Tri(hex-5-en-1-yl)phosphate was synthesized as described elsewhere [36].

### 3.3.5. Poly(tri(hex-5-en-1-yl)phosphate) (poly-2) by ATMET Polymerization

In a Schlenk tube fitted with a magnetic stirring bar, tri(hex-5-en-1-yl)phosphate (2) (2 g, 5.81 mmol) was placed under an argon atmosphere at  $60\text{ }^{\circ}\text{C}$ . Then, Grubbs catalyst 1<sup>st</sup> gen. (33.45 mg, 40.65  $\mu\text{mol}$ , 0.7 mol%) was added. The polymerization was carried out at a controlled vacuum of  $5 \times 10^{-2}$  mbar to

remove the evolving ethylene. When the viscosity increased, the flask was filled with argon and the reaction was terminated by adding ethyl vinyl ether (0.4 mL). The product was precipitated twice into hexane and dried at reduced pressure to give a viscous off-white polymer (yields 85–96%).

$^1\text{H}$ NMR (300 MHz, 298 K,  $\text{CDCl}_3$ ):  $\delta/\text{ppm} = 5.81$  (ddt,  $J = 16.9, 10.2, 6.6$  Hz),  $5.40$  (m,  $J = 5.5, 5.1$  Hz),  $4.99$  (t,  $J = 13.9$  Hz),  $4.03$  (m, 6H),  $2.08$  (qd,  $J = 14.8, 12.0, 8.3$  Hz, 6H),  $1.68$  (h,  $J = 6.9$  Hz, 6H),  $1.47$  (dp,  $J = 15.1, 7.5$  Hz, 6H).

$^{31}\text{P}\{\text{H}\}$  NMR (121.5 MHz, 298 K,  $\text{CDCl}_3$ ):  $\delta/\text{ppm} = -0.66$ .

### 3.3.6. Epoxy Resins

All epoxy resins were prepared using bisphenol A diglycidylether (DGEBA) (Araldite MY740, Bodo Möller Chemie GmbH, Offenbach am Main, Germany) as the epoxide agent and 2,2'-dimethyl-4,4'-methylene-bis-(cyclohexylamine) (DMC) (Sigma Aldrich Co. LLC/Merck KgaA, Darmstadt, Germany) as the amine hardener. The materials were mixed, poured into aluminum molds of desired dimensions, then hardened at 150 °C for 3h. The flame retarded epoxy resins were produced in the same manner, except 10 wt.-% of the mixture was replaced with the respective flame retardant.

## 4. Conclusions

The herein presented aromatic and aliphatic, hyperbranched, halogen-free polyphosphoesters (hbPPEs) were synthesized by olefin metathesis polymerization and investigated as a flame retardant (FR) in epoxy resins. The impact on the  $T_g$  of the matrix was different for all tested materials. However, in all cases, the addition of aliphatic FRs 2 and poly-2 resulted in a higher or equivalent decrease of  $T_g$  compared to the aromatic FRs.

Regarding their flame retardant properties, the aromatic FRs proved a significant increase in residue yield and thermal stability in pyrolysis investigations compared to their aliphatic counterparts: the aromatic moieties acted as char precursors, thereby retaining significant residue yields. Moreover, condensed phase analysis concluded the formation of P-species for all tested resins with FRs.

Investigations with the cone calorimetry proved a significant effect of all FRs on epoxy resins during a developing fire. The aliphatic FRs were more effective on the tested matrix due to their greater overlap in decomposition temperature and thus better matrix interaction. The greater interaction resulted in a stronger reduction of peak of heat release rate (PHRR) and fire growth rate (FIGRA = max. (HRR/ $t$ )) than those resins with aromatic FRs. Especially 2 reduced the PHRR of EP significantly due to the formation of a voluminous char layer that insulated the underlying polymer. Moreover, 2 was very active in the gas phase, as evidenced by a reduction in the effective heat of combustion (EHC). While pyrolytic investigations proved high residue yields and interaction with the matrix for poly-2, it did not exhibit the same type of FR efficacy as 2 in cone calorimeter tests due to a less pronounced reactivity with the matrix in form of phosphorylation. The aromatic FRs were less effective in lowering PHRR and FIGRA in cone calorimeter measurements than the aliphatic counterparts, however, their efficacy in creating high residue yields in pyrolysis measurements should not go unnoted. The aromatic FRs might be more suited for materials with higher decomposition temperatures to increase the matrix-FR interaction. Moreover, the addition of a synergist may promote chemical interaction.

**Supplementary Materials:** The following are available online: Table S1: Polymerization conditions of 1 with Grubbs Hoveyda 2<sup>nd</sup> in 1-chloronaphthalene generation catalyst at 40 °C in solution., Figure S1: SEC curves (VWD-Signal 270 nm) of poly-1 in DMF polymerized with Grubbs 1st generation catalyst and Grubbs Hoveyda 2nd generation catalyst at 40 °C., Figure S2:  $^1\text{H}$  NMR (300 MHz in  $\text{CDCl}_3$  at 298 K) spectra of 4-vinylphenol., Figure S3:  $^1\text{H}$ -NMR (500 MHz in  $\text{CDCl}_3$  at 298 K) spectra of 1., Figure S4:  $^{31}\text{P}\{\text{H}\}$ -NMR (121 MHz in  $\text{CDCl}_3$  at 298 K) spectra of 1., Figure S5:  $^1\text{H}$ -MR (300 MHz in  $\text{CDCl}_3$  at 298 K) spectra of poly-1., Figure S6:  $^{31}\text{P}\{\text{H}\}$ -NMR (121 MHz in  $\text{CDCl}_3$  at 298 K) spectra poly-1., Figure S7:  $^1\text{H}$ -MR (300 MHz in  $\text{CDCl}_3$  at 298 K) spectra of poly-2., Figure S8:  $^{31}\text{P}\{\text{H}\}$ -NMR (121 MHz in  $\text{CDCl}_3$  at 298 K) spectra of poly-2., Figure S9: TGA-FTIR spectrum of 2 (top, black), identifying the main decomposition products (1,5-hexadiene; 5-hexen-1-ol and phosphate species, comparison shown in gray below) at specific decomposition temperature (259 °C) using references from NIST library., Figure S10: TGA-FTIR spectrum of poly-2 (top, blue), identifying the main decomposition products

(1,3-hexadiene (c,t) and 2-octene (c,t) and trans-1,4-hexadiene, comparison shown in gray below) at specific decomposition temperature (216 °C, 259 °C) using references from NIST library, Figure S11: TGA-FTIR spectrum of **1** (top, red), identifying the main decomposition products (p-tolyl acetate; p-cresol; 4-ethylphenol and bisphenol A, comparison shown in gray below) at specific decomposition temperature (143 °C, 470 °C) using references from NIST library., Figure S12: TGA-FTIR spectrum of poly-1 (top, green), identifying the main decomposition products (phenol and benzene, comparison shown in gray below) at specific decomposition temperature (447 °C and 487 °C) using references from NIST library., Figure S13: TGA-FTIR spectrum of EP-2 (top, black), identifying the main decomposition products (5-hexen-1-ol; phosphate species and decomposition products of the matrix, a comparison is shown in gray below) at specific decomposition temperature (266 °C, 373 °C) using references from NIST library., Figure S14: TGA-FTIR spectrum of EP-poly-2 (top, blue), identifying the main decomposition products (5-hexen-1-ol; oct-2-en-4-ol and decomposition products of the matrix, a comparison is shown in gray below) at specific decomposition temperature (287 °C, 349 °C) using references from NIST library., Figure S15: TGA-FTIR spectrum of EP-1 (top, red), identifying the main decomposition products (p-n-propylphenol and decomposition products of the matrix, a comparison is shown in gray below) at specific decomposition temperature (203 °C, 371 °C, 437 °C) using references from NIST library., Figure S16: TGA-FTIR spectrum of EP-poly-1 (top, green), identifying the main decomposition products (4-(3-hydroxyisoamyl)phenol and decomposition products of the matrix, a comparison is shown in gray below) at specific decomposition temperature (375 °C, 482 °C) using references from NIST library., Figure S17: Results from hot-stage FTIR measurements, comparing the condensed phase spectra of EP-FRs at 100 °C., Figure S18: Results from hot-stage FTIR measurements, comparing the condensed phase spectra of EP-FRs at 300 °C., Figure S19: Results from hot-stage FTIR measurements, comparing the condensed phase spectra of EP-FRs at 500 °C., Figure S20: Results from hot-stage FTIR measurements, comparing the condensed phase spectra of EP-FRs at 600 °C, underlined bands are typical to DGEBA-DMC., Table S2: Glass transition temperatures ( $T_g$ ) of the flame retardant containing epoxy resins (measured by DSC), Figure S21: Mass loss (bottom) and mass loss rate (top) over  $T$  of neat epoxy resin and flame retardant containing epoxy resins from TGA measurements ( $10 \text{ K min}^{-1}$ ;  $\text{N}_2$ )., Table S3: TGA data of the flame retardant containing epoxy resins.  $T_{5\%}$ : Temperature at which 5% mass-loss happened;  $T_{\text{max}}$ : Temperature of maximum degradation; Residue: Residue at 700 °C., Figure S22: Total heat released (THR) of epoxy resin and epoxy resin with flame retardant measured by cone calorimeter., Table S4: Results from cone calorimeter measurements of the flame retardant containing epoxy resins., Figure S23: Cross-linking of **1** at 300 °C in a silicon form for 2 h, producing a hard, cross-linked PPE resin., Figure S24: Chemical structure of Diglycidyl ether of Bisphenol A (DGEBA) and 2,2'-Dimethyl-4,4'-methylene-bis(cyclohexylamine) (DMC).

**Author Contributions:** Conceptualization, J.C.M., A.B., M.M.V., B.S. and F.R.W.; methodology, J.C.M., A.B. and M.M.V.; validation, J.C.M., A.B., M.M.V., B.S. and F.R.W.; formal analysis, J.C.M. and A.B.; investigation, J.C.M., A.B., M.M.V. and D.P.; resources, B.S. and F.R.W.; data curation, J.C.M., A.B., M.M.V. and D.P.; writing—original draft preparation, J.C.M. and A.B.; writing—review and editing, J.C.M., A.B., B.S. and F.R.W.; visualization, J.C.M. and A.B.; supervision, B.S. and F.R.W.; project administration, J.C.M., A.B., M.M.V., B.S. and F.R.W.; funding acquisition, B.S. and F.R.W.

**Funding:** Please add: This research was funded by the Deutsche Forschungsgemeinschaft, grant number DFG WU 750/8-1 and SCHA 730/15-1, and the Excellence Initiative in the context of the graduate school of excellence “MAINZ” (Materials Science in Mainz), grant number DFG/GSC 266.

**Acknowledgments:** The authors thank Angelika Manhart (MPIP, Germany) for synthetic assistance. Frederik R. Wurm and Jens C. Markwart thank Katharina Landfester (MPI-P, Germany).

**Conflicts of Interest:** The authors declare no conflict of interest.

## References

1. Alexander, B.; Jens, C.M.; Frederik, R.W.; Bernhard, S. Matrix matters: Hyperbranched flame retardants in aliphatic and aromatic epoxy resins. *Polym. Degrad. Stab.* **2019**, *108*, 986. [[CrossRef](#)]
2. Perret, B.; Pawlowski, K.; Schartel, B. Fire retardancy mechanisms of arylphosphates in polycarbonate (PC) and PC/acrylonitrile-butadiene-styrene. *J. Therm. Anal. Calorim.* **2009**, *97*, 949–958. [[CrossRef](#)]
3. Despinasse, M.-C.; Schartel, B. Influence of the structure of aryl phosphates on the flame retardancy of polycarbonate/acrylonitrile-butadiene-styrene. *Polym. Degrad. Stab.* **2012**, *97*, 2571–2580. [[CrossRef](#)]
4. Schartel, B.; Perret, B.; Dittrich, B.; Ciesielski, M.; Krämer, J.; Müller, P.; Altstädt, V.; Zang, L.; Döring, M. Flame retardancy of polymers: The role of specific reactions in the condensed phase. *Macromol. Mater. Eng.* **2016**, *301*, 9–35. [[CrossRef](#)]
5. Morgan, A.B.; Wilkie, C.A. *Flame Retardant Polymer Nanocomposites*; Wiley: Hoboken, NJ, USA, 2007.
6. Müller, P.; Schartel, B. Melamine poly(metal phosphates) as flame retardant in epoxy resin: Performance, modes of action, and synergy. *J. Appl. Polym. Sci.* **2016**, *133*. [[CrossRef](#)]



7. Velencoso, M.M.; Battig, A.; Markwart, J.C.; Schartel, B.; Wurm, F.R. Molecular firefighting—how modern phosphorus chemistry can help solve the challenge of flame retardancy. *Angew. Chem. Int. Ed. Engl.* **2018**, *57*, 10450–10467. [[CrossRef](#)]
8. Schartel, B. Phosphorus-Based flame retardancy mechanisms—Old hat or a starting point for future development? *Mater.* **2010**, *3*, 4710–4745. [[CrossRef](#)]
9. Lu, S.-Y.; Hamerton, I. Recent developments in the chemistry of halogen-free flame retardant polymers. *Prog. Polym. Sci.* **2002**, *27*, 1661–1712. [[CrossRef](#)]
10. Bauer, K.N.; Liu, L.; Andrienko, D.; Wagner, M.; Macdonald, E.K.; Shaver, M.P.; Wurm, F.R. Polymerizing phosphonates: A fast way to in-chain poly(phosphonate)s with adjustable hydrophilicity. *Macromol.* **2018**, *51*, 1272–1279. [[CrossRef](#)]
11. Steinbach, T.; Wurm, F.R. Poly(phosphoester)s: A new platform for degradable polymers. *Angew. Chem. Int. Ed.* **2015**, *54*, 6098–6108. [[CrossRef](#)]
12. Monge, S.; Canniccionni, B.; Graillot, A.; Robin, J.-J. Phosphorus-containing polymers: A great opportunity for the biomedical field. *Biomacromolecules* **2011**, *12*, 1973–1982. [[CrossRef](#)] [[PubMed](#)]
13. Ye, J.; Liang, G.; Gu, A.; Zhang, Z.; Han, J.; Yuan, L. Novel phosphorus-containing hyperbranched polysiloxane and its high performance flame retardant cyanate ester resins. *Polym. Degrad. Stab.* **2013**, *98*, 597–608. [[CrossRef](#)]
14. Kim, Y.H. Hyperbranched polymers 10 years after. *J. Polym. Sci. Part. A Polym. Chem.* **1998**, *36*, 1685–1698. [[CrossRef](#)]
15. Täuber, K.; Marsico, F.; Wurm, F.R.; Schartel, B. Hyperbranched poly(phosphoester)s as flame retardants for technical and high performance polymers. *Polym. Chem.* **2014**, *5*, 7042–7053. [[CrossRef](#)]
16. Gao, C.; Yan, D. Hyperbranched polymers: From synthesis to applications. *Prog. Polym. Sci.* **2004**, *29*, 183–275. [[CrossRef](#)]
17. Henke, H.; Brüggemann, O.; Teasdale, I. Branched macromolecular architectures for degradable, multifunctional phosphorus-based polymers. *Macromol. Rapid Commun.* **2017**, *38*, 1600644. [[CrossRef](#)] [[PubMed](#)]
18. Wang, Q.F.; Shi, W.F. Synthesis and thermal decomposition of a novel hyperbranched polyphosphate ester used for flame retardant systems. *Polym. Degrad. Stab.* **2006**, *91*, 1289–1294. [[CrossRef](#)]
19. Deng, J.; Zhu, S.W.; Shi, W.F. Effect of molecular chain structure of the cured epoxy resin containing hyperbranched (3-hydroxyphenyl) phosphate on expansion and flame retardance. *J. Appl. Polym. Sci.* **2004**, *94*, 2065–2070. [[CrossRef](#)]
20. Deng, J.; Shi, W.F. Synthesis and effect of hyperbranched (3-hydroxyphenyl) phosphate as a curing agent on the thermal and combustion behaviours of novolac epoxy resin. *Eur. Polym. J.* **2004**, *40*, 1137–1143. [[CrossRef](#)]
21. Chen, X.; Jiao, C.; Li, S.; Sun, J. Flame retardant epoxy resins from bisphenol-A epoxy cured with hyperbranched polyphosphate ester. *J. Polym. Res.* **2011**, *18*, 2229–2237. [[CrossRef](#)]
22. Chen, X.; Zhuo, J.; Jiao, C. Thermal degradation characteristics of flame retardant polylactide using TG-IR. *Polym. Degrad. Stab.* **2012**, *97*, 2143–2147. [[CrossRef](#)]
23. Pawlowski, K.H.; Schartel, B. Flame retardancy mechanisms of triphenyl phosphate, resorcinol bis(diphenyl phosphate) and bisphenol A bis(diphenyl phosphate) in polycarbonate/acrylonitrile–butadiene–styrene blends. *Polym. Int.* **2007**, *56*, 1404–1414. [[CrossRef](#)]
24. Weil, E.D. Fire-Protective and flame-retardant coatings—A State-of-the-Art Review. *J. Fire Sci.* **2011**, *29*, 259–296. [[CrossRef](#)]
25. Weil, E.D.; Levchik, S.V. *Flame Retardants for Plastics and Textiles: Practical Applications*; Carl Hanser Verlag GmbH Co KG: München, Germany, 2015. [[CrossRef](#)]
26. Marsico, F.; Wagner, M.; Landfester, K.; Wurm, F.R. Unsaturated polyphosphoesters via acyclic diene metathesis polymerization. *Macromol.* **2012**, *45*, 8511–8518. [[CrossRef](#)]
27. Steinbach, T.; Alexandrino, E.M.; Wahlen, C.; Landfester, K.; Wurm, F.R. Poly(phosphonate)s via olefin metathesis: Adjusting hydrophobicity and morphology. *Macromol.* **2014**, *47*, 4884–4893. [[CrossRef](#)]
28. Steinbach, T.; Alexandrino, E.M.; Wurm, F.R. Unsaturated poly(phosphoester)s via ring-opening metathesis polymerization. *Polym. Chem.* **2013**, *4*, 3800–3806. [[CrossRef](#)]

29. Steinmann, M.; Markwart, J.; Wurm, F.R. Poly(alkylidene chlorophosphate)s via acyclic diene metathesis polymerization: A general platform for the postpolymerization modification of poly(phosphoester)s. *Macromolecules* **2014**, *47*, 8506–8513. [CrossRef]
30. Mutlu, H.; de Espinosa, L.M.; Meier, M.A.R. Acyclic diene metathesis: A versatile tool for the construction of defined polymer architectures. *Chem. Soc. Rev.* **2011**, *40*, 1404–1445. [CrossRef]
31. Cowie, J.M.G.; Arrighi, V. *Polymers: Chemistry and Physics of Modern Materials*, 3rd ed.; CRC Press: Boca Raton, FL, USA, 2007.
32. Schartel, B.; Wilkie, C.A.; Camino, G. Recommendations on the scientific approach to polymer flame retardancy: Part 1—Scientific terms and methods. *J. Fire Sci.* **2016**, *34*, 447–467. [CrossRef]
33. Rakotomalala, M.; Wagner, S.; Döring, M. Recent developments in halogen free flame retardants for epoxy resins for electrical and electronic applications. *Materials* **2010**, *3*, 4300–4327. [CrossRef]
34. Ciesielski, M.; Schäfer, A.; Döring, M. Novel efficient DOPO-based flame-retardants for PWB relevant epoxy resins with high glass transition temperatures. *Polym. Adv. Technol.* **2008**, *19*, 507–515. [CrossRef]
35. Braun, U.; Balabanovich, A.I.; Schartel, B.; Knoll, U.; Artner, J.; Ciesielski, M.; Döring, M.; Perez, R.; Sandler, J.K.W.; Altstädt, V.; et al. Influence of the oxidation state of phosphorus on the decomposition and fire behaviour of flame-retarded epoxy resin composites. *Polymer* **2006**, *47*, 8495–8508. [CrossRef]
36. Markwart, J.C.; Battig, A.; Zimmermann, L.; Wagner, M.; Fischer, J.; Schartel, B.; Wurm, F.R. Systematically controlled decomposition mechanism in phosphorus flame retardants by precise molecular architecture: P–O vs. P–N. *ACS Appl. Polym. Mater.* **2019**, *1*, 1118–1128. [CrossRef]
37. Linstrom, P.J.; Mallard, W.G. NIST Chemistry WebBook, NIST Standard Reference Database Number 69. Available online: <https://doi.org/10.18434/T4D303> (accessed on 27 August 2019).
38. Socrates, G. *Infrared and Raman Characteristic Group Frequencies: Tables and Charts*; Wiley: Hoboken, NJ, USA, 2004.
39. Hesse, M.; Meier, H.; Zeeh, B. *Spektroskopische Methoden in der organischen Chemie*; Thieme Verlag: Stuttgart, Germany, 2005.
40. Levchik, S.V.; Weil, E.D. Thermal decomposition, combustion and flame-retardancy of epoxy resins—a review of the recent literature. *Polym. Int.* **2004**, *53*, 1901–1929. [CrossRef]
41. Levchik, S.V.; Camino, G.; Luda, M.P.; Costa, L.; Muller, G.; Costes, B. Epoxy resins cured with aminophenylmethylphosphine oxide—II. Mechanism of thermal decomposition. *Polym. Degrad. Stab.* **1998**, *60*, 169–183. [CrossRef]
42. Bishop, D.P.; Smith, D.A. Combined pyrolysis and radiochemical gas chromatography for studying the thermal degradation of epoxy resins and polyimides. I. The degradation of epoxy resins in nitrogen between 400 °C and 700 °C. *J. Appl. Polym. Sci.* **1970**, *14*, 205–223. [CrossRef]
43. Lee, L.-H. Mechanisms of thermal degradation of phenolic condensation polymers. II. Thermal stability and degradation schemes of epoxy resins. *J. Polym. Sci. Part. A Gen. Pap.* **1965**, *3*, 859–882. [CrossRef]
44. Ciesielski, M.; Burk, B.; Heinzmann, C.; Döring, M. *2-Fire-retardant High-performance Epoxy-based Materials. In Novel Fire Retardant Polymers and Composite Materials*; Wang, D.-Y., Ed.; Woodhead Publishing: Cambridge, UK, 2017; pp. 3–51. [CrossRef]
45. Thomas, L.C. *Interpretation of the Infrared Spectra of Organophosphorus Compounds*; Heydon: London, UK, 1974.
46. Battig, A.; Markwart, J.C.; Wurm, F.R.; Schartel, B. Hyperbranched phosphorus flame retardants: Multifunctional additives for epoxy resins. *Polym. Chem.* **2019**, *10*, 4346–4358. [CrossRef]
47. Schartel, B.; Hull, T.R. Development of fire-retarded materials—Interpretation of cone calorimeter data. *Fire Mater.* **2007**, *31*, 327–354. [CrossRef]
48. Ricks-Laskoski, H.L.; Chaloux, B.L.; Deese, S.M.; Laskoski, M.; Miller, J.B.; Buckley, M.A.; Baldwin, J.W.; Hickner, M.A.; Saunders, K.M.; Christensen, C.M. Tetrazolation of side chains and anhydrous conductivity in a hydrophobic polymer. *Macromol.* **2014**, *47*, 4243–4250. [CrossRef]





## Supporting Information

for

### **Aromatic vs. aliphatic hyperbranched polyphosphoesters as flame retardants in epoxy resins**

*Jens C. Markwart<sup>‡[1,2]</sup>, Alexander Battig<sup>‡[3]</sup>, , Maria M. Velencoso<sup>[1]</sup>, Dennis Pollok<sup>[1]</sup>, Bernhard Schartel<sup>\*[3]</sup>, Frederik R. Wurm<sup>\*[1]</sup>*

<sup>1</sup> Max-Planck-Institut für Polymerforschung, Ackermannweg 10, 55128 Mainz, Germany;  
wurm@mpip-mainz.mpg.de

<sup>2</sup> Bundesanstalt für Materialforschung und -prüfung (BAM), Unter den Eichen 87, 12205 Berlin,  
Germany; bernhard.schartel@bam.de

<sup>3</sup> Graduate School Materials Science in Mainz, Staudinger Weg 9, 55128 Mainz, Germany

<sup>‡</sup> These authors contributed equally to this work.

#### **Corresponding author:**

\*E-mail: wurm@mpip-mainz.mpg.de; bernhard.schartel@bam.de

**Table S1.** Polymerization conditions of **1** with Grubbs Hoveyda 2<sup>nd</sup> in 1-chloronaphthalene generation catalyst at 40 °C in solution.

1 <sup>st</sup> addition					
Polymer	%mol Catalyst	Time (min)	Mn (g/mol)	Mw (g/mol)	D
1.2	0.32	60	1300	1400	1.1
1.3 <sup>i</sup>	0.65	60	1700	2400	1.4
1.5 <sup>ii</sup>	0.65	45	-	-	-
1.15	0.81	120	3000	8700	2.9
2 <sup>nd</sup> addition (after sampling of 1 <sup>st</sup> addition)					
Polymer	%mol Catalyst	Time (min)	Mn (g/mol)	Mw (g/mol)	D
1.2	0.32	60	1756	2390	1.36
1.3	0.65	30	4185	56306	13.45
1.5	0.32	25	4875	55333	11.35

<sup>i</sup> in bulk. <sup>ii</sup> cross-linked.

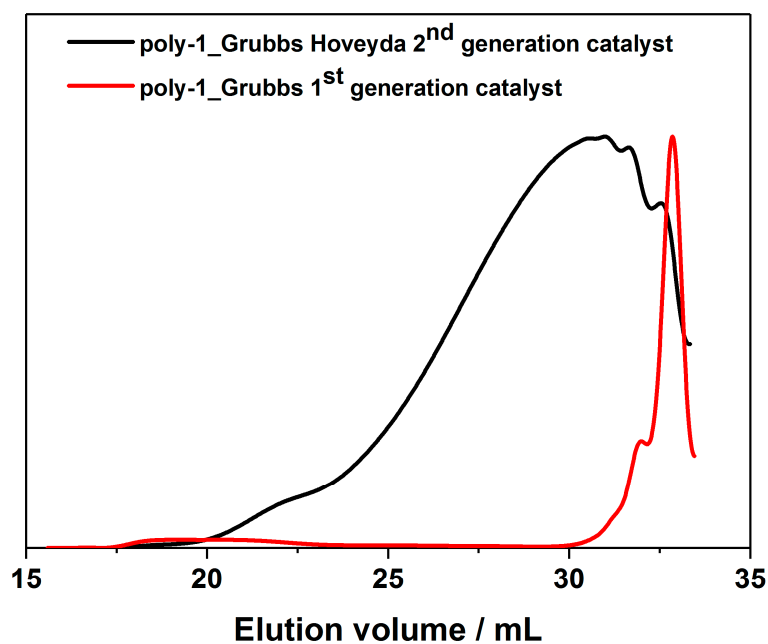


**Figure S1.** SEC curves (VWD-Signal 270 nm) of **poly-1** in DMF polymerized with Grubbs 1st generation catalyst and Grubbs Hoveyda 2nd generation catalyst at 40 °C.

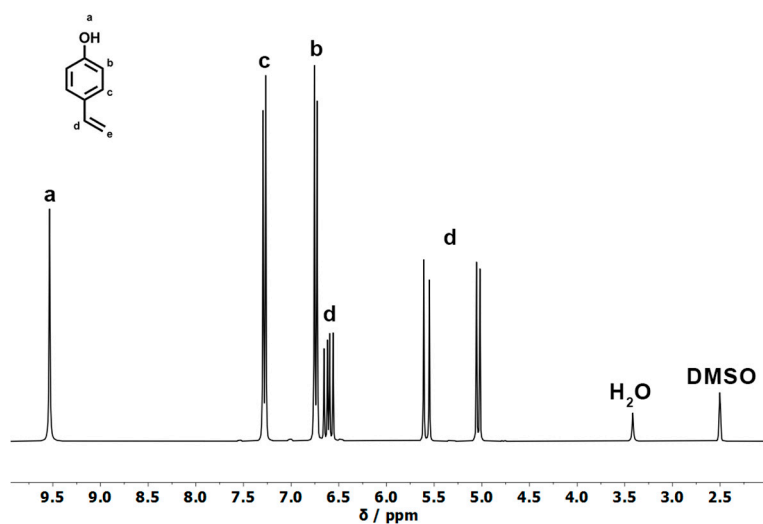


**Figure S2.**  $^1\text{H}$  NMR (300 MHz in  $\text{CDCl}_3$  at 298 K) spectra of 4-vinylphenol.

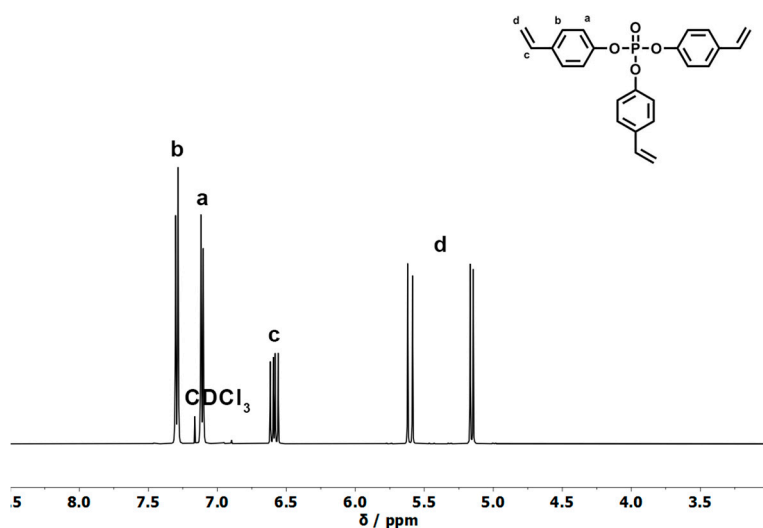


**Figure S3.**  $^1\text{H}$ -NMR (500 MHz in  $\text{CDCl}_3$  at 298 K) spectra of **1**.

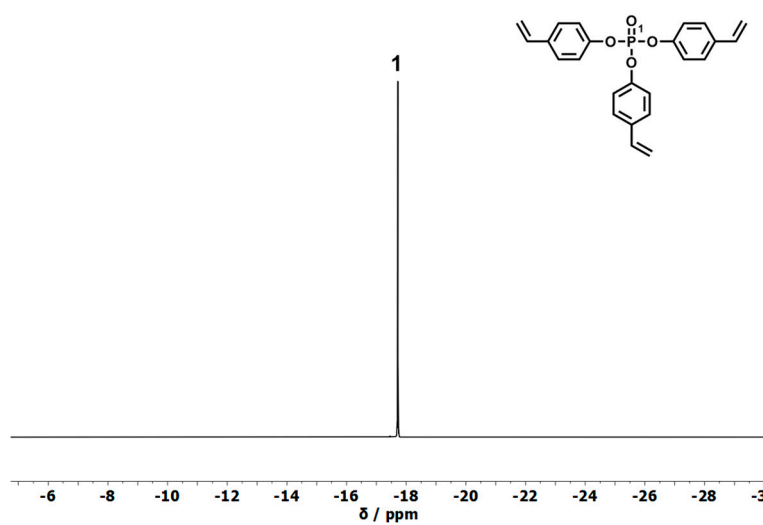


**Figure S4.**  $^{31}\text{P}$   $\{^1\text{H}\}$ -NMR (121 MHz in  $\text{CDCl}_3$  at 298 K) spectra of **1**.

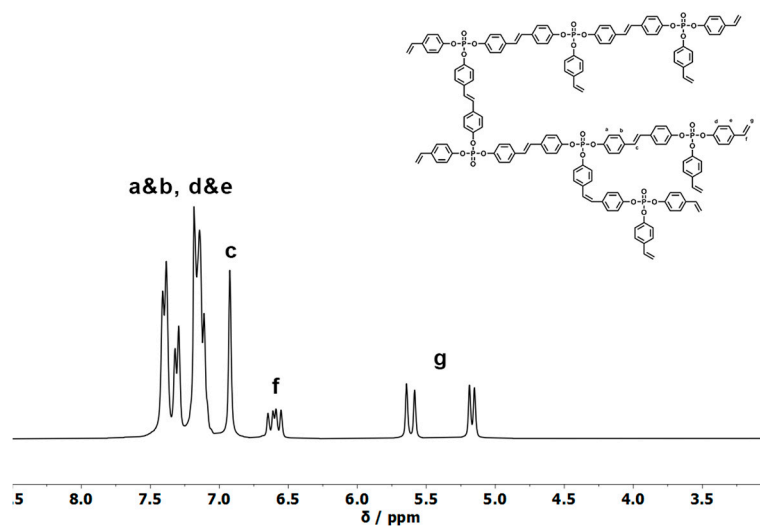


Figure S5.  $^1\text{H}$ -MR (300 MHz in  $\text{CDCl}_3$  at 298 K) spectra of **poly-1**.

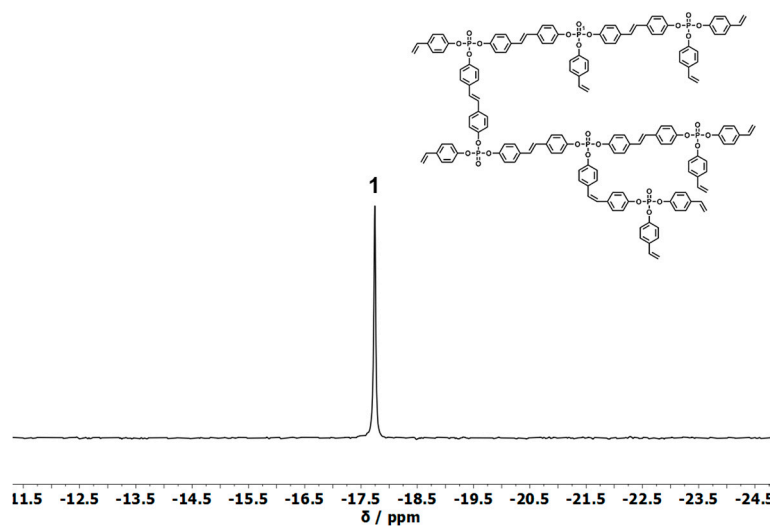


Figure S6.  $^{31}\text{P}$  {H}-NMR (121 MHz in  $\text{CDCl}_3$  at 298 K) spectra of **poly-1**.

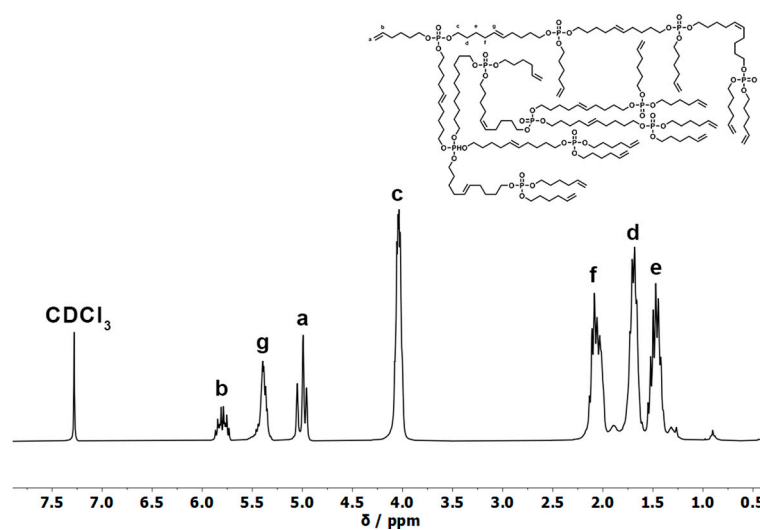
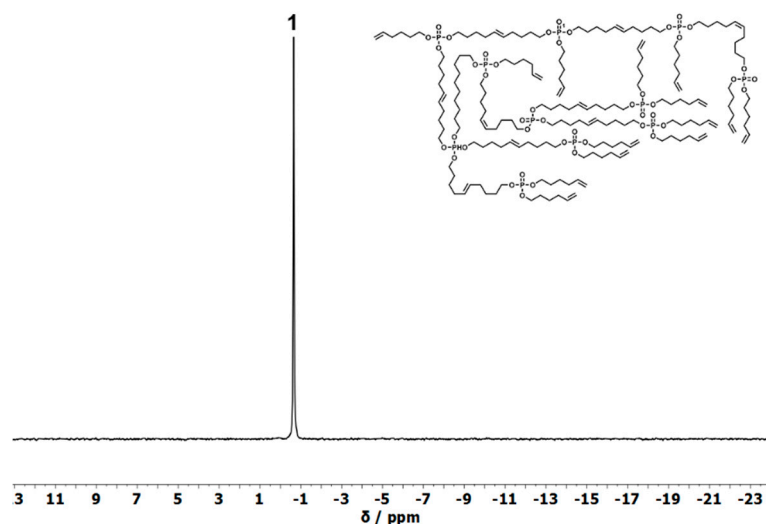
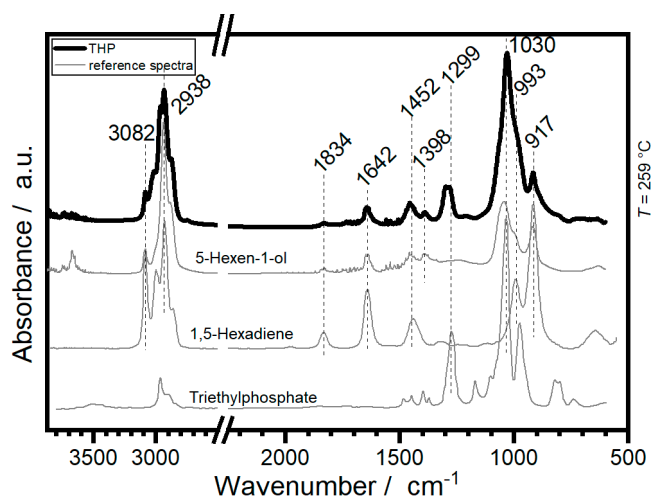


Figure S7.  $^1\text{H}$ -MR (300 MHz in  $\text{CDCl}_3$  at 298 K) spectra of **poly-2**.



**Figure S8.**  $^{31}\text{P}$  {H}-NMR (121 MHz in  $\text{CDCl}_3$  at 298 K) spectra of **poly-2**.



**Figure S9.** TGA-FTIR spectrum of **2** (top, black), identifying the main decomposition products (1,5-hexadiene; 5-hexen-1-ol and phosphate species, comparison shown in gray below) at specific decomposition temperature (259 °C) using references from NIST library.[1]

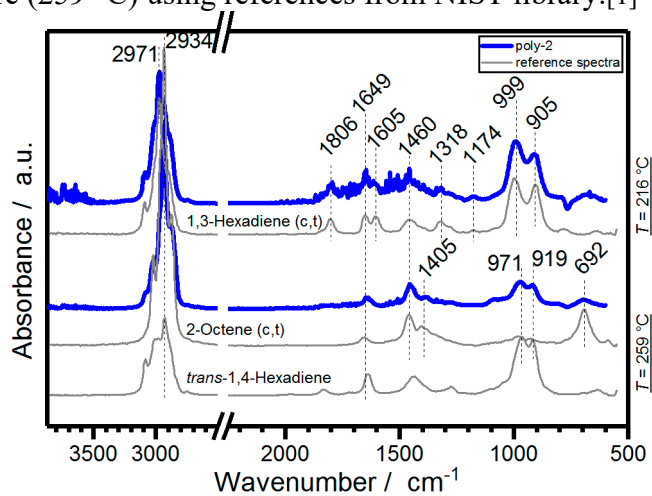


**Figure S10.** TGA-FTIR spectrum of **poly-2** (top, blue), identifying the main decomposition products (1,3-hexadiene (c,t) and 2-octene (c,t) and trans-1,4-hexadiene, comparison shown in gray below) at specific decomposition temperature (216 °C, 259 °C) using references from NIST library.[1]

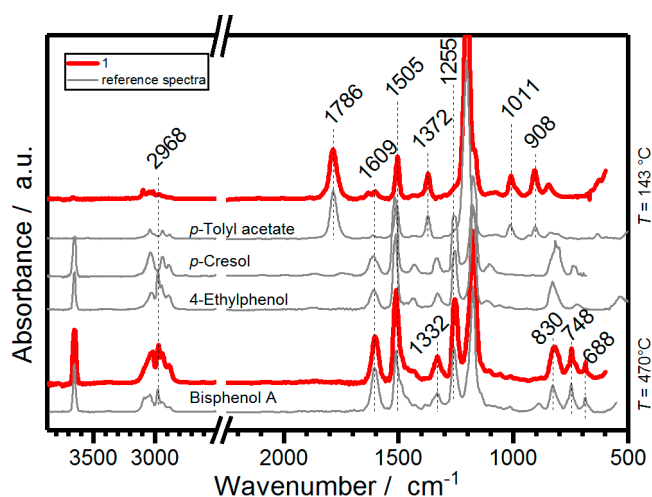


**Figure S11.** TGA-FTIR spectrum of **1** (top, red), identifying the main decomposition products (p-tolyl acetate; p-cresol; 4-ethylphenol and bisphenol A, comparison shown in gray below) at specific decomposition temperature (143 °C, 470 °C) using references from NIST library.[1]

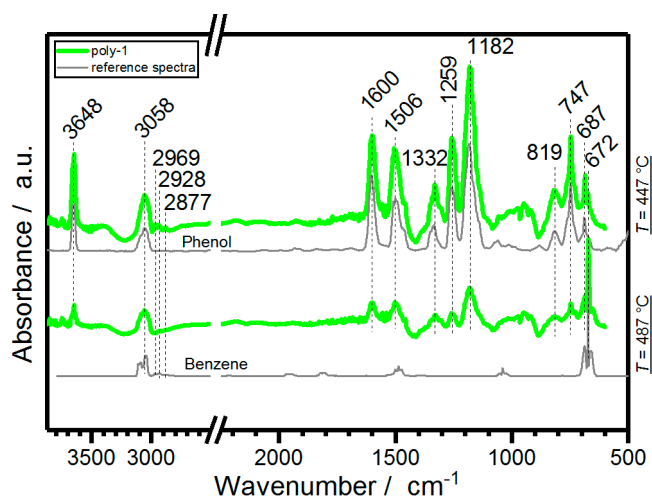


**Figure S12.** TGA-FTIR spectrum of **poly-1** (top, green), identifying the main decomposition products (phenol and benzene, comparison shown in gray below) at specific decomposition temperature (447 °C and 487 °C) using references from NIST library.[1]

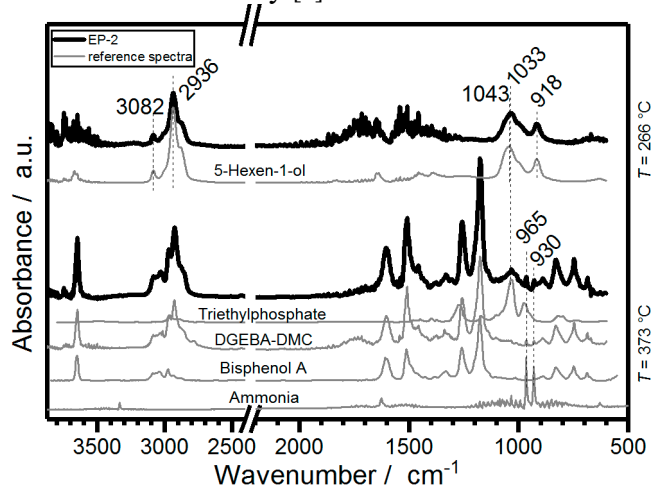


**Figure S13.** TGA-FTIR spectrum of **EP-2** (top, black), identifying the main decomposition products (5-hexen-1-ol; phosphate species and decomposition products of the matrix, a comparison is shown in gray below) at specific decomposition temperature (266 °C, 373 °C) using references from NIST library.[1]

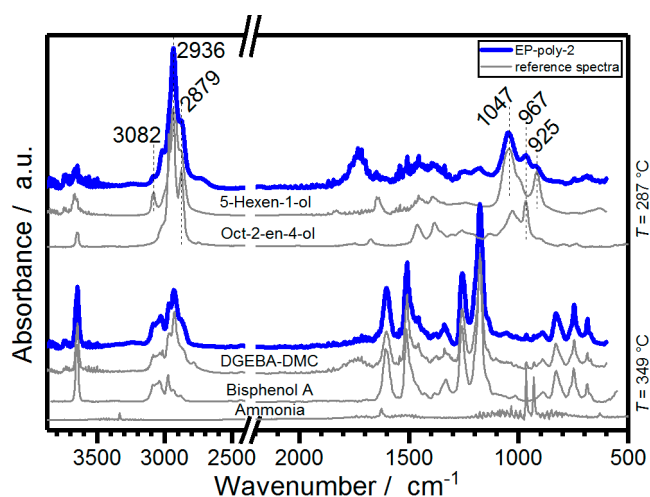


**Figure S14.** TGA-FTIR spectrum of **EP-poly-2** (top, blue), identifying the main decomposition products (5-hexen-1-ol; oct-2-en-4-ol and decomposition products of the matrix, a comparison is shown in gray below) at specific decomposition temperature (287 °C, 349 °C) using references from NIST library.[1]

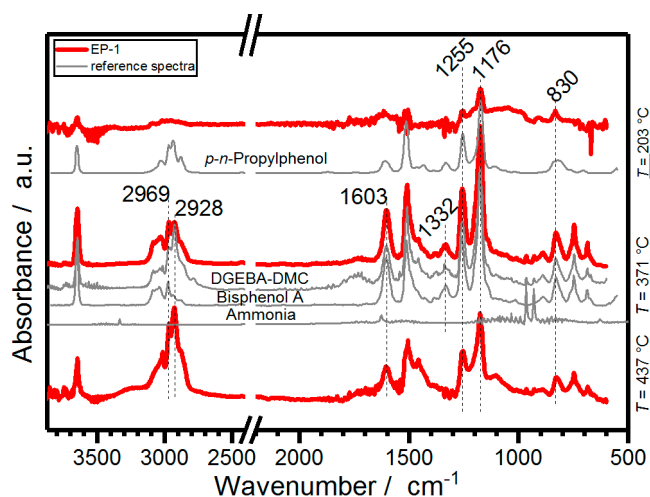


**Figure S15.** TGA-FTIR spectrum of **EP-1** (top, red), identifying the main decomposition products (p-n-propylphenol and decomposition products of the matrix, a comparison is shown in gray below) at specific decomposition temperature (203 °C, 371 °C, 437 °C) using references from NIST library.[1]

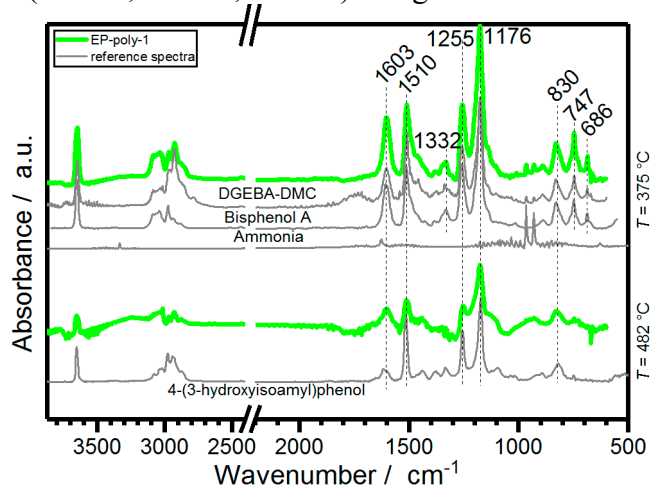


**Figure S16.** TGA-FTIR spectrum of **EP-poly-1** (top, green), identifying the main decomposition products (4-(3-hydroxyisoamyl)phenol and decomposition products of the matrix, a comparison is shown in gray below) at specific decomposition temperature (375 °C, 482 °C) using references from NIST library.[1]



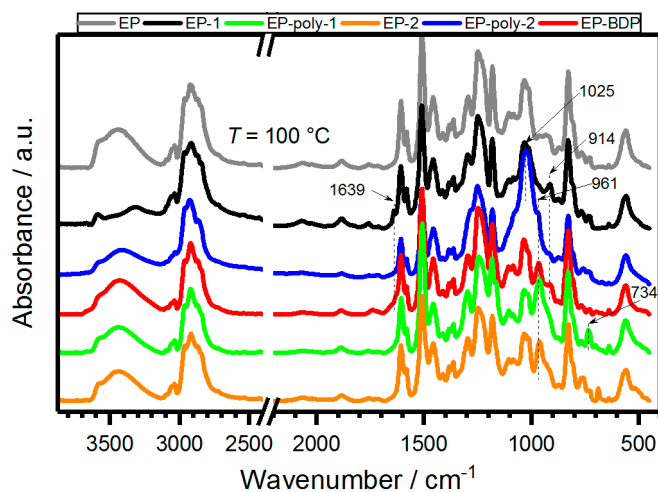


**Figure S17.** Results from hot-stage FTIR measurements, comparing the condensed phase spectra of EP-FRs at 100 °C.

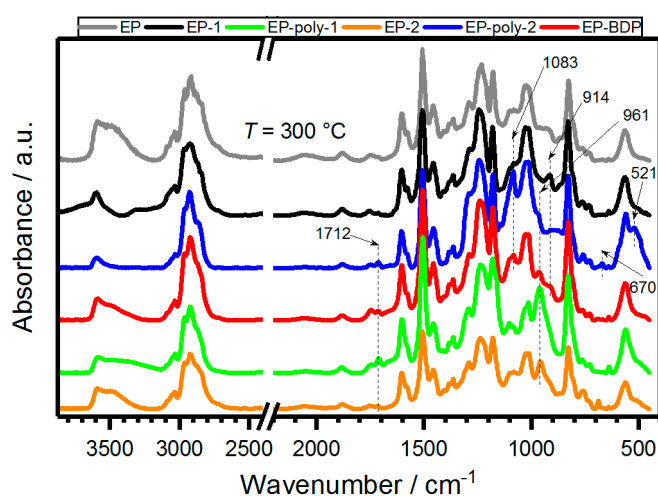


**Figure S18.** Results from hot-stage FTIR measurements, comparing the condensed phase spectra of EP-FRs at 300 °C.

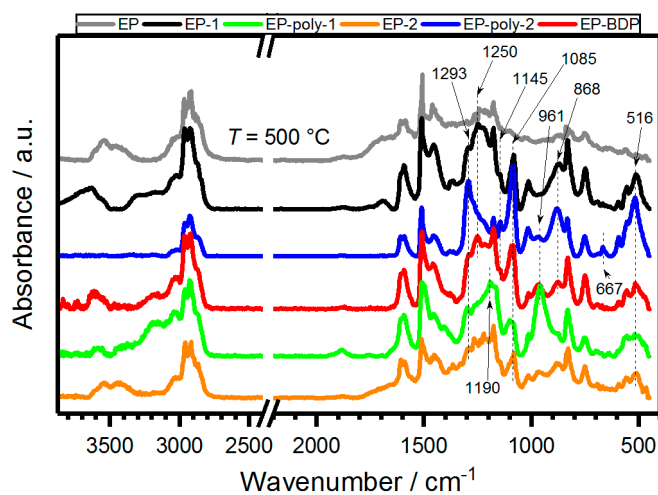


**Figure S19.** Results from hot-stage FTIR measurements, comparing the condensed phase spectra of EP-FRs at 500 °C.

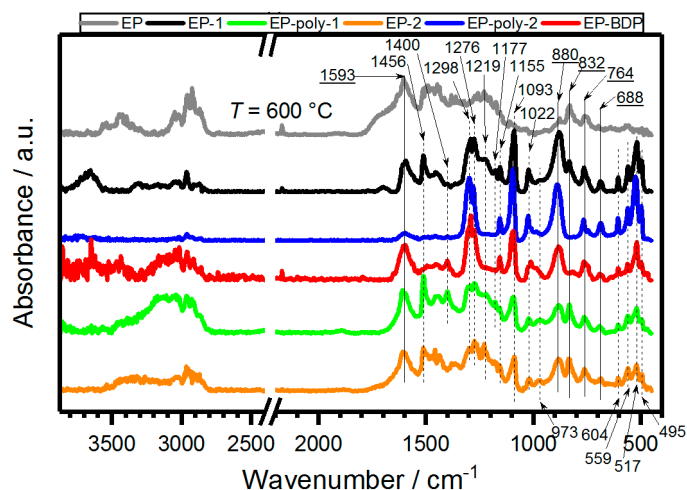


**Figure S20.** Results from hot-stage FTIR measurements, comparing the condensed phase spectra of **EP-FRs** at 600 °C, underlined bands are typical to DGEBA-DMC.

**Table S2.** Glass transition temperatures ( $T_g$ ) of the flame retardant containing epoxy resins (measured by DSC).

Material	$T_g$
EP-1	149 ± 1
EP-poly-2	127 ± 3
EP- 2	113 ± 1
EP-poly-2	154 ± 2

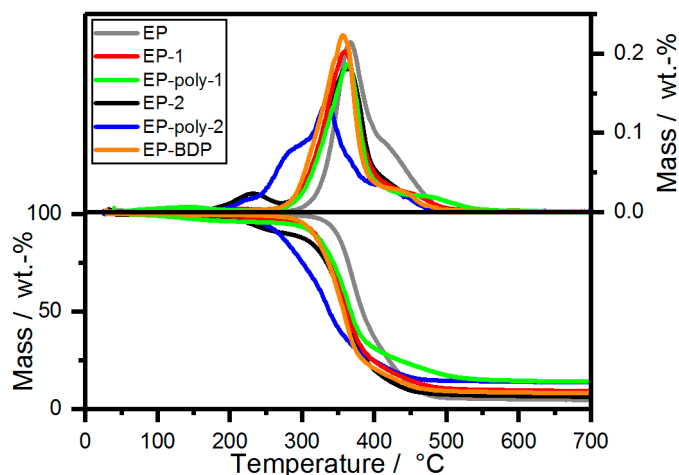


**Figure S21.** Mass loss (bottom) and mass loss rate (top) over  $T$  of neat epoxy resin and flame retardant containing epoxy resins from TGA measurements (10 K min<sup>-1</sup>; N<sub>2</sub>).

**Table S3.** TGA data of the flame retardant containing epoxy resins.  $T_{5\%}$ : Temperature at which 5% mass-loss happened;  $T_{max}$ : Temperature of maximum degradation; Residue: Residue at 700 °C.

Material	$T_{5\%} / ^\circ\text{C}$	$T_{max} / ^\circ\text{C}$	Residue / wt.-%
DGEBA-DMC (EP)	$338 \pm 1$	$372 \pm 1$	$4.5 \pm 0.1$
EP-1	$279 \pm 1$	$359 \pm 1$	$9.1 \pm 0.2$
EP-poly-1	$299 \pm 3$	$361 \pm 1$	$14.7 \pm 0.5$
EP-2	$231 \pm 1$	$367 \pm 0$	$5.1 \pm 0.1$
EP-poly-2	$249 \pm 3$	$337 \pm 2$	$13.3 \pm 0.2$
EP-BDP	$304 \pm 1$	$357 \pm 0$	$8.2 \pm 0.1$

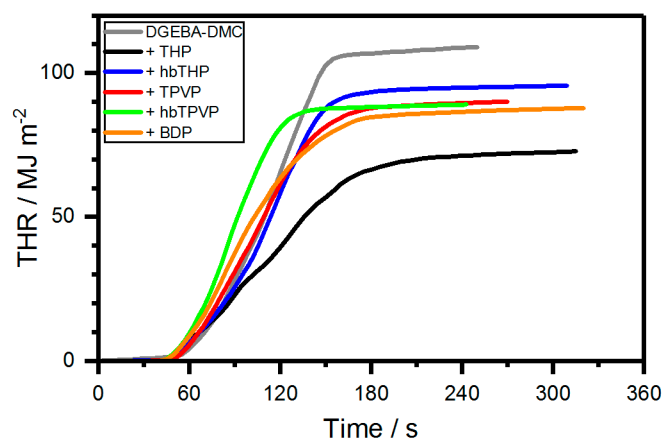


**Figure S22.** Total heat released (THR) of epoxy resin and epoxy resin with flame retardant measured by cone calorimeter.

**Table S4.** Results from cone calorimeter measurements of the flame retardant containing epoxy resins.

Material	THE / $\text{MJ m}^{-2}$	PHRR / $\text{kW m}^{-2}$	Residue / wt.-%	EHC / $\text{MJ kg}^{-1}$	FIGRA / $\text{kW m}^{-2} \text{s}$
DGEBA-DMC (EP)	$108 \pm 3$	$1696 \pm 180$	$0.7 \pm 0.1$	$26.9 \pm 1.0$	$15.5 \pm 2.3$
EP-1	$88 \pm 1$	$1194 \pm 100$	$5.3 \pm 0.0$	$23.3 \pm 0.2$	$11.2 \pm 0.0$
EP-poly-1	$92 \pm 4$	$1969 \pm 353$	$7.0 \pm 1.5$	$25.0 \pm 1.5$	$15.0 \pm 0.7$
EP-2	$78 \pm 6$	$885 \pm 16$	$9.2 \pm 0.1$	$21.7 \pm 1.8$	$9.0 \pm 0.2$
EP-poly-2	$95 \pm 0$	$1248 \pm 32$	$5.1 \pm 0.7$	$24.9 \pm 0.2$	$9.0 \pm 0.0$
EP-BDP	$87 \pm 1$	$1180 \pm 41$	$3.1 \pm 0.2$	$22.7 \pm 0.2$	$11.0 \pm 0.7$



**Figure S23.** Cross-linking of **1** at 300 °C in a silicon form for 2 h, producing a hard, cross-linked PPE resin.

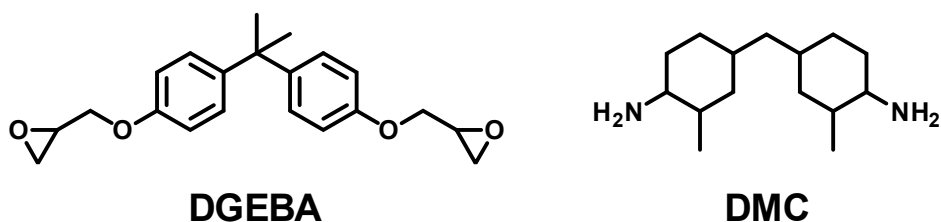


**Figure S24.** Chemical structure of Diglycidyl ether of Bisphenol A (DGEBA) and 2,2'-Dimethyl-4,4'-methylene-bis(cyclohexylamine) (DMC).



**3 cm**

**Figure S25.** Residue of EP-1 after cone calorimeter measurement, exhibiting a moderate protective layer effect from the formation of a rigid char layer.



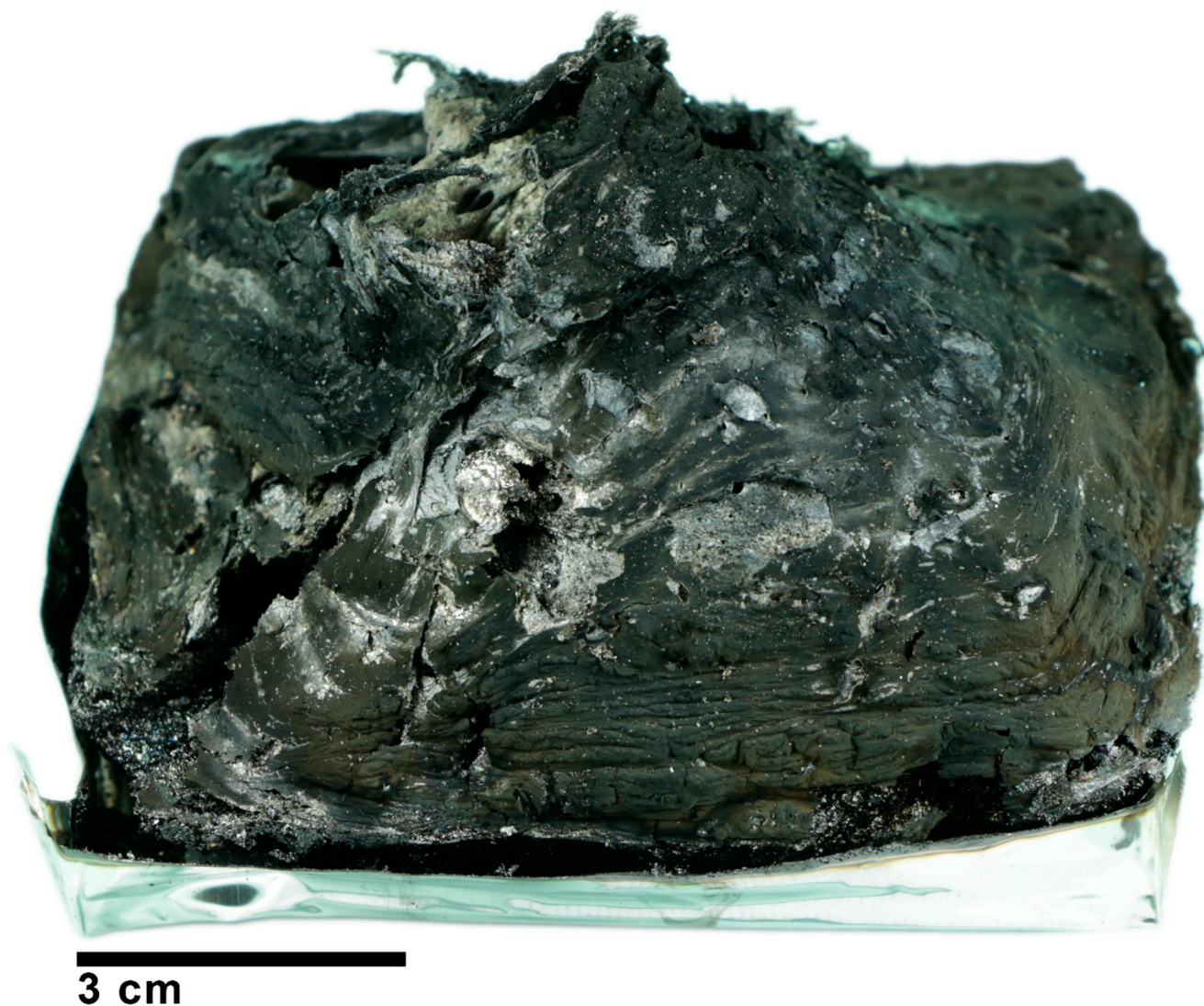


**Figure S26.** Residue of EP-2 after cone calorimeter measurements, exhibiting a strong protective layer from the large voluminous, multicellular char.

### References

1. Linstrom, P.J.; Mallard, W.G. NIST Chemistry WebBook, NIST Standard Reference Database Number 69. Available online: <https://doi.org/10.18434/T4D303> (accessed on 27.08.2019).

## 5.5. Matrix matters: Hyperbranched flame retardants in aliphatic and aromatic epoxy resins

Alexander Battig, Jens C. Markwart, Frederik R. Wurm, Bernhard Schartel, *Polym. Degrad. Stab.* **2019**, 170, 108986.

DOI link: <https://www.doi.org/10.1016/j.polymdegradstab.2019.108986>

This article was accepted and published.

### Author contribution:

- Conceptualizing the frame of the work
- Chose the polymer materials, approach, loading, sample preparation and testing
- Pyrolytic investigations of the flame retardants (FRs)
  - Thermogravimetric analysis
  - Evolved gas and condensed phase FTIR
  - Pyrolysis gas chromatography / mass spectrometry
  - Pyrolysis combustion flow calorimeter
- Material and fire testing of FR-containing epoxy resins
  - Differential scanning calorimeter
  - Cone calorimeter, LOI and UL-94
  - Scanning electron microscopy, photography
- Collection, analysis, and interpretation of the data.
- Provided figures throughout the article, including decomposition mechanism
- Scientific discussion, conclusions, and writing the manuscript
- Proofread and spell-checked all versions of the article

## Abstract

We synthesized a library of phosphorus-based flame retardants (phosphates and phosphoramides of low and high molar mass) and investigated their behavior in two epoxy resins (one aliphatic and one aromatic). The pyrolytic and burning behavior of the two resins (via TGA, TG-FTIR, Hot stage FTIR, Py-GC/MS, PCFC, DSC, LOI, UL-94, Cone calorimeter) are analyzed and compared to the results of flame retardant (FR)-containing composites. A decomposition pathway incorporating the identified modes of action and known chemical mechanisms is proposed. The overlap of decomposition temperature ( $T_{dec}$ ) ranges of matrix and FR determines the efficacy of the system. Low molar mass FRs strongly impact material properties like  $T_g$  but are very reactive, and high molar mass variants are more thermally stable. Varying P-O and P-N content of the FR affects decomposition, but the chemical structure of the matrix also guides FR behavior. Thus, phosphates afford lower fire load and heat release in aliphatic epoxy resins, and phosphoramides can act as additives in an aromatic matrix or as reactive FRs in aliphatic ones. The chemical structure and the structure-property relationship of both FR and matrix are central to FR performance and must be viewed not as two separate but as one codependent system.





# Matrix matters: Hyperbranched flame retardants in aliphatic and aromatic epoxy resins



Alexander Battig <sup>a,1</sup>, Jens C. Markwart <sup>b,1</sup>, Frederik R. Wurm <sup>b,\*\*</sup>, Bernhard Schartel <sup>a,\*</sup>

<sup>a</sup> Bundesanstalt für Materialforschung und -prüfung (BAM), Unter den Eichen 87, 12205, Berlin, Germany

<sup>b</sup> Max Planck Institute for Polymer Research, Ackermannweg 10, 55128, Mainz, Germany

## ARTICLE INFO

### Article history:

Received 14 June 2019

Received in revised form

24 September 2019

Accepted 26 September 2019

Available online 5 October 2019

### Keywords:

Flame retardant

Phosphate

Phosphorus

Phosphoramidate

Epoxy resin

Hyperbranched polymer

## ABSTRACT

We synthesized a library of phosphorus-based flame retardants (phosphates and phosphoramidates of low and high molar mass) and investigated their behavior in two epoxy resins (one aliphatic and one aromatic). The pyrolytic and burning behavior of the two resins (via TGA, TG-FTIR, Hot stage FTIR, Py-GC/MS, PCFC, DSC, LOI, UL-94, Cone calorimeter) are analyzed and compared to the results of flame retardant (FR)-containing composites. A decomposition pathway incorporating the identified modes of action and known chemical mechanisms is proposed. The overlap of decomposition temperature ( $T_{dec}$ ) ranges of matrix and FR determines the efficacy of the system. Low molar mass FRs strongly impact material properties like  $T_g$  but are very reactive, and high molar mass variants are more thermally stable. Varying P–O and P–N content of the FR affects decomposition, but the chemical structure of the matrix also guides FR behavior. Thus, phosphates afford lower fire load and heat release in aliphatic epoxy resins, and phosphoramidates can act as additives in an aromatic matrix or a reactive FRs in aliphatic ones. The chemical structure and the structure-property relationship of both FR and matrix are central to FR performance and must be viewed not as two separate but as one codependent system.

© 2019 Elsevier Ltd. All rights reserved.

## 1. Introduction

Phosphorus-based FRs (P-FRs) have gained added attention as suitable alternatives to halogenated FRs. Primarily, this is due to heightened health and environmental concerns over halogen-containing formulations. P-FRs offer a broad range of application for many polymer types, as reactive or additive components, mainly due to the chemical versatility of phosphorus [1–4]. Moreover, their mode of action can be adjusted to suit a specific application by altering the P-FR composition: Recently, a study conducted on the ratio of P–O to P–N bonds highlighted the change in mode of action and decomposition mechanism of low molar mass P-FRs in epoxy resins [5]. Additionally, by polymerizing these low molar mass P-FRs into hyperbranched (hb) polymers, the effect of complex architecture on the flame retardancy of epoxy resins was investigated, and the effectiveness of hb polymers as

multifunctional FRs was elucidated [6].

The interaction between decomposition compounds of FR and matrix affect the combustion efficiency, peak of heat release rate, and effective heat of combustion in fire scenarios [7,8]. Previous works have shown that one underlying mode of action is the formation of aromatic char precursors and the stabilizing role of phosphorus in them [9]. Critically, this effect is maximized when the overlap of decomposition temperature ( $T_{dec}$ ) ranges of matrix and FR is greatest [10–12]. Investigation of the previously synthesized low molar mass monomeric FRs (mFRs) and the polymeric hyperbranched FRs (hbFRs) in an epoxy resins (EP) concluded that the FR's mode of action is alterable by the presence of nitrogen in the P-binding sphere (P–N vs. P–O) [5]. Moreover, its chemical interaction capabilities are increased by polymerization, mainly due to the shift to higher  $T_{dec}$ . Furthermore, the role of sulfur in the flame retardancy of hbFRs is the subject of another investigation. These changes in the chemical composition and architecture led to higher residue yields and more effective flame retardancy of a bisphenol A based epoxy resin (EP-B) [6].

The structure-property relationship of the FR and matrix are crucial to effective flame retardancy. As it stands, the modes of action and chemical FR mechanisms previously proposed for mFRs

\* Corresponding author.

\*\* Corresponding author.

E-mail addresses: [wurm@mpip-mainz.mpg.de](mailto:wurm@mpip-mainz.mpg.de) (F.R. Wurm), [bernhard.schartel@bam.de](mailto:bernhard.schartel@bam.de) (B. Schartel).

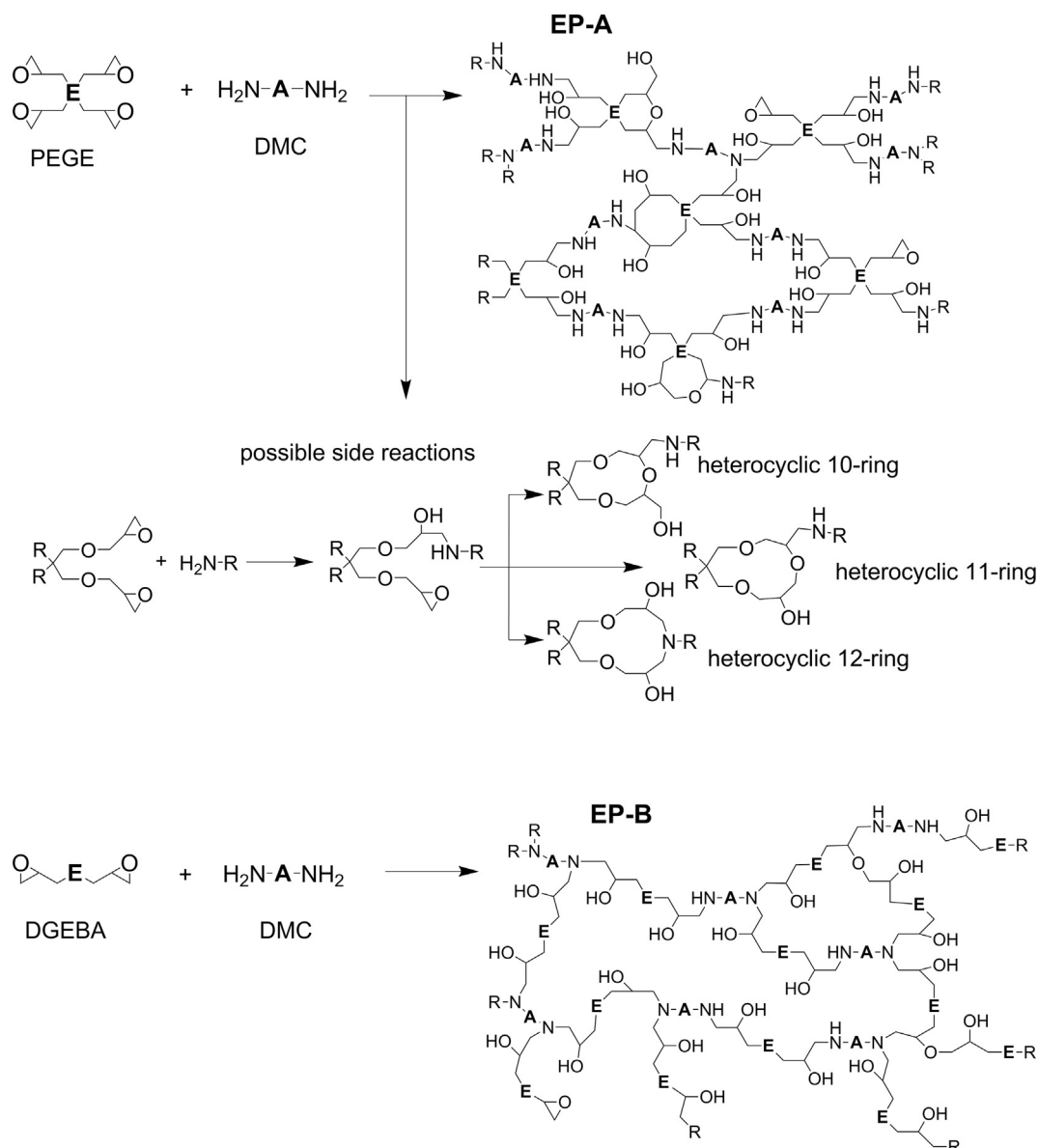
<sup>1</sup> These authors contributed equally.

and hbFRs are based on their performance in an aromatic, bisphenol A-based polymer resin. However, a fuller understanding of the FRs' capabilities may be gained from examining their performance in an aliphatic epoxy resin (EP-A) and comparing the results to the previously examined EP-B, which is precisely the approach proposed in the following manuscript.

The aliphatic epoxy resin EP-A (Scheme 1) has been previously investigated in use as fiber-reinforced composites and as a basis for reactive phosphorus-based FR-crosslinking agents [13,14]. Its epoxide agent is based on pentaerythritol, a main component (carbon-source) in intumescent systems [15,16]. Pentaerythritol glycidyl ether has further been investigated as a chain extender and plasticizing agent for bisphenol A systems [17], as well as a starting material for polyurethanes [18].

We have investigated the flame retardancy effects of previously synthesized and characterized monomeric and hyperbranched polymeric FRs in aliphatic and aromatic epoxy resins. As a means to compare the efficacy of these FRs in the respective matrices, an

industrially available FR, previously proven effective in epoxy resins, namely bisphenol A bis(diphenyl phosphate) (BDP), was used as a benchmark. This work aims at understanding the fundamental chemical interactions at play of phosphates and phosphoramides – as low molar mass and hyperbranched polymeric variants – in two distinct epoxy resin systems. By comparing the results, greater insight into the mode of action and chemical mechanisms surrounding these P-FRs may be gained. More significantly, investigating these FRs in different matrices expands the understanding of the FR-matrix system and the codependence of the two on effective flame retardancy. This work is not aimed at optimizing the performance of the materials, but rather at observing their behavior in divergent matrices and extrapolating their function by means of multi-method pyrolysis and fire behavior investigations.



**Scheme 1.** General synthesis scheme of EP-A (top) and EP-B (bottom) and schematic representation of matrices (E: epoxy component PEGE; A: amine component DMC).

## 2. Materials and Methods

All materials (Table 1) were used without further purification.

The aliphatic epoxide agent pentaerythritol tetraglycidyl ether (PEGE, ipox CL 16) was supplied by ipox chemicals GmbH (Lau-pheim, Germany). The aromatic epoxide agent diglycidyl ether of Bisphenol A (DGEBA, Araldite MY740) was supplied by Bodo Müller Chemie GmbH (Offenbach am Main, Germany). The amine component 2,2'-dimethyl-4,4'-methylene-bis-(cyclohexylamine) (DMC) was purchased from Sigma Aldrich Co. LLC/Merck KgaA (Darmstadt, Germany). The benchmark FR bisphenol A bis(diphenyl phosphate) (BDP) was supplied by Albemarle (Louvain-la-Neuve, Belgium). The mFRs and hbFRs were previously synthesized and characterized [5,6]: starting from  $\text{POCl}_3$ , mE was produced via esterification with hex-5-en-1-ol, and mA was prepared via amidation with hex-5-en-1-amine. hbE and hbA were produced via a radical thiol-ene polyaddition, combining mE or mA as monomers, respectively, with 1,2-ethanethiol as comonomer and azoisobutyronitrile (AIBN) as a radical initiator. Purities and chemical structures were identified via  $^1\text{H}$  and  $^{31}\text{P}$  {H} NMR.

All epoxy resin samples (with or without FR) were prepared as follows (Table 2): the epoxide agent (PEGE or DGEBA) was poured into in a 1 L polypropylene cup. For FR-containing composites, 10 wt.-% of the total batch was replaced with the FR. The amount of FR, and therefore P-content regarding weight equivalents, was identical in both systems. The FR was mixed with the epoxide agent with a wooden spatula. Once the components were fully mixed, the amine component DMC was added, and the mixture was again stirred until homogenous. The contents were poured into prepared aluminum molds sized 100 mm × 100 mm × 4 mm (for cone calorimeter specimens) or 130 mm × 130 mm × 3 mm (for LOI or UL-94 specimens). UL-94 and LOI samples were cut from the mold into appropriate specimen sizes according to their respective standards.

Nuclear magnetic resonance (NMR) analysis,  $^1\text{H}$ ,  $^{31}\text{P}$  {H},

$^1\text{H}$ ,  $^1\text{H}$ -COSY and  $^1\text{H}$ ,  $^{31}\text{P}$ -HMBC NMR spectra were recorded with Bruker Avance spectrometers operating with 300 or 500 MHz frequencies in deuterated chloroform or deuterated N,N-dimethylformamide as a solvent. The calibration of the spectra was done against the solvent signal. The spectra were analyzed using MestReNova 9 from Mestrelab Research S.L.

Powdered samples for TGA-FTIR, PCFC and hot stage FTIR measurements were obtained using a CryoMill (RETSCH, Germany) under liquid nitrogen cooling.

Thermogravimetric analysis (TGA) measurements were performed on a TG 209 F1 Iris (Netzsch Instruments, Selb, Germany). 10 mg powdered samples were used for EPs and EPs with FRs, and 5 mg samples for pure FRs. Samples were heated from 30 to 900 °C at a rate of 10 K min<sup>-1</sup> under a 30 ml min<sup>-1</sup> nitrogen flow.

Evolved gas analysis of TGA samples was conducted using a Fourier transform infrared spectrometer Tensor27 (Bruker Optics, Ettlingen, Germany) (TG-FTIR). The machines were coupled by a 1.0 m transfer line heated to 270 °C.

Condensed phase FTIR spectra during pyrolysis were gathered using a FTIR600 hot-stage cell (Linkam Scientific Instruments Ltd., Chilworth, UK) fitted to a Vertex70 FTIR spectrometer (Bruker Optics, Ettlingen, Germany). The measuring range was 4000 to 400 cm<sup>-1</sup> at a resolution of 0.4 cm<sup>-1</sup>. Approx. 5 mg of powdered material was pressed into a potassium bromide platelet ( $d = 1$  cm;  $w = 0.1$  cm) and placed into the hot-stage cell. Under a nitrogen flow of 300 ml min<sup>-1</sup>, the samples were heated from 30 to 600 °C at a rate of 10 K min<sup>-1</sup>.

Pyrolysis Gas Chromatography - Mass Spectrometry (Py-GC/MS) measurements were performed using a PY3030iD micro-furnace double-shot pyrolyzer (Frontier Laboratories, Japan) coupled via a split/splitless inlet port to a 7890B gas chromatograph (Agilent Technologies, USA) and combined with a 5977B mass selective detector (Agilent Technologies, USA). The EI ionization energy of the MSD was 70 eV and the scan range was 15–50 amu. 150 μg

**Table 1**  
Material names, abbreviations, and chemical structures.

Name	Short name	Chemical structure	P content (calc) [%]
Pentaerythritol tetraglycidyl ether	PEGE		–
Diglycidyl ether of bisphenol A	DGEBA		–
2,2'-Dimethyl-4,4'-methylene-bis-(cyclohexylamine)	DMC		–
Tri(hex-5-en-1-yl) phosphate	mE		9.0
hb-Phosphoester	hbE		7.1
Tri(hex-5-en-1-yl) phosphoramidate	mA		9.1
hb-Phosphoramidate	hbA		7.1
Bisphenol A diphenyl phosphate	BDP		8.1

**Table 2**  
Composition of tested epoxy resin and composite specimen.

Material	Composition [g] (exemplary 500 g batch)											
	EP-A	+ mE	+ hbE	+ mA	+ hbA	+ BDP	EP-B	+ mE	+ hbE	+ mA	+ hbA	+ BDP
PEGE	301	271	271	271	271	271	—	—	—	—	—	—
DGEBA	—	—	—	—	—	—	370	333	333	333	333	333
DMC	199	179	179	179	179	179	130	117	117	117	117	117
mE	—	50	—	—	—	—	—	50	—	—	—	—
hbE	—	—	50	—	—	—	—	—	50	—	—	—
mA	—	—	—	50	—	—	—	—	—	50	—	—
hbA	—	—	—	—	50	—	—	—	—	—	50	—
BDP	—	—	—	—	—	50	—	—	—	—	—	50
P cont. [%]	0	0.9	0.7	0.9	0.7	0.8	0	0.9	0.7	0.9	0.7	0.8

samples were pyrolyzed at 500 °C in a helium atmosphere by a gravimetric fall into the pyrolysis zone. All evolved pyrolysis products were separated under a helium flow of 1 ml min<sup>-1</sup> using an Ultra Alloy + -5 capillary column of a length of 30 m, and inner diameter of 0.25 mm, and a film thickness of 0.25 μm. The temperature of the column was held for 2 min at 40 °C, then increased to 300 °C at a rate of 10 K min<sup>-1</sup> and held for 10 min. The temperature of the gas chromatograph injector was 300 °C, and it was operated in a split mode of 1:300. The NIST 14 MS library was used for peak assignment.

Pyrolysis flow combustion calorimetry (PCFC) measurements were conducted on a microscale combustion calorimeter (Fire Testing Technologies Ltd., East Grinstead, UK). 5 mg powdered samples were pyrolyzed at a heating rate of 1 K s<sup>-1</sup> from 150 to 750 °C. The combustor temperature was set to 900 °C. The gas flow of nitrogen was 80 ml min<sup>-1</sup> and 20 ml min<sup>-1</sup> for oxygen.

Differential scanning calorimetry (DSC) measurements were conducted on a Netzsch 204 FR “Phoenix” (Netzsch Instruments, Selb, Germany). 5 mg samples were taken from the bulk material. In the range of -80 to 180 °C, three heating and two cooling runs were conducted at a rate of 10 K min<sup>-1</sup> under a 30 ml min<sup>-1</sup> nitrogen flow. The second and third heating run was used to determine *T<sub>g</sub>*.

Underwriter's Laboratory 94 (UL-94) testing was performed in vertical and then in horizontal orientation in accordance with EN 60695-11-10. Samples sized approx. 125 mm × 12 mm × 3 mm were stored at 50% relative humidity and 23 °C for at least 80 h prior to testing.

Limiting oxygen index (LOI) testing was conducted in accordance with ISO 4589-2. Type IV samples sized 125 mm × 6 mm × 3 mm were used after storage at 50% relative humidity and 23 °C for at least 80 h.

Forced-flaming measurements were conducted using a cone calorimeter (Fire Testing Technology Ltd., East Grinstead, UK) in accordance with ISO 5660. Samples sized 100 mm × 100 mm × 4 mm were stored at 50% relative humidity and 23 °C for at least 48 h prior to testing. Samples were irradiated with a heat flux of 50 kW m<sup>-2</sup> at a distance of 35 mm between specimen and cone heater, thus simulating a developing fire [19,20]. Measurements were conducted in duplicate, unless the margin of error was greater than 10%, whereupon a third specimen was measured.

### 3. Results and Discussion

#### 3.1. Pyrolysis – Decomposition temperature and mass loss

The pyrolytic decomposition temperature (*T<sub>dec</sub>*) and mass loss of the epoxy resin matrices EP-A and EP-B, as well as the flame retardants mE, hbE, mA, hbA, and BDP, were investigated via TGA (Fig. 1a & Table 3).

The mass loss and mass loss rate curves of EP-A and EP-B (Fig. 1a)

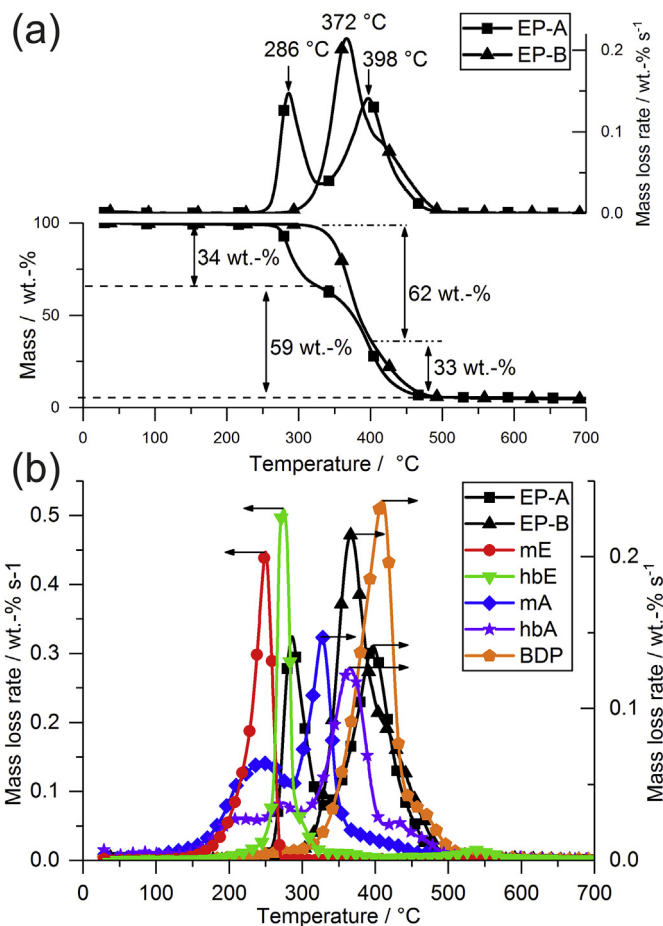


**Fig. 1.** Results from TGA measurements. a) Mass loss (bottom) and mass loss rate (top) of epoxy resins EP-A and EP-B; b) Mass loss rates of FRs and EPs, indicating decomposition temperature ranges.

outline the difference in thermal stability of the two materials. The onset temperature *T<sub>5%</sub>* (the temperature at 5% mass loss) of EP-A was 276 °C, and that of EP-B was 338 °C. Noticeably, EP-A exhibited two distinct decomposition steps, while EP-B's mass loss occurred in one step with a slight shoulder. The first decomposition step of EP-A, identified by the temperature at peak mass loss rate, occurred at 286 °C and corresponded to about 34 wt.-% mass loss, while the second step at 398 °C amounted to a 59 wt.-% mass loss. For EP-B, the main decomposition step (*T<sub>max</sub>*) at 372 °C amounted to a 62 wt.-% mass loss, while the shoulder at about 424 °C constituted a loss of about 33 wt.-%. Both materials retained similar residues at 700 °C (4.6 wt.-% for EP-A and 4.5 wt.-% for EP-B).

**Table 3**  
Results from TGA measurements of pure FRs and the epoxy resin matrices EP-A and EP-B.

	$T_{5\%}$ /°C	$T_1$ /°C	ML <sub>1</sub> /wt.-%	$T_2$ /°C	ML <sub>2</sub> /wt.-%	$T_{\max}$ /°C	ML <sub>max</sub> /wt.-%	$T_3$ /°C	ML <sub>3</sub> /wt.-%	Residue (700 °C) / wt.-%
EP-A	276 ±2	—	—	286 ±2	34.8 ±0.3	398 ±1	58.8 ±1.2	—	—	4.6 ±0.3
EP-B	338 ±1	—	—	—	—	372 ±1	62.0 ±0.8	424 ±5	33.2 ±0.3	4.5 ±0.1
mE	195 ±3	—	—	—	—	250 ±2	95.7 ±1.4	—	—	2.8 ±0.8
hbE	242 ±2	—	—	—	—	280 ±1	83.3 ±0.2	—	—	11.2 ±1.4
mA	181 ±2	236 ±10	36.1 ±0.5	—	—	317 ±10	46.4 ±0.3	—	—	15.6 ±0.8
hbA	190 ±3	212 ±2	11.1 ±1.2	273 ±3	14.2 ±2.3	361 ±3	47.1 ±0.5	430 ±4	7.9 ±0.8	17.8 ±0.4
BDP	331 ±1	—	—	—	—	415 ±6	85.5 ±2.2	467 ±3	11.8 ±1.3	1.8 ±0.9

The pure FRs have been previously characterized in detail [5,6], and Fig. 1b summarizes the mass loss rates of these materials during pyrolysis. Additionally, Table 3 summarizes the results from TGA measurements for all materials. mE decomposed in a single step ( $T_{5\%} = 195$  °C,  $T_{\max} = 250$  °C). For the hyperbranched polymeric variant hbE,  $T_{5\%}$  (242 °C) and  $T_{\max}$  (280 °C) were shifted to higher temperatures due to increased thermal stability of the hb-structure [6]. Notably, the residue yield at 700 °C of hbE (11.2 wt.-%) was four times higher than that of mE (2.8 wt.-%). mA decomposed in two steps, the first at 236 °C (36 wt.-% mass loss) and the second at 317 °C (46 wt.-% mass loss), retaining a residue of 15.6 wt.-% at 700 °C. The hyperbranched polymeric phosphoramidate hbA exhibited a higher  $T_{\max}$  compared to mA, comparable to the shift seen from mE to hbE. While  $T_{5\%}$  was only slightly higher than mA, hbA decomposed in multiple steps over a large temperature range, exhibiting four peak mass loss rates at 212 °C (11 wt.-% mass loss), 273 °C (14 wt.-% mass loss),  $T_{\max}$  at 361 °C (47 wt.-% mass loss), and 430 °C (8 wt.-% mass loss). The residue yield at 700 °C was 18 wt.-%, an increase of 14% compared to mA.

The benchmark FR BDP decomposed in a single decomposition step with a shoulder. Its  $T_{5\%}$  was at 331 °C and  $T_{\max}$  at 415 °C, accounting for an 85 wt.-% mass loss. Thus, BDP was the most thermally stable FR used in this study. The shoulder at approx. 467 °C presented a mass loss of 12 wt.-%, preserving a residue of only about 2 wt.-% at 700 °C.

### 3.2. Pyrolysis – Evolved gas analysis of EP

There have been several in-depth investigations into the thermal decomposition of EP-B [21–23]. Although flame retardancy of EP-A has been investigated previously [13,24], less is known about the pyrolytic evolved gases corresponding to the mass loss steps of EP-A. To understand the flame retardancy effects of the FRs on the polymer, the decomposition steps of the matrix must be more closely identified. To this end, pyrolysis – gas chromatography/mass spectrometry (Py-GC/MS) enables a more in-depth analysis of the evolved gases during pyrolysis. Two single-shot measurements were measured at specific temperatures:  $T = 325$  °C (Fig. 2a) and 500 °C (Fig. 2b). They represent the end of a mass loss step, as indicated by a minimum of the mass loss rate curve of EP-A in TGA experiments. Thus, products from the decomposition step at  $T = 286$  °C can be observed separately from the step at  $T = 398$  °C. Notably, the spectra at 500 °C contain information of decomposition products of both steps and not only the second. By analyzing the difference in spectra, a clearer image of the decomposition mechanism is presented.

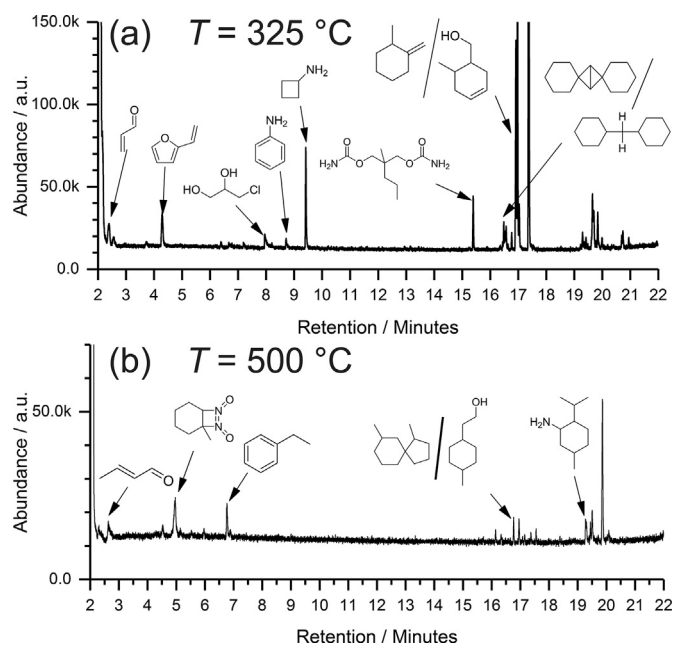


**Fig. 2.** Gas chromatograph of EP-A taken at (a) 325 °C and (b) 500 °C (B) via Py-GC/MS. Molecules matching MS spectra at specific retention times are noted with arrows.

The chromatograph in Fig. 2a reveals the production of several specific decomposition products from the EP-A matrix at 325 °C: At low retention times (2–10 min), low molar mass molecules were identified via comparative mass spectra, such as acrolein at 2.39 min (Figure S1), 2-vinylfuran at 4.29 min (Figure S2), 3-chloro-1,2-propanediol at 7.95 min (Figure S3), aniline at 8.72 min (Figure S4), and cyclobutylamine at 9.42 min (Figure S5). At higher retention times, the mass spectra resembled meprobamate at 15.39 min (Figure S6) and dispiro[cyclohexane-1,2'-bicyclo(1.1.0)butane-4',1''-cyclohexane] at 16.48–16.57 min (Figure S7). Additionally, 1-methyl-2-methylenecyclohexane and 6-methyl-3-cyclohexane-1-methanol at 16.97 min (Figure S8) were among the products identified as decomposition products from their mass spectra.

Fig. 2b exhibits those products pyrolyzed at 500 °C. Notably, the spectrum is significantly different to Fig. 2a. At low retention times (2–8 min), the mass spectral data saw similarities with 2-butenal at 2.66 min (Figure S9), 1,2-dinitroso-2-methyl-cyclohexane at 4.54 min (Figure S10), and ethylbenzene at 6.77 min (Figure S11). At



higher retention times, the mass spectra resembled 2-(4-methylcyclohexyl) ethanol or 1,7-dimethylspiro[4.5]decane at 16.76 min (Figure S12), as well as neomenthylamine at 19.30 min (Figure S13).

It should be noted that the NIST 14 library was utilized for structure identification purposes. Several fragmentations in the mass spectra do not fully correspond to the fragmentation pattern of the molecules mentioned above. However, their fragmentation pattern closely resembles these products, and they provide clues to the decomposition mechanism of EP-A. By using TGA-FTIR, corroborating evidence to the presence of these decomposition products may be gained.

By coupling the TGA to a Fourier transform infrared spectrometer (FTIR) via a transfer line, FTIR-spectra from the evolved gases at specific decomposition steps were captured. The gas spectra at the two main decomposition steps of EP-A are plotted in Fig. 3, along with reference spectra of decomposition products.

Notable decomposition products in the spectrum at 24.7 min were water (approx.  $4000\text{--}3475\text{ cm}^{-1}$  and  $2100\text{--}1275\text{ cm}^{-1}$ ), carbon dioxide ( $2360$  and  $669\text{ cm}^{-1}$ ), carbon monoxide ( $2185$  and  $2107\text{ cm}^{-1}$ ), and hydrochloric acid (approx.  $3100\text{--}2550\text{ cm}^{-1}$ ), the latter resulting from epichlorohydrin, an educt in the production of pentaerythritol tetraglycidyl ether. The decomposition of epichlorohydrin also yielded acrolein from the epoxy group, as identified via the large (C=O) band at  $1731\text{ cm}^{-1}$  as well as  $1154\text{ cm}^{-1}$ , and especially the sharp band at  $951\text{ cm}^{-1}$ . The presence of cyclobutylamine was identified by  $1121\text{ cm}^{-1}$  and the broad (N–H) band around  $750\text{ cm}^{-1}$ , while the sharp band at  $744\text{ cm}^{-1}$  corresponded to furan.

At 36.0 min, notable decomposition products include water, methane ( $3016\text{ cm}^{-1}$ ), carbon dioxide, carbon monoxide, and ammonia ( $965$  and  $931\text{ cm}^{-1}$ ). Notably, HCl is not present in the spectrum at 36.0 min. The carbonyl (C=O) band at  $1731\text{ cm}^{-1}$  is predominantly visible, providing evidence for the evolution of aldehydes such as propenal at 2.66 min. The band at  $2960\text{ cm}^{-1}$  signaled the production of ethylbenzene, which correlates with its presence at 6.77 min.

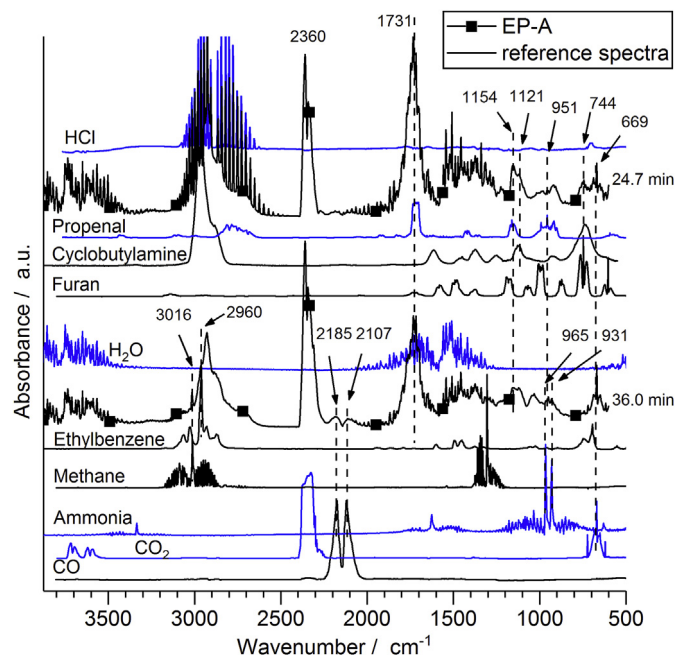


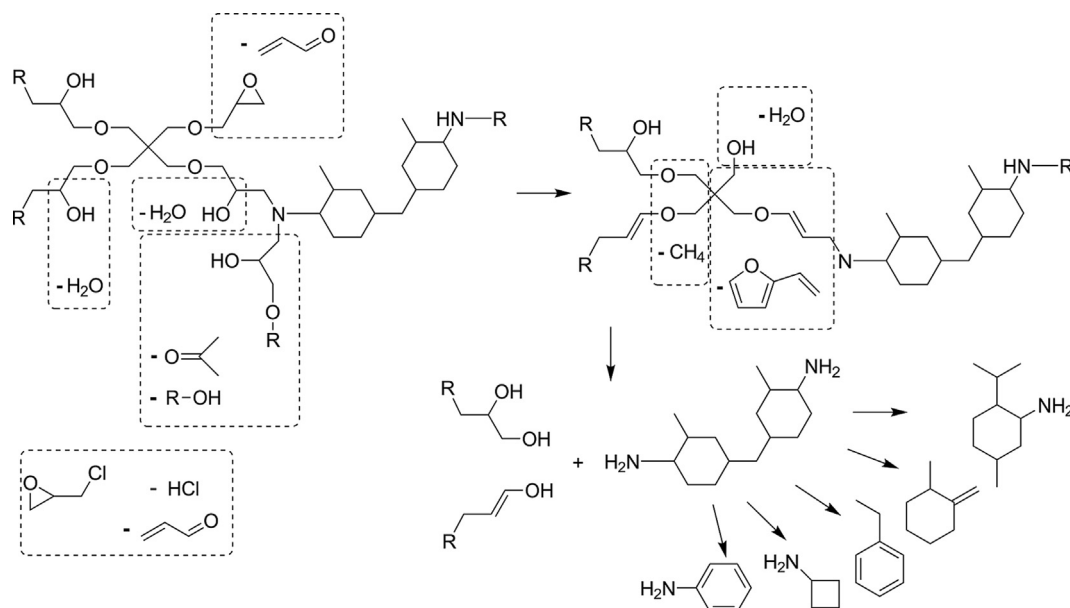
Fig. 3. Evolved gas FTIR spectra of EP-A at the main decomposition steps ( $t = 24.7$  and  $36.0$  min) and comparative spectra (blue lines: main decomposition products).

From the data gathered from Py-GC/MS and TG-FTIR, a decomposition mechanism of EP-A (Scheme 2) is proposed. The two decomposition steps (see Fig. 1a) correspond to specific mechanisms: Above  $280\text{ }^{\circ}\text{C}$ , unreacted epoxide moieties decomposed to form acrolein, and (unreacted) amine components produced cyclobutylamine, aniline, etc. Unreacted epichlorohydrin provided the hydrochloric acid seen in Fig. 3 at 24.7 min. Water and ketones were released from secondary hydroxyls. Additionally, some rearrangements and dehydration of the cyclic hydrocarbons from the amine component formed aromatic moieties. These decomposed at higher temperatures, along with more densely cross-linked moieties, resulting in the second decomposition step which peaked at  $398\text{ }^{\circ}\text{C}$ . Here, the decomposition of aromatic moieties resulted in the production of ethylbenzene, and hydrolysis of amines led to the evolution of ammonia. The decomposition of aromatic structures at this temperature correlated with the decomposition step of EP-B, which is based on the aromatic bisphenol A structure. EP-B displayed a maximum mass loss at  $372\text{ }^{\circ}\text{C}$  and has a shoulder in the same temperature range as EP-A's second mass loss step, indicating that aromatic decomposition occurs in this temperature range.

The characterization of EP-A is crucial to understanding the flame retardancy effects of the FRs, as the interaction between FR and matrix during decomposition determines the efficacy of the FR system.

### 3.3. Material properties of EPs and EP-FRs

One of the principal properties of polymeric materials is the glass-transition temperature ( $T_g$ ). It determines the functional temperature range of the material. In the  $T_g$  plots of the matrices EP-A and EP-B (Fig. 4), there is a noticeable difference of approx.  $50\text{ }^{\circ}\text{C}$  between them: the  $T_g$  of EP-A was  $105\text{ }^{\circ}\text{C}$ , while EP-B's  $T_g$  was  $155\text{ }^{\circ}\text{C}$ . As EP-B contains aromatic rings, its  $T_g$  is inherently higher due to increased stiffness of the polymer chains [25]. The incorporation of a FR additive into a polymer resin has the potential to change the material properties of the matrix. Most additives act as plasticizers and reduce  $T_g$  of the material due to a reduction in the cross-linking density [26], and this phenomenon was observable in the  $T_g$ s of EP-A and EP-B with FRs. More specifically, the low molar mass FRs mE and mA decreased  $T_g$  more strongly than the polymeric hbFRs. The relatively low impact of the hbFRs on  $T_g$  has been previously studied and is linked to the higher molar mass compared to mFRs [6]. Notably, the addition of BDP decreased  $T_g$  between  $19$  and  $22\text{ }^{\circ}\text{C}$ , which is in the same range as the hbE, but not hbA, as its presence increased the  $T_g$  of EP-A. This behavior highlights the versatility of hbFRs in different epoxy resin matrices, especially given that hbFRs are aliphatic and BDP is aromatic. mE lowered  $T_g$  of the matrices by  $30\text{--}42\text{ }^{\circ}\text{C}$ , while hbE only lowered  $T_g$  by  $14\text{--}22\text{ }^{\circ}\text{C}$ . Similarly, mA lowered  $T_g$  by  $24\text{--}36\text{ }^{\circ}\text{C}$ . hbA exhibited very different behavior in EP-A than in EP-B: in the aromatic matrix,  $T_g$  was lowered by  $12\text{ }^{\circ}\text{C}$ , while in the aliphatic matrix,  $T_g$  was increased by  $24\text{ }^{\circ}\text{C}$ . This behavior is explained by the varied reactivity of the epoxy resin matrix: Previous investigations proved that phosphoramides act as additives in EP-B, as  $^{31}\text{P}$  and  $^1\text{H}$  NMR showed no reaction with phenyl glycidyl ether [5]. However, the glycidol groups in EP-A possess a different reactivity. To assess whether phosphoramides compete with the amine component DMC during the curing process, mA was mixed with glycidol and left to react under the same curing conditions, and a  $^1\text{H}$  NMR was measured afterward (Figure S14). The highlighted areas in Figure S14 signify that mA reacted with glycidol, as the mixture of the two at curing conditions contained different signals than the two individual components. From the  $^1\text{H}$  NMR spectra, the signals of the amide protons (highlighted blue,



Scheme 2. Proposed decomposition mechanism of EP-A.

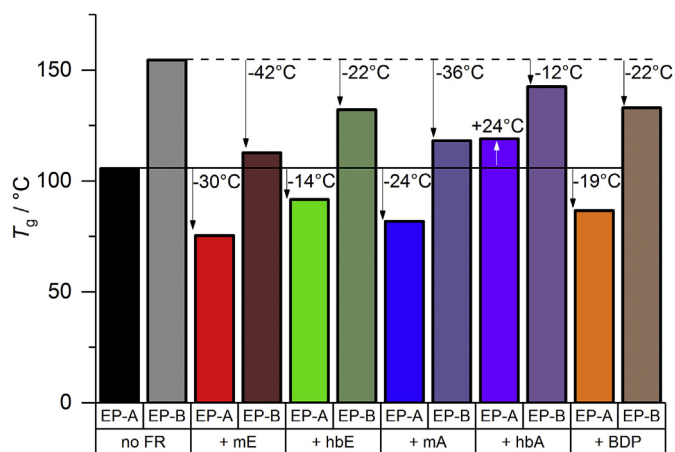


Fig. 4. Glass-transition temperatures ( $T_g$ ) of EP-A and EP-B, and FR composites thereof via DSC measurements. Change in  $T_g$  of the FR-containing composites to the respective epoxy resin is noted.

Figure S14) and the epoxy methylene and methine groups (highlighted gray) disappear. Moreover, Figure S15 ( $^1\text{H}^1\text{H-COSY}$ ) highlights the correlation between the methylene groups obtained from the glycidol and the methylene groups of the hexenyl side-chain, proving the successful reaction of the phosphoramidate with glycidol. This is further supported by Figure S16, which shows a correlation of the two methylene groups with the phosphorus and the disappearance of the amide proton. It follows that phosphoramidates compete with DMC in EP-A, but not in EP-B formulations. Therefore, the increase in  $T_g$  is the result of hbA acting as a reactive FR instead of an additive. The effect is stronger for hbA than for mA due to the presence of many net-points in hbA not present in mA. Thus, the macromolecular structure of hbA helped promote cross-linking in EP-A, yielding a higher  $T_g$ . This toughening effect of the epoxy resin has been previously described [27,28], yet the results herein point to the ability of a single hbFR to act either as an additive or a reactive FR based on the chemical structure of the epoxide-component.

### 3.4. Pyrolysis – Decomposition temperature and mass loss of EP-FRs

The addition of FRs to a polymer matrix typically alters its decomposition behavior. In Fig. 5a, the mass loss and mass loss rate of EP-A is presented along with its FR containing variants, and Fig. 5b shows the same for EP-B. The results of TGA measurements of all FR-containing materials are summarized in Table 4.

During thermal decomposition, specific reactions ultimately control the decomposition mechanism, e.g. hydrolysis, rearrangements, etc. For FR-containing polymers, the decomposition pathway of the matrix is influenced by the decomposing FR: as the matrix and FR decompose, their respective decomposition products react with another, ideally forming thermally stable residues. This interaction between FR and matrix presupposes that the partially decomposed matrix may interact freely with the partially decomposed FR, yet this interaction is greatest if both materials decompose in the same temperature range, i.e. at the same “time”. It follows then that the interaction between matrix and FR is greatest if the overlap of  $T_{\text{dec}}$  is also greatest, as has been previously shown to be the case [10–12].

Resins with the low molar mass FRs mE and mA exhibited low  $T_{5\%}$  due to the additional mass loss steps below 300 °C, a result of the FRs vaporizing in this temperature range. The polymeric FRs hbE and hbA also lowered  $T_{5\%}$  in both EP-A and EP-B, but the effect was less pronounced and is supposed to be related to a decrease in cross-linking density leading to a decreased thermal stability [26]. Those resins containing BDP exhibited the weakest impact on  $T_{5\%}$  due to BDP's high thermal stability ( $T_{\text{max}} = 415$  °C).

In the range of the second decomposition step ( $T_{\text{max}2}$ ), the changes of the corresponding mass loss ( $\text{ML}_{\text{max}2}$ ) of EP-A with FRs were caused by the reaction of the FRs with the decomposing polymer matrix, either prior to or in this temperature range. Notably,  $T_{\text{dec}}$  of the pure FRs closely match the  $T_{\text{dec}}$  ranges of EP-A: mE ( $T_{\text{max}} = 250$  °C) and hbE ( $T_{\text{max}} = 280$  °C) decompose close to  $T_{\text{max}1}$  of EP-A at 286 °C, while mA ( $T_{\text{max}} = 317$  °C) decomposes between the two maxima, and hbA ( $T_{\text{max}} = 361$  °C) decomposes close to  $T_{\text{max}2}$  at 398 °C. For EP-B, the main decomposition step at  $T_{\text{max}1} = 372$  °C is more closely aligned to mA and hbA, than mE or



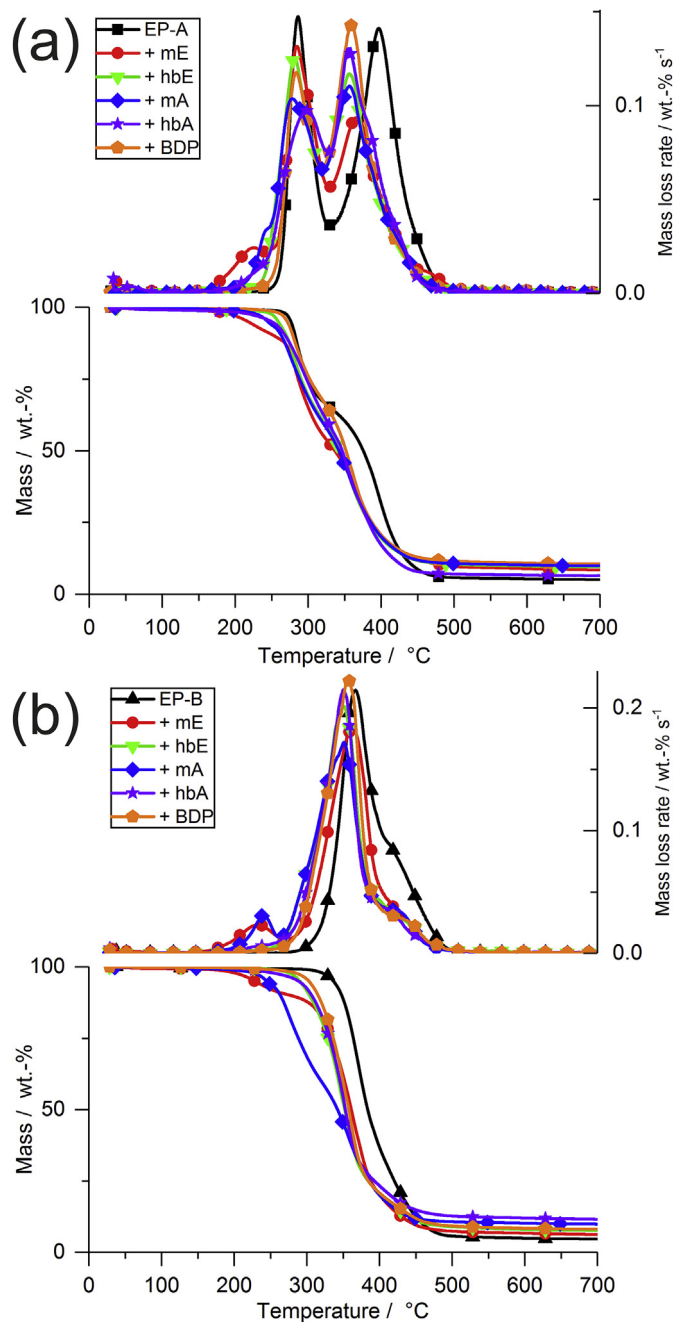


**Fig. 5.** (a) Mass loss (bottom) and mass loss rate (top) of EP-A and FR-containing resins, and (b) mass loss (bottom) and mass loss rate (top) of EP-B and FR-containing resins.

hbE; as a result, the increase in residue yields reflect this behavior. As previously described, the first decomposition step is tied to dehydration and cyclisation, while the second decomposition step is related to the breakdown of aromatic moieties. Those FRs that decompose closely to  $T_{\max 1}$  may phosphorylate the matrix, which ultimately leads to cross-linking at higher temperatures. Moreover, the change in  $T_{\max 2}$  as well as the reduction in mass loss results from the interaction of P-species with aromatic components forming polyaromatic residue. This correlates well with the increase in residue at 700 °C for all FRs. Therefore, the increased overlap between FR and matrix  $T_{\text{dec}}$ -ranges led to improved chemical interaction, resulting in higher residue yields.

Calculated residue yields were obtained by adding the residue of each individual component at their respective content, simulating a decomposition of the products without interaction. The measured residue yields are significantly higher than the calculated values, meaning that chemical interaction between the components during pyrolysis must cause this increase. All FRs increased residue yields of EP-A at 700 °C: mE and mA increased residue yields by a factor of 1.8 and 2.0, respectively, while hbE and hbA increased residues by a factor of 2.0 and 1.6, respectively. BDP increased residues by a factor of 2.1. For EP-B, mE and mA increased residues by a factor of 1.1 and 1.7, respectively, while hbE and hbA increased residues by a factor of 1.7 and 1.8, respectively. BDP had the greatest impact on EP-B, increasing residues by a factor of 1.8.

### 3.5. Pyrolysis – Evolved gas analysis of EP-FRs

The evolved gases from TGA measurements were analyzed via FTIR, and the spectra of EP-A at  $T_{\max 1}$  and  $T_{\max 2}$  are displayed in Fig. 6a and c, respectively; these spectra are rescaled to highlight the fingerprint region in Fig. 6b and d, respectively. Fig. 7a shows the spectra of EP-B with FRs at  $T_{5\%}$ , while the spectra at  $T_{\max}$  are compiled in Fig. 7b, and a rescaled version is plotted in Fig. 7c.

The spectra of EP-A with FRs in Fig. 6a and c demonstrate that all materials produce many of the same gases during decomposition, namely water, carbon dioxide, and carbon monoxide, as well as hydrochloric acid at  $T_{\max 1}$  (Fig. 6a) and methane at  $T_{\max 2}$  (Fig. 6c). More closely, the evolution of P-containing species was identified via the band near 1030  $\text{cm}^{-1}$  in Fig. 6b and d for EP-A/mE, as indicated by the comparative spectra of pure mE. Moreover, while the evolution of ammonia was prevalent in all spectra at  $T_{\max 2}$  (Fig. 6c and d), as indicated by the two bands at 960 and 930  $\text{cm}^{-1}$ .

The spectra in Fig. 7a correspond to evolved gases at  $T_{5\%}$  from resins with mE, hbE, mA, and hbA, respectively. For EP-B/mE and EP-B/mA, TGA measurements indicated a mass loss of approx. 10 wt.-% at about 240 °C, prior to the main decomposition step. Although such a mass loss step was missing for the resins with hbE and hbA, similar products to those from EP-B with mFRs were identified in the spectra at  $T_{5\%}$ . The reason lies in the production of hex-5-ene-1-ol for the phosphate-containing mE and hbE, or hex-5-ene-1-amine for the phosphoramidate-containing mA and hbA. These products may result from hydrolysis of P–O or P–N, respectively, as has been previously described [5], and the process may provide further P-species than can interact with the decomposing matrix. Fig. 7b illustrates that all materials exhibited mostly identical decomposition products at  $T_{\max}$  for EP-B, predominantly bisphenol A, as well as carbon monoxide and water, as previously described [5,6]. An additional absorption band appeared in the spectra of EP-B/mE, which was highlighted in Fig. 7c: the band at 1030  $\text{cm}^{-1}$  was among the main signals in the TG-FTIR spectrum of pure mE at its  $T_{\max}$ . The appearance of this band corresponds to a P-based signal, as many P-signals overlap in this region, e.g.  $\nu_{\text{as}}$  (P–O–C) or  $\nu_{\text{s}}$  (P–OH).

### 3.6. Pyrolysis – Condensed phase activity of EP-FRs via TG-FTIR

During thermal decomposition, the condensed phase interaction of FR and matrix may lead to the formation of polyaromatic compounds, and P-species play a significant role as networking points. Condensed phase FTIR spectra via hot-stage FTIR provide insight into the change in chemical surrounding during pyrolysis of the materials, and offer clues to the interaction of the matrix and FR.

The FRs investigated herein have been previously shown to act in the condensed phase with EP-B, either through phosphorylation of the matrix, the formation of polyphosphates as inorganic glasses,

**Table 4**  
Results from TGA measurements of the epoxy matrices EP-A and EP-B and the FR-containing resins.

Material	$T_{5\%}$ /°C	$T_1$ /°C	$ML_1$ /wt.-%	$T_{max1}$ /°C	$ML_{max1}$ /wt.-%	$T_{max2}$ /°C	$ML_{max2}$ /wt.-%	$\mu$ (700 °C) /wt.-%	$\mu$ (calc) /wt.-%
EP-A	276 ± 2	—	—	286 ± 2	34.8 ± 0.3	398 ± 1	58.8 ± 1.2	4.6 ± 0.3	—
+ mE	218 ± 1	226 ± 1	13.0 ± 0.1	285 ± 1	33.4 ± 0.5	368 ± 3	45.5 ± 1.2	8.2 ± 0.7	4.4
+ hbE	257 ± 2	—	—	280 ± 1	37.8 ± 0.1	356 ± 1	52.4 ± 0.4	9.3 ± 0.2	5.3
+ mA	244 ± 1	241 ± 1	6.8 ± 0.2	281 ± 1	32.6 ± 0.1	357 ± 1	50.9 ± 0.1	9.2 ± 0.3	5.7
+ hbA	253 ± 1	—	—	299 ± 1	39.2 ± 0.2	356 ± 1	51.9 ± 0.1	7.5 ± 0.1	5.9
+ BDP	271 ± 1	—	—	282 ± 1	31.8 ± 0.5	358 ± 1	57.8 ± 0.6	9.8 ± 0.3	4.2
EP-B	338 ± 1	—	—	372 ± 1	62.0 ± 0.8	424 ± 5	33.2 ± 0.3	4.5 ± 0.1	—
+ mE	231 ± 1	233 ± 1	8.9 ± 0.1	337 ± 1	77.8 ± 0.1	422 ± 1	7.4 ± 0.2	5.1 ± 0.6	4.3
+ hbE	289 ± 1	—	—	351 ± 1	54.6 ± 0.1	424 ± 6	23.2 ± 0.7	7.7 ± 0.1	5.2
+ mA	245 ± 2	243 ± 1	7.1 ± 0.4	352 ± 1	74.1 ± 0.3	415 ± 1	10.7 ± 0.1	7.6 ± 0.2	5.6
+ hbA	283 ± 1	—	—	351 ± 1	74.7 ± 0.3	421 ± 1	12.9 ± 0.2	8.0 ± 0.2	5.8
+ BDP	304 ± 1	—	—	357 ± 1	74.6 ± 0.2	423 ± 1	16.1 ± 0.3	8.2 ± 0.1	4.2

$\mu$  = residue.

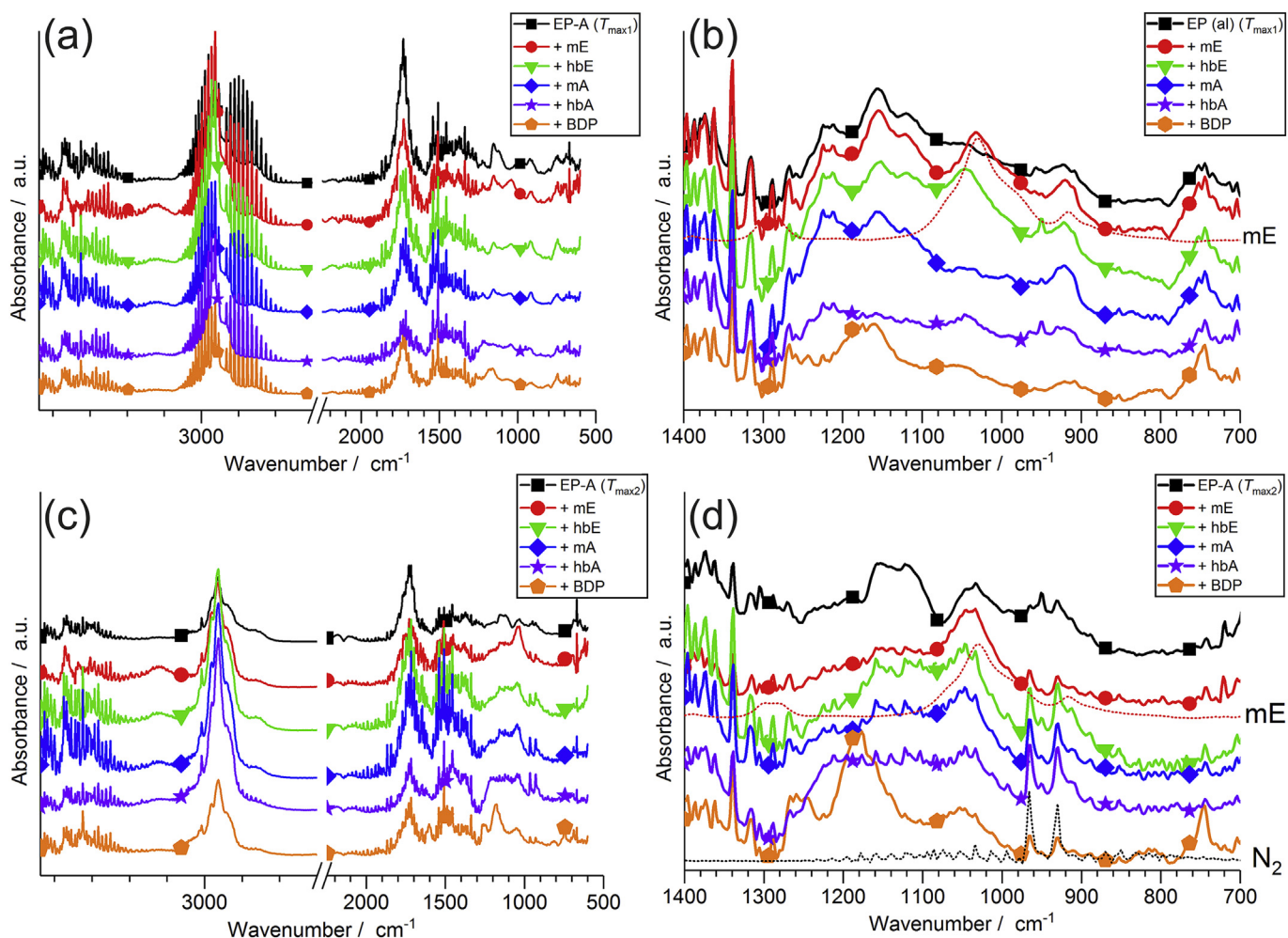


**Fig. 6.** Evolved gas spectra of pyrolysis products of EP-A at specific decomposition temperatures via TG-FTIR. (a) Spectra at  $T_{max1}$ , and (b) rescaled spectra between 1400 and 700  $\text{cm}^{-1}$ . (c) Spectra at  $T_{max2}$ , and (d) rescaled spectra between 1400 and 700  $\text{cm}^{-1}$ .

or as (poly)phosphazenes, phosphorus oxynitrides, etc. [29–31] Therefore, the effect of FRs on EP-B in the condensed phase are not discussed further.

Fig. 8 displays the condensed phase FTIR spectra of EP-A with FRs at key temperatures corresponding to various stages of decomposition: before the first decomposition step (100 °C; top), between two decomposition steps (325 °C; 2nd from top), end of the second decomposition step (500 °C, 2nd from bottom), and

final residues at the end of the experiment (600 °C; bottom).

For the pure resin EP-A, the first decomposition step entailed the decrease of water signals above 3200  $\text{cm}^{-1}$  (ether or secondary alcohol bonds) and decreased absorption of characteristic fingerprint signals near 1100 and 750  $\text{cm}^{-1}$  (either saturated hydrocarbons or possibly C–Cl bonds from epichlorohydrin). At 325 °C, the increased absorption around 1750–1650  $\text{cm}^{-1}$  pointed to dehydration of saturated hydrocarbons, as this region is common for

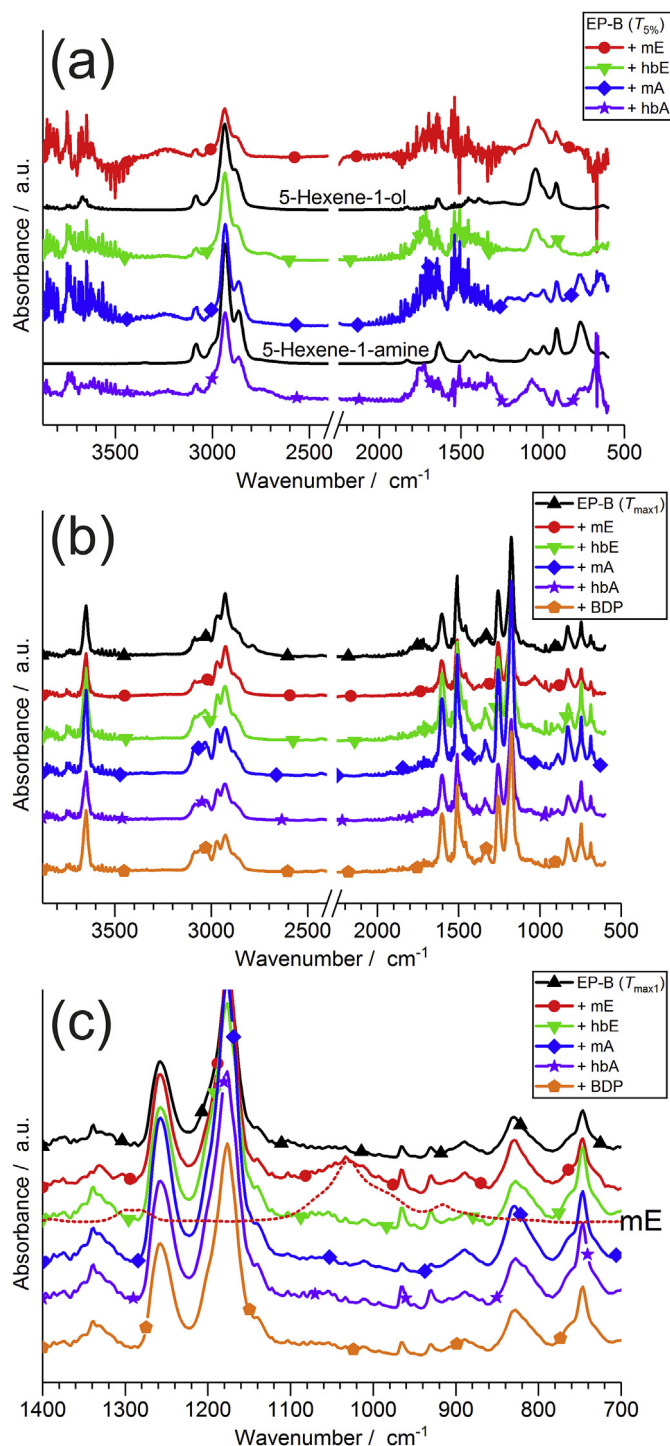


**Fig. 7.** Evolved gas spectra of pyrolysis products of EP-B at specific decomposition temperatures via TG-FTIR. (a) Spectra at  $T_{5\%}$ ; (b) Spectra at  $T_{\text{max}}$ , and (c) rescaled spectra between 1400 and 700  $\text{cm}^{-1}$ .

stretching vibrations of (C=C) bonds. Additionally, amides, ketones, aldehydes, and esters show characteristic signals in this region, therefore implying hydrolysis of ether bonds. The decrease of the ether absorption band at 1100  $\text{cm}^{-1}$  provides further evidence of this process, further supporting the proposed mechanism in Scheme 2. The disappearance of the signal at 750  $\text{cm}^{-1}$  (possibly epichlorohydrin) may explain the appearance of hydrochloric acid in the FTIR spectra of this decomposition step (see Fig. 6a). The

comparison of the spectra before and after the second decomposition step of EP-A (325 °C and 500 °C) revealed that the ether bands at 1100  $\text{cm}^{-1}$  disappeared in the pure EP-A spectrum, and the broad absorption around 1750–1650  $\text{cm}^{-1}$  reduced to only containing a signal at 1600  $\text{cm}^{-1}$ , which corresponds to secondary amides, or phenol-based signals. The broad absorption band >3000  $\text{cm}^{-1}$  at 500 °C pointed to the formation of unsaturated hydrocarbons, but it is also a common range for (N–H) hydrogen bonding. At 600 °C, the main signals from hydrocarbons at around 3000  $\text{cm}^{-1}$  disappeared and only the signal at 1600  $\text{cm}^{-1}$  remained prominent.

With the addition of FRs, the condensed phase spectra of EP-A were altered: At 100 °C, the spectra of EP-A/mE and EP-A/mA exhibited sharp bands at 3075, 1640, and 911  $\text{cm}^{-1}$ , which correspond to signals present in 1,5-hexadiene. Moreover, those resins with phosphate-containing FRs mE and hbE displayed a band at 1259  $\text{cm}^{-1}$  that was also present in the ATR spectrum of pure mE, belonging to the stretching vibration of phosphate (P=O) [8,32]. The spectra of EP-A with BDP at 100 °C further contained characteristic bands pertaining to pure BDP, namely at 1588, 1489, 1194, 1163, 957, 836, and 688  $\text{cm}^{-1}$ .

When comparing the spectra at 100 °C to that of 325 °C, the bands at 3075, 1640, and 911  $\text{cm}^{-1}$  from 1,5-hexadiene disappeared for both EP-A/mE and EP-A/mA, which correlated with the decomposition mechanisms described previously. The signals from BDP persisted, as this material only decomposed at higher temperatures (compare Fig. 1b), as visible in the spectra at 500 °C.

At 500 °C, several specific bands appeared in all spectra of EP-A with FRs, namely 1284  $\text{cm}^{-1}$  [ $\nu(\text{P}=\text{O})$ ], 1157  $\text{cm}^{-1}$  [ $\text{R}_2(\text{P}=\text{O})\text{OH}$  or  $\text{P}-\text{O}-\text{C}_{\text{aryl}}$ ], 1082  $\text{cm}^{-1}$  [ $\nu(\text{P}-\text{Ph})$  or  $\text{P}-\text{O}-\text{C}_{\text{alkyl}}$ ], 1020  $\text{cm}^{-1}$  [ $\nu(\text{P}-\text{OH})=\text{O}$ , or  $\text{PO}_4^-$ ], 880  $\text{cm}^{-1}$  [ $\text{P}-\text{O}-\text{P}$  or  $\delta_{\text{wag}}(\text{P}-\text{H})$ ], and 524  $\text{cm}^{-1}$  [ $\nu_{\text{skel}}(\text{C}-\text{C})$ ] [8,32]. These signals gained in intensity and sharpness at 600 °C, and the signal at 1284  $\text{cm}^{-1}$  split in two: 1293  $\text{cm}^{-1}$  [ $\nu(\text{P}=\text{O})$ ] and 1276  $\text{cm}^{-1}$  [ $\nu_{\text{sym}}(\text{P}-\text{CH}_3)$ ]. Additionally, new signals at 688, 605, 560, and 495  $\text{cm}^{-1}$ , belonging to phenols and P-species, appeared. These bands, which are also present in residues of these FRs in EP-B [5,6], points towards the chemical integration of P-species into the residue, and this condensed phase mechanism was responsible for the residue increase in TGA and PCFC measurements. For EP-A/mA and EP-A/hbA, the band at 1339  $\text{cm}^{-1}$  corresponded to  $\nu(\text{P}=\text{N}-\text{Ar})$  [33] or  $\text{P}=\text{N}-\text{P}$  compounds as their vibration occurs in this wavenumber range [34]; their appearance pointed to the presence of phosphazenes.

### 3.7. Fire testing of EP-FRs via cone calorimeter

An effective method to ascertain the flame-retardancy potential is by comparing the forced-flaming combustion of pure and FR-containing polymer matrices by cone calorimeter. The method yields crucial information on heat release rate (HRR), peak of HRR (PHRR), fire load (= total heat release, THE), mass loss, and heat release per mass loss (= effective heat of combustion, EHC). The results of cone calorimeter measurements of EP-A (Fig. 9a) and EP-B (Fig. 9b), with and without FRs, help illustrate the FR effect on the two distinct matrices. Table 5 summarizes the main results for EP-A and EP-B.

In Fig. 9a, the addition of FRs altered the shape of the HRR curve, most notably for EP-A/hbA. All FRs increased PHRR of EP-A (1881  $\text{kW m}^{-2}$ ) apart from hbE (reduction of 11%). hbA had the largest impact on PHRR (3172  $\text{kW m}^{-2}$ ), increasing it by a factor of 1.7. As changes in the PHRR correlate strongly with the protection layer effect [8,35], the addition of hbA led to a decreased protection layer, thus increasing the flux of fuel into the fire. This was made evident by THR at flame-out (= THE): hbA in EP-A increased THE by 10%, while the other FRs decreased THE by 12% on average. The



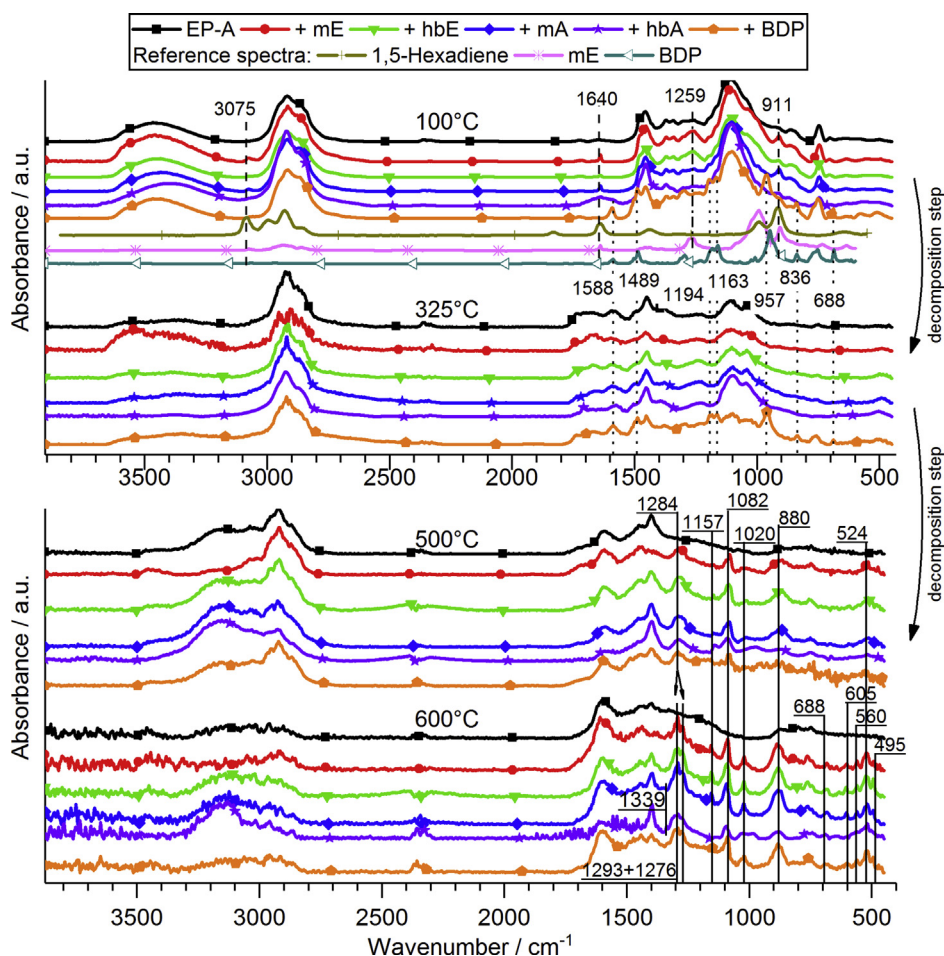


**Fig. 8.** Condensed phase FTIR spectra taken at specific temperatures via hot-stage FTIR. Vertical dashed line: bands from 1,5-hexadiene; vertical dash-dotted line: signal from pure mE (comparative); vertical dotted line: bands from BDP; full lines: phosphorus signals.

addition of FRs into EP-A increased residue yields up to 6.3 wt.-% for mA and 5.5 wt.-% for hbA, while the phosphate FRs mE and hbE only increased char yield to 3.6 and 3.5 wt.-%, respectively. Notably, there is a slightly higher P-content in the resins with mE and mA compared to hbE and hbA, yet both phosphates in EP-A produce similar residue yields, and mA's increase in residue compared to hbA in EP-A cannot only be explained by the different P-contents. While residue yields give insight into the mass converted into fuel during combustion, the relationship between fire load per mass loss, i.e. EHC, provides better insight into the FR-effect. EP-A had an EHC of  $22.0 \text{ MJ kg}^{-1}$  and the addition of most FRs reduced this value by about 10%, from  $19.2 \text{ MJ kg}^{-1}$  for BDP up to  $21.2 \text{ MJ kg}^{-1}$  for mA. However, hbA increased EHC of EP-A to  $25.3 \text{ MJ kg}^{-1}$ , an increase of 15%. Moreover, the reduction of EHC is strong evidence for the gas-phase activity of P-FRs [8]. Therefore, mE and hbE are more effective FRs in EP-A than mA and hbA: they lowered fire load, showed some protective layer effects, increased residue yield, and lowered EHC by exhibiting an effective gas-phase mode of action. The phosphoramidate-containing FRs proved less effective in EP-A, as both mA and hbA increased PHRR and had little influence on EHC. When taking the heat of combustion of the volatiles into account (cf. Figure S17, Table S1), the poor flame retardancy of EP-A/hbA is attributed to the strong contribution of the FR to the heat, as well as the lack of protective layer effects. The latter were caused by a low interaction between matrix and FR, resulting from the FR interacting with itself rather than with the matrix during

decomposition, similarly to phosphorus-FRs in PC/ABS blends [36].

Fig. 9b exhibits HRR and THR curves over time from EP-B as a pure resin and with FR additives. The results highlight the change in interaction between FR and polymer matrix: For EP-B, all FRs lowered fire loads and increased char yields. The phosphate-containing FRs mE, hbE, and BDP lowered THE and PHRR more strongly than the amide-containing FRs mA and hbA. Phosphates incurred higher mass loss, but lower EHCs. Phosphoramidate-containing FRs in EP-B led to significantly higher residue yields compared to the pure resin, but both mA and hbA had subdued effects on PHRR and EHC: hbA exhibited lower PHRR but higher EHC, and mA showed the opposite effect. However, the relative changes in PHRR and EHC of phosphoramidate-containing FRs were much lower in EP-B than in EP-A: hbA decreased PHRR in EP-B (although it increased it in EP-A) and the increase in EHC was only 5% (versus 15% in EP-A).

For both matrices, the benchmark material BDP effectively lowered THE of the matrices EP-A and EP-B. BDP exhibited predominantly a gas phase mechanism and a minor condensed phase mechanism, as evidenced by the reduction in EHC and small increase in residue, respectively.

The residues after fire testing (Figure S18) further illustrated the efficacy of phosphates in EP-A and EP-B to produce voluminous, multicellular residues with more effective protection layer effects than phosphoramidates, which created a dense, brittle char. The difference in char formation was further illustrated in reaction to

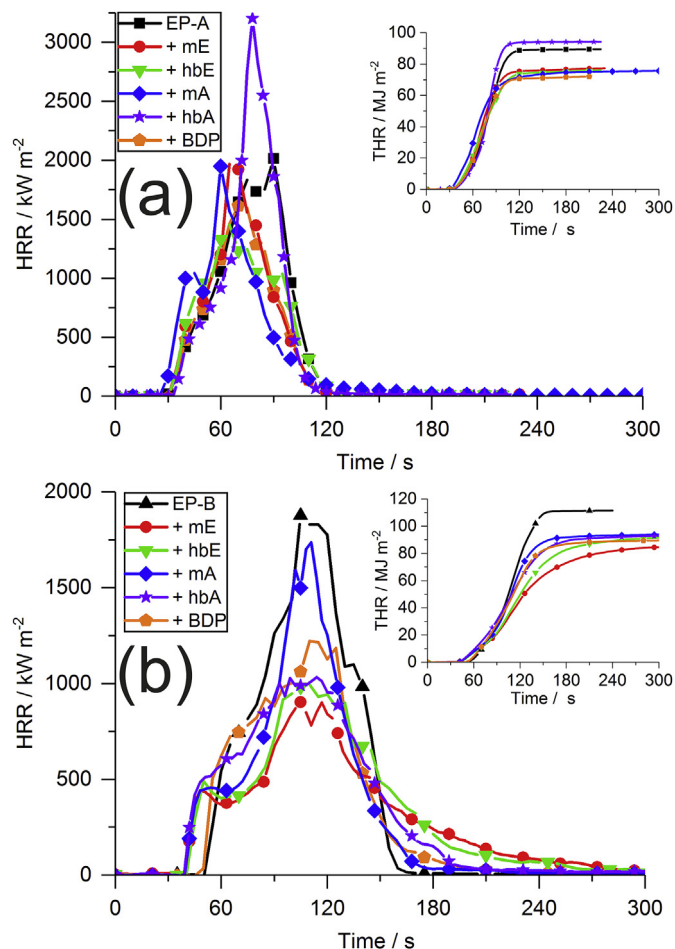


**Fig. 9.** Heat release rate (HRR) and total heat release (THR) over time of (a) EP-A and FR-containing composites, and (b) EP-B and FR-containing composites, respectively, from cone calorimeter measurements.

**Table 5**  
Results of cone calorimeter measurements at a heat flux of  $50 \text{ kW m}^{-2}$ .

	THE / $\text{MJ m}^{-2}$	PHRR / $\text{kW m}^{-2}$	Residue / wt.-%	EHC / $\text{MJ kg}^{-1}$
EP-A	$86.5 \pm 2.1$	$1881 \pm 133$	$1.7 \pm 0.1$	$22.0 \pm 0.6$
+ mE	$74.4 \pm 1.4$	$1933 \pm 35$	$3.6 \pm 0.1$	$19.4 \pm 0.4$
+ hbE	$76.7 \pm 2.5$	$1672 \pm 220$	$3.5 \pm 0.1$	$20.0 \pm 0.7$
+ mA	$79.0 \pm 2.6$	$2287 \pm 337$	$6.3 \pm 0.7$	$21.2 \pm 1.2$
+ hbA	$96.0 \pm 2.3$	$3172 \pm 29$	$5.5 \pm 1.6$	$25.3 \pm 0.2$
+ BDP	$74.9 \pm 4.4$	$1992 \pm 379$	$2.6 \pm 0.1$	$19.2 \pm 1.1$
EP-B	$108.4 \pm 2.6$	$1696 \pm 180$	$0.7 \pm 0.1$	$26.9 \pm 1.0$
+ mE	$78.1 \pm 6.5$	$885 \pm 16$	$9.2 \pm 0.1$	$21.6 \pm 1.8$
+ hbE	$89.8 \pm 3.0$	$953 \pm 41$	$7.5 \pm 0.6$	$24.3 \pm 0.6$
+ mA	$91.6 \pm 1.2$	$1833 \pm 96$	$8.4 \pm 0.2$	$25.3 \pm 1.0$
+ hbA	$95.5 \pm 2.3$	$1189 \pm 155$	$12.1 \pm 2.7$	$28.2 \pm 2.4$
+ BDP	$87.5 \pm 1.2$	$1180 \pm 41$	$3.1 \pm 0.2$	$22.7 \pm 0.2$

small flames tests, i.e. limiting oxygen index (LOI) and Underwriter's Laboratory 94 (UL-94) tests (Table S2). All FRs generally increased the oxygen index of EP-A and EP-B, phosphoramidates in EP-A burned with a reduced horizontal burn speed compared to phosphates, as their dense char was more successful at preventing horizontal flame spread. In EP-B, hbFRs lowered burn speeds by forming stable chars, compared to the more voluminous but fragile char that mFRs formed due to their high volatility.

An effective method to visualize flame retardancy is by Petrella plot, which graphs fire load (= THE) over fire growth rate (= PHRR/

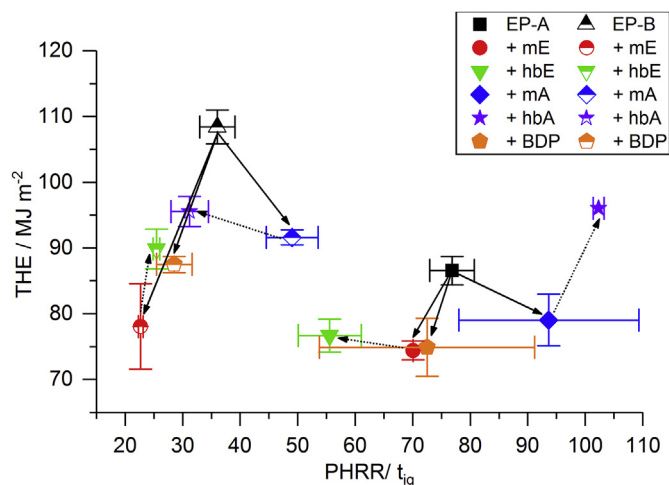


**Fig. 10.** Petrella-plot of EP-A and EP-B with FRs, assessing fire load versus fire growth rate. Solid lines: monomeric/polymeric FR; dashed lines: difference between monomeric and hb polymeric FR.

$t_{ig}$ ) [37]. Ideally, the addition of FRs leads to a reduction of both (i.e. shift to lower left corner of graph). Fig. 10 depicts the Petrella-plot of EP-A and EP-B resin formulations. For EP-A, phosphate-containing FRs improved both fire growth rate and fire load. When comparing mE to hbE, the polymeric FR slightly increased THE but decreased  $\text{PHRR}/t_{ig}$ . For phosphoramidate-containing FRs, mA decreased fire load, but increased the fire growth rate, and hbA increased both. The behavior is different for EP-B: the phosphate-containing FRs improved flame retardancy by the greatest amount, yet both phosphoramidate-containing FRs lowered THE, with hbA lowering both fire load and fire growth rate.

### 3.8. Modes of action and molecular mechanism

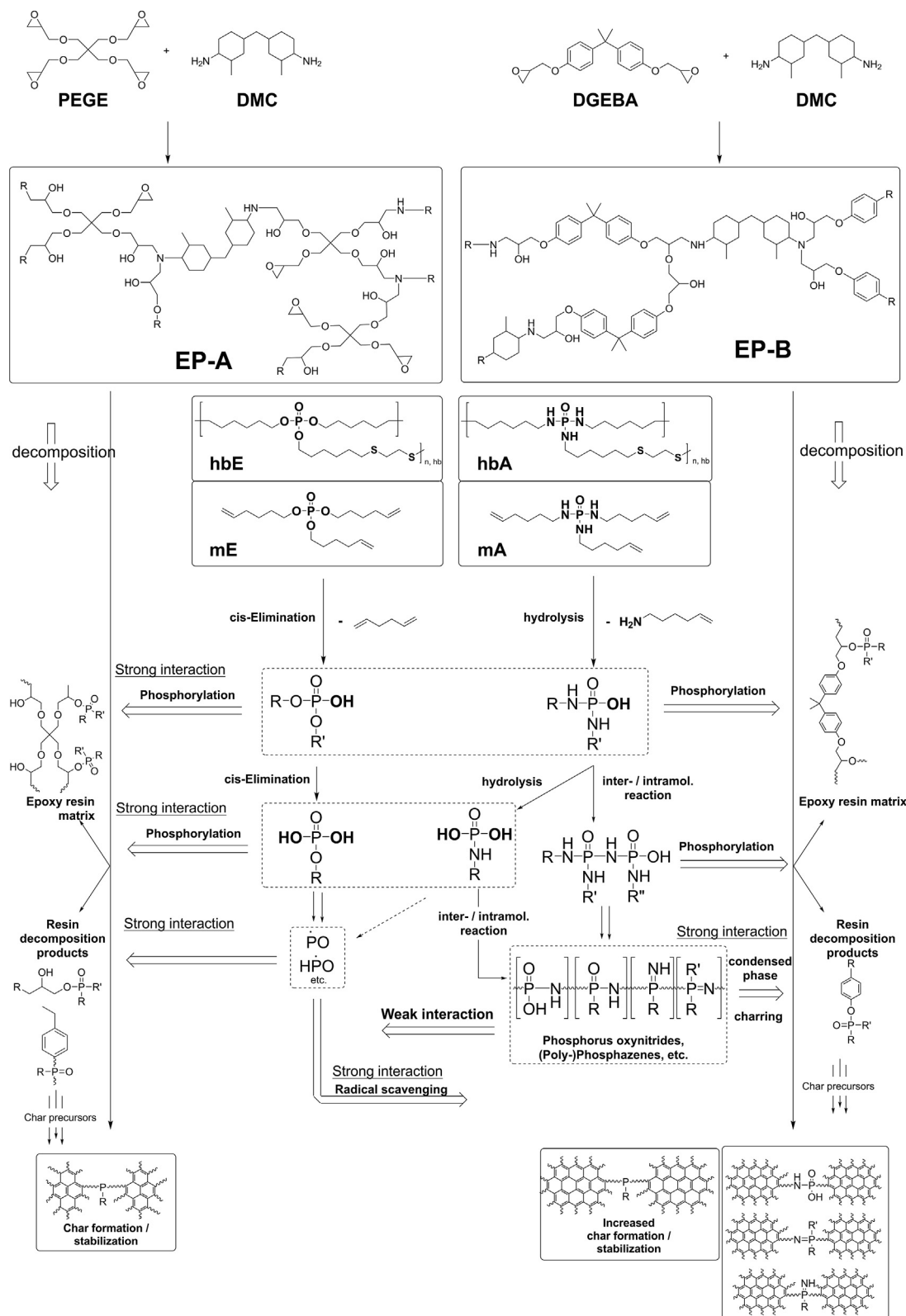
As previously investigated [5,6], the addition of mE, mA, hbE, or hbA to EP-B increased residue yields in both pyrolysis and flaming investigations: the FRs or their decomposition products interact either directly with the matrix or its decomposition products via phosphorylation, thus catalyzing the formation of polyaromatic char and acting as a char stabilizer [9]. Moreover, EP-B contains aromatic rings which can act as char precursors, further enhancing the charring potential in the presence of P-FRs. mA and hbA were shown to be more active in the condensed phase, especially through the formation of (poly-)phosphazenes/phosphorus oxynitrides [5,6]. For mE and hbE, the phosphate-moiety is susceptible to *cis*-elimination [5,38], leading to more active phosphate-species, which acted in the condensed and, via radical scavenging, in the gas phase. As previous investigations showed, phosphates were more likely to undergo *cis*-eliminations, while phosphoramidates were more likely to undergo hydrolysis reactions [5].

EP-A, on the other hand, is aliphatic and contains four epoxide groups per epoxy moiety; bisphenol A in EP-B only contains two. Therefore, the polymer network of EP-A has a different network density, and more importantly, a higher polarity. As investigated, the polymer matrix of EP-A decomposes in two steps under pyrolysis, and some of those steps yield aromatic components via rearrangement or dehydrogenation, which can act as char precursors. Moreover, the incorporation of FRs led to residue yields that were higher than the calculated sum of the individual components, signaling the interaction of matrix and FR. Additionally,  $T_{max}$  of mE and hbE were closer to  $T_{max1}$  of EP-A, while  $T_{max}$  mA and hbA were closer to  $T_{max}$  of EP-B. The chemical interaction was more

pronounced for these specific FRs with a specific matrix, because the  $T_{dec}$ -ranges of matrix and FR more closely matched, meaning that decomposition products of both materials were more likely to react with another.

In flaming conditions, the difference between phosphoramidate-

and phosphate-containing FRs became more apparent in EP-A: The addition of mE and hbE increased residue yields and led to a substantial reduction in EHC (mE: 12%; hbE: 9%) and THE (mE: 14%; hbE: 11%). These results are explained by the effective fuel fixation caused by increased interaction of matrix and FR, as well as the



**Scheme 3.** Proposed main decomposition pathways of epoxy resin matrices with FRs, and interaction between the two.

proven gas-phase activity/ flame poisoning of the phosphate-containing FRs. The addition of mA and hbA to EP-A did not improve the fire performance in the same way that it did for EP-B. The reason for this may be a less pronounced chemical interaction and the resulting change in condensed phase activity. mA and hbA more greatly promoted char formation in EP-B due to the interaction with bisphenol A-derived aromatic char precursors. Lacking those precursors in EP-A, these phosphoramidate-containing FRs formed P–N compounds that, although retaining fuel in the form of residue, did not offer a good protection layer effect. Poor protective layers cause increased mass flux into the flame, resulting in higher PHRR. Furthermore, hbA itself decomposes via hydrolysis and produces hex-5-ene-1-amine [6], which additionally increases the fire load of the sample. Moreover, EP-A is more polar than EP-B, which may further impede the phosphoramidate-containing FRs from interacting with the decomposing matrix.

Scheme 3 illustrates the proposed decomposition mechanism of the FRs and their interaction with the decomposing matrices EP-A or EP-B. While hbFRs have a decomposition pathway distinct from the mFRs, they share general decomposition mechanisms. More importantly, hbFRs contain thiol-ether bonds, which propagate cross-linking reactions. Phosphate-based FRs undergo *cis*-eliminations, while phosphoramidate-based FRs undergo hydrolysis [5]. Both steps lead to a P-hydroxyl-group, which may interact with the epoxy resin matrix or decomposition products thereof via phosphorylation. The higher epoxide-group content in EP-A leads to a higher content of secondary hydroxyl groups; therefore, phosphorylation of EP-A is more likely than in EP-B. As the phosphate-based FRs have a lower  $T_{dec}$ , they are more likely to phosphorylate these hydroxyls before key functional groups of EP-A are lost due to advanced decomposition. Hence, they have a stronger interaction in the condensed phase, which explains the reduction in fire load of EP-A, as increased phosphorylation leads to higher fuel storage. Furthermore, the phosphate-based FRs more readily form P-based radicals, thus acting strongly in the gas phase in both EP-A and EP-B. This radical scavenging mechanism is strong for phosphate-based FRs and explains the strong decrease in EHC of all matrices. The phosphoramidate-based FRs are less likely to interact with the decomposing aliphatic matrix, in part because these FRs may undergo inter-/ intramolecular reactions with themselves, leading to the production of phosphorus oxynitrides or (poly-)phosphazenes, as seen in condensed phase FTIR via the presence of P=N compounds. A similar auto-reaction was shown for aryl phosphates in PC/ABS blends, where an FR was shown to crosslink with itself rather than enhance charring [36]. Phosphoramidate-based FRs proved effective in the condensed phase in EP-B due to interaction with aromatic moieties, especially given that mA and hbA decompose in similar temperature ranges as EP-B. For EP-A, these aromatic moieties form only after rearrangements or dehydrogenation and are not readily available reaction partners; therefore, the interaction between phosphoramidate-based FRs and EP-A is weak in the condensed phase. Lacking reaction partners, phosphorus oxynitrides or (poly-)phosphazenes offer little protective layer effects, and contribute to increasing fire loads; this increased THE in fire tests of mA and hbA in both resins. Although the phosphoramidate-based FRs produced a substantial residue yield, previous investigations have shown that not quantity, but residue morphology and properties thereof are paramount in flame retardancy [8].

#### 4. Conclusion

A systematic library of phosphorus-based FRs (phosphate and phosphoramidate as low and high molar masses) was prepared and investigated in two chemically different epoxy resins, one aliphatic and one aromatic. Investigations of the pyrolytic decomposition via

TGA-FTIR, pyrolysis-GC/MS, hot stage FTIR, and PCFC, as well as fire behavior of the pure matrices provided a background into understanding how the FR-containing composites behaved under pyrolysis and fire testing conditions.

The chemical decomposition mechanisms of the FRs are essential to understand their mode of action. However, also the chemical structure of the polymer matrix strongly influences the possible reactions during fire. The reaction between decomposition products of both matrix and FR are crucial to achieve efficient flame retardancy. Moreover, the importance of  $T_{dec}$  overlap between FR and polymer matrix cannot be understated. When this overlap of FR and matrix is highest, the chemical interaction is greatest, leading to effective flame retardancy in the form of higher char yield, reduced PHRR and lower THE. The presented results provide some crucial tools to potentially optimize matrix-FR-systems:

hbFRs exhibited a slightly less pronounced reactivity but a higher thermal stability than mFRs. This means that  $T_{dec}$  is tunable via molecular weight. Especially for the multifunctional hbFRs, this may prove useful for processing, especially given their decreased impact on  $T_g$ . The overlap in temperature range between FR and matrix can thus be increased if the molar mass of the FR is adjusted.

Phosphoramides typically possess a higher  $T_{dec}$  compared to structurally analogous phosphates, but phosphates exhibit a stronger gas phase mode of action. Crucially, altering the P–O and P–N content results in varying degrees of chemical interaction between matrix and FR. Depending on the properties of the matrix, the FR can be shifted from additive to reactive FR for epoxy resins, thus acting as a toughening agent, further highlighting the chemical versatility of these materials as FRs.

It must be carefully considered how the efficacy or mechanisms of FRs are evaluated, as these may change depending on the polymer's chemical composition. Even within the realm of epoxy resins, alterations to the chemical structure of the material affect flame retardancy. The results of this study help underline that the chemical structure–property relationship of the flame retardant and the matrix matters when investigating the FR-efficacy and mode of action of these synthesized FRs.

#### Acknowledgement

The authors thank the Deutsche Forschungsgemeinschaft (DFG) for funding (DFG SCHA 730/15-1; WU 750/8-1).

Alexander Battig thanks Patrick Klack for his assistance with the cone calorimeter, and Dr. Katharina Kebelmann for her assistance with the Py-GC/MS.

Jens C. Markwart is the recipient of a fellowship through funding of the Excellence Initiative (DFG/GSC 266) in the context of the graduate school of excellence "MAINZ" (Materials Science in Mainz). Jens C. Markwart and Frederik R. Wurm thank Prof. Dr. Katharina Landfester (MPI-P, Germany).

#### Appendix A. Supplementary data

Supplementary data related to this article can be found at <https://doi.org/10.1016/j.polydegradstab.2019.108986>.

#### References

- [1] M.M. Velencoso, A. Battig, J.C. Markwart, B. Scharrel, F.R. Wurm, *Angew. Chem. Int. Ed.* 57 (2018) 10450–10467.
- [2] F. Marsico, M. Wagner, K. Landfester, F.R. Wurm, *Macromolecules* 45 (2012) 8511–8518.
- [3] M. Steinmann, J. Markwart, F.R. Wurm, *Macromolecules* 47 (2014) 8506–8513.
- [4] T. Steinbach, F.R. Wurm, *Angew. Chem. Int. Ed.* 54 (2015) 6098–6108.
- [5] J.C. Markwart, A. Battig, L. Zimmermann, M. Wagner, J. Fischer, B. Scharrel, F.R. Wurm, *ACS Appl. Polym. Mater.* 1 (2019) 1118–1128.



- [6] A. Battig, J. Markwart, F.R. Wurm, B. ScharTEL, *Polym. Chem.* 10 (2019) 4346–4358.
- [7] A.F. Grand, C.A. Wilkie, *Fire Retardancy of Polymeric Materials*, CRC Press, 2000.
- [8] B. ScharTEL, B. Perret, B. Ditttrich, M. Ciesielski, J. Krämer, P. Müller, V. Altstädt, L. Zang, M. Döring, *Macromol. Mater. Eng.* 301 (2016) 9–35.
- [9] U. Braun, A.I. Balabanovich, B. ScharTEL, U. Knoll, J. Artner, M. Ciesielski, M. Döring, R. Perez, J.K.W. Sandler, V. Altstädt, T. Hoffmann, D. Pospiech, *Polymer* 47 (2006) 8495–8508.
- [10] K.H. Pawlowski, B. ScharTEL, *Polym. Int.* 56 (2007) 1404–1414.
- [11] M.C. Despinasse, B. ScharTEL, *Polym. Degrad. Stab.* 97 (2012) 2571–2580.
- [12] B. Perret, K.H. Pawlowski, B. ScharTEL, *J. Therm. Anal. Calorim.* 97 (2009) 949–958.
- [13] A. Toldy, B. Szolnoki, G. Marosi, *Polym. Degrad. Stab.* 96 (2011) 371–376.
- [14] A. Toldy, B. Szolnoki, I. Csontos, G. Marosi, *J. Appl. Polym. Sci.* (2014) 131.
- [15] M. Jimenez, S. Duquesne, S. Bourbigot, *Surf. Coat. Technol.* 201 (2006) 979–987.
- [16] J. Alongi, Z.D. Han, S. Bourbigot, *Prog. Polym. Sci.* 51 (2015) 28–73.
- [17] T. Misaki, T. Hirohata, M. Yoshii, T. Hamasaki, *J. Appl. Polym. Sci.* 37 (1989) 2617–2625.
- [18] M. Fleischer, H. Blattmann, R.J.G.C. Mülhaupt, *Green Chem.* 15 (2013) 934–942.
- [19] B. ScharTEL, T.R. Hull, *Fire Mater.* 31 (2007) 327–354.
- [20] B. ScharTEL, M. Bartholmai, U. Knoll, *Polym. Adv. Technol.* 17 (2006) 772–777.
- [21] J. Artner, M. Ciesielski, O. Walter, M. Döring, R.M. Perez, J.K.W. Sandler, V. Altstädt, B. ScharTEL, *Macromol. Mater. Eng.* 293 (2008) 503–514.
- [22] L.-H. Lee, *J. Polym. Sci. - Part A Gen. Pap.* 3 (1965) 859–882.
- [23] D.P. Bishop, D.A. Smith, *J. Appl. Polym. Sci.* 14 (1970) 205–223.
- [24] A. Toldy, N. Toth, P. Anna, G. Marosi, *Polym. Degrad. Stab.* 91 (2006) 585–592.
- [25] J.M.G. Cowie, V. Arrighi, *Polymers: Chemistry and Physics of Modern Materials*, CRC press, 2007.
- [26] M. Ciesielski, B. Burk, C. Heinzmann, M. Döring, in: D.-Y. Wang (Ed.), *Novel Fire Retardant Polymers and Composite Materials*, Woodhead Publishing, 2017, pp. 3–51, <https://doi.org/10.1016/B978-0-08-100136-3.00002-9>, ch. 2.
- [27] L. Boogh, B. Pettersson, J.A.E. Manson, *Polymer* 40 (1999) 2249–2261.
- [28] R. Mezzenga, L. Boogh, J.A.E. Manson, *Compos. Sci. Technol.* 61 (2001) 787–795.
- [29] S.V. Levchik, in: A.B. Morgan, C.A. Wilkie (Eds.), *Flame Retardant Polymer Nanocomposites*, John Wiley & Sons, Inc., 2006, pp. 1–29, <https://doi.org/10.1002/9780470109038.ch1>.
- [30] E.D. Weil, *Fire Retardancy of Polymeric Materials*, 2000, pp. 115–145.
- [31] S.V. Levchik, G.F. Levchik, A.I. Balabanovich, E.D. Weil, M. Klatt, *Angew Makromol. Chem.* 264 (1999) 48–55.
- [32] M. Hesse, H. Meier, B. Zeeh, *Spektroskopische Methoden in der organischen Chemie*, Georg Thieme Verlag, 2005.
- [33] L.C. Thomas, *Interpretation of the Infrared Spectra of Organophosphorus Compounds*, Heyden London, 1974.
- [34] I.N. Zhmurova, A.A. Kisilenko, A.V. Kirsanov, *J. Gen. Chem. USSR* 32 (1962) 2544. &
- [35] S. Brehme, B. ScharTEL, J. Goebbels, O. Fischer, D. Pospiech, Y. Bykov, M. Döring, *Polym. Degrad. Stab.* 96 (2011) 875–884.
- [36] E. Wawrzyn, B. ScharTEL, M. Ciesielski, B. Kretschmar, U. Braun, M. Döring, *Eur. Polym. J.* 48 (2012) 1561–1574.
- [37] R. Petrella, *J. Fire Sci.* 12 (1994) 14–43.
- [38] S. Gaan, P. Rupper, V. Salimova, M. Heuberger, S. Rabe, F. Vogel, *Polym. Degrad. Stab.* 94 (2009) 1125–1134.

## Matrix Matters: Hyperbranched Flame Retardants in Aliphatic and Aromatic Epoxy Resins

Alexander Battig,<sup>a,1</sup> Jens C. Markwart,<sup>b,1</sup> Frederik R. Wurm,<sup>b,\*\*</sup> and Bernhard Schartel<sup>a,\*</sup>

<sup>a</sup> Bundesanstalt für Materialforschung und -prüfung (BAM), Unter den Eichen 87, 12205 Berlin, Germany.

<sup>b</sup> Max Planck Institute for Polymer Research, Ackermannweg 10, 55128 Mainz, Germany.

<sup>1</sup> these authors contributed equally

\* corresponding author: Bernhard Schartel, Bundesanstalt für Materialforschung und -prüfung (BAM), Unter den Eichen 87, 12205 Berlin, Germany. bernhard.schartel@bam.de;

\*\* corresponding author: Frederik R. Wurm, Max-Planck-Institut für Polymerforschung, Ackermannweg 10, 55128 Mainz, Germany. wurm@mpip-mainz.mpg.de

### Pyrolysis-Gas Chromatography/Mass Spectrometry spectra

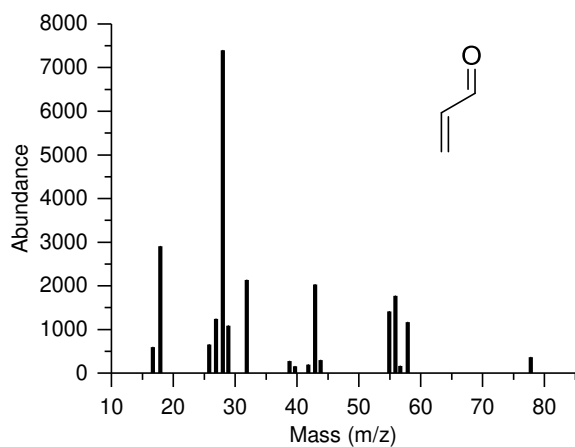


Figure S1. Mass spectrum of pyrolysis products of EP-A at 325 °C at 2.39 min, corresponding to acrolein.

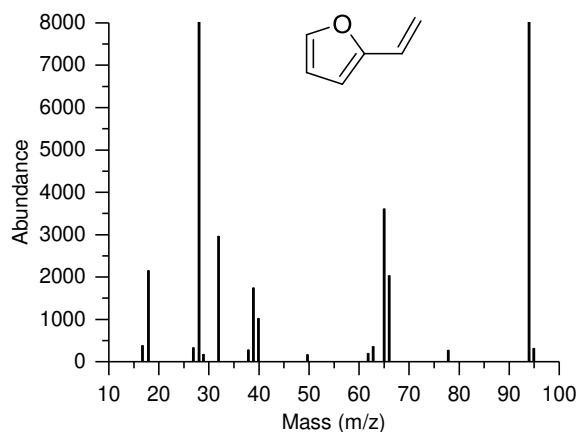


Figure S2. Mass spectrum of pyrolysis products of EP-A at 325 °C at 4.29 min, corresponding to 2-vinylfuran.

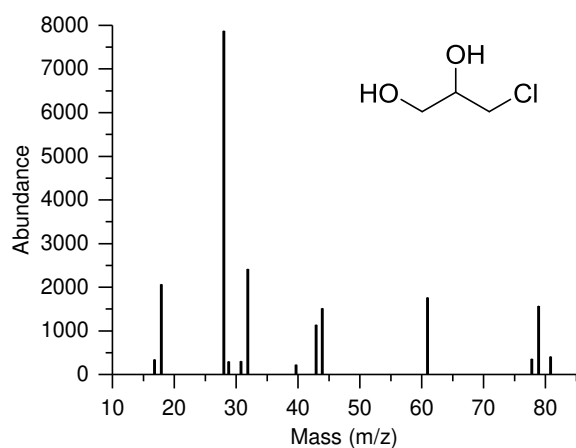


Figure S3. Mass spectrum of pyrolysis products of EP-A at 325 °C at 7.95 min, corresponding to 3-chloro-1,2-propanediol.

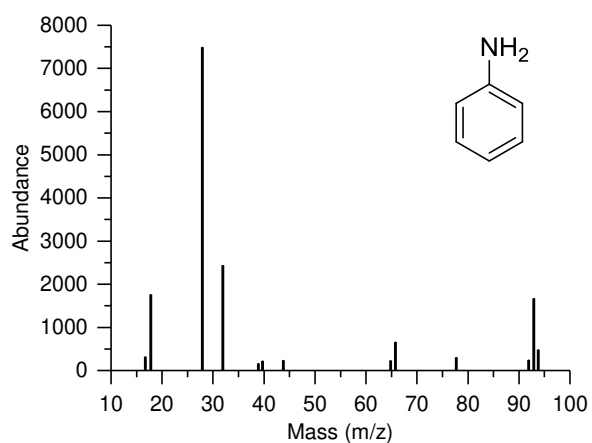


Figure S4. Mass spectrum of pyrolysis products of EP-A at 325 °C at 8.72 min, corresponding to aniline.

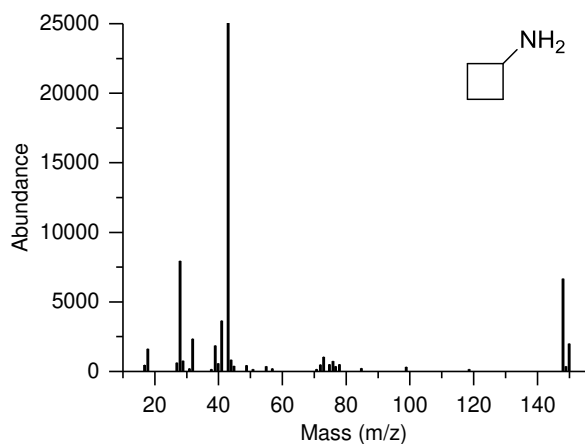


Figure S5. Mass spectrum of pyrolysis products of EP-A at 325 °C at 9.42 min, corresponding to cyclobutylamine.

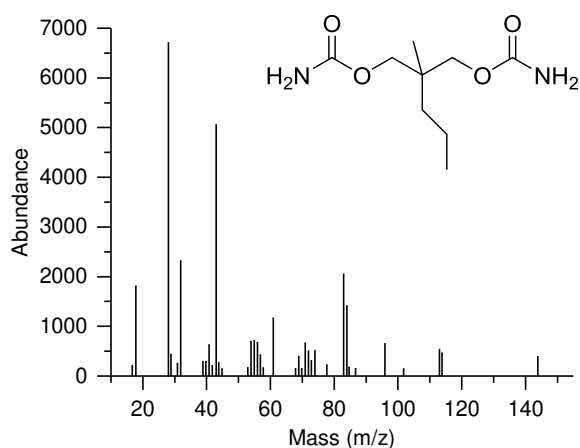


Figure S6. Mass spectrum of pyrolysis products of EP-A at 325 °C at 15.39 min, corresponding to mebroamate.

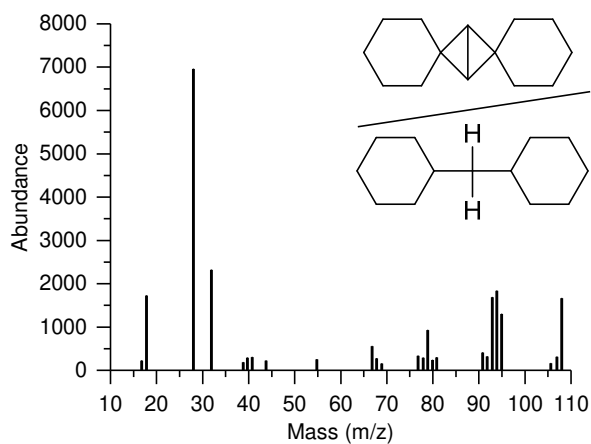


Figure S7. Mass spectrum of pyrolysis products of EP-A at 325 °C at 16.49 min, identified as dispiro[cyclohexane-1,2'-bicyclo(1.1.0)butane-4',1''-cyclohexane], which may correspond to 4,4'-methylene-bis(cyclohexane).

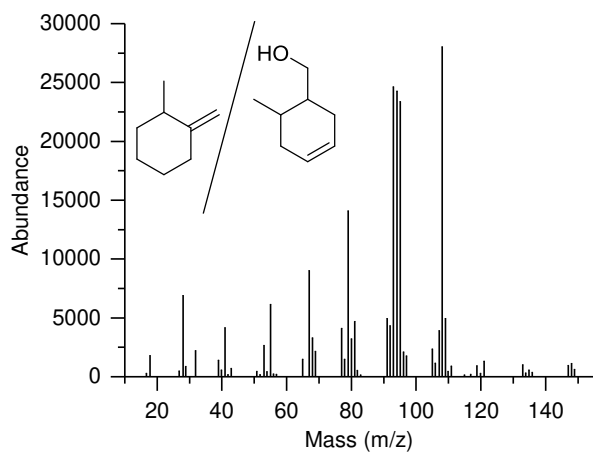


Figure S8. Mass spectrum of pyrolysis products of EP-A at 325 °C at 16.97 min, corresponding to 1-methyl-2-methylenecyclohexane and/or 6-methyl-3-cyclohexane-1-methanol.

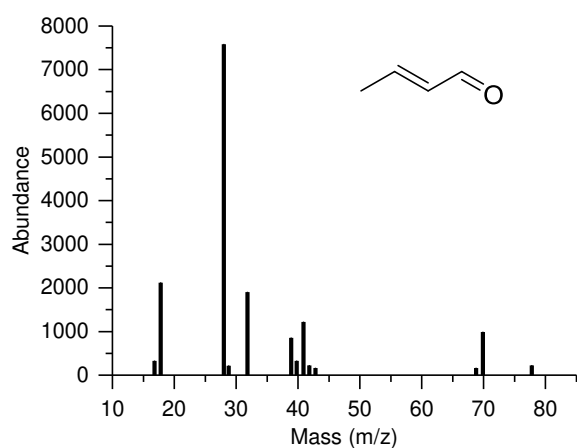


Figure S9. Mass spectrum of pyrolysis products of EP-A at 500 °C at 2.66 min, corresponding to 2-butenal.

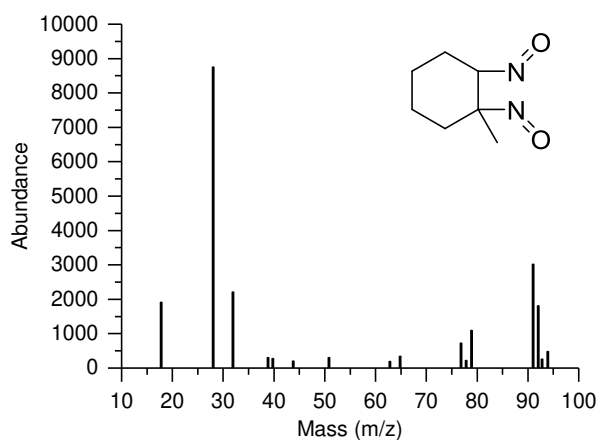


Figure S10. Mass spectrum of pyrolysis products of EP-A at 500 °C at 4.54 min, corresponding to 1,2-dinitroso-2-methyl-cyclohexane.

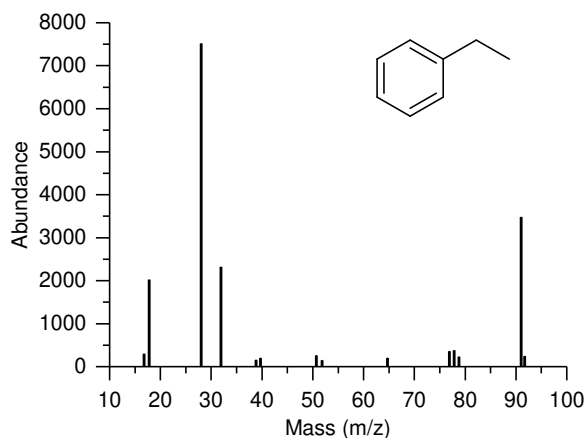


Figure S11. Mass spectrum of pyrolysis products of EP-A at 500 °C at 6.77 min, corresponding to ethylbenzene.

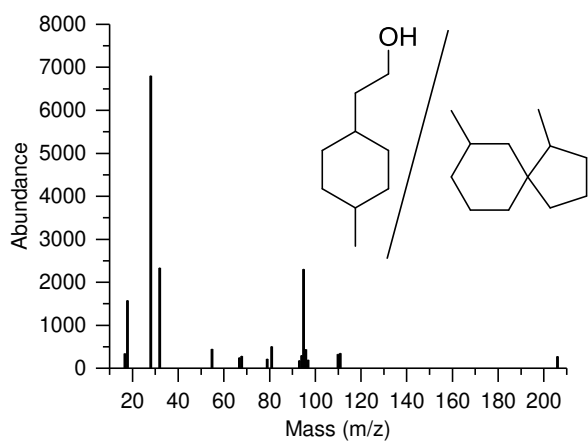


Figure S12. Mass spectrum of pyrolysis products of EP-A at 500 °C at 16.76 min, corresponding to 2-(4-methylcyclohexyl) ethanol, or 1,7-dimethylspiro[4.5]decane.

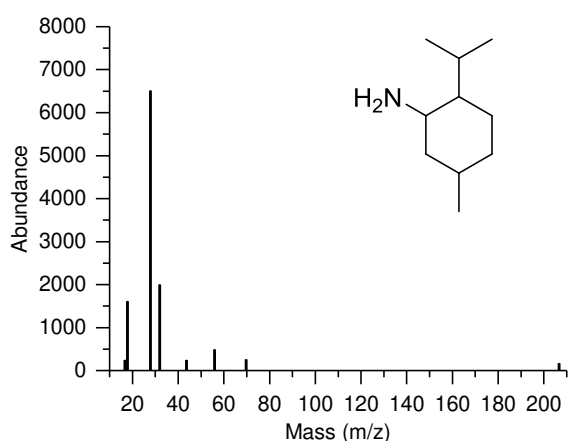


Figure S13. Mass spectrum of pyrolysis products of EP-A at 500 °C at 19.30 min, corresponding to neomenthylamine.

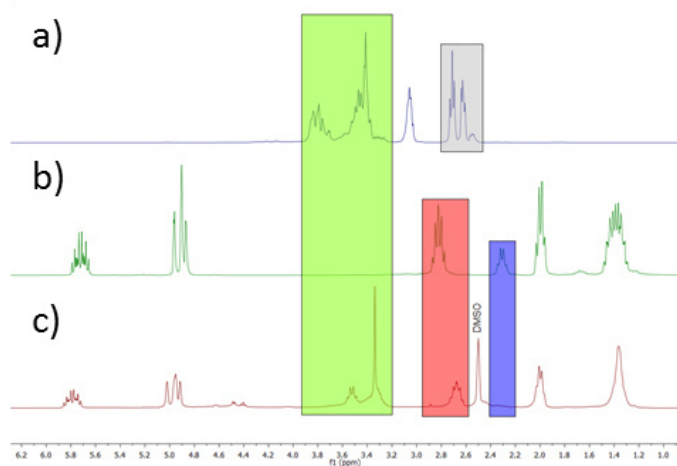


Figure S14. a)  $^1\text{H-NMR}$  (250 MHz in  $\text{CDCl}_3$  at R.T.) of glycidol; b)  $^1\text{H-NMR}$  (300 MHz in  $\text{CDCl}_3$  at R.T.) of mA; c)  $^1\text{H-NMR}$  (300 MHz in  $d\text{-DMSO}$  at R.T.) of mA reacted with glycidol.

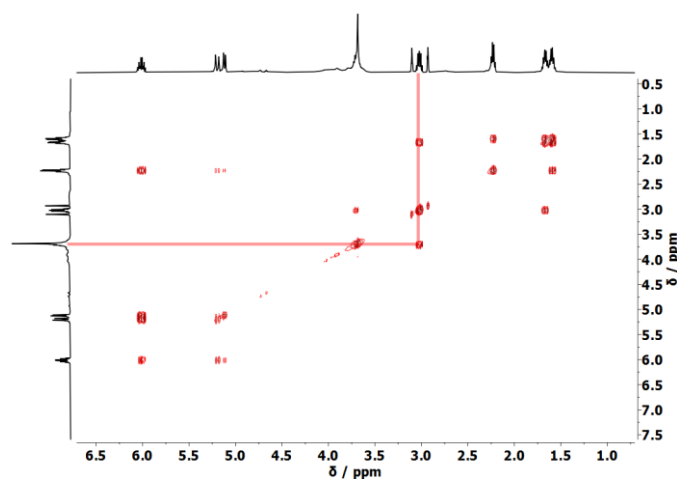


Figure S15.  $^1\text{H-}^1\text{H COSY}$  (250 MHz in  $\text{DMF-}d$  at R.T.) of mA reacted with glycidol.



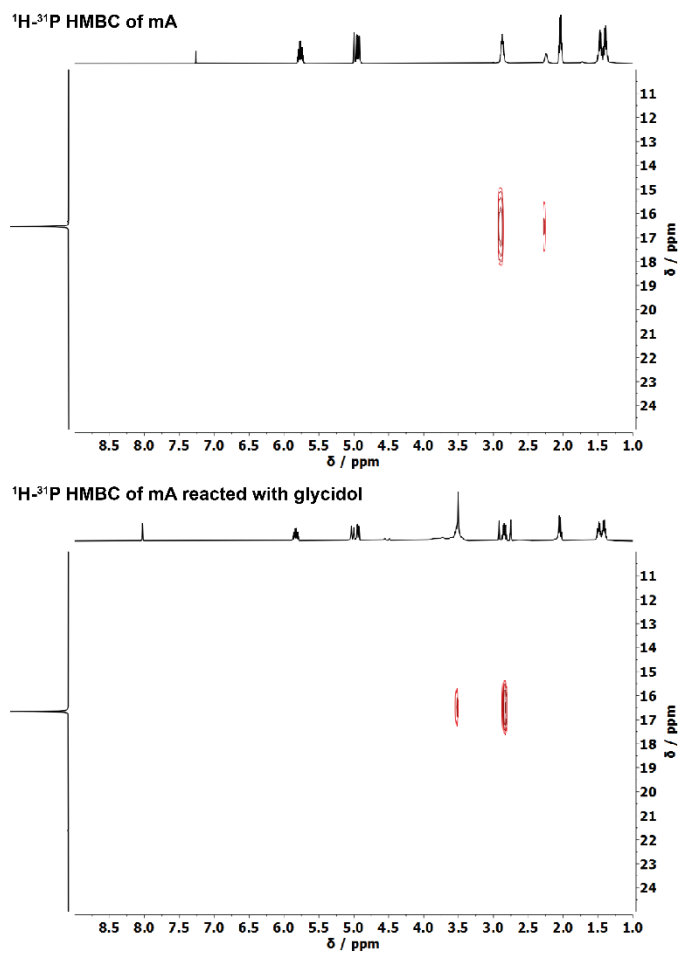


Figure S16.  $^1\text{H}$ - $^{31}\text{P}$  HMBC of mA (top) (250 MHz in  $\text{CDCl}_3$  at R.T.) and  $^1\text{H}$ - $^{31}\text{P}$  HMBC of mA reacted with glycidol (bottom) (250 MHz in  $\text{DMF-}d$  at R.T.), indicating the reaction of mA with glycidol.

### Heat of combustion of EP-FRs

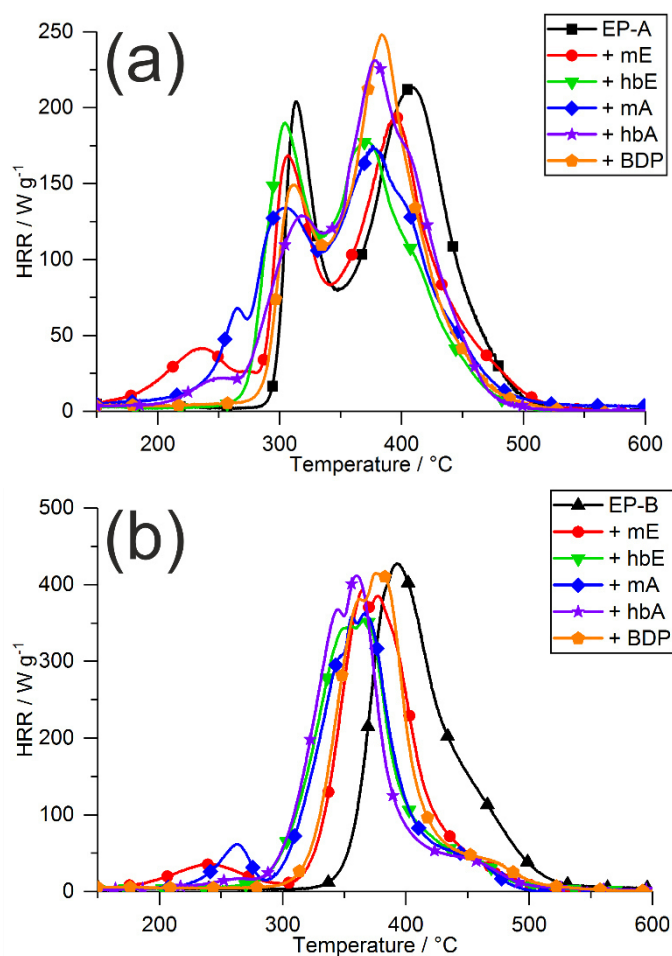


Figure S17. Heat release rate curves of (a) EP-A with FRs, and (b) EP-B with FRs via PCFC measurements.

In a fire, the gaseous products from pyrolytic decomposition at the gas / condensed phase interface feed the diffusion flame. Determining the heat of complete combustion via PCFC is useful in assessing the heat release of volatiles and provides an insight into the combustibles and possible flame-retardant modes of action such as flame dilution. It should be noted that the results from PCFC cannot be compared to forced-flaming conditions via cone calorimetry, as flame poisoning, a crucial mode of action for P-FRs, is not detectable in PCFC. The heat release curves from PCFC measurements of EP-A with FRs are plotted in Figure S17a, Figure S17b depicts those curves from EP-B with FRs, and Table S1 summarizes the results.

When mE and mA were present in resins, a small increase in heat release appeared at approx. 250 °C. Notably, the hbFRs exhibited a less pronounced increase in heat release in the same temperature range as the low molar mass FRs. This small increase in heat release coincides with the mass loss step near 250 °C in TGA measurements (Figures 5a and 5b). Thus, the volatiles from this decomposition step contribute to the heat release; moreover, FTIR analysis pointed to the production of hex-5-ene-1-ol or hex-5-ene-1-amine in Figure 7a.

The addition of FRs increased the residue yields of both EP-A and EP-B similarly: mE increased residue yield by a factor of 2.1 in EP-A and by 1.2 in EP-B, while the increase factor for hbE was 2.1 in EP-A and 2.7 in EP-B. The addition of mA into EP-A increased residues by a factor of 3.7, but it only increased residues by a factor of 2.9 in EP-B. In contrast, hbA's residue increase factor was 2.8 in EP-A and 3.0 for EP-B. Phosphoramidate-containing FRs caused higher residue yields than those containing phosphates due to greater overlap in  $T_{dec}$ -range (compare Figure 1b). BDP attained higher residue yields in EP-B (factor: 3.0) than in EP-A (factor: 1.5), which correlates well with previous TGA measurements.

The heat of complete combustion ( $h^0_c$ ), which is the ratio of total heat release and mass loss, may change for flame-retarded materials if incombustible gases such as water, CO<sub>2</sub>, or ammonia are released. The  $h^0_c$  of EP-A and EP-B was altered by the addition of FRs in different ways: both mE and mA increased  $h^0_c$  by 1% in EP-A and by 2% in EP-B, respectively. On the other hand, hbE decreased  $h^0_c$  by 3% in EP-A and by 1% in EP-B, while hbA increased  $h^0_c$  in EP-A and decreased it in EP-B. The polymeric FR hbA may have a higher affinity to the aromatic matrix EP-B during decomposition, causing the release of more incombustible gases during pyrolysis.

Table S1. Results from pyrolysis and complete combustion of the volatiles of EP-A and EP-B resins with FRs via PCFC measurements.

	HRC / J g <sup>-1</sup> K <sup>-1</sup>	THE / kJ g <sup>-1</sup>	Residue / wt.-%	h <sup>0</sup> <sub>c</sub> / kJ g <sup>-1</sup>
EP-A	223 ±8	24.3 ±0.1	1.7 ±0.1	25.1 ±0.1
+ mE	202 ±3	24.5 ±0.2	3.6 ±0.1	25.3 ±0.2
+ hbE	194 ±3	22.7 ±0.1	3.5 ±0.1	24.4 ±0.1
+ mA	186 ±6	23.5 ±0.1	6.3 ±0.7	25.3 ±0.1
+ hbA	232 ±2	24.9 ±0.2	4.8 ±0.2	26.1 ±0.1
+ BDP	255 ±7	23.0 ±0.2	2.6 ±0.1	24.6 ±0.3
EP-B	434 ±7	32.0 ±0.3	2.1 ±0.1	32.7 ±0.1
+ mE	432 ±9	32.7 ±0.3	2.5 ±0.5	33.5 ±0.4
+ hbE	447 ±1	30.5 ±0.3	5.7 ±0.1	32.3 ±0.4
+ mA	386 ±4	31.1 ±0.4	6.1 ±0.1	33.5 ±0.1
+ hbA	398 ±31	30.0 ±0.3	6.4 ±0.2	32.0 ±0.2
+ BDP	255 ±7	30.1 ±0.4	6.2 ±0.1	32.1 ±0.4

#### **Reaction to small flames via LOI and UL-94**

Reaction-to-small-flame tests, i.e. limiting oxygen index (LOI) and Underwriter’s Laboratory 94 (UL-94), help to determine the behavior of a given material in the incipient fire stage. Vertical and horizontal flame-spread give insight into the flammability of the material: flame-retarded materials often reach higher oxygen indices (OI) or better UL-94 ratings (e.g. V-0) than their base matrix due to gas or condensed phase activity such as flame poisoning or char formation, or alternatively through enhanced dripping.

Table S2 summarizes the results from LOI and UL-94 measurements and highlights the change in behavior compared to the base material. The addition of FRs increased charring, which was able to snuff downward flame spread and led to increased OI. The addition of FRs led to an OI increase between 2 – 5 vol.-% in EP-A, and an average increase of 4.4 vol.-% in EP-B. Notably, mE and hbE attained slightly higher OI values in EP-A than in EP-B, while mA and hbA, and especially BDP, raised OI more strongly in EP-B than in EP-A. The addition of BDP led to the highest OI in EP-B (24.0 vol.-%), yet it presented the lowest OI in EP-A (21.6 vol.-%). The change in behavior resulted from the lack of chemical interaction during combustion, as indicated from TGA results.

Table S2. Results from reaction to small flame tests LOI and UL-94 of EP-A and EP-B with FRs.

	OI / vol.-%	$\Delta$ OI / vol.-%	UL-94 class	Burn speed / mm min <sup>-1</sup>	rel. $\Delta$ (Burn speed)
EP-A	19.7 $\pm$ 0.3	–	HB40	43.0 $\pm$ 0.8	–
+ mE	24.5 $\pm$ 0.2	+ 4.8	HB	31.1 $\pm$ 0.3	- 28%
+ hbE	24.4 $\pm$ 0.3	+ 4.7	HB	35.1 $\pm$ 0.2	- 18%
+ mA	23.3 $\pm$ 0.2	+ 3.6	HB	30.1 $\pm$ 6.5	- 30%
+ hbA	22.1 $\pm$ 0.2	+ 2.4	HB	25.2 $\pm$ 6.5	-41%
+ BDP	21.6 $\pm$ 0.2	+ 1.9	HB	27.7 $\pm$ 1.5	- 36%
EP-B	18.7 $\pm$ 0.3	–	HB	31.7 $\pm$ 3.6	–
+ mE	23.2 $\pm$ 0.3	+ 4.5	HB	30.0 $\pm$ 1.6	- 5%
+ hbE	22.1 $\pm$ 0.2	+ 3.4	HB	27.7 $\pm$ 4.4	- 13%
+ mA	22.9 $\pm$ 0.2	+ 4.2	HB	38.3 $\pm$ 2.9	+ 21%
+ hbA	23.3 $\pm$ 0.2	+ 4.6	HB	22.0 $\pm$ 0.7	- 31%
+ BDP	24.0 $\pm$ 0.2	+ 5.3	HB	19.6 $\pm$ 3.6	- 38%

All tested materials burned intensely in UL-94 vertical tests, owing to the high fire load of the epoxy resins; thus, all materials required horizontal tests. EP-A burned with an average burn speed of 43.0 mm s<sup>-1</sup>, reaching only an HB40 classification. The addition of FRs decreased the horizontal burn speed by 18–41%, the lowest value belonging to EP-A/hbA. Similarly, the addition of FRs to EP-B altered the horizontal burning speed. Notably, while the addition of mA increased burn speed in EP-B, it lowered the horizontal burn speed in EP-A. This is attributed to the increased heat of combustion of mA in EP-B, but not in EP-A. Moreover, hbA decreased the burning speed in both matrices, but impacted EP-A most strongly, a result of its reactive FR properties in this matrix. However, while the materials gained some improvement through the addition of FRs, the high fire load of the epoxy resins could not be overcome by the FRs. While OI and burning speed generally improved with FR addition, higher FR loadings may be necessary to attain higher OI and V-classification of high-performance materials.

## Residue Analysis

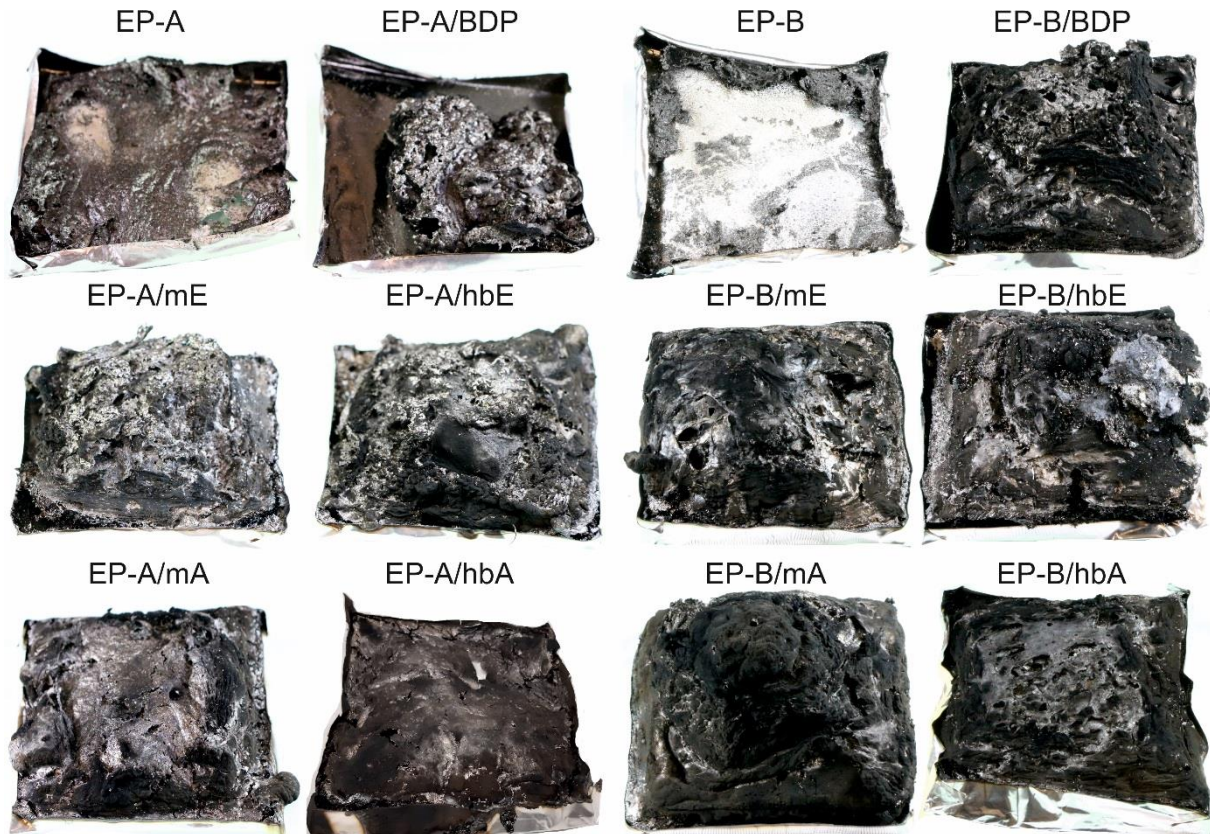


Figure S18. Residues from cone calorimeter measurements of EP-A and EP-B resins and FR containing composites.

The specimen residues after cone calorimeter measurements provide a valuable insight into the mode of action of the tested FRs. Figure S18 presents the residues of EP-A and EP-B resins and their FR containing composites. Notably, EP-A and EP-B burned almost completely with little residue remaining. The addition of BDP to the matrices increased the residue amount, yet the morphology of EP-B/BDP was different than that of EP-A/BDP: although the difference in residue amount is only about 0.5 wt.-%, EP-B/BDP was more voluminous and resembled a multicellular char layer. Consequently, BDP formed a more effective protective layer, thus explaining the strong reduction of PHRR for EP-B but not EP-A. The phosphate FRs mE and hbE more strongly reduced PHRR in EP-B than in EP-A for the same reason, as the residue surface of EP-A/mE and EP-A/hbE were frayed and less voluminous than that of EP-B/mE and EP-B/hbE. For the phosphoramidate FRs mA and hbA, the lack of a strong multicellular char acting as a protective layer resulted in the increased PHRR compared to EP-A and EP-B. Instead, the residues

were dense and brittle and offered scant protective layer effects. The incorporation of mA into the matrices generally increased PHRR because the dense char acted as a thermal conductor to the underlying material, thereby increasing the release of volatiles. Notably, EP-A/mA had the shortest burning time (Figure 9a). For hbA, the difference in PHRR between EP-A and EP-B is due to the difference in volume and the multicellular structure of EP-B/hbA.



## 5.6. Sulfur's Role in the Flame Retardancy of Thio-Ether–linked Hyperbranched Polyphosphoesters in Epoxy Resins

Alexander Battig, Jens C. Markwart, Frederik R. Wurm, Bernhard Schartel, *Europ. Polym.*

*J.* **2020**, 122, 109390.

DOI link: <https://www.doi.org/10.1016/j.eurpolymj.2019.109390>

This article was accepted and published.

Author contribution:

- Conceptualizing the frame of the work
- Chose the polymer materials, approach, loading, sample preparation and testing
- Pyrolytic investigations of the flame retardants (FRs)
  - Thermogravimetric analysis
  - Evolved gas and condensed phase FTIR
  - Pyrolysis gas chromatography / mass spectrometry
  - Pyrolysis combustion flow calorimeter
- Material and fire testing of FR-containing epoxy resins
  - Differential scanning calorimeter
  - Cone calorimeter, LOI and UL-94
  - Scanning electron microscopy, photography
- Collection, analysis, and interpretation of the data.
- Provided figures throughout the article, including decomposition mechanism
- Scientific discussion, conclusions, and writing the manuscript
- Proofread and spell-checked all versions of the article

## Abstract

Hyperbranched polyphosphoesters are promising multifunctional flame retardants for epoxy resins. These polymers were prepared via thiol-ene polyaddition reactions. While key chemical transformations and modes of actions were elucidated, the role of sulfur in the chemical composition remains an open question. In this study, the FR-performance of a series of phosphorus-based flame retardant additives with and without sulfur (thio-ethers or sulfones) in their structure are compared. The successful synthesis of thio-ether or sulfone-containing variants is described and verified by  $^1\text{H}$  and  $^{31}\text{P}$  NMR, also FTIR and MALDI-TOF. A decomposition process is proposed from pyrolytic evolved gas analysis (TG-FTIR, Py-GC/MS), and flame retardancy effect on epoxy resins is investigated under pyrolytic conditions and via fire testing in the cone calorimeter. The presence of sulfur increased thermal stability of the flame retardants and introduced added condensed phase action. Likely, sulfur radical generation plays a key role in the flame-retardant mode of action, and sulfones released incombustible  $\text{SO}_2$ . The results highlight the multifunctionality of the hyperbranched polymer, which displays better fire performance than its low molar mass thio-ether analogue due to the presence of vinyl groups and higher stability than its monomer due to the presence of thio-ether groups.



# Sulfur's role in the flame retardancy of thio-ether-linked hyperbranched polyphosphoesters in epoxy resins

Alexander Battig<sup>a,1</sup>, Jens C. Markwart<sup>b,c,1</sup>, Frederik R. Wurm<sup>b,\*</sup>, Bernhard Schartel<sup>a,\*</sup>

<sup>a</sup> Bundesanstalt für Materialforschung und -prüfung (BAM), Unter den Eichen 87, 12205 Berlin, Germany

<sup>b</sup> Max Planck Institute for Polymer Research, Ackermannweg 10, 55128 Mainz, Germany

<sup>c</sup> Graduate School Materials Science in Mainz, Staudinger Weg 9, 55128 Mainz, Germany

## ARTICLE INFO

### Keywords:

Phosphoester  
Hyperbranched  
Sulfur  
Thio-ether  
Flame retardant  
Epoxy resin

## ABSTRACT

Hyperbranched polyphosphoesters are promising multifunctional flame retardants for epoxy resins. These polymers were prepared via thiol-ene polyaddition reactions. While key chemical transformations and modes of actions were elucidated, the role of sulfur in the chemical composition remains an open question. In this study, the FR-performance of a series of phosphorus-based flame retardant additives with and without sulfur (thio-ethers or sulfones) in their structure are compared. The successful synthesis of thio-ether or sulfone-containing variants is described and verified by <sup>1</sup>H and <sup>31</sup>P NMR, also FTIR and MALDI-TOF. A decomposition process is proposed from pyrolytic evolved gas analysis (TG-FTIR, Py-GC/MS), and flame retardancy effect on epoxy resins is investigated under pyrolytic conditions and via fire testing in the cone calorimeter. The presence of sulfur increased thermal stability of the flame retardants and introduced added condensed phase action. Likely, sulfur radical generation plays a key role in the flame-retardant mode of action, and sulfones released incombustible SO<sub>2</sub>. The results highlight the multifunctionality of the hyperbranched polymer, which displays better fire performance than its low molar mass thio-ether analogue due to the presence of vinyl groups and higher stability than its monomer due to the presence of thio-ether groups.

## 1. Introduction

Polymeric flame retardants (FRs) based on phosphorus (P) are gaining increased attention, [1] not only because they more closely adhere to the requirements of REACH, but particularly due to their ability to mitigate some of the drawbacks of low molar mass variants, e.g. leaching or blooming out of the matrix, which diminish material properties such as glass-transition temperature ( $T_g$ ). Especially hyperbranched (hb) polymers have been recently investigated, as these materials act as multifunctional FRs in polymer resins, thereby exhibiting good miscibility, low impact on  $T_g$ , and effective flame retardancy at low loadings [2]. Hyperbranched polymers may be produced in a one-pot synthesis, as opposed to the highly symmetrical dendrimers; [3] this ease of synthesis is a major contributor to the use of these complex-shaped polymers in a wide array of fields [4,5]. The choice of reaction type is highly relevant to the material properties and application, and a wide range of synthetic approaches have been described [6,7]. Previously, P-based A<sub>3</sub> and more recently AB<sub>2</sub>-type hb-polymers were synthesized, [8,9] and their efficacy as FRs for bisphenol A-based and

pentaerythritol-based epoxy resins (EPs) was proven [10,11]. Another approach to attain P-based hb-polymers is via an A<sub>2</sub> + B<sub>3</sub>-type reaction: in previous works, P-based polymeric hyperbranched FRs (hb-FRs) were synthesized and their efficacy as additive FRs in bisphenol A-based epoxy resins (EPs) were demonstrated [12]. The hb-FRs were synthesized via thiol-ene polyaddition using ethanedithiol as an A<sub>2</sub>-unit and low molar mass P-based FRs with systematically varied P-O and P-N contents as B<sub>3</sub>-units. These low molar mass FRs were previously synthesized and investigated as additives in EP [13]. Research into the low molar mass FRs and their hb-polymeric variants indicated that conversion to polymers generally improved thermal stability and decreased impacts on  $T_g$ . However, the comparison between hb-polymers and their monomers did not fully consider the role of the sulfur (S)-containing A<sub>2</sub>-component and how its presence may affect flame retardancy.

In this work, the role of S-containing compounds, i.e. thio-ethers and sulfones, in the flame retardancy of P-based FRs is investigated to gain a better understanding of the impact of the A<sub>2</sub>-linker of hb-FRs. Two S-containing low molar mass P-FRs are synthesized and their

\* Corresponding authors.

E-mail addresses: [wurm@mpip-mainz.mpg.de](mailto:wurm@mpip-mainz.mpg.de) (F.R. Wurm), [bernhard.schartel@bam.de](mailto:bernhard.schartel@bam.de) (B. Schartel).

<sup>1</sup> These authors contributed equally.

performance as additives in bisphenol-A-based EPs are compared to that of the previously synthesized hb-FR (**hbPPE**) and its non-S-containing monomer (**mPE**). To better compare the performance of low molar mass FRs to that of **hbPPE**, a thio-ether-containing compound (**mPE-S**) is prepared via thiol-ene reaction of **mPE** with ethanethiol. Additionally, **mPE-S** is oxidized to form a sulfone-containing compound (**mPE-S-ox**).

The use of sulfur in flame retardancy has been investigated for a wide array of flame retardants and polymers. The role of sulfur oxidation was investigated for P-esters in bisphenol A, where it was found that flame retardancy increased with increasing levels of oxidation state [14]. Several S-containing FRs have been previously investigated in polycarbonates (PC), many of them as aromatic sulfonate salts [15]. Although the flame-retardant modes of action are not completely clear, one investigation stipulated that Fries-rearrangement was accelerated by aromatic sulfonates in PC, causing higher cross-linking but a faster decomposition [16]. Moreover, extensive investigations into the flame-retardant action of elemental sulfur, sulfides, and disulfides were performed, highlighting that these compounds decompose to form sulfur radicals, which may promote cross-linking reactions [17,18]. Sulfone-containing FRs were shown to release sulfur dioxide into the gas-phase, [19] which acts not only as a fuel-diluent thus reducing the combustion efficiency, but was shown to act as a radical-scavenger [20,21]. Additionally, P-containing sulfones have been investigated as a toughening agent and flame retardant for epoxy resins [22]. Other S-based FRs include sulfamic acid-based salts, i.e. ammonium sulfamate, or diammonium imidobisulfonate, which proved as effective FRs for cotton and wool, [23] polyamide 6, [24,25] and polymethyl methacrylate or polystyrene [26]. Furthermore, P and S-containing FRs have also been investigated in PC [27] and in thermoplastic polyurethanes [28].

By analyzing the difference between S- and non-S-containing low molar mass FRs, new light may be shed on the role that S plays in effective flame retardancy of hb-FRs. Furthermore, by assessing the flame-retardant action of S-containing low molar mass FRs (S-FRs), additional information on the mode of action of hb-FRs may be gained, thus potentially helping improve future formulations.

## 2. Materials and methods

All chemicals were purchased from commercial suppliers as reagent grade and used without further purification. Bisphenol A bis(diphenyl phosphate) (BDP) was supplied by Albemarle (Louvain-la-Neuve, Belgium). Diglycidyl ether of Bisphenol A (DGEBA, Araldite MY740) was supplied by Bodo Müller Chemie GmbH (Offenbach am Main, Germany). 2,2'-Dimethyl-4,4'-methylene-bis-(cyclohexylamine) (DMC) was purchased from Merck KGaA (Darmstadt, Germany).

### 2.1. Syntheses

#### **mPE**, **hbPPE**

**mPE** was prepared as previously described, [13] by the reaction of phosphoryl chloride with 5-hexene-1-ol. **hbPPE** was prepared as previously described, [12] where **mPE** was allowed to react with 1,2-ethanedithiol using azobisisobutyronitrile (AIBN) as an initiator.

#### **mPE-S**

**mPE-S** (56.5 g; 164.0 mmol; 1.0 eq.) was added to a dried 250 mL, round-bottomed flask under an argon atmosphere. Then, ethanethiol (48.5 mL; 656.2 mmol; 4.0 eq.) was slowly added while stirring the solution and cooling the flask with a water bath at room temperature. After a few minutes, AIBN (808.1 mg; 4.9 mmol; 0.03 eq.) was added and the mixture was stirred overnight at 40 °C. The crude mixture was concentrated at reduced pressure to give a yellowish oil in quantitative yields.

<sup>1</sup>H NMR (300 MHz, Chloroform-*d*, δ): 4.01 (q, *J* = 6.7 Hz, 6H), 2.51

(q, *J* = 7.3 Hz, 12H), 1.68 (dd, *J* = 12.9, 6.2 Hz, 6H), 1.63 – 1.51 (m, 6H), 1.39 (s, 12H), 1.24 (t, *J* = 7.4 Hz, 9H). (Fig. S1)

<sup>31</sup>P {H} NMR (121 MHz, Chloroform-*d*, δ): –0.67 (s, 1P). (Fig. S2)

#### **mPE-S-ox**

**mPE-S** (33.0 g; 62.2 mmol; 1.0 eq.), dissolved in *N,N*-dimethylformamide (DMF) (125 mL), was added to a 250 mL, round-bottomed flask. Then, B(OH)<sub>3</sub> (82.9 mg; 1.2 mmol; 0.02 eq.) and 35% H<sub>2</sub>O<sub>2</sub> (55 mL; 621.7 mmol; 10.0 eq.) were added while stirring the solution and cooling the flask with a water bath. The reaction was allowed to continue overnight at 75 °C. The crude mixture was transferred to a separation funnel, where dichloromethane (DCM) and water were added. The water phase was washed two more times with DCM and the combined organic layers were washed with NaHCO<sub>3</sub> solution, 10% aqueous hydrochloric acid solution and brine. The organic layer was dried over magnesium sulfate, filtered and concentrated at reduced pressure to give a white wax in quantitative yields.

<sup>1</sup>H NMR (300 MHz, Chloroform-*d*, δ): 4.00 (q, *J* = 6.6 Hz, 6H), 2.95 (q, *J* = 7.4 Hz, 12H), 1.82 (dd, *J* = 6.4, 5.7 Hz, 6H), 1.68 (dd, *J* = 6.6 Hz, 6H), 1.43 (m, 12H), 1.37 (t, *J* = 7.5 Hz, 9H). (Fig. S3)

<sup>31</sup>P {H} NMR (121 MHz, Chloroform-*d*, δ): –0.71 (s, 1P). (Fig. S4)

MALDI-TOF: 627.25 [M + H]<sup>+</sup>, 649.24 [M + Na]<sup>+</sup>, 665.21 [M + K]<sup>+</sup> (Calculated M<sup>+</sup>: 626.24).

### Sample preparation

Epoxy resin samples were prepared in the following manner: DGEBA was placed into in a 1 L polypropylene cup and, where applicable, the FR (10 wt.-% loading) was added. With a wooden spatula, the mixture was blended until homogenous. DMC was then added next, then all components were stirred until fully mixed. Finally, the contents were poured into prepared aluminum molds. For cone calorimeter measurements, samples sized 100 mm × 100 mm × 4 mm were used.

### 2.2. Methods

<sup>1</sup>H, <sup>31</sup>P {H}, and <sup>13</sup>C {H} nuclear magnetic resonance (NMR) spectra were recorded with Bruker Avance spectrometers operating with 250, 300, 500, and 700 MHz frequencies in deuterated chloroform or deuterated dimethyl sulfoxide as a solvent. The calibration of the spectra was done against the solvent signal. The spectra were analyzed using MestReNova 9 from Mestrelab Research S.L.

Matrix-assisted laser desorption/ionization – time of flight (MALDI – TOF) measurements were carried out with a Reflex I mass spectrometer (Bruker, Bremen, Germany), equipped with a 337 nm nitrogen laser. The spectra were recorded in the linear mode with the Bruker HIMAS detector at an acceleration voltage of 30 kV. 2-[(2E)-3-(4-*tert*-Butylphenyl)-2-methylprop-2-enylidene]malononitrile (DCTB) was used as a matrix. To avoid fragmentation in MALDI-TOF mass spectrum (MS) measurements, the laser power required for the desorption/ionization process was carefully adjusted slightly above threshold.

A TG 209 F1 Iris (Netzsch Instruments, Selb, Germany) was used for thermogravimetric analysis (TGA) measurements. A CryoMill (RETSCH, Germany) was used to mill epoxy resin-based samples into powder under liquid nitrogen. Pure FR samples (5 mg) or powdered polymer samples (10 mg) were heated at a constant heating rate (10 K min<sup>-1</sup>) from 30 to 900 °C under a nitrogen flow (30 mL min<sup>-1</sup>). A Fourier transform infrared spectrometer Tensor27 (Bruker Optics, Ettlingen, Germany) was used for evolved gas analysis of TGA samples (TG-FTIR). A heated (270 °C) transfer line connected TGA with FTIR. A Vertex70 FTIR spectrometer (Bruker Optics, Ettlingen, Germany) with an attached FTIR600 hot-stage cell (Linkam Scientific Instruments Ltd., Chilworth, UK) was used to measure condensed phase FTIR (range: 4000 – 400 cm<sup>-1</sup>; resolution 0.4 cm<sup>-1</sup>). Samples (5 mg) were mixed with potassium bromide (150 mg) and pressed into a platelet (pressure: 7 t). Under a constant heating rate (10 K min<sup>-1</sup>) and constant nitrogen

flow ( $300 \text{ mL min}^{-1}$ ), the platelets were heated from 30 to  $600^\circ\text{C}$ .

A PY3030iD micro-furnace single-shot pyrolyzer (Frontier Laboratories, Japan) coupled via a split/ splitless inlet port to a 7890B gas chromatograph (Agilent Technologies, USA) and combined with a 5977B mass selective detector (Agilent Technologies, USA) was used to measure pyrolysis gas chromatography – mass spectrometry (Py-GC/MS). The mass spectrometer detector (ionization energy =  $70 \text{ eV}$ ) had a scan range of  $15 - 50 \text{ amu}$ . Samples ( $150 \mu\text{g}$ ) were pyrolyzed ( $T = 500^\circ\text{C}$ ) via gravimetric fall into the pyrolysis zone under helium atmosphere. Using an Ultra Alloy + 5 capillary column (length =  $30 \text{ m}$ ; inner diameter =  $0.25 \text{ mm}$ ; film thickness =  $0.25 \mu\text{m}$ ), evolved pyrolysis products were separated under a constant flow of helium ( $1 \text{ mL min}^{-1}$ ). The column temperature ran for 2 min at  $40^\circ\text{C}$ , then heated ( $10 \text{ K min}^{-1}$ ) to  $300^\circ\text{C}$  and held for 10 min. The gas chromatograph injector ( $T = 300^\circ\text{C}$ ) ran a split of 1:300. Peak assignments and product identification were done with the aid of the NIST 14 MS library.

A microscale combustion calorimeter (Fire Testing Technologies Ltd., East Grinstead, UK) was used for pyrolysis flow combustion calorimetry (PCFC) measurements. At a constant heating rate ( $1 \text{ K s}^{-1}$ ) and constant gas flow (nitrogen:  $80 \text{ mL min}^{-1}$ ; oxygen:  $20 \text{ mL min}^{-1}$ ), powdered samples ( $5 \text{ mg}$ ) were pyrolyzed from  $150$  to  $750^\circ\text{C}$ , and the evolved gases were combusted at  $900^\circ\text{C}$ .

A Netzsch 204 FR “Phoenix” (Netzsch Instruments, Selb, Germany) was used to measure differential scanning calorimetry (DSC). Samples from the bulk material ( $5 \text{ mg}$ ) were measured at a constant heating/cooling rate ( $10 \text{ K min}^{-1}$ ) from  $-80 - 180^\circ\text{C}$ . Three heating and two cooling runs were measured, and data was collected from the second and third heating run to determine the glass transition temperature.

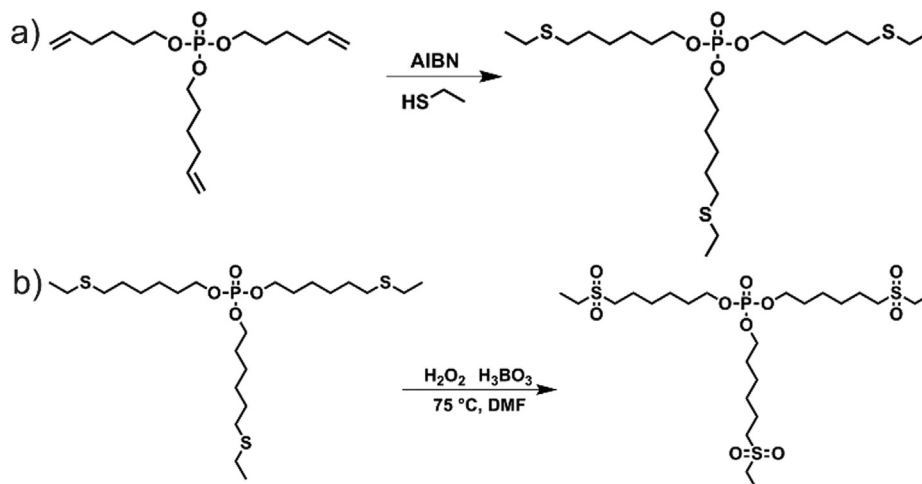
A cone calorimeter (Fire Testing Technology Ltd., East Grinstead, UK) was used for forced-flaming combustion experiments according to ISO 5660. Samples ( $100 \text{ mm} \times 100 \text{ mm} \times 4 \text{ mm}$ ) were stored in a climate control ( $T = 23^\circ\text{C}$ ; RH = 50%) for at least 48 h before testing. To simulate a developing fire, [29,30] a distance between sample and heater of  $35 \text{ mm}$  and a heat flux of  $50 \text{ kW m}^{-2}$  was chosen. Tests were conducted in duplicate, unless the margin of error was greater than 10%, whereupon a third measurement was conducted.

### 3. Results and discussion

#### 3.1. Synthesis of FRs

**mPE** was synthesized by the reaction of 5-hexen-1-ol with phosphoryl chloride as previously described [13].

The synthesis of **mPE-S** was performed in a single reaction step from



**Scheme 1.** Synthesis schemes of thio-ether and sulfone-containing FRs: (a) **mPE** and ethanethiol were allowed to react via thiol-ene-reaction with AIBN as initiator to form **mPE-S**; (b) **mPE-S** was oxidized with hydrogen peroxide with boronic acid as a catalyst to form **mPE-S-ox**.

**mPE** and ethanethiol by a thiol-ene-reaction (Scheme 1a). Further purification, such as distillation or chromatography, was not necessary. The resulting compound was a liquid at room temperature and had a calculated P-content of 5.84 wt.-%. It was soluble in aromatic (e.g. toluene) and halogenated solvents (e.g. dichloromethane and chloroform), and insoluble in water. Successful synthesis of **mPE-S** was followed by  $^1\text{H}$  NMR spectroscopy (Fig. 1a). After the thiol-ene-reaction, the resonances of the double bonds at  $8.83 - 5.70 \text{ ppm}$  and  $5.02 - 4.93 \text{ ppm}$  vanished, and a new resonance signal at  $2.51 \text{ ppm}$  for the methylene groups next to the thio-ether was detected. The  $^{31}\text{P}$  NMR spectrum (Fig. 1 b) revealed a single signal at  $-0.67 \text{ ppm}$ , which is typical for phosphates.

In a second reaction, **mPE-S** was oxidized with hydrogen peroxide using boronic acid as a catalyst (Scheme 1 b) at  $75^\circ\text{C}$  overnight to form **mPE-S-ox**. After oxidation to the sulfone, the resonance of the methylene groups next to the sulfone group shifted downfield to  $2.95 \text{ ppm}$  in  $^1\text{H}$  NMR (Fig. 1 c), which is characteristic and has been reported for similar compounds [31]. In addition, the successful oxidation to the sulfone and not to the sulfoxide was supported by IR spectroscopy, as indicated by the characteristic frequencies at  $1299 \text{ cm}^{-1}$  and  $1124 \text{ cm}^{-1}$  (Fig. 2a) [32] and MALDI-TOF mass spectrometry (Fig. 2b).

The polymeric FR **hbPPE** was prepared via a thiol-ene reaction of **mPE** with ethanedithiol. Its synthesis has been previously described and will not be further illustrated here [12].

#### 3.2. Pyrolysis – Decomposition temperature and mass loss of FRs

All FRs were characterized by their mass loss under pyrolytic conditions via thermogravimetric analysis (TGA) (Table 2). The mass loss and mass loss rate curves of **mPE-S** and **mPE-S-ox** (Fig. 3a) highlighted that both S-FRs are more thermally stable than **mPE**. The beginning of decomposition, i.e. the temperature at 5 wt.-% mass loss ( $T_{5\%}$ ), of **mPE-S** was approx.  $30^\circ\text{C}$  higher than that of **mPE**, and  $T_{5\%}$  of **mPE-S-ox** was approx.  $10^\circ\text{C}$  higher than that of **hbPPE**. The temperature of maximum decomposition rate ( $T_{\text{max}}$ ) of **mPE-S** was in the same temperature region as that of **hbPPE**, and **mPE-S-ox** decomposed at slightly higher temperatures ( $T_{\text{max}} = 286^\circ\text{C}$ ). The increased thermal stability stems from the thio-ether or sulfone groups, which are more thermally stable than allyl-groups. By “end-capping” the vinyl groups of **mPE**, added thermal stability is afforded to **mPE-S**. Furthermore, sulfone groups are more thermally stable than thio-ether groups, as **mPE-S-ox** degraded at elevated temperatures compared to **mPE-S**. When comparing the residues at  $700^\circ\text{C}$ , the residue of **mPE-S** was higher than that of **mPE** by a factor of 2.7. Moreover, the residue of **mPE-S-ox** was in the same range as that of **hbPPE**. The presence of thio-ethers altered the decomposition

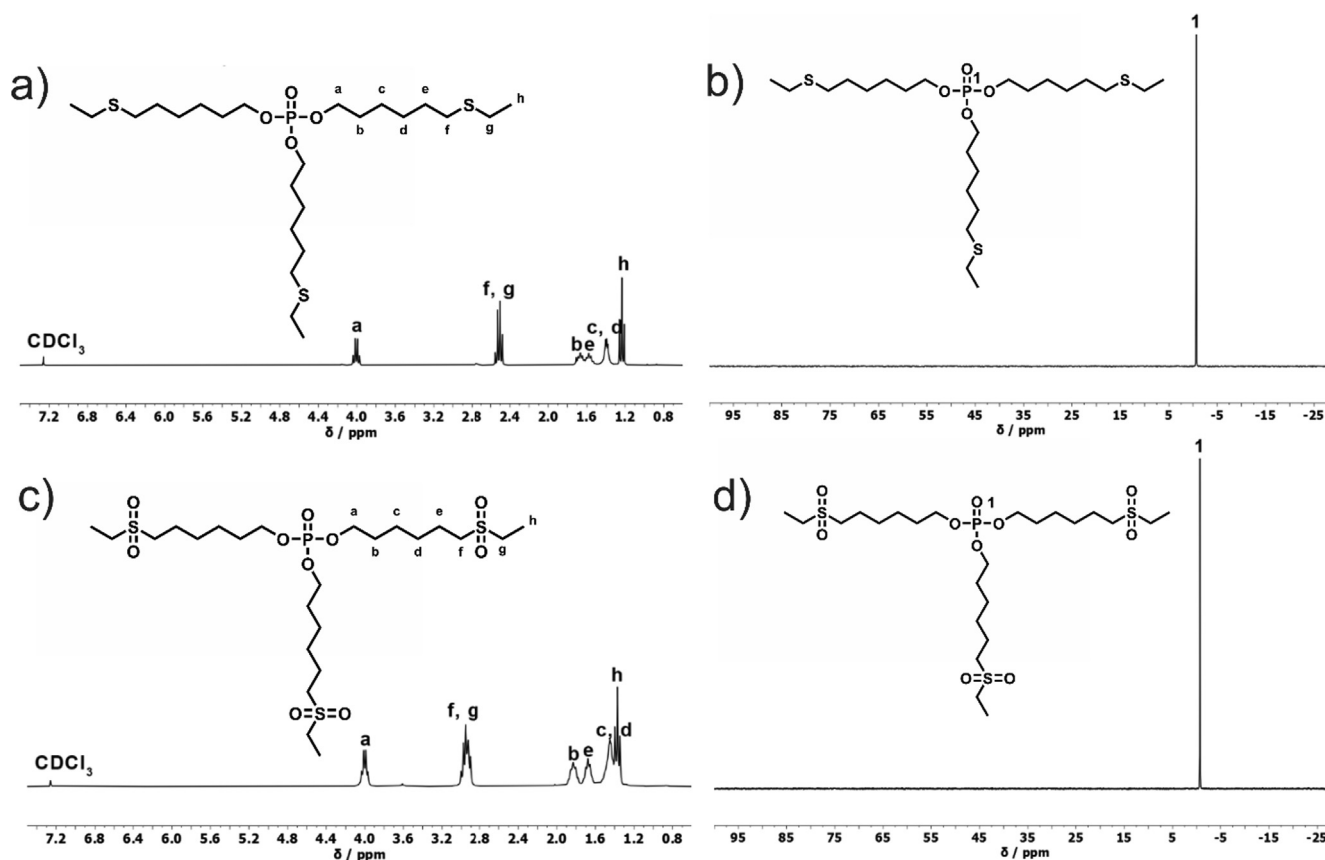


Fig. 1. (a)  $^1\text{H}$  NMR (300 MHz in  $\text{CDCl}_3$  at 298 K) of **mPE-S**; (b)  $^{31}\text{P}$  {H} NMR (121 MHz in  $\text{CDCl}_3$  at 298 K) of **mPE-S**; (c)  $^1\text{H}$  NMR (300 MHz in  $\text{CDCl}_3$  at 298 K) of **mPE-S-ox**;  $^{31}\text{P}$  {H} NMR (121 MHz in  $\text{CDCl}_3$  at 298 K) of **mPE-S-ox**.

of **mPE** by replacing the highly reactive vinyl group; moreover, the thio-ether bond decomposed to form sulfur radicals. As it has been shown that radical formation plays a significant role in flame retardancy, [33] the higher residue yield is explained by sulfur radicals undergoing cross-linking reaction with the decomposing FR.

### 3.3. Pyrolysis – Evolved gas analysis of FRs

The evolved gases during pyrolytic decomposition were analyzed via thermogravimetric analysis coupled with Fourier transform infrared spectroscopy (FTIR) (Fig. 4), and via pyrolysis coupled with gas chromatography and subsequent mass spectrometry (Py-GC/MS) (Fig. 5). The decomposition products of **mPE** and **hbPPE** were previously investigated: the main products corresponded to 5-hexen-1-ol, where the  $\omega$ -OH group was identified via FTIR by the band at  $1043\text{ cm}^{-1}$ , and 1,5-hexadiene, where the vinyl group exhibited a strong band at  $916\text{ cm}^{-1}$  [34]. The vinyl function, which was visible for all tested FRs, resulted from *cis*-eliminations, where the scission of the (PO)-C bond resulted in an vinyl group [13]. **hbPPE** exhibited an additional absorption band at  $1271\text{ cm}^{-1}$  which matched a signal from ethanedithiol, [35] indicating the presence of S in the decomposition spectrum. For **mPE-S**, the FTIR spectrum exhibited an absorption band at  $1267\text{ cm}^{-1}$  which was nearly identical to the band seen in **hbPPE** and comparatively 1-hexanethiol [35]. Thus, this band relates to thio-ether or thiol groups. Moreover, the spectrum showed similarities to 5-hexen-1-ol via the band at  $1043\text{ cm}^{-1}$ , implying that the decomposition product contained signals of both  $\omega$ -OH and thio-ether groups caused by the hydrolytic scission of the P-O bond, resulting in the production of 6-(ethylsulfanyl)-1-hexanol. For **mPE-S-ox**, the decomposition spectrum displayed strong absorption at  $1339$  and  $1142\text{ cm}^{-1}$  belonging to characteristic sulfone groups, [34] as evidenced by the comparative spectrum of 1,1-

sulfonylbispropane [35]. Furthermore, the development of 1-hexanol was underlined by the absorption at  $1043\text{ cm}^{-1}$  and confirmed by Py-GC/MS.

Py-GC/MS measurements of the FRs (Fig. 5) provided further evidence of the evolution of specific decomposition products identified in FTIR spectra of the evolved gases (Fig. 4). The presence of 5-hexene-1-ol in the FTIR spectrum of **mPE** was verified in the mass spectrum at a retention time of 6.63 min (Fig. S6). For **mPE-S**, the production of ethanethiol at 2.26 min (Fig. S2) and diethyl sulfide at 3.38 min (Fig. S5) were observed. Identical to **hbPPE**, **mPE-S** decomposed to form tetrahydro-2-methyl-2H-thiopyran (7.79 min, Fig. S9), 2-ethyltetrahydro thiophene (8.21 min, Fig. S10), and thiepane (9.29 min, Fig. S11). Notably, **mPE-S-ox** formed  $\text{SO}_2$ , as implied by the mass spectrum at 1.92 min (Fig. S1), as well as 1-hexanol at 6.68 min (Fig. S7). The formation of  $\text{SO}_2$  for sulfones has been noted in literature [19]. **mPE-S-ox** decomposed to form a tetrahydrofuran-like material; the mass spectrum of 2-propyl-tetrahydrofuran showed similarities to the mass spectrum at 7.75 min (Fig. S8), yet 2-ethyl-tetrahydrofuran is more reasonably formed when considering the C-atom amount. Notably, the mass spectrum at 8.21 min of **mPE-S-ox** shared similarities with 2-ethyltetrahydro thiophene, possibly stemming from unreacted thio-ether groups. The production of 1,5-hexadiene was present in the chromatograms of **mPE**, **mPE-S**, and **hbPPE** at 2.63 min (Fig. S3). However, for **mPE-S-ox** the evolution of 1-hexene was observed at 2.64 min (Fig. S4).

The decomposition mechanisms for **mPE** [13] and **hbPPE** [12] have been described previously, and generally involved *cis*-eliminations and hydrolysis reactions. From the evolved gas analyses from FTIR and Py-GC/MS measurements, a decomposition process for the S-FRs is proposed (Scheme 2):

The decomposition of several thio-ether [36] and of sulfone



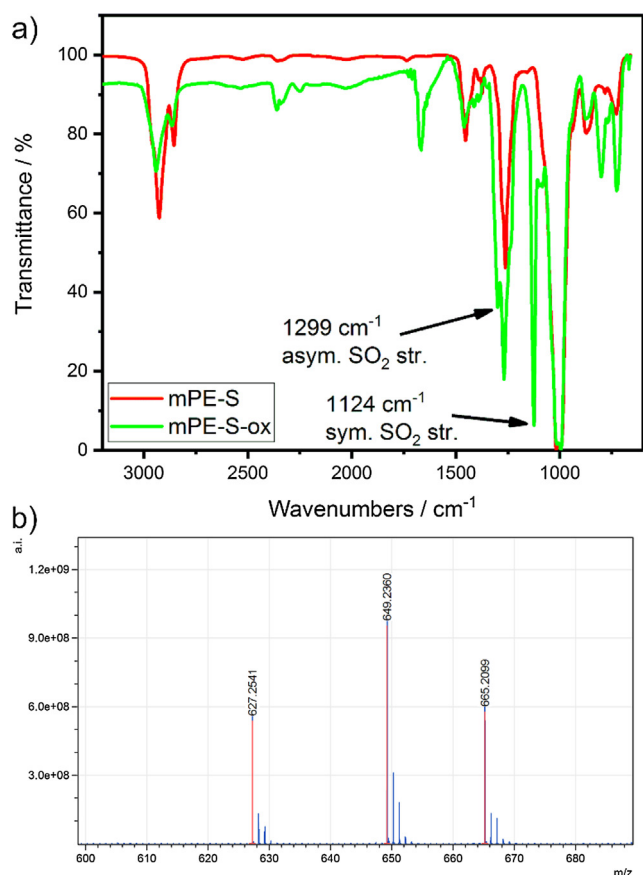


**Fig. 2.** (a) FTIR spectra of mPE-S and mPE-S-ox, highlighting the asymmetrical and symmetrical SO<sub>2</sub> stretching frequencies; (b) MALDI of mPE-S-ox with DCBT as matrix (left to right: [M + H]<sup>+</sup>, [M + Na]<sup>+</sup>, and [M + K]<sup>+</sup>).

**Table 1**  
Material abbreviation, names, chemical structures, and calculated phosphorus content.

Abbreviation	Name	Chemical structure	P-content (calc.)
mPE	Tri(hex-5-en-1-yl)phosphate		9.0 wt.-%
mPE-S	Tris[6-(ethyl thio)hexyl]phosphate		5.8 wt.-%
mPE-S-ox	Tris[6-(ethyl sulfonyl)hexyl]phosphate		4.9 wt.-%
hbPPE	hb-Poly(phosphate)		7.0 wt.-%
BDP	Bisphenol A bis(diphenyl phosphate)		8.5 wt.-%
DGEBA	Diglycidyl ether of bisphenol A		-
DMC	2,2'-dimethyl-4,4'-methylene-bis-(cyclohexylamine)		-

[37,38]-containing compounds have been described in literature and involve the production of S-radicals. For **mPE-S**, *cis*-elimination leads to the production of 6-(ethylsulfonyl)-1-hexene, which further decomposes via the homolytic cleavage of the C-S bond, thus producing the products (a), (b), (c), and (d) (Scheme 2), depending on which C-S bond is cleaved. The beta-scission of (a) leads to the formation of 1,5-hexadiene, which was identified in Py-GC/MS, and the recombination reaction of (b) and (c) leads to the formation of diethyl sulfide, which was also detected. Hydrogen atom abstraction of (b) leads to ethanethiol, which was observed at 2.26 min, and hydrogen transfer of (d) and cyclisation reactions lead to the formation of tetrahydro-2-methyl-2H-thiopyran, 2-ethyltetrahydro thiophene, and thiopane. For **mPE-S-ox**, the driving force of decomposition is the release of SO<sub>2</sub>: sulfone-containing olefins undergo a transfer of the β-hydrogen atom to the sulfone-group and subsequent elimination of a vinyl functionalized olefin and sulfinic acid, the latter rapidly decomposing to form SO<sub>2</sub> and alkyl radicals [39]. Hydrolysis or *cis*-elimination reactions of **mPE-S-ox** form 1-(ethylsulfonyl) hexanol or 1-(ethylsulfonyl)-hex-5-en, respectively. Both products decompose via the aforementioned pathway, and via hydrogen atom transfer reactions 1-hexanol or 1-hexene are produced; both compounds were identified in Py-GC/MS. The decomposition of **hbPPE** is expanded (Scheme 2) to more precisely describe the production of several measured compounds: while hydrolysis or *cis*-elimination reactions of terminal groups lead to the production of 5-hexene-1-ol or 1,5-hexadiene, respectively, *cis*-elimination of linear or dendritic units yields thio-ether-containing compounds. These thio-ethers undergo cyclisation and elimination reactions to form cyclic thio-ethers, but they also undergo homolytic C-S bond cleavage to form radical compounds: the vinyl-functionalized alkyl radical undergoes β-scission to yield 1,5-hexadiene, and previously reported [12] thiirane and 1,4-dithiane are formed from elimination reactions and subsequent dimerization, respectively.

### 3.4. Material properties – Resin blends

In most cases, additives act as plasticizers in polymer resins:



**Table 2**  
Results from thermogravimetric analysis (TGA) of FRs and EP.

Material	$T_{5\%}/^{\circ}\text{C}$	$T_{\text{max}}/^{\circ}\text{C}$	$\text{ML}_{\text{max}}/\text{wt.}\%$	$T_{\text{shoulder}}/^{\circ}\text{C}$	$\text{ML}_{\text{shoulder}}/\text{wt.}\%$	Residue (700 °C)/wt.-%
mPE	195 ± 3	250 ± 2	95.7 ± 1.4	–	–	2.8 ± 0.8
mPE-S	228 ± 4	277 ± 0	90.2 ± 1.6	–	–	7.5 ± 0.2
mPE-S-ox	252 ± 4	286 ± 2	83.4 ± 0.0	–	–	11.8 ± 0.5
hbPPE	242 ± 2	280 ± 1	83.3 ± 0.2	–	–	11.2 ± 1.4
DGEBA-DMC	338 ± 1	372 ± 1	62.0 ± 0.8	424 ± 5	33.2 ± 0.3	4.5 ± 0.1
BDP	331 ± 1	415 ± 6	85.5 ± 2.2	467 ± 3	11.8 ± 1.3	1.8 ± 0.9

Onset temperatures ( $T_{5\%}$ ); temperature of maximum decomposition rate ( $T_{\text{max}}$ ); mass loss of decomposition step at  $T_{\text{max}}$  ( $\text{ML}_{\text{max}}$ ); temperature of additional decomposition step, i.e. “shoulder” ( $T_{\text{shoulder}}$ ); mass loss of decomposition step at shoulder ( $\text{ML}_{\text{shoulder}}$ ).

additives affect the cross-linking density of the material, altering its mechanical properties and affecting the glass-transition temperature ( $T_g$ ) [40]. The impact of the FRs on the  $T_g$  of EP was determined via differential scanning calorimetry (DSC) (Fig. 6a) DGEBA-DMC had a  $T_g$  of 155 °C, and the addition of FRs lowered it between 21 and 38 °C (Fig. 6b). EP with BDP (EP/BDP) had a  $T_g$  of ca. 134 °C; EP with hbPPE (EP/hbPPE) and EP with mPE-S-ox (EP/mPE-s-ox) displayed  $T_g$ s in a similar temperature range, i.e. 132 and 129 °C, respectively. Resins with mPE (EP/mPE) and mPE-S (EP/mPE-S) exhibited the lowest  $T_g$ s at 117 and 118 °C, respectively. DSC measurements identified that the thio-ether-containing mPE-S affected the  $T_g$  of EP similarly to the allyl-functionalized mPE, indicating that “end-capping” did not improve the impact on  $T_g$ . Furthermore, the sulfone-containing mPE-S-ox had a reduced impact on  $T_g$  of EP, comparable to that of hbPPE. This phenomenon can be explained by the bulky sulfone groups that affect the free-volume of the matrix, thus altering the energy needed to attain a flowing process of the polymer chain, resulting in increased  $T_g$  [41].

### 3.5. Pyrolysis – Decomposition temperature and mass loss of resin blends

The pyrolytic decomposition of EP and of EP-FRs were investigated via TGA (Fig. 7a): the mass loss of EPs with S-FRs illustrated that the low  $T_{5\%}$  and approx. 10 wt.-% mass loss near 230 °C exhibited by EP/mPE was not shared by EP/mPE-S or EP/mPE-S-ox (Table 2), implying that “end-capping” the vinyl-groups increased the thermal stability of the EP-FRs. This is further exemplified by the low  $T_{\text{max}}$  of EP/mPE compared to the S-FR-containing EPs;  $T_{\text{max}}$  of EP/mPE-S and of EP/mPE-S-ox were both in the same range as  $T_{\text{max}}$  of EP/BDP and of EP/hbPPE, i.e. about 15 – 20 °C lower than  $T_{\text{max}}$  of EP. Moreover, the residue yields at 700 °C of S-FR-containing EPs were higher than that of EP/mPE (Fig. 7b). The addition of mPE to resins increased residue yields at 700 °C by about 13%, which is the lowest among the tested FRs. However, mPE-S-ox and mPE-S had a greater impact on residue,

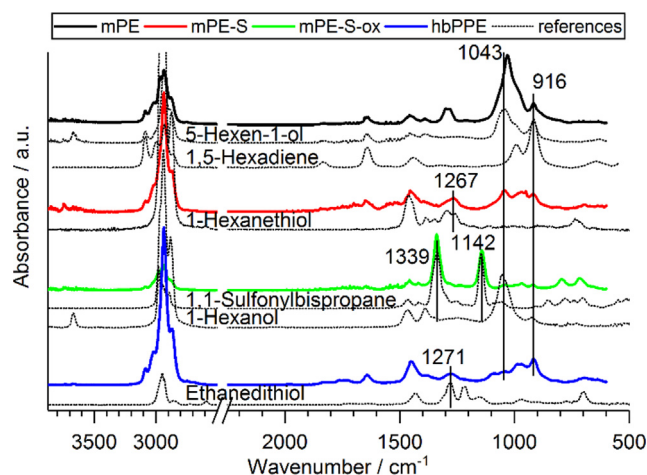


**Fig. 4.** FTIR spectra of pyrolytic decomposition products of FRs at  $T_{\text{max}}$  via thermogravimetric analysis coupled with Fourier transform infrared spectroscopy (TG-FTIR).

increasing yields by 41% compared to pure EP (residue = 4.5 wt.-%). When comparing EP/mPE to the S-FRs, the thio-ether “end-capping” led to an increase in residue yield of 24% (Table S1). The sulfone-containing FR did not additionally yield higher residues compared to the thio-ether. The presence of sulfur increased the thermal stability of mPE, leading to increased interaction with the decomposing matrix, thus producing higher char yields. Moreover, the presence of sulfur in FRs may promote cross-linking reactions by generating sulfur-radicals, as noted in the decomposition of the pure FRs. The oxidation state of sulfur did not play a role in the increase of residue. EP with hbPPE exhibited higher pyrolytic residues than those EPs with low molar mass S-FRs, even though pure mPE-S-ox had similar residue yields as pure

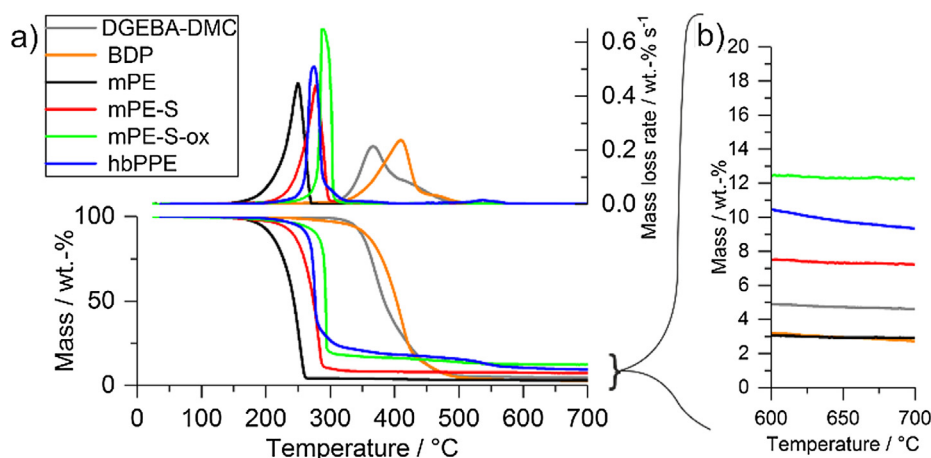


**Fig. 3.** (a) Mass loss (bottom) and mass loss rate (top) of pyrolytic decomposition of pure FRs and EP via TGA; (b) Comparison of residue remaining between 600 and 700 °C of pure FRs and EP.

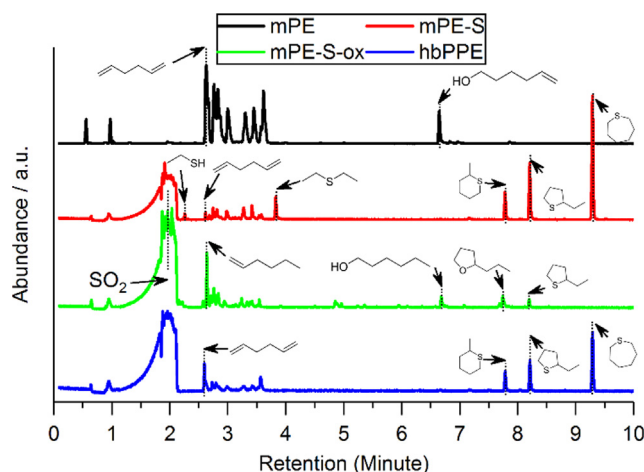


Fig. 5. Gas chromatograms of FRs from Pyrolysis-Gas Chromatography/Mass Spectrometry (Py-GC/MS) measurements.

**hbPPE.** The presence of sulfur in FRs improved the residue yields of EP in pyrolysis, thus helping to explain the high residue yields of EP/hbPPE. Additionally, the presence of certain S-species may act as a synergist with P-based flame retardants; previous investigations into halogenated flame retardants for polystyrene proved some cooperative effects of disulfides and sulfonamides [42].

### 3.6. Pyrolysis – Evolved gas analysis of resin composites

Evolved gas analysis of the resin blends further illustrated the FR modes of action: FTIR analysis of the pyrolytic decomposition products (Fig. 8) highlighted the evolution of specific products prior to the main decomposition step (Fig. 8a), namely 5-hexen-1-ol for EP/mPE and EP/hbPPE. For EP/mPE-S, the spectrum shared similarities with 1-hexanol, especially via the absorption band at  $1048\text{ cm}^{-1}$  and the lack of absorption at  $917\text{ cm}^{-1}$  which corresponds to  $\delta_{\text{oop}}(\text{C-H})$  of the vinyl groups. The spectrum of EP/mPE-S-ox at  $312^\circ\text{C}$  exhibited decomposition products from the epoxy matrix, especially from phenol products, identified by the absorption bands at  $1175$  and  $749\text{ cm}^{-1}$ . Moreover, the spectrum shared similarities with the evolved gas of pure mPE-S-ox, as identified by the band at  $1140\text{ cm}^{-1}$  belonging to  $\nu_s(\text{SO}_2)$ , thus implying that some  $\text{SO}_2$ -species progressed into the gas phase. The spectra at the main decomposition step (Fig. 8b) showed the decomposition of the epoxy matrix, as evidenced by the similarities of all spectra with that of EP. As previously reported, [13] the spectrum of EP/mPE exhibited mPE signals even at the main decomposition step, most probably due to phosphorylation of the resin caused by the strong reactivity of mPE.

The resin blends were analyzed by means of pyrolysis combustion flow calorimetry (PCFC) to further understand how the evolved gas affects the gas phase. Although some FRs are known to act in the gas phase via radical scavenging, this mode of action cannot be detected in PCFC due to the complete oxidation of the pyrolysis products in the combustion zone. However, PCFC (otherwise known as micro cone calorimetry, i.e. MCC) may be used to measure fuel dilution effects, as the evolution of incombustible gases do not contribute to oxygen consumption, i.e. heat release. The production of incombustible gases can be quantified by changes in the heat of complete combustion ( $h_c^0$ ). The plot of HRR vs. time (Fig. 9) of PCFC measurements pointed to a decrease in PHRR for most flame retardant-containing EPs, with mPE-S-ox lowering the PHRR of EP by 21% ( $340\text{ W g}^{-1}$ , as opposed to  $429\text{ W g}^{-1}$  of EP). EP/mPE-S-ox also displayed the lowest heat release capacity (HRC), THE, and  $h_c^0$ , followed by EP/mPE-S (Table S2). The low molar mass S-FRs produced incombustible products during pyrolytic decomposition: For mPE-S-ox,  $\text{SO}_2$ -release was identified in Py-

GC/MS measurements, and PCFC results of EP/mPE-S-ox further illuminate that its release is a gas-phase mode of action of this FR. Moreover, mPE-S produced a S-containing compound during pyrolysis, i.e. 1-hexanethiol or a derivative thereof. As this product further decomposed, it produced incombustible gases, as indicated by the reduction in  $h_c^0$ . Notably, hbPPE did not have the same effect in lowering  $h_c^0$  as mPE-S or mPE-S-ox in EP; this is mainly due to the presence of linear and terminal units in the structure of hbPPE, which decomposed to form 1,5-hexadiene, analogous to mPE. The release of this compound contributed to the combustion heat, thus explaining the increase in  $h_c^0$  for EP/mPE compared to EP. Thus, the thio-ether groups competed with the vinyl-groups in hbPPE, leading to only moderate reduction in  $h_c^0$  of EP/hbPPE compared to EP.

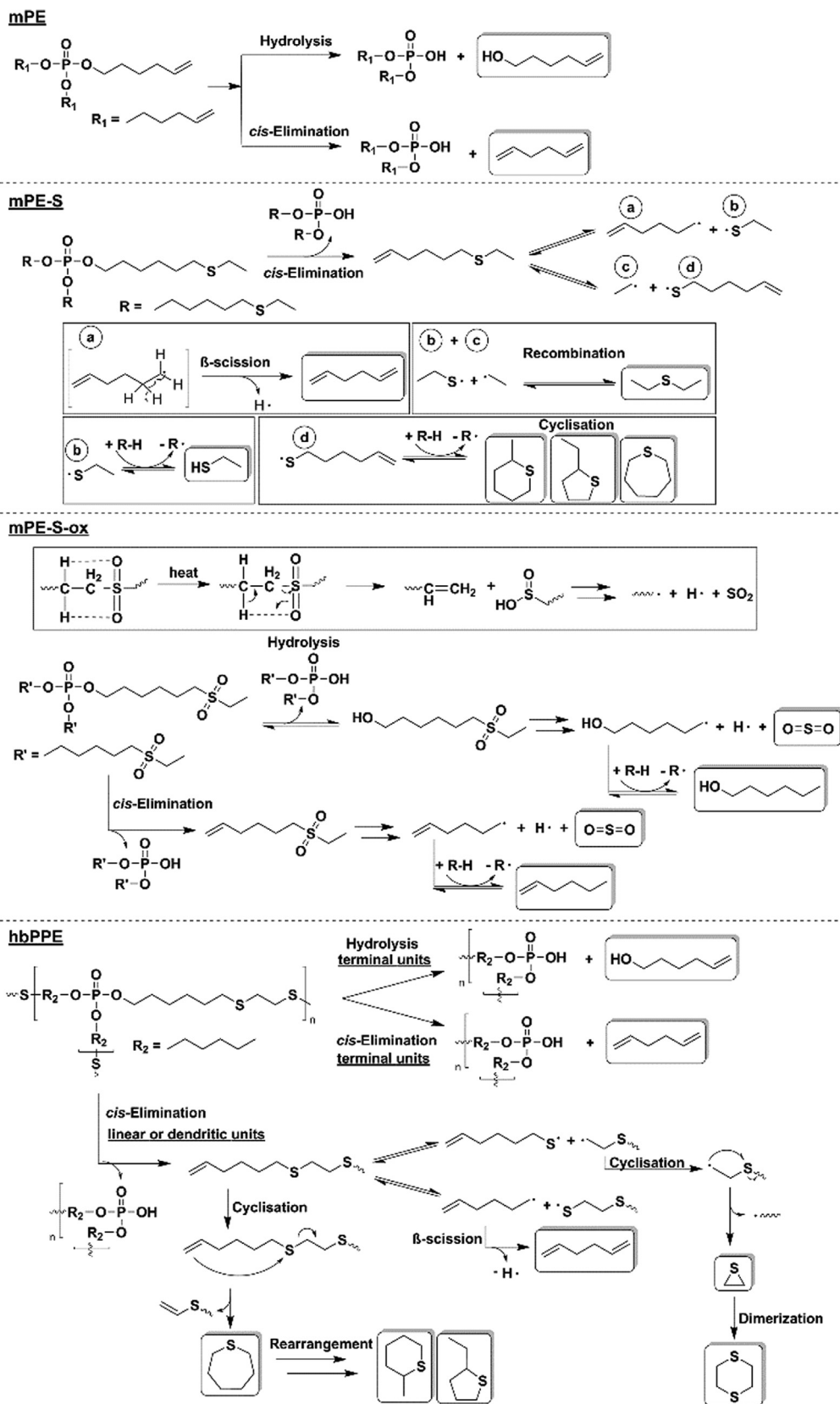
### 3.7. Pyrolysis – Condensed phase activity of resin blends

The condensed phase spectra from hot-stage FTIR measurements (Fig. 10) portrayed the change in specific absorption bands for all FR-containing EP blends. For EP/mPE-S-ox, the band of asymmetrical  $\nu(\text{SO}_2)$  was visible at  $1125\text{ cm}^{-1}$  between  $100$  and  $500^\circ\text{C}$ , indicating its presence even after the main decomposition step of EP. Moreover, both EP/mPE-S and EP/mPE-S-ox exhibited an absorption band at  $744\text{ cm}^{-1}$  at  $600^\circ\text{C}$ , which correspond to S-containing species such as  $\nu(\text{C-S})$  of  $\text{O}=\text{CH-S-Ar}$ ,  $\nu_s(\text{S-O-C})$  of  $\text{S-O-CH}_2\text{-R}$ , or  $\nu_s(\text{P}=\text{S})$  of various P and S-containing compounds [32,34]. The spectra of the S-containing EP-FRs and EP/hbPPE did not exhibit absorption bands at  $1511$ ,  $1456$  and  $832\text{ cm}^{-1}$ , where EP, EP/mPE, and EP/BDP showed signals. These bands originate from Bisphenol A-based compounds; their disappearance for EP/mPE-S, EP/mPE-S-ox, and EP/hbPPE indicates that S-FRs have a different decomposition pathway.

While the volatility of the low molar mass FRs was significantly reduced after thiol-ene reaction and oxidation (cf. TGA measurements in Fig. 3), the additional thio-ethers or sulfones affected the FR's reactivity. Phosphorylation is a major contributor to the condensed phase mode of action of P-FRs: the interaction between hydroxyl groups in the resin matrix and P-species leads to increased charring [43]. However, this process changed when polar groups such as thio-ether or sulfone were present. Thus, although all FR are active in the condensed phase and S-containing FRs exhibited higher residue amounts in EP in pyrolysis measurements (Table 3), the type of residue is notably different from sulfur-free to sulfur-containing FRs. It has been reported that the production of sulfonic acid further promotes char formation [44,45]. The presence of S-containing species may point to such a process for the tested FRs.

### 3.8. Fire testing of resin blends

Fire testing via cone calorimeter measurements was effective in examining the modes of action of the various FRs and especially the S-FRs. From the results (Table 3), a reduction of the total heat evolved (THE = total heat release [THR] at flame-out) of all EP-FRs was noted, although the degree of reduction was distinct for each FR. mPE had the strongest impact on reducing the fire load of EP, lowering THE by 28% (Fig. 11 b). The S-FRs mPE-S-ox and mPE-S exhibited a less pronounced fire load reduction of EP, only lowering its THE by 8 and 11%, respectively, whereas the benchmark FR BDP and the hyperbranched polymeric FR hbPPE both lowered THE of EP by 17 and 19%, respectively. The HRR curves (Fig. 11a) shed some light on the modes of action of the low molar mass S-FRs: About 30 s after ignition, the curves of EP/mPE and EP/hbPPE exhibited a reduction in HRR and displayed a plateau-like area resultant from the formation of a protective char layer. This plateau was also visible for EP/mPE-S and EP/mPE-S-ox, but the reduction in HRR was less pronounced; furthermore, the peak of heat release rate (PHRR) of EP/mPE-S-ox was higher than that of EP/mPE-S, indicating that the protective layer effect was stronger for the thio-ether-containing FR than for the sulfone-containing one. This point



**Scheme 2.** Proposed decomposition scheme of mPE, mPE-S, mPE-S-ox, and hbPPE. Substances in solid boxes were identified in FTIR or Py-GC/MS and comparative spectra.

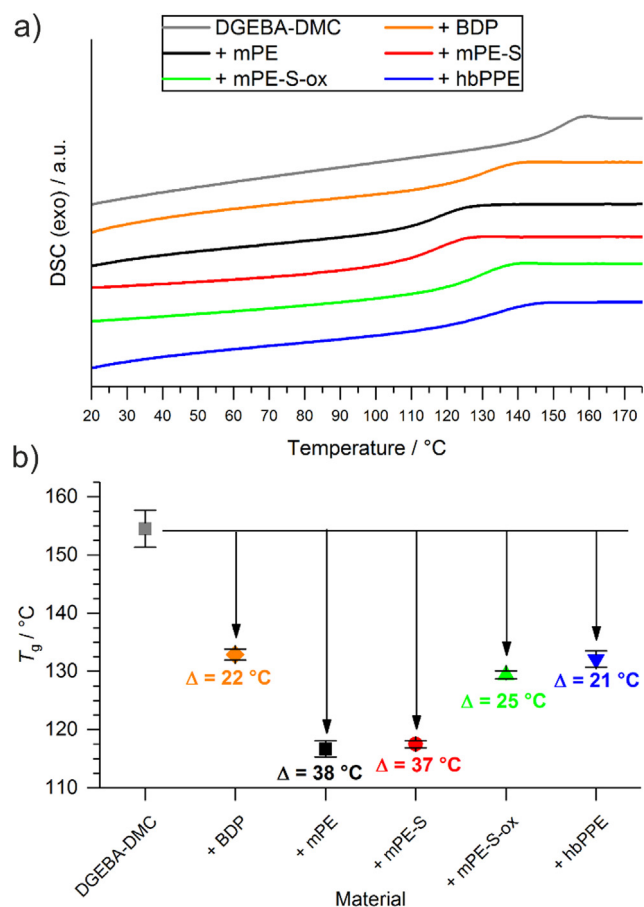


**Fig. 6.** (a) Differential scanning calorimetry (DSC) measurements of the second heating run of EP and EP-FRs; (b) Relative change in glass-transition temperature ( $T_g$ ) of EP-FRs compared to EP.

was strengthened by the fact that **EP/mPE-S** and **EP/hbPPE** had similar PHRR values; both contain thio-ether groups. The changes to THE and PHRR can be visualized via Petrella-plot, where the fire load, i.e. THE, is plotted versus the fire growth index, i.e. PHRR/time to ignition ( $t_{ig}$ ) (Fig. 11c) [46]. Both low molar mass S-FRs were able to lower fire load and fire growth index of EP in a similar manner, with **mPE-S** lowering THE of EP more strongly. However, **mPE** and **hbPPE** were more effective in lowering the fire load and fire growth rate of EP, illustrating that these materials were more able to bind fuel or create a strong protective layer than the S-FRs. This is further exemplified by the residue yields: while all FRs increased char yields (Fig. 11d), **EP/mPE-S-ox** had the second lowest char yield of all tested materials, the lowest exhibited by **EP/BDP**. Moreover, the char yield of **EP/mPE-S** was in a similar range to that of **EP/hbPPE**, further highlighting that thio-ether-containing FRs were more effective in storing fuel in the form of carbonaceous char than sulfone-containing FRs in EP blends. The S-FRs were able to create higher residue amounts in pyrolytic investigations of EP than during fire tests, and the low char yield also helps explain the higher fire loads of **EP/mPE-S** and **EP/mPE-S-ox** compared to the other EP-FRs. The low char yield in fire tests resulted from a reduced phosphorylation of the matrix, i.e. a low reactivity of the FR's decomposition products with the decomposing matrix. Moreover, **mPE-S** and **mPE-S-ox** have a lower P-content than **mPE** or **hbPPE** (Table 1), thus explaining the lower residue yields and higher fire loads in EP blends resulting from a reduced P-based condensed and gas phase activity. Fire tests proved that the high volatility and reactivity of **mPE**, as well as its higher P-content, was more effective in binding fuel compared to the thio-ether and sulfone-containing FRs. As evolved gas analysis highlighted the production of  $SO_2$  for the sulfone-containing FR, its gas

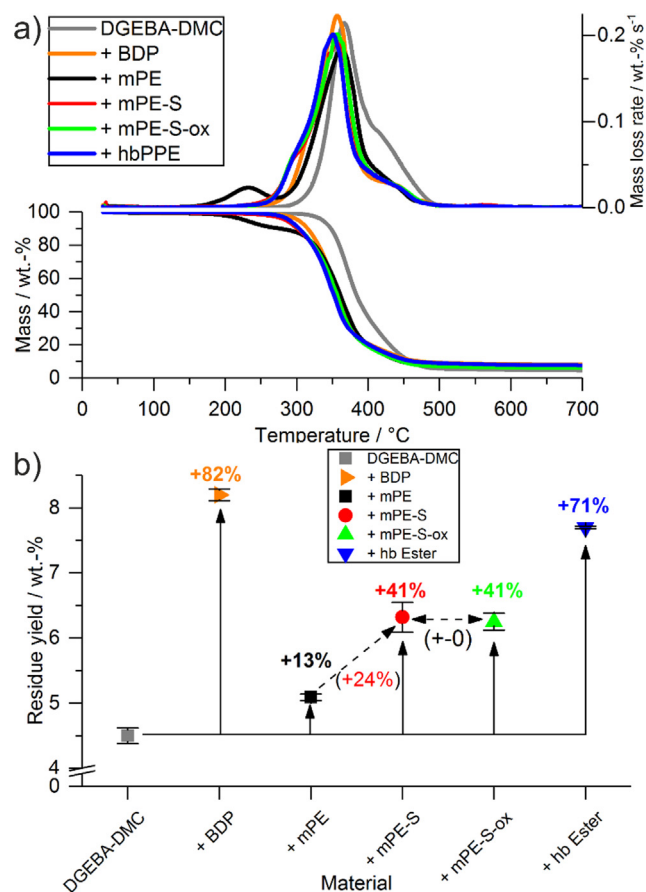


**Fig. 7.** (a) Mass loss (bottom) and mass loss rate (top) versus temperature via thermogravimetric analysis (TGA); (b) Change in residue yields at 700 °C of EP-FRs compared to EP.

diluting effect may be the main mode of action; however, it is plausible that the release of  $SO_2$  inhibited the FR to effectively bind fuel in the condensed phase. Furthermore, the reduced P-content of **mPE-S-ox** further explains the lower residue yield and protective layer effect in EP, as well as a higher fire load.

#### 4. Conclusion

To gain further insight into the flame-retardant effect of polymeric hyperbranched polyphosphoesters (**hbPPE**), the material was compared to two sulfur-containing low molar mass variants of the monomeric phosphoester **mPE**.

Pyrolytic decomposition investigations of the FRs illustrated that the increased thermal stability and higher residue yield of **hbPPE** compared to its monomer **mPE** stemmed not only from its higher molecular mass, but also from thio-ether groups present in **hbPPE**: the thio-ether-containing FR **mPE-S** displayed a higher  $T_{dec}$  and residue yield than **mPE**, and the sulfone-containing **mPE-S-ox** proved even more thermally stable and retained higher residues than **mPE-S**. The presence of sulfur altered the decomposition pathway of the P-FRs: thio-ethers promoted the production of S-radicals which cross-linked to promote residue yield, while sulfonates decomposed to release incombustible  $SO_2$ .

In epoxy resins, the sulfur-containing FRs affected the glass-transition temperature of the resin less strongly than the sulfur-free **mPE**. Moreover, the presence of sulfur decreased the volatility of the P-FRs and encouraged an overlap of decomposition temperatures of FR and matrix, thus improving chemical reactivity. Moreover, the presence of sulfur increased condensed phase activity, and several sulfur species



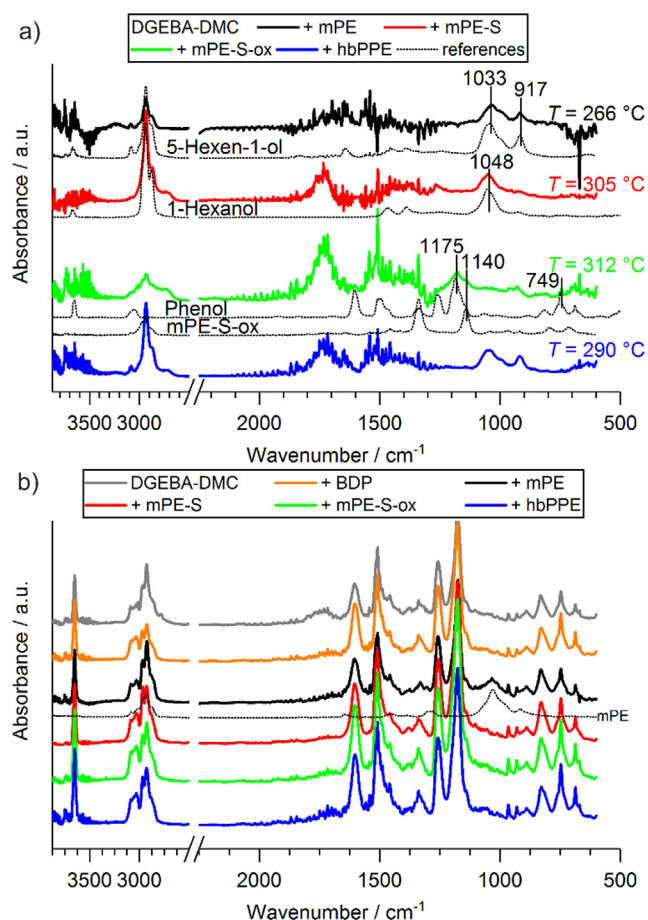


Fig. 8. TG-FTIR spectra of pyrolytic decomposition products at (a) decomposition step prior to main step, and at (b) main decomposition step.

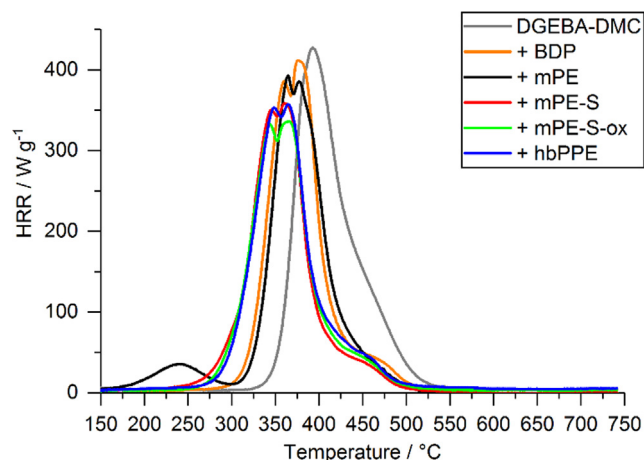


Fig. 9. Heat release rates over time of EP and EP-FRs from pyrolysis combustion flow calorimetry (PCFC).

were identified in the residues via FTIR. Fire tests of FR-containing epoxy resins exemplified that **hbPPE**'s effectiveness as an FR was not rooted solely in the presence thio-ether groups, but the occurrence of both vinyl and thio-ether groups.

The results of this study highlight that the presence of sulfur in **hbPPE** played a significant role to the multifunctional qualities of the hyperbranched P-FR, mainly by improving thermal stability, reducing the impact on  $T_g$  of epoxy resins, and adding additional chemical decomposition mechanisms in the condensed phase and thus improving

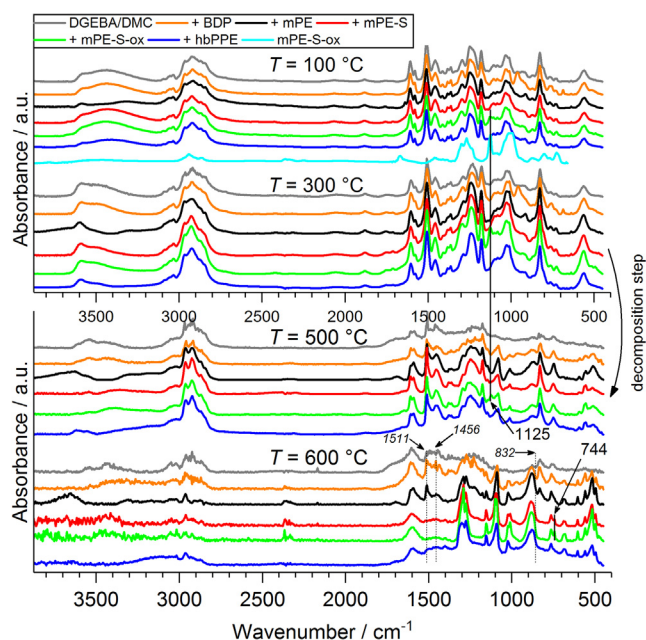


Fig. 10. Condensed phase FTIR spectra from hot stage FTIR measurements of EP and EP-FRs at specific temperatures (100, 300, 500, 600 °C). Dotted lines/italic numbers: bands not present in S-FRs.

Table 3

Results from cone calorimeter measurements.

	THE/MJ m <sup>-2</sup>	PHRR/kW m <sup>-2</sup>	μ/wt.-%	EHC/MJ kg <sup>-1</sup>
EP	108.4 ± 2.6	1696 ± 180	0.7 ± 0.1	26.9 ± 1.0
EP/BDP	87.5 ± 1.2	1180 ± 41	3.1 ± 0.2	22.7 ± 0.2
EP/mPE	78.1 ± 6.5	885 ± 16	9.2 ± 0.1	21.6 ± 1.8
EP/mPE-S	96.5 ± 0.7	958 ± 51	7.7 ± 0.0	25.2 ± 0.6
EP/mPE-S-ox	99.3 ± 5.0	1219 ± 26	4.7 ± 0.5	27.5 ± 0.4
EP/hbPPE	89.8 ± 3.0	953 ± 41	7.5 ± 0.6	24.3 ± 0.6

Total heat evolved (THE = total heat released at flame-out); peak of heat release rate (PHRR); char yield (μ); effective heat of combustion (EHC).

residue yields.

### CRedit authorship contribution statement

**Alexander Battig:** Conceptualization, Methodology, Investigation, Writing - original draft, Writing - review & editing, Visualization. **Jens C. Markwart:** Investigation, Resources, Writing - original draft, Writing - review & editing. **Frederik R. Wurm:** Conceptualization, Supervision, Funding acquisition, Writing - review & editing. **Bernhard Schartel:** Conceptualization, Supervision, Funding acquisition, Writing - review & editing.

### Declaration of Competing Interest

The authors declare that they have no known competing financial interests or personal relationships that could have appeared to influence the work reported in this paper.

### Acknowledgements

Funding: This work was supported by the Deutsche Forschungsgemeinschaft [DFG SCHA 730/151; DFG WU 750/8-1].

Alexander Battig thanks Dr. Katharina Kebelmann (BAM) for help with Py-GC/MS measurements and Patrick Klack (BAM) for support with the cone calorimeter. Jens C. Markwart is the recipient of a fellowship through funding of the Excellence Initiative (DFG/ GSC 266) in

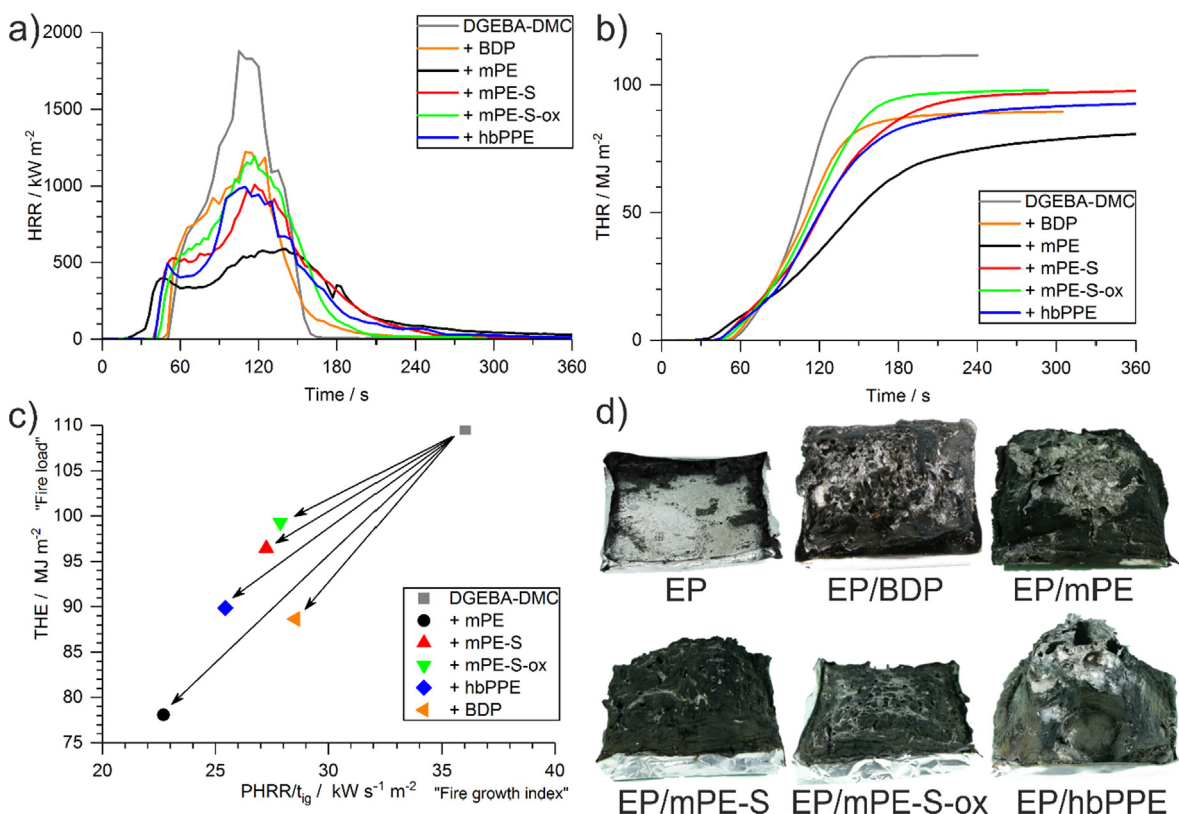


**Fig. 11.** (a) Heat release rate (HRR) versus time of EP and EP-FRs; (b) Total heat release (THR) versus time of EP and EP-FRs; (c) Petrella-plot of EP and EP-FRs; (d) Residue photographs (10 cm × 10 cm aluminum tray base) of EP and EP-FRs after cone calorimeter measurements.

the context of the graduate school of excellence "MAINZ" (Materials Science in Mainz). Frederik R. Wurm and Jens C. Markwart thank Prof. Dr. Katharina Landfester (MPIP) for support.

## Appendix A. Supplementary material

Supplementary data to this article can be found online at <https://doi.org/10.1016/j.eurpolymj.2019.109390>.

## References

- M.M. Velencoso, A. Battig, J.C. Markwart, B. Scharrel, F.R. Wurm, Molecular fire-fighting-how modern phosphorus chemistry can help solve the challenge of flame retardancy, *Angew Chem. Int. Ed.* 57 (2018) 10450–10467.
- Q.F. Wang, W.F. Shi, Kinetics study of thermal decomposition of epoxy resins containing flame retardant components, *Polym. Degrad. Stab.* 91 (2006) 1747–1754.
- C.J. Hawker, J.M.J. Fréchet, Preparation of polymers with controlled molecular architecture - a new convergent approach to dendritic macromolecules, *J. Am. Chem. Soc.* 112 (1990) 7638–7647.
- Q. Cao, P.S. Liu, Hyperbranched polyurethane as novel solid-solid phase change material for thermal energy storage, *Eur. Polym. J.* 42 (2006) 2931–2939.
- A. Asif, W.F. Shi, Synthesis and properties of UV curable waterborne hyperbranched aliphatic polyester, *Eur. Polym. J.* 39 (2003) 933–938.
- B.I. Voit, A. Lederer, Hyperbranched and highly branched polymer architectures-synthetic strategies and major characterization aspects, *Chem. Rev.* 109 (2009) 5924–5973.
- C.R. Yates, W. Hayes, Synthesis and applications of hyperbranched polymers, *Eur. Polym. J.* 40 (2004) 1257–1281.
- F. Marsico, A. Turshatov, R. Pekoz, Y. Avlasevich, M. Wagner, K. Weber, D. Donadio, K. Landfester, S. Balushev, F.R. Wurm, Hyperbranched unsaturated polyphosphates as a protective matrix for long-term photon upconversion in air, *J. Am. Chem. Soc.* 136 (2014) 11057–11064.
- J.C. Markwart, A. Battig, T. Kuckhoff, B. Scharrel, F.R. Wurm, First phosphorus AB<sub>2</sub> monomer for flame retardant hyperbranched polyphosphoesters: AB<sub>2</sub> vs. A<sub>2</sub> + B<sub>3</sub>, *Polym. Chem.* 10 (2019) 5920–5930, <https://doi.org/10.1039/c9py01156k>.
- K. Täuber, F. Marsico, F.R. Wurm, B. Scharrel, Hyperbranched poly(phosphoester)s as flame retardants for technical and high performance polymers, *Polym. Chem.-Uk* 5 (2014) 7042–7053.
- A. Battig, J.C. Markwart, F.R. Wurm, B. Scharrel, Matrix matters: hyperbranched flame retardants in aliphatic and aromatic resins, *Polym. Degrad. Stab.* 170 (2019), <https://doi.org/10.1016/j.polydegradstab.2019.108986>.
- A. Battig, J. Markwart, F.R. Wurm, B. Scharrel, Hyperbranched phosphorus flame retardants: multifunctional additives for epoxy resins, *Polym. Chem.-Uk* 10 (2019) 4346–4358.
- J.C. Markwart, A. Battig, L. Zimmermann, M. Wagner, J. Fischer, B. Scharrel, F.R. Wurm, Systematically controlled decomposition mechanism in phosphorus flame retardants by precise molecular architecture: P-O vs P-N, *ACS Appl. Polym. Mater.* 1 (2019) 1118–1128.
- B.A. Howell, Y.G. Daniel, The impact of sulfur oxidation level on flame retardancy, *J. Fire Sci.* 36 (2018) 518–534.
- S.V. Levchik, E.D. Weil, Overview of recent developments in the flame retardancy of polycarbonates, *Polym. Int.* 54 (2005) 981–998.
- J. Green, Mechanisms for flame retardancy and smoke suppression -a review, *J. Fire Sci.* 14 (1996) 426–442.
- W. Pawelec, A. Holappa, T. Tirri, M. Aubert, H. Hoppe, R. Pfaendner, C.E. Wilen, Disulfides - effective radical generators for flame retardancy of polypropylene, *Polym. Degrad. Stab.* 110 (2014) 447–456.
- J. Wagner, P. Deglmann, S. Fuchs, M. Ciesielski, C.A. Fleckenstein, M. Döring, A flame retardant synergism of organic disulfides and phosphorous compounds, *Polym. Degrad. Stab.* 129 (2016) 63–76.
- U. Braun, U. Knoll, B. Scharrel, T. Hoffmann, D. Pospiech, J. Artner, M. Ciesielski, M. Döring, R. Perez-Gratero, J.K.W. Sandler, V. Altstädt, Novel phosphorus-containing poly(ether sulfone)s and their blends with an epoxy resin: thermal decomposition and fire retardancy, *Macromol. Chem. Phys.* 207 (2006) 1501–1514.
- C.L. Rasmussen, P. Glarborg, P. Marshall, Mechanisms of radical removal by SO<sub>2</sub>, *P Combust. Inst.* 31 (2007) 339–347.
- M.R. Zachariah, O.I. Smith, Experimental and numerical-studies of sulfur chemistry in H<sub>2</sub>-O<sub>2</sub>-So<sub>2</sub> flames, *Combust. Flame* 69 (1987) 125–139.
- R.M. Perez, J.K.W. Sandler, V. Altstädt, T. Hoffmann, D. Pospiech, M. Ciesielski, M. Döring, U. Braun, A.I. Balabanovich, B. Scharrel, Novel phosphorus-modified polysulfone as a combined flame retardant and toughness modifier for epoxy resins, *Polymer* 48 (2007) 778–790.
- M. Lewin, Flame retarding of polymers with sulfamates. 1. Sulfation of cotton and wool, *J. Fire Sci.* 15 (1997) 263–276.
- M. Lewin, J. Brozek, M.M. Martens, The system polyamide/sulfamate/dipentaerythritol: flame retardancy and chemical reactions, *Polym. Adv. Technol.* 13 (2002) 1091–1102.
- M. Lewin, J. Zhang, E. Pearce, J. Gilman, Flammability of polyamide 6 using the sulfamate system and organo-layered silicatel, *Polym. Adv. Technol.* 18 (2007) 737–745.
- J.Y. He, G. Cai, C.A. Wilkie, The effects of several sulfonates on thermal and fire retardant properties of poly(methyl methacrylate) and polystyrene, *Polym. Adv.*

- Technol. 25 (2014) 160–167.
- [27] W. Zhao, B. Li, M.J. Xu, L.L. Zhang, F.M. Liu, L.M. Guan, Synthesis of a novel flame retardant containing phosphorus and sulfur and its application in polycarbonate, *Polym. Eng. Sci.* 52 (2012) 2327–2335.
- [28] Y.H. Chen, H.Q. Peng, J.H. Li, Z.X. Xia, H. Tan, A novel flame retardant containing phosphorus, nitrogen, and sulfur, *J. Therm. Anal. Calorim.* 115 (2014) 1639–1649.
- [29] B. ScharTEL, T.R. Hull, Development of fire-retarded materials - interpretation of cone calorimeter data, *Fire Mater.* 31 (2007) 327–354.
- [30] B. ScharTEL, M. Bartholmai, U. Knoll, Some comments on the main fire retardancy mechanisms in polymer nanocomposites, *Polym. Adv. Technol.* 17 (2006) 772–777.
- [31] M.S.F. Lie Ken Jie, O. Bakare, <sup>1</sup>H- and <sup>13</sup>C-NMR studies on sulfinyl and sulfonyl derivatives of positional isomers of methyl thialaurate, *Chem. Phys. Lipids*, 61 (1992) pp. 139–147.
- [32] G. Socrates, *Infrared and Raman characteristic group frequencies: tables and charts*, John Wiley & Sons, 2004.
- [33] G. Camino, L. Costa, Performance and mechanisms of fire retardants in polymers - a review, *Polym. Degrad. Stab.* 20 (1988) 271–294.
- [34] M. Hesse, H. Meier, B. Zeeh, *Spektroskopische Methoden in der organischen Chemie*, Georg Thieme Verlag, 2005.
- [35] P.J. Linstrom, Mallard, W.G., NIST Standard Reference Database Number 69, in, 2018.
- [36] J.P. Machon, A. Nicco, Thermal decomposition reactions of oligomeric thioethers of polythioethene and polythiotrimethylene, *Eur. Polym. J.* 7 (1971) 1693–2000.
- [37] F. Vögtle, L. Rossa, Pyrolysis of sulfones as a synthetic method, *Angew. Chem.-Int. Ed. English* 18 (1979) 515–529.
- [38] E. Wellisch, E. Gipstein, O.J. Sweeting, Thermal decomposition of polysulfones, *J. Appl. Polym. Sci.* 8 (1964) 1623–1631.
- [39] E. Wellisch, O.J. Sweeting, E. Gipstein, Thermal decomposition of sulfinic acids, *J. Org. Chem.* 27 (1962) 1810–2000.
- [40] M. Ciesielski, B. Burk, C. Heinzmann, M. Döring, Fire-retardant high-performance epoxy-based materials, in: D.-Y. Wang (Ed.), *Novel Fire Retardant Polymers and Composite Materials*, Woodhead Publishing, 2017, pp. 3–51.
- [41] J.M.G. Cowie, V. Arrighi, *Polymers: chemistry and physics of modern materials*, CRC Press, 2007.
- [42] J. Eichhorn, Synergism of free radical initiators with self-extinguishing additives in vinyl aromatic polymers, *J. Appl. Polym. Sci.* 8 (1964) 2497–2524.
- [43] B. ScharTEL, B. Perret, B. Dittrich, M. Ciesielski, J. Krämer, P. Müller, V. Altstädt, L. Zang, M. Döring, Flame retardancy of polymers: the role of specific reactions in the condensed phase, *Macromol. Mater. Eng.* 301 (2016) 9–35.
- [44] A. Ballistreri, G. Montaudo, E. Scamporrino, C. Puglisi, D. Vitalini, S. Cucinella, Intumescent flame retardants for polymers. 4. The polycarbonate aromatic sulfonates system, *J. Polym. Sci. Pol. Chem.* 26 (1988) 2113–2127.
- [45] A. Nodera, T. Kanai, Thermal decomposition behavior and flame retardancy of polycarbonate containing organic metal salts: effect of salt composition, *J. Appl. Polym. Sci.* 94 (2004) 2131–2139.
- [46] R. Petrella, The assessment of full-scale fire hazards from cone calorimeter data, *J. Fire Sci.* 12 (1994) 14–43.



## Supplemental Information

### “Sulfur’s Role in the Flame Retardancy of Thio-Ether–linked Hyperbranched Poly(phosphoesters) in Epoxy Resins”

Alexander Battig,<sup>a,‡</sup> Jens C. Markwart,<sup>b,c,‡</sup> Frederik R. Wurm,<sup>\*,b</sup> and Bernhard Schartel<sup>\*,a</sup>

<sup>a</sup> Bundesanstalt für Materialforschung und -prüfung (BAM), Unter den Eichen 87, 12205 Berlin, Germany.

<sup>b</sup> Max Planck Institute for Polymer Research, Ackermannweg 10, 55128 Mainz, Germany.

<sup>c</sup> Graduate School Materials Science in Mainz, Staudinger Weg 9, 55128 Mainz, Germany.

<sup>‡</sup> these authors contributed equally

<sup>\*</sup> corresponding authors:

Bernhard Schartel, Bundesanstalt für Materialforschung und -prüfung (BAM), Unter den Eichen 87, 12205 Berlin, Germany. [bernhard.schartel@bam.de](mailto:bernhard.schartel@bam.de);

Frederik R. Wurm, Max-Planck-Institut für Polymerforschung, Ackermannweg 10, 55128 Mainz, Germany. [wurm@mpip-mainz.mpg.de](mailto:wurm@mpip-mainz.mpg.de)

#### Pyrolysis–Gas Chromatography/ Mass Spectrometry

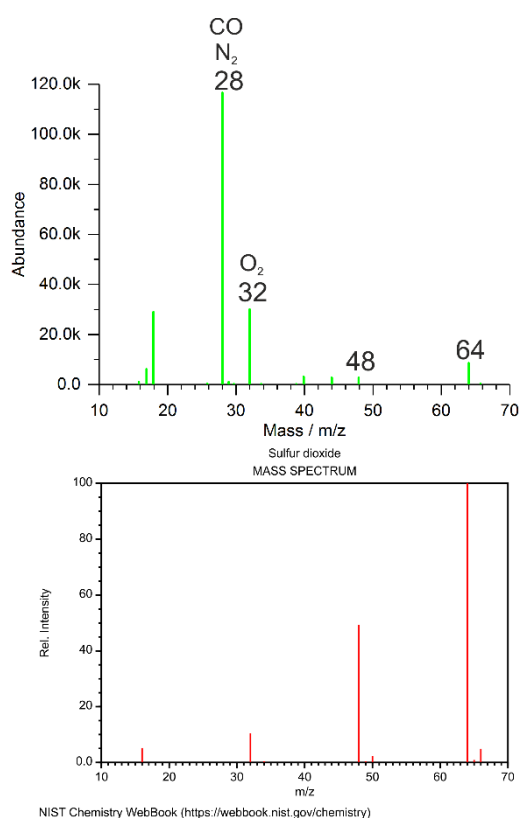


Figure S1. Mass spectrum of mPE-S-ox at 1.92 min, and a comparative spectrum of sulfur dioxide from the NIST database.<sup>1</sup>

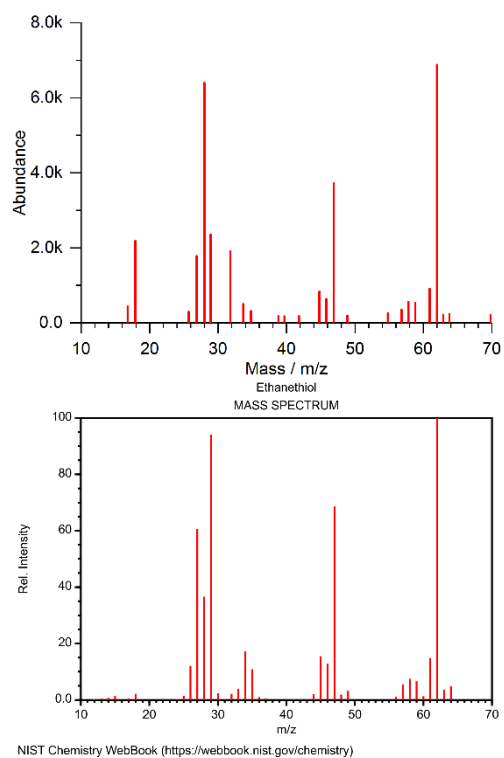


Figure S2. Mass spectrum of mPE-S at 2.26 min, and a comparative spectrum of ethanethiol from the NIST database.<sup>1</sup>

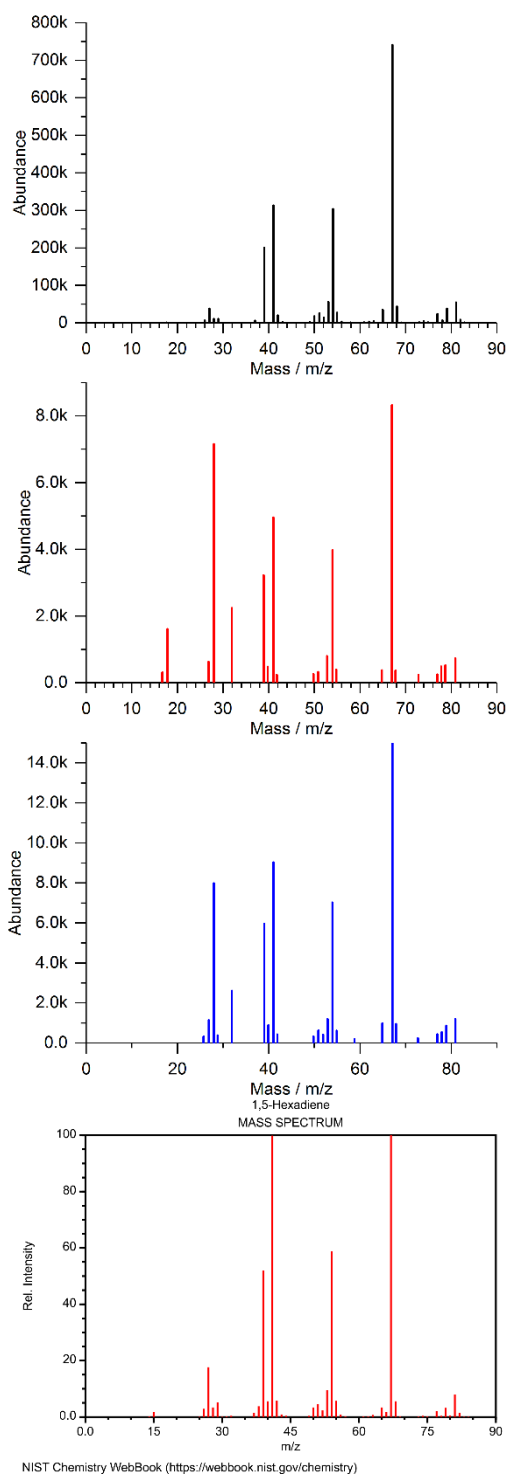


Figure S3. Mass spectra of mPE, mPE-S, and hbPPE at 2.63 min, and a comparative spectrum of 1,5-hexadiene from the NIST database.<sup>1</sup>

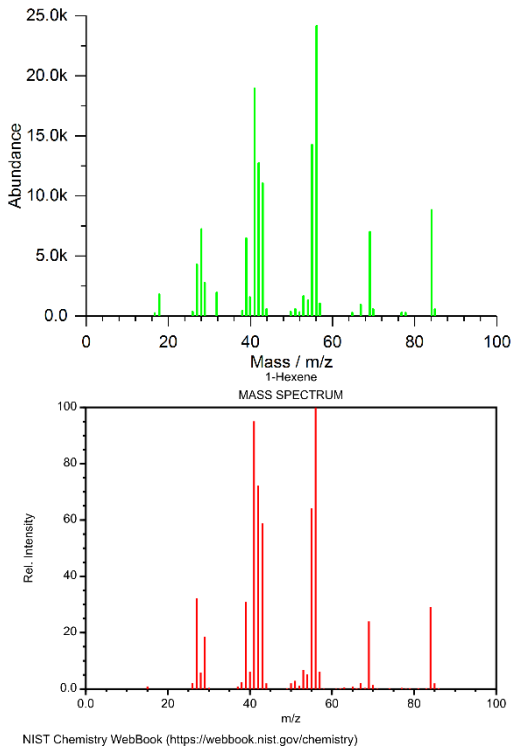


Figure S4. Mass spectrum of mPE-S-ox at 2.64 min, and a comparative spectrum of 1-hexene from the NIST database.<sup>1</sup>

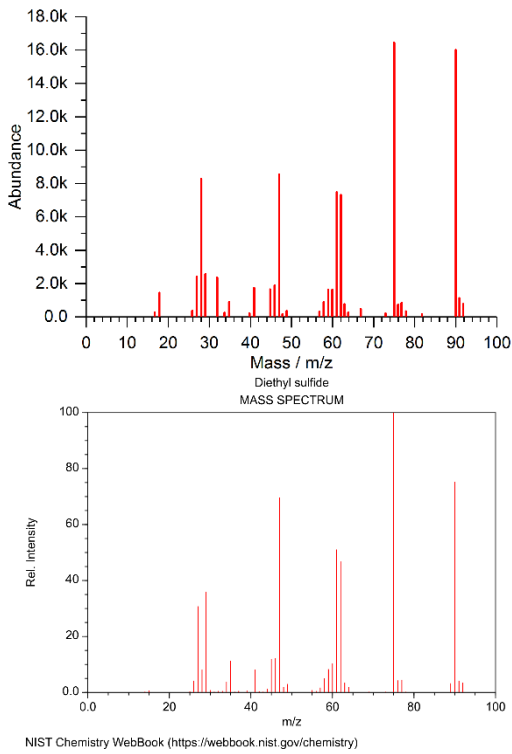


Figure S5. Mass spectrum of mPE-S at 3.38 min, and a comparative spectrum of diethyl sulfide from the NIST database.<sup>1</sup>

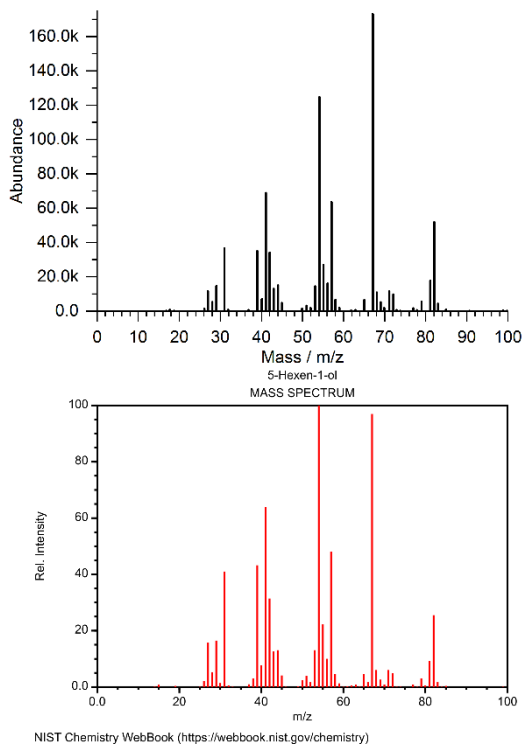


Figure S6. Mass spectrum of mPE at 6.63 min, and a comparative spectrum of 5-hexene-1-ol from the NIST database.<sup>1</sup>

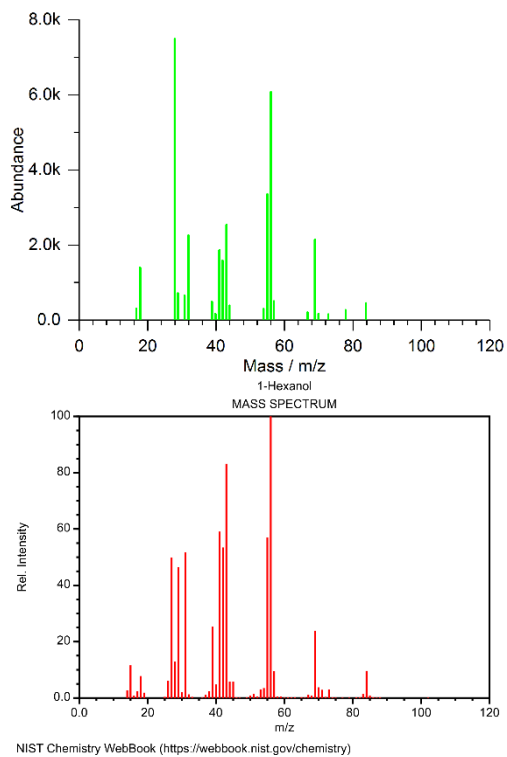


Figure S7. Mass spectrum of mPE-S-ox at 6.68 min, and a comparative spectrum of 1-hexanol from the NIST database.<sup>1</sup>

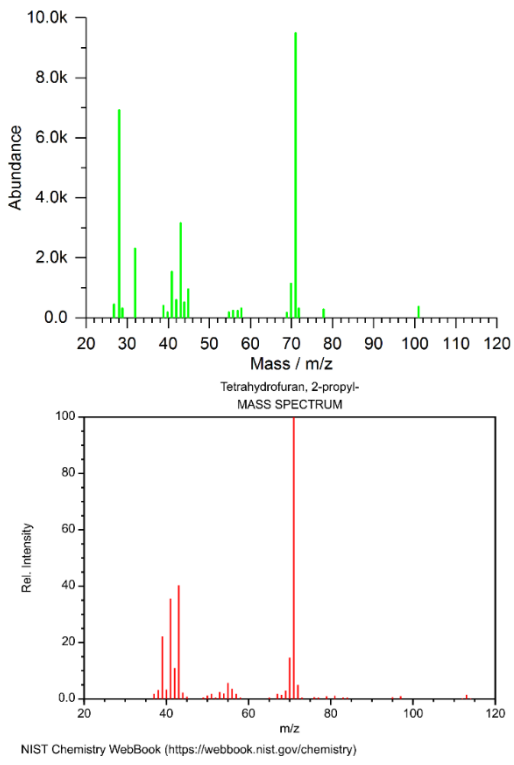


Figure S8. Mass spectrum of mPE-S-ox at 7.75 min, and a comparative spectrum of 2-propyl tetrahydrofuran from the NIST database.<sup>1</sup>

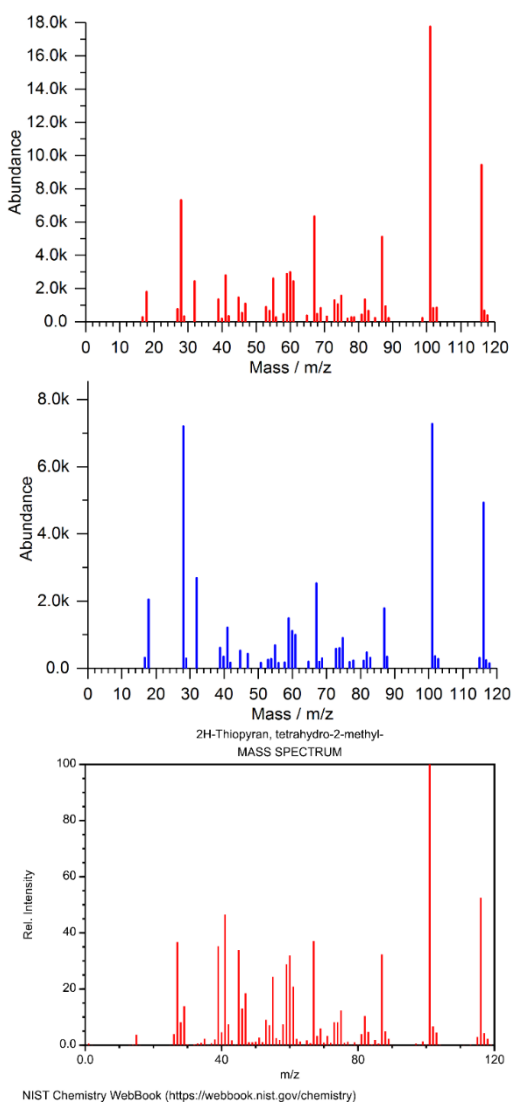


Figure S9. Mass spectra of mPE-S and hbPPE at 7.79 min, and a comparative spectrum of tetrahydro-2-methyl 2H-thiopyran from the NIST database.<sup>1</sup>



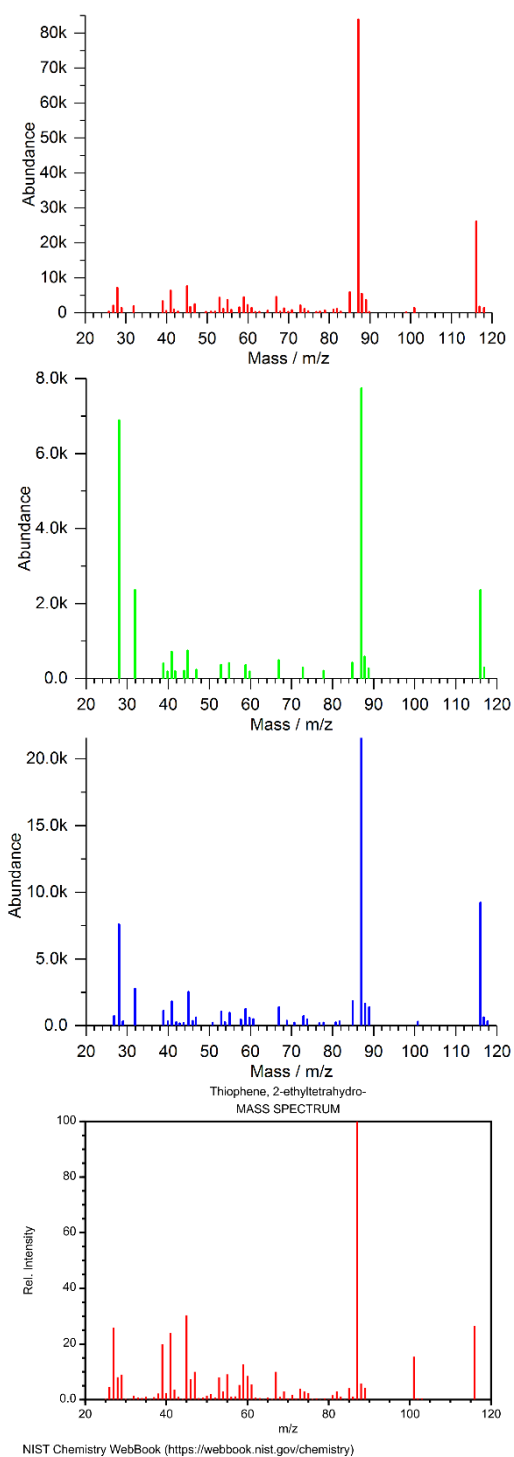


Figure S10. Mass spectra of mPE-S, mPE-S-ox, and hBPPE at 8.21 min, and a comparative spectrum of 2-ethyltetrahydro thiophene from the NIST database.<sup>1</sup>

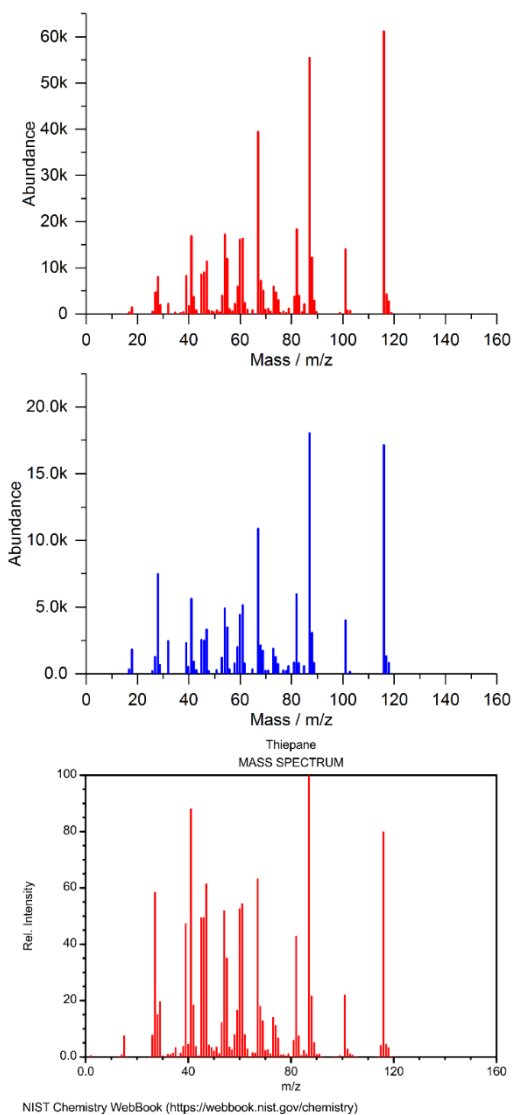


Figure S11. Mass spectrum of mPE-S and hbPPE at 9.29 min, and a comparative spectrum of thiopane from the NIST database.<sup>1</sup>

## Thermogravimetric Analysis

Table S1. Results from thermogravimetric analysis (TGA) of EP and EP-FRs.

	$T_{5\%}$ / °C	$T_1$ / °C	ML <sub>1</sub> / wt.-%	$T_{max}$ / °C	ML <sub>max</sub> / wt.-%	$T_2$ / °C	ML <sub>2</sub> / wt.-%	Residue (700 °C) / wt.-%	Residue (calc) / wt.-%
EP	338 ±1	-	-	372 ±1	62.0 ±0.8	424 ±5	33.2 ±0.3	4.5 ±0.1	-
EP/BDP	304 ±1	-	-	357 ±1	74.6 ±0.2	423 ±1	16.1 ±0.3	8.2 ±0.1	4.2
EP/mPE	231 ±1	233 ±1	8.9 ±0.1	337 ±1	77.8 ±0.1	422 ±1	7.4 ±0.2	5.1 ±0.6	4.3
EP/mPE-S	286 ±1	294 ±1	9.8 ±0.2	358 ±1	73.0 ±0.1	434 ±1	8.8 ±0.1	6.3 ±0.2	4.7
EP/mPE-S-ox	289 ±2	286 ±1	10.2 ±0.2	356 ±0	73.1 ±0.3	430 ±0	9.6 ±0.6	6.3 ±0.1	5.3
EP/hbPPE	289 ±1	-	-	351 ±1	54.6 ±0.1	424 ±6	23.2 ±0.7	7.7 ±0.1	5.2

Onset temperature ( $T_{5\%}$ ); decomposition temperature of step prior to  $T_{max}$  ( $T_1$ ); mass loss of decomposition step at  $T_1$  (ML<sub>1</sub>); temperature at maximum mass loss rate ( $T_{max}$ ); mass loss of  $T_{max}$  (ML<sub>max</sub>), decomposition temperature of step after  $T_{max}$  ( $T_2$ ); mass loss of  $T_2$  (ML<sub>2</sub>).

## Pyrolysis Combustion Flow Calorimetry

Table S2. Results from PCFC measurements

	HRC / J g <sup>-1</sup> K <sup>-1</sup>	PHRR / W g <sup>-1</sup>	THE / kJ g <sup>-1</sup>	Residue / wt.-%	$h_c^0$ / kJ g <sup>-1</sup>
EP	434 ±7	429 ±4	32.0 ±0.3	2.0 ±0.1	32.7 ±0.3
EP/BDP	413 ±1	381 ±3	30.1 ±0.4	6.2 ±0.1	32.1 ±0.4
EP/mPE	431 ±9	389 ±6	32.7 ±0.3	2.5 ±0.5	33.5 ±0.1
EP/mPE-S	396 ±13	353 ±4	30.4 ±0.1	4.9 ±0.6	31.9 ±0.3
EP/mPE-S-ox	349 ±7	340 ±7	30.0 ±0.2	4.9 ±0.1	31.5 ±0.2
EP/hbPPE	447 ±1	439 ±5	30.5 ±0.3	5.7 ±0.1	32.4 ±0.4

Heat release capacity (HRC); Peak of heat release rate (PHRR); Total heat evolved (THE); heat of complete combustion ( $h_c^0$ ).

## References

1. Linstrom, P. J., Mallard, W.G., NIST Standard Reference Database Number 69. 2018.

## 5.7. First phosphorus AB<sub>2</sub> monomer for flame-retardant hyperbranched polyphosphoesters: AB<sub>2</sub> vs. A<sub>2</sub> + B<sub>3</sub>

Jens C. Markwart, Alexander Battig, Thomas Kuckhoff, Bernhard Schartel, Frederik R. Wurm, *RSC Polym. Chem.* **2019**, 10, 5920-5930. - Published by The Royal Society of Chemistry

DOI link: <https://www.doi.org/10.1039/c9py01156k>

This article was accepted and published.

Author contribution:

- Aided in conceptualizing the frame of the work
- Chose the polymer materials, approach, loading, sample preparation and testing
- Pyrolytic investigations of the flame retardants (FRs)
  - Thermogravimetric analysis
  - Evolved gas and condensed phase FTIR
  - Pyrolysis gas chromatography / mass spectrometry
  - Pyrolysis combustion flow calorimeter
- Material and fire testing of FR-containing epoxy resins
  - Differential scanning calorimeter
  - Cone calorimeter, LOI and UL-94
  - Residue photography
- Collection, analysis, and interpretation of the data.
- Provided figures throughout the article, including decomposition mechanism
- Authored the results and discussion chapter with respect to flame-retardancy
- Scientific discussion, conclusions, maintained communication of all authors
- Proofread and spell-checked all versions of the article

## Abstract

Branched polymers are an important class of polymers with a high number of terminal groups, lower viscosity compared to their linear analogs and higher miscibility, which makes them especially interesting for flame retardant applications, where the flame retardants (FR) are blended with another polymer matrix. Hyperbranched polyphosphoesters (*hbPPEs*) are gaining more and more interest in the field of flame retardancy, as low molar mass FRs often have the disadvantage of blooming out or leaching, which is not desired in consumer products. Here, we present the first phosphorus-based  $AB_2$  monomer for the synthesis of *hbPPEs* and assess its flame-retardant performance in an epoxy resin compared to a *hbPPE* synthesized by an  $A_2+B_3$  approach. The *hbPPE* synthesized from an  $AB_2$  monomer exhibited a slightly higher performance compared to a similar *hbPPE*, which was prepared by  $A_2+B_3$  polyaddition, probably due to its higher phosphorus content.



Cite this: *Polym. Chem.*, 2019, **10**, 5920

# First phosphorus AB<sub>2</sub> monomer for flame-retardant hyperbranched polyphosphoesters: AB<sub>2</sub> vs. A<sub>2</sub> + B<sub>3</sub>†

Jens C. Markwart, <sup>‡a,b</sup> Alexander Battig, <sup>‡c</sup> Thomas Kuckhoff,<sup>a</sup> Bernhard Schartel <sup>\*c</sup> and Frederik R. Wurm <sup>\*a</sup>

Branched polymers are an important class of polymers with a high number of terminal groups, lower viscosity compared to their linear analogs and higher miscibility, which makes them especially interesting for flame retardant applications, where the flame retardants (FR) are blended with another polymer matrix. Hyperbranched polyphosphoesters (*hb*PPEs) are gaining more and more interest in the field of flame retardancy, as low molar mass FRs often have the disadvantage of blooming out or leaching, which is not desired in consumer products. Here, we present the first phosphorus-based AB<sub>2</sub> monomer for the synthesis of *hb*PPEs and assess its flame-retardant performance in an epoxy resin compared to a *hb*PPE synthesized by an A<sub>2</sub> + B<sub>3</sub> approach. The *hb*PPE synthesized from an AB<sub>2</sub> monomer exhibited a slightly higher performance compared to a similar *hb*PPE, which was prepared by A<sub>2</sub> + B<sub>3</sub> polyaddition, probably due to its higher phosphorus content.

Received 1st August 2019,  
Accepted 24th September 2019

DOI: 10.1039/c9py01156k

rsc.li/polymers

## Introduction

Hyperbranched (*hb*) polymers, with their high number of terminal groups, lower viscosity, and higher matrix miscibility compared to their linear analogs, are especially interesting as flame-retardant additives, as effective blending with a polymer matrix is essential.<sup>1–5</sup> Moreover, flame retardants (FRs) with complex architectures have a decreased impact on the material properties of polymers.<sup>6,7</sup>

The synthesis of such dendritic polymers can be achieved by multi-step dendrimer syntheses, which are time-consuming, often need several purification steps and therefore unattractive for large scale, flame-retardant applications.<sup>1,8</sup> In contrast, *hb* polymers are readily available by one polymerization step, *e.g.* by polycondensation of commercially available A<sub>2</sub> + B<sub>3</sub> monomer mixtures. *hb* polymers do not exhibit an architecture as perfect as dendrimers, because the polymers are statistically branched with structural and molar mass dispersities. Despite

these architectural differences, *hb* polymers still retain many of the particular properties of dendrimers.<sup>1,3</sup>

Here, we present, to the best of our knowledge, the first phosphorus-based AB<sub>2</sub> monomer for the synthesis of *hb* polyphosphoesters (*hb*PPEs), which are promising candidates as halogen-free flame-retardant additives.

To date, *hb*PPEs were synthesized by A<sub>2</sub> + B<sub>3</sub> approaches or by using AB\* inimers, for which representative examples are given in Scheme 1. Penczek *et al.* prepared a family of oligomers with acidic end groups by an A<sub>2</sub> + B<sub>3</sub> approach by addition of H<sub>3</sub>PO<sub>4</sub> to a bisphenol A based epoxy resins.<sup>9</sup> Liu *et al.* described a water-soluble *hb*PPE through a self-condensing ring-opening polymerization of an AB\* inimer (2-(2-hydroxyethoxy)ethoxy-2-oxo-1,3,2-dioxaphospholane).<sup>10</sup> More recently, we used radical polyaddition of phosphorus-based B<sub>3</sub>-monomers with dithiols to prepare *hb*PPEs, polyphosphoramidates, and -amides to elucidate their decomposition mechanism as flame-retardant additives in epoxy resins.<sup>11</sup>

Previous studies used *hb*PPEs due to their biocompatibility and biodegradability for mostly biomedical<sup>12,13</sup> or optical applications.<sup>14</sup> With the ban of some halogenated FRs, phosphorus-based derivatives as effective alternatives are in growing demand in recent years.<sup>15–18</sup> Moreover, polymeric FRs are interesting as they exhibit less blooming out or leaching compared to low molar mass FRs, which is not desired in consumer products.<sup>19</sup> In addition, the thermal stability of low molar mass FRs is usually lower, thus limiting their processability. In comparison, oligomeric or polymeric FRs exhibit

<sup>a</sup>Physical Chemistry of Polymers, Max Planck Institute for Polymer Research, Ackermannweg 10, 55128 Mainz, Germany. E-mail: wurm@mpip-mainz.mpg.de

<sup>b</sup>Graduate School Materials Science in Mainz, Staudinger Weg 9, 55128 Mainz, Germany

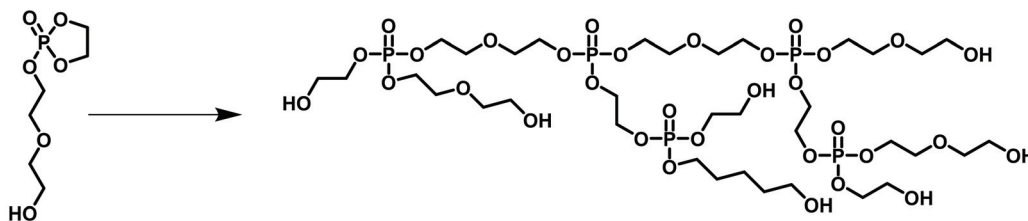
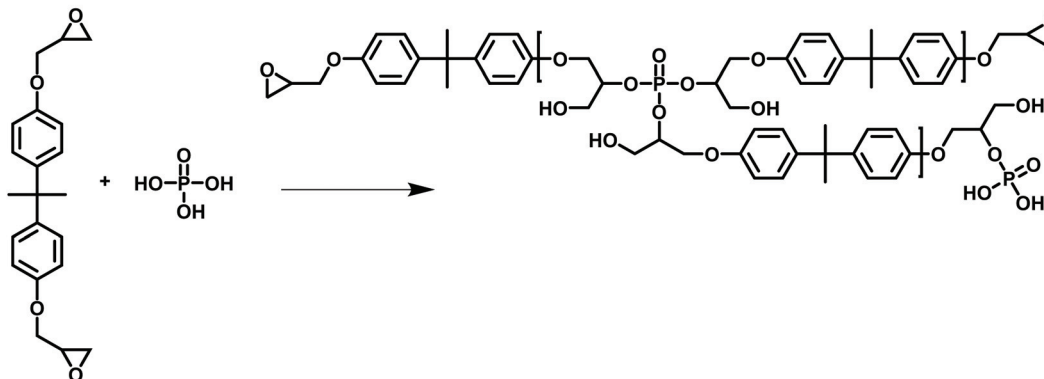
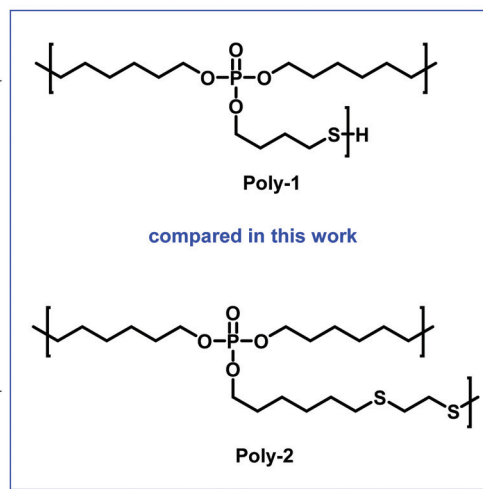
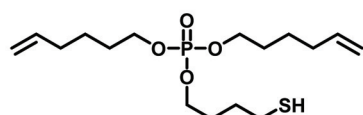
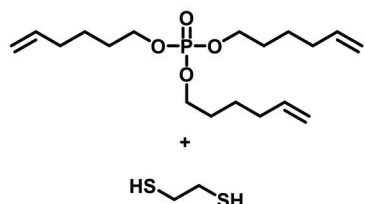
<sup>c</sup>Bundesanstalt für Materialforschung und -prüfung (BAM), Unter den Eichen 87, 12205 Berlin, Germany

†Electronic supplementary information (ESI) available. See DOI: 10.1039/c9py01156k

‡These authors contributed equally to this work.



## a) Inimer approach (by Liu et al.):

b) A<sub>2</sub> + B<sub>3</sub> approach (by Penczek et al.):c) AB<sub>2</sub> approach (this work):d) A<sub>2</sub> + B<sub>3</sub> approach (our previous work):

**Scheme 1** Examples of *hbPPEs* in literature: (a) *hbPPEs* via inimer approach by Yan et al.<sup>10</sup> (b) A<sub>2</sub> + B<sub>3</sub> approach by Penczek et al.<sup>9</sup> (c) this work: AB<sub>2</sub> monomer and (d) the comparison A<sub>2</sub> + B<sub>3</sub> approach by Battig et al.<sup>11</sup>

increased thermal stability and therefore higher effectiveness, which leads to improved chemical interaction during decomposition, yielding higher char yields and better overall flame retardancy.<sup>11,20,21</sup> Furthermore, FRs with different architectures have been investigated, stressing the impact of complex chemical structure on the mechanical properties and glass-transition temperature ( $T_g$ ) of the polymer matrix.

With the first example of an AB<sub>2</sub>-type phosphate monomer for radical polycondensation, we present a straightforward approach to *hbPPEs* and thus avoid the chance of cross-linking during the synthesis. In addition, the versatile monomer

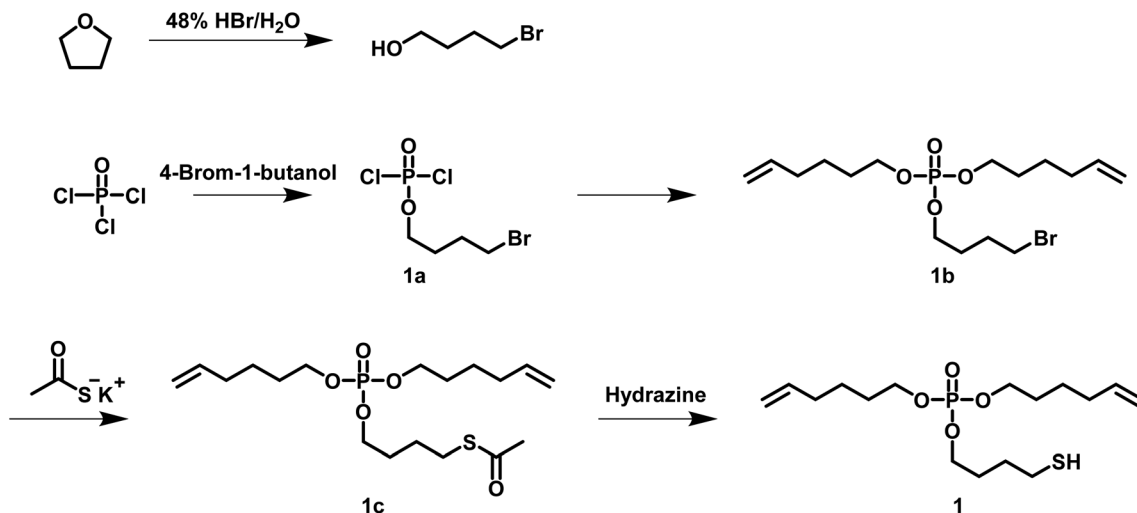
design, which was exemplarily used for **1**, allows further tuning of the P-content or the hydrophilicity, *i.e.* matrix compatibility, by variation of the alkyl-spacers, which makes the herein presented approach also applicable for other polymer matrices.

## Results and discussion

For the synthesis of hyperbranched (*hb*) polymers, two common approaches exist: The AB<sub>*n*</sub> and A<sub>*n*</sub> + B<sub>*m*</sub> approach.<sup>22</sup> In







Scheme 2 Synthesis scheme of di(hex-5-en-1-yl)(4-mercaptobutyl)phosphate (**1**).

the  $AB_n$  approach, first envisioned by Flory in 1952, only a single monomer with an  $AB_n$  ( $n \geq 2$ ) structure is used.<sup>23</sup> When A and B groups react selectively with each other, a statistically branched polymer without cross-linking is generated.<sup>24</sup>

In the  $A_n + B_m$  approach, two monomers are used for polymerization ( $A_n$  and  $B_m$  ( $n, m \geq 2$ )), with the most common method being the  $A_2 + B_3$  approach, as several monomers are commercialized. However, to obtain soluble polymers, the polymerization needs to be terminated before the gel point, which requires adjustment of the reaction conditions, or adjustment of the monomer feed-ratio, *etc.* for each monomer set.<sup>24–26</sup>

For the synthesis of a *hb* polyphosphoester (*hbPPE*) via the  $AB_n$  approach, an  $AB_2$  phosphoester with two different reactive groups (A and B) was prepared: di(hex-5-en-1-yl)(4-mercaptobutyl)phosphate (**1**) was synthesized in a four step reaction, starting from  $POCl_3$  and 4-bromobutan-1-ol (Scheme 2). 4-Bromobutan-1-ol was obtained from refluxing THF with HBr for several hours, followed by neutralizing with  $NaHCO_3$  and extraction with DCM, according to a literature protocol.<sup>27</sup> An excess  $POCl_3$  was reacted with 4-bromobutan-1-ol. Removing the excessive amount of  $POCl_3$  gives compound **1a**. **1a** was used in the next step without further purification and treated with 5-hexen-1-ol to give compound **1b**. The electrophilic alkyl bromide in **1b** renders it a versatile precursor for various modifications like the introduction of other functional groups or as a monomer for ADMET itself. **1b** was mixed with potassium thioacetate and stirred overnight to obtain compound **1c**, which was purified by solvent extraction. The final  $AB_2$ -monomer **1** for radical polyaddition was obtained after treating **1c** with hydrazine, which cleaved the thioacetate group and released the free thiol. Monomer **1** is a liquid at room temperature and has a phosphorus content of 8.84 wt%. It is soluble in most organic solvents (*e.g.* toluene, tetrahydrofuran, ethyl acetate, acetone, dichloromethane and chloroform), but insoluble in water. It is important to mention that the butyl

spacer between thiol and phosphorus is essential for the monomer stability: a similar monomer structure with an ethyl spacer was recently used to prepare linear PPEs with pendant 2-acetylthioethyl side chains.<sup>28</sup> In this case, the pendant group acted as a protective group for the P-OH group after treatment with hydrazine, followed by a 3-*exo-tet* mechanism to release the P-OH group after cleavage of the phosphoester.

$^1H$  NMR spectroscopy (Fig. 1a) of **1** revealed two distinct resonances at 2.60 ppm (methylene group next to the thiol) and 1.36 ppm (SH). The olefinic signals were detected as multiplets in the region of 5.80 ppm and 5.00 ppm. The methylene group next to the double bond was found at 2.09 ppm and the methylene group next to the P-O group had a resonance at 4.05 ppm. The remaining signals of the methylene units were detected between 1.81 ppm and 1.45 ppm. The  $^{31}P$  NMR spectrum shows a single signal at  $-0.68$  ppm (Fig. 1c).

Compound **1** was used as  $AB_2$  monomer for the radical thiol-ene polyaddition to produce *hb poly-1* (Scheme 3). The statistically branched polymer with dendritic (D), linear (L), and terminal (T) units (*cf.* Scheme 3) was obtained as a viscous oil with a  $T_g$  of *ca.*  $-88$  °C (Fig. 1i). The  $^1H$  NMR pattern of **poly-1** was very similar to that of **1** (Fig. 1b); however, with increasing degree of polymerization, the olefinic resonances, the methylene group next to the S-H group and the S-H signal decreased. Due to signal overlap, calculation of a degree of branching was not possible. The polymerization was followed by GPC and NMR by taking samples throughout the reaction and calculating the ratio between the methylene groups next to the P-O ( $n_{Ester}$ ) and the double bond ( $n_{Double-bond}$ )  $n_{Double-bond}/n_{Ester}$  (marked blue in Fig. 1f). During polymerization, a new resonance appeared at 2.54 ppm representing the methylene groups next to the thioethers. Polymerization was conducted at different temperatures (50 °C, 70 °C, and 90 °C) with 0.03 eq. AIBN and additionally with different amounts of AIBN (0.03 eq., 0.06 eq. and 0.09 eq.) at 70 °C (*e.g.* Fig. 1h).



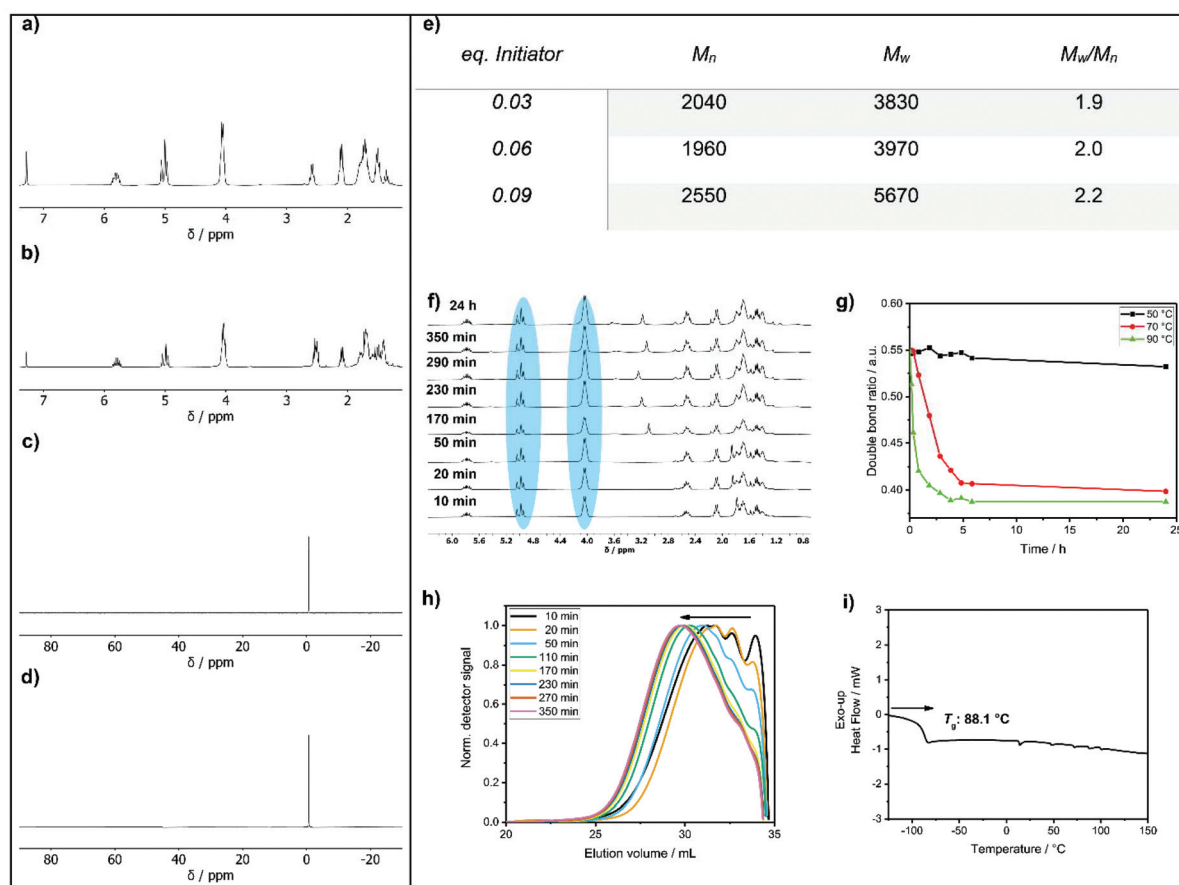
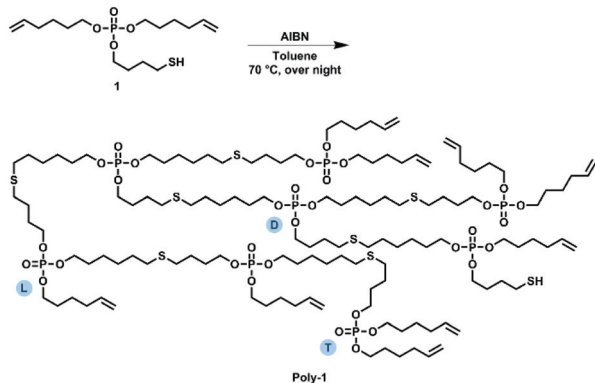


**Fig. 1**  $^1\text{H}$  NMR spectra of **1** (a) and **poly-1** (b);  $^{31}\text{P}$  NMR spectra of **1** (c) and **poly-1** (d). (e) Molar masses of the polymer at different initiator equivalents; (f)  $^1\text{H}$  NMR kinetic of the polymerization of **1** at 90 °C and 0.03 eq. AIBN. (g) Polymerization kinetics measured by NMR (change of  $n_{\text{Double-bond}}/n_{\text{Ester}}$  over time) at different temperatures (50 °C, 70 °C and 90 °C). (h) GPC kinetics of the polymerization of **1** with 0.09 eq. AIBN (measured in DMF). (i) Differential scanning calorimetry (DSC) of **poly-1** with a  $T_g$  at 88.1 °C.



**Scheme 3** Hyperbranching polymerization of monomer **1** to **poly-1** by radical thiol-ene polyaddition.

From the NMR data, only very slow reaction kinetics were detected at 50 °C, while at elevated temperatures (70 °C), no further reaction was observed after 7 h (Fig. 1g). With increasing initiator concentration, a slight increase in molar mass was observed (Fig. 1e). The  $^{31}\text{P}$  NMR resonance of **poly-1**

remained relatively unchanged compared to the monomer with a single signal at  $-0.70$  ppm (Fig. 1d). As the degree of polymerization increased,  $n_{\text{Double-bond}}/n_{\text{Ester}}$  became smaller.

For the flame retardancy investigations, the resulting polymer had an  $M_w$  of  $5500 \text{ g mol}^{-1}$  with an  $M_w/M_n$  of 2.39 (GPC in DMF). **Poly-1** was used as an additive flame retardant (FR) in epoxy resins, and the FR properties were compared to a similar *hbPPE* prepared by the  $A_2 + B_3$  approach (**poly-2**, Scheme 1),  $M_w$  of  $11300 \text{ g mol}^{-1}$  with an  $M_w/M_n$  of 3.29 (GPC in THF),<sup>11</sup> and a commercial phosphate-based FR, namely bisphenol A bis(diphenyl phosphate) (**BDP**), which was already used in epoxy resins like DGEBA/DMC.<sup>19,29</sup> The ratio  $n_{\text{Double-bond}}/n_{\text{Ester}}$ , an indication of the amount of terminal double bonds, was identical for **poly-1** and **poly-2** (0.39). Looking at the phosphorus content, **poly-1** exhibits the same amount of P when compared to the monomer. In contrast, for **poly-2** the P content varied, depending on the monomer ratio and workup procedure. The theoretical phosphorus content deviated from the measured phosphorus content after precipitation. The theoretical phosphorus content of **poly-2** is 5.1 wt%, the measured phosphorus content by elemental analysis is 7.7 wt%.



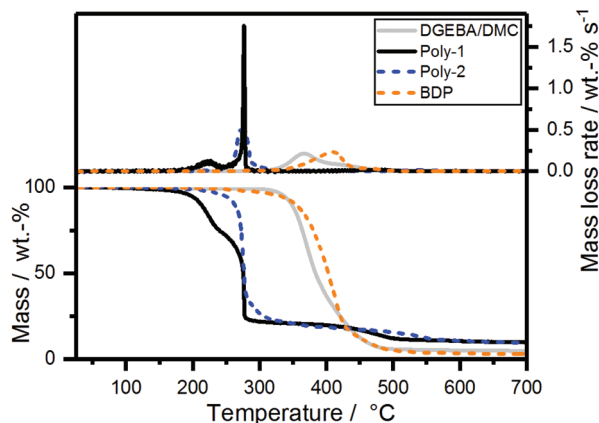


Fig. 2 Mass loss (bottom) and mass loss rate (top) over  $T$  of **poly-1**, **poly-2**, bisphenol A bis(diphenyl phosphate) and neat epoxy resin from TGA measurements ( $10\text{ K min}^{-1}$ ;  $\text{N}_2$ ).

### Pyrolysis: thermal decomposition of FRs *via* TGA

The pyrolytic decomposition of the FRs was investigated using thermogravimetric analysis (TGA) (Fig. 2). During burning, the thermal decomposition of the material feeds volatile fuel into the flame zone, where exothermal combustion reactions, *i.e.* oxidation, occur. However, at the solid/gas interface, the reactions in the anaerobic pyrolysis zone determine the fire behavior. This model is accurate for polymeric materials in developing fires, which are simulated in the cone calorimeter, but also reaction-to-small-flame tests such as UL94 and LOI. Therefore, investigations into the pyrolytic reactions of FRs and FR-containing polymers *via* TGA in nitrogen atmosphere are an important analytical tool to understand the chemical mechanisms underlying the FR's modes of action.<sup>30</sup>

The mass loss curve of **poly-2** exhibited a main single decomposition step at 274 °C with a gradual decomposition thereafter (Fig. 2). **Poly-1** exhibited an additional decomposition step at *ca.* 226 °C, followed by the second decomposition step at the same temperature as **poly-2**. The additional decomposition step might be rationalized with the cleavage of the terminal alkyl-SH group, similar to the mechanism described previously by Markwart *et al.*,<sup>28</sup> which was confirmed by the presence of tetrahydrothiophene (from pyrolysis-(Py)-GC/MS measurements at 250 °C (Fig. S6 and S8†) and TGA-FTIR measurements (Fig. S16†)). The amount of residue at 700 °C was very similar for both polymers (**poly-1**: 9.7 wt%, **poly-2**: 9.3 wt%).

### Pyrolysis: evolved gas analysis of FRs *via* TG-FTIR

Evolved gas analysis during pyrolysis of **poly-1** was performed *via* Py-GC/MS and TG-FTIR measurements. The analysis of epoxy resin (EP) and **poly-2** has been previously described in detail and will therefore not be discussed herein.<sup>11,31</sup> For **poly-1**, two single-shot Py-GC/MS measurements at varied pyrolysis temperatures (250 °C and 500 °C) were conducted to isolate the decomposition products in the first decomposition step. The gas chromatogram at 250 °C (Fig. S6†) displays a single

large signal at 5.62 min retention time, while at 500 °C (Fig. S7†), additional signals between 2.60–3.56 min were detected, as well as minor signals >5.62 min. The mass spectrum at 5.62 min was identified as tetrahydro thiophene (Fig. S8 and S9†), thus confirming the cleavage of alkyl-SH groups of **poly-1** during the first decomposition step seen in TGA. The signals between 2.60–3.56 min corresponded to 1,5-hexadiene (Fig. S10 and S11†) and its thermal rearrangement products. The rearrangement is proven by the presence of cyclohexane (Fig. S12 and S13†) at 3.56 min, a product of cyclization of 1,5-hexadiene. At 6.57 min, the signal was identified as 5-hexen-1-ol (Fig. S14 and S15†) resulting from hydrolysis of the phosphate-moiety.

### Pyrolysis: EP-FR preparation and material properties

The FR-performances of **BDP**, **poly-1**, and **poly-2** were studied in an epoxy resin (EP) based on bisphenol A diglycidylether (DGEBA) and 2,2'-dimethyl-4,4'-methylene-bis-(cyclohexylamine) (DMC). All epoxy plates were prepared in the following manner: DGEBA was mixed with the respective FR (loading: 10 wt%) until homogenous. Then, DMC was added, and the mixture was poured into appropriately sized aluminum molds, followed by curing for 30 min at 90 °C, 30 min at 120 °C, and 1 h at 150 °C. Additive FRs can act as plasticizers in epoxy resins, thus reducing the glass transition temperature ( $T_g$ ) of the resulting composite. Differential scanning calorimetry (DSC) measurements revealed that the flame retardant containing epoxy resins (EP-FRs) lowered  $T_g$  by an average of 24 °C: **Poly-1** had the strongest impact on the  $T_g$  of EP, lowering it by about 30 °C to 124 °C ( $T_{g, EP} = 155\text{ °C}$ ), while **poly-2** and **BDP** had a similar impact on the  $T_g$  of EP ( $T_{g, EP-poly2} = 132\text{ °C}$ ;  $T_{g, EP-BDP} = 133\text{ °C}$ ). The impact of FRs on the  $T_g$  of EP is presented in Fig. S20,† and the change of  $T_g$  relative to EP is noted.

### Pyrolysis: thermal decomposition and evolved gas analysis of EP-FRs *via* TGA and TG-FTIR

The decomposition behavior of EP-FRs was investigated by analyzing the mass loss and evolved gas during pyrolytic decomposition *via* TGA coupled with FTIR (Table S2†). A significant change in decomposition behavior was observable for all EP-FRs, as the mass loss and mass loss rate curves (Fig. 3) and the change in residue yields at 700 °C proved. The pure epoxy decomposed with an onset temperature ( $T_{5\%}$ ) of 338 °C and reached the temperature of maximum mass loss rate ( $T_{max}$ ) at 372 °C. EP decomposed in a single main step with a mass loss equal to 62 wt%. Following the main decomposition step, a shoulder beginning at 424 °C with a mass loss of 33 wt% was observed. At 700 °C, the residue yield was 4.5 wt%. The mass loss and evolved gas analysis of the epoxy resin (DGEBA/DMC) has been extensively investigated; therefore, it will not be discussed further.<sup>32,33</sup> When **BDP** was added to the resin (EP-**BDP**), the composite decomposed similarly to the pure EP, but  $T_{5\%}$  was lowered by about 33 °C, and  $T_{max}$  was 15 °C lower than EP. This change is attributed to a reduction in cross-linking density of the EP-system when additives are present.<sup>34</sup> The plateau which started at 423 °C exhibited a



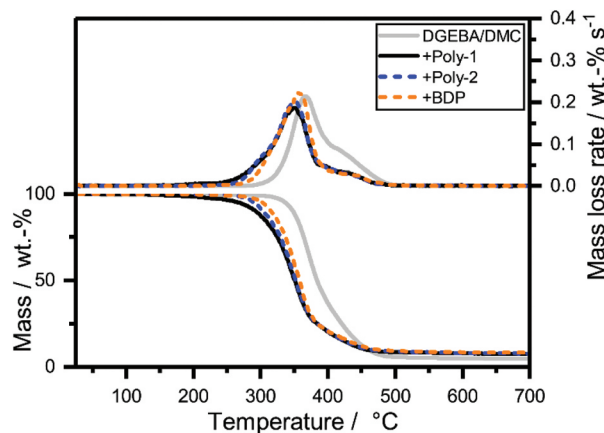


Fig. 3 Mass loss (bottom) and mass loss rate (top) over  $T$  of EP-FRs from TGA measurements ( $10\text{ K min}^{-1}$ ;  $\text{N}_2$ ).

lower decomposition rate compared to pure EP. An increase in mass loss at  $T_{\text{max}}$  to 75 wt% and a decrease to 16 wt% at the shoulder was observable. An explanation for this phenomenon is the interaction of the FR with the decomposing matrix.<sup>35</sup> More specifically, the phenol-derivates and cycloalkanes are bound; these exhibit a production rate maximum in this temperature range.<sup>36</sup> As a result, the residue yield of EP-BDP increased to 8.1 wt%, which is nearly twice that of pure EP.

All *hb*-FR containing EPs (EP-*hb*-FRs) exhibited a decomposition behavior similar to EP-BDP. The  $T_{5\%}$  of EP was lowered by 70 °C for **poly-1** and 47 °C for **poly-2**.  $T_{\text{max}}$  was also lowered when FRs were present, on average by approx. 16 °C. The lower  $T_{5\%}$  of EP-**poly-1** compared to EP-**poly-2** is caused by the additional decomposition step in **poly-1**. All residue yields of EP-FRs were in a similar range, and all investigated FRs increased the residue of EP (7.9 and 7.7 wt% for **poly-1** and **poly-2**, respectively, and 8.1 wt% for BDP). The neat EP had a residue yield of only 4.6 wt%. This increase in residue indicates that the tested FRs interact with the decomposing matrix. As a result, thermally stable residues are formed.

From the evolved gas analysis of EP-FRs via TG-FTIR (Fig. S17†), two distinct decomposition products were visible for EP-**poly-1** and EP-**poly-2**, the first appearing in the range of about 290 °C and the second between 360–380 °C. At ca. 290 °C, the spectra of EP-**poly-1** and EP-**poly-2** exhibited the evolution of 5-hexen-1-ol, a product of either hydrolysis or transesterification. Its presence indicates that *hb*-FRs are active near  $T_{5\%}$ , forming either lower molecular phosphates (hydrolysis) which are active in the condensed phase, or phosphorylating the polymer matrix (transesterification), thus forming char precursors. The condensed phase mode of action is additionally proven by hot-stage FTIR (Fig. S19†). At 360–380 °C, all spectra are identical to EP, as the matrix decomposes in this temperature range.

#### Pyrolysis: condensed phase analysis of EP-FRs via hot-stage FTIR

The condensed phase mode of action of **poly-1** and **poly-2** in EP was proven by hot-stage FTIR measurements (Fig. S18 and

S19†). Fig. S18† displays the unique signals of EP-**poly-1** at 300 °C, namely 1146 and 1108  $\text{cm}^{-1}$ , which are shifted to slightly lower wavenumbers and increase in intensity at 500 °C (Fig. S19†). These signals may correspond to  $\nu(\text{P}=\text{O})$  of  $\text{R}_2-(\text{P}=\text{O})-\text{OH}$  resulting from the cleavage of terminal alkyl-SH groups which occurs more readily than cleavage of terminal hexene-moieties, as observed in Py-GC/MS (Fig. S8†) and TG-FTIR measurements (Fig. S16†) of **poly-1**. It is conceivable that **poly-1** is more reactive than **poly-2** in terms of phosphorylation of the epoxy resin matrix, especially given the increase in residue yields of fire testing and pyrolysis (Tables S1 and S2,† respectively). At 600 °C, the hot-stage FTIR spectrum of EP-**poly-1** exhibits many bands that are also present in EP-**poly-2** and EP-BDP, which have already been previously described as phosphorus signals.<sup>11</sup> Moreover, additional bands at 1400, 1125, 1010, 974, and 585  $\text{cm}^{-1}$  are present. Many types of compounds, including vinylene-moieties, cyclic aliphatic hydrocarbons, and secondary or tertiary alcohols, present signals at these wavenumbers. While the identification of specific compounds in hot-stage FTIR is not always possible, it is certain that the spectrum of EP-**poly-1** presents clear signals that are distinct and different from EP, thereby proving a condensed-phase spectrum of **poly-1** in EP.

#### Fire testing: forced flaming conditions

All EP-*hb*-FRs reduced the fire load (THE) of EP. **Poly-1** decreased the fire load of EP by 21%, whereas **poly-2** decreased the fire load by 17% and BDP by 19%. **Poly-1** reduced THE of EP more strongly than **poly-2** because it was able to retain more fuel in the condensed phase, as evidenced by its higher residue yield (Fig. 4d). This fuel retention may be caused by the higher reactivity of **poly-1** compared to **poly-2**: as **poly-1** has a lower  $T_{5\%}$ , its decomposition products may interact earlier with the decomposing matrix than **poly-2**, therefore increasing char yield, *i.e.* fuel fixation, and thus lowering THE. The tested FRs lowered the peak of heat release rate (PHRR) of EP by ca. 30% for BDP and **poly-1**, and by 44% for **poly-2**. The HRR curves (Fig. 4a) indicate that the formation of a protective char layer on the sample surface resulted in a plateau-like shape approx. 30 s after ignition, reducing PHRR by shielding the underlying material from irradiation. All FRs increased residue yields in the order EP-**poly-1** > EP-**poly-2** > EP-BDP. EP-**Poly-1** exhibited the highest residue amount (11.5 wt%) and EP-BDP showed the lowest (3.1 wt%). The residues after fire testing (Fig. 4d) help visualize the differences in fire performance of **poly-1** and **poly-2** in EP: The residue of EP-**poly-2** was more voluminous than that of EP-**poly-1**, pointing to higher gas emission, similar to intumescent FR systems. This large char volume was effective in shielding some of the underlying material, acting as a protective layer and thereby reducing PHRR of EP.<sup>37</sup> However, EP-**poly-1** exhibited a lower THE and higher residue yield than EP-**poly-2**, because the thermal properties of its char were greater. As a result, **poly-1** was better able to bind fuel in the condensed phase in the form of char, which increased residue yields and thus reduced the fire load, *i.e.* THE. Although EHC of both materials were nearly





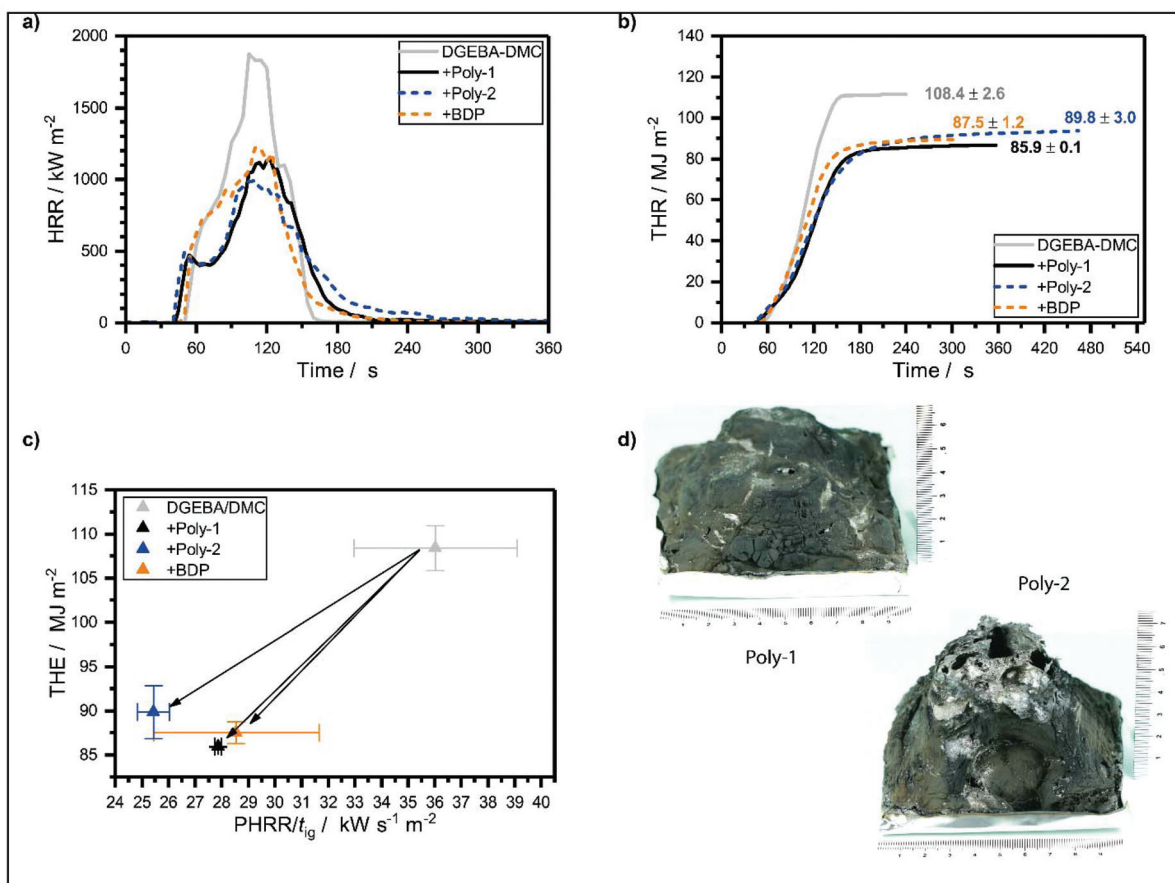


**Fig. 4** (a) Heat release rate (HRR) of epoxy resin and epoxy resin with FRs. (b) Total heat released (THR) of epoxy resin and epoxy resin with FRs. (c) Petrella plot of the different epoxy resins with all FRs having a positive effect (lowering THE and PHRR/ $t_{ig}$ ). (d) Char residues of EP-poly-1 and EP-poly-2 after cone calorimeter test. Residue of EP-poly-2 is more voluminous than that of EP-poly-1, pointing to higher gas emission, similar to intumescent FR systems.

identical, the change in char characteristics explains the difference in fire performance, as the residue morphology and its properties often determine effective flame retardancy.<sup>35</sup>

Additionally, the effective heat of combustion (EHC) was reduced by the release of P-containing volatiles. These P-containing volatiles acted in the gas phase as radical scavengers, *i.e.* by lowering the concentration of highly reactive radicals (H<sup>•</sup>, HO<sup>•</sup>, CO<sup>•</sup>, *etc.*) through P<sup>•</sup> or PO<sup>•</sup> radicals. The resulting flame inhibition led to less complete combustion; additionally, P enhanced charring thus stored fuel in the condensed phase, all of which resulted in a reduction of THE (Fig. 4b).

To further assess fire behavior and flame retardancy, the fire load (THE) is often plotted against the fire growth index (PHRR/ $t_{ig}$ , Fig. 4c),<sup>38</sup> because THE describes heat release quantitatively, however it does not describe the release rate. PHRR/ $t_{ig}$  is a means of describing the time-dependent flashover potential or fire growth index, *i.e.* the severity of a fire, or peak heat release potential; however, it is not quantitative. The investigated FRs reduced both PHRR/ $t_{ig}$  and THE of EP, which had a PHRR/ $t_{ig}$  of 36 kW m<sup>-2</sup> s<sup>-1</sup> and a THE of 110 MJ m<sup>-2</sup>. EP-Poly-1 had a performance similar to EP-BDP: BDP reduced THE of EP by 19% to 88 MJ m<sup>-2</sup> and Poly-1 reduced it by 21% to

86 MJ m<sup>-2</sup>. The PHRR/ $t_{ig}$  was reduced by 21% to 29 kW s<sup>-1</sup> m<sup>-2</sup> and by 23% to 28 kW s<sup>-1</sup> m<sup>-2</sup> for BDP and Poly-1, respectively. Poly-2 exhibits a higher THE compared to Poly-1 and BDP but has a stronger reduction in PHRR/ $t_{ig}$ . The graph visualizes the overall good flame-retardancy potential of the *hb*-FRs: a shift to the lower-left corner of the coordinate system indicates a reduction of overall heat and fire growth. Both *hb*-FRs lower both values on a similar level to the benchmark material, proving their efficacy for this polymer resin system. Moreover, Poly-1 exhibited lower fire loads than Poly-2 in EP; this implies that Poly-1 was more able to bind fuel in the condensed phase, as proven by the higher overall char yield. On the other hand, Poly-2 reduced the fire growth rate more strongly than Poly-1 in EP: this resulted from the better thermal barrier properties of EP-Poly-2's char, which lowered PHRR, as well as the higher thermal stability of Poly-2 which led to an increased  $t_{ig}$ .

## Conclusion

Hyperbranched polymers, especially polyphosphoesters, are interesting candidates as polymeric flame retardants. *hb*PPes



were previously prepared by  $A_n + B_m$  approaches, which might result in cross-linked PPEs, as adjustment of the monomer feed-ratio or termination before the gel point needs to be carefully conducted. Herein, we presented the first phosphorus-based  $AB_2$  monomer (**1**), allowing the synthesis of *hb*PPEs in a single polyaddition step without the chance of undesired cross-linking.

In addition to the simplified polymerization procedure, **poly-1** exhibited a slightly higher performance compared to similar *hb*PPEs (**poly-2**), prepared by  $A_2 + B_3$  polyaddition, probably due to its higher phosphorus content. This work further extends the possibilities for the preparation of branched polyphosphoesters, which might be used in biofriendly flame retardant applications or biomedical applications.

## Experimental section

### Materials

All chemicals were purchased from commercial suppliers as reagent grade and used without further purification.

Samples for TGA-FTIR and hot-stage FTIR were milled prior to use. Powdered specimens were obtained using a RETSCH CryoMill under liquid nitrogen cooling.

### DSC

For Differential Scanning Calorimetry (DSC), a Mettler Toledo DSC 823<sup>e</sup> was used. With a heating and cooling rate of 10 K min<sup>-1</sup>, three measurements of heating, cooling and heating were performed. The measurements were done in a nitrogen atmosphere with a flow rate of 30 mL min<sup>-1</sup>.

EP-FRs were measured on a Netzsch 204 F1, type Phoenix. Two cooling and three heating runs were performed on 5 mg bulk material samples; the rate was 10 K min<sup>-1</sup>, the temperature range was -80 to 180 °C, and the nitrogen flow rate was 30 mL min<sup>-1</sup>. The second and third heating rate were used to determine  $T_g$ .

### TGA

For the thermogravimetric analysis (TGA) of the neat flame retardants, a Mettler Toledo TGA/DSC 3+ in a nitrogen atmosphere was used. Using 10 mg of the sample, the measurements were performed in a range from 25 °C to 700 °C with a heating rate of 10 K min<sup>-1</sup>.

### TG-FTIR

Pyrolysis investigations into mass loss and evolved gas analysis were performed *via* thermogravimetric analysis (TGA) on a Netzsch TG 209, type Iris, which was coupled *via* transfer line to a Bruker Tensor 27 infrared spectrometer (FTIR). For TG-FTIR measurements of EP and EP-FRs, 10 mg powdered samples were used, while for pure *hb*-FRs, 5 mg samples were measured. Measurements were conducted from 30–900 °C (10 K min<sup>-1</sup>) under a 30 ml min<sup>-1</sup> nitrogen purge. Evolved gases passed through a transfer line heated to 270 °C into the

FTIR gas cell which was also heated to 270 °C. The measuring range was 4000–400 cm<sup>-1</sup> with a resolution of 1 cm<sup>-1</sup>.

### Hot stage FTIR

Pyrolysis investigations of the condensed phase activity were performed on a Bruker Vertex 70 FTIR equipped with a Linkam FTIR600 hot stage cell. Powdered EP and EP-FR samples (*ca.* 5 mg) were mixed with 150 mg KBr in a mortar and pestle, then pressed into a platelet at 7 bar. Specimens were heated from 30–600 °C at a rate of 10 K min<sup>-1</sup> under a nitrogen atmosphere. The measuring range was 4000–400 cm<sup>-1</sup> with a resolution of 0.4 cm<sup>-1</sup>.

### Pyrolysis-gas chromatography-mass spectrometry (Py-GC/MS)

Pyrolytic evolved gas analysis was performed on a pyrolysis-gas chromatograph/mass spectrometer using a Frontier Lab PY3030iD micro-furnace single-shot pyrolyzer connected to an Agilent Technologies 7890B gas chromatograph *via* a split/splitless inlet port. An Agilent Technologies 7890B mass selective detector was combined with the gas chromatograph; the ionization energy (EI) was 70 eV and the scan range was 15–550 amu. 150 µg samples were pyrolyzed under helium atmosphere and inserted into the pyrolyzer *via* gravimetric fall; the temperature was 500 °C, except for measurements of **poly-1**, where the pyrolyzer temperature was set to 250 °C for an additional measurement. All evolved pyrolysis products were separated under a helium flow of 1 mL m<sup>-1</sup> in an Ultra Allow+ 5 capillary column with a length of 30 m, inner diameter of 0.25 mm, and film thickness of 0.25 µm. First, the column was heated to 40 °C and held there for 2 min, then heated at a rate of 10 K min<sup>-1</sup> up to 300 °C, where it was kept for 10 min. The GC injector was operated in a split mode of 1 : 300; the interface temperature was 300 °C. MS peak assignments were made using the NIST 14 MS library.

### Cone calorimeter

Fire testing was conducted on an FTT cone calorimeter operating at a heat flux of 50 kW m<sup>-2</sup> according to ISO 5660, simulating a developing fire.<sup>39</sup> Samples sized 100 mm × 100 mm × 4 mm were conditioned at 23 °C and 50% RH for at least 48 h, then measured at a distance of 35 mm from the cone heater, as a distance of 25 mm was not suitable for the large residues of the materials.<sup>40</sup>

### GPC

GPC measurements were performed in DMF (+LiBr 1 g L<sup>-1</sup>) with a PSS SecCurity system (Agilent Technologies 1260 Infinity). Sample injection was performed by a 1260-ALS auto-sampler (Waters) at 60 °C. SDV columns (PSS) with dimensions of 300 × 80 mm, 10 µm particle size, and pore sizes of 10 000, 1000, and 100 Å were employed. The IR 1260 RID detector and UV-vis 1260-VWD detector (Agilent) were used for detection. Calibration was achieved using poly(styrene) standards provided by Polymer Standards Service.



## Elemental analysis

Elemental analysis was run on an Elementar Vario EL cube.

## NMR

Nuclear magnetic resonance (NMR) analysis,  $^1\text{H}$ ,  $^{31}\text{P}$  {H} and  $^{13}\text{C}$  {H} NMR spectra were recorded with Bruker Avance spectrometers operating with 250, 300, 500 and 700 MHz frequencies in deuterated chloroform, deuterated dimethyl sulfoxide or deuterated *N,N*-dimethylformamide as a solvent. The calibration of the spectra was done against the solvent signal. The spectra were analyzed using MestReNova 9 from Mestrelab Research S.L.

### 4-Bromobutan-1-ol

The synthesis was done according to a literature procedure.<sup>27</sup> In a 1 L flask, THF (270 mL, 3.33 mol) was added to hydrobromic acid (48%, 180 g, 1.06 mol). The mixture was refluxed for two hours, transferred into an Erlenmeyer flask, and the reaction was neutralized by the addition of  $\text{NaHCO}_3$  under strong  $\text{CO}_2$  development. The aqueous solution was extracted with dichloromethane and the organic layers were combined and dried with  $\text{Na}_2\text{SO}_4$ . The solvent was removed at reduced pressure, yielding the product (47.3 g, 29%), which was used without further purification.

$^1\text{H}$  NMR (250 MHz,  $\text{CDCl}_3$ ):  $\delta$  [ppm] = 4.01 (s, 1H), 3.69 (t,  $J$  = 6.4 Hz, 2H), 3.44 (t,  $J$  = 6.6 Hz, 2H), 2.05–1.79 (dd,  $J$  = 8.0, 6.6 Hz, 2H), 1.79–1.62 (dd,  $J$  = 8.5, 6.4 Hz, 2H).

### 4-Bromobutyl phosphorodichloridate (1a)

To a dried three-necked, 500 mL round bottom flask equipped with two 100 mL dropping funnels, 0.522 mol phosphoryl chloride (80.00 g, 47.62 mL, 521.78 mmol, 5.0 eq.) were added to ice-cooled, dry toluene (100 mL) under argon atmosphere. 4-bromobutan-1-ol (15.97 g, 9.51 mL, 104.36 mmol, 1.0 eq.) dissolved in dry toluene (50 mL) and pyridine (8.25 g, 8.42 mL, 104.36 mmol, 1.0 eq.) dissolved in dry toluene (50 mL) were added to the above flask dropwise, keeping the temperature at 0 °C. After stirring overnight at room temperature, pyridine hydrochloride was removed as a white solid by filtration. The filtrate containing the alkylene dichlorophosphate in toluene was concentrated at reduced pressure. 4-Bromobutyl phosphoro-dichloridate was obtained as a colourless liquid (yield: 21.6 g, 77%).

$^1\text{H}$  NMR (300 MHz, 298 K,  $\text{CDCl}_3$ ,  $\delta$ /ppm): 4.43–3.34 (m, 2H), 3.49–3.43 (t,  $J$  = 5.8 Hz, 2H), 2.07–1.95 (m, 4H).

$^{31}\text{P}$ {H} NMR (202 MHz, 298 K,  $\text{CDCl}_3$ ,  $\delta$ /ppm): 7.21.

### 4-Bromobutyldi(hex-5-en-1-yl) phosphate (1b)

To a dry three-necked, 500 mL round bottom flask fitted with a 250 mL dropping funnel, 5-hexen-1-ol (17.61 g, 21.11 mL, 175.29 mmol, 2.1 eq.) and pyridine (13.87 g, 14.15 mL, 175.29 mmol, 2.1 eq.) were added to dry toluene (100 mL) under an argon atmosphere. **1** (22.53 g, 83.47 mmol, 1.0 eq.) dissolved in dry toluene (100 mL) was added to the above flask dropwise at room temperature. After stirring overnight, pyri-

dine hydrochloride was removed as a white solid by filtration. The organic solution was washed with sodium bicarbonate solution, 10% hydrochloric acid, and sodium chloride solution. The organic layer was dried over anhydrous sodium sulfate, filtered, and the solvent was removed at reduced pressure. 4-Bromobutyldi(hex-5-en-1-yl) phosphate was obtained as a yellow liquid (yield: 30.2 g, 88%).

$^1\text{H}$  NMR (300 MHz, 298 K,  $\text{CDCl}_3$ ,  $\delta$ /ppm): 5.90–5.68 (m, 2H), 5.06–4.92 (m, 4H), 4.40–3.92 (m, 6H), 3.69–3.61 (t,  $J$  = 6.3 Hz, 2H), 3.48–3.40 (t,  $J$  = 6.3 Hz, 2H), 2.21–2.05 (m, 4H), 2.05–1.74 (m, 4H), 1.74–1.59 (m, 4H), 1.53–1.41 (m, 4H).  $^{31}\text{P}$ {H} NMR (202 MHz, 298 K,  $\text{CDCl}_3$ ,  $\delta$ /ppm): –0.71.

### Di(hex-5-en-1-yl)(4-acetylthiobutyl)phosphate (1c)

To a dry one-necked, 500 mL round bottom flask, **2** (29.05 g, 73.11 mmol, 1.0 eq.) and potassium thioacetate (9.18 g, 80.42 mmol, 1.1 eq.) were dissolved in acetone (100 mL). After stirring overnight at room temperature, potassium bromide was removed as a white solid by filtration. Acetone was removed at reduced pressure and the residue was dissolved in toluene (100 mL). The mixture was washed with sodium bicarbonate solution, 10% hydrochloric acid and sodium chloride solution. The organic layer was dried over anhydrous sodium sulfate, filtered and the solvent was removed at reduced pressure to isolate *S*-(4-((bis(hex-5-en-1-yloxy)phosphoryl)oxy)butyl)ethanethioate (yield: 27.7 g, 96%).

$^1\text{H}$  NMR (300 MHz, 298 K,  $\text{CDCl}_3$ ,  $\delta$ /ppm): 5.87–5.70 (m, 2H), 5.06–4.92 (m, 4H), 4.23–3.94(m, 6H), 3.92–2.82 (m, 4H), 2.32 (s, 3H), 2.13–2.02 (m, 4H) 1.79–1.63 (m, 8H), 1.54–1.42 (m 4H).

$^{31}\text{P}$ {H} NMR (202 MHz, 298 K,  $\text{CDCl}_3$ ,  $\delta$ /ppm): –0.55.

### Di(hex-5-en-1-yl)(4-mercaptopbutyl)phosphate (1)

**1c** (26.78 g, 68.24 mmol, 1.0 eq.) was dissolved in dichloromethane (100 mL) in a dry one-necked, 500 mL round bottom flask. Then 1 M hydrazine in THF (102.36 mL, 102.36 mmol, 1.5 eq.) was added dropwise. After stirring overnight at room temperature, the mixture was washed with sodium bicarbonate solution, 10% hydrochloric acid and sodium chloride solution. The organic layer was dried over anhydrous sodium sulfate, filtered and concentrated *in vacuo*. The remaining liquid was purified by column chromatography (3 : 7 ethyl acetate/petroleum ether) to obtain an off-white oil (yield: 5.8 g, 24%).

$^1\text{H}$  NMR (300 Hz, 298 K,  $\text{CDCl}_3$ ,  $\delta$ /ppm): 5.88–5.70 (m, 2H), 5.06–4.92 (m, 4H), 4.10–3.98 (m, 6H), 2.62–2.50 (m, 2H), 2.14–2.02 (m, 4H), 1.88–1.58 (m, 8H), 1.54–1.41 (m, 4H), 1.34 (t,  $J$  = 7.9 Hz, 1H).

$^{31}\text{P}$ {H} NMR (202 MHz, 298 K,  $\text{CDCl}_3$ ,  $\delta$ /ppm): –0.68.

## Poly-1

**Poly-1** was prepared by a radical thiol-ene polyaddition. 33 g (94.2 mmol; 1.0 eq.) of the previously synthesized monomer **1** were dissolved in 230 mL toluene and added to a reactor fitted with a mechanical stirrer under an argon atmosphere. As a radical initiator, 1.4 g azobisisobutyronitrile (AIBN) (8.5 mmol; 0.1 eq.) was used. The solution was heated at 90 °C for





24 hours. The crude mixture was then concentrated and dried at reduced pressure until constant weight (yield: 32.5 g, 98.5%).

$^1\text{H}$  NMR (300 Hz, 298 K,  $\text{CDCl}_3$ ,  $\delta/\text{ppm}$ ): 5.88–5.70 (m, 2H), 5.06–4.92 (m, 4H), 4.10–3.98 (m, 6H), 2.62–2.50 (m, 4H), 2.14–2.02 (m, 4H), 1.88–1.58 (m, 8H), 1.54–1.41 (m, 4H).

$^{31}\text{P}\{\text{H}\}$  NMR (202 MHz, 298 K,  $\text{CDCl}_3$ ,  $\delta/\text{ppm}$ ): –0.70.

## Poly-2

The synthesis was done according to a literature procedure.<sup>11</sup>

## Poly-1 for kinetic studies

In a 25 mL Schlenk tube, **1** (405 mg, 1.16 mmol) was dissolved in toluene (2.7 mL) under an argon atmosphere. AIBN (0.03, 0.06, or 0.09 eq.) was added to the Schlenk tube and the mixture was heated to 70 °C or 90 °C. After specific reaction times, samples (each 0.2 mL) were taken and terminated in air for the analysis of the polymerization kinetics. The crude product was dried *in vacuo* and analyzed by  $^1\text{H}$ ,  $^{31}\text{P}$  NMR, and GPC.

$^1\text{H}$  NMR (300 Hz, 298 K,  $\text{CDCl}_3$ ,  $\delta/\text{ppm}$ ): 5.88–5.70 (m, 2H), 5.06–4.92 (m, 4H), 4.10–3.98 (m, 6H), 2.62–2.50 (m, 4H), 2.14–2.02 (m, 4H), 1.88–1.58 (m, 8H), 1.54–1.41 (m, 4H).

$^{31}\text{P}\{\text{H}\}$  NMR (202 MHz, 298 K,  $\text{CDCl}_3$ ,  $\delta/\text{ppm}$ ): –0.70.

## Epoxy preparation

All epoxy resins were prepared using bisphenol A diglycidylether (DGEBA) (Araldite MY740, Bodo Möller Chemie GmbH, Offenbach am Main, Germany) as the epoxide agent and 2,2'-dimethyl-4,4'-methylene-bis-(cyclohexylamine) (DMC) (Sigma Aldrich Co. LLC/Merck KGaA, Darmstadt, Germany) as the amine hardener. The materials were mixed, poured into aluminum molds of desired dimensions, then hardened at 150 °C for 3 h. The flame retarded epoxy resins were produced in the same manner, except 10 wt% of the mixture was replaced with the respective flame retardant.

## Author contributions

The manuscript was written through contributions of all authors. All authors have given approval to the final version of the manuscript.

## Conflicts of interest

There are no conflicts to declare.

## Acknowledgements

The authors thank the Deutsche Forschungsgemeinschaft (DFG WU 750/8-1; SCHA 730/15-1) for funding. Jens C. Markwart is the recipient of a fellowship through funding of the Excellence Initiative (DFG/GSC 266) in the context of the graduate school of excellence "MAINZ" (Materials Science in

Mainz). F. R. Wurm and Jens C. Markwart thank Prof. Dr. Katharina Landfester (MPI-P, Germany) for support. Alexander Battig thanks Dr. Katharina Kebelmann and Patrick Klack for their support with Py-GC/MS and the cone calorimeter. Open Access funding provided by the Max Planck Society.

## References

- 1 J. Liu, W. Huang, Y. Pang and D. Yan, *Chem. Soc. Rev.*, 2015, **44**, 3942–3953.
- 2 M. D. Lechner, K. Gehrke and E. H. Nordmeier, *Makromolekulare Chemie: Ein Lehrbuch für Chemiker, Physiker, Materialwissenschaftler und Verfahrenstechniker*, Springer, Berlin Heidelberg, 2014.
- 3 B. I. Voit and A. Lederer, *Chem. Rev.*, 2009, **109**, 5924–5973.
- 4 B. Schartel and J. H. Wendorff, *Polym. Eng. Sci.*, 1999, **39**, 128–151.
- 5 K. Täuber, F. Marsico, F. R. Wurm and B. Schartel, *Polym. Chem.*, 2014, **5**, 7042–7053.
- 6 B. Perret, B. Schartel, K. Stöß, M. Ciesielski, J. Diederichs, M. Döring, J. Krämer and V. Altstädt, *Eur. Polym. J.*, 2011, **47**, 1081–1089.
- 7 B. Perret, B. Schartel, K. Stöß, M. Ciesielski, J. Diederichs, M. Döring, J. Krämer and V. Altstädt, *Macromol. Mater. Eng.*, 2011, **296**, 14–30.
- 8 C. R. Yates and W. Hayes, *Eur. Polym. J.*, 2004, **40**, 1257–1281.
- 9 S. Penczek, K. Kaluzynski and J. Pretula, *J. Appl. Polym. Sci.*, 2007, **105**, 246–254.
- 10 J. Liu, W. Huang, Y. Pang, X. Zhu, Y. Zhou and D. Yan, *Biomacromolecules*, 2010, **11**, 1564–1570.
- 11 A. Battig, J. C. Markwart, F. R. Wurm and B. Schartel, *Polym. Chem.*, 2019, **10**, 4346–4358.
- 12 J. Khandare, M. Calderón, N. M. Dagia and R. Haag, *Chem. Soc. Rev.*, 2012, **41**, 2824–2848.
- 13 Y. Zhou, W. Huang, J. Liu, X. Zhu and D. Yan, *Adv. Mater.*, 2010, **22**, 4567–4590.
- 14 F. Marsico, A. Turshatov, R. Peköz, Y. Avlasevich, M. Wagner, K. Weber, D. Donadio, K. Landfester, S. Balushev and F. R. Wurm, *J. Am. Chem. Soc.*, 2014, **136**, 11057–11064.
- 15 M. M. Velencoso, A. Battig, J. C. Markwart, B. Schartel and F. R. Wurm, *Angew. Chem., Int. Ed.*, 2018, **57**, 17.
- 16 P. Wen, X. Wang, W. Xing, X. Feng, B. Yu, Y. Shi, G. Tang, L. Song, Y. Hu and R. K. K. Yuen, *Ind. Eng. Chem. Res.*, 2013, **52**, 17015–17022.
- 17 J. Li, C. Ke, L. Xu and Y. Wang, *Polym. Degrad. Stab.*, 2012, **97**, 1107–1113.
- 18 K.-C. Cheng, C.-C. Wang, J.-I. Ruan, C.-H. Wu and C.-W. Li, *Polym. Adv. Technol.*, 2018, **29**, 2529–2536.
- 19 M. Rakotomalala, S. Wagner and M. Döring, *Materials*, 2010, **3**, 4300.
- 20 K. H. Pawlowski and B. Schartel, *Polym. Int.*, 2007, **56**, 1404–1414.



- 21 B. Perret, K. H. Pawlowski and B. Schartel, *J. Therm. Anal. Calorim.*, 2009, **97**, 949.
- 22 C. Gao and D. Yan, *Prog. Polym. Sci.*, 2004, **29**, 183–275.
- 23 P. J. Flory, *J. Am. Chem. Soc.*, 1952, **74**, 2718–2723.
- 24 D. Yan, C. Gao and H. Frey, *Hyperbranched Polymers: Synthesis, Properties, and Applications*, Wiley, 2011.
- 25 P. J. Flory, *J. Am. Chem. Soc.*, 1941, **63**, 3083–3090.
- 26 C. Walling, *J. Am. Chem. Soc.*, 1945, **65**, 441–447.
- 27 H. Tan, H. Liu, X. Chen, H. Chen and S. Qiu, *Org. Biomol. Chem.*, 2015, **13**, 9977–9983.
- 28 J. C. Markwart and F. R. Wurm, *Tetrahedron*, 2018, **74**, 7426–7430.
- 29 M. Ciesielski, A. Schäfer and M. Döring, *Polym. Adv. Technol.*, 2008, **19**, 507–515.
- 30 B. Schartel, C. A. Wilkie and G. Camino, *J. Fire Sci.*, 2016, **34**, 447–467.
- 31 J. C. Markwart, A. Battig, L. Zimmermann, M. Wagner, J. Fischer, B. Schartel and F. R. Wurm, *ACS Appl. Polym. Mater.*, 2019, **1**, 1118–1128.
- 32 L.-H. Lee, *J. Polym. Sci., Part A: Gen. Pap.*, 1965, **3**, 859–882.
- 33 D. P. Bishop and D. A. Smith, *J. Appl. Polym. Sci.*, 1970, **14**, 205–223.
- 34 M. Ciesielski, B. Burk, C. Heinzmann and M. Döring, in *Novel Fire Retardant Polymers and Composite Materials*, ed. D.-Y. Wang, Woodhead Publishing, 2017, pp. 3–51, DOI: 10.1016/B978-0-08-100136-3.00002-9.
- 35 B. Schartel, B. Perret, B. Dittrich, M. Ciesielski, J. Krämer, P. Müller, V. Altstädt, L. Zang and M. Döring, *Macromol. Mater. Eng.*, 2016, **301**, 9–35.
- 36 B. Perret, K. Pawlowski and B. Schartel, *J. Therm. Anal. Calorim.*, 2009, **97**, 949–958.
- 37 S. Brehme, B. Schartel, J. Goebbels, O. Fischer, D. Pospiech, Y. Bykov and M. Döring, *Polym. Degrad. Stab.*, 2011, **96**, 875–884.
- 38 R. V. Petrella, *J. Fire Sci.*, 1994, **12**, 14–43.
- 39 B. Schartel and T. R. Hull, *Fire Mater.*, 2007, **31**, 327–354.
- 40 B. Schartel, M. Bartholmai and U. Knoll, *Polym. Degrad. Stab.*, 2005, **88**, 540–547.



## Supplementary Information

### First phosphorus AB<sub>2</sub> monomer for flame-retardant hyperbranched polyphosphoesters: AB<sub>2</sub> vs A<sub>2</sub>+B<sub>3</sub>

*Jens C. Markwart<sup>‡[a, c]</sup>, Alexander Battig<sup>‡[b]</sup>, Thomas Kuckhoff<sup>[a]</sup>, Bernhard Schartel<sup>\*[b]</sup>, Frederik R. Wurm<sup>\*[a]</sup>*

#### Corresponding author:

\*E-mail: wurm@mpip-mainz.mpg.de; bernhard.schartel@bam.de

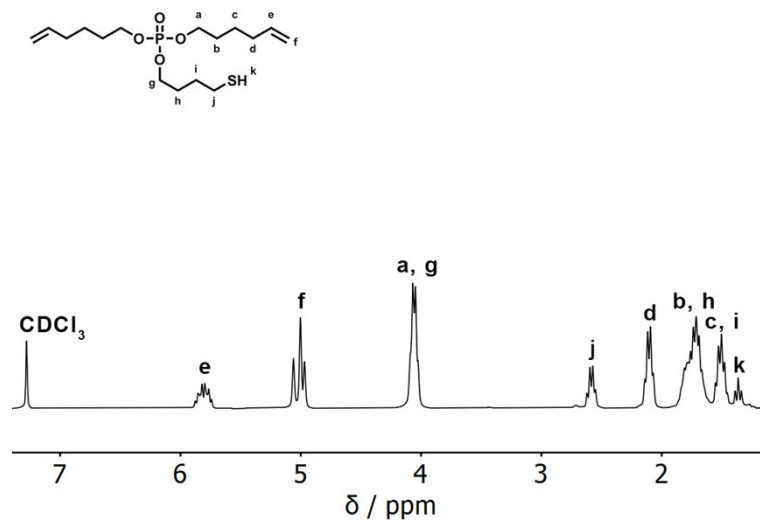


**Figure S1.**  $^1\text{H-NMR}$  (300 MHz in  $\text{CDCl}_3$  at 298 K) of **1**.

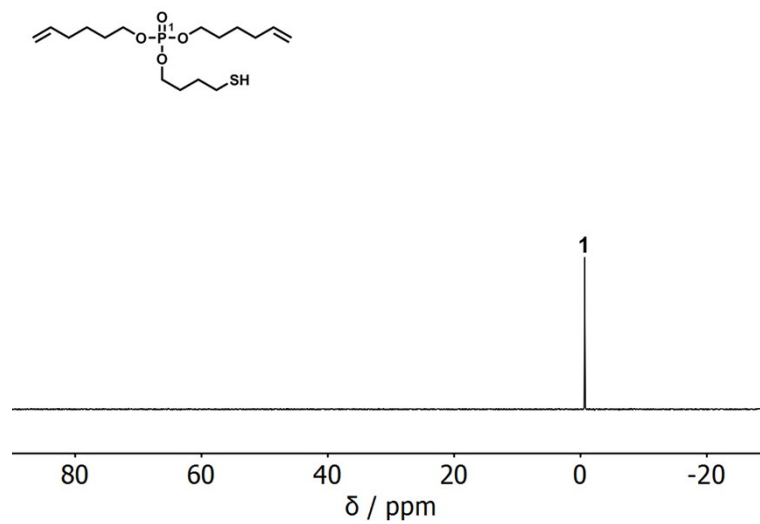


**Figure S2.**  $^{31}\text{P} \{^1\text{H}\}$ -NMR (121 MHz in  $\text{CDCl}_3$  at 298 K) of **1**.

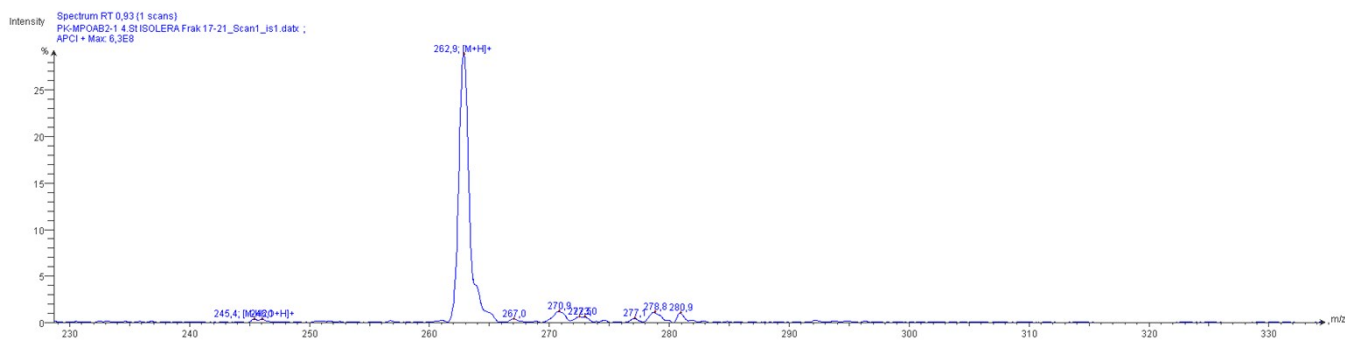


**Figure S3.** ASAP-MS of **1**  $[\text{M}+\text{H}]^+$  262.9  $m/z$ .

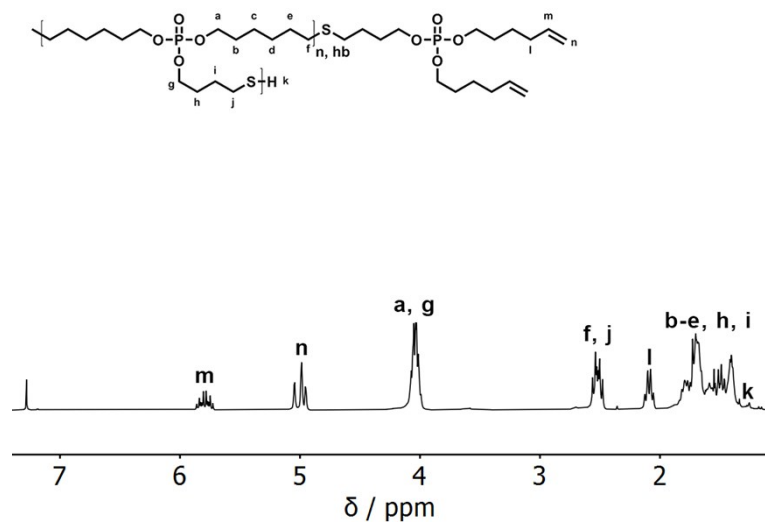


**Figure S4.**  $^1\text{H-NMR}$  (300 MHz in  $\text{CDCl}_3$  at 298 K) of **poly-1**.

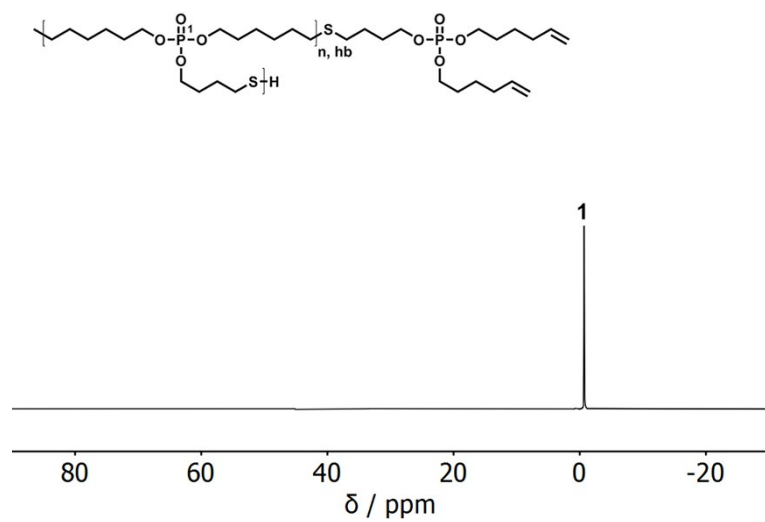


**Figure S5.**  $^{31}\text{P} \{^1\text{H}\}$ -NMR (121 MHz in  $\text{CDCl}_3$  at 298 K) of **poly-1**.

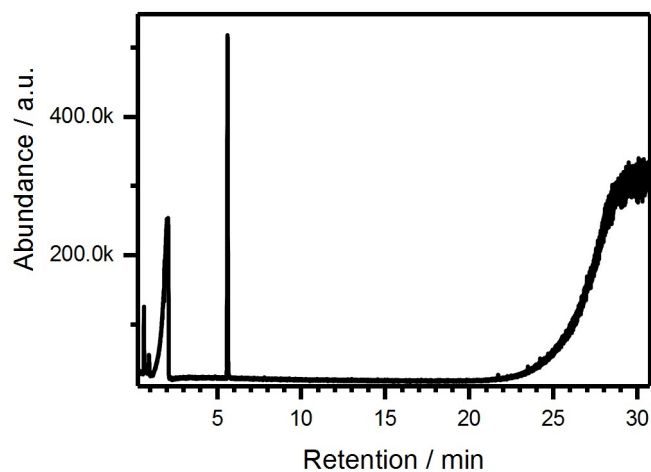


**Figure S6.** Total ion chromatogram of pyrolysis GC MS of **poly-1** measured at 250 °C (first decomposition step).

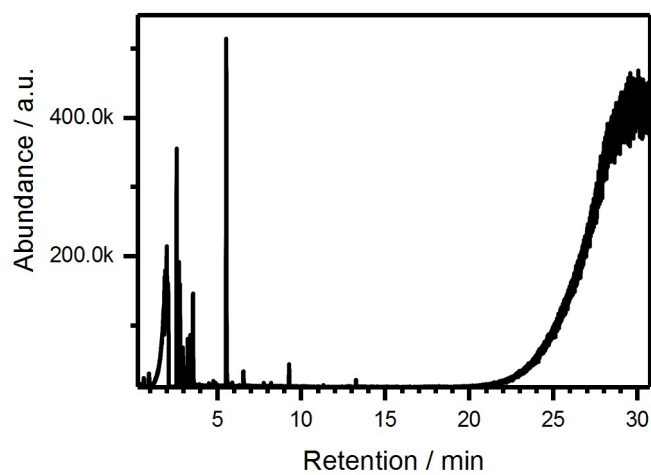


**Figure S7.** Total ion chromatogram of pyrolysis GC MS of **poly-1** measured at 500 °C (full decomposition).

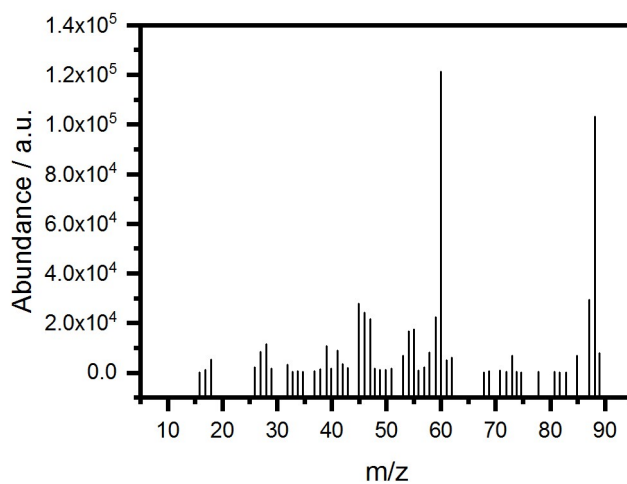


**Figure S8.** Mass spectrum at 5.62 min in the pyrolysis GC MS total ion chromatogram of **poly-1** at 250 °C, identified by NIST 14 library as tetrahydro thiophene.

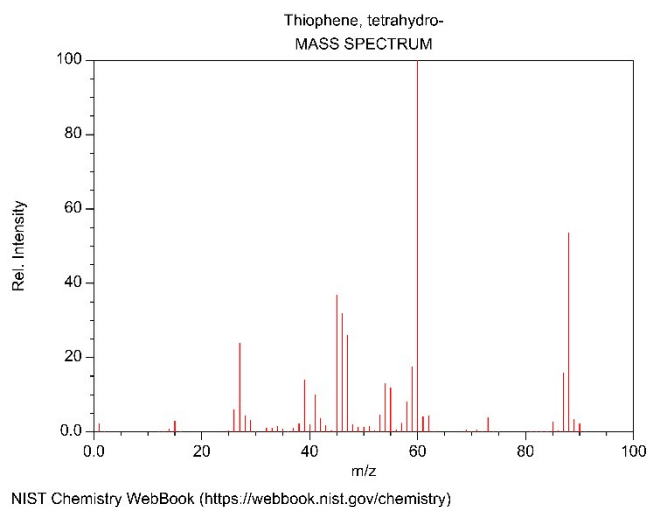


**Figure S9.** Comparative spectra of tetrahydro thiophene from NIST chemistry webbook.

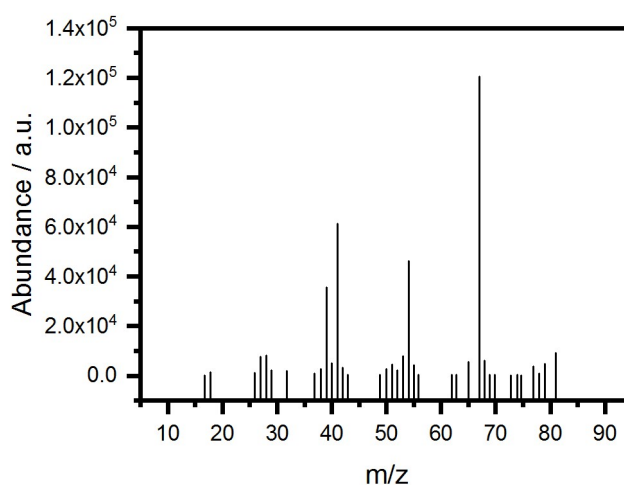


**Figure S10.** Mass spectrum at 2.60 min in the pyrolysis GC MS total ion chromatogram of **poly-1** at 500 °C, identified by NIST 14 library as 1,5-hexadiene.



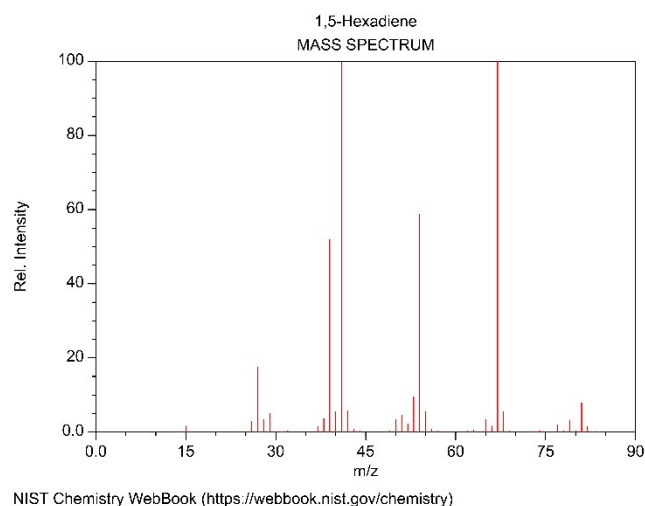


**Figure S11.** Comparative spectra of 1,5-hexadiene from NIST chemistry webbook.

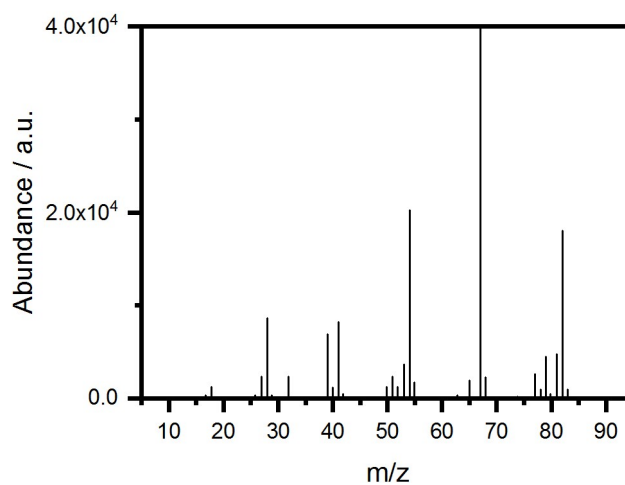


**Figure S12.** Mass spectrum at 3.56 min in the pyrolysis GC MS total ion chromatogram of **poly-1** at 550 °C, identified by NIST 14 library as cyclohexene.

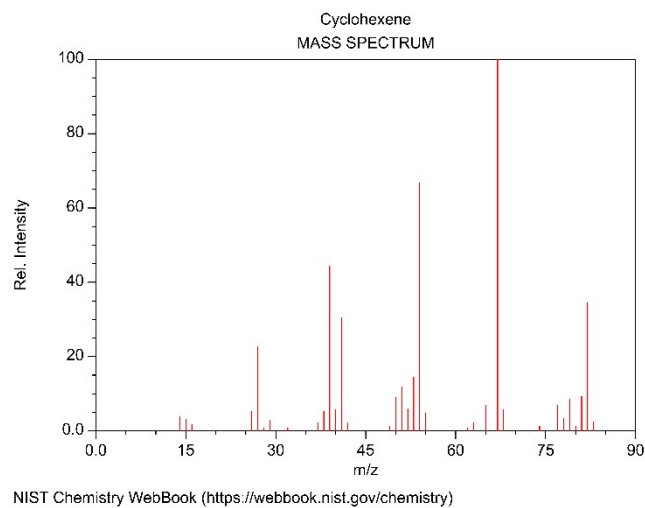


**Figure S13.** Comparative spectra of cyclohexene from NIST chemistry webbook.

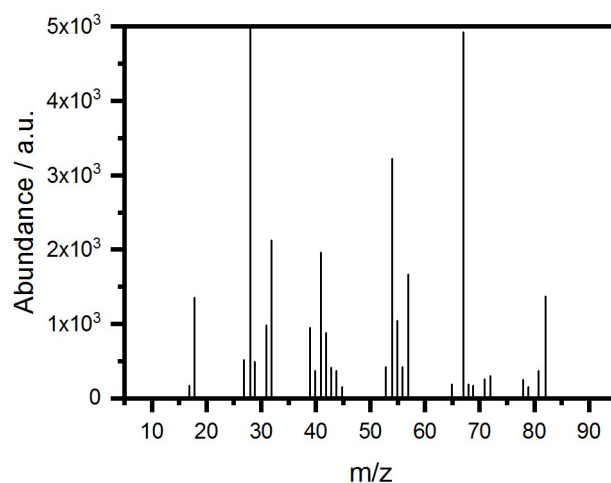


**Figure S14.** Mass spectrum at 6.57 min in the pyrolysis GC MS total ion chromatogram of **poly-1** at 500 °C, identified by NIST 14 library as 5-hexen-1-ol.

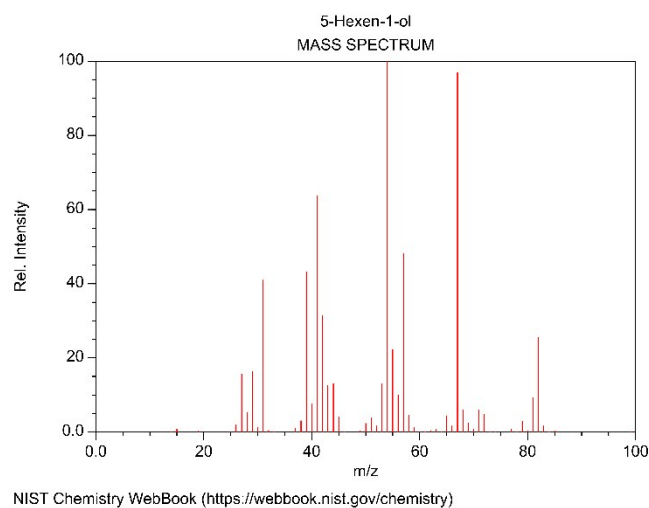


**Figure S15.** Comparative spectra of 5-hexen-1-ol from NIST chemistry webbook.

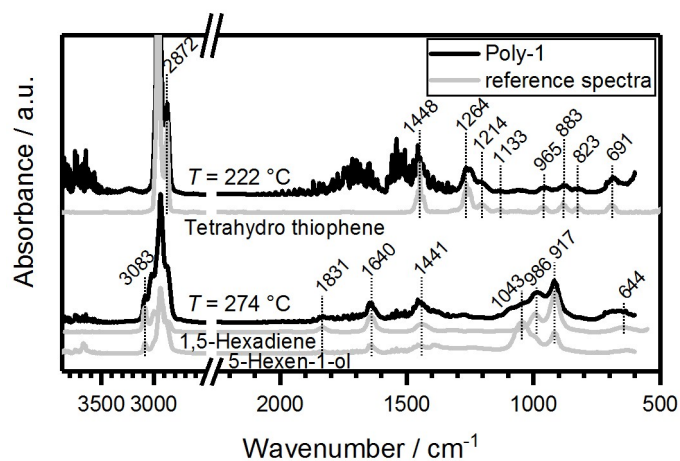


**Figure S16.** TGA-FTIR spectrum of **poly-1**, identifying the main decomposition products (tetrahydro thiophene; 1,5-hexadiene; 5-hexen-1-ol) at specific decomposition temperatures (222 °C, 274 °C) using references from NIST library.

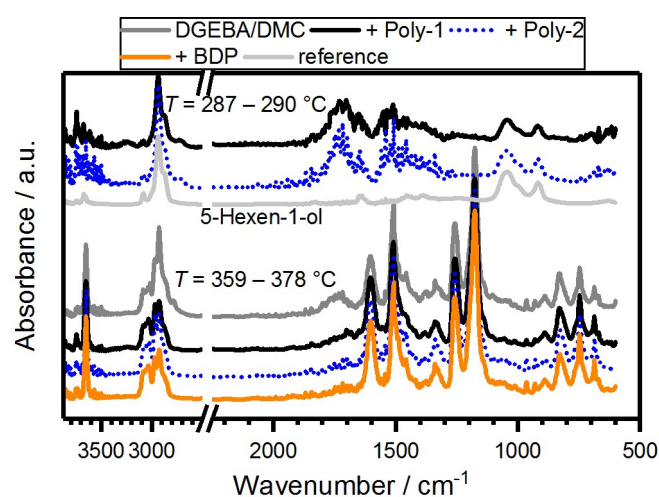


**Figure S17.** Evolved gas analysis of **EP-FRs** during pyrolysis via TGA coupled with FTIR (TG-FTIR), comparing the products at ca. 290 °C and ca. 360 – 380 °C.

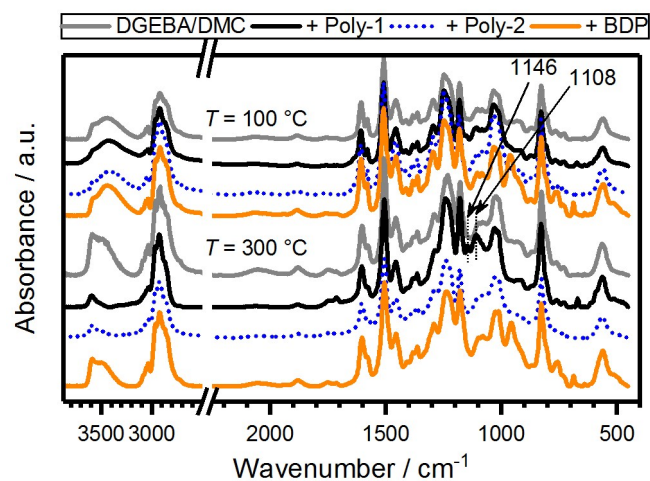


**Figure S18.** Results from hot-stage FTIR measurements, comparing the condensed phase spectra of EP-FRs at 100 °C and 300 °C.

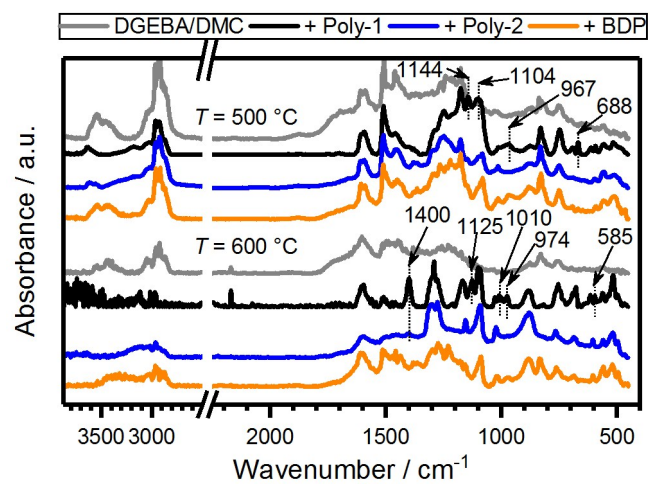


**Figure S19.** Results from hot-stage FTIR measurements, comparing the condensed phase spectra of EP-FRs at 500 °C and 600 °C.

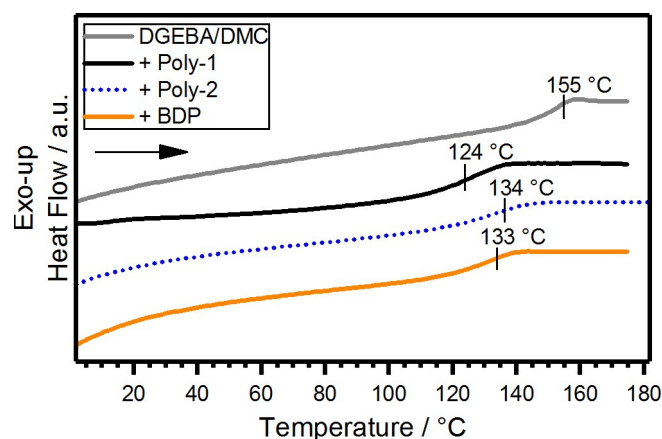


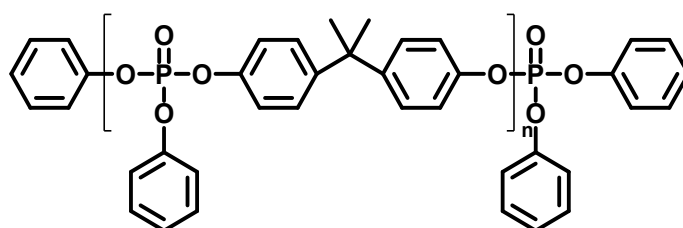
**Figure S20.** Results from DSC measurements, comparing glass-transition temperatures ( $T_g$ ) of EP and EP-FRs.

**Table S1.** Results from cone calorimeter measurements of EP-FRs, comparing total heat evolved (THE; = total heat released at flame-out), peak of heat release rate (PHRR), time to ignition ( $t_{ig}$ ), residue yield, and effective heat of combustion (EHC; = THE / total mass loss).

	EP	EP-poly-1	EP-poly-2	EP-BDP
THE / MJ m <sup>-2</sup>	108.4 ± 2.6	85.9 ± 0.0	89.8 ± 3.0	87.4 ± 1.2
PHRR / kW m <sup>-2</sup>	1696 ± 180	1170 ± 32	953 ± 41	1180 ± 41
$t_{ig}$ / s	47 ± 1	39 ± 2	38 ± 3	42 ± 6
Residue / wt.-%	0.7 ± 0.1	11.5 ± 0.8	7.5 ± 0.6	3.1 ± 0.2
EHC / MJ kg <sup>-1</sup>	26.9 ± 1.0	24.3 ± 0.2	24.3 ± 0.6	22.7 ± 0.2

**Table S2.** TGA results of EP and EP-FRs, comparing onset temperature ( $T_{5\%}$ ), temperature of maximum mass loss rate ( $T_{max}$ ), and residue at 700 °C.

	EP	EP-poly-1	EP-poly-2	EP-BDP
$T_{5\%}$ / °C	338 ± 1	268 ± 1	289 ± 1	304 ± 1
$T_{max}$ / °C	372 ± 1	350 ± 0	351 ± 1	357 ± 0
Residue / wt.-%	4.5 ± 0.1	7.9 ± 0.3	7.7 ± 0.0	8.2 ± 0.1



**Scheme S1.** Chemical structure of bisphenol A bis(diphenyl phosphate) (BDP).

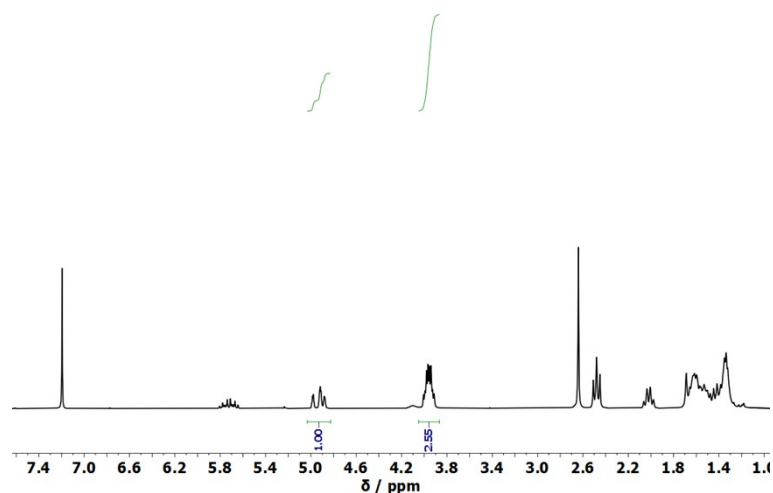


**Figure S21.**  $^1\text{H-NMR}$  (300 MHz in  $\text{CDCl}_3$  at 298 K) of **poly-2** showing a ratio of  $n_{\text{Double-bond}}/n_{\text{Ester}}$  of 0.39.

**Table S3.** Elemental analysis of **poly-2**. %C, %H, %N and %S was measured, the other values were calculated as follows:  $\%O\&P = 100 - (\%C + \%H + \%N + \%S)$ ;  $\%P_{\%O\&P} = M(P) / (4 * M(O) + M(P)) * 100\%$ ;  $\%P = \%O\&P * \%P_{\%O\&P} / 100\%$ .

	%C	%H	%N	%S	%O&P	%P <sub>%O&amp;P</sub>	%P
<i>Poly-2</i>	55.23	8.66	0	12.48	23.64	33	7.7

## 6. Summary

Due to the chemical versatility of phosphorus, phosphorus-based compounds are an important group of halogen-free flame retardants (FRs). Especially additive flame retardants may be applied in a wide range of polymer materials, and many organophosphorus-based additives have been proven effective at low loadings with reduced impact on material properties compared to conventional inorganic variants. Moreover, polymeric organophosphorus FRs are less prone to leach or bloom out of the polymer matrix. Recently, phosphorus-based polymeric FRs with complex shapes have gained attention due to their ability to further increase miscibility with and immobilization in the polymer matrix, as well as reduce the impact on material properties like glass-transition temperature, present a high functional group content, be effective at low loadings, and exhibit an increased biocompatibility.

In this work, phosphorus-based hyperbranched polymers are investigated as multifunctional flame-retardant additives to epoxy resins. In the first steps, a library of phosphorus-based flame retardants was synthesized, and their chemical structure verified, predominantly by  $^1\text{H}$  and  $^{31}\text{P}$  {H} NMR analysis, gel permeation chromatography (GPC), and in some cases via MALDI-TOF. These compounds varied in their molar mass (low molar mass monomers; hyperbranched polymers), in the chemical surrounding of phosphorus (systematically varied P-O and P-N content), aromaticity, polymerization type (ATMET;  $\text{AB}_2$  vs.  $\text{A}_2+\text{B}_3$ ), and sulfur oxidation state (thioether vs. sulfone). These compounds' pyrolysis behavior was characterized multi-methodically, and a chemical decomposition pathway was presented. The fire behavior and pyrolytic decomposition of an epoxy resin was characterized and compared to resins with 10 wt.-% loadings of the respective flame retardants to indicate the mode of action and reveal the chemical interaction between matrix and additive.

The multi-methodic approach involved investigations of the pyrolytic decomposition of the flame retardants, and the comparison of pyrolysis and fire behavior of an epoxy resin with a flame-retarded formulation. Several methods were used to identify the decomposition



products in the gas and the condensed phase, including thermogravimetric analysis, infrared spectroscopy, pyrolysis-gas chromatography/ mass spectrometry, pyrolysis combustion flow calorimetry, elemental analysis, and scanning electron microscopy. Fire tests included reaction-to-small-flames tests, e.g. limiting oxygen index and UL-94, and forced flaming tests via cone calorimeter. By interpreting the combined results, a decomposition mechanism and chemical interaction pathway was proposed to explain the detected modes of action.

The polymer matrix was an epoxy resin based on diglycidyl ether of bisphenol A (DGEBA). In an additional investigation, the efficacy of the flame retardants in DGEBA-based resins with a pentaerythritol tetraglycidyl ether-based epoxy resin was compared. DGEBA is among the most commonly used resin educts and has a wide range of applications in the electronic and electric industry, as well as in aviation and automobiles, where high-performance polymers with special properties are used. Hence, the material properties, i.e. glass transition temperature, of the matrix were investigated via differential scanning calorimetry. The hyperbranched polymers exhibited a reduced or similar effect on glass-transition temperature compared to the commercially available benchmark FR, i.e. bisphenol A diphenyl phosphate (BDP).

The investigations showed that the chemical surrounding of phosphorus plays a crucial role in the decomposition pathway and the resultant flame-retardant modes of action: while phosphoramides function primarily in the condensed phase, phosphoesters function in both gas and condensed phase. Moreover, hyperbranched polymers exhibited a high thermal stability, thus increasing the interaction between epoxy resin and flame retardant. It was shown that the resin type plays a significant role in the flame-retardancy potential due to thermal decomposition temperature overlap. This effect was also highlighted in investigations of aliphatic and aromatic FR formulations, as aromatic compounds were more thermally stable, yet aromatic hyperbranched polymers lacked chemical interaction due to their elevated decomposition temperature in comparison to the resin. Furthermore, the role of sulfur in the hyperbranched polymers' linker group was elucidated and shown to add flame-retardant functionality via thiyl-radical generation. Studies of the polymerization type ( $A_2+B_3$  or  $AB_2$ )

highlighted the increased flame-retardancy potential of AB<sub>2</sub> polymers due to higher phosphorus content. The herein presented results illuminate the multifunctional qualities of phosphorus-based hyperbranched polymers as effective flame retardants for epoxy resins and provide an insight into their chemical interaction and mode of action in pyrolytic and flaming conditions. The research presented within this work helps to understand the way in which hyperbranched flame retardants function and may improve future formulations in the ever-evolving landscape of flame retardancy of polymers.

## 7. Zusammenfassung

Phosphorbasierte Verbindungen sind eine wichtige Gruppe der halogenfreien Flammschutzmittel (FSM) aufgrund der chemischen Vielseitigkeit von Phosphor. Insbesondere additive Flammschutzmittel können in einer großen Vielfalt an Polymerwerkstoffen eingesetzt werden, und viele additive Organophosphorverbindungen haben sich bereits bei geringer Füllmenge als wirksam erwiesen. Materialeigenschaften werden hierbei im Vergleich zu herkömmlichen anorganischen Varianten weniger beeinträchtigt werden. Des Weiteren neigen polymere Organophosphorverbindungen weniger dazu aus der Polymermatrix auszulaugen oder auszublühen. Phosphor-basierte Polymere mit komplexen Strukturen haben in letzter Zeit aufgrund ihrer vielfältigen vorteilhaften Eigenschaften für Aufmerksamkeit gesorgt. Darunter zählen ihre gute Mischbarkeit mit sowie hohe Fixierung in Polymermatrices, ihre niedrigere Auswirkung auf Materialeigenschaften wie Glasübergangstemperatur, dem hohen Gehalt an funktionellen Gruppen, ihre Wirksamkeit bei niedrigen Füllmengen, und ihrer erhöhten Biokompatibilität.

In dieser Arbeit werden hyperverzweigte Polymere als multifunktionale additive Flammschutzmittel für Epoxidharze untersucht. Zunächst wurden dazu eine Reihe an phosphorbasierten Flammschutzmittel synthetisiert. Deren chemische Struktur wurde primär per  $^1\text{H}$  und  $^{31}\text{P}$  {H} NMR, Gelpermeationschromatographie (GPC) und in einigen Fällen mittels MALDI-TOF verifiziert. Die Flammschutzmittel variierten in ihrer Molmasse (niedermolekulare Monomere; hyperverzweigte Polymere), in der chemischen Umgebung des Phosphors (systematisch variierender Gehalt an P-O- und P-N-Bindungen), ihrer Aromatizität, dem Polymerisationstyp (ATMET,  $\text{AB}_2$  versus  $\text{A}_2+\text{B}_3$ ) und der Oxidationszahl des Schwefels (Thioether versus Sulfon). Das Pyrolyseverhalten dieser Verbindungen wurde multimethodisch charakterisiert und ein chemischer Abbauweg wurde erstellt. Das Brandverhalten und die pyrolytische Zersetzung eines Epoxidharzes wurde ebenso charakterisiert und mit Harzen mit 10 Gew.-% Füllmengen der jeweiligen FSM verglichen, um die Wirkungsweise zu identifizieren und die chemische Wechselwirkung zwischen Matrix und Additiv aufzuzeigen.

Der multimethodische Ansatz umfasste Untersuchungen zur pyrolytischen Zersetzung der Flammschutzmittel, sowie der Vergleich von Pyrolyse- und Brandverhalten eines Epoxidharzes mit einer flammgeschützten Variante. Zur Identifizierung der Zersetzungsprodukte in der Gas- und der kondensierten Phase wurden verschiedene Methoden angewendet, einschließlich thermogravimetrischer Analyse, Infrarotspektroskopie, Pyrolyse–Gaschromatographie/ Massenspektrometrie, Pyrolysis Combustion Flow Kalorimetrie, Elementaranalyse und Rasterelektronenmikroskopie. Brandprüfungen umfassten Entflammbarkeitsprüfungen, z.B. durch den Sauerstoffindex und der UL-94-Brennkammer, sowie Flammentests über das Cone-Kalorimeter. Durch Interpretation der jeweiligen Ergebnisse wurde ein Zersetzungsmechanismus und ein chemischer Wechselwirkungsweg vorgeschlagen, um die ermittelten Wirkungsmechanismen zu erklären.

Bei der Polymermatrix handelt es sich um ein Epoxidharz auf Basis von Diglycidylether von Bisphenol A (DGEBA). Bei einer weiteren Untersuchung wurde die Wirksamkeit der Flammschutzmittel in DGEBA-basierten Harzen mit einem Pentaerythrittetraglycidylether-basierten Epoxidharz verglichen. DGEBA gehört zu den am häufigsten verwendeten Harzedukten und hat ein breites Anwendungsspektrum in der Elektronik- und Elektroindustrie, sowie in der Luftfahrt und im Automobilbereich, wo Hochleistungspolymere mit besonderen Eigenschaften eingesetzt werden. Aus diesem Grund wurden die Materialeigenschaften der Matrix, wie Glasübergangstemperatur, mittels dynamische Differenzkalorimetrie (DSC) untersucht. Verglichen mit dem im Handel erhältlichen Referenz-FSM Bisphenol A–Diphenylphosphat (BDP), zeigten die hyperverzweigten Polymere eine verringerte oder ähnliche Wirkung auf die Glasübergangstemperatur der Matrix.

Die Untersuchungen zeigten, dass die chemische Umgebung des Phosphors eine entscheidende Rolle für den Abbauweg und die daraus resultierenden flammhemmenden Wirkmechanismen spielt: Während Phosphoramide hauptsächlich in der kondensierten Phase wirken, waren Phosphoester sowohl in der Gas- als auch in der kondensierten Phase wirksam. Darüber hinaus zeigten hyperverzweigte Polymere eine hohe thermische Stabilität, wodurch die Wechselwirkung zwischen Epoxidharz und Flammschutzmittel erhöht wurde. Es konnte

gezeigt werden, dass die Art des Harzes aufgrund der thermischen Zersetzungstemperaturüberlappung eine signifikante Rolle zum effektiven Flammenschutz beiträgt. Dies wurde auch bei Untersuchungen von aliphatischen und aromatischen FSM-Formulierungen beobachtet. Aromatische Verbindungen waren dabei thermisch stabiler als aliphatische. Aromatische hyperverzweigte Polymere hingegen wiesen nur geringe chemische Wechselwirkungen auf, da ihre Zersetzungstemperaturen höher als die der Matrix waren. Darüber hinaus wurde die Rolle von Schwefel in der Linkergruppe von hyperverzweigten Polymeren aufgeklärt und gezeigt, dass Schwefel über die Bildung von Thiyl-Radikalen eine flammhemmende Funktion bietet. Untersuchungen des Polymerisationstyps ( $A_2+B_3$  oder  $AB_2$ ) haben außerdem das erhöhte Flammschutzpotential von  $AB_2$ -Polymeren aufgrund eines höheren Phosphorgehalts aufgedeckt. Die hier vorgestellten Ergebnisse veranschaulichen die multifunktionalen Eigenschaften von phosphorbasierten hyperverzweigten Polymeren als wirksame Flammenschutzmittel für Epoxidharze und geben einen Einblick in deren chemische Wechselwirkung und Wirkungsweise unter pyrolytischen und flammenden Bedingungen. Die Forschungsergebnisse dieser Arbeit veranschaulichen, wie hyperverzweigte Flammenschutzmittel funktionieren und haben das Potential zukünftige Formulierungen in der sich ständig weiterentwickelnden Landschaft der Flammenschutzmittel für Polymeren zu verbessern.

## 8. References

1. G. L. Nelson, *Fire Retardancy of Polymeric Materials*. Marcel Dekker, New York, 2000, 1-26.
2. U. Fink and J. Troitzsch, *Plastics Flammability Handbook*. Carl Hanser Verlag, Munich, Germany, 2004, 8-32.
3. R. Geyer, J. R. Jambeck and K. L. Law, *Science Advances*, 2017, **3**, e1700782.
4. L. V. McAdams and J. Gannon, *Wiley-Interscience, Encyclopedia of Polymer Science and Engineering.*, 1986, **6**, 322-382.
5. B. Ellis, *Chemistry and technology of epoxy resins*, Springer, 1993.
6. J. L. Massingill and R. S. Bauer, in *Applied Polymer Science: 21st Century*, 2000, DOI: 10.1016/b978-008043417-9/50023-4, pp. 393-424.
7. G. Gibson, in *Brydson's Plastics Materials*, Elsevier, 2017, pp. 773-797.
8. E. A. Weil and S. V. Levchik, in *Flame Retardants for Plastics and Textiles: Practical Applications*, ed. C. Hamilton, Carl Hanser Verlag GmbH & Co. KG, Munich, 2nd edn., 2015, DOI: 10.3139/9781569905791.010 ch. 10, pp. 241-264.
9. P. Langemeier and C. Scheuer, *Reinforced Plastics*, 2010, **54**, 36-39.
10. *Epoxy Resins Market, [By Formulation Type (DGBEA, DGBEF, Novolac, Aliphatic, Glycidylamine, and, Others); By Application (Paints & Coatings, Adhesives, Composites, Electrical & Electronics, Wind Turbines, and Others); By Regions]: Market size & Forecast, 2018 - 202*, Report MSR1695248, 2019.
11. Y. C. Zheng, S. P. Li, Z. L. Weng and C. Gao, *Chemical Society Reviews*, 2015, **44**, 4091-4130.
12. L. H. Sperling, *Introduction to physical polymer science*, Wiley, Hoboken, N.J., 4th edn., 2006.
13. J. G. Quintiere, *Principles of fire behavior*, CRC Press, 2016.
14. J. H. Troitzsch, *Chemistry today*, 1998, **16**.
15. B. Schartel and T. R. Hull, *Fire and Materials*, 2007, **31**, 327-354.
16. E. D. Weil and S. V. Levchik, *Flame Retardants for Plastics and Textiles: Practical Applications*, Carl Hanser Verlag GmbH Co KG, 2nd edn., 2015.
17. S. V. Levchik, in *Flame Retardant Polymer Nanocomposites*, eds. A. B. Morgan and C. A. Wilkie, John Wiley & Sons, Inc., 2006, DOI: 10.1002/9780470109038.ch1, pp. 1-29.
18. G. J. Minkoff, *Chemistry of combustion reactions*, Butterworths, 1962.
19. R. Lyon, in *Handbook of Building Materials for Fire Protection*, ed. C. Harper, McGraw-Hill, New York, New York, 2004, pp. 3.1-3.51.
20. G. Camino, L. Costa and M. P. Luda di Cortemiglia, *Polymer Degradation and Stability*, 1991, **33**, 131-154.
21. S. Bourbigot and M. Le Bras, in *Plastics Flammability Handbook*, ed. J. Troitzsch, Carl Hanser Verlag GmbH & Co. KG, Munich, 2004, DOI: 10.3139/9783446436695.005, pp. 133-172.
22. M. Lewin and E. Weil, in *Fire retardant materials*, eds. A. R. Horrocks and D. Price, Woodhead Publishing Ltd., 2001, DOI: 10.1533/9781855737464.31, ch. 2, pp. 31-68.
23. *Additives for Polymers*, 2017, **2017**, 10-11.
24. *Specialty Chemicals Update Program: Flame Retardants*, IHS Markit, 2017.
25. M. Lewin, *Journal of Fire Sciences*, 1999, **17**, 3-19.
26. M. Lewin, *Chim Oggi*, 1997, **15**, 41-41.
27. S. Shaw, *Reviews on environmental health*, 2010, **25**, 261-306.
28. S. Kitamura, N. Jinno, S. Ohta, H. Kuroki and N. Fujimoto, *Biochem Bioph Res Co*, 2002, **293**, 554-559.

29. P. L. Lallas, *American Journal of International Law*, 2001, **95**, 692-708.
30. S. V. Levchik and E. D. Weil, *Journal of Fire Sciences*, 2006, **24**, 345-364.
31. B. Schartel, *Materials*, 2010, **3**, 4710-4745.
32. S. V. Levchik and E. D. Weil, in *Advances in Fire Retardant Materials*, eds. A. R. Horrocks and D. Price, Woodhead Publishing Ltd., 2008, DOI: Doi 10.1533/9781845694701.1.41, ch. 3, pp. 41-66.
33. A. H. Landrock, *Handbook of Plastic Foams: Types, Properties, Manufacture and Applications*, Elsevier Science, 1995.
34. F. Celebi, O. Polat, L. Aras, G. Gunduz and I. M. Akhmedov, *Journal of Applied Polymer Science*, 2004, **91**, 1314-1321.
35. T. Saito and H. Ohishi, *Journal*, 1981.
36. R. M. Perez, J. K. W. Sandler, V. Altstädt, T. Hoffmann, D. Pospiech, J. Artner, M. Ciesielski, M. Döring, A. I. Balabanovich, U. Knoll, U. Braun and B. Schartel, *Journal of Applied Polymer Science*, 2007, **105**, 2744-2759.
37. B. Perret, B. Schartel, K. Stoss, M. Ciesielski, J. Diederichs, M. Döring, J. Krämer and V. Altstädt, *Macromolecular Materials and Engineering*, 2011, **296**, 14-30.
38. E. N. Peters, *Journal of Applied Polymer Science*, 1979, **24**, 1457-1464.
39. U. Braun and B. Schartel, *Macromolecular Chemistry and Physics*, 2004, **205**, 2185-2196.
40. E. Michels and H. Staendeke, *Phosphorus Sulfur*, 1987, **30**, 637-640.
41. E. Gallo, B. Schartel, U. Braun, P. Russo and D. Acierno, *Polymers for Advanced Technologies*, 2011, **22**, 2382-2391.
42. U. Braun, A. I. Balabanovich, B. Schartel, U. Knoll, J. Artner, M. Ciesielski, M. Döring, R. Perez, J. K. W. Sandler, V. Altstädt, T. Hoffmann and D. Pospiech, *Polymer*, 2006, **47**, 8495-8508.
43. E. Wawrzyn, B. Schartel, M. Ciesielski, B. Kretzschmar, U. Braun and M. Doring, *European Polymer Journal*, 2012, **48**, 1561-1574.
44. E. D. Weil, S. V. Levchik, M. Ravey and W. M. Zhu, *Phosphorus Sulfur*, 1999, **144**, 17-20.
45. S. Rabe, Y. Chuenban and B. Schartel, *Materials*, 2017, **10**, 23.
46. J. Green, in *Fire Retardancy of Polymeric Materials*, eds. A. F. Grand and C. A. Wilkie, Marcel Dekker, Inc., New York, 1st edn., 2000, ch. 5, pp. 147-170.
47. M. M. Velencoso, A. Battig, J. C. Markwart, B. Schartel and F. R. Wurm, *Angew Chem Int Edit*, 2018, **57**, 10450-10467.
48. J. Green, *Journal of Fire Sciences*, 1996, **14**, 353-366.
49. M. Ciesielski, B. Burk, C. Heinzmann and M. Döring, in *Novel Fire Retardant Polymers and Composite Materials*, ed. D.-Y. Wang, Woodhead Publishing, 2017, DOI: 10.1016/B978-0-08-100136-3.00002-9, ch. 2, pp. 3-51.
50. K. A. Salmeia and S. Gaan, *Polymer Degradation and Stability*, 2015, **113**, 119-134.
51. X. Wang, Y. A. Hu, L. Song, W. Y. Xing and H. D. Lu, *J. Polym. Sci. Pt. B-Polym. Phys.*, 2010, **48**, 693-705.
52. A. Dumitrascu and B. A. Howell, *Polymer Degradation and Stability*, 2012, **97**, 2611-2618.
53. *Journal*, 2006, 1-849.
54. M. Rakotomalala, S. Wagner and M. Döring, *Materials*, 2010, **3**, 4300-4327.
55. K. H. Pawlowski and B. Schartel, *Polymer International*, 2007, **56**, 1404-1414.
56. B. Perret, K. H. Pawlowski and B. Schartel, *Journal of Thermal Analysis and Calorimetry*, 2009, **97**, 949-958.



57. L. Zang, S. Wagner, M. Ciesielski, P. Müller and M. Döring, *Polymers for Advanced Technologies*, 2011, **22**, 1182-1191.
58. B. Schartel, A. I. Balabanovich, U. Braun, U. Knoll, J. Artner, M. Ciesielski, M. Döring, R. Perez, J. K. W. Sandler, V. Altstädt, T. Hoffmann and D. Pospiech, *Journal of Applied Polymer Science*, 2007, **104**, 2260-2269.
59. A. Lederer and W. Burchard, *Hyperbranched Polymers: Macromolecules in between deterministic linear chains and dendrimer structures*, Royal Society of Chemistry, 2015.
60. B. I. Voit and A. Lederer, *Chemical Reviews*, 2009, **109**, 5924-5973.
61. D. Yan, C. Gao and H. Frey, *Hyperbranched polymers: synthesis, properties, and applications*, John Wiley & Sons, 2011.
62. B. Schartel and J. H. Wendorff, *Polym Eng Sci*, 1999, **39**, 128-151.
63. C. J. Hawker, R. Lee and J. M. J. Frechet, *Journal of the American Chemical Society*, 1991, **113**, 4583-4588.
64. S. E. Stiriba, H. Frey and R. Haag, *Angew Chem Int Edit*, 2002, **41**, 1329-1334.
65. M. Calderon, M. A. Quadir, S. K. Sharma and R. Haag, *Adv Mater*, 2010, **22**, 190-218.
66. P. Y. Wen, X. F. Wang, W. Y. Xing, X. M. Peng, B. Yu, Y. Q. Shi, G. Tang, L. Song, Y. Hu and R. K. K. Yuen, *Industrial & Engineering Chemistry Research*, 2013, **52**, 17015-17022.
67. K. C. Cheng, C. C. Wang, J. L. Ruan, C. H. Wu and C. W. Li, *Polymers for Advanced Technologies*, 2018, **29**, 2529-2536.
68. K. Täuber, F. Marsico, F. R. Wurm and B. Schartel, *Polym Chem-Uk*, 2014, **5**, 7042-7053.
69. P. J. Flory, *Journal of the American Chemical Society*, 1952, **74**, 2718-2723.
70. T. Emrick, H. T. Chang and J. M. J. Frechet, *Macromolecules*, 1999, **32**, 6380-6382.
71. M. Jikei, S. H. Chon, M. Kakimoto, S. Kawauchi, T. Imase and J. Watanebe, *Macromolecules*, 1999, **32**, 2061-2064.
72. J. M. J. Frechet, M. Henmi, I. Gitsov, S. Aoshima, M. R. Leduc and R. B. Grubbs, *Science*, 1995, **269**, 1080-1083.
73. M. Suzuki, A. Ii and T. Saegusa, *Macromolecules*, 1992, **25**, 7071-7072.
74. P. Kubisa, *J Polym Sci Pol Chem*, 2003, **41**, 457-468.
75. A. Battig, J. C. Markwart, F. R. Wurm and B. Schartel, *Polym Chem-Uk*, 2019, **10**, 4346-4358.
76. A. B. Lowe, *Polym Chem-Uk*, 2010, **1**, 17-36.
77. E. Wawrzyn, B. Schartel, M. Ciesielski, K. Bernd, U. Braun and M. Döring, *European Polymer Journal*, 2012, **48**, 1561-1574.
78. F. Marsico, M. Wagner, K. Landfester and F. R. Wurm, *Macromolecules*, 2012, **45**, 8511-8518.
79. M. R. Acocella, C. E. Corcione, A. Giuri, M. Maggio, A. Maffezzoli and G. Guerra, *Rsc Adv*, 2016, **6**, 23858-23865.
80. A. Battig, J. C. Markwart, F. R. Wurm and B. Schartel, *Polymer Degradation and Stability*, 2019, **170**.
81. W. Grellmann and S. Seidler, *Kunststoffprüfung*, Carl Hanser Verlag GmbH Co KG, 2015.
82. R. E. Lyon and M. L. Janssens, in *Encyclopedia of Polymer Science and Technology*, John Wiley & Sons, Inc., 2002, DOI: 10.1002/0471440264.pst135.pub2.
83. M. L. Janssens, *Fire Technol*, 1991, **27**, 234-249.
84. Shimadzu, Pyrolysis gas chromatography mass spectrometry, ([www.shimadzu.com/an/gcms/n9j25k0000e4swe.html](http://www.shimadzu.com/an/gcms/n9j25k0000e4swe.html), 2019).



## **Statement of Authorship / Selbstständigkeitserklärung**

I hereby certify that the herein presented dissertation was authored by myself and was completed using only the cited literature and sources.

Hiermit versichere ich, dass die vorliegende Dissertation selbstständig und lediglich unter Benutzung der angegebenen Quellen und Hilfsmittel verfasst habe.

Berlin, 04.09.2020

Alexander Battig